Cranfield University

M. H. Raffles

Elid Superfinishing of Spherical Bearings

School of Applied Sciences

PhD THESIS

Cranfield University

School of Applied Sciences

PhD THESIS

2007

Mark H. Raffles

Elid Superfinishing of Spherical Bearings

Supervisors: Professors David Stephenson, Paul Shore

Academic Years 2003 to 2007

ABSTRACT

Driven by a requirement to extend the lifespan of self-aligning lined spherical bearings, this research investigates the use of Elid (electrolytic in-process dressing) as a method of improving ball surface finish. Elid is a continuous and self-regulating electro-chemical dressing process that modifies the surface of a grinding, lapping, or superfinishing wheel. It provides improved grit protrusion, impedes wheel loading / glazing and promotes effective cutting.

The characteristics of the newly-developed Elid superfinishing process are in many ways fundamentally different to conventional superfinishing. The main difference is that the use of super-abrasives prevents the wheel from self-sharpening; the normal mechanism by which dulled conventional abrasives are removed and a wheel's surface refreshed. Because the wheel's performance and condition is continually maintained in-process by the Elid system, metal resin bonded (MRB) wheels containing very small super-abrasives can be used. It is the utilization of these fine abrasives (30 to 0.12 μm) that enables surface roughness values below 5 nm Ra to be consistently produced on the spherical surface of corrosion-resistant steel balls.

This research provides an in-depth understanding of the Elid spherical superfinishing process; investigating the most effective use of the Elid system, wheel dressing requirements and process performance. Optimisation is provided in terms of evaluating the critical operating parameters, the most effective superfinishing cycle and the implications to the complete ball production chain. A range of techniques are used to evaluate processing performance and ball output quality. These include in-process monitoring of Elid and wheel spindle power levels, analysis of wheel condition, rates of ball surface generation and material removal, ball finish and form. Although predominantly concentrated on corrosion-resistant steel, testing is also conducted on titanium and various ball coatings.

In investigating various ways of using the Elid system, this work considers electro-discharge truing, pre-process dressing, Elid 1, Elid 2, Elid 3, and Elid combined with electrolytically assisted superfinishing. The initial process solution of Elid 3 (electrode-less) superfinishing provides the capability of working on all standard size balls, however the dressing system lacks stability. The development of a fixturing system that has a small separate electrode enables Elid 1 (conventional) to be used on the majority

of ball sizes. Elid 1 allows more aggressive and consistent dressing, a faster rate of ball material removal and thus a substantially reduced processing time.

Results with a #12,000 wheel show that surface quality is vastly improved through the use of Elid whilst maintaining current production standards of form accuracy. Surface finishes of 2nm Ra are achieved, which is an order of magnitude better than balls currently produced using barrelling / polishing. Processing times are equivalent or faster when using Elid 1. Alternatively, consistently sub 10 nm Ra finishes can be reached with a #2,000 wheel using Elid 2 (interval dressing). Generally MRB-CBN wheels provide a more effective carbide cutting action than conventional superfinishing wheels.

Controlling wheel condition and achieving full and even ball to wheel conformity are the two most significant contributory factors to the success of Elid spherical superfinishing. Insufficient control of these factors results in poor output quality. Monitoring of wheel spindle and Elid power usage provides useful information in assessing the condition of the wheel and identifying potential problems. High spindle power correlates with fast material removal and is a result of high loads and a free cutting action. Elid processing can be employed for improving surface finish after the conventional honing stage, or after cylindrical grinding for improving both ball form and finish.

ACKNOWLEDGEMENTS

I would like to thank the following people for their invaluable assistance in conducting and completing this research:

- John Hedge, Technician, for his unfailing support and advice during the intensive testing periods.
- Other technical staff, Andrew Baldwin, Alan Heaume, for their assistance.
- Workshop staff, particularly Paul, for their assistance with the fixturing.
- Supervisors Professors' David Stevenson and Paul Shore, for their comments, advice, and guidance.
- The industrial sponsors NMB Minebea UK Ltd, in particular Paul Smith, Steve Essam, Jamie Back and Tony Richardson.
- Wheel manufactures FujiDie and Darmann abrasives.
- My partner, Lisa Mitchell, who helped me extensively with proof reading as well as provided moral support and encouragement.
- My parents, who assisted with proof reading.

TABLE OF CONTENTS

INTRODUCTION

Chapter 1

1.1 Scope

This research investigates the use of Elid (electrolytic in-process dressing) as a method of superfinishing balls used in spherical bearings, in order to improve surface finish and extend bearing life. Superfinishing is a new use of the Elid method that differs substantially from Elid grinding. Several distinct types of Elid are tested, including Elid 2 and Elid 3, which adds significantly to the existing knowledge base and literature available on these types. The use of Elid superfinishing in the production of spherical ball bearings has not been studied before. The research will therefore add substantially to the current understanding, particularly pertaining to metal-resin bond (MRB) wheels and spherical surfaces. The focus is to develop this new finishing process in order to provide an efficient, repeatable, and usable method of achieving sub 10nm Ra surface finishes whilst maintaining ball form accuracies. Elid superfinishing is compared to standard production methods, as well as to non-Elid processing using very fine abrasive wheels. Alternative ball materials, principally titanium, are examined along with steel. This thesis does not cover the superfinishing of other components with spherical surfaces, or other components of different geometries. Although the improved surface finish achieved through this new processing method is of benefit because it extends bearing life, the life extension achieved is not assessed within this body of work.

1.2 Statement of Research Objectives / Purpose for Research

The aim of this research is to deliver a working process to achieve sub 10nm Ra surface finish on spherical bearings.

There is a particular requirement for the ability to produce spherical ball bearings to a variety of standards; including the potential to improve surface finish and surface integrity, as well as to reach the desired quality in the most cost efficient way. This PhD is a collaborative research project, between NMB Minebea UK Ltd in Lincoln and Cranfield University, undertaken to realise the following goals:

(1) Further the understanding of the Elid 3 process using MRB wheels.

(2) Improve the understanding of Elid as it pertains to the superfinishing of a ball's spherical surface.

(3) Achieve an improved surface finish over and above the best currently available for the purpose of extending the life of the bearing. Provide a way to reduce the surface roughness to below 10nm Ra, currently unachievable at NMB.

(4) Shorten the process route and provide an improved alternative to the current superfinishing processes. Enable roughing and finishing operations to be completed on one machine.

(5) Assess the most suitable point for Elid to enter the current process chain.

(6) In-process monitoring of the Elid superfinishing system leading to a simple to use process with easy detection of undesirable processing conditions.

(7) Optimisation in terms of efficiency and output quality providing a highly repeatable product for use in production.

(8) In addition to providing a method of processing balls made from hardened bearing steel, evaluate the performance when Elid superfinishing is applied to balls made from titanium.

1.3 Background of Research Participants

NMB-Minebea U.K. Ltd is a market leader in the design and manufacture of precision Rod End, Self-Aligning Spherical Bearings and Lined Bushes. The company is focused on high quality at competitive costs, based on innovation, development and technical expertise. The Lincoln site is the headquarters of European operations, offering high performance standard products and tailored design solutions primarily to the aerospace and automotive industries.

Cranfield University is well recognized by industrial and commercial sponsors as being a world leader for strategic and applied research, development and design. Cranfield is a small almost entirely postgraduate University, however the focus on industrial partnership provides contract research income that places it among the largest and top UK universities. Part of the School of Applied Sciences, the precision machining laboratories, are among the best equipped in Europe and at the forefront of grinding research and development.

This research is also funded in part by the Engineering and Physical Sciences Research Council. The EPSRC is the main UK government agency for funding research and training in engineering and the physical sciences.

1.4 Types and Applications of Spherical Bearings

Self-aligning spherical bearings function as joints and are used extensively in the automotive and aerospace industries. The most prominent producer of this type of bearing (60% market share) is the industrial sponsor NMB Minebea [1, 2].

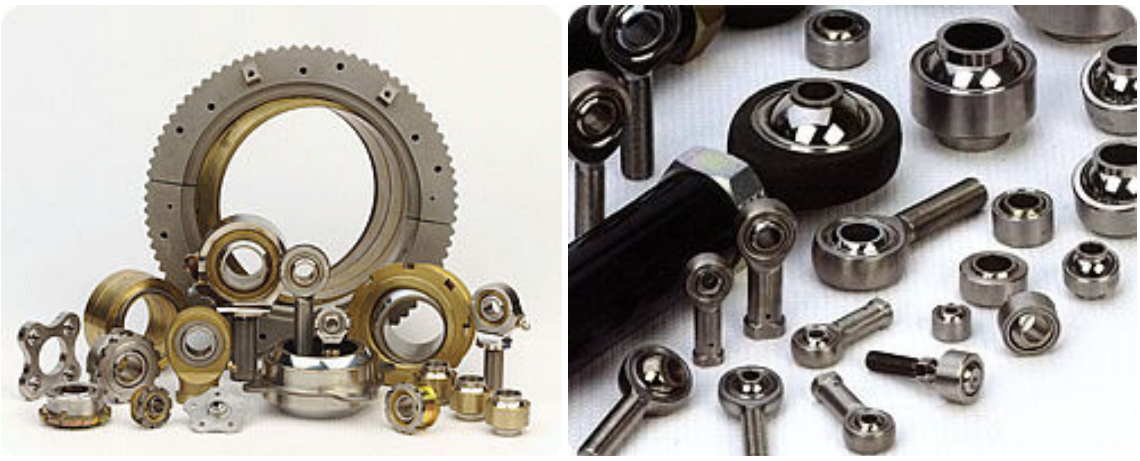

Figure 1 - Selection of spherical bearings & rod ends [2].

Spherical bearings are often used at high pressures and subjected to various (but relatively slow) rotational and misalignment movements and speeds, as well as environmental conditions. Long life applications, such as bearings used in helicopter rotors, require optimum surface characteristics in order to achieve the required performance and reliability.

This research considers the production of balls that correspond to the standard NMB Minebea UK catalogue range of spherical bearings. Within the standard range are a number of distinctions that relate to the type of spherical bearing and can ultimately affect the manufacture and requirements of the bearing ball. These are:

- The bearing's size, including whether it is metric or imperial, narrow or wide series.
- Whether it is lined (figure 2), or metal to metal (figure 3)
- If it is a high angle bearing (figure 3)

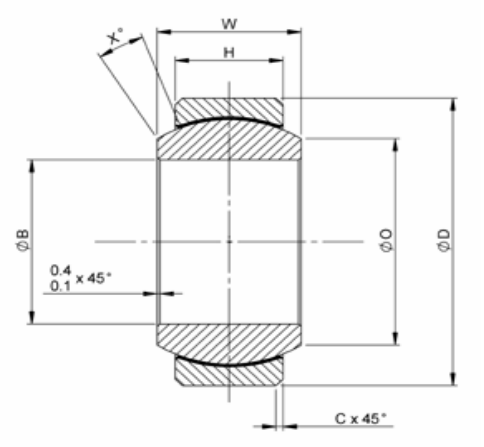

Figure 2 - MND Series
(Metric, Narrow, Lined, Chamfered) [1]

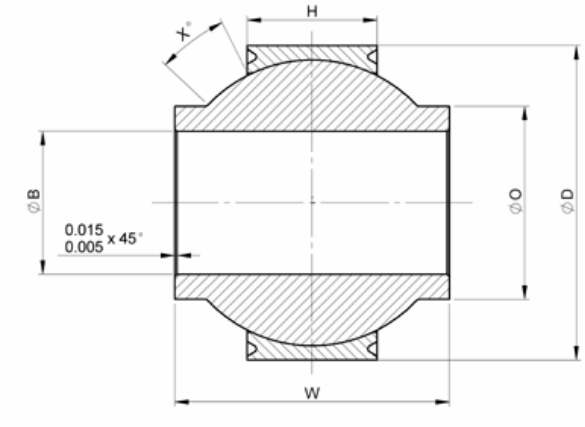

Figure 3 - RBTWG Series
(High Angle, Imperial, Metal to Metal, Grooved) [1]

P/N	Bore (B)	Width (W)	Face O/D (O)	Ball O/D
RNB08	0.5	0.5	0.6	0.781
MNRFB08GA	0.315	0.59	0.512	0.781
RBJB208 EXP D3	0.75	0.56	0.951	1.104
RNDEB14	0.875	0.875	0.980	1.375
RBFB16AB	1.000	1.875	1.276	1.9685

Figure 4 - Dimensional information of balls used in this research (Inches)

Taking into consideration the standard range of sizes for lined spherical bearings, ball outside diameters (O/D) vary from 11 to 82 mm. This research concentrates on optimising the process to produce a tailored ball surface to work with the liner systems. With metal to metal bearings very fine finishes are not necessarily associated with extended bearing life and a different surface topography is required to achieve this. As described later in the thesis, the balls from both high angle bearings and small size bearings cannot be superfinished using Elid 1. Outside the remit of this research, the ability of Elid superfinishing to produce very smooth surfaces could be applied to ball pins, bushes, bearing raceways, and various bespoke bearing applications.

Various materials are used for spherical balls but this research concentrates predominantly on the standard ball material, AMS5630. This is similar to AISI 440C and is a corrosion resistant bearing steel, the composition of which can be seen in figure 5. Titanium is increasingly being used as a ball or ball substrate material as it offers a considerable weight saving advantage over steel. The potential of Elid superfinishing as a method to produce a suitable bearing surface on Ti6Al4V is also evaluated.

Properties	Value
Material & Treatment	AMS5630 (Hardened [HT11])
Ultimate Tensile Strength	1750
Yield Strength (MPa)	1280
Modulus of Elasticity, Tension (GPa)	200
Hardness (Hv)	58 - 62
Density (g/cm3)	7.75
CTE, linear 20°C (µm/m-°C)	10.2
Heat Capacity (J/g-°C)	0.46
Maximum continuous service Temp in Air (°C)	760

Element	Maximum	Minimum
Carbon	1.20	0.95
Silicon	1.00	-
Manganese	1.00	-
Phosphorus	0.040	-
Sulphur	0.030	-
Chromium	18.00	16.00
Molybdenum	0.65	0.40
Nickel	0.75	-
Copper	0.50	-

Figure 5 - Mechanical Properties & Chemical composition of AMS5630 corrosion-resistant steel

There are various ball coatings used to extend bearing life in aggressive environments or high cycle applications. In this research Elid superfinishing is tested on Apticote 100T Chrome-coated titanium balls and nitrided titanium balls. A hardwearing Tungsten Carbide and Graphite coating (Balinit C) is applied using physical vapour deposition (PVD) to a thickness of 1 µm after ball processing. As the resultant surface finish is highly dependent on the initial surface finish its combination with Elid superfinishing can be considered where the longest bearing life spans are required.

1.5 Tribology, Friction and Wear

Tribology is an integral aspect of bearing design; the topography of contacting surfaces affects the wear properties and mechanisms. In order to produce a bearing capable of extended life it is necessary to understand how surface topography, as well as surface and sub-surface metallurgy, affect both friction and wear. Bearing surfaces are highly engineered and the resulting surface characteristics are dependent on the process type and capabilities.

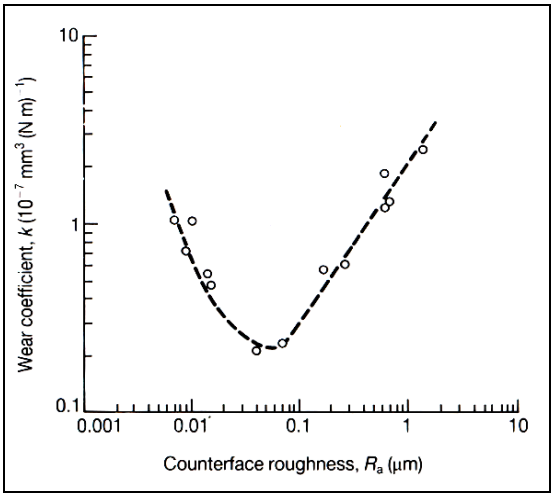

Figure 6 - Wear rate of ultra-high molecular weight polyethylene (UHMWPE) sliding against a steel counter-face, as a function of the roughness of steel surface [3]

As shown in figure 6, low wear rates can be achieved at surface roughness values corresponding to the change in wear mechanisms [3]. The predominant wear mechanism for a smooth surface will result from interfacial (adhesive) wear. Cohesive wear from surface perturbations will be minimal. Third body contaminants and chemical effects at the surface also play an important role. For polymers the transition between wear mechanisms typically occurs at counter-face Ra values between 0.01 to 1 μm. This would suggest that the lowest wear rate does not always correspond to the smoothest surface finish. Under certain conditions a strongly adhered and stable transfer film of highly oriented PTFE adheres to the counter-face material, preventing further transfer and resulting in low friction and wear rates at very smooth counterface finishes. The condition of the transfer film, typically 5 to 10 nm thick, is precarious and requires slow sliding speeds.

Dynamic life testing of lined spherical bearings conducted at NMB prior to the commencement of this PhD, found bearing life was extended when smoother than standard surfaces were employed due to reduced wear in the liner [4]. It is the bearing life extension provided by the combination of liner systems ('D' and 'RE' in particular) and very smooth ball surfaces that is the driving force behind the development of the Elid superfinishing process.

There are numerous different liner systems employed at NMB Minebea UK Ltd, and various others throughout the NMB group. The use of a self-lubricating liner provides maintenance free operation throughout a bearing's lifespan. The 'D' liner system is one of the most effective and widely used types available. Associated performance includes a static load capacity of 541MPa, a dynamic capacity of 258 MPa, an operating temperature range between –54C to +200C, and a low coefficient of friction (figure 7). 'D' liner consists of woven textiles containing Nomex and PTFE yarns and resins. In addition, it is also enriched with extra PTFE at the bearing surface. The 'RE' liner system consists of PTFE flock and Nomex fibre with Vinyl Phenolic resin matrix, enriched with PTFE.

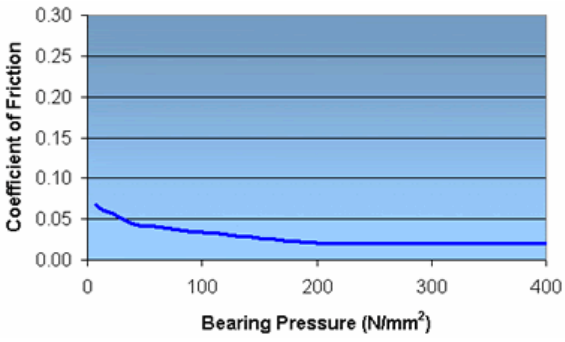

Figure 7 - Dynamic Coefficient of Friction – Type D liner [1]

On contact the surface asperities of both the rigid ball and compliant PTFE liner materials result in elastic deformation of the liner against the ball. With lined spherical

bearings, wear predominantly occurs in the soft liner material as it is abraded away by the harder counter-face of the ball. The measurement of axial / radial bearing play during life testing is used to evaluate bearing wear. Both in testing and in actual operation an excessive amount of bearing play denotes the end of the bearing's usable life. An initially high rate of wear generally occurs during the bedding-in stage. This is often followed by a steady state period before the wear rate begins to rise until the bearing is deemed to have failed. Figure 8 shows the life of bearings superfinished with standard techniques and those produced to a much finer surface finish (examples 3, 4 and 5). Examples with an improved surface finish significantly increased bearing life.

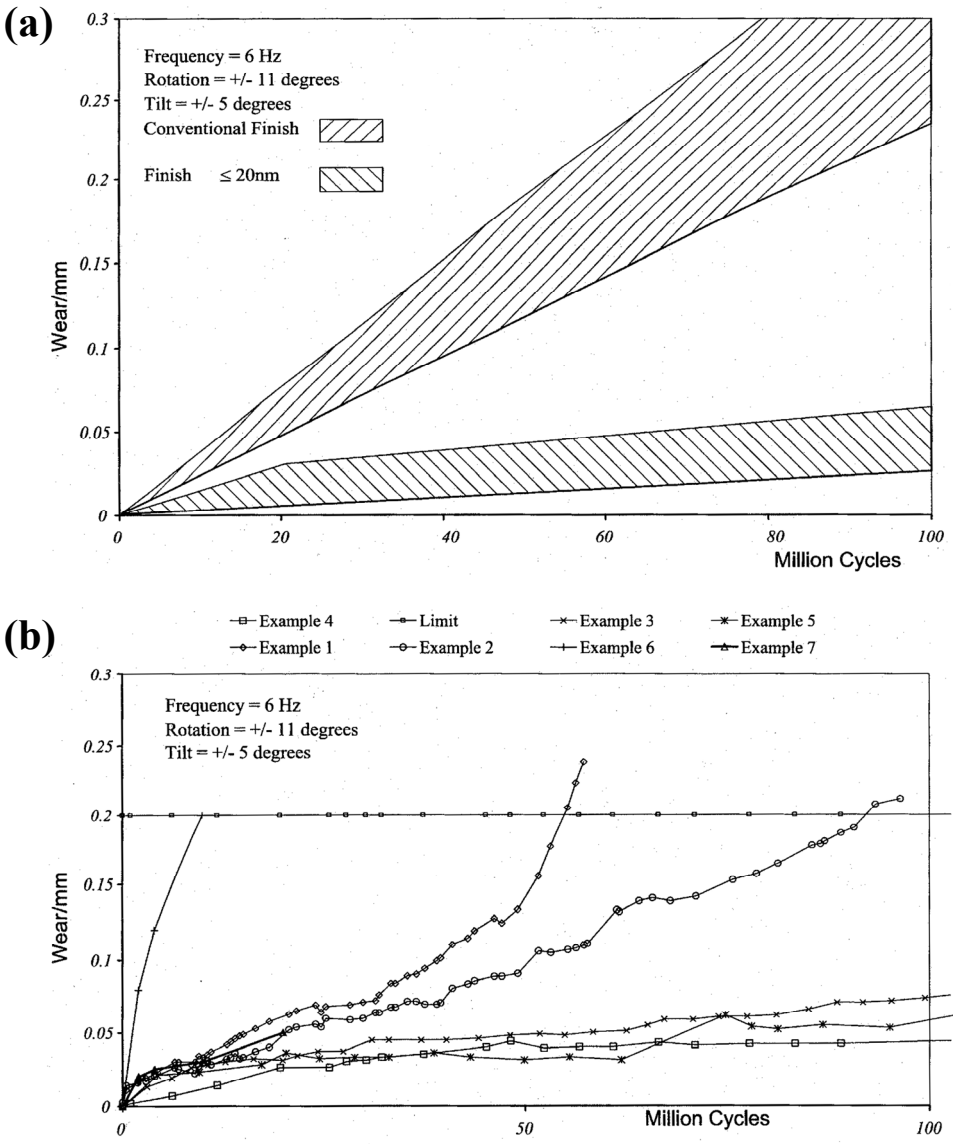

Figure 8 - Dynamic bearing life testing of standard, coated, and Elid superfinished spherical bearings, (a) Graphical comparison showing the influence of surface finish, (b) wear test results - [4]

1.6 Details of the Conventional NMB Ball Process chain

The existing NMB process chain used to produce the spherical surface of a ball is shown in figure 9. It consists of turning, heat treatment, cylindrical grinding, honing, and either polishing or barrelling. Production is carried out in batches that generally range from 50 to 200 bearings. The route the ball takes around the factory can vary as required and thus times will change. Differences in times due to the size of the ball should be minimal for the standard size range of balls.

Figure 9 – STANDARD BALL SPHERICAL SURFACE PRODUCTION DETAILS

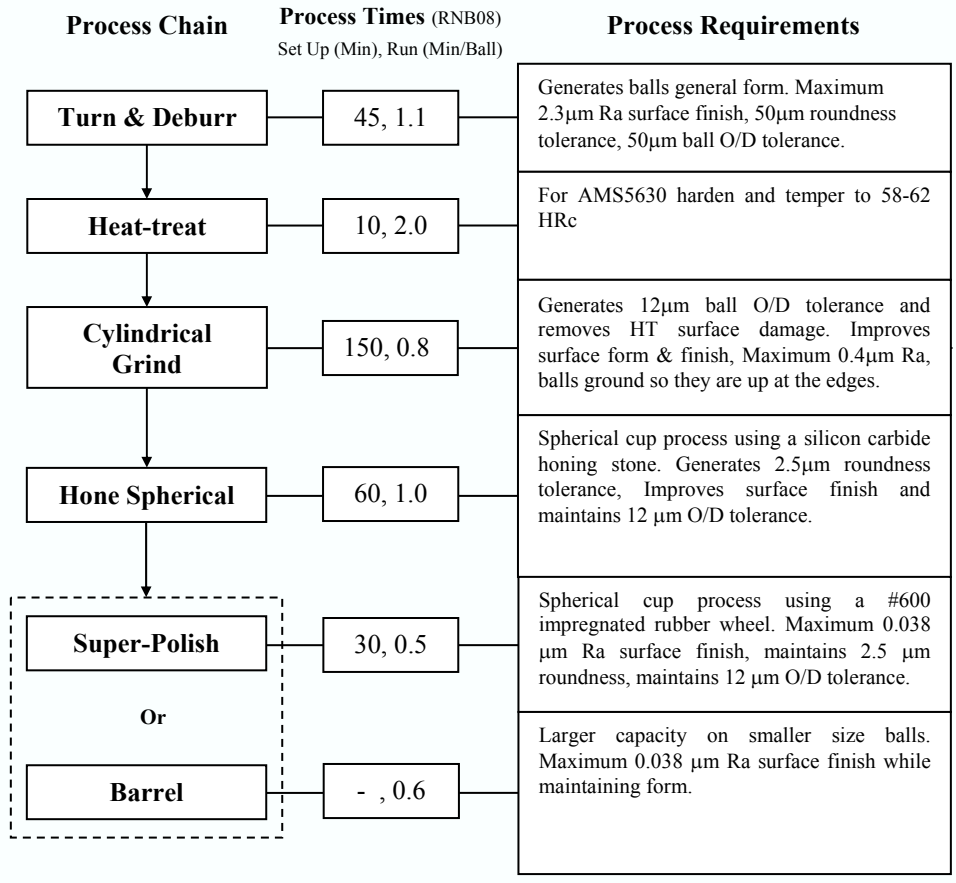

The cost of an RNB08 ball is £4.98, of which 27p is materials, 89p is labour, and £3.82 is overheads (batch size dependent). The manufacturing drawing for RNB08 balls can be seen in appendix B1.

1.6.1 Turn & Deburr

Produced on CNC lathes, the general form of the balls is generated to within a 50μm tolerance band on the ball roundness and ball O/D. Any failure to meet this requirement is generally a result of set-up errors or tool wear. Along with tool wear the machines are capable of monitoring load, machine power usage, displacement, and speeds. For an RNB08 ball the set-up time is around 45 minutes and a run time of about 70 seconds per ball. The material is turned in the as-received fully annealed condition prior to being heat treated.

1.6.2 Heat-treatment

Heat-treatment of AMS 5630 consists of preheating (40 minutes at 780C), heating to hardening temperature (80 minutes at 1050C), oil quenching, sub-zero treatment (210 minutes -70 C), and tempering (130 minutes at 175C). Heat-treatment takes around 11 hours per load; set-up time is negligible and only consists of loading and unloading. As the capacity to heat-treat RNB08 balls (~1000 per load) exceeds the size of batches, a requirement for a large enough quantity of balls to be heat-treated can be a bottle-neck in the system. Batches of balls of differing size are combined. The hardening and low temperature tempering of the balls to between 58 and 62 HRc, results in the creation of a surface layer that must be fully removed by subsequent processing.

1.6.3 Cylindrical Grind Spherical

The ball faces are ground before cylindrical grinding the spherical surface, with either face being used as the datum reference. Whether the bore requires grinding first depends on the holding method used to grind the spherical. On the shoe centre-less NC machines the spherical is ground before the bore, due to the problem of spherical - bore concentricity. On the CNC machines the bore is ground first and the spherical surface is ground on a mandrel. One problem with this is distortion, or squashing, when the mandrel is removed. The cylindrical grinding operation typically uses vitrified bond grinding wheels containing CBN abrasive grits #80 - #100 mesh size. In a cycle time of ~48 seconds, the cylindrical grinding process reduces the O/D by 120 μm and is responsible for achieving a 12 μm tolerance band.

1.6.4 Superfinish Spherical (Honing)

There are two machines at NMB for standard superfinishing, a CNC machine with an auto loading system and an NC machine with manual loading on a rotating loader. The CNC machine is used for honing as well as polishing. Workpiece holding is a roller-centric method with vertical play in one of the driving rollers. Approximately two thirds of the production is of a standard catalogue type and the remainder are specialist products. Machine set up takes around one hour.

The honing process uses green silicon carbide stones that are the same size and shape as the MRB Elid wheels used in this research. A choice of hard or soft grades is available depending on the requirements. An estimate of the number of balls produced from each stone in its usable life is 400 – 500 balls. The stones are bonded onto their reusable steel mountings with Loctite and the grinding surface is roughly shaped, by hand, with a metal stylus tool. Resultant stone wear / bedding-in, and the spindle rotation self-generate the spherical surface of the wheel more accurately. There is no noticeable difference in the process variability or quality from newly shaped, to a state where the spherical surface is fully formed. The process uses an oil-based cutting fluid lubricant.

The honing process is broken up into 3 sub-sections: roughing, finishing and spark-out. These are CNC controlled and run continuously in cycle, the difference being the z-axis position of the wheel spindle. For the finishing and spark-out process this is varied and thus force applied through the spring is varied. The wheel spindle speeds are up to 2500rpm (3000 max) for smaller sizes, and the drive roller rotation is up to 145rpm. The ratio of wheel to ball spindle speed is around 1 to 1. This results in a skewed crosshatch patterning of scratches being introduced onto the ball surface.

Visual reading and adjustment of dial gauges (x and y directions) are used for centring the ball to the wheel at the start of a run. No adjustment is made to account of variances through the batch. It is possible to visually inspect the surface of the ball after the honing process to determine if there is a problem. The O/D of each ball is gauged to determine whether it is within tolerance. First on and last off balls are roundness measured up and down the ball.

1.6.5 Superfinish Spherical (Polishing)

Polishing is generally the same set-up as with honing. However the polishing process uses faster speeds with larger loads and more fluid. There is no spark out used in the polishing process and the wheel is encouraged to rapidly move off the ball at the end of the run. This prevents any caught up debris damaging the surface. In addition to the roller-centric superfinishing machines, the machine used for Elid at NMB is occasionally used for honing and polishing. Factors influencing the use of Elid on the roller-centric machine relate to the development of electrical insulation of the ball and wheel fixturing.

1.6.6 Superfinish Spherical (Barrelling)

Barrelling operations (tumbling, rumbling, vibratory-finishing) combine an abrasive media, water solution and the components being processed, into a container. The relative kinetic motion (rotary, centrifugal, or vibratory) between the components and the abrasives provides a cutting or polishing action. Two types of barrelling operations are used for two main reasons. (1) To remove ball edges after cylindrical grinding and (2) to achieve final finishing after honing. Various grades of stones / abrasives are used and most of the standard bearings undergo some form of barrelling operation.

High energy vibratory-finishing operations used for final finishing typically take 2 hours per run. Batches of small size balls, such as RNB08, are processed with balls wired together to prevent damage caused by collisions. The capacity of large ball sizes becomes limited, as on occasion they requiring processing individually in a chamber. Its use as a finishing operation is therefore best suited for small ball sizes. It is not possible to just barrel the balls with finer abrasive in order to get the required sub 10 nm Ra finishes because it would take an excessively long time. In addition the carbides in the ball's surface would be removed at a slower rate, resulting in a dappled surface with large peaks.

1.6.7 Inspection & Crack Detection (NDT)

Non-destructive testing (NDT) in the form of die penetrant or magnetic particle inspection is performed on a sample of balls after superfinishing. Neither the swaging process, nor subsequent operations involved in the production of a complete spherical bearing, affect the ball. After completion the bearing goes back for 100% NDT.

LITERATURE REVIEW

This research is multidisciplinary in nature and spans many aspects of science and engineering. The following literature review provides a brief outline of many of the relevant topic areas, for which a comprehension is required, in order to evaluate Elid superfinishing. Before reviewing the Elid process it is worth looking at general abrasive processing. The literature on Elid grinding is extensive. However, as its application for the spherical superfinishing of bearing balls is new, no published literature is available. The review of the Elid literature will initially cover the basic principles, before reviewing the different configurations, types and performance of wheels and fluids in more depth. Finally brief details will be given on the processing of titanium, and the methods of in-process monitoring used.

Chapter 2 - General Abrasive Processing

Abrasive processes such as grinding, honing and superfinishing, involve the removal of workpiece material through the abrasive action of hard particles embedded in a wheel or stone. They are generally used as a finishing operation when fine surface finishes and high dimensional accuracy are required. The definitions of the various abrasive processes are in some cases ambiguous, in particular concerning the current research.

According to Shaw [5], grinding processes can be divided into two regimes that relate to the primary concern of the process, (1) stock removal grinding and (2) form and finish grinding. The distinction between abrasive processes is often based on the rate of workpiece material removal. Metzger [6] distinguishes honing from grinding as it is not a high-speed material removal process, and superfinishing is characterised by Knight [7] as having comparatively lower stock removal rates and producing smoother surface finishes than honing. McKee [8] defines honing as the application of an abrasive stick or stone to the internal hole or bore of a component, whereas superfinishing is the application to an external surface. Lapping applies to a number of loose abrasive flat finishing operations; lap-grinding on the other hand uses a wheel with fixed abrasives. Operations involving free-flowing abrasives, such as barrelling, are termed mass finishing.

Many aspects of the well established literature covering the principles and theory of abrasive processing are relevant to the current Elid superfinishing research. As the current research uses very fine abrasives (#500 to #120,000 mesh wheels) and is subject to low rates of material removal, only the precision end of grinding is of relevance. Unlike conventional Elid grinding, in this research Elid is applied to a constant force process. These aspects are classically associated with lapping, honing and superfinishing. However metal bonded superabrasive wheels are used that do not rely on the self-sharpening mechanism and are normally associated with precision grinding. In order to resolve any ambiguities this process is referred to as an Elid spherical superfinishing process.

2.1 Abrasive Wheels / Stone Details

There are three main elements that make up the structure of bonded abrasives, such as grinding wheels and honing stones (figure 10). These are (1) the type of abrasive, (2) the bonding material and (3) the wheel's porosity. The relative proportions of the three elements affect the performance of a particular wheel. A wheel with an open structure has a large degree of porosity which provides clearance for grinding chips. Dense wheels with relatively little porosity generally obtain better surface finishes and dimensional control [9].

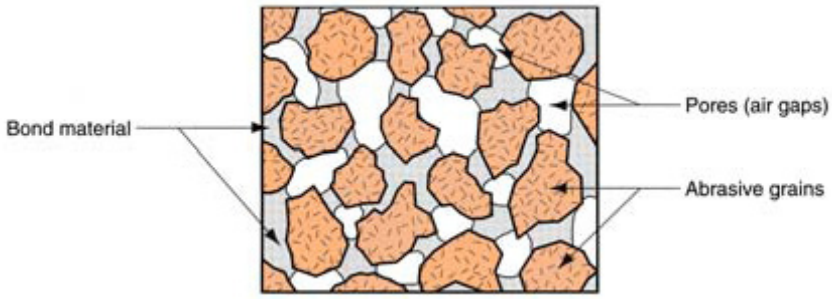

Figure 10 - Grinding wheel structure [9]

Two standardized specification systems, one for conventional abrasive wheels and one for superabrasive wheels, are employed to provide information about a particular wheel (appendix A). Conventional abrasives include various types of (Al_2O_3) aluminium oxides denoted by an (A) and (SiC) silicon carbides denoted by a (C), with a prefix number used by the manufacturer to indicate the individual abrasives in their range. Superabrasive wheels refer to those which either use diamond (D) or cubic boron nitride (B) as the abrasive.

Factors such as hardness, wear resistance, strength, impact resistance and fracture toughness, are specific to the abrasive types. Figure 11 shows the Knoop hardness values of different abrasive grits in comparison to steel. However, hardness values alter depending on the temperature at which they are used (figure 12). CBN for example reacts with water at 800 °C but is stable in air up to approximately 1300 °C, whereas diamond graphitizes at temperatures above 800 °C in air [5]. Another problem with the use of diamond is its affinity to the carbon present in steel [6]. This is the main reason why CBN is preferred for grinding steel. Both CBN and diamond have good thermal conductivity and are not electrically conductive.

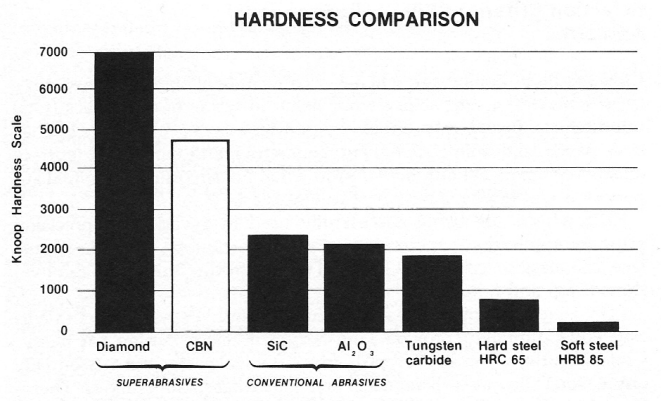

Figure 11 - Abrasive hardness comparison chart [10]

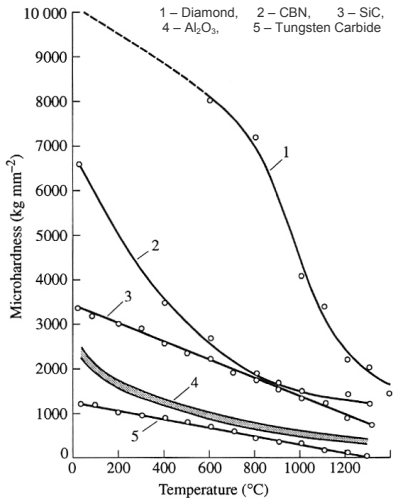

Figure 12 - The variation of Knoop hardness with temperature for several hard materials. [Loladze and Bockuchava in 5]

Along with the high wear resistance and hardness value of the various abrasives available, it is necessary to consider the degree of toughness or friability required. Friability describes the abrasives capacity to fracture when cutting edges become dulled. Conventional abrasives are more friable than superabrasives. As superabrasives remain sharper for longer they generate less grinding heat than would otherwise be caused by dull conventional abrasives ploughing the workpiece surface. Superabrasive wheels also wear at a much slower rate.

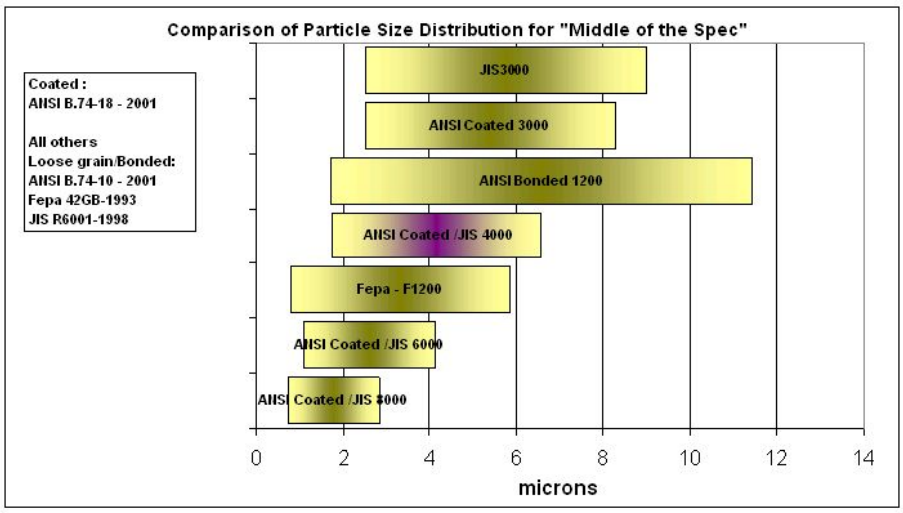

Figure 13 - Comparison of Particle Size Distribution – [11]

The size of the abrasive contained within the wheel is denoted by the abrasive mesh number. A larger number denotes a smaller grit size. There is a large variation between

the different specifications for micro-grit sizes, making comparisons difficult (figure 13). The relationship between mesh number and abrasive size, as referred to in this research, is shown in figure 14. The size of the abrasive used is the overriding factor that controls both the rate of material removal and quality of the surface finish achieved. When grinding it is recommended that the coarsest grit compatible to the surface quality requirements of the job should be used [6].

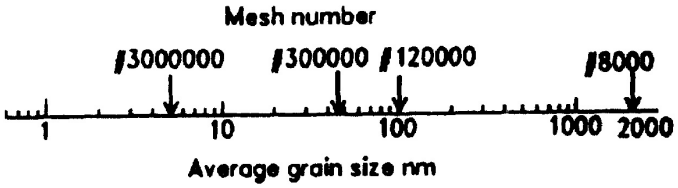

Figure 14 - Relationship between mesh number and abrasive size used – [12]

Grit concentration denotes how much superabrasive is held within the abrasive portion of the wheel; the size of the abrasive portion is specified by the superabrasives depth. The Elid superfinishing wheels in this thesis use a 75 concentration, meaning that there are 3.3 carats per cm^3, or 18.75% by volume, contained within a wheel. Elid wheel grit concentration is typically 50 to 125. Higher concentrations can offer longer wheel life and faster material removal.

The wheel's bonding material is characterized by its mechanical properties and its ability to retain abrasives (hardness, grade, strength). The harder the wheel grade, the longer it will last (A denoting softest, Z denoting hardest). However, the wear of the bonding material must keep pace with the renewal of abrasive in the wheel. Softer bonds often produce better finishes, faster cutting, less chatter and are used at a high rpm.

There are four types of bond available, Resin (B), Metal (M), Vitrified (V) and electroplated bonds. Vitrified bonds are commonly employed for superfinishing and precision grinding. They are ceramic, glass-type bonds which are generally porous, rigid, hard and brittle. Vitrified bonded wheels are used in chapter 25 as an alternative to processing with Elid. Metal bonds are generally hard, tough and stable and exhibit a reduced rate of wheel wear. Difficulties in truing, wheel loading, glazing and a requirement for frequent re-dressing, have been identified as major problems with metal bonded wheels. The use of Elid in combination with metal bonded wheels addresses these issues. The softer resin bonds, as well as rubber bonded wheels, are capable of achieving high levels of surface finish.

It is important to consider the grinding system as a whole, including the workpiece, the grinding machine and the grinding wheel [6]. The choice of wheel needs to take into account the interaction with the workpiece. For example, hard materials generally require a soft bond and a fine abrasive. The aggressiveness and configuration of the grinding operation also influences wheel selection. A larger grit size and a soft bond are often employed where an area contact is used, as the force on each grit is reduced.

2.2 General Grinding

Many fundamental aspects of conventional grinding remain the same across the range of other abrasive processes. Even when the abrasive size becomes very small, or a constant force is applied, the process remains one where numerous randomly orientated individual metal cutting points engage the workpiece. Figure 15 outlines the interactions at the grinding zone.

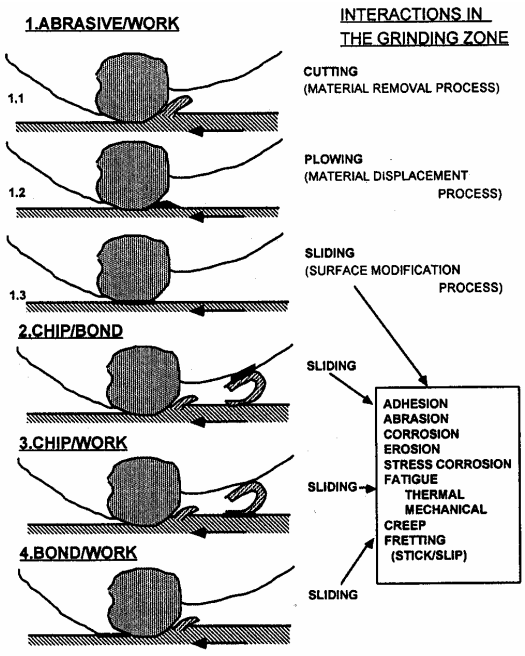

Figure 15 - Wheel and workpiece interaction [13]

The interaction between the wheel and the workpiece results in normal and tangential force components being set up on each abrasive that comes into contact with the workpiece. In force controlled grinding the magnitude of the normal force is predetermined. The tangential force increases proportionally to the normal force, in addition to being affected by the contact conditions at the grinding interface. The application of insufficient normal force may, for example, cause the abrasive to rub against the workpiece surface as opposed to cutting. This will result in the abrasives dulling and wear flats forming at the contact points. Although good surface finishes can be achieved when grinding under these conditions, very low workpiece removal rates are achieved as material is not removed but plastically deformed.

Although accelerated by adverse working conditions or chemical attack, dulling of the grits (attritious wear) is dependent on the distance slid and is therefore unavoidable (figure 16). It is essential that the abrasives are refreshed and that some wheel wear occurs, in order to maintain an effective cutting action and acceptable rates of workpiece material removal.

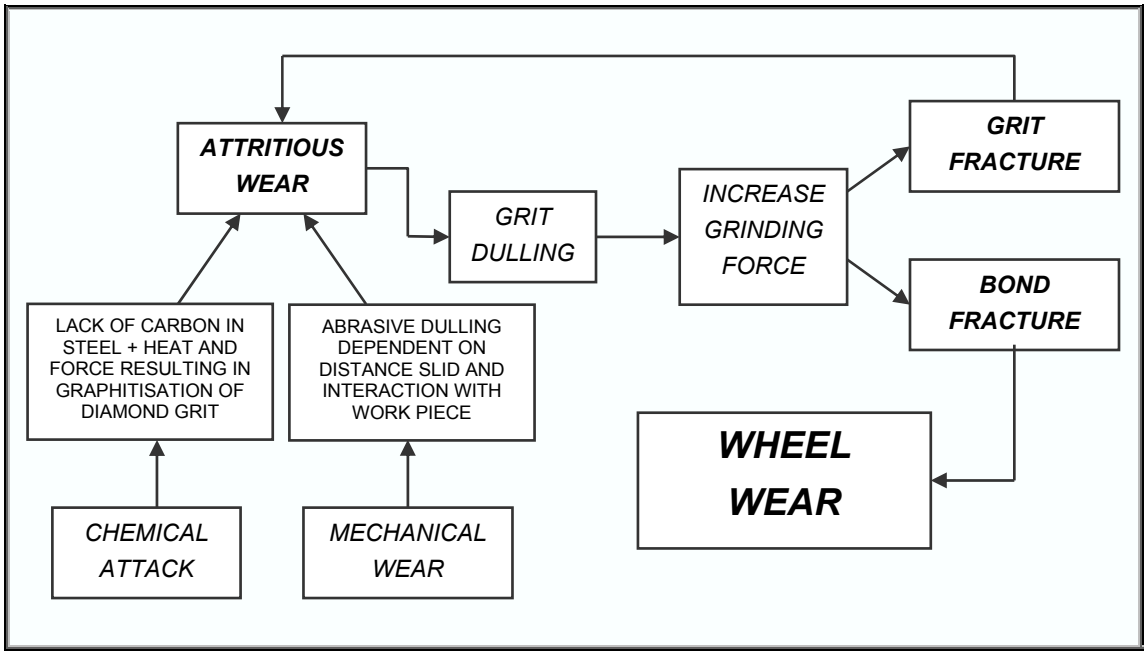

Figure 16 - Wear mechanisms involved in grinding - [after 14]

The wear of the wheel can be analyzed in terms of the frequency of the bond fracture or quantity of grit loss [14]. Under idealized conditions a grinding wheel's cutting performance can be continually maintained by the wear mechanism of the wheel [15]. When grinding, this mechanism relies on a delicate balance between the forces acting on the grits, the ease with which they fracture and the strength with which they are held within the bonding material. As the sharp abrasives begin to dull, the forces acting on them begin to increase. This can cause the abrasives to fracture revealing sharp new edges. Alternatively when the grit holding strength is surpassed, bond fracture occurs and the grit is ejected. The presence of large, hard carbides in hardened steel, for example, is a source of mechanical wear on abrasive grits and can cause micro-cracks.

Although this mechanism is often effective for stock removal grinding it can be inadequate, especially when considering form and finish grinding. Therefore some other form of wheel dressing is required [14].

2.3 General Superfinishing

Superfinishing operations are employed after grinding, either to introduce a cross hatched pattern of scratches (for lubrication through oil retention), or when a very fine mirror surface finish is required. Abrasive stones, wheels or tape, oscillate while applying pressure on the workpiece. The motions are arranged so that grits should never repeat the same path around the workpiece. Although it is not employed for large scale form generation, superfinishing is commonly used on round workpieces to improve roundness and reduce friction. It is intended to remove minute surface defects and not as a bulk material removal process.

When superfinishing, the input surface finish of the workpiece drives the self-sharpening mechanism. As a result the superfinishing process is intrinsically linked to the previous processing operation and the condition of the input workpiece [16]. The input of a component with a rough finish abrades the surface of the wheel, causing it to wear until the surface finish of the component is improved. As the abrasives begin to dull on the improved smooth surface of the component, excellent surface finishes can be achieved. The introduction of the next component being manufactured again abrades the surface of the wheel. The grinding interface is flooded with coolant which reduces friction and heat and removes debris. As the conformity between the contacting surface of the wheel and workpiece improves during a cycle, the fluid film pressure equalises across the interface reducing material removal.

During a superfinishing investigation [17], workpiece material removal was found to be of two different regimes, (1) flattening of a rough, as-received, surface and (2) bulk material removal after steady state surface finish is reached. This is demonstrated in figure 17, by the recorded vertical decline in removal rate at the point where steady state surface finish is achieved. Therefore, this particular stone is only capable of surface improvement and not bulk material removal.

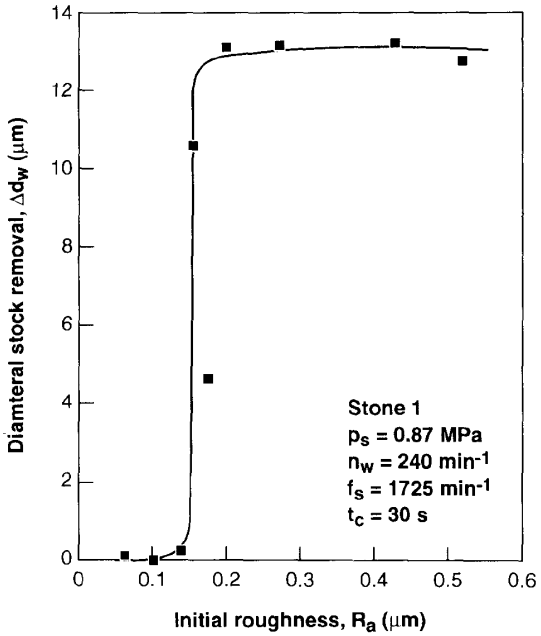

Figure 17 – Effect of input surface roughness on material removal [17]

Typical input roughness values of 0.25 to 0.38 μm Ra allow a stone to cut aggressively, improving finish down to values of 0.13 to 0.025 μm Ra [16]. A more consistent superfinishing process can only be achieved by improving the input form and finish consistency. A higher productivity can therefore be achieved by modifying the previous operation.

Smearing of the workpiece material as the dulled abrasives plough the surface can act to smooth a component's surface. Although surface finish may be improved, surface structure is not; the softer, re-deposited material can be unstable under load. Excessive processing with dulled abrasives may also result in thermal damage to the workpiece.

In addition to the input condition of the workpiece, figure 18 outlines solutions to overcome a variety of problems experienced during superfinishing.

Figure 18 - Common Superfinishing Problems And how To Correct Them - [16]

Condition	Increase	Decrease	Other
Excessive stone wear	spindle RPM	stone/wheel pressure; reciprocation/ oscillation	use harder abrasive product
Insufficient stock removal	abrasive pressure reciprocation/ oscillation rate	spindle RPM	use softer abrasive product; use coarser grit abrasive product
Rough finish	spindle RPM	stone/wheel pressure; reciprocation/ oscillation rate	use finer and/or harder abrasive product
Undesirable smooth finish	reciprocation/ oscillation rate; abrasive pressure	spindle RPM	use coarser and/or softer abrasive product
Excessive heat generated	coolant flow rate	stone/wheel pressure	use softer abrasive product
Out-of-round parts	reciprocation/ oscillation rate	stone/wheel pressure; spindle RPM	use softer abrasive product
Glazing of abrasive surface	reciprocation/ oscillation rate; abrasive pressure	spindle RPM	use finer and/or softer abrasive product
Loading of abrasive surface	reciprocation/ oscillation rate	spindle RPM	use finer and/or softer abrasive product

2.4 Cup wheels

With processes such as grinding with cup wheels, honing and superfinishing, the surface contact is large and often results in higher removal rates, improved form accuracy and better surface finishes [6]. Cup wheels are used for various grinding and superfinishing operations where there are geometric considerations [18]. Parts such as ball and socket joints, ball pins and spherical bearings are able to be manufactured with high geometric accuracy, in addition to fine levels of surface finish.

When used for superfinishing, cup wheels allow heat-treated surfaces to be mirror finished on one machine as an alternative to performing a hard-turning and subsequent polishing operation [19].

The use of an area contact enables surface peaks to be bridged, reducing waviness and improving component form in addition to finish. However the fluctuating contact between wheel and workpiece can result in unstable working conditions. Moreover the wide cutting area can cause problems of insufficient fluid penetration, leading to workpiece damage and a loss in the freeness of cutting. The use of a wheel with a low grit concentration improves self-sharpening and ensures the freeness of cut. Additional consideration needs to be paid to the application of grinding fluid (chapter 24).

2.5 Specific Grinding Energy

Assessment of specific grinding energy is one of the fundamental parameters for characterising the effectiveness of a grinding process. It is defined as the energy consumed per unit volume of material removed and is shown in the equation, where P_m is the net grinding power and Q_w is the volumetric removal rate.

$$u = \frac{P_m}{Q_w}$$

A realistic process model should be able to account for the magnitude of specific energy and its dependence on the operating conditions. The specific energy is higher for grinding compared to turning, due to the large number and random orientation of active abrasive grits. This results in individual abrasives engaging the workpiece differently, with many not involved in material removal but elastically or plastically deforming the workpiece surface (figure 15). Energy is transferred into the workpiece material, rather than being removed in the chips.

The specific energy increases more rapidly as the size of the abrasive is reduced. This is known as the ‘Size Effect’ and means that when grinding with very fine abrasives, specific energy levels are very high. Hwang et al. [20] related an increase in specific energy at smaller depths of cut to an increase in ploughing of the workpiece surface, caused as a result of rounded tipped abrasives. The size effect was found to diminish and constant specific energy levels were recorded, when the depth of cut was increased to over half the average tip radius.

Chapter 3 - Introduction to Elid Processes

Electrolytic in-process dressing, or Elid, is a method of dressing a metal bonded grinding wheel during the grinding process. As dressing is uninterrupted, an effective wheel surface of sharp protruding abrasives is continually maintained. By reducing wheel loading and promoting effective cutting, it lowers grinding forces and enables the use of very fine superabrasives. It provides a method of processing materials that are traditionally hard to machine and is capable of achieving high dimensional accuracy and nano-surface finishes. Along with reducing workpiece scratches and sub-surface damage, reduced component corrosion and extended fatigue life can be achieved [21, 22].

Although Elid has been shown to have many benefits over non-Elid techniques, it has found limited application in actual production environments. This may be in part due to a reluctance to adopt the new technology but also because it is often slower and perceived as problematic. An increased processing efficiency can however be attained through the maintenance of effective cutting and the elimination of processing stages, such as the need to perform a polishing operation. Although ultimately lower, grinding forces can become erratic and unstable when using Elid [23]. The problems associated with the Elid 1 technique also apply when evaluating Elid 2 and further complications arise when using an Elid 3 technique.

3.1 Elid History

In the 1960s Norton Company reversed the polarity of the electrolytic grinding process, resulting in a new method of dressing a grinding wheel [24]. The method referred to as Elid was developed by the Ohmori materials fabrication laboratory of RIKEN (Institute of Physical and Chemical Research). Hitoshi Ohmori was one of the first proponents of this technique in the late 1980s. In early research, Murata et al. (1985) [25] found Elid to be effective for grinding hard and brittle materials, such as ceramics, with sub #400 metal bonded diamond wheels. Ohmori and Nakagawa (1990) [26], utilized Elid with sub #1000 wheels achieving fine surface finishes. Research and development in this field continues around the world.

3.2 Existing Elid Applications and Configurations

The Elid process has been applied to numerous materials and a multitude of applications; a few of which are shown in figure 19. Elid systems can be fitted to existing machine tools and have been used in a number of different configurations. These include cylindrical grinding, surface grinding with cup wheels and the machining of asymmetric shapes. It has also been applied to the manufacture of micro-components and the machining of micro-holes.

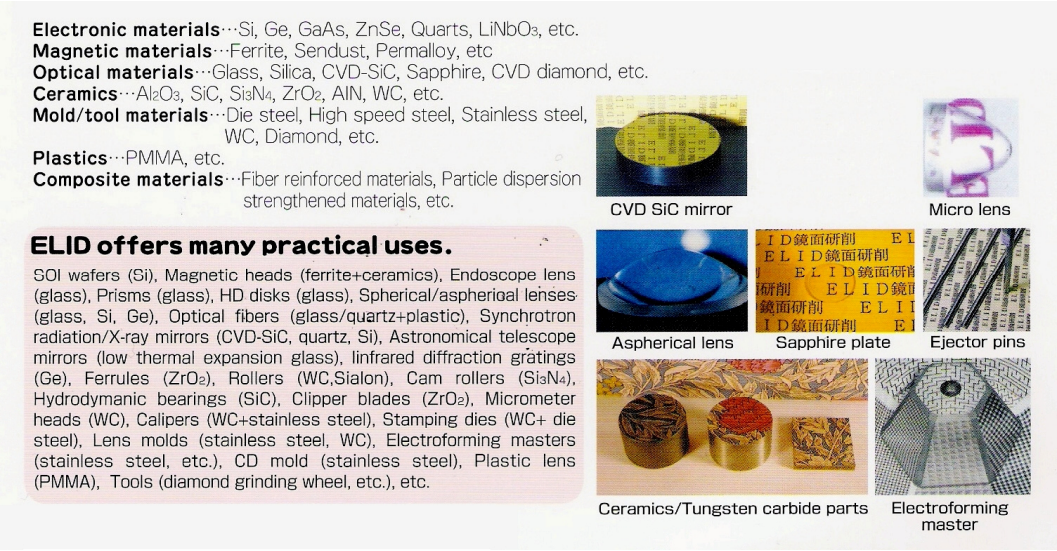

Figure 19 - Elid material and applications [27]

The vast majority of Elid research is concerned with Elid 1 precision grinding, although the Elid principle has also been applied in a lapping configuration in several papers. Of particular relevance to this research is the application to hardened steels and titanium. Elid 3 has not been studied extensively. Of probably the most relevance to this research is the application of Elid in a honing configuration, using metal-resin bonded superabrasives on bearing steel [7], however only one piece of research is available referring to Elid honing.

3.3 Elid Types & Definitions

Over the last 20 years research and development of the technology has resulted in several different and distinct methods of using Elid. These are outlined by Rahman et al. [28] and can be characterised as:

- **Elid 1** - This is the conventional and most commonly studied Elid system, where a separate electrode is used.
- **Elid 2** - Interval dressing. This involves stopping grinding and periodically redressing with a separate electrode.
- **Elid 3** - Electrode-less electrolytic dressing. This uses the component being ground as the electrode and dressing occurs at the grinding interface.
- **Elid 3A** - Electrode-less electrolytic dressing using alternating current. Both the wheel and workpiece are oxidised.

Where possible an Elid 1 system using a separate electrode is used. As this is not always possible, Elid 2 and Elid 3 have been developed. Increased control of Elid power values has been developed through the application of computer control. These processes are known variously as Optimum Elid [29], ECD / EcoDress [24] (Chapter 12).

3.4 The Basic Elid 1 System

Figure 20 shows an example of Elid 1 using a cylindrical grinding configuration. This system consists of an Elid power supply connected to a metal bonded wheel and a separate electrode. The electrode gap used in almost all Elid papers is typically between 0.1 to 0.3 mm [30, 31, 23, 32, 33]. This gap is flooded with an aqueous electrolyte that also acts as the grinding coolant. The electrode typically covers between 1/4 and 1/6 of a proportion of the wheel's free surface [23, 32].

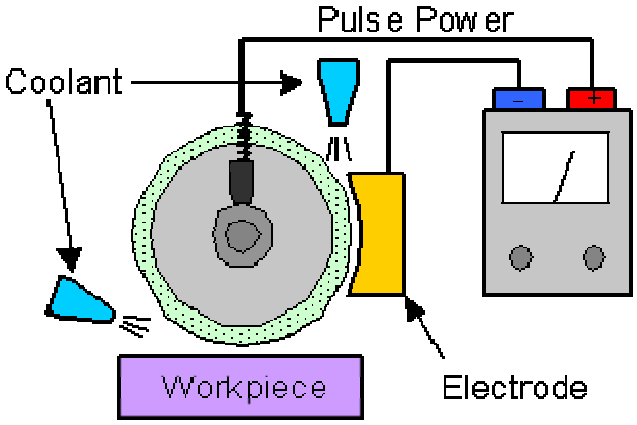

Figure 20 - Illustration of Elid 1 cylindrical grinding [34]

Electrodes are becoming increasingly sophisticated particularly when grinding micro-components [22]. Conductive materials such as carbon, copper and stainless steel can be used for the electrode. Electrode design for large grinding wheels should ideally generate a dynamic pressure, caused by fluid entering the electrode-wheel gap.

3.5 The Elid Process Model

Figure 21 illustrates the Elid cycle. After wheel truing, pre-process dressing is conducted. A pulsed, square wave, direct current is then passed through the water-based grinding fluid and between the grinding wheel and the electrode. This erodes the wheel's metallic bond material into its ions, or converts it into hydroxides and oxides. As the bond material recedes, a non-conductive insulating layer is formed on the dressed surface. This suppresses further electrochemical dissolution of the metallic bond and creates a condition of good grit protrusion, enabling an effective cutting action. When grinding commences the friable oxide layer is gradually depleted, which in turn stimulates the anodic reaction, causing it to regenerate. As the abrasive grits wear, the material removal mechanism changes from a low energy cutting action to a higher energy ploughing or sliding action. The combination of the reduced holding force of the bond material and the increased force of grinding with worn grits, results in the abrasives being ejected and wheel wear occurring [35, 28, 36].

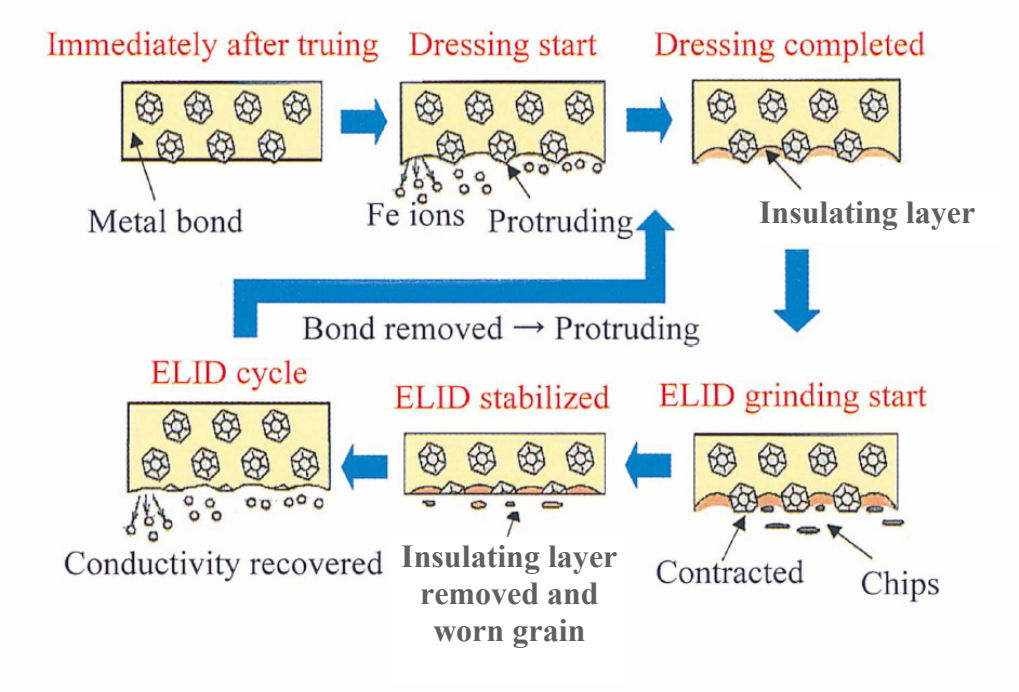

Figure 21 - Elid 1 mechanism for Cast Iron Bonded (CIB) wheels [36]

Chapter 4 - Electro-Discharge Truing (EDT)

The process of truing is conducted to form or correct the required shape of an abrasive wheel and resolve errors in its rotating motion. Mechanical methods of truing are most commonly used and account for the majority of research. A detailed assessment of a typical conventional rotary diamond truing process is provided by Shih et al. [37, 38]. Some of the beneficial properties of superabrasive metal bonded grinding wheels, such as their hard abrasives, high bond strength and wear resistance, also make them difficult to true [39]. Using mechanical methods of truing on these wheels will result in a short truing wheel life and only a limited period of satisfactory performance.

A method known as electro-discharge truing (EDT) has been developed and used in numerous pieces of research [28, 40, 41, 42, 43, 44], as a preferred method of truing prior to Elid processing. EDT is particularly suitable when used in conjunction with Elid because the contacts, fluid, insulation and power source used for Elid are also suitable for EDT.

Electro-discharge truing is a process of spark erosion (figure 22). The wheel bonding material is melted by the spark and is easily removed. It is suitable for use with all metal and metal-resin bonded wheels, small and thin walled wheels, as well as micro-wheels, as small as 0.1 mm in diameter [28, 41, 45]. It can provide precise forming of various shapes, is highly efficient, and as it is a non-contact process, forces remain low.

Figure 22 - EDT process [46]

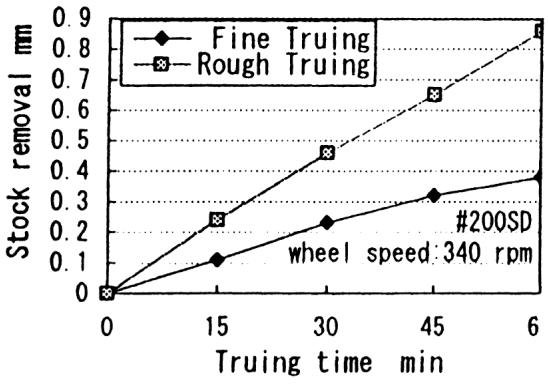

Figure 23 - Efficiency of rough & fine EDT [46]

4.1 Truing parameters

The EDT process is influenced by a number of electrical and non-electrical parameters, a few of which are shown in figure 24. There is a general consensus around the effect of parameters on material removal efficiency and resultant form accuracy.

- Higher electrical parameters increase removal efficiency (for rough truing 150V, 60A in [46], figure 23)
- Lower electrical parameters increase accuracy (for fine truing 120V, 48A, τ on:off: 12:3 μs in [46])
- Slow wheel speeds are recommended [22, 46] and, as demonstrated in figure 24d, result in an increase in truing efficiency [39].
- A small depth of cut (2 μm) is recommended [22, 46].
- A fast feed rate is recommended (100 mm/min in [46], 40 mm/min in [22]).

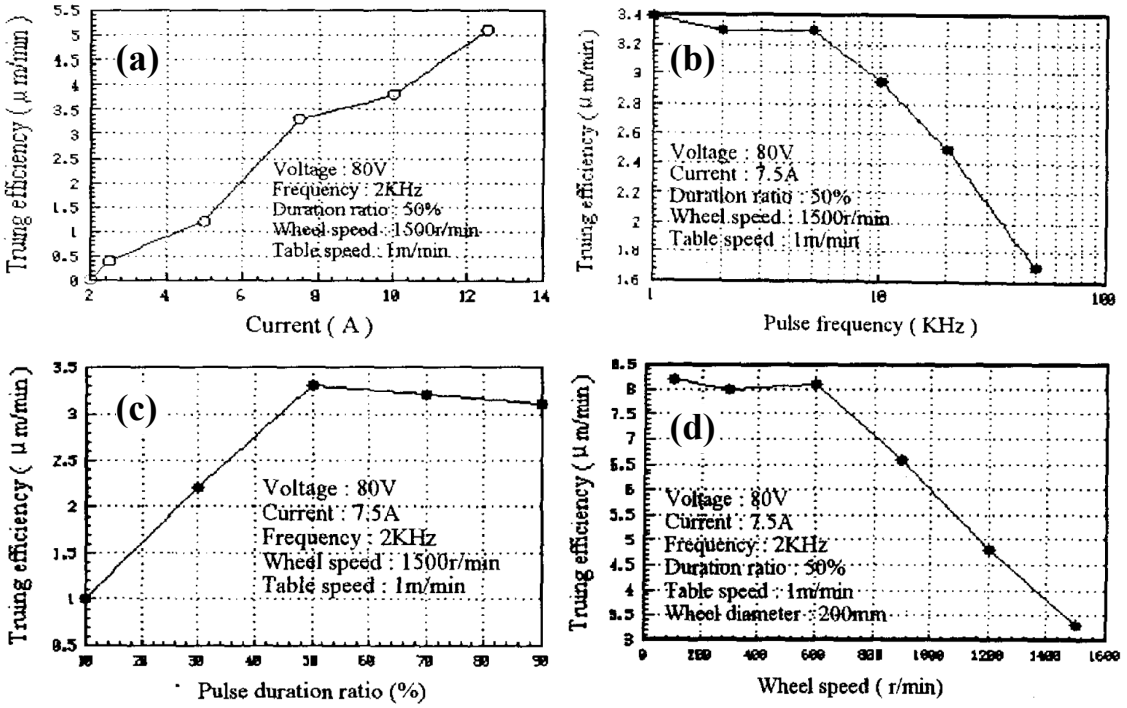

Figure 24 - Effect of various parameters on truing efficiency (wheel material removal rate) [39]

Good results were achieved by several authors, regardless of the set-up, configurations or wheel types used. For example, an assessment of profile accuracy of a 150mm x W50 mm wheel recorded a straightness of 6 μm and roundness of 2 μm [46].

The use of fluid is another parameter that can be varied when electro-discharge truing. Little or no coolant was used by Qian et al. [40, 42] in order to prevent electrolysis and attain optimal precision. The improvement in wheel runout went from 40 μm to 4 μm. However this took an incredibly long four hours to achieve. Zhang et al [45] investigated EDT performance using a condenser capacity of between 10uf to 0.01uf, a voltage of between 60 and 100 Volts, both in air and using a coolant. Truing efficiency increased significantly when coolant was used. Truing in air produced a distinct wheel surface that was considered to be of poorer quality.

Material removal when using a fluid is a combination of electrolytic dissolution and spark erosion. Wheel material that has been oxidized through electrolysis is more easily removed by a discharging spark than non-oxidized material. This increases the removal rate over and above the simple addition of the electrochemical and electro-discharge mechanisms [45].

4.2 Effect on Wheel Condition

Microscope analysis of the wheel's condition after truing [39, 46, 47] demonstrates that the wheel bonding material is melted and removed by the spark erosion. Wang et al [39] analyzed the same portion of a wheel's surface before and after truing. During the truing process, some abrasives were removed and some were obscured by re-solidified bond material. However, the protrusion of other grits was improved and new abrasives were also revealed. The EDT process did not damage the abrasive grits. This is in contrast to mechanical methods of truing where the grits are removed (figure 25) [47].

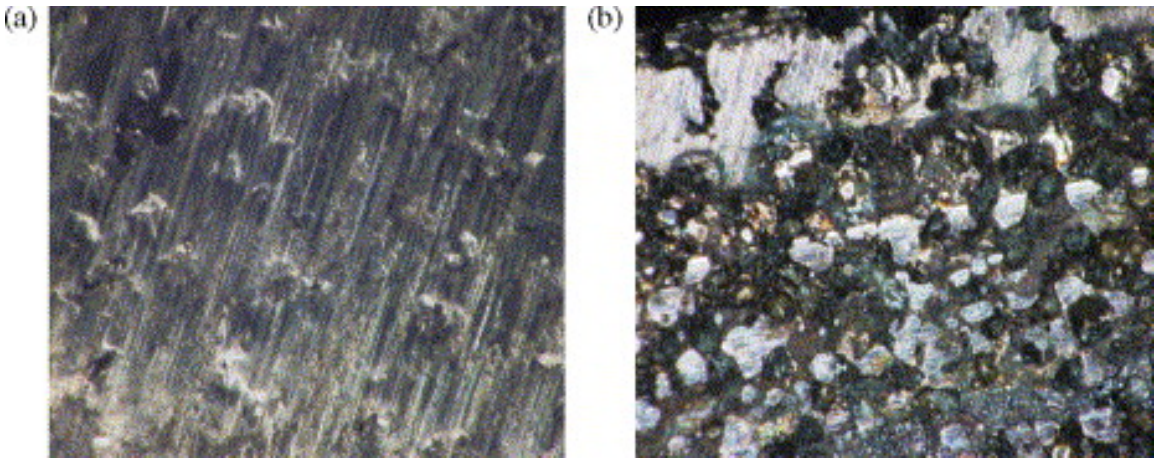

Figure 25 - Wheel surface topographies (mag: 175×).
(a) after mechanical truing, (b) after dry-ECD assisted truing. [47]

The volume of material removed by a spark should be less than the size of the abrasive contained in the wheel [39]. When using finer abrasive wheels, electrical parameters should be set to minimize efficiency in order to retain abrasives. The conflict between efficiency and generation of a suitable wheel surface can be resolved by adopting less aggressive parameters at the end of the truing stage.

When superfinishing spherical bearing balls in the current research, only the general form of the wheel needs to be generated by truing. A subsequent bedding-in process is used to get the final, accurate form and Elid dressing is used to create the optimum wheel surface condition. As outlined in chapter 15, the tests conducted produced a vastly increased rate of material removal (1.2 mm/min) to that presented in the literature.

Chapter 5 - Oxide Layer Growth

5.1 Electrochemistry

Elid superfinishing is an electrochemical method of oxidising / dressing a grinding wheel, involving a forced electrical potential being imposed on an electrolyte-filled circuit. The creation of an electrochemical cell between the electrodes results in an oxidation reaction at the anode (wheel) and a reduction reaction at the cathode (separate electrode / component). As anodic dissolution of a metal-resin bonded (MRB) wheel's copper bond material occurs, atoms lose electrons, become ions, and go into solution. Electrons are received at the cathode and depending on the exact conditions, can combine with metal ions in the solution and begin to plate out, or form hydroxyl $(OH)^-$ ions in the grinding fluid [7, 48].

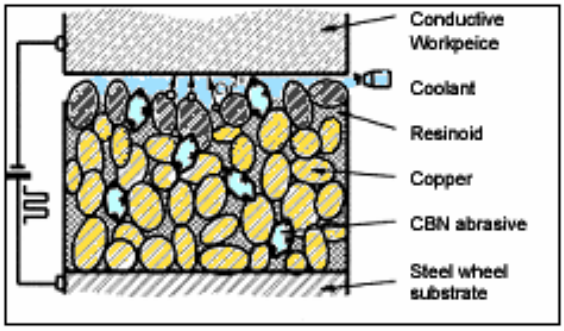

Figure 26 - Elid 3 electrochemical cell and MRB wheel Structure [after Qian & Ohmori (2001) in 40]

As a result of the electrochemical oxidation reaction, an insulating or oxide layer forms on the surface of the wheel (figure 26). The oxide layer is defined as the thickness of oxidized material on the surface of the wheel. Measurement of wheel wear using a photoelectric optical sensor [32] revealed that the size of the wheel increased by 0.2 mm from a trued state, after dressing. As the size of the wheel generally increases when an oxide is formed, the wear of the wheel is described by the term etch layer. The etch layer is defined as the change in the wheel radius, excluding the insulating layer, after pre-process dressing [41, 49].

5.2 Pre-process Dressing Time

After wheel truing it is necessary to condition the grinding surface of the wheel. This process is termed pre-process dressing, as opposed to in-process or interval dressing. Assessing Elid power values provides information on the growth of the oxide layer. When the power levels have stabilised the layer will have reached steady state thickness. Using cast iron fibre bonded diamond (CIFB-D) wheels [33], the Elid power

values (60V, 30I, 2us on & off) began to level off after 15 minutes but took 90 minutes to level off totally. When pre-process dressing an MRB wheel [22], the time required for voltage and current values to stabilize was 80 minutes (figure 27). However, in other papers using MRB wheels, the power levels stabilized between 5 and 20 minutes [12, 30]. Results outlined in this thesis demonstrate that power values recovered significantly faster than reported in the literature (anywhere between 10 seconds and 5 minutes).

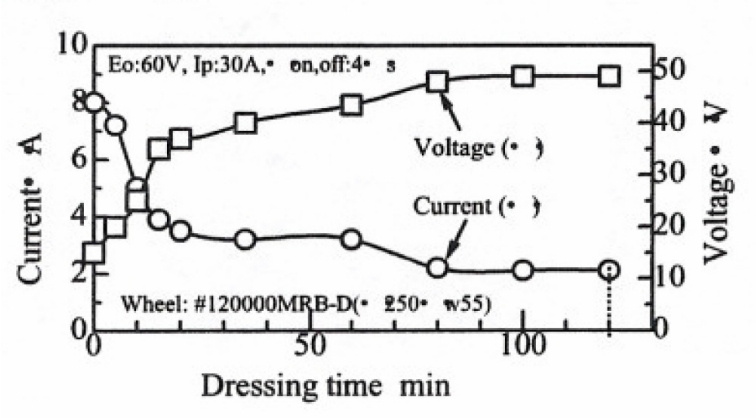

Figure 27 - Electrolytic dressing of MRB-D wheel [22]

After pre-process dressing, the colour of the wheel's surface changed from copper, when new and unused, to green [22]. This is seen on some occasions when pre-process dressing in this thesis, however there are also occasions when the wheel's surface turns black and when it has a more bluish appearance.

5.3 Determination of Oxide Layer Growth

A theoretical rate of corrosion is determined by Faraday's equation below [50]. However even a simple electrochemical system can be affected by numerous factors. These include voltage / current levels, electrode gap, polarisation, electrolyte pH, fluid conductivity and temperature to name but a few.

$$w = \frac{iAtM}{nF}$$

w = Weight of material corroded (g)

i = Current density, I/A, (A/m^2)

A = Area (m^2)

t = Time (s)

M = Atomic mass of metal

n = Valence of the metal ion

F = Faraday's constant (96500 C)

Numerous authors formulate the rate at which a wheel surface is oxidized [51, 52]. When compared to experimental results, theoretical analysis was found to be capable of predicting the required pre-process dressing time [21]. The situation becomes more complicated when used as part of a grinding process and in particular with Elid 3 superfinishing, where electrolysis occurs at the grinding interface, the electrode separation gap is dynamic and fluid access is restricted.

The development of an Elid grinding system that assesses the thickness of the insulating layer in-process, using both capacitor and eddy current type gap sensors, shows the possibility of controlling the Elid grinding process by assessment of the insulating layer thickness [53].

5.4 Determination of Oxide Growth during Elid Grinding

Bifano [54] continues to develop equations relating to the growth of the oxide layer from pre-process dressing to during Elid grinding. The wear rate of the wheel is related to the theoretical oxide layer growth. The oxide layer will reach a steady state thickness. No oxide layer will be present if the wear of the layer is greater than its growth. Wear on the diamond abrasive is independent of electrolysis. The wear rate of the wheel is controlled by the erosion of the bond and set to a level that suits wear on the diamond grit. If the oxide layer is too thick it can obscure the abrasives and the removal rate will drop. Therefore an appropriate balance must be found between layer growth and wheel wear.

Assessing the linearity and thus stability of material removal (figure 28), demonstrated that only the use of a high current level, pulsed current and a 0.002M electrolyte achieved stable material removal. If the wheel gets loaded or the abrasive grits become dulled, as happens when no dressing is used, then material removal drops. In order for efficient cutting to be sustained, the time taken for an abrasive to become dulled should be larger than the time taken for the bond to erode a distance equal to the abrasive diameter. When removing material effectively it was observed that a green copper I oxide was formed on the surface of the wheel and when it was not effective a black copper II oxide was prevalent.

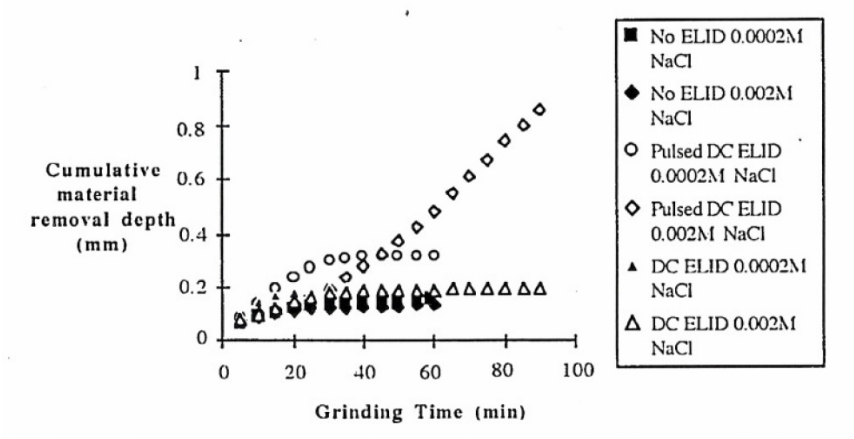

Figure 28 - Effect of Elid wave form and electrolyte Conductivity on work-piece material removal. [54]

5.5 Effect of Elid Power Parameters

The influence that the Elid electrical parameters (voltage, current, duty, waveform, and gap) have on both the process performance and wheel's morphology has been investigated by several authors.

5.5.1 Waveform

The use of a high frequency pulsed DC rectangular waveform is standard for Elid grinding. Ohmori et al. [49] compared DC pulsed, DC continuous, and AC power supply wave forms. The fastest rate of wheel dressing / wheel surface oxidation, as well as the thickest oxide layer, was produced when a continuous direct current was used (figure 29). This could be due to the increased current passed. A gradual reduction in working current, along with a thin insulating layer (referred to as isolating layer) but a thick etch layer, was observed when AC current was used. The wheel's material is being eroded away rapidly while not forming a sufficient insulating layer of oxide. The working current reflects the formation of non-conducting oxides on the surface of the wheel.

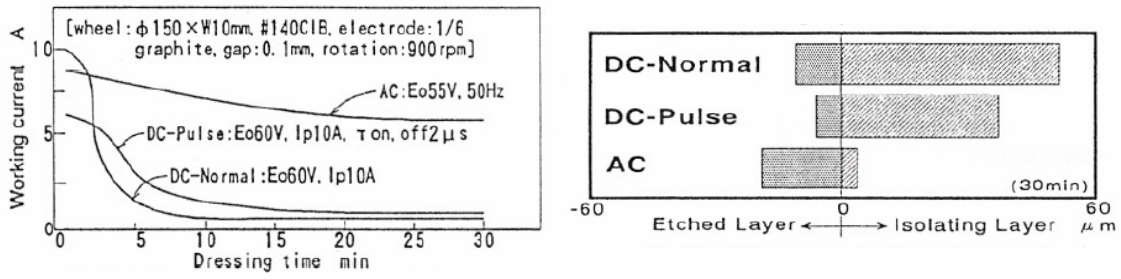

Figure 29 - Effect of waveform on working current, oxide layer thickness and etch layer thickness. – [49]

The oxide film is considered too thick when using a direct current [22] possibly because it obscures the abrasive. The characteristics of the waveform used, affect not only the insulating layer but the resultant surface finish. Continuous DC achieved 20 nm Ra, 110 nm Rmax, while pulse DC achieved 8 nm Ra, 50 nm Rmax.

5.5.2 Voltage and Current Level

Zhang et al. [41] carried out experiments with a 1.4 mm cast iron bond diamond (CIB-D) wheel, in order to investigate electrical behaviour during pre-dressing and the affect it had on the oxide and etch layers. Figures 30 and 31 show the working voltage during dressing and the resultant oxide and etch layers formed using different current levels. Due to the extensive bubbling (gas evolved due to electrolysis) experienced when a current of 20 amps was used, an insulating oxide layer did not form on the surface of the wheel as it was rapidly eroded. This prevented stabilization of the working voltage. When using current ranging from 1 to 3 amps, the larger the current the thicker the oxide layer and the thinner the etch layer.

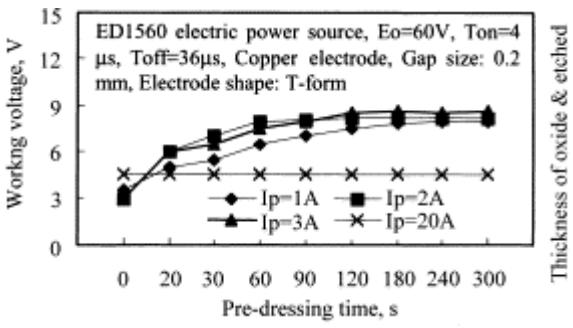

Figure 30 - Relationship of working voltage with dressing time for different peak currents. [41]

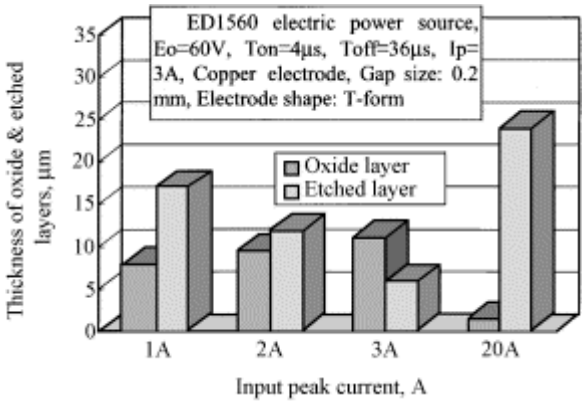

Figure 31 - Thickness of the oxide layer or etched layer vs. peak electric current. [41]

Itoh et al [30] investigated the pre-process dressing behaviour and grinding performance (figure 32) for metal-resin bonded (MRB) grinding wheels, employing currents of 10, 20 and 30 amps. The higher Elid current levels decreased more rapidly and all levels stabilized between 20 to 40 minutes. The thickness of the etch layer was found to increase with increased current, however little variation was found in insulating layer thickness. Stable material removal and surface finish are recorded when using currents of both 10 and 30 amps.

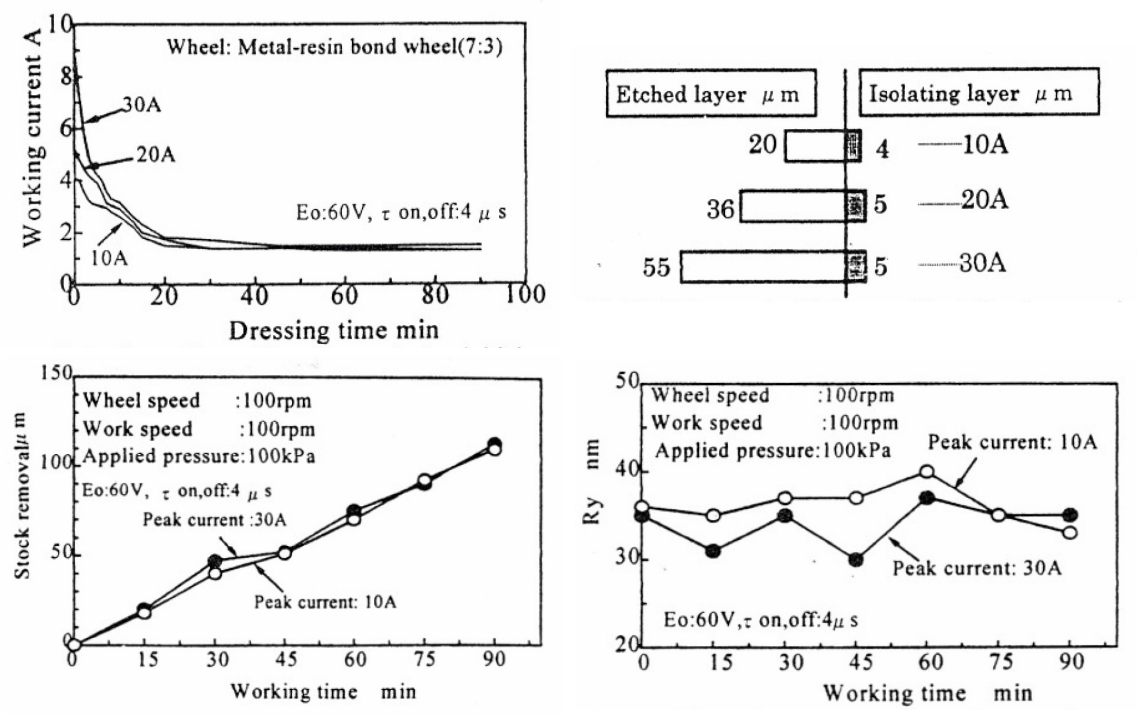

Figure 32 - Effects of peak current on dressing behaviour and lap-grinding performance [30]

5.5.3 Effect of Electrode Gap

Using a factorial design experimental method, Pavel et al. [21] examined the effects of current level, wheel speed and electrode gap on the pre-dressing insulating layer thickness of a CIB-D wheel. Both current and gap were statistically significant (p-values of 0.0049 and 0.0167 respectively), whereas wheel rpm produced no effect over the measured range of 300 to 500 rpm. As demonstrated by the regression equation below, an increased current and a reduced dressing gap reduced the required dressing time. At the highest current tested (13 amps) and the smallest gap (0.1mm), the minimum dressing time was achieved (61.87 minutes).

Pre-dressing time (mins) = 304.688 − (20.9375 * current in amps) + (293.75 * gap in mm).

Figure 33 illustrates the relationship between Elid current, inter-electrode gap and wheel oxide layer thickness for a CIB wheel with optimized Elid [35, 55]. At low current levels the insulating layer thickness decreases as the electrode gap is increased.

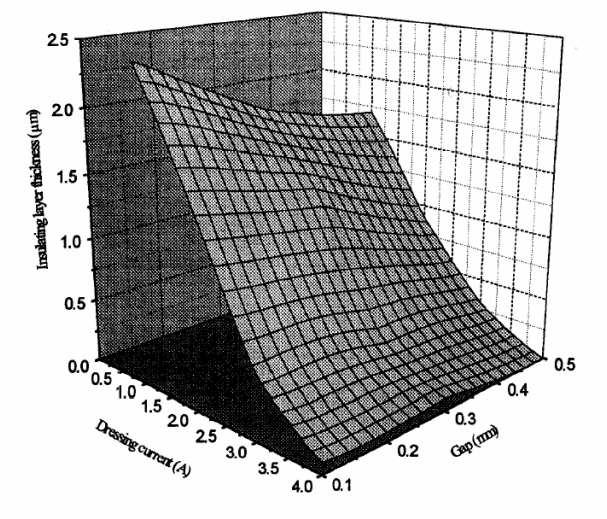

Figure 33 - Insulating layer thickness according to dressing current and gap. [35]

5.5.4 Duty Ratio / Effect of τon & τoff Times

The current duty ratio is defined as the percentage of time that the current is flowing for a given square wave cycle. t_{on} is the ON time and t_{off} is the OFF time. When larger on times are used, the working current is increased and effectively produces stronger dressing.

$$\text{Current duty ratio}(R_c) = \frac{t_{on}}{t_{on} + t_{off}} \times 100(\%)$$

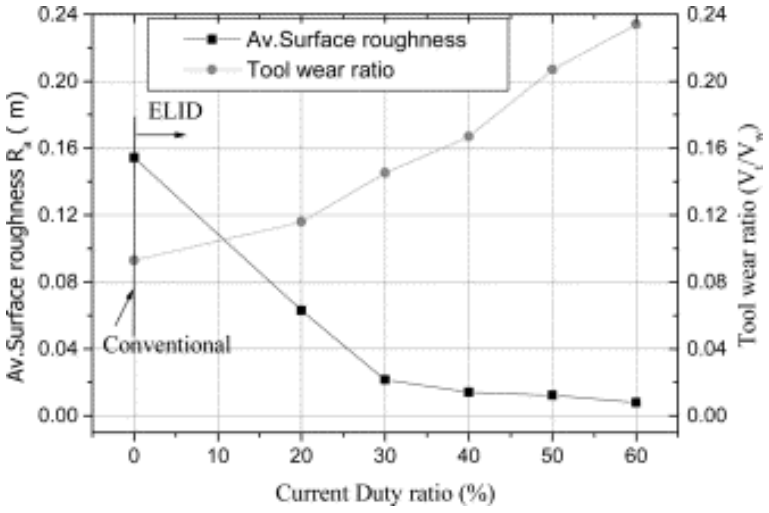

Figure 34 - Effect of duty factor on surface roughness and tool wear ratio - [23]

Higher normal and tangential forces were experienced when a low duty ratio (30%) was used compared to a high duty ratio (60%). Increasing the duty ratio reduces the normal force and was found to improve stability [23]. Increasing the duty ratio also increases tool wear, as the wheel is eroded more quickly. This provides an improvement to the component surface finish (figure 34), as a thicker oxide layer provides damping with grits held loosely and entirely within it. The ejected grits provide a loose abrasive polishing action that promotes an improved surface finish.

Chapter 6 - Elid Grinding Fluids

The fluid used is a fundamental factor to consider when evaluating abrasive processes in general. This chapter looks at the effect of grinding fluids, particularly those used with Elid. In abrasive processing, fluids are used to cool the grinding interface, provide lubrication, remove debris and improve finish. The fluid must be environmentally sound, able to suppress metal corrosion, not foam, be easily filtered, and be cost effective [6].

When using Elid, a water-based fluid must be used to enable electrolysis. When compared to the more conventional oil-based fluids, the use of a water-based fluid has a number of advantages and disadvantages. Water-based fluids are considered to be less efficient at removing debris than oil-based fluids when superfinishing, due to their lower permeability [56]. Because of the area contact between wheel and workpiece, conventional superfinishing processes use oil-based fluids, which also provide better lubricity. The advantages of using water-based fluids are that they are more environmentally friendly and are better at cooling.

As the fluid is a significant factor involved in dressing behaviour and resultant wheel's surface structure, the relationship when using a fluid for Elid is more complicated than for non-Elid grinding. It is important to consider not only the type of fluid used but also the entire fluid system (fluid delivery, filtration, cooling, etc). Metal and resin bond wheels are not as porous as vitrified wheels; therefore there is less or no need to match the fluid velocity to the wheel speed [6]. However the optimum positioning of the fluid nozzle remains critical.

6.1 Evaluation of Elid Fluid Types

Various fluids have been designed for use with Elid. The wheel manufacturer Fujidie [57] states that the ideal fluid should be alkaline (pH 11) with high electrical conductivity (>2 mS/cm) after dilution. The recommended 1:50 dilution ratio of coolant to water is used by numerous authors [22, 32, 41, 57]. With an Elid grinding process the fluid has two roles. (1) As an electrolyte its electrochemical properties influence the dressing performance and wheel structure. (2) As a grinding fluid it must possess the ability to lubricate, penetrate and cool. Both aspects influence the grinding process and responses such as grinding force [41]. Zhang et al. [41] examined three different fluids, looking at the pre-dressing stage and insulating / etch layers.

Grinding fluids	AFG-M type (Noritake), diluted by water, 50:1 Coolant A (Kyodo oil), diluted by water, 50:1 Coolant B (Kyodo oil), diluted by water, 50:1

Fluid type	Properties	Coolant A	Coolant B	AFG-M
Original fluid	Color	Yellow-green	Yellow-green	Yellow-green
	Density (35°C)	1,07 g/cm^3	1,07 g/cm^3	1,07 g/cm^3
Diluted fluid	Color	Slightly green	Slightly green	Slightly green
	pH value	10.5	10.5	10.5
	Surface tension ($\times 10^{-3}$)	38 N/m	32 N/m	55 N/m
	Permeation time	130 s	110 s	>15 min
	Electric conductivity	1400 μs/cm	1380 μs/cm	1450 μs/cm

Figure 35 - Properties of the three kinds of grinding fluids [41]

Figure 35 shows the properties of the fluids tested. Coolants A and B were specifically developed to improve the small hole grinding process, as well as to extend wheel life. As demonstrated in figure 36, the working voltage increased more dramatically with the AFG-M fluid, which also resulted in a thinner oxide layer and thicker etch layer in comparison to coolants A & B. When assessing the grinding forces, coolant A maintained the lowest force and required less frequent Elid 2 redressing than the other fluids. The authors conclude than the choice of fluid is an important variable when using Elid and either AFG-M or type A are considered suitable. Fluid type B was considered unsuitable due to insufficient grit protrusion resultant from the strong oxide layer growth and good permeability.

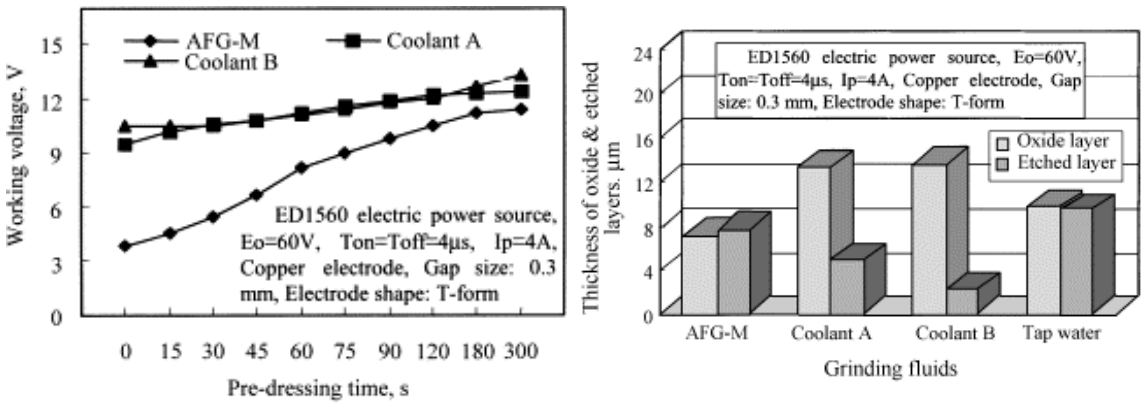

Figure 36 - Influence of fluid type on working current, Insulating layer and etched layer thickness using cobalt–cast iron compound bond [41]

Four kinds of grinding fluid of varying properties, as detailed in figure 37, were evaluated by Ohmori and Nakagawa [49]. Fluid (A) results in standard electrical behaviour of CIB wheels while fluid (D) achieves a similar but faster rate of current decline. A very gradual, linear, decline in working current is experienced by fluids (B) and (C). It is suggested that the higher current value of fluid (B) than (C) is a result of fluid (B) having a higher ionization rate of the wheel's bond material. Evaluating the thicknesses of etch and insulating layers, demonstrates that fluids (A) and (D) achieve a thick insulating layer in accordance with their non-linear electrical dressing behaviour. As a result of the high linear current during pre-process dressing, fluid (B) produced the thinnest insulating layer and the thickest etch layer.

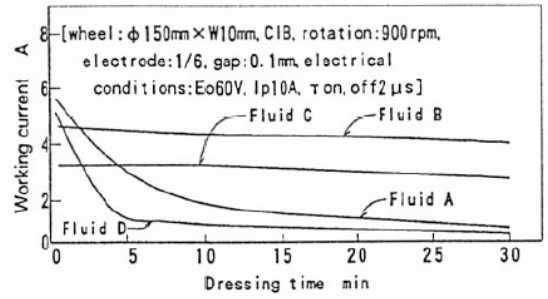

Properties \ Fluid type	Fluid A	Fluid B	Fluid C	Fluid D
Density(15℃) g/cm³	1.09	1.13	1.12	1.08
pH ×30	10.8	9.6	9.6	9.9
pH ×50	10.7	9.4	9.5	9.9
Conductivity (20℃) μS/cm ×30	2700	3700	1250	1600
Conductivity (20℃) μS/cm ×50	1800	2400	800	1100
Surface tension mN/m ×30	63.0	-	64.0	53.0
Surface tension mN/m ×50	64.0	-	65.0	54.0

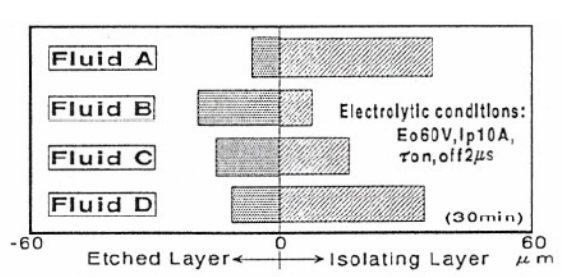

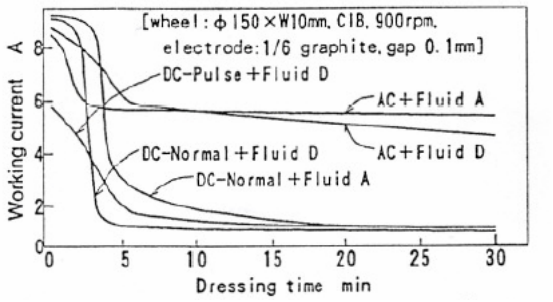

Figure 37 - Influence of fluid type on working current, Insulating layer and etched layer thickness [49].

The waveform characteristics, in combination with the fluid used, affected the electrical / dressing properties of particular combinations. As expected, a continuous direct current produced a faster decline than a pulsed DC wave and the use of alternating current achieved the least significant decline. Although once again fluid (D) declines quicker than fluid (A).

Using #1000, 4000, and 8000 bronze-bonded wheels Ueda et al. [56] investigated Elid 1 lap-grinding, including work-piece oscillation (superfinishing) for Al_2O_3 and soft steel. The influence of five different grinding fluids (figure 38) and concentrations (figure 39) was investigated along with numerous other factors.

Symbol of coolants	A_c	B_c	C_c	D_c	E_c
Coolant type JIS	W2-2	—	—	W2-1	—
Fatty acid - its derivative mass%	22	7	—	11	—
Alkanolamine mass%	15	30	30	13	—
Refined mineral oil mass%	5	—	—	—	85
Surface active agent mass%	—	—	—	30	—
Rust inhibitor mass%	10	—	30	15	—
Others mass%	5.9	0.4	1.3	0.5	15
Water mass%	42.1	62.6	38.7	31.5	—
Sulfur mass%	—	—	—	—	0.7
Chlorine mass%	2.5	—	—	—	1.2
Fatty oil mass%	—	—	—	—	12
pH (×30)	9.4	9.4	9.8	8.7	—
Surface tension (×30) 10^{-3} N/m	38	68.2	72	35.5	—

Figure 38 – characteristics of coolants [56]

Fluid resistivity increased as the fluid concentration (referred to as dilution) decreases, with the exception of 100 % where high values are recorded for fluids (C) and (D). For fluid (D) on soft steel, optimal material removal is achieved when using a 2% concentration. This is in line with what is recommended by Fujidie for their fluid.

Unit : Ωcm

Symbol of coolants	A_c	B_c	C_c	D_c
100% dilution	198	142	1 308	812
10% dilution	245 (360*)	253 (—)	351 (500*)	285 (390*)
5% dilution	394 (400*)	368 (—)	458 (—)	359 (480*)
3.3% dilution	— (634)	— (168)	— (1 024)	— (—)
2% dilution	691 (1 085)	718 (1 056)	633 (1 573)	635 (—)
1% dilution	1 285 (—)	856 (—)	786 (—)	979 (—)

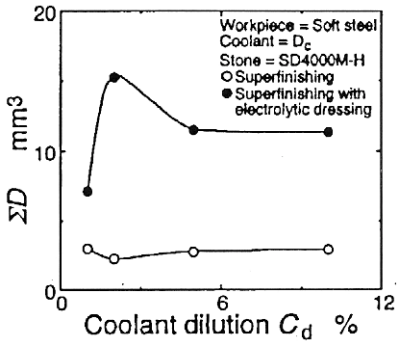

Figure 39 - Influence of concentration on resistivity and material removal [56]

There is a large difference in material removal when using different fluids (figure 40). Fluid (B) achieves the highest rate on Al_2O_3. Lower rates were recorded when processing without Elid but there was also an interaction between the use of Elid and fluid type. The largest difference in material removal was recorded, when using fluid (D) on steel, between Elid and non-Elid. However there is little difference when using fluid (C) on steel. On Al_2O_3 there was little difference in surface finish when using oil or water-based fluids. On soft steel the surface finish was worse when using Elid with a water-based fluid than when the Elid was not used.

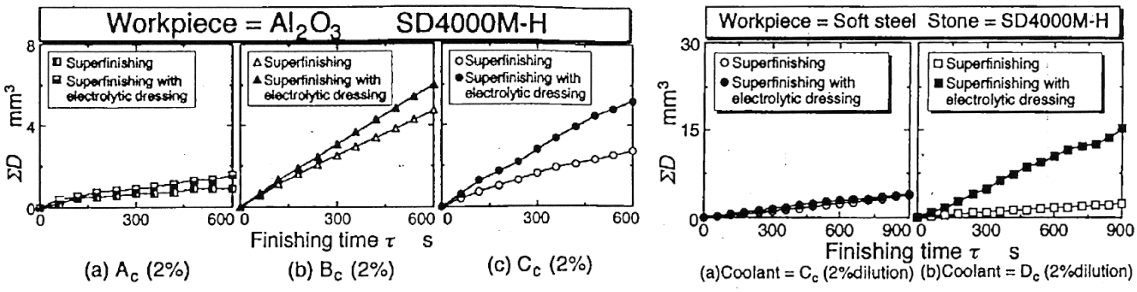

Figure 40 - Influence of fluid type and use of Elid on material removal [56]

The water, with which the electrolytic grinding fluid is diluted, has an effect on the wheel's insulating layer thickness and ultimately the grinding performance. This was investigated while grinding using a #6000 SB-D wheel [22]. The difference in insulating layer thickness is shown in figure 41. A surface finish of 5.4 nm Ra, 36 nm Rmax, is produced when using tap water. However an improvement is recorded when ground (distilled) water is used, 2.4 nm Ra, 18 nm Rmax. This is because distilled water has a lower conductivity, which aids dressing effectiveness. Fluid conductivity needs to be kept low and will rise during use.

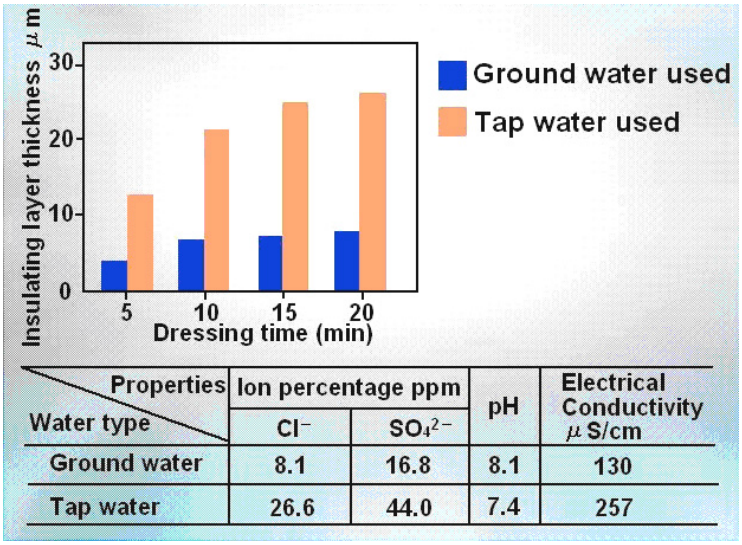

Water type \ Properties	Ion percentage ppm		pH	Electrical Conductivity μS/cm
	Cl^-	SO_4^{2-}		
Ground water	8.1	16.8	8.1	130
Tap water	26.6	44.0	7.4	257

Figure 41 - Difference in insulating layer thickness according to water [22]

Dowel fluid [58] is a water-based, fully-synthetic coolant that can be used in place of oil soluble fluids. It is not specifically designed for use with Elid but is recommended for use in moderate to heavy duty machining operations, particularly on cast iron, stainless steel, brass and aluminium. Dowel contains various additives which improve lubrication, inhibit corrosion, reduce foaming and improve high pressure performance. Its use was examined as alternative to the Noritake CEM fluid used throughout testing in this research (chapter 24).

Chapter 7 - Details of Elid Wheel Types

Elid wheels use superabrasives and require the high bonding strength and electrical properties of a metal bonding material. Traditionally metal bonded wheels are stable but as a result of their high strength and hardness they exhibit a slow rate of wear and are difficult to true. They are susceptible to wheel loading, glazing and require frequent dressing. The use of Elid with metal bonded wheels allows in-process dressing and controls wheel wear, thus improving the condition at the wheel's grinding surface. Figure 42 outlines the range of Elid wheels that are available and / or have been researched.

References	Elid Wheel Type
[57, 49]	(CIB) - Cast iron bond (FCI*)
[59, 30]	(CIFB) - Cast Iron fibre bond
[57, 49]	(CICB) - Cobalt modified cast-iron bonded (FCI-X*)
[49]	(CB) - Cobalt bond
[49, 46]	(CIBB) - Hybrid cast iron (50%) bronze (50%) bond
[57, 49, 54]	(BB) - Bronze bond (FSI-2*)
[60]	Carbon resin bonded wheels
[7, 62]	Elid honing stones with aluminium, iron, copper, and resin bonds
[57]	Iron resin hybrid bond.
[57, 40, 43]	(MRB) - Metal resin hybrid bonded (KFSI-2*), (KFSI-2Q*)
[27]	(SD) - Synthetic diamond abrasive
[27]	(CBN) - Cubic boron nitride abrasive
[27]	(DB) - Composite abrasives
[61, 27]	(CeO_2) - Cerium oxide abrasive and composite with diamond
[27]	(SiO2) - Silicon Oxide abrasives

Figure 42 - Various Elid Wheels (* - Fujidie wheel code)

The most commonly used and extensively researched type of Elid wheel is known as cast iron bond (CIB). These are produced by mixing cast iron powders and fine abrasives into a mould before sintering [45]. CIB wheels can be used for a wide range of applications and are commercially available from several wheel manufacturers [57, 62]. One manufacturer, Fujidie, recommends abrasive mesh sizes ranging from #80 for high efficiency roughing to #30,000 for mirror surface grinding and finishing. Both cast iron bond and Cerium oxide wheels have shown successful results when grinding / lap-grinding titanium [61, 63, 64]

The addition of cobalt to the cast iron bond (CICB) improves grinding performance. It is recommended for roughing to middle finishing, with mesh sizes ranging from #80 to #8000. A reduced initial pre-process dressing time is stated as the purpose of adding the cobalt by Fujidie [57]. However, Ohmori and Nakagawa [49] demonstrated that where a 50/50 ratio of cast iron to cobalt was used, Elid power stabilisation during pre-process dressing took longer with cobalt than iron.

In the USA, bronze bonded grinding wheels have traditionally been used for machining ceramics and the use of iron-bonded wheels is less common. Bifano et al. [54] explored the use of bronze bonded wheels with Elid. Bronze bonded wheels have also been used for rotary grinding using cup wheels and are particularly suited to high efficiency grinding of hard-to-grind materials (#60-#8,000) [57].

A prototype, metal-free, carbon resin bonded diamond Elid wheel was evaluated by Itoh et al. [60]. An oxygen-rich layer formed at the surface of the wheel, which possessed higher friction than the base material and wore more easily. When compared to CIB wheels an improved finish was achieved (30nm P-V with an #8000 wheel), reportedly as a result of the compliance of the wheel's resin constituent, however cutting quality was poor.

KFSI-2Q wheels (metal resin hybrid bonded wheels with increased porosity) were shown to be unsuccessful on titanium but the increased porosity may prove beneficial when grinding other materials such as bearing steel. Apart form MRB wheels, there is no other commercially available wheel that is capable of Elid 3 (electrode-less) grinding. Research, reviewed in chapter 10, used experimental Elid honing stones that along with a resin constituent, contained combinations of iron, aluminium, and copper.

7.1 Comparative Performance of Elid Wheel Types

Ohmori and Nakagawa [49] compared the dressing and grinding performance of various Elid wheels with a #140 mesh size. Pre-process dressing performance for three wheels is illustrated in figure 43, with the corresponding thickness of insulating layer. Working current for the cast iron bond wheel rapidly declines as a result of the easy oxidation and formation of a thick oxide layer. The bronze bond does not form a thick oxide layer and the current reduces gradually. Hybrid bonded wheels produced intermediate dressing characteristics according to their constituent parts.

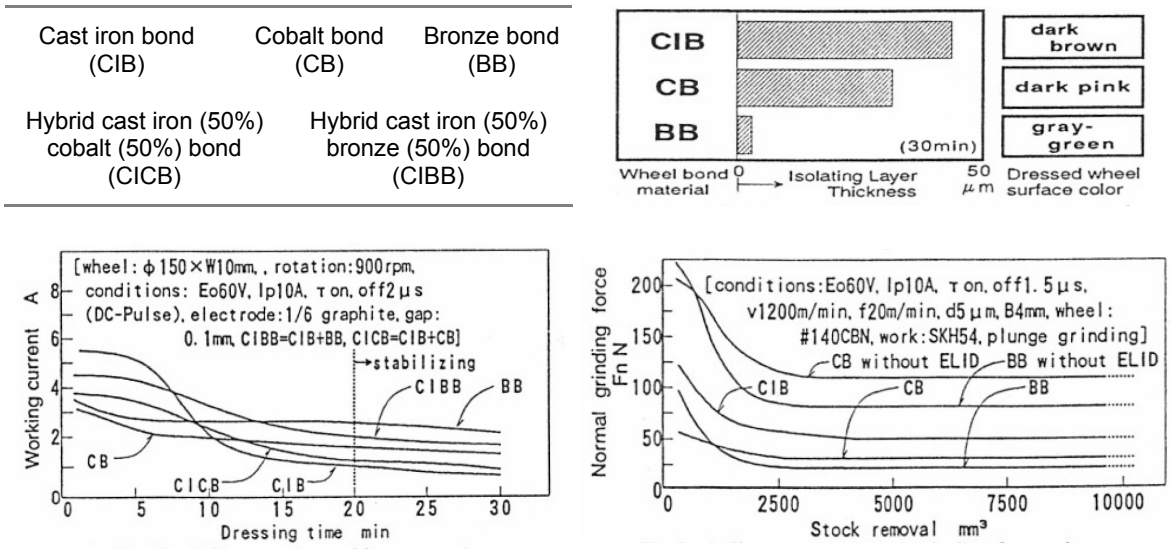

Figure 43 - Difference In Insulating layer thickness, working current, and normal grinding force change according to wheel bond material [49]

According to Ohmori and Nakagawa [49] confirmation that wheels producing a thinner insulating layer generate lower grinding forces is provided by figure 43. The reason stated for this is that wheels which produce a thinner oxide layer have a faster electrolysing rate.

7.2 Metal Resin bond Wheels

Metal-resin hybrid bonded Elid wheels (MRB), as used in the current research, were developed by the Ohmori team in the mid to late 1990s. The advantage of MRB wheels is twofold:

- The non-conductive resin provides a separation gap between the electrically charged wheel and workpiece allowing them to be used for Elid 3 grinding (#325 to #12,000) [30, 40, 43, 57].
- The resin in the wheel adds compliance to the wheel's grinding surface making them particularly suited for lap-grinding using ultra fine abrasives (#30,000 to #3,000,000) [12, 30, 31, 57].

The spherical ball superfinishing studied in this research is Elid 3 and is closely related to constant pressure lap-grinding.

7.2.1 MRB development - metal : resin ratio

Early MRB wheel development studies were conducted into Elid 3 ball-nose grinding [31] and Elid 1 lap grinding [30, 31]. Three wheel compositions containing 3:7, 5:5, and 7:3 parts copper to phenol resin were investigated by Itoh et al. [30], during the development of metal-resin bonded wheels. Decreasing the non-conductive resin portion (figure 44) increases the resistance of the wheel as a whole and has an enormous influence on the dressing characteristics. According to Itoh et al. [30] a resistance below 0.5 Ωmm is suitable for Elid.

Metal : Resin	Electrical Resistivity
3 : 7	1733.3 Ωmm
5 : 5	0.32 Ωmm
7 : 3	0.13 Ωmm

Figure 44 - Electrical resistivity according to MRB wheel mixing ratio [30]

Both 5:5 and 7:3 ratios exhibited a typical, non-linear, decline in current as a non-conductive layer of copper oxide (Cu_2O) built up on the surface during pre-process dressing (figure 45). Increased metal constituent produced a slower rate of working current stabilization. Elid 1 lap-grinding tests with #8,000 wheels (figure 46) revealed that stable material removal was achieved with the use of a 7:3 ratio but not a 5:5 ratio. A 7:3 ratio was commonly employed thereafter.

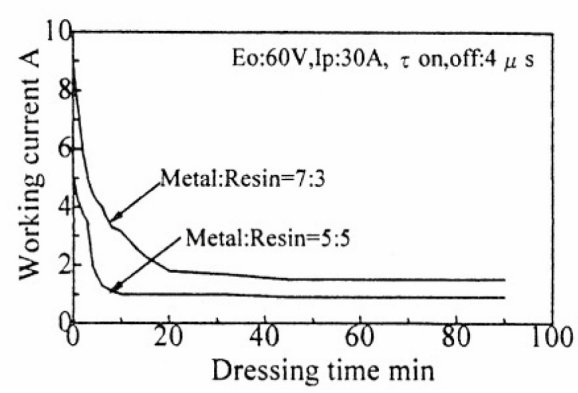

Figure 45 - Difference in pre-process dressing behaviour of working current according to MRB wheel mixing ratio [30]

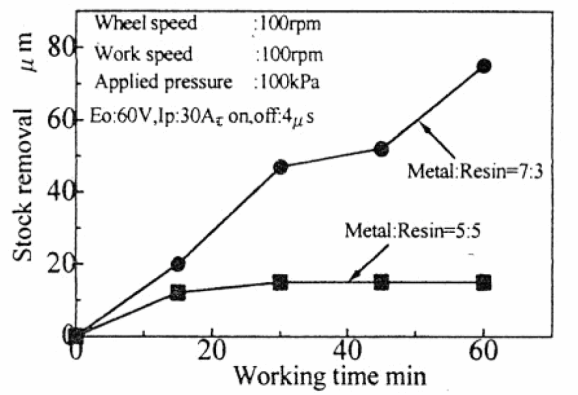

Figure 46 - Relation between grinding time and grinding efficiency according to MRB wheel mixing ratio [30]

7.2.2 Improved surface finish performance using MRB wheels

MRB wheels are the first choice when lap-grinding for optimal surface finish and in this respect have demonstrated superior finishing performance over CIB wheels [30]. A comparison between a metal-resin bond and a cast iron fibre bond wheel (both #8000),

showed faster current stabilization with the MRB wheel, a reduced material removal rate and an improved surface finish; Ra 3.2 nm compared to 7.4 nm (figures 47 & 48).

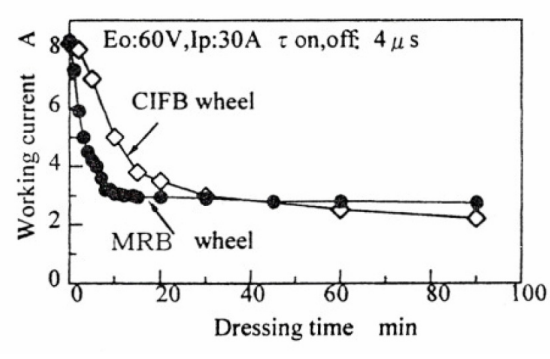

Figure 47 - Difference in electrical behaviour of initial dressing between cast iron fibre bond wheel and metal-resin bond wheel [30]

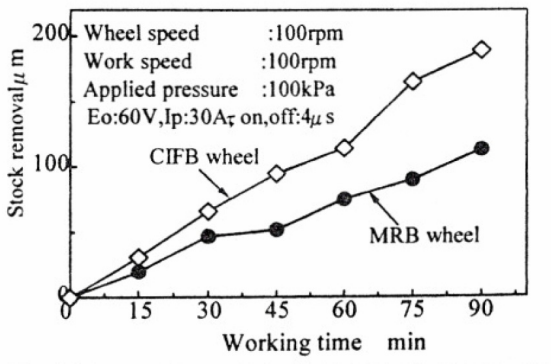

Figure 48 - Comparison of stock removal between cast iron fibre bond wheel and metal-resin bond wheel [30]

This is attributed to the formation of an elastic film at the electrolyzed surface of the wheel. As the wheel's metal component is removed through electrolysis a compliant porous structure of resin is left behind. The recession of abrasives into this compliant layer provides a more even pressure distribution of abrasives onto the surface of the workpiece [12, 22]. The increased elasticity also reduces the grit depth of cut and increases the number of active grits removing material from the workpiece (figure 49). As the grit depth of cut is reportedly smaller and more consistent, the surface finish is improved; as the number of active grits is increased, so is the material removal efficiency. Although it is not mentioned, enhanced damping characteristics may also play a role in improving finish.

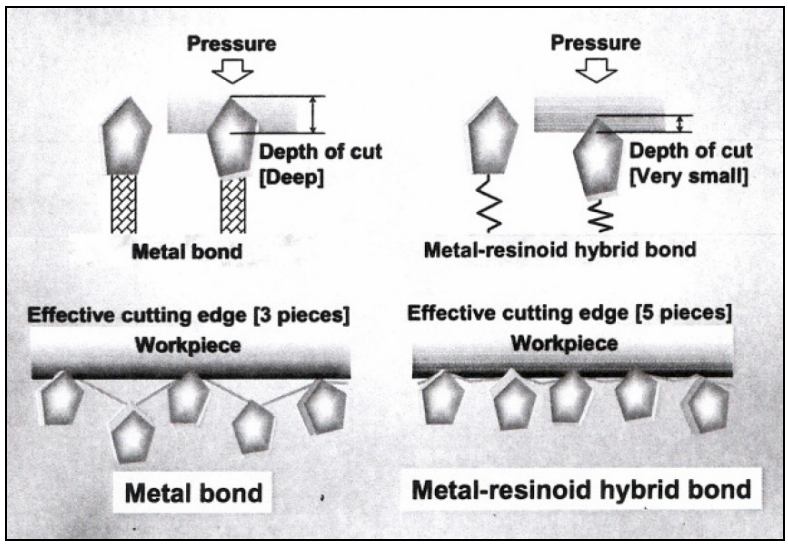

Figure 49 - Schematic illustration of grinding wheel surface with elasticity [22]

7.3 Effect of wheel bond strength

While Elid superfinishing, Ueda et al. [56] measured workpiece material removal using two bronze bonded #4000 mesh wheels with bonding strengths of 140 MPa and 200 MPa (figure 50). Both recorded linear material removal from the AL_2O_3 workpiece; the harder bonded wheel recorded an increased rate of 1.66 mm^3 per minute compared to the softer bond of 0.5 mm^3 per minute. The reason for the improvement observed when using a harder bond is reportedly because it controls the cutting ability of the stone.

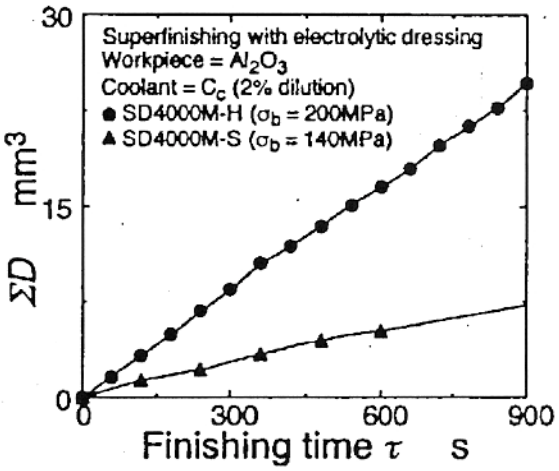

Figure 50 - Influence of bending strength of SD stone - [56]

7.4 Elid Wheel Wear

Fathima et al. [32] investigated the wear mechanisms involved in Elid grinding, while studying the vertical groove grinding of BK7 glass with a CIB wheel. When using the Elid method, wheel wear differs in some fundamental ways when compared to conventional grinding because the formation of an oxide layer within which the abrasives are held reduces the grit holding strength. The wheel wear mechanism is dominated by the electrochemical erosion of the bonding material that ultimately leads to micro fracture of the oxide layer (figure 51). This occurs when it reaches a critical thickness and can no longer withstand the grinding forces it experiences. If the depth of the oxide layer is greater than the grit size when fracture occurs, then new and unused grits are lost along with old and worn ones. Breakage of the oxide layer can cause instability in grinding parameters; grinding force for example.

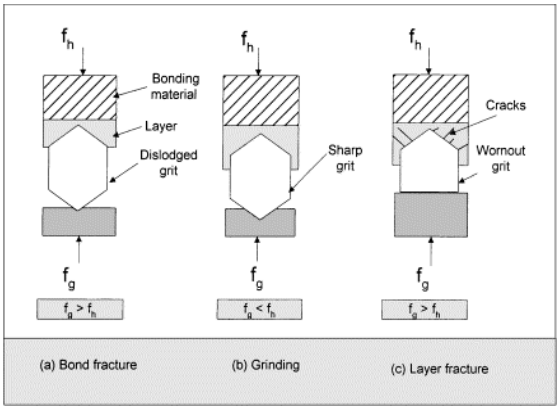

Figure 51 - Elid grinding wear mechanism [32]

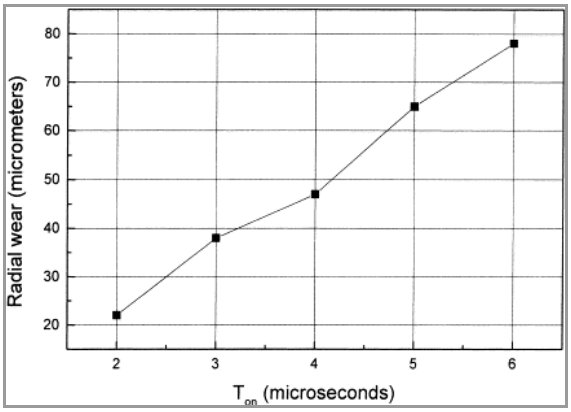

Figure 52 - Radial wear vs. T_{on} time [32]

Through the selection of Elid power values that influence the oxide layer, the Elid process provides a method of controlling the rate at which wheel wear occurs, thus preventing loading and glazing and providing ejection of worn abrasives. A reduced on pulse (τon) reduces wheel wear (figure 52) and can be used with coarse abrasive grits where an increased grinding efficiency is required. Improved surface finish is achieved when grinding using longer pulse on times, as this produces a thicker oxide layer. A thicker oxide layer accentuates the wheel compliance and further reduces the grit depth of cut as well as maintaining optimal dressed conditions. The use of more aggressive dressing / increased wheel wear necessitates that a balance be struck between whether the improvement in surface finish is justified by the reduction in grinding ratio. This relationship is often non-linear with a tipping point at which further reductions in grinding ratio no longer achieve an improvement in surface finish.

The resin constituent in MRB wheels makes the wheel wear mechanism differ slightly from that outlined for CIB wheels. The oxidized surface of an MRB wheel does not flake off in the same manner that a CIB wheel does, as the resin in the wheel requires mechanical abrasion to wear it away.

Chapter 8 - Elid 1 Grinding

The vast majority of work conducted using Elid is focused on Elid 1 grinding, which has been employed in numerous configurations. This chapter examines several papers that are relevant to the current research, looking at the results achieved with various set-ups and the subsurface characteristics of Elid.

8.1 Elid 1 Cylindrical Grinding with CIB Wheels

An Elid 1 set-up was employed by Qian et al. [44] to investigate the cylindrical grinding of bearing bushes (figure 53). The paper compares cylindrical Elid 1 grinding with honing and electro-finishing and finds that it clearly produces better surface finishes. With a #4000 mesh CIB-CBN wheel, finish values of 20nm Ra, 200nm Rz, zero skew and a surface slope of 0.2 were achieved. The Elid system produced slower removal rates, improved medium band and reduced high band waviness values, compared to honing and electro-finishing. Comparisons of residual compressive stress introduced through processing showed that the Elid process produced a shallower and less compacted surface. This system is a possible alternative to the current NMB cylindrical grinding operation.

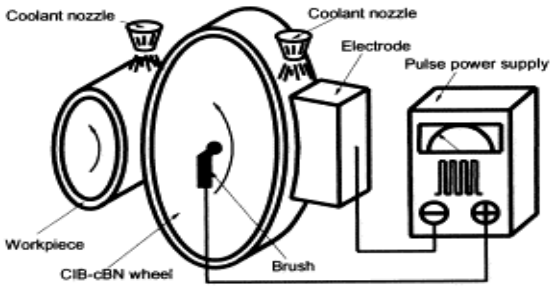

Figure 53 - Principle of cylindrical ELID grinding [44]

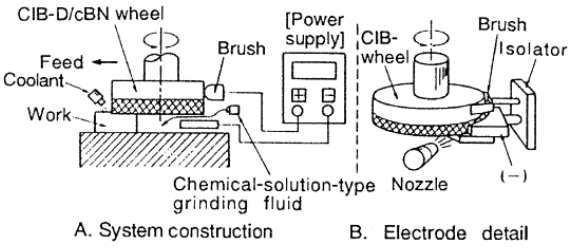

Figure 54 - Electrolytic in-process dressing (ELID), [after Ohmori and Nakagawa in 65]

8.2 Elid 1 Face Grinding with CIB Cup Wheels

It has been demonstrated that optical quality surface finishes, repeatedly below 10 nm Ra, can be achieved using large abrasive sizes (76 μm) when a precision machine tool is used [65]. Two CBN cup wheel types, resin bond and CIB + Elid, are compared when position controlled grinding bearing steel M50 (figure 54). Long contact times at the contacting flat face of the wheel on the workpiece are identified as providing a

secondary finishing cutting action, similar to a large number of spark-out passes. Controlling this aspect of grinding ensures the best finish and minimal sub-surface damage. When using Elid, less carbide pullout is observed and the surface finish is not compromised when feed rate is increased. This is due to the in-process dressing providing continual renewal of sharp grits and the resultant lower grit cutting force. Dulled grits do provide improved finish through a burnishing action and this effect is reduced when grinding with Elid, but to the benefit of surface integrity.

8.3 Elid 1 grinding for spherical lens fabrication

Optical components, such as spherical lenses, need to be produced with high shape accuracy, very low surface roughness and no surface damage. This is traditionally achieved using a long process chain, finishing with loose abrasive polishing. When manufacturing micro-lenses, problems exist with the fabrication of grinding and lapping tools. In addition, loose abrasive polishing of micro-components is time-consuming and degrades the form accuracy.

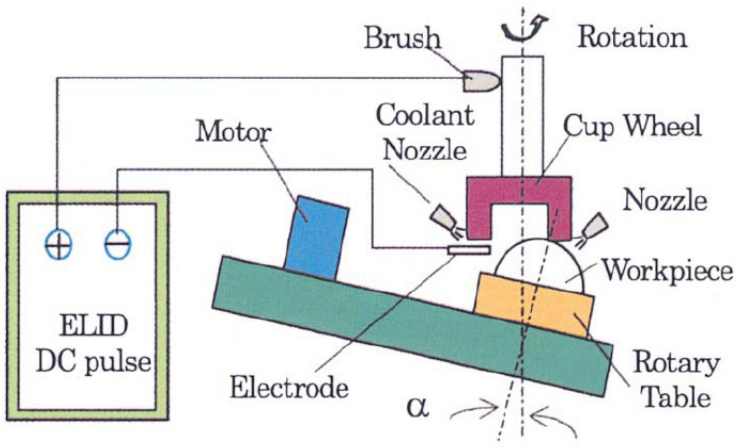

Figure 55 - Spherical lens fabrication using cup grinding wheels with Elid 1 – [66]

Elid 1 was used with a tilted rotary table and CIB cup wheels (figure 55) to grind spherical lenses [66]. Using #600 and #4000 wheels, much better surface finish was achieved with ELID than without ELID. Surface profile accuracy was also improved through the use of Elid. The same configuration was also used successfully for the fabrication of micro-lenses (1 mm in diameter).

8.4 Ductile-brittle transition

A ductile mode material removal mechanism can be achieved when grinding brittle material, such as BK7 glass, by the use of the Elid method. Whereas brittle material removal results in a rough surface finish and a large degree of micro-cracks / subsurface damage, removal in a ductile mode produces very smooth, optical quality surface finishes [67]. A brittle - ductile transition is dependent on the control of grinding parameters such as depth of cut, feed rate, etc. Ductile mode removal results in lower grinding forces than brittle mode.

Ductile mode machining of optical quality glass is achieved through a mechanism of plastically deformed chip removal. Under correctly controlled grinding conditions, subsurface damage in the workpiece is all but eliminated and nanometre surface finishes are achieved. The brittle – ductile transition marks the boundary of this removal mechanism. As demonstrated in figure 56 the transition occurs using different abrasive sizes on different workpiece materials. Large changes in the output surface finish are associated with the ductile – brittle material removal transition [22].

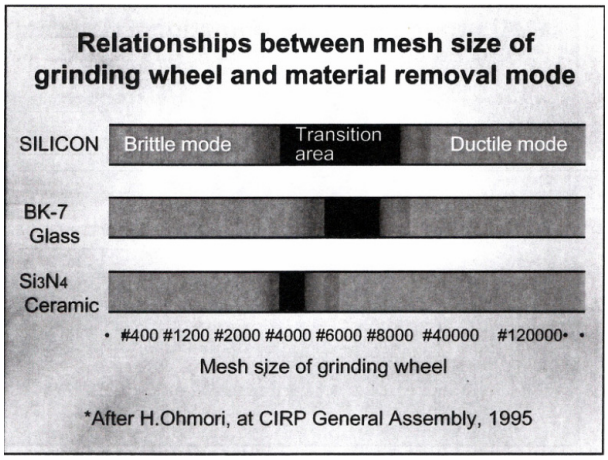

Figure 56 - Ductile – brittle transitions - [22]

8.5 Comparisons of Elid and conventional grinding

Several authors [25, 32, 49], using various grinding configurations, have demonstrated that grinding forces are lower when using Elid compared to conventional non-Elid methods. Machining vertical grooves with CIB wheels, Lim et al. [23] compared grinding forces, feed rate, tool wear and surface finish for non-Elid, Elid and Elid duty ratio. Normal and tangential grinding forces, although ultimately lower when using Elid, are inherently unstable and fluctuate in accordance with variations in the insulating oxide layer (figure 57).

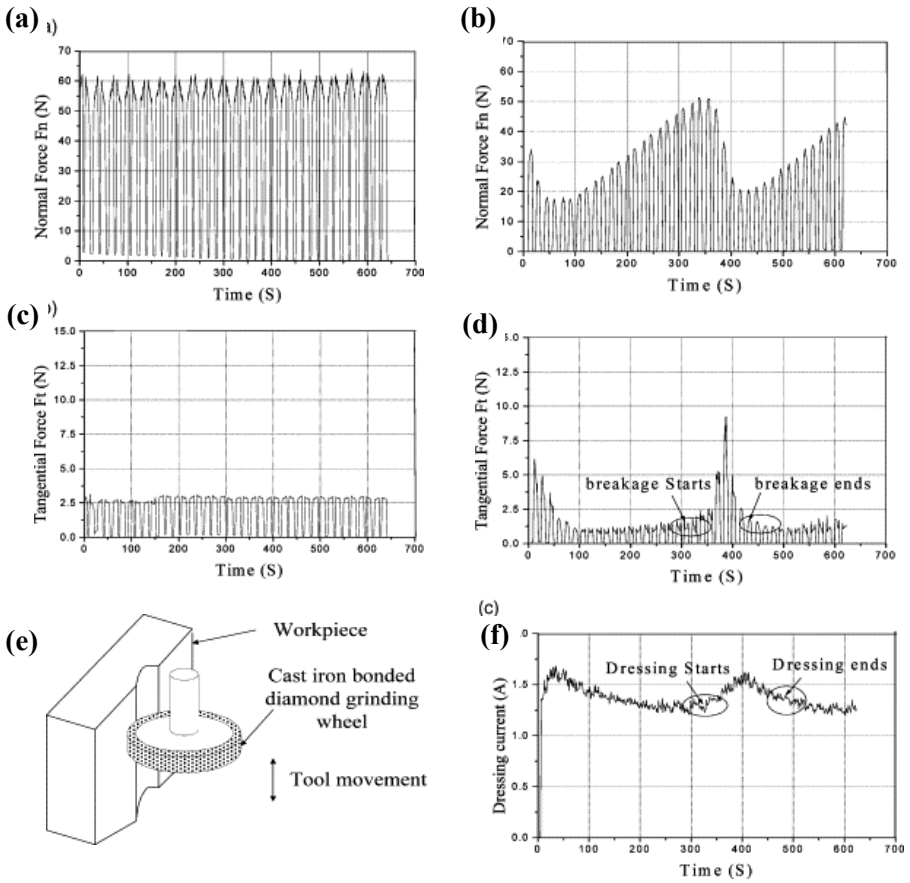

Figure 57 - (a) Normal force conventional, (b) Normal force Elid, (c) Tangential force conventional, (d) Tangential force Elid, (e) Grinding configuration, (f) Elid current - [23]

The continual refreshment of the Elid dressed grinding surface prevents the normal force from reaching comparatively high values, nevertheless the wheel's fluctuating condition causes a pattern of periodic rise and fall in force. The tangential force rapidly varies in line with the breaking and recovery of the oxide layer. An effective grinding process requires conditions to remain constant during operation. Variations in force indicate that the process lacks stability.

Increasing the feed rate and / or depth of cut increases the dressing current, normal force and tangential force. Excessive feed rates, in this case exceeding 400 mm/min, result in an increased oxide layer removal, leading to poor wheel condition and workpiece surface quality. Although feed rates and depth of cut are not applicable to the superfinishing of bearing balls, the common consensus is that more aggressive grinding parameters, i.e. faster feed rates and larger depths of cut, generate increased heat leading to a poorer surface finish. The improvement in wheel condition that processing using Elid provides, results in a better surface finish compared to non-Elid methods using equivalent depths of cut and feed rates [46].

8.6 Corrosion response of Elid

Processing using the Elid method can provide an improved resistance to workpiece corrosion. A range of CIB-D Elid wheels was used to assess corrosion performance and sample surface finish [68]. In addition, Elid processing is compared to samples produced using 400 – 2000 grit emery paper and 0.3 μm alumina suspension. Higher pitting potential (Epit) was recorded when the 316 stainless steel samples were prepared with Elid wheels containing finer abrasives (figure 58). This demonstrates that processing with finer abrasives, which ultimately results in a smoother surface finish, endowed the samples with improved corrosion properties.

Processing Method	Ra Surface Finish (nm)	Ecorr - Corrosion Potential (mV vs S.C.F)	Epit - Pitting Potential (mV vs S.C.F)	Ipass - Passive Current Density (10^{-4} mA/cm^2)
# 325 Elid grinding	~ 35	-142	52	-
# 2000 Elid grinding	~ 25	-23	330	2.00
# 8000 Elid grinding	~ 10	43	427	0.86
Polishing with a 0.3 μm Alumina suspension	~ 10	-131	310	3.32

Figure 58 - Surface finish and polarization test results on 316 stainless steel samples. Corrosion tests used a three electrode electrochemical cell connected to a computer driven potentiostat. [After 68]

The #8000 Elid ground samples, of equivalent surface finish to those polished with alumina, demonstrated superior corrosion performance. EDX analysis revealed that the Elid processed surfaces contained higher levels of oxygen and carbon. The improvement in corrosion performance with Elid was attributed to the creation of a very thin and stable oxide film on the specimen's surface that inhibits further corrosion. It was suggested that this is formed as a result of the electrochemical process causing a reaction between oxygen and the heated specimen.

Chapter 9

Elid Grinding With Restricted Electrode Access

To overcome the space restrictions involved in grinding certain features and components, both Elid 2 and Elid 3 have been developed.

9.1 Elid 2 - Interval Dressing

The process of Elid 2 (electrolytic interval dressing) involves a periodic cycle of separate dressing and grinding operations. The interval dressing stage follows the same procedure as for Elid pre-process dressing, however as there is no room to fit in a separate electrode, the Elid system is not used while actually grinding. With this method the benefits of Elid can be applied to the small hole grinding of micro-components (figure 59) [28, 40, 41, 42, 43, 45]. Using conventional methods to grind small holes in hard materials poses numerous problems, many of which are also relevant for spherical superfinishing. Difficulties are experienced with the following:

- conditioning small wheels
- maintaining static grinding conditions
- ensuring fluid access in order to provide effective dressing, cooling, lubrication, and debris removal
- minimizing wheel wear and compensating for it
- achieving the required grinding speeds and finding suitable grinding parameters
- achieving satisfactory grinding efficiency
- reaching a high degree of form accuracy and surface finish

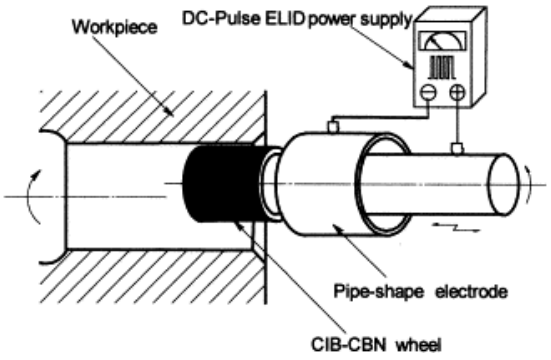

Figure 59 - Elid 2 Small Hole Machining Set-up [40]

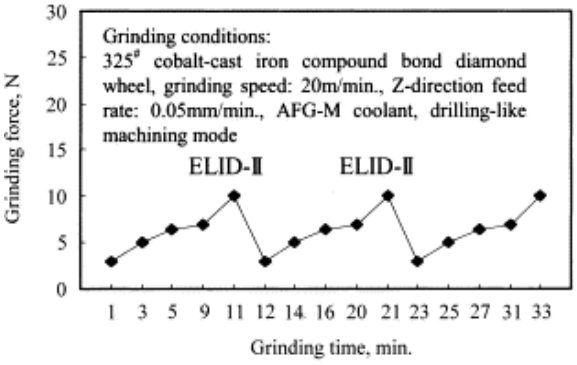

Figure 60 - Typical Elid 2 Force characteristics [41]

Using wheels with a 1 to 2.5 mm diameter, Zhang et al [41] found the Elid 2 method to be effective on Al_2O_3 specimens. Using these small wheels the characteristics of the Elid process were distinct; the type of grinding fluid and electrical parameters used had a large influence on the resultant wheel's grinding surface. Correct selection of Elid dressing parameters provided good grit protrusion while also being able to minimize and control wheel wear. The periodic dressing was governed by the rise in grinding forces during processing. Re-dressing the wheel when the forces reached a critical value maintained static grinding conditions. A periodic pattern is seen in figure 60. The average grinding force was reduced by increasing the spindle speed and reducing the feed rate. The distance ground before the wheel required re-dressing was increased by increasing the spindle speed and the feed rate. Optical microscope analysis revealed that no crack marks were present at either the entrance or exit of the ground hole.

Elid 2 research by Qian et al. [40, 42, 43] investigated the internal cylindrical grinding of ceramics, hardened steels and bearing steels. Using a #4000 CIB-D wheel the process achieved mirror surface finishes, 20 nm Ra and 128 nm Rz on bearing steel (figure 61). The pipe type electrode, as shown in figure 59, produced better results when compared to an arc type electrode. The larger coverage of the wheel's grinding surface by the pipe type electrode resulted in a higher dressing current being drawn and produced a better component finish. Assessing the surface finish response when varying grinding parameters, the same effects were observed when Elid 2 grinding as are experienced when performing conventional Elid 1. Surface finish was improved by reducing traverse speed and depth of cut, as well as by increasing wheel speed. The worst surface finish results were achieved when no dressing was used (figure 62).

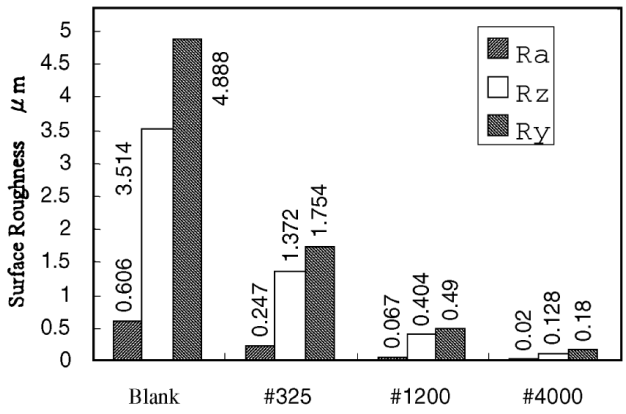

Figure 61 - Surface finish produced on bearing steel using Elid 2 and different mesh CIB wheels [42]

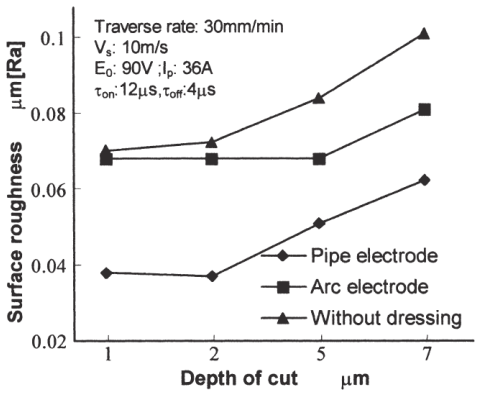

Figure 62 - Effect of electrode type on surface finish [42]

In the case of the current research, using a ball type electrode will result in almost total coverage of the wheel's grinding surface when either pre-process dressing or interval dressing. Elid 2 can be used with CIB wheels, which are not suitable for Elid 3 grinding but may be advantageous over MRB wheels due to their reportedly improved removal rates. When using ELID 2 on wheels with a long internal surface, it is reportedly difficult to achieve a sufficient degree of dressing. Dressing times can be lengthy with time spent dressing at the expense of grinding and thus overall efficiency. These aspects were a driving cause for the development of the Elid 3 process.

9.2 Elid 3 - Electrode-less

Elid 3 is defined as 'electrode-less electrolytic in-process dressing'. The process was patented by Hitoshi Ohmori and the Institute of Physical and Chemical Research (Saitama, JP) in 2000 [69]. It is a newly developed type of Elid grinding and little research has been published on it. This system has been applied to the grinding of small holes [40, 43], as illustrated in figure 63, as well as lapping and free form grinding with a ball-nosed wheel [31]. Work on spherical ball superfinishing with this system has also been conducted by Minebea Co Ltd (Japan), with a European patent application published in 2001 [70]. The experimental configuration discussed includes an option of rotational movement of the wheel around the centre position of the ball for the purpose of improving ball roundness.

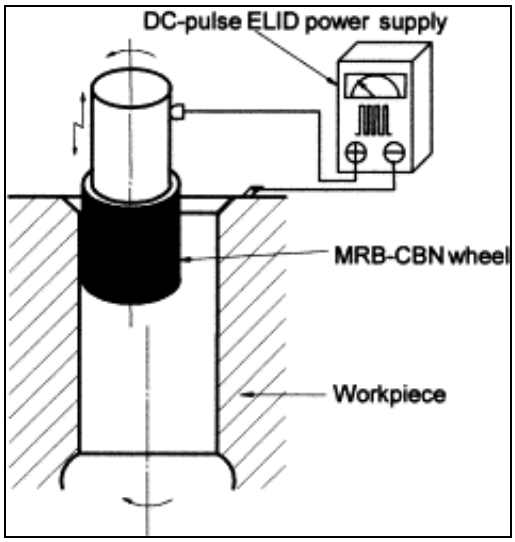

Figure 63 - Elid 3 Small Hole Machining Set-up. [40]

As the Elid 3 process does not use a separate electrode, electrolysis, or dressing, takes place between a conductive workpiece (the cathode) and the grinding wheel (the anode). Dressing occurs in-process at the grinding interface. The mechanism presented in the literature of how Elid 3 works with these wheels is limited.

A brief development study of the Elid 3 method was performed by Matsuzawa et al. [31]. When Elid 3 lap-grinding silicon, an oxide layer was formed on the surface of the wheel at a peak current of 30 amps and a voltage of 60 volts. Using an S35C steel workpiece, 4 Amps and 20 volts resulted in the formation of a wheel oxide layer. Better surface roughness was achieved when a greater applied load of 16 kgf was used. An Ra surface finish of 24 nm was achieved on the steel sample using a #1200 wheel. Sparking between the ball-nosed wheel and the workpiece occurred using a current of 10 Amps. Improved performance was achieved when the depth of cut was below 10 μm for an #80 wheel and below 5 μm for a #200 wheel.

Work conducted by Qian et al. using Elid 2 and CIB wheels [42], is continued employing an Elid 3 set-up with MRB wheels [40, 43], allowing comparisons to be drawn. Figure 64 outlines the details of experimentation. The research is similar to this thesis as both use Fujidie MRB-CBN wheels in an Elid 3 set-up on hardened steel.

Machine tool	Mug27/30-22 [Mitsui Seiki Kogyo Co. Ltd.]	
Grinding wheel	1A1 CIB–CBN wheel:	∅30×L20, #325, #1200, #4000
	1A1 MRB–CBN wheel:	∅30/∅20×L20, #1200, #2000, #4000
		∅2.5×L5, #325, #1200, #4000
ELID power	SUE-87 (peak value: 150 V, 30 A)	
Coolant	2% dilution of chemical coolant AFM-G	
Workpieces	SKD11(HRc 62), SKH51(HRc 56)	∅36×L30/∅26×L60
	WC-Co	∅26×L60
	Bearing steel (HRc 58)	∅36×L15 mm
	Alumina (Al_2O_3: 93.8%)	∅36×L30 mm
	Oil nozzle SCM420 (HRc 60)	∅4×L12.5 mm

Figure 64 - Experimental details [40]

One problem highlighted with Elid 3 grinding [40, 43] is spark discharge between the workpiece and wheel. This is reportedly caused by insufficient dressing, insulating layer characteristics, grinding chips and high electric parameters. Mirror surface grinding is only achievable when electrical discharge is prevented. This requires the correct selection of electrical and grinding parameters. These are low open voltage, low peak current and low duty factor of pulse amplitude. As grinding chips are one cause of sparking, a low feed rate should be used to minimize the effects. Abrasives remained protruding from the wheel's surface both after pre-process dressing and after grinding. However, the oxide present after pre-dressing was removed during grinding, leaving a porous structure.

The use of MRB wheels enables mirror surfaces to be easily achieved and there was only a small difference in roughness between the use of #2000 and #4000 wheels. Using the #1200, #2000, and #4000 MRB wheels, surface finishes of 25nm, 6nm, and 4nm respectively were achieved on hardened steel bearing rings (figure 65). A coarser abrasive MRB wheel with Elid 3 produced comparable levels of surface finish to a finer abrasive CIB wheel with Elid 2.

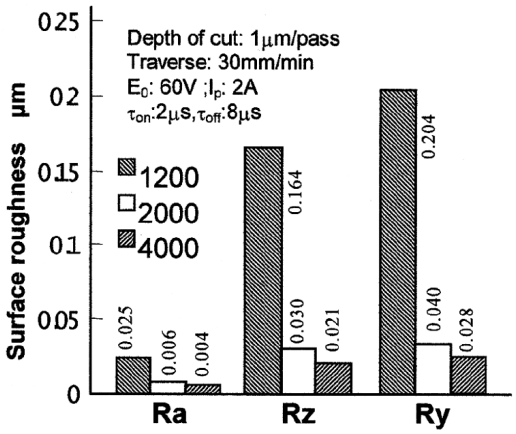

Figure 65 - Surface roughness results [40, 43]

Internal Elid 3 grinding was also investigated on a kerosene engine nozzle [40]. The levels of surface finish achieved using the 2.5 mm diameter wheels were not as good as those achieved on the hardened steel bearing ring samples. This was due to the poor grinding conditions. The wheel was too small and wheel wear was rapid. The process did not produce a hole of consistent diameter. This was reportedly due to poor wheel mounting; although attempts to maximize stiffness were made, as the wheel has such a small diameter it also possessed poor stiffness.

When compared to CIB wheels, MRB wheels reportedly wear at a higher rate and possess lower integral wheel strength.

$$\text{G - Ratio} = \frac{\text{Volume removed from workpiece}}{\text{Volume removed from wheel}}$$

The G-ratio (grinding ratio) is significantly lower for MRB wheels than for CIB wheels. Values of 55 and 12 were achieved for #1200 and #4000 MRB wheels. It is stated that CIB wheels typically achieve values over 100. Recommendations are made that CIB wheels be used initially with an Elid 2 set-up, followed by an Elid 3 grinding system with MRB wheels for final finishing, particularly when small wheel diameters are employed. When spherical superfinishing in this thesis, wheel wear is not regarded as a problem; the wheel maintains its shape and diameter as it wears and only the length is reduced.

9.3 Elid 3A and Combined Elid + EDM

Elid 3A is an electrode-less process as described for Elid 3, however a pulsed, square wave, alternating power source is used as opposed to the pulsed direct current used for all other Elid types. The result of this is that electrolysis occurs at both the wheel and the workpiece. This provides some advantages over an electrode-less process using direct current, as it reportedly eliminates sparking occurring at the grinding interface [Lim et al. in 28]. This results in a reduction in surface damage. Figure 66 demonstrates the process which is essentially a combination of a conventional electrochemical grinding process and an Elid process. The depth of cut is set so that it is within the layer of oxidised material on the surface of the workpiece.

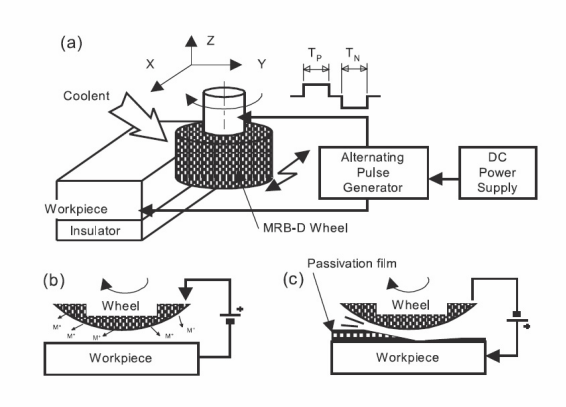

Figure 66 - Schematic diagram of ELID-IIIA (a) ELID-3 machining system with alternating current. (b) ELID without electrode. (c) Electrolysis of work-piece. [Lim et al 2000, 2001 in 28]

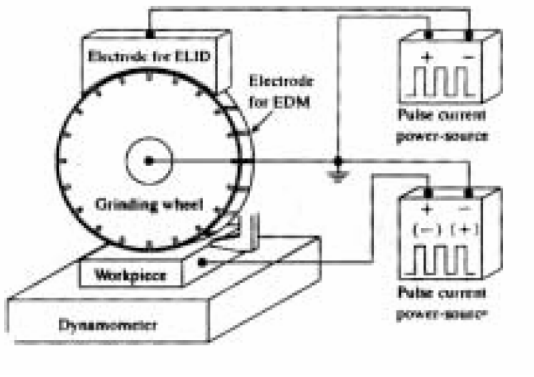

Figure 67. Combined ELID and EDM setup [Okuyama 2001 In 28]

Okuyama et al. [71] proposed a new combination machining method of ELID-grinding and EDM, as illustrated in figure 67. In comparison with conventional ELID-grinding, grinding forces were reduced but surface finish deteriorated. When a pulsed DC- power-source was used, finish improved. A similar configuration was tested in chapter 26.

Chapter 10 - Constant Force Elid Processing

10.1 Elid Lap-grinding

Elid lap-grinding is a constant force process that uses metal and metal-resin bonded grinding wheels (figure 68). The process uses a slow workpiece speed (typically 50 to 100 rpm) and a faster wheel speed (typically 100 - 200 rpm with a 300mm wheel). Unlike conventional grinding, lap-grinding does not require the use of a very precise, stiff and expensive machine tool to achieve very good levels of surface finish. The adoption of constant force processing allows grinding aggressiveness to remain static and the required removal rate / processing time to vary.

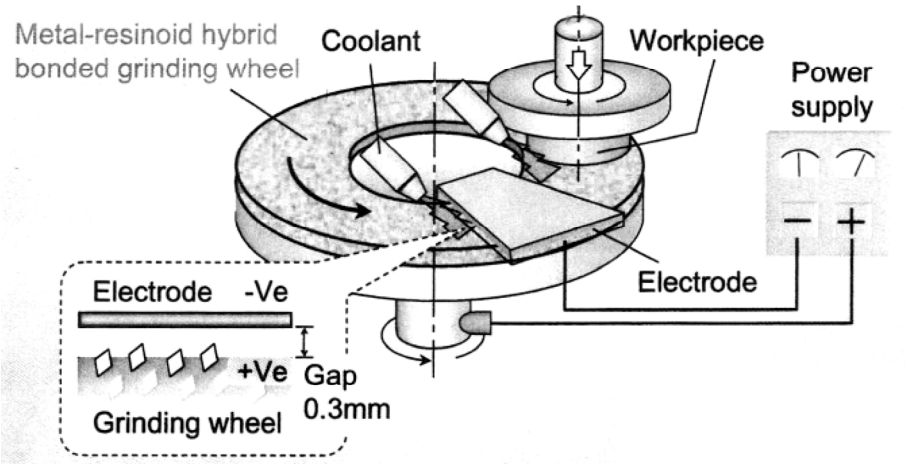

Figure 68 - Schematic illustration of Elid lap-grinding [22]

10.1.1 General Surface Finish & Efficiency

Figure 69 outlines the surface finish results and material removal rates achieved when Elid lap-grinding with various wheels and workpiece materials. The levels of surface finish reported in the literature for Elid lap-grinding should be the ultimate goal for the current research. Both are constant force processes and although superfinishing of spherical bearing balls adds additional geometric considerations and uses smaller, thin walled wheels, comparable levels of surface finish should be approached. As with surface finish the efficiency of material removal during lap-grinding should be aspired to. However, the smaller wheel-work contact area and reduced free wheel area available for dressing during spherical superfinishing limit the efficiency somewhat.

Ref.	Details	Mesh No.	Workpiece	Finish (nm)	Material Removal (µm/min)
[30]	7:3 MRB-D	#8,000	Monocrystalline Silicon	3.2 Ra, 28 Ry	1.2
	CIFB-D			7.4 Ra, 60 Ry	2
[31]	7:3 MRB-D (Elid 3 lap-grinding)	#1,200	Silicon	50 Ra, 300 Rz, 426 Ry	-
			S35C	24 Ra, 104 Rz, 167 Ry	-
[12]	7:3 MRB-D Applied pressure 0.1 or 0.15 MPa, wheel speed 100 rpm, workpiece speed 100 rpm	#8,000	Monocrystalline Silicon	22.3 P-V	1.1
			BK7 Glass	~20 P-V	-
		120,000	Monocrystalline Silicon	3.3 P-V	0.14
			BK7 Glass	~ 4 P-V	-
		3,000,000	Monocrystalline Silicon	0.38 Ra, 2.8 P-V	0.02
			BK7 Glass	2.5 P-V	-
[61]	Cerium oxide, iron bonded wheel	#20,000	Ti-6Al-4V	~ 8 Ra, 81 Ry	-
[33]	Cast iron fibre bond diamond (CIFB-D)	#1,200	Silicon	~ 66 Ra	~ 40
			Tungsten Carbide	~ 18 Ra	~ 12
		#4,000	Silicon	~ 18 Ra	~ 7
			Tungsten Carbide	~ 4 Ra	~ 3
		#8,000	Silicon	~ 8 Ra	~ 2
			Tungsten Carbide	~ 3 Ra	~ 1
[72]	CIB-D	#120,000	Silicon	1.2 Ra, 8.0 Rmax	-
		#3,000,000	Silicon	0.329 Ra, 2.34 P-V	-
			Glass	0.325 Ra, 2.36 P-V	-
[22]	CIB-D	#8000	CVD-SiC	3.6 Ra, 30.0 Ry	-
			WC	4.0 Ra, 28.5 Ry	-
			BK7 (glass)	5.7 Ra, 40.5 Ry	-
	MRB-D	#8000	WC	2.0 Ra, 14.0 Ry	-
			Si	3.0 Ra, 24.5 Ry	-

Figure 69 - Summary of surface finish results from Elid lap grinding papers

10.1.2 Comparison to non-Elid lap-grinding

Whilst Elid grinding has demonstrated the ability to produce very high quality surface finishes, loose abrasive polishing can achieve equivalent levels. Where Elid really offers a benefit is in the ability to produce high quality surface finishes whilst maintaining very precise form. The surfaces produced with Elid are defect free and high levels of material removal are achieved. When the performance of Elid lap-grinding is compared to non-Elid lap-grinding, both using metal bonded wheels (figures 70 to 72), surface finish is better, material removal is higher, and greater consistency is achieved with Elid [12, 22, 33].

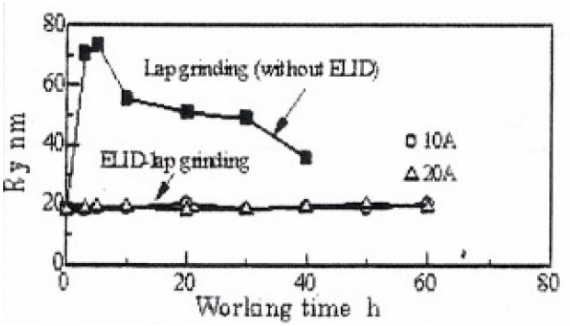

Figure 70 - Change in surface roughness for lap-grinding with and without the use of Elid. (#8000CIB-D wheel on WC workpiece) [22]

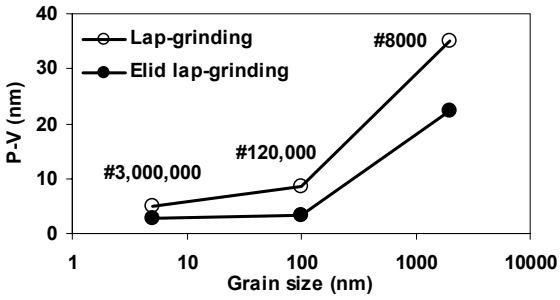

Figure 71 - Effect of Elid and abrasive size on surface finish. (MRB-D wheel on silicone workpiece) - [From data in 12]

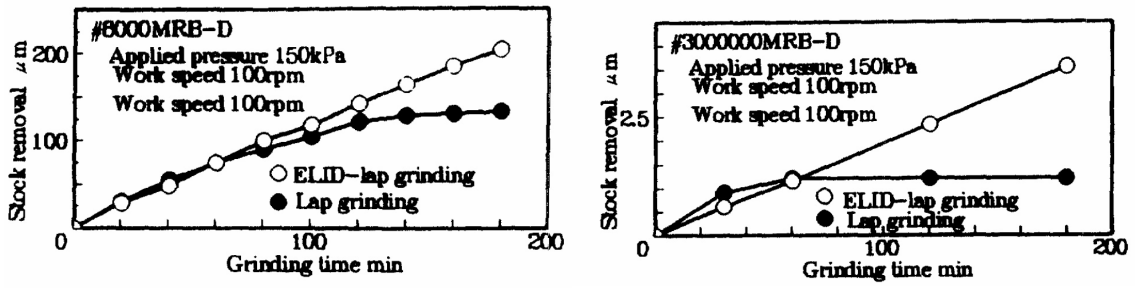

Figure 72 - Effect of Elid and abrasive size on material removal. (MRB-D wheel on silicone workpiece) - [12]

Using Elid 1 lap-grinding and MRB-D wheels #8,000, #120,000, and #3,000,000, stable grinding has been achieved, producing a P-V finish of 2.8 nm on silicon and 2.5 nm on glass with the #3,000,000 wheel [12]. When compared to conventional fine abrasive lap grinding, all mesh size Elid wheels showed an improvement in finish and a stable stock removal rate. Using the #8000 wheel the improvement was from 35 nm P-V without Elid to 22.3 nm P-V with Elid. Improved surface finish was reportedly due to the formation of an elastic film at the grinding interface providing a more even grit depth of cut.

10.1.3 Effects of workpiece material

The workpiece material plays a large role in the performance and results of abrasive processing in general. Polishing of soft steel, for example, results in a greater degree of wheel loading and thus requires stronger electrolytic dressing [56].

10.1.4 Effect of abrasive size

Investigating Elid 1 lap grinding of silicon and tungsten carbide with CIFB-D wheels, Itoh et al. [33] evaluated the effect of abrasive size on surface finish and removal rate (figure 73).

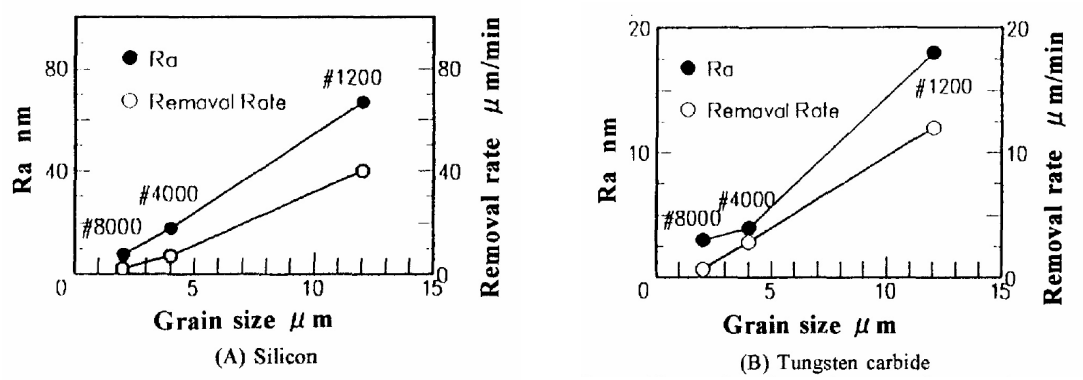

Figure 73 - Surface roughness and removal rate against abrasive size for lap-grinding differing workpiece materials with CIFB-D wheels [33]

The change in material removal mechanism, from brittle to ductile, is affected by material type as well as abrasive size. The brittle - ductile transition occurs using an #8000 wheel on silicon and a #4000 wheel on tungsten carbide. An additional surface finish improvement of a silicon sample can be achieved by grinding silicon and tungsten carbide together [33].

As abrasive size reduces there is a corresponding improvement in surface finish and retardation of removal rate. Although the overriding goal of Elid grinding is to achieve a very fine surface finish it must do so at an acceptable and efficient rate. These requirements are often in conflict with each other and are strongly dependent on abrasive size [30].

10.1.5 Applied Pressure

The applied pressure between the contacting surfaces of the wheel and workpiece influences the processing performance. Figure 74 shows that surface finish worsened when the contact pressure was increased over 0.15 MPa; the material removal rate increased with increased pressure. A contact pressure of 0.3 MPa is recommended [22]. Larger contact pressures of 1 to 3 MPa were investigated by Ueda et al. [56] using an Elid 1 lap-grinding configuration involving an oscillating motion.

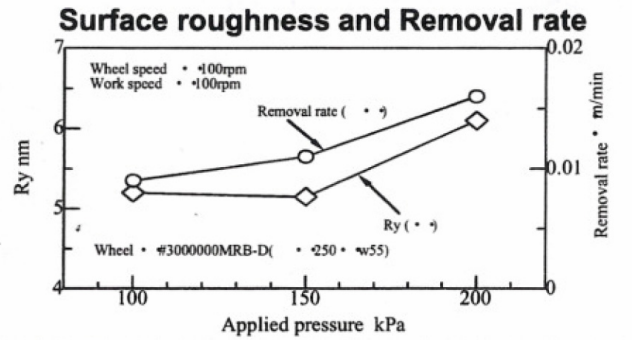

Figure 74 - Effect of contact pressure on finish and removal rate (CVD-SiC finished by #3,000,000 MRB wheel) [22]

10.2 Constant Force Elid Grinding

An improvement in surface finish can be achieved by employing a constant in-feed pressure as an alternative to the use of a preset in-feed speed and depth of cut. Ohmori and Nakagawa [72] compared the two techniques using #3,000,000 and #120,000 CIB-D wheels on a rotary surface grinder.

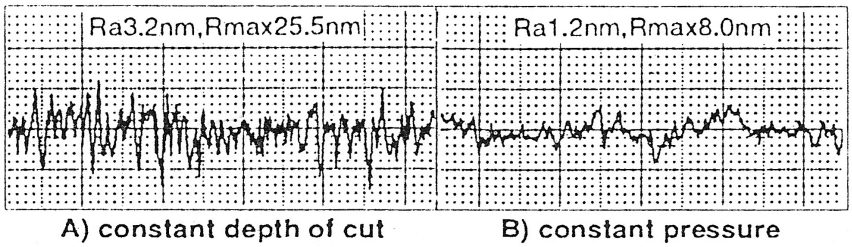

Figure 75 - Effect of grinding configuration on finish (#120,000 CIB-D) [72]

Using a pre-defined feed rate and a 20 microns depth of cut, the surface finish improved as smaller abrasives were employed but only down to a wheel mesh size of #40,000. The use of even finer abrasives, such as the #120,000 wheel, resulted in a worsening of finish. This limitation does not occur when maintaining a constant in-feed pressure. The finish is not only comparatively better (figure 75) but continues to improve as the abrasive size is reduced. A #3,000,000 (0.5nm) wheel, the smallest mesh size available, is capable of producing a very impressive, atomic quality surface finish of 0.3 nm Ra.

Bifano et al. [54] investigated constant force Elid grinding with a bronze bonded diamond wheel. As shown in figure 76 a gradual decline in material removal rate is observed when no wheel dressing is performed. After 26 cuts the material removal has decreased dramatically. When the Elid system is turned on, material removal efficiency rapidly increases, returning to the wheel's original starting performance within 3 cuts.

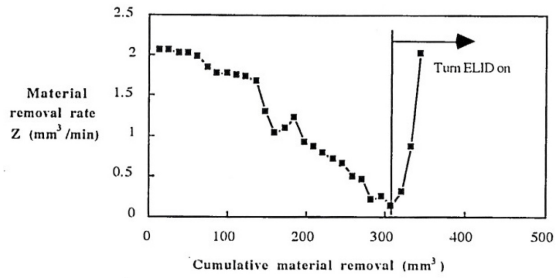

Figure 76 - Restoration of wheels performance after Elid dressing. - [54]

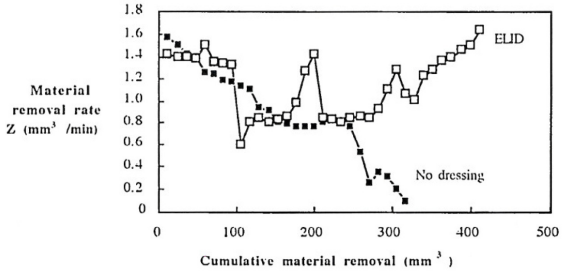

Figure 77 - Material removal performance with and without the use of Elid. -[54]

When comparing cut off sawing performance with and without the use of Elid, it can be seen that the material removal rate remains at a high level when Elid is used, although it does fluctuate somewhat (figure 77). Removal rates that are relatively large but fluctuating are not highlighted as a problem by the authors, however in this thesis they are. Large fluctuations in removal rates translate to very large differences in the processing time required to reach the desired surface finish.

The wheel wear resultant when using Elid was compared to the more conventional dressing method of a porous ceramic abrasive stick [54]. When a consistent cutting time was maintained by periodic stick re-dressing, the wheel wear rate was approximately the same as with Elid. A cumulative wheel wear rate of 0.087mm^3 per mm^3 of workpiece material removed was achieved (figure 78). One concern highlighted was the deterioration of the wheel's trueness after a prolonged dressing period. It was seen to degrade from 25 μm to 125 μm over a 3 hour period of continuous Elid dressing.

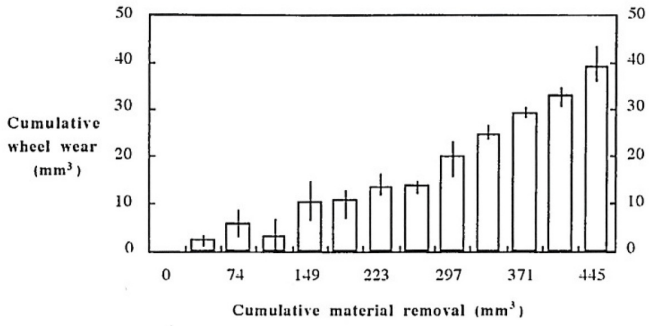

Figure 78 - Wheel wear with Elid for CVD silicon carbide. - [54]

10.3 Elid Honing

Work conducted by Knight [7] investigating the application of Elid to a honing operation is of particular relevance and worth an in-depth review. A selection of metal and metal-resin bonded honing stones, produced by Wendt Boart, were tested in an Elid 3 configuration against a cylindrical roller bearing's inner raceway (SAE 52100). The research along this avenue was ultimately deemed unsuccessful.

Following a diamond truing operation, an additional one second electrolytic pre-process dressing operation of an iron bonded #4000 CBN honing stone was found to produce an open stone surface with good grit protrusion. A freer cutting action was produced when using electrolytically dressed stones. A free-cutting action can however diminish the burnishing action that is often capable of achieving a superior surface finish. The abrasive truing procedure failed to produce an exactly conforming profile. The conventional bedding-in procedure was hampered by the hardness and wear resistance of the stones metal bond.

During Elid honing a low recorded voltage of less than one volt indicated that metal to metal contact between the stone and workpiece had occurred. A stable inter-electrode gap can be maintained by the abrasive grits, or by the formation of an insulating layer of oxide that can be rapidly repaired when damaged. Fluid must penetrate the stone's surface effectively to allow electrolysis to occur. A reduction in stone size and the use of multi nozzles are suggested as methods to improve the ability of the fluid to penetrate the stone - workpiece area interface.

Electrolytic dressing of a copper-resin bonded diamond stone resulted in dissolution of the stone's copper bond material with the copper ions plating-out onto the workpiece surface. This occurred at a point corresponding to where the insulating layer of the stone had broken down. Unlike the copper bonded stones, the other stones tested (Fe for example) were able to form a solid precipitate ($Fe(OH_2)$) and did not deposit material onto the workpiece surface. Although inconsistent, the formation of an Elid separation layer between the copper-resin stone and workpiece was verified via monitoring of Elid voltage levels. Frequent redressing of the stone (Elid 2) was required to maintain the insulating layer without the surface of the workpiece abrading it away. The copper bond material did not form a precipitate or oxide layer on the stone's surface, with the electrical separation reported to be the result of oxidised workpiece material loading onto the stone's surface. The Elid separation layer could be easily rubbed off.

Problems with sparking between the stone and workpiece existed when Elid honing with both the iron and the copper resin stones. Postulated causes of the sparks were:

(1) Poor conditions and control of the small size inter-electrode gap with the breakdown of the insulating layer causing rapid electrical discharge.
(2) Grinding chips breaking through the insulating layer to form an electrical bridge.
(3) The heat generated by the passage of the electrical current causing the evolution of oxygen and hydrogen gas.

It was suggested that good fluid access and a pulsed wave provide time for the gasses to dissipate. The frequency of sparking was seen to diminish as the surface finish improved and the use of high-frequency pulsing, low current levels was used to minimise the detrimental effects. When the detrimental effects of sparking were minimised, consistent high quality surface finishes of 15 nm Ra were achieved with a 2 to 4 μm abrasive in a cycle time of 30 seconds. The process time was considered too long for this application but is not necessarily excessive with regard to this doctoral research.

Although no Elid honing was conducted, pre-process dressing and analysis of three #4000 diamond stones (Fe resin bond, Al resin bond, and Fe Al resin bond) was carried out. Typically characteristic power values were recorded when pre-process dressing was performed, whereby there was a rise in voltage and a fall in current as the stone was dressed. Subsequent analysis of the iron resin bond stone revealed a very rough and heavily oxidised surface that easily flaked off and was deemed too thick and weak. The ease and degree of oxidation was enhanced as a result of a fine iron powder being used in the stone's construction. The aluminium bonded stone oxidised rapidly, forming a thin film with an open and porous stone structure. The stone containing an equal proportion of iron and aluminium displayed an appearance combining the two constituents. It was suggested that the abrasive properties of the oxide layer, in addition to the abrasive grits, contribute to the processing mechanism. When using a combination of metal and resin bond stones the abrasive grits at the active surface of the stone are held within the non-conductive resin portion of the stone that remains after dressing.

Chapter 11 - Grinding Titanium

The use of titanium offers a weight saving advantage over steel; however the manufacture of titanium components presents numerous difficulties. Titanium exhibits poor machinability and is one of the most difficult materials to grind, due in large part to its thermal properties [5, 73].

Ti-6Al-4V is an alpha-beta titanium alloy used for general purpose applications which accounts for approximately 50% of the total titanium market. The allotropic transformation (hexagonal closed packed to body centred cubic) is affected by the alloying elements; aluminium raises this temperature and vanadium lowers it [50]. The beta transus temperature of Ti-6Al-4V is between 995 - 1010 ^{0}C [63] and various heat-treatments are available. Exposure to atmospheric oxygen at elevated temperatures can result in the formation of an alpha rich case at the material's surface. This can lead to an increase in hardness and reductions in fatigue strength, material toughness and UTS.

Properties	Value
Material & Treatment	Ti-6Al-4V (Annealed)
Tensile Strength, MPa	895
Yield Strength, MPa	825
Modulus of Elasticity, Tension, GPa	110
Hardness, Hv	340
Density, g/cm^3	4.43
Thermal Conductivity, W/mK	7.3

Element	Maximum	Reason for Inclusion
Aluminium	6.15	Alpha stabiliser
Vanadium	4.3	Beta stabiliser
Iron	0.16	Increases strength
Oxygen	0.18	Alpha stabiliser
Carbon	0.01	Alpha stabiliser
Nitrogen	<0.01	Alpha stabiliser
Hydrogen	0.003	Beta stabiliser
Titanium	Remainder	

Figure 79 - Mechanical Properties & Chemical composition of Titanium alloy IMI 318 (Ti-6Al-4V)

Titanium exhibits high strength at elevated grinding temperatures and strong work hardening characteristics [74]. This results in high grinding forces. The high toughness inhibits an effective cutting action with ploughing of the workpiece generating high specific grinding energies and friction, thus increased temperatures. It is highly reactive and has a chemical affinity with almost all abrasive materials, as well as bonding materials. Chemical affinities cause titanium chips to adhere to abrasive or bond material [5]. In a self perpetuating cycle, high material reactivity dulls abrasives, increases loading, friction, temperatures and thus increases reactivity.

Titanium has a thermal conductivity only one sixth that of steel and a lower volumetric specific heat. This prevents quick dispersion of heat and can result in localised heat damage of the workpiece. Titanium is half as stiff (modulus of elasticity) as steel which can produce problems of chatter, rubbing and poor dimensional stability [74].

The mechanical properties and high reactivity impose limitations on processing titanium. Grinding often results in wheel loading, grit plucking / fracture and excessive tool wear or failure. Additional problems include wheel workpiece welding, rubbing, galling, smearing and the deterioration of surface integrity [73]. The introduction of tensile stress, or the failure to create compressive stress, at a component's surface results in a reduction in fatigue life. Titanium is also susceptible to poor surface roughness, micro-cracking and surface burning [75]. Factors affecting surface finish when grinding titanium were explored by Turley [59].

As titanium can be quite adherent when machined, the ground surface is likely to exhibit more sideways flow caused by ploughing. Workpiece material adhered to the abrasive can be re-deposited onto the workpiece surface [59]. Due to the often larger loads or a recently dressed wheel, extensive abrasive fracture or removal can result in the creation of surface craters or embedded abrasives [14].

11.1 Parameters for Grinding Titanium

Minimization of the heat generated by the grinding process is essential to prevent degradation of surface integrity. Several authors recommend low wheel speeds that are 1/3 that of conventional operating speeds [5, 73], as this generates less heat. It is essential that ample grinding fluid reaches the grinding zone. Rapid oxidation of grinding chips presents a risk of ignition to oil-based grinding fluid, so water-based fluid is preferred. Inorganic salts of heavy alkali metals are the most effective [5]. The high pressure application of inorganic water-based fluid that contains high pressure additives is common. Cryogenic grinding was found to be a less effective lubricant and it is also difficult and uneconomic [5, 63]. Authors disagree over which abrasive types offer the best performance but several have tested silicon carbide [5, 63, 73, 76]. Very fine wheels are not suitable due to an inability for fluid to penetrate the grinding interface, increased abrasive wear, etc.

11.2 Elid Grinding of Titanium

An investigation into the grinding of titanium alloys was conducted by Wang [63] that looked into the use of Elid, along with other possible methods such as cryogenic grinding. A CIB cup wheel containing 76 μm diamond abrasives was tested against Ti-6Al-4V specimens using the Elid 1 method. The best surface finish value achieved through Elid grinding was 180 nm Ra, achieved at a depth of cut of 10 μm. However this was worse than results achieved with a non-Elid resin bonded wheel. Elid grinding displayed an ability to maintain levels of surface finish at the larger depths of cut of 25 μm. This was thought to be because the use of Elid prevents wheel loading and clogging, with evidence of an effective cutting mechanism and good grit protrusion. However, analysis of the wheels revealed that the weak holding strength of the oxide layer was unable to prevent removal of the abrasives.

Grinding with cup wheels was found to improve finish compared to peripheral surface grinding [63]. Diamond outperformed Al_2O_3 abrasive and resulted in an improved component fatigue life. Water-based fluids produced a better surface finish than liquid nitrogen coolant. A slow table speed and a fast wheel speed achieved an improved response when non-Elid grinding, as it reduced chip size and loading on the wheel.

Using a Cerium oxide #20,000 iron bonded grinding wheel in an Elid 1 lap polishing set-up, Ti-6Al-4V was polished to an Ra surface finish below 10nm [61]. Although there was no noticeable difference in the average Ra values (figure 80) when compared to loose alumina abrasive polishing, higher Ry values (maximum height of the profile) and deep grinding marks were observed when using the Elid process. Elid did however endow the titanium workpiece with an improved corrosion resistance in the passive state (figure 81).

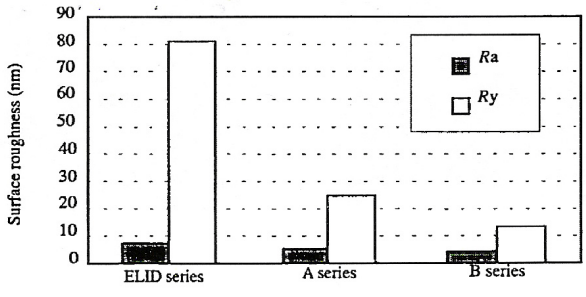

Figure 80 - Surface finish results [61]

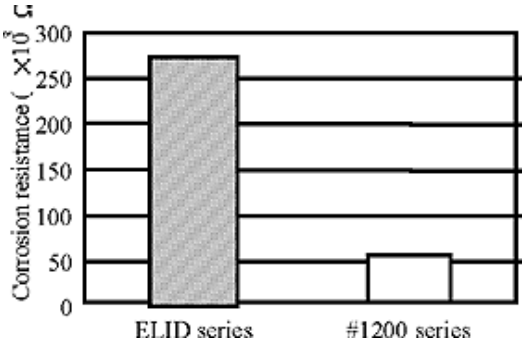

Figure 81 - Workpiece corrosion resistance [64]

The Elid process can improve the corrosion resistance of the workpiece [61, 64] by aiding the diffusion of oxygen into the workpiece surface, thus forming a thick and potentially stable oxide layer. In potentio-dynamic polarization measurements, the diffused oxygen accelerates the rate that at which the oxide layer is reformed and inhibits dissolution of metal ions. Direct contact between the workpiece and the wheel (anode) results in a positive potential at the specimen. This causes hydroxide ions (OH^-) evolved at the cathode / electrode and transported in the fluid, to oxidise the workpiece surface.

An increase in nano-hardness of a titanium workpiece was achieved when processing using the Elid method through the diffusion of carbon into its surface [64]. Measuring an indentation depth approximately equal to the diffused layer (~100 nm), the Elid ground specimen achieved a nano-hardness of 535 Hv compared to 450 Hv when polishing with SiC. The carbon is thought to diffuse from the diamond abrasive during Elid processing. Although increased hardness is potentially beneficial to titanium spherical bearings, there are better ways in which this can be achieved, such as the use of coatings or heat-treatment.

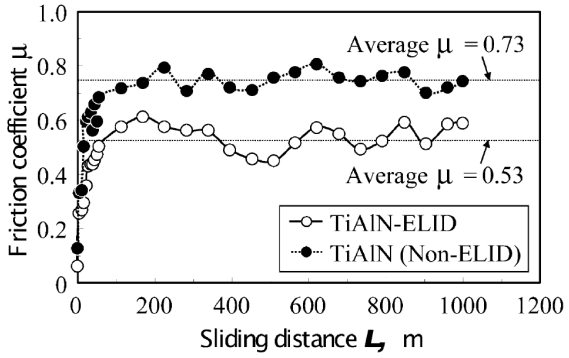

Figure 82 - Relationship between friction coefficient and sliding distance [77]

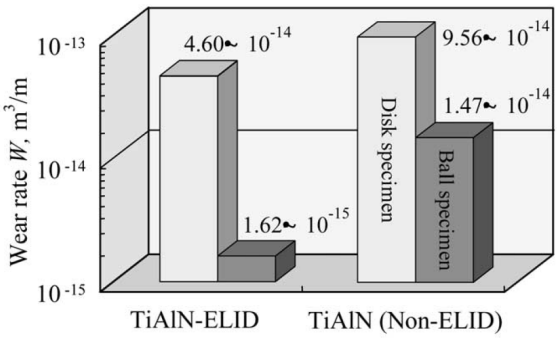

Figure 83 - Wear rate of disk and ball specimens [77]

Excellent levels of surface finish, typically 2.4 nm Ra, were achieved by Katahira et al. [77] when Elid grinding a TiAlN film with a #30,000 CIB-D wheel. Through Elid grinding substantially improved tribological characteristics were observed, in part due to the improvement in surface finish and in part due to the creation of a workpiece oxide layer on top of the TiAlN film. Ball-on-disk wear tests of the surfaces produced showed that, as a result of Elid grinding, the friction coefficient was reduced by one third and there was a substantial reduction in wear (figures 82 & 83).

Chapter 12 - Methods of In-Process Monitoring

In the move towards increased efficiency, reliability and precision, process monitoring becomes an essential requirement in controlling the exacting conditions of the grinding process. In-process monitoring enables the earliest detection of faults and poor grinding conditions, which would inevitably lead to increased scrap or a poorer end product. A number of in-process methods have been developed to assess the performance of grinding processes. Assessment of grinding mechanisms and conditions can be achieved by monitoring acoustic emission [78, 79, 80], eddy current [53], grinding forces [23, 81], temperature [82], Elid power and control, and machine power usage. There are also direct in-process measurements, such as form, surface finish [83, 84, 85, 86] and wheel wear [32, 87]. However the fine nature of this type of superfinishing, as well as the slow removal rates, preclude many types of monitoring. Both spindle and Elid power monitoring are used for this research and are discussed in more detail below.

12.1 Monitoring and Control of Elid Power Supply Values

Monitoring Elid power supply activity provides information on how well the wheel is dressed. The Elid power supply's ammeter displays the average output current. The Elid power supply's voltmeter displays the output voltage when set to 'out' and the source power voltage when set to 'in'. These values can be read directly from the display or data logged via a computer connection.

As has been shown in earlier chapters, the Elid power values are related to the growth and removal of oxide on the wheel's surface. In addition to monitoring Elid power levels, several systems have been developed that incorporate feedback control including:

(1) Optimum in-process electrolytic dressing [29, 35, 55, 88].
(2) EcoDress / Electro-chemical in-process Controlled Dressing (ECD) [24, 89, 90].
(3) A system developed by Boland [91]

They are essentially the same thing; employing computer controlled changes to the Elid power supply values. When using Elid there is a natural stabilizing mechanism; the removal of the insulating oxide layer from the grinding surface of the wheel stimulates the oxidation of newly revealed metallic bonding material. The feedback control methods magnify these effects resulting in a thicker oxide formation on the wheel's

surface whilst maintaining low Elid power values. This produces better stability of the insulating layer and worn grit ejection, resulting in reported improvements in efficiency, quality and reliability. Eco-dress provides a reported increase in grit protrusion compared to Elid.

12.2 Monitoring of Spindle Power

In-process monitoring of motor load during grinding provides invaluable information about grinding forces, friction and specific energy. It can be used to determine how well the wheel is dressed, predict the component's surface finish, determine removal rate and evaluate the process mechanisms. An example of using an in-process method to evaluate the grinding mechanism is given by Bifano and Fawcett [92]. Assessment of specific grinding energy is used to determine the ductile-brittle material removal transition when grinding brittle materials.

Grinding spindle power was monitored using a Hall Effect sensor by Shih et al [37] to investigate wheel truing, wear mechanisms and grinding forces. Using two types of diamond truing tools, rod and particle, an analysis of a large number of truing passes was conducted. The calculated drift adjusted power change was converted into its tangential force component by dividing it by surface speed. When comparing grinding forces after truing, higher values were recorded after using a rod diamond tool than a particle diamond tool. It was proposed that this was a result of the wheel having a higher overlap ratio when rod diamond trued. Power monitoring was able to identify abrasive wear and fracture during operation.

A continuation of work by Shih [38] on rotary truing of CBN, SiC and diamond wheels investigated the effects of feed, speed ratio and overlap ratio. Again power values were converted to the tangential force and specific energy during truing and grinding. A trend of increasing grinding force at higher specific truing energy and better surface finish at higher grinding force was recorded.

In-process measurements of power monitoring, workpiece size reduction and stone wear were recorded by Puthanangady and Malkin [17], during experimental investigation of an external cylindrical superfinishing process. The forces and specific energy were able to be separated into chip-formation, ploughing and sliding components. A linear relationship was found between spindle power and applied contact pressure for the three 500 grit abrasive vitrified bond alumina stones.

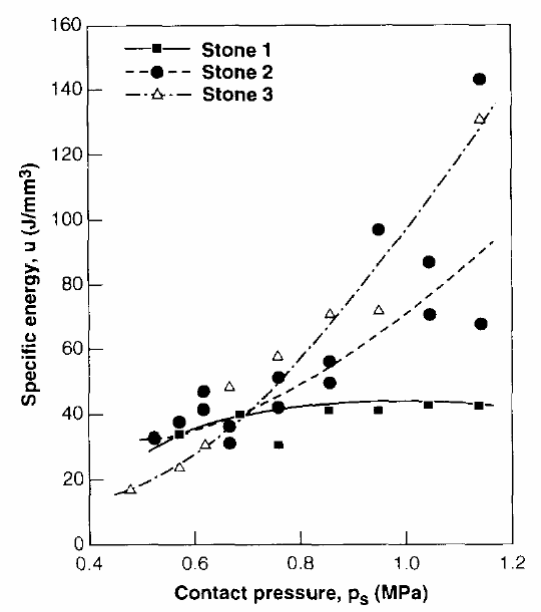

Figure 84 - Specific energy vs. contact pressure during superfinishing [17]

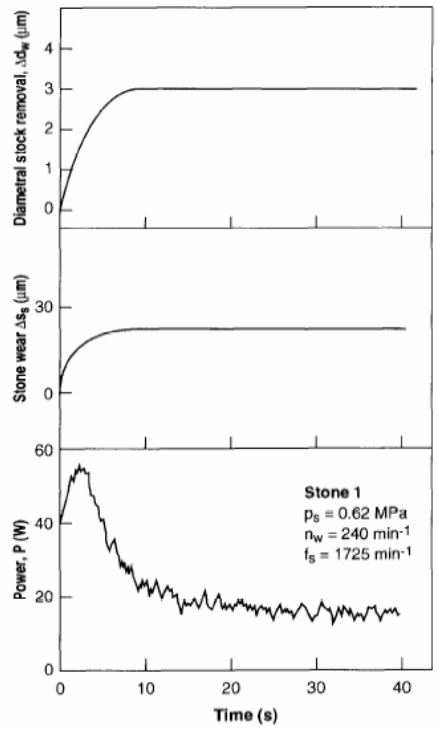

Figure 85 - Diametral stock removal, radial stone wear and power vs. time during superfinishing [17]

Two of the stones recorded increased removal rates at lower pressures 0.5 MPa but the third achieved maximum removal at contact pressures over 0.75 MPa. This information produced a plot of specific energy shown in figure 84. As is the norm for a superfinishing process, increased stone wear or self-sharpening leads to an increased material removal rate. When investigating the time-dependent behaviour of superfinishing stone No.1, a lower pressure produced a progressive decrease in power, stone wear and workpiece material removal (figure 85).

EXPERIMENTAL

Chapter 13

Testing was conducted at both NMB in Lincoln and at Cranfield University. Initial Elid 3 superfinishing tests were predominantly conducted at NMB and on two sizes of AMS5630 steel balls, titanium Ti6Al4V balls and briefly on Apticote 100T chrome-coated titanium balls. At Cranfield the use of a CNC precision machine tool [93] enabled experiments to be conducted with more accuracy and control. The system developed allowed the investigation of Elid 1, 2 and 3 configurations, EDT, ball and flat specimens, and Elid in combination with electrolytically-assisted superfinishing.

13.1 Basic Elid Superfinishing System

A basic Elid superfinishing system consists of a machine tool, DC pulse electrical power source, electrolyte fluid and an MRB superfinishing wheel. The conductive wheel is connected to the positive terminal of the Elid power supply, making it the anode. Depending on the type of Elid used, either the workpiece fixturing or the workpiece itself is made the cathode (-). Elid 3 superfinishing does not use a separate electrode; in-process dressing is achieved at the grinding interface and implemented at full contact during superfinishing. When Elid 1 is used, the component being processed is insulated from the electrical circuit with dressing occurring between the wheel and a separate electrode.

The superfinishing carried out in this research was a constant force process involving a spherical area contact between ball and wheel. The wheel spindle applied load via a spring; load being determined as a result of calibrated spring stiffness and compression through z-axis linear movement. A 1:50 dilution ratio of Noritake CEM to tap water was used as the superfinishing fluid and was applied in a flood application to the ball's spherical surface at the grinding interface. Although alternative wheels were investigated, the majority of research involved the use of MRB-CBN superfinishing wheels.

13.2 Experimental System at NMB

The Elid 3 machine system at NMB is shown in figures 86 to 89. Electrical contact with the ball is made via a carbon rod rubbing on the steel ball fixture, which locates on the ball face. Different Tuffnel holders are used for different size balls and provide electrical insulation to the rest of the machine. The wheel spindle is not isolated and the machine itself is made the positive earth. At NMB the pattern of honing marks is used to determine if it is aligned correctly. A proximity sensor controls the position of the wheel spindle and the applied load.

Figure 86 - Elid superfinishing machine at NMB

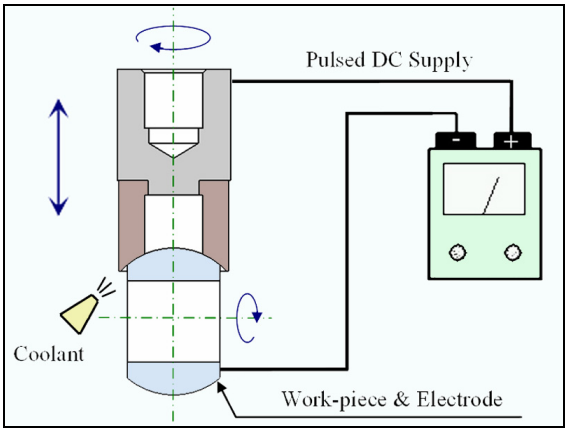

Figure 87 - Elid 3 arrangement for spherical superfinishing

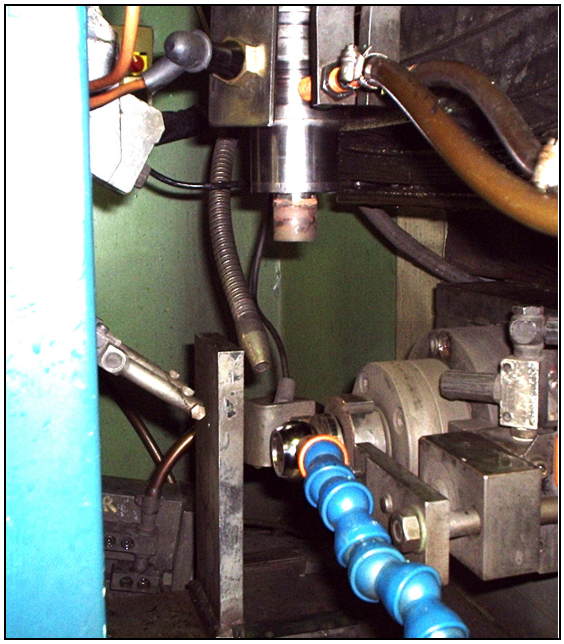

Figure 88 - Elid superfinishing machine at NMB

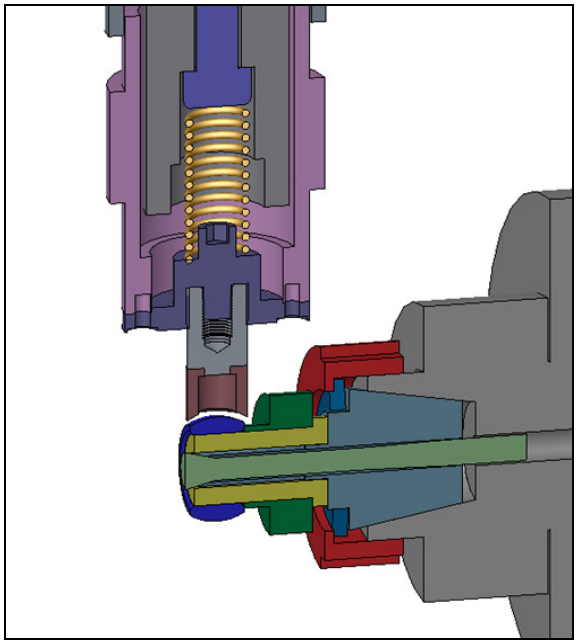

Figure 89 - Sectioned model of Elid 3 superfinishing machine / setup at NMB

13.3 Experimental System & Design of Fixturing at Cranfield

To enable spherical balls to be ground at Cranfield using a CNC precision controlled machine tool [93], a ball and wheel fixturing had to be designed. The system took considerable time to set up but was essential to allow experimentation to be conducted with high levels of accuracy and control. The fixturing, designed by the researcher using CAD and manufactured in Cranfield's workshops, replicates the operation of the machine tool used at NMB. The machine system used at Cranfield is shown in figures 90 to 93, and the fixturing drawings along with additional pictures are shown in appendices B & C.

Figure 90 - Precision Machine Tool at Cranfield (TetraForm C)

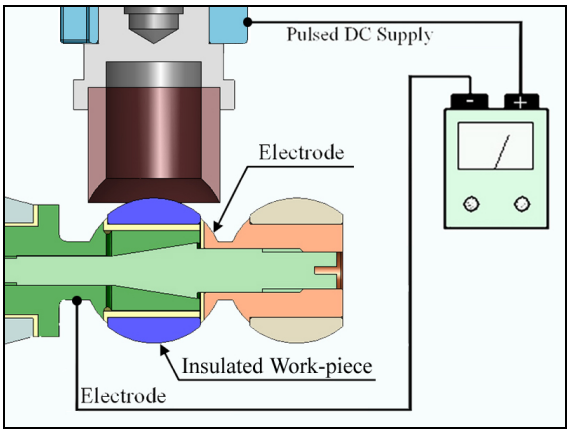

Figure 91 - Elid 1 arrangement for spherical superfinishing

Electrical contact of the ball and wheel spindles was made through a brush copper contact running on the steel fixturing. Both the superfinishing wheel and ball were electrically insulated from the rest of the machine. As the spring was compressed after making initial grinding contact, the wheel and inner wheel fixturing receded into the outer wheel fixturing along a needle roller bearing, lubricated with a silicone based lubricant. The use of a needle roller bearing provided a number of line contacts that ensure smooth movement whilst maintaining stiffness in the x and y directions. An expanding collet that located and fixed the ball via its face and bore was designed to work in conjunction with Tetraform's removable truing spindle. The limited working space available on Tetraform, in particular the height, placed restrictions on the design. However, this was successfully overcome allowing for a 10 mm spring compression to be achieved on both new and fully worn superfinishing wheels.

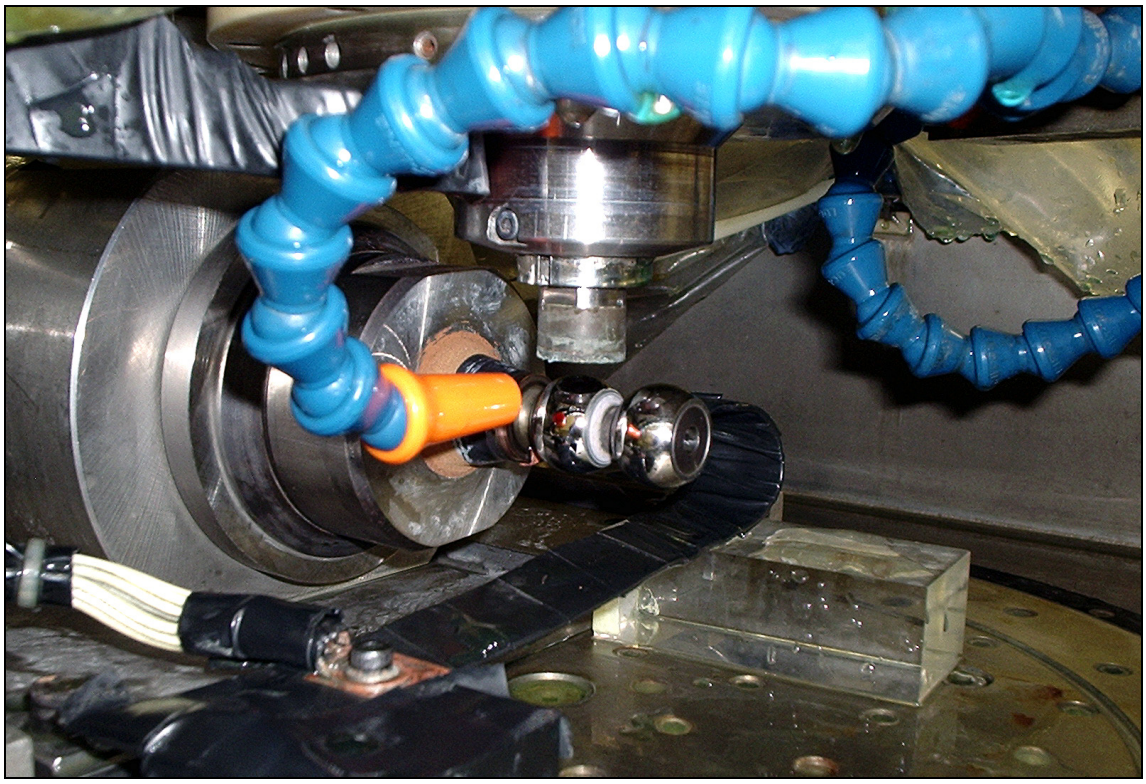

Figure 92 - Photograph of Elid 1 superfinishing set-up / fixturing at Cranfield

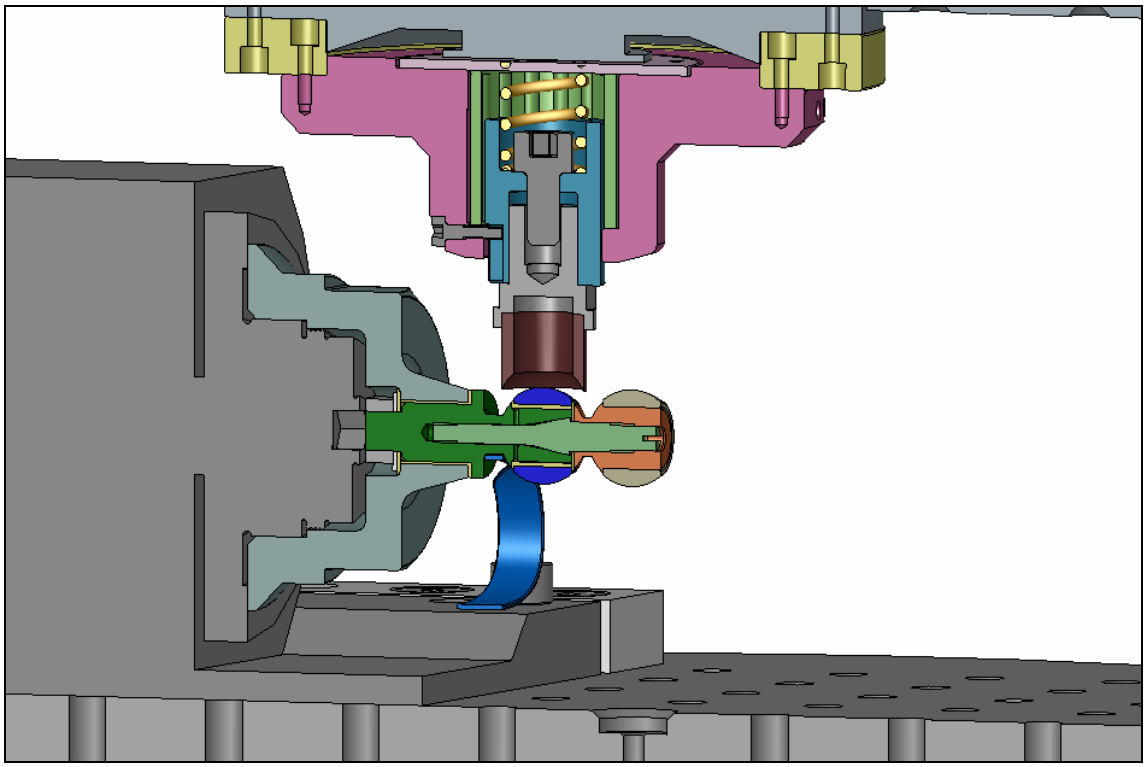

Figure 93 - Sectioned model of Elid 1 superfinishing set-up / fixturing at Cranfield

Elid power values were logged via a connection to a computer data acquisition system (Labview). Wheel spindle motor load was also monitored by making use of the Quantum Hall Effect [94]. The Universal Power Cell module [95] is able to determine spindle power by performing an instantaneous vector multiplication of voltage and current. Power is monitored as opposed to current, as this provides equal sensitivity at both high and low loads.

Elid 2 (interval dressing) can be conducted prior to a processing run on a separate, adjacent ball. Exchanging the insulating nylon washer for one made of steel connects the ball being processed onto the electrical circuit, thus changing the process into Elid 3. Operation in an Elid 3 configuration is effectively the same as that described for the NMB machine.

The electrolytic dressing action of Elid should be concentrated at the spherical grinding surface of the superfinishing wheel. As the surface of a metal bonded wheel oxidises through the Elid process, it forms an insulating layer. This can result in it no longer being the most energy efficient site to be oxidized. As the wheel fixturing, or at NMB the entire machine tool, is also an anode, stray currents can erode material from these sites as well. To minimize the effect of stray currents and concentrate the electrolytic corrosion at the wheel's grinding surface, as much of the machine and fixturing at Cranfield were isolated / insulated as possible.

13.3.1 Ball Geometric Criteria for Elid 1 Superfinishing

The geometric criteria described in figure 94 must be met to enable the use of a separate electrode, thereby creating an Elid 1 system. The wheel's internal diameter (A) must be larger than the width of the ball (B) to allow the entire grinding surface of the wheel to be accessed when Elid is used. If the wheel's I/D overlaps onto the ball then dressing of that part of the wheel will be severely hampered. The overlapped area will ultimately become glazed and become the only part of the wheel that is in direct contact with the ball. Setting (A) to between 0.3 to 2.0 mm larger than the width of the ball provides sufficient clearance and also allows for electrical insulation.

A = Wheel I/D

B = Ball Width

C = Wheel Wall Thickness

D = Collet Shaft Thickness

E = Ball O/D

F = Electrode Diameter

$$D = \left(\sqrt{\left(\frac{E}{2}\right)^2 - \left(\frac{A}{2} + C\right)^2} \right) - 0.2$$

$$A \geq B + 0.3\,mm$$

$$A \leq B + 2.0\,mm$$

$$C \geq 2.5\,mm$$

$$D \geq 3\,mm$$

$$F = E - 0.5\,mm$$

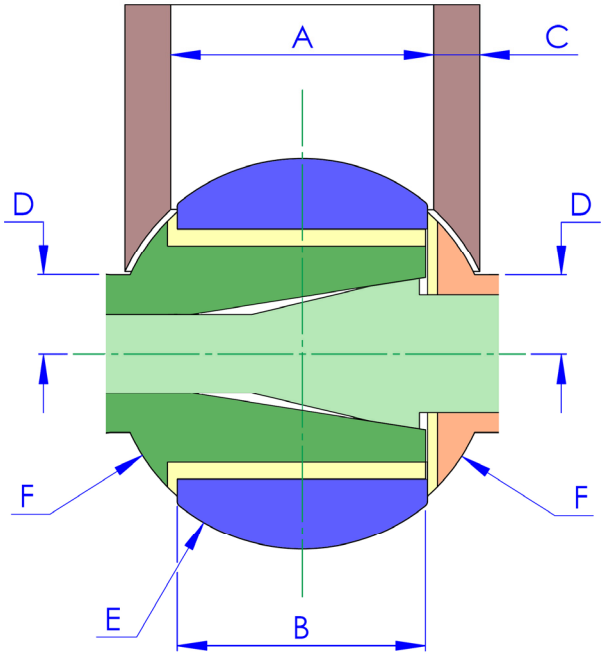

Figure 94 - Ball Geometric Criteria for Elid 1 Superfinishing

The wall thickness of the wheel (C) must be greater than 2.5 mm in order for it to retain a minimum integral strength. If space constraints allow, (C) should be set considerably larger as appropriate to the ball / wheel size, whilst ensuring that excessive wrap around does not occur. A balance between wheel wall thickness (C) and collet shaft thickness (D) is required. For the ball fixturing to possess the required stiffness and strength, (D) must be larger than 3 mm if the ball is to be secured using the standard locking pin method. An electrode gap of 0.25 $\pm$ 0.05 mm is required for Elid 1 superfinishing (E & F). This was produced by Elid superfinishing 0.5 mm from the diameter of the first ball tested, thus shaping the collet.

Elid 1 can be used on over half the NMB standard catalogue range of balls, although small ball sizes and high angle balls are precluded. Ball sizes larger than RWD08, RND08, MND12 and MWD12 are able to be Elid 1 superfinished using this fixturing method.

13.4 Generalized Description of Standard Operating Procedure

The standard operating procedure consists of the following:

(1) Install the fixturing, checking electrical insulation and contacts
(2) Balance the wheel fixturing, including measurements of spindle concentricity
(3) Ensure correct ball to wheel alignment and conformity
(4) Electro discharge true the wheel
(5) Pre-process dress the wheel
(6) Bed in of wheel to ball / test run / dummy runs

After insulation of the fixturing and its correct operation has been confirmed, accurate ball to wheel alignment must be ensured and complete conformity achieved. The importance of correct alignment and conformity is demonstrated in chapter 17. Prior to truing, correct alignment must also be achieved.

As new wheels do not come pre-formed, truing is required to form a spherical grinding surface that corresponds to the ball being superfinished. Truing should continue until complete ball to wheel conformity exists and the slight positional and rotational variations of a particular set-up are accounted for. Although a reasonably large degree of damage to the wheel's grinding surface can be tolerated, truing should be performed if it is excessively chipped, particularly if the chipped edges progress to a width that overlaps onto the ball width (Elid 3 only). Truing is required when using a previously used wheel on a new set-up and is beneficial if it has been simply removed and re-installed. When electro-discharge truing, normal spindles speeds can be used; the grinding zone should be flooded with coolant and truing aggressiveness reduced towards the end of the truing cycle.

Pre-process dressing of the wheel is required to remove damage caused as a result of truing, to achieve a suitable grinding surface, and to prevent metal to metal contact when Elid 3 superfinishing. This research used a gap of 0.2 mm and normal superfinishing speeds were used as slower speeds offered no advantage. Only a short initial pre-process dress of the wheel should be conducted (~2 minutes) as it is preferable for the Elid layer to generate under normal superfinishing conditions. Chapter 15 investigates truing and pre-process dressing behaviour and performance.

Bedding-in the wheel with the Elid on, further improves ball to wheel conformity and helps develop the required wheel condition at its grinding surface. Initially only a minimal load should be applied, gradually increasing to the full superfinishing load over approximately 5 minutes. Performing a test run confirms correct ball to wheel conformity and dressing performance. If the test run appears satisfactory, based on the criteria (a to e), then experimentation / production runs can begin. Experiments that were particularly sensitive to processing variability also incorporated a number of dummy runs, in order to provide a more static wheel condition and consistent performance for testing.

(a) A good surface quality that is consistent and defect free over the entirety of the ball's spherical surface
(b) The ball's p-v spherical roundness is below 2.5 μm
(c) A satisfactory removal rate is achieved
(d) The Elid system is actively working during superfinishing
(e) The wheel spindle power readings appear normal

Alterations to the ball to wheel alignment, conformity, or condition of the wheel's grinding surface will correct the majority of problems.

13.5 Experimental Parameters

As a typical example, the fixed processing information relevant during various tests is shown below.

Cranfield machine tool, Elid power supply	Tetraform C, Fuji-Die - ED-921
Work-piece P/N, Material, Dimensions	RNB08, AMS5630, O/D 19.836 mm, Faces 12.67 mm
Superfinishing wheel type, Dimensions	#12000, MRB-CBN, O/D 14.65, I/D 8.00 mm (Elid 3)
Wheel truing, Dressing methods	EDT, No-dressing, Elid 1, 2, 3, Abrasive stick
Elid Power Settings (Voltage, Current, Duty)	60V, 20A, 10% or 90V, 40A, 50% or 90V, 40A, 70%
Elid 2 dressing gap	0.2 mm
Ball spindle speed (crown) across static wheel	1.0 m/s @ 963 rpm
Wheel spindle speed (O/D) across static ball	4.0 m/s @ 5125 rpm
Combined speed (wheel I/D, ball far side)	1.41 m/s @ 5125, 963 rpm
Combined speed (wheel O/D, ball near side)	4.77 m/s @ 5125, 963 rpm
Run time	5 minutes
Spring compression, Applied force	2.75 mm, 67.6 N
Spherical area in contact, Applied pressure	112.62 mm^2, 0.6 MPa
Fluid type, Nozzle size, Position, Fluid flow	CEM, 1 x ¼" nozzle, Interface centre , ~0.1 litres / sec

Figure 95 - Typical / standard RNB08 experimental parameters. [Used for material removal stability tests]

In order to minimize the influence of ball size on processing performance, it is most appropriate to consider the contact pressure between the wheel's grinding surface and the ball. Contact pressures of 0.5, 1.0, and 1.5 MPa were achieved when applying the forces of 45N, 90N, 135N respectively. For RNB08 balls, an rpm of 963 converts to 1 m/s. A wheel speed of 5215 rpm and a load of 67.6N were used to maintain consistency for comparisons across tests. Due to the configuration employed relative superfinishing spindle speeds vary at differing points

This research investigated a range of different Elid (Fujidie) and very fine abrasive non-Elid (Darmann [96]) wheel types. In addition to seven metal-resin bond (MRB) wheels containing CBN abrasives from 30 μm to 0.14 μm in size, are MRB wheels containing 2 μm Alumina and Cerium oxide. A cast iron bond wheel containing 8 μm diamond, as well as non-Elid 10 μm Silicon carbide + alumina and 5 μm alumina wheels are also tested. It should be pointed out that although an abrasive size of 30 μm is considered large within the context of this research, it is classified as being fine when considering it for normal grinding or even superfinishing processes.

Experimentation employed both factorial designs [97, 98, 99] and individual comparative experiments, in order to best evaluate this process. The formalized design of a factorial experiment evaluates the various factors in a much more rigorous way in terms of finding statistically significant effects and relationships. Parameters under investigation include; wheel type, abrasive size, Elid type and aggressiveness, spindle speeds, applied load, system stiffness, processing time, fluid type and application, ball material and size. Optimization considers process parameters and system design, as well as the overall implications to the complete process chain.

13.6 Assessment of Superfinishing Performance

A range of techniques are used both in-process and post-process to evaluate performance. Various measurements of form and finish were taken using both profilometry and interferometry. Process efficiency was measured in terms of ball weight reduction / material removal, rate of ball roundness and surface finish generation.

13.6.1 Surface Roughness Characterisation

The majority of surface finish results were measured across the ball (figure 96), as this best represents the variation of finish quality over the entire surface. When measurements were taken around the centre of balls of consistent quality, they produced values typically one to two nanometres rougher than those measured across the ball. Measurements taken around the ball are perpendicular to the honing / superfinishing marks and are therefore expected to be slightly higher. However, inconsistencies in the profile across the ball, that are not represented when measuring around the ball, result in the breakdown of the trend.

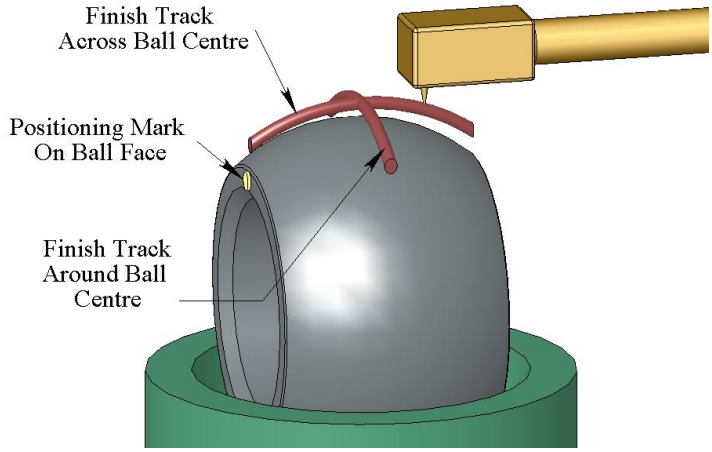

Figure 96 - Surface Finish Measurement

Using a 'Taylor Hobson Form Talysurf 120L' at Cranfield, surface finish measurements were taken over the entirety of the ball surface (from one face to the other). On the 'Mitutoyo CS-3000 talysurf' at NMB and in accordance with the standardised ISO measurement procedure, a smaller measurement length was evaluated (0.4 mm). Both methods used a Gaussian filler and cut-off of Lc=0.08 (upper) and Ls=0.0025 (lower). Typically measurements at Cranfield produced slightly larger roughness values and a more accurate general representation of surface quality. Surface finish parameters investigated include Ra, Rq, Rst, Rku, Rp, Rv, Rz, Rt, and Rdq [3, 100].

A ‘Wyko Topo 3D phase shift interferometer tp307026’ was also used to assess surface finish alongside talysurf measurements. This normally involved taking a number of measurements on random areas of a ball. In addition, ball surfaces were also briefly assessed using a ‘Wyko RST interferometer’, ‘Fisba µphase ophthalmic compact interferometer’, and ‘Taylor Hobson CCI 6000 interferometer’.

13.6.2 Ball Form Measurements

Measurement of ball O/D taken using a micrometer was the primary method of determining ball size. This provides a more accurate assessment than those produced by talysurf or interferometers where a diameter is fitted to the partial surface measured. Using a talysurf produced a greater degree of variation in the results, as errors in ball form can amplify O/D errors. A comparator gauge provides the most accurate method of assessing the variation within a batch, however its accuracy in determining ball size is dependent on careful set up.

Ball spherical roundness was measured using a ‘Mitutoyo Roundtest RA-114’ at NMB and a ‘Taylor Hobson TalyCenta’ at Cranfield. In all experiments the roundness ‘up & down’ the ball (figure 97) is significantly worse than roundness ‘around’ the centre of the ball.

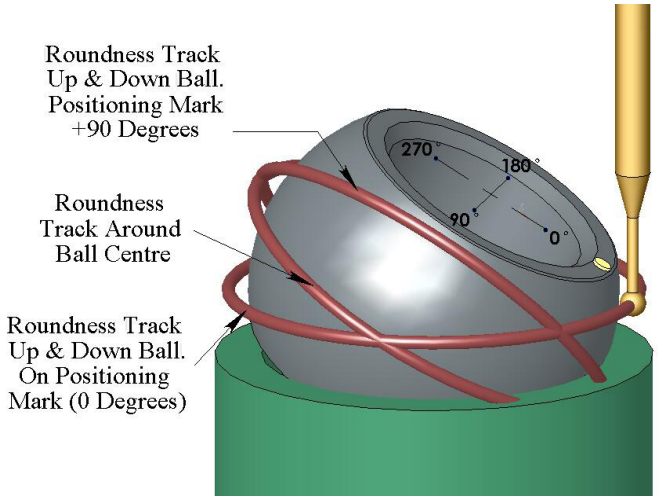

Figure 97 - Ball Roundness Measurement

Ball waviness measurements are available when finish measurements are taken using the Taylor Hobson talysurf. Although they are considered to be less accurate than the roundness measurements, they provide additional information.

13.6.3 Ball Spherical Generation Rate

Both measurements of form and surface finish were used to assess the rate at which a ball's surface was improved by the Elid superfinishing process. Accurate assessment of ball generation requires processing conditions to remain stable over extended stop-start periods. In addition, part formed ball surfaces that are in transition are often irregular over their measured profile, making them subject to the point of measurement. Evaluating efficiency and the required processing time by this method was a lot more time-consuming than measuring ball material removal. As there is a reliable relationship between the removal of ball material and the generation of a ball's form and finish, it was material removal that was the primary indicator of improvements made to processing efficiency. Nevertheless, as it is ball form and finish that is ultimately of interest, a set of generation plots is provided whilst Elid 1, 2 and 3 superfinishing.

13.6.4 Material Removal Rate

Measuring the weight reduction of the components before and after the processing run provides an easy and accurate method of determining material removal that is independent of geometry. Weight reduction can be related to volume of material removed (7.75mg/mm^3), or O/D reduction (3 mg per micron off RNB08 O/D). Long process times can be used to increase accuracy; however this is dependent upon run conditions being static throughout. Nevertheless, this is the most appropriate method of easily assessing process efficiency. Process efficiency and conditions of stable material removal for particular testing conditions / superfinishing cycles are confirmed by monitoring for a constant rate of ball material removal over an extended period.

Density of AMS5630 = 0.00775 grams per cubic millimetre
Volume of RNB08 ball at mid drawing limits = 1777.91699 cubic millimetres
Mass = 13.77886 grams

Reduce the ball O/D by 1 µm.
Volume = 1777.52222 cubic millimetres
Mass = 13.77580 grams

Change in mass = 3.06 mg or [3 mg reduction per 1 µm removed from the ball O/D]

13.6.5 Wheel Wear

Wheel wear was determined through the assessment of changing touch point position between ball and wheel. An accurate electronic contact probe (Marprobe) position at R2 in figure 104 (section 13.7) was used in combination with the machine tool's z-axis position.

> Wheel length reduction = (Touch point at start – Touch point at end) – reduction in ball radius.

13.6.6 Microscopy

The visual quality of balls produced in this research is very closely linked to surface finish. A low magnification binocular microscope, situated next to the machine tool, was used to provide a rapid assessment of surface quality without the time consuming process of measuring ball finish. This approach was particularly useful when experimenting to improve processing efficiency and is an effective method for identifying small ball defects. The surfaces of the balls and wheels were assessed using optical and scanning electron microscopes.

13.6.7 Precision, and Degree of Accuracy

As is to be expected, a lesser degree of variation was observed, in surface finish (figure 98), when measurements are simply repeated, compared to when the ball is removed and then re-measured at different points (figure 99). The same holds true for roundness measurements (figure 100). A larger variation in results is observed when removing and re-measuring balls that are less round (heat-treated and cylindrically ground balls) compared to balls with a high degree of roundness (honed, polished, and Elid ground balls).

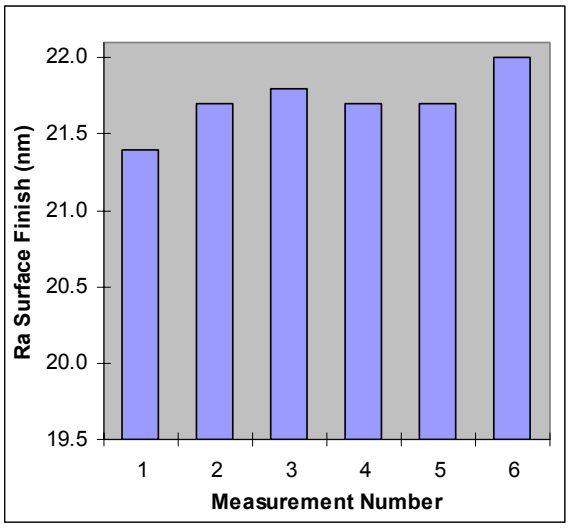

Figure 98 - RBFB16AB repeated ball finish measurement over the same track (Taylor Hobson talysurf, across ball)

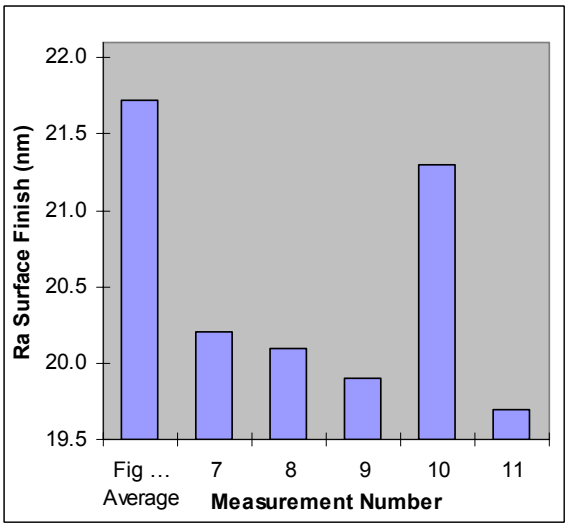

Figure 99 - RBFB16AB ball finish measurement over six different tracks on the same ball (Taylor Hobson talysurf, across ball)

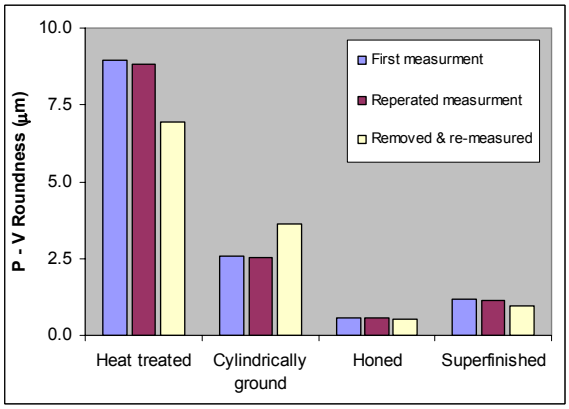

Figure 100 - Measurement repeatability of Taylor Hobson TalyCenta.

Figure 101 - Effect of interrupting the superfinishing run

Interrupting the superfinishing processing, in order to take measurements, was found to slightly increase material removal / rate of surface generation, however the effect was marginal (figure 101).

Due to the small quantity of material removed from the ball, particularly when conducting Elid 3 superfinishing tests, an accurate assessment of ball material removal is essential. Measurements of a control ball that was not processed along with the ball that was superfinished, were taken to ensure measurements remained accurate. This data (figure 102) demonstrates the accuracy of the scales. The use of long running times, averaging of repeated measurements, and averaging of sets of tests, further improved assessment of material removal accuracy.

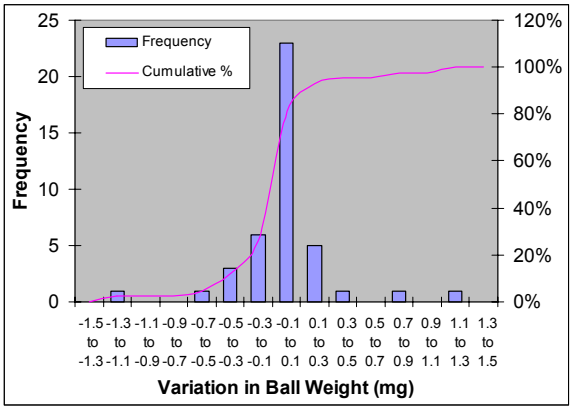

Figure 102 - Frequency graph of repeated measurement of control ball.

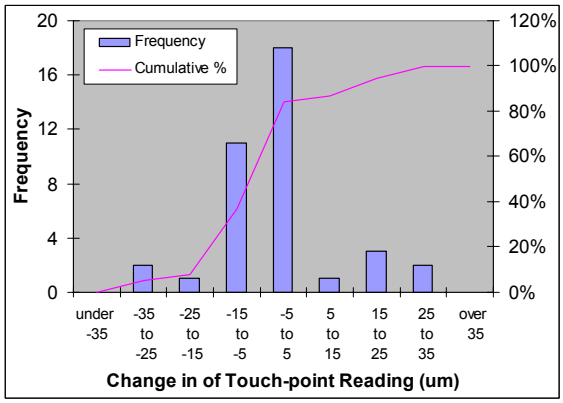

Figure 103 - Frequency graph of showing the accuracy of measuring the ball and wheel touch-point position.

Likewise the accuracy of wheel wear measurements is dependent on the running time and number of touch-point measurements taken. The accuracy with which touch can be assessed is demonstrated by repeating touch-point measurements where no wheel wear occurred (figure 103).

13.7 Cranfield Machine Calibration

Various measurements were taken to evaluate the performance of the fixturing and provide information that relates to geometric considerations of spherical superfinishing (figure 104).

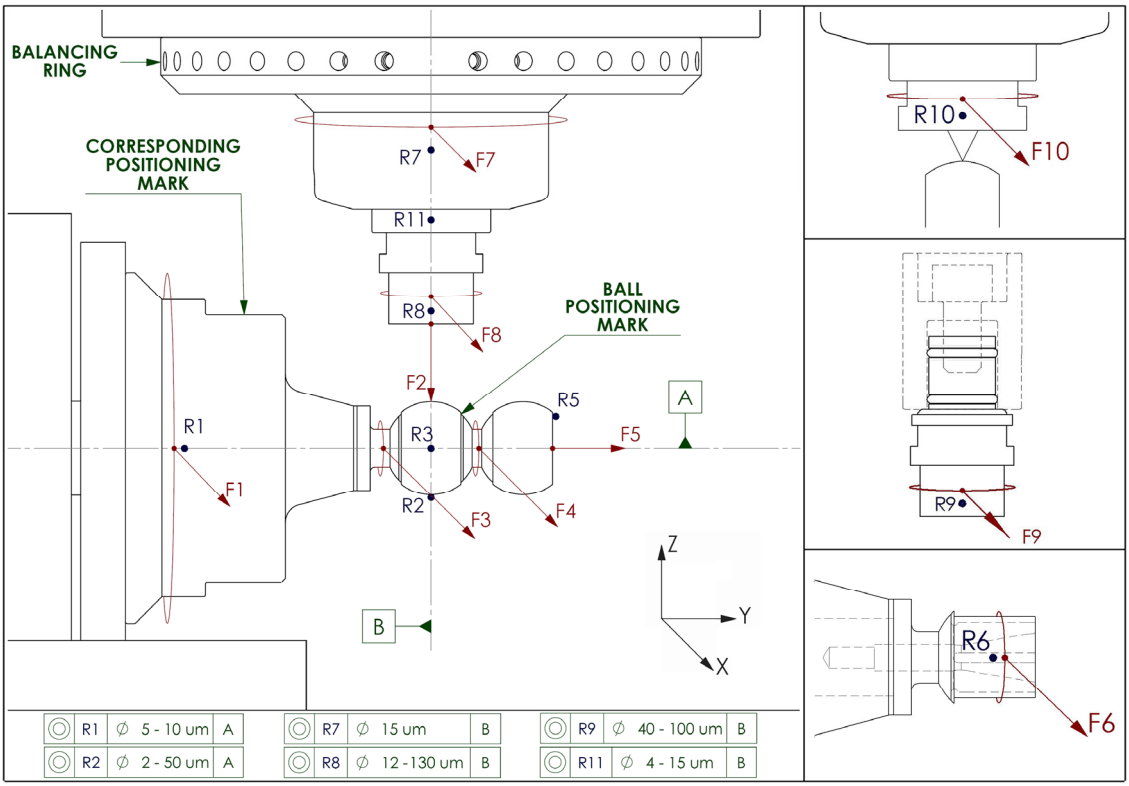

Figure 104 - Locations of stiffness measurements taken on ball and wheel spindles and fixturing

13.7.1 Spindle Balancing

Wheel spindle vibration was measured using VibroPort equipment each time the wheel fixturing was installed. After balancing, by adding counter-weighting screws to the balancing ring, the results revealed a reduction in error (appendix D4). An acceptable level of error was achieved; 25 to 60 nm after balancing over the available machine speed range and 25 nm at the common operating speed of 5215 rpm. The results demonstrate that the addition of the relatively large weight of the wheel fixturing did not adversely affect Tetraform's performance. Subsequent re-installations produced equivalent values.

13.7.2 Concentricity & Ball Installation

The Marprobe contact sensor was used to measure spindle and fixturing concentricity. The concentricity of the wheel fixturing is good, when measured at point (R7) and the linear bearing of the wheel fixturing does not introduce substantial error (4 to 15 μm at point R11). Measurements on the wheel O/D (R8 & R9) varied considerably between different wheels and critically when re-installing the same wheel. Concentricity error was generally larger when mounting the wheel against rubber o-rings (R9). The actual concentricity error at the spherical grinding surface of the wheel is likely to be very small after truing and bedding. This results in a situation where superfinishing is performed with full but skewed conformity between ball and wheel. The poor repeatability with which wheels can be removed and re-installed (130 μm max) means that the wheel must be trued each time a wheel is re-installed.

Measurements taken at point (R1), ranged from 5 to 10 μm. On the spherical surface of the ball (R2), the concentricity error increases due to variation in ball manufacture and the use of plastic insulating sleeves on the ball fixturing. Superfinishing runs were conducted when ball and fixturing concentricity errors were cancelled / minimized and only when total concentricity error was below 50 μm. Conducting a run with a concentricity error larger than 50 μm is likely to cause the wheel to fracture. Once the minimum concentricity error had been found, the ball was marked on its face to allow it to be removed and re-installed with the minimum influence on result accuracy.

A laser [87] was used to measure the positional repeatability of balls being loaded onto the collet. This involved recording the machine's x-axis position when the beam was broken by the ball. Very consistent results were recorded; the ball's position only varied within a range of 3.5 μm.

13.7.3 Static Spindle Stiffness

The stiffness of the ball spindle (positions 1 to 6 on figure 104) and the wheel spindle (7 to 10) were assessed by suspending weights and measuring displacement via the Marprobe. Although relatively crude, this technique was an accurate and effective method of assessing static system stiffness, the results of which are presented in appendices D1 & D2, and summarised by figure 105.

Appling a force at (F1) and measuring the displacement at (R1) provided a radial stiffness profile of the ball spindle on its own. There is only a marginal decrease in stiffness observed as the lever arm length is increased and the loading position moved onto the ball fixturing (F3 R3, F2 R2 and F4 R3). Stiffness also remains constant when the ball and locking pin are removed (F6 R6). Appling the load with the wheel, in the same manner as it is during superfinishing (F2 R2), a displacement of 29 μm was recorded at 180 N. The axial stiffness of the ball spindle and fixturing (F5 R5) was greater than the radial stiffness.

Loading Position	Stiffness (μm / N) [Trend line]	
	No Additional Load	69.5N Superfinishing Load in Place
F1 R1	0.071	-
F2 R2	0.139	-
F3 R3	0.099	0.071
F4 R3	0.180	0.130
F5 R5	0.029	-
F6 R6	0.129	-
F7 R7	0.028	-
F8 R8	0.225	0.053
F9 R9	1.432	0.250
F10 R10	-	0.377

Figure 105 - Summary of spindle & fixturing stiffness

Measurements of static wheel spindle and wheel fixturing stiffness reveal that higher stiffness occurs on the wheel spindle (F7 R7) compared to on the grinding wheel (F8 R8). This is partly due to the increase in the distance from the spindle bearings and partly due to the slight play in the liner wheel fixturing bearing. As intended, mounting the wheel against rubber o-rings (F9 R9) increased the flexibility substantially.

In order to assess the combined stiffness of the wheel and ball spindles, measurements were taken when a typical superfinishing load of 70N was applied by the wheel to the ball. System stiffness values (at F3 R3, F4, R3, F8 R8, and F9 R9) all increased and increased most prominently on the wheel spindle. Appling a point load (F10 R10), as opposed to using the wheel, did not increase the system stiffness as it did not increase the system constraint.

The tetrahedral structure of Tetraform was designed to maximize dynamic stiffness. However as the wheel spindle uses an air bearing, the initial displacement deflects into the air gap for between 10 to 15 microns when static. As none of the stiffness results exceed a displacement of over 15 microns (other than those involving the use of rubber o-rings), the fixturing is not the principal factor in influencing the overall system stiffness.

The various springs used to apply the load during superfinishing were calibrated using a load cell (appendix D3). This provides static stiffness measurements of the springs and wheel fixturing in the z-direction. As the spring is partially compressed in the fixturing a sharp rise in load is observed on contact. The increase in load with displacement is generally linear and consistent along the same path when measurements are repeated. Large increases in load were occasionally recorded, particularly at larger displacements, possibly due to the bearing sticking; however off-centre loading did not adversely affect consistency. Somewhat stiffer values are recorded by the springs and fixturing than by the springs on their own.

13.7.4 NMB Machine Calibration

At NMB, spindle calibration between dial value and rpm was achieved via tachometer measurements. The plots produced for the ball and wheel spindles can be seen in appendices D6 & D7. They show that the maximum spindle speed capacity of ball and wheel are 1838 rpm and 13343 rpm respectively.

The applied force generated from vertical displacement of the wheel spindle was determined by compressing each of the five optional springs in a load cell. A plot is shown in appendix D8. The spring used during the majority of testing at NMB was spring number 5. Dynamic stiffness of the system during superfinishing, as well as the rate at which the wheel is removed from the ball, at the end of the processing cycle, are both important factors which would promote the use of stiff springs with minimal displacement. Better accuracy of the applied loading would come from the use of a less stiff spring with a larger displacement.

RESULTS & DISCUSSION

Chapter 14

Standard NMB Ball Production Outputs

This chapter evaluates the output quality achieved after the standard NMB production operations are used to produce the spherical surface of a ball. This provides information relating to the input condition of balls used for Elid superfinishing, as well as providing a baseline with which Elid processed balls can be compared. Additional pictures, graphs, etc for this chapter are presented in appendix E.

14.1 Microscopy

14.1.1 Material Structure & Hardness

The standard ball material used at NMB is AMS5630. This is equivalent to 440C and is a martensitic stainless bearing steel. Optical microscope pictures taken of the etched AMS5630 bulk material structure after heat-treatment (figure 106), show that there are larger primary and tempered secondary chromium carbide phases. The carbides are evenly distributed throughout a ball's cross section.

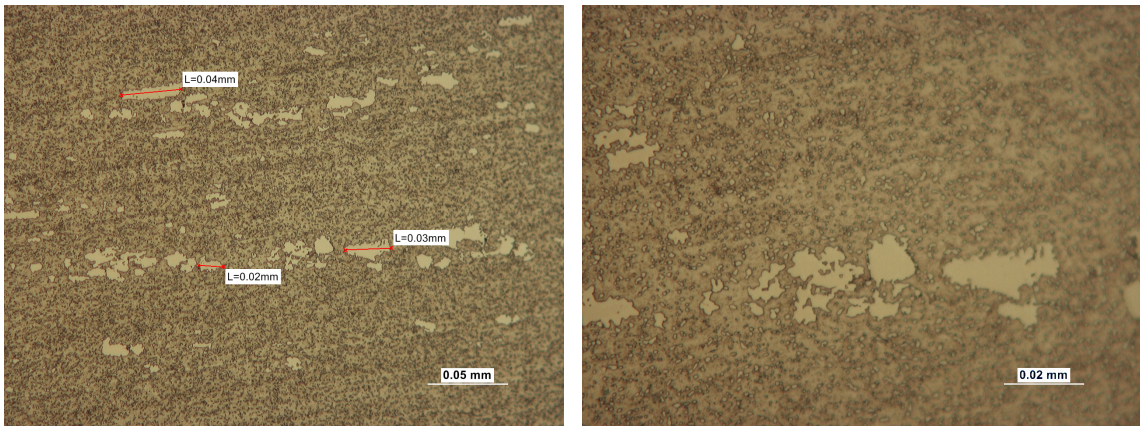

Figure 106 - Optical microscope images of etched AMS 5630 structure

Micro-hardness measurements performed when using a light load exclusively on the large carbides of the sample shown above, reveal that the hardness of the carbides is between 925 and 1100 Hv. Measurements performed away from the primary carbides

and at a larger load, determined the general hardness of the bulk material, producing values around 700 Hv (~60 HRc).

Hardness is normally checked on the ball face. However, in order to determine if the various processes result in a thermal softening of the ball material, measurements were taken on the spherical surface. After heat-treatment, hardness was consistent across the spherical surface and was found to be reliably between 58 to 62 HRc, in line with NMB heat-treatment specification HT11. Measurements on the spherical surface after barrelling, as well as Elid superfinishing, also achieved hardness results within this range. This suggests that neither the standard NMB processing operations nor Elid superfinishing results in a significant degree of softening.

14.1.2 Ball Visual Appearance

Figure 107 shows the progressive improvement in visual quality of RNB08 balls after heat-treatment, cylindrical grinding, honing and barrelling. Full ball pictures were taken with a plain white background reflected in the ball's surface to highlight surface details.

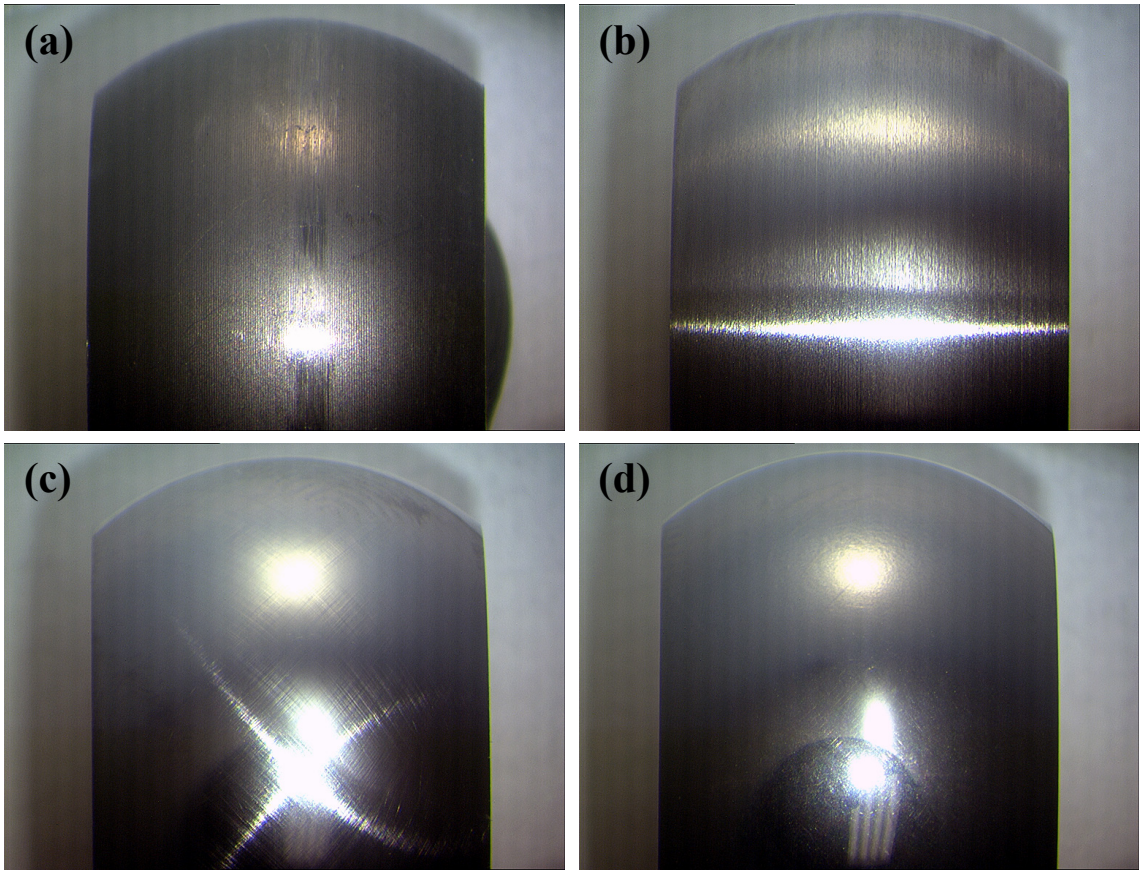

Figure 107 - Pictures of RNB08 balls at various points in the NMB ball production chain -
(a) After Heat-treatment, (b) After Cylindrical Grinding, (c) After Honing, (d) After Barrelling

14.1.3 Balls after Heat-Treatment

Heat-treatment oxidises the ball's surface. The patterning from the turning process remains visible. The heat-treated balls evaluated had an irregular, rougher band around their centre where the surface has been disturbed (figure 107a). Optical and Scanning Electron Microscope assessment of the surface of a heat-treated ball (figure 108) demonstrates both the coarse, but regular, turning marks and the surface structure of the ball.

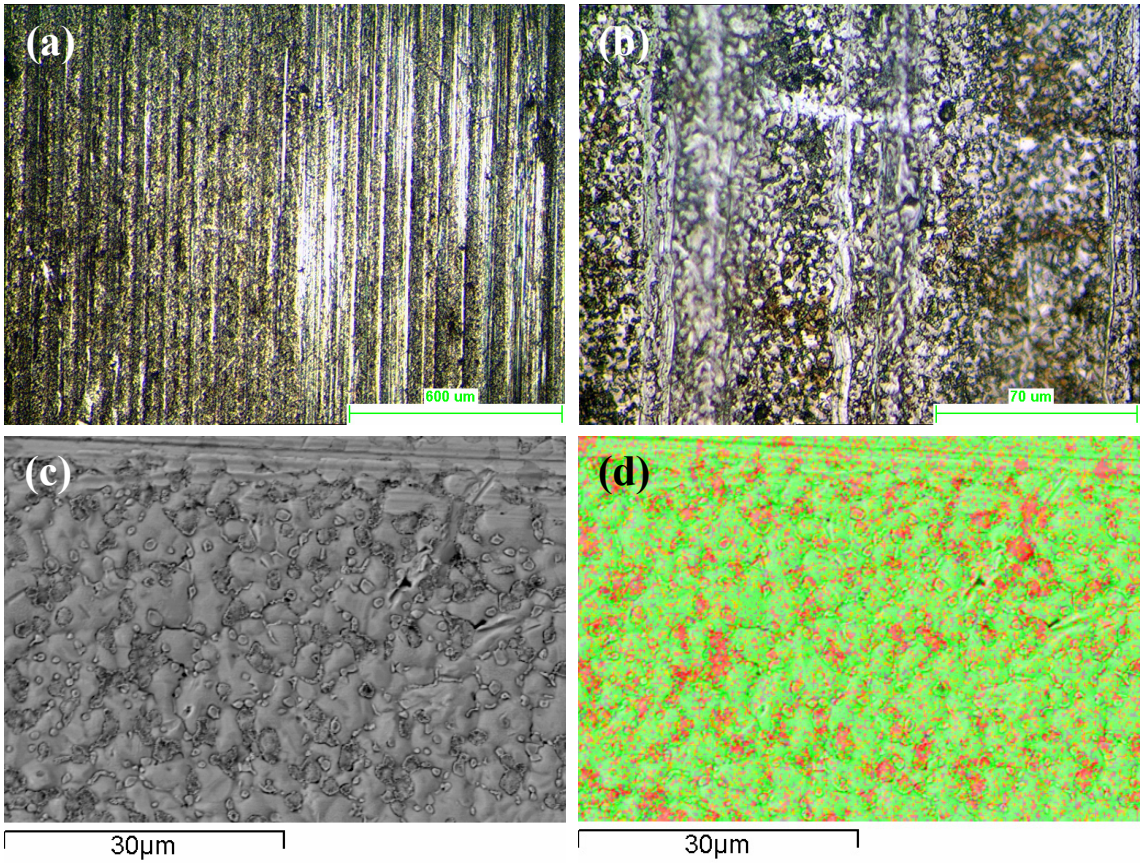

Figure 108 - Heat-treated RNB08 ball"s surface - (a) Low magnification optical microscope images (b) High magnification optical microscope images (c) SEM image, (d) Overlaid x-ray map of Chromium.

14.1.4 Balls after Cylindrical Grinding

Cylindrical grinding has to remove all trace of the heat-treated surface consisting of heat damaged surface layers. The appearance of a ball after cylindrical grinding and for subsequent process stages is of an even and consistent quality over its entirety. Cylindrical grinding removes 120 µm from the balls O/D and introduces a surface made up of relatively coarse circumferential grinding marks (figure 109).

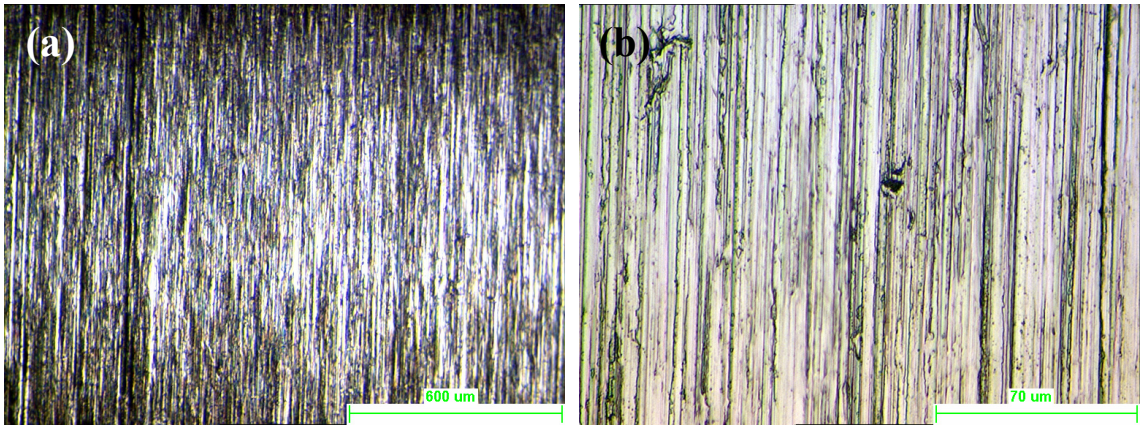

Figure 109 - Cylindrically ground RNB08 ball's surface - (a) Low magnification optical microscope images (b) High magnification optical microscope images

14.1.5 Balls after Honing

Honed balls have a smoother feel and improved appearance (figure 107c). A spiralling cross hatch pattern is introduced during honing which is dependent on the ball to wheel speed ratio.

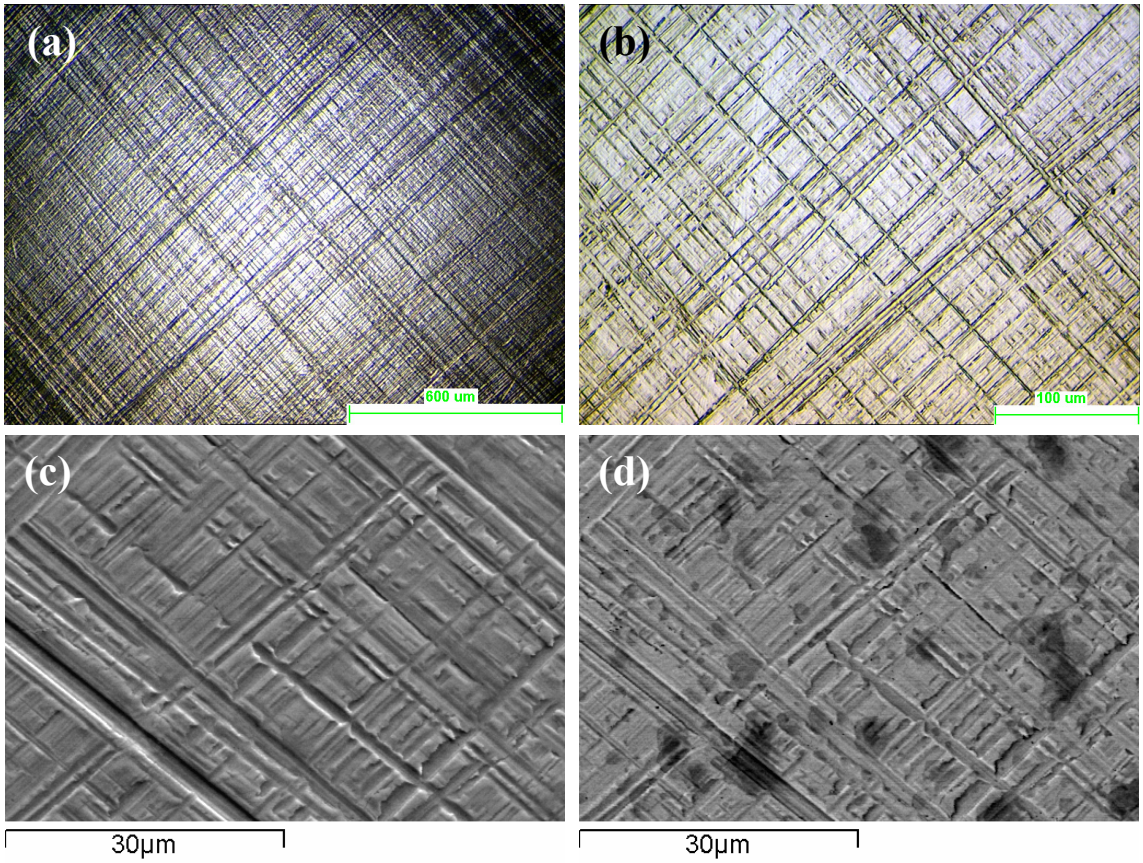

Figure 110 - Honed RNB08 ball's surface at crown - (a) Low magnification optical microscope images (b) High magnification optical microscope images (c) SEM image, (d) Backscatter SEM image

The surface introduced by the honing process (figure 110) is made up of a large number of 'U' shaped valleys cross hatched on top of each other. The backscatter image provides information about the surface structure, highlights the chromium carbides and demonstrates that they are being cut effectively at this stage.

14.1.6 Balls after Barrelling

The barrelling stage removes the visually distinct honing marks from the surface of the ball (figure 107d). To the naked eye, the finish produced appears to be of a high surface quality. However, the reflections on its surface lack the sharpness of image that is achieved after Elid superfinishing.

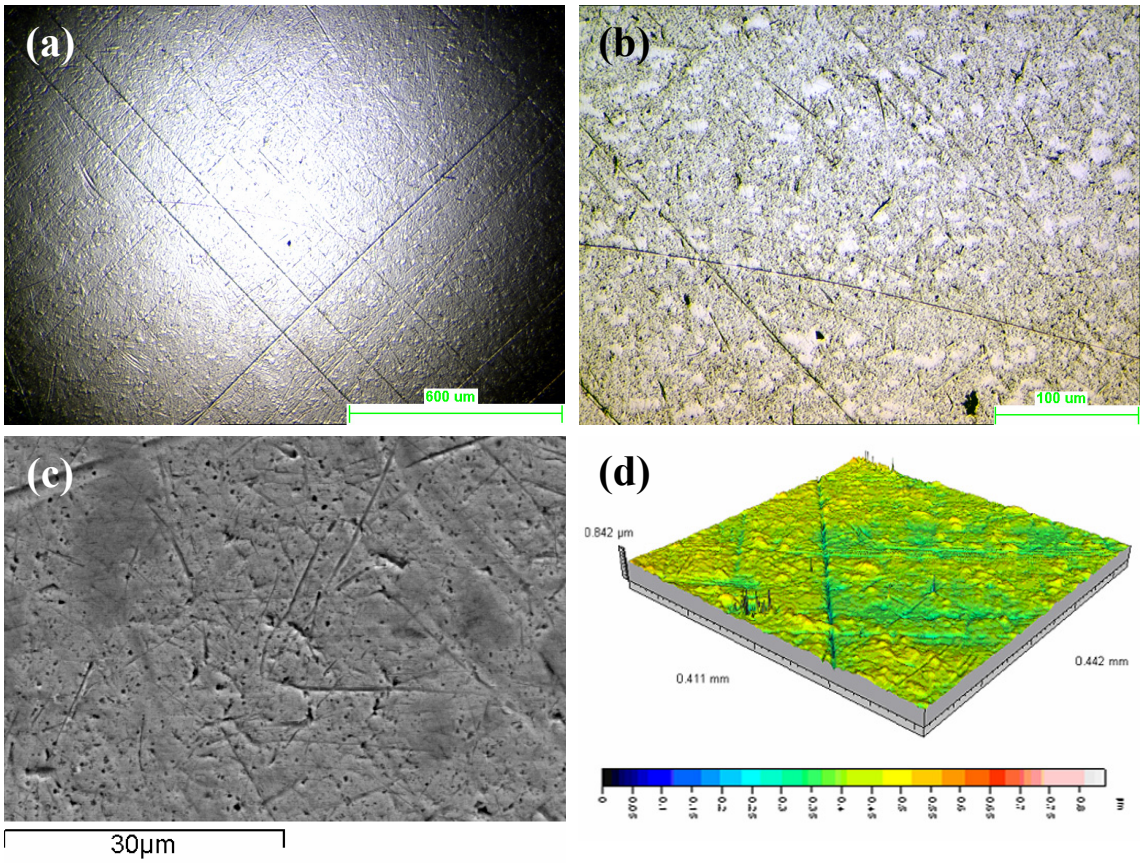

Figure 111 - Barrelled RNB08 ball's surface - (a) Low magnification optical microscope images (b) High magnification optical microscope images (c) SEM image, (d) Interferometer area profile

When viewed using an optical microscope, particularly at low magnification (figure 111a), a barrelled surface has a dappled appearance. Although the vast majority of honing marks are removed, several remain. At higher magnification (figure 111 b & c) the surface appears blemished with scattered smooth regions that correspond to the dappled appearance. X-ray mapping the surface reveals that these areas are rich in

chromium and depleted in iron, confirming these as chromium carbides. An interferometer area profile quantified them as being surface peaks. Although intrinsically necessary, the size and dispersion of the carbides in bearing materials can reduce fatigue life and ultimately limit the level of surface finish attainable. The increased hardness of the carbide phase impinges on the ability of the polishing process, particularly when using conventional abrasives, to evenly remove material from the workpiece surface.

14.1.7 Balls after Super-polishing

Whereas small ball sizes (such as RNB08) can be barrelled, larger ball sizes (RBFB16AB) have to be super-polished. Microscope analysis of balls that were finished by the standard NMB super-polishing operation did not demonstrate any difference to those that were barrelled (figure 112).

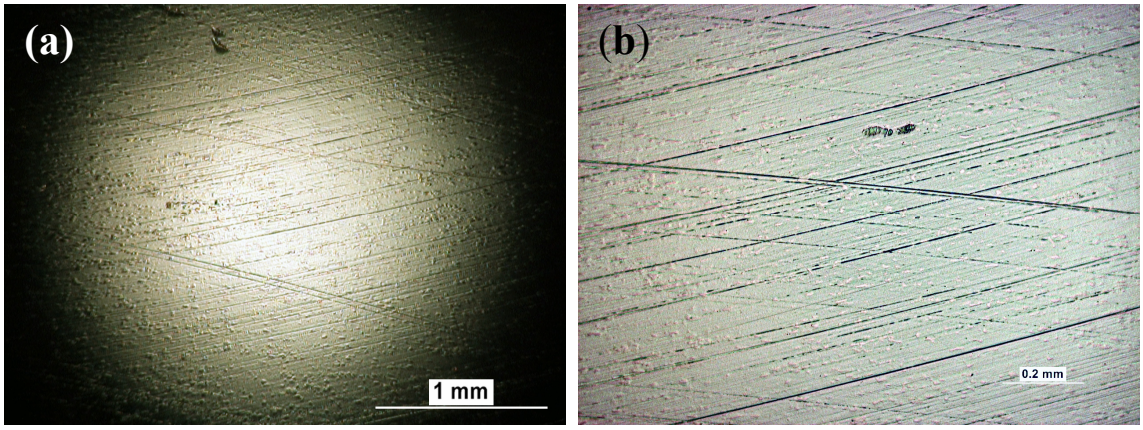

Figure 112 - Super-polished RBFB16AB ball's surface - (a) Low magnification optical microscope images (b) Medium magnification optical microscope images

14.2 Surface Finish

Surface finish measurements taken on balls after heat-treatment, cylindrical grinding, honing and barrelling, are presented in figures 113, 114 and summarized in figure 115. Corresponding examples of the profiles produced on a Taylor Hobson talysurf are shown in appendix E3.

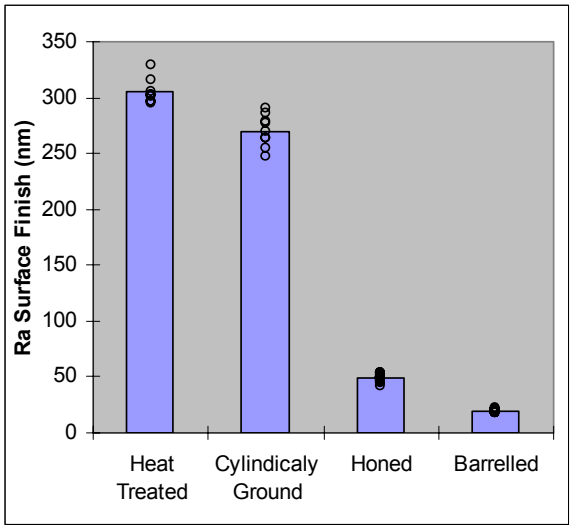

Figure 113 - RNB08 batch Ra surface finish results of the standard NMB processing operations. (Taylor Hobson talysurf, across ball)

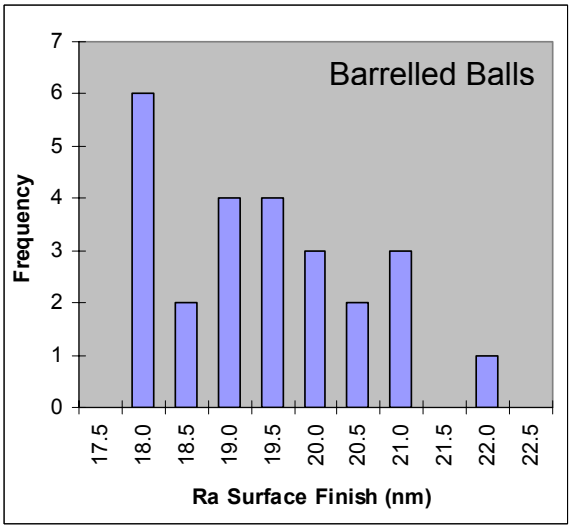

Figure 114 - Histogram showing distribution of Ra surface finish results for a barrelled RNB08 batch of balls (Taylor Hobson talysurf, across ball)

	Heat-Treated			Cylindrical Ground			Honed			Barrelled		
	Mean	Max	St.Dev	Mean	Max	St.Dev	Mean	Max	St.Dev	Mean	Max	St.Dev
Ra (nm)	305	329	12	270	291	15	49	54	3	19	22	1.1
Rq (nm)	404	499	41	346	370	18	64	72	4	28	36	3.1
Rp (nm)	960	1039	36	634	674	26	120	136	7	53	56	2.0
Rv (nm)	645	773	75	850	897	35	189	216	13	89	113	9
Rz (nm)	1605	1787	106	1484	1570	58	309	351	19	142	167	10
Rt (nm)	5387	12408	2915	3309	5659	976	770	1227	172	479	986	174
Rsk	0.6	0.8	0.2	-0.6	-0.5	0.1	-0.9	-0.7	0.2	-1.6	-0.8	0.7
Rku	8.0	32.7	10.0	4.1	6.7	1.1	5.2	7.9	1.1	16	65	15
Rdq (°)	5.9	6.5	0.4	9.1	9.5	0.2	2.7	3.1	0.2	1.1	1.2	0.1

Figure 115 - RNB08 Batch surface finish results of the standard NMB processing operations (Taylor Hobson talysurf, across ball)

After each stage of the process chain, surface finish not only improves but becomes more consistent. The results at each processing stage surpass the requirements provided by the manufacturing drawing (appendix B1). The upper roughness tolerance for cylindrical grinding (406 nm Ra) is achieved prior to this operation being conducted.

The finish of a standard NMB ball when fully processed must be below 38.1 nm Ra. The barrelled RNB08 balls measured achieve an average of 19.2 nm Ra and a standard deviation of 1.1 nm Ra. The small variation between balls is approximately equal to the variation observed when repeating measurement at different points on the same ball. The finish distribution of barrelled balls (figure 114) exhibits a slight skew of 0.5 with results clustered towards the lowest value of 17.6 nm Ra.

14.2.1 Additional finish parameters

As the size of the surface perturbations are reduced by the various processes, the measurements of average roughness (Ra, Rq) and peak to valley roughness (Rz, Rt) decrease. Changes in surface skew (Rsk) denote a shift in symmetry of the surface profile mean. A move towards negative values shows that surface valleys (Rv) are increasingly dominant over the surface peaks (Rp). An increase in kurtosis is recorded as the balls proceed through the process chain; this denotes an increase in the sharpness of perturbations. Lower surface slope (Rdq) values are produced by honing and barrelling, compared to turning and cylindrically grinding.

14.2.2 Completed Ball Comparisons (Roughness)

Figure 116 presents Ra surface finish measurements from four separate batches of standard NMB superfinished balls. Individual roughness measurements (circles) and the set average result (columns) are shown, providing a comparison of batches of balls, measurement systems, measurement type, barrelling and super-polishing operations.

Comparing columns 1 and 2 demonstrates that finish measurements taken using a Wyko phase shift interferometer are generally in good agreement with those taken on a Talysurf (figure 116, columns 1 & 2). Measurements of six RNB08 balls (column 3) that came from a different batch to those in column 1, recorded close average values and are of equal quality and consistency.

Although the average quality is similar, there is a larger degree of variation seen within the RNDEB14 batch (column 4) than the RNB08 batch (column 1). This may be because the RNB08 balls were barrelled, which is a mass finishing operation, whereas RNDEB14 balls were individually super-polished. The process capability values (Cpk) for the barrelled RNB08 balls (column 1) and super-polished RNDEB14 balls (column 4) were 5.49 and 1.73 respectively. Both are above 1 and are therefore satisfactory.

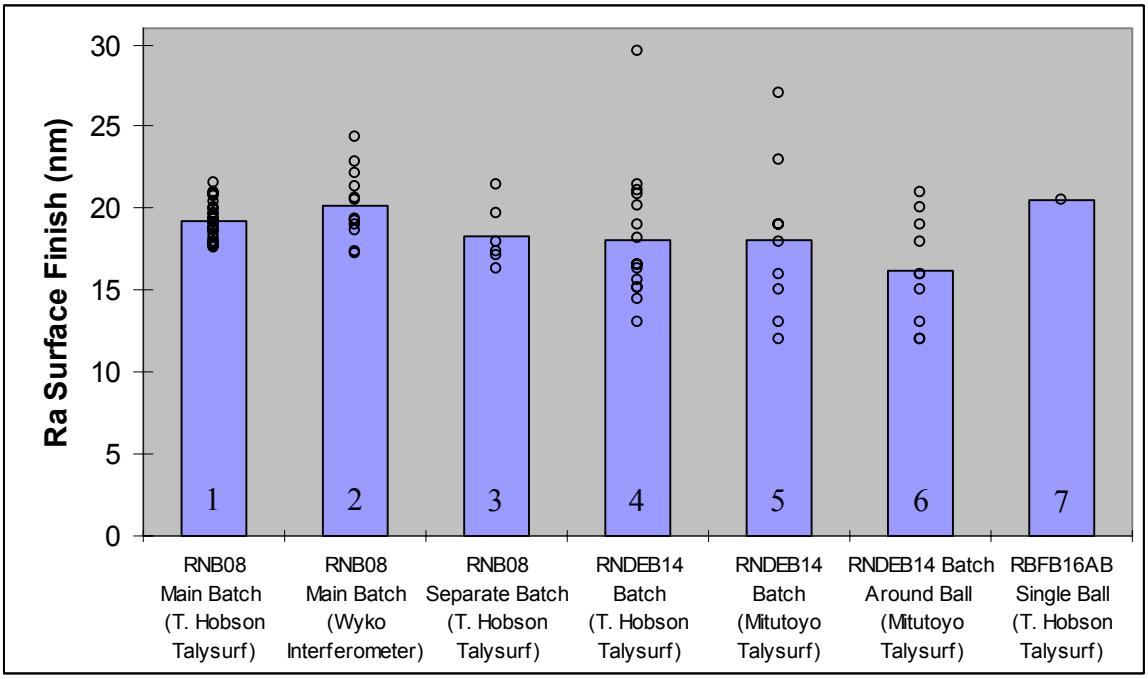

Figure 116 - A variety of Ra surface finish measurements providing a comparison of batches of balls, measurement systems, barrelling and polishing processes.

Measurements of RNDEB14 balls on Cranfield's Taylor Hobson and NMB's Mitutoyo talysurf (columns 4 & 5) produced mean Ra values of 18 nm and 17.7 nm respectively. A slightly lower average finish was recorded when measurements were taken around the ball centre (columns 5 & 6) compared to across the ball.

Repeated measurement of a standard polished RBFB16AB ball produced an increased degree of variation in results when it was removed and re-measured rather than simply repeating the measurement over the same track. Values varied by 0.6 nm when re-measuring and by 1.6 nm when measuring along different tracks.

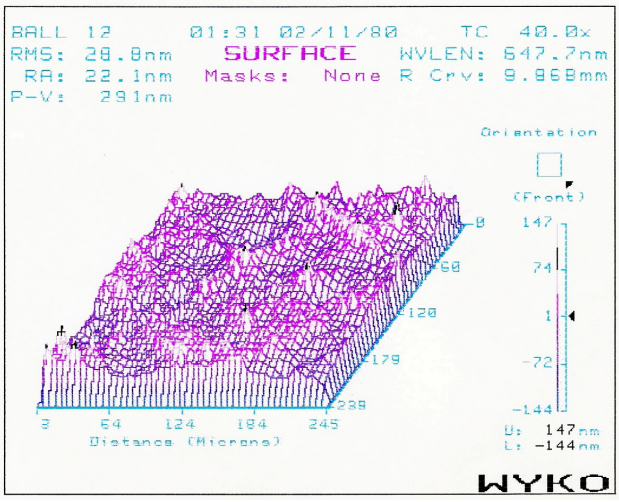

Figure 117 - Barrelled Surface
(Wyco phase shift interferometer)

14.3 Ball Form

14.3.1 Ball Size

Measurements of RNB08 balls show a reduction in their size through the process stages (figures 118 - 120). Cylindrical grinding removes 120 µm off the balls O/D, which consists of the oxidised heat-treated surface layer. The honing process reduces the radius by a further 10 µm as the form is generated and surface finish improved. Barrelling can be classified as a non material removal operation, which only reduces the ball radius by an exceptionally small amount.

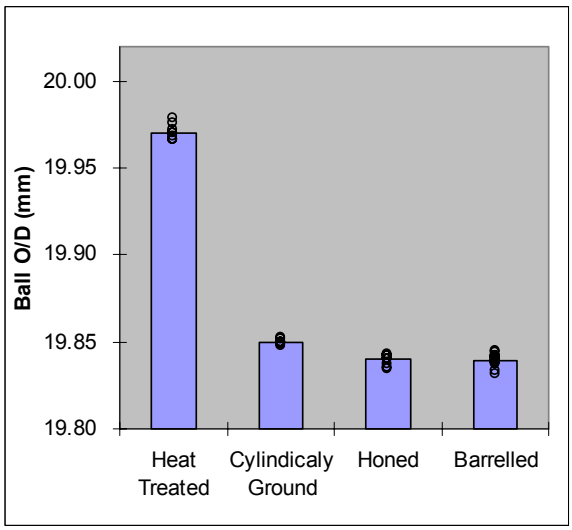

Figure 118 - RNB08 batch ball O/D results of the standard NMB processing operations. (Micrometer)

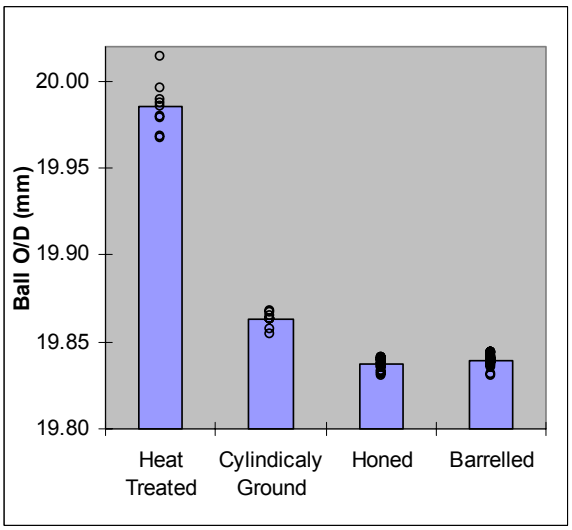

Figure 119 - RNB08 batch ball size results of the standard NMB processing operations. (Taylor Hobson talysurf, measuring radius across ball)

	Heat-Treated			Cylindrical Ground			Honed			Barrelled		
	Mean	Max	St.Dev	Mean	Max	St.Dev	Mean	Max	St.Dev	Mean	Max	St.Dev
Ball Size, (mm) Micrometer	19.970	19.979	0.0048	19.850	19.853	0.0016	19.840	19.843	0.0031	19.840	19.845	0.0037
Ball Size, (mm) Talysurf	19.985	20.014	0.0152	19.863	19.868	0.0046	19.837	19.842	0.0036	19.839	19.844	0.0033
Waviness, Wt (µm) Talysurf	5.104	5.447	0.216	3.376	3.890	0.278	0.115	0.149	0.019	0.110	0.163	0.023
Roundness P-V (µm) TalyCenta	7.90	10.59	1.83	4.21	5.74	0.70	0.73	1.33	0.37	0.88	2.37	0.70

Figure 120 - RNB08 batch ball form results of the standard NMB processing operations

Control of the range of balls O/D values within a batch is more critical than the exact diameter of a ball. According to the more accurate micrometer measurements, the range of ball O/Ds after heat-treatment varies by 12.5 μm. This is better than the required 50 μm drawing tolerance range and is very close to the final ball swaging prerequisite of 12 μm. It is the responsibility of the cylindrical grinding operation to create consistent ball size. Sampling the output from this stage recorded a reduction in the range to 5 μm. This value slightly increased through honing and barrelling operations, which achieve ranges of 9.0 μm and 12.5 μm respectively. Consistency worsens through honing as it is a constant force process that relies on processing time and the self-sharpening mechanism to control material removal. Polishing and barrelling operations traditionally degrade form accuracy.

Measurements taken using a talysurf (figure 119) recorded a larger spread of O/D values, particularly after the heat-treatment (47 μm) and cylindrical grinding (14 μm) stages. This is because the ball's diameter is calculated by fitting an average diameter to the measured profile across the ball. The value is susceptible to errors in ball roundness, which are largest when measured across the ball and before the honing operation. Therefore the improvement in consistency achieved after honing (10.6 μm) can be attributed to the reduction in form error.

Ball O/D measurements taken on super-polished RNDEB14 balls also demonstrated slightly more variation when using the talysurf compared to using a comparator gauge.

14.3.2 Ball Form Error

As demonstrated by figures 120 - 122, the honing operation is responsible for generating the required 2.5 μm ball roundness. Neither the super-polishing nor barrelling operations appreciably degrade the form of the ball. Measurements of Wt (peak to valley) waviness recorded on the talysurf produced lower values and more consistent results than roundness measurements. Talycenta measurements 'up & down' the ball follow the standard measuring method used at NMB. Examples of the raw profiles produced when using both methods can be found in appendices E2 & E4. Levels of ball form error are of an equal magnitude to Rt surface finish values. This means that a significant proportion of form error is in fact made up by the surface roughness of the ball. Improving the finish to nanometre levels also improves ball form to the required levels. When processing 'out of round' balls, the form reaches steady state conditions before the finish does.

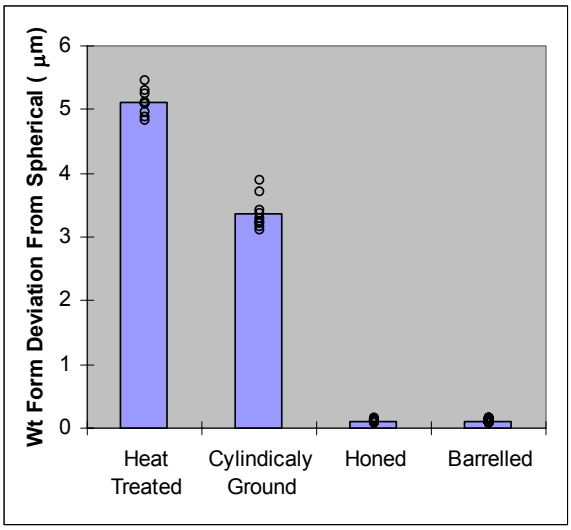

Figure 121 - RNB08 Batch Wt form deviation results of the standard NMB processing operations. (Taylor Hobson talysurf, across ball)

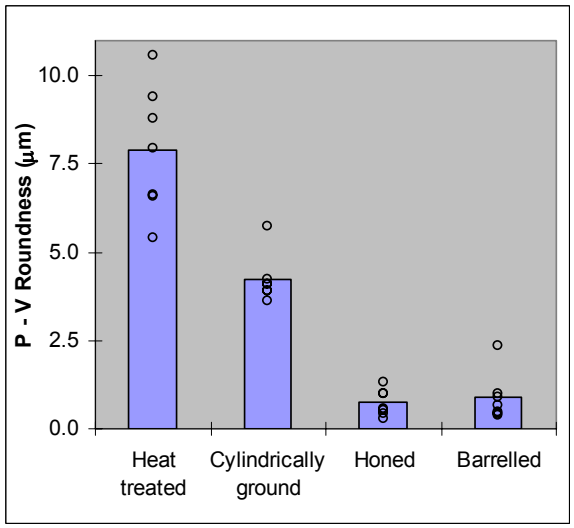

Figure 122 - RNB08 Batch peak to valley roundness results of the standard NMB processing operations. (Taylor Hobson TalyRound, up & down ball)

14.3.3 Completed Ball Comparisons (Form)

The degree of variation is likely to be larger between balls from different batches than between those from the same batch (figure 123). Roundness measurements on RNDEB14 balls are poorer than those from RNB08 balls. In addition to being less round the RNDEB14 balls were 'up at the edges'. It is not known whether this is due to ball size, polishing as opposed to barrelling, or natural variation between batches. Balls recorded larger values when measurements are taken up and down the ball compared to circumferentially around a ball. Control of roundness up and down the ball is critical.

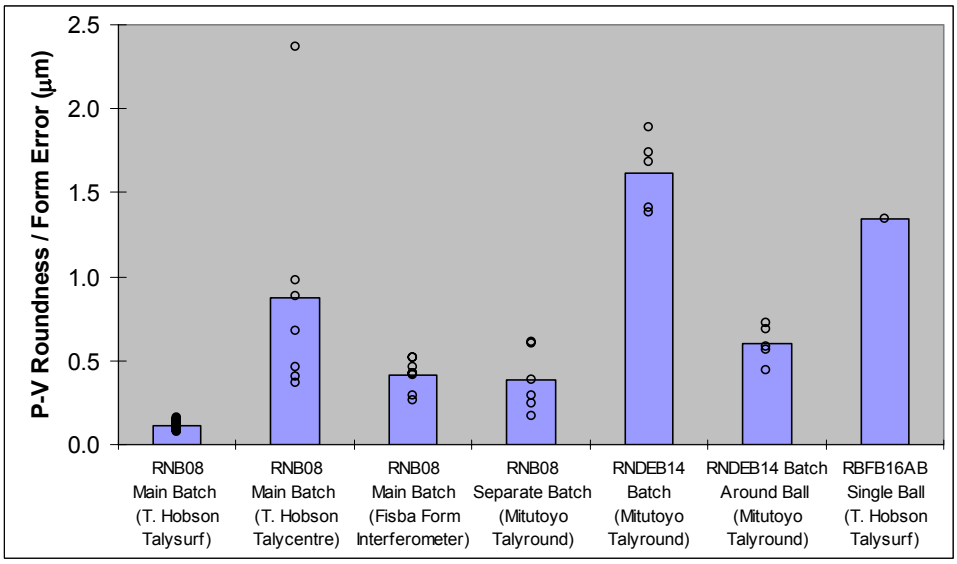

Figure 123 - A variety of ball roundness / form error measurements providing a comparison of batches of balls, measurement systems, barrelling and polishing processes.

Chapter 15 - Conditioning of MRB wheels

15.1 Analysis of MRB Wheel structure

Figure 124 shows a new and unused MRB-CBN superfinishing wheel. Mounting and polishing a piece of a #12,000 MRB wheel for metallurgical analysis revealed information about its structure (figure 125). The lighter portions are an amalgam of copper and plastic, and the darker regions are pores in the wheel structure. Micro-hardness testing performed on this sample produced hardness values that ranged between 29 and 71 Hv. X-ray mapping was unable to identify the resin portion. Etching the sample followed by ultrasonic cleaning eroded the copper from the surface and left behind what is assumed to be the resin constituent. According to the available literature on KFSI-2 wheels, they consist of a 7:3 ratio of copper to phenol resin. The concentration of abrasive in all the wheels used is 75%. Figure 127 shows the CBN abrasives from the #500 Wheel. This is the largest size of abrasive used in this research.

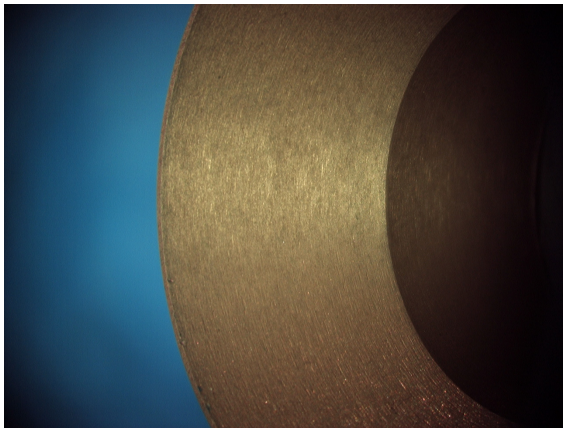

Figure 124 - Picture of new and unused RBFB16AB #4000 MRB-CBN wheel's surface

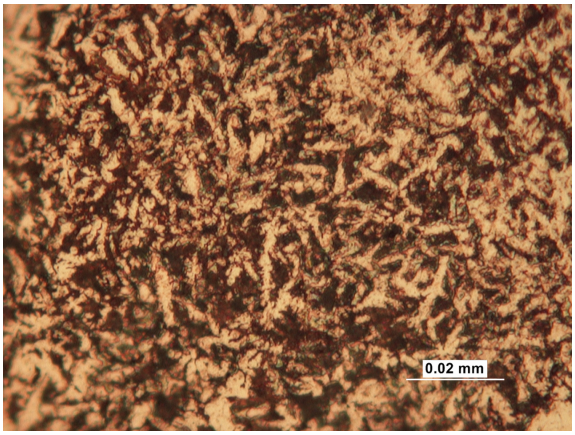

Figure 125 - Bulk #12000 wheel structure (sectioned & polished)

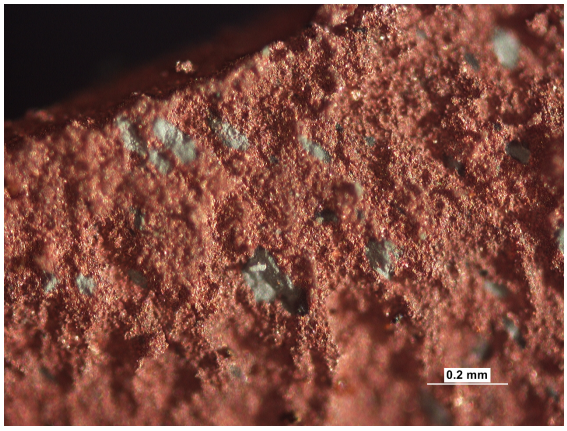

Figure 126 - Bulk #12000 wheel Structure (broken edge)

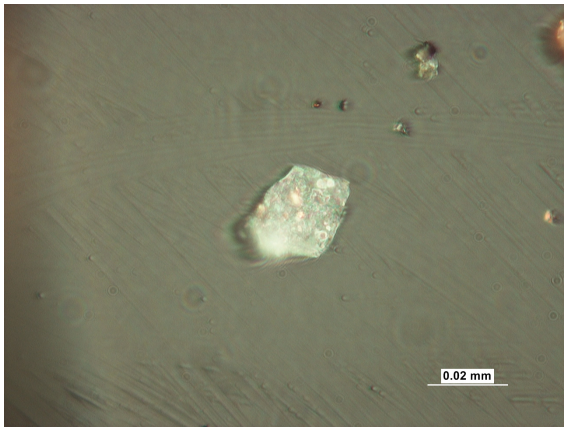

Figure 127 - CBN abrasive from a #500 MRB wheel

15.2 Wheel Truing

15.2.1 Diamond coated truing ball

A diamond coated truing ball was used to generate the required form of the wheel (figure 128). This method enables truing of the wheel whilst still on the machine. In order to be considered successful, it must achieve the following:

- form new wheels and reform broken or chipped wheels rapidly and easily
- maintain a suitably long usable life
- accurate creation of wheel form at the grinding surface
- result in a wheel's surface that is not damaged beyond what can be recovered by re-dressing

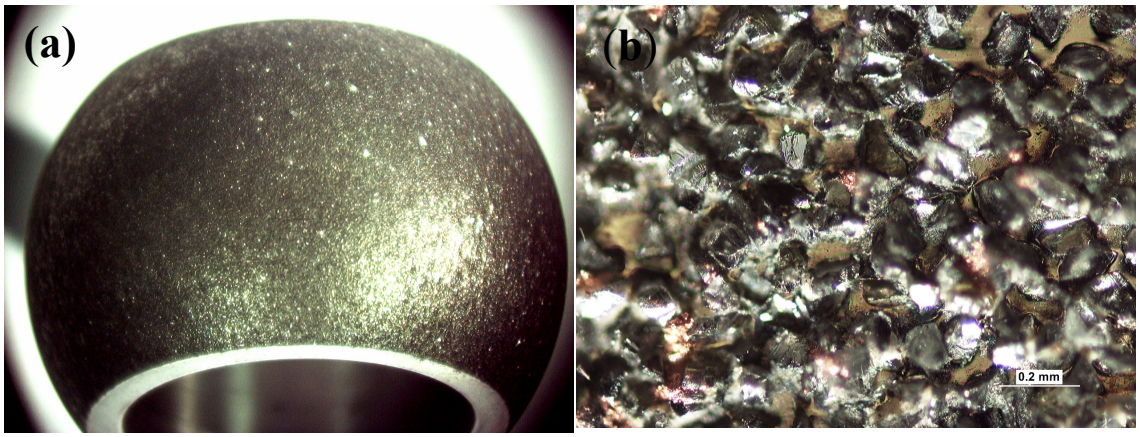

Figure 128 - Diamond coated truing ball (a) Full ball picture, (b) Optical microscope image

When testing the truing ball on RNB14 wheels, rapid re-forming of the wheels' shape was achieved. For the #4000 wheel, full generation from a lapped flat starting surface was achieved in 20 seconds. The broken edges of the #500 wheel were reformed in 10 seconds. The second time it was trued there was no increase in the time taken to re-form the #4000 wheel. However as it would be necessary to destroy several wheels to determine the usable life, this factor has not been determined. Prior to commencing grinding, the wheels were pre-process dressed with Elid. Full area contact was made between the ball and wheel, thus demonstrating that the correct wheel form had been achieved. The ball surface quality after grinding was good and the time that the surface was generated in was comparable to other results. This suggests that the surface of the wheel was not damaged by the truing process.

15.2.2 Electro-Discharge Truing

Electro-Discharge Truing (EDT) can be used as an alternative to mechanical methods of truing. When passing through the point where initial grinding contact is made, electrical sparking can occur between the ball and wheel. In terms of normal Elid superfinishing operation, sparking between the ball and wheel is unacceptable and must be eliminated.

The electrical discharge of the Elid power supply does however have a practical use and can be used effectively to true the superfinishing wheel. Maintaining the ball and wheel at the point of grinding contact, results in extensive sparking and rapid erosion of the wheel. In order to continue spark eroding the wheel as its length is reduced, accurate control of the machine's z-axis position is required in order to maintain the exact touch point of the ball and wheel contact. Figure 129 shows the Elid power activity recorded and the length reduction of the MRB wheel when Electro-discharge truing.

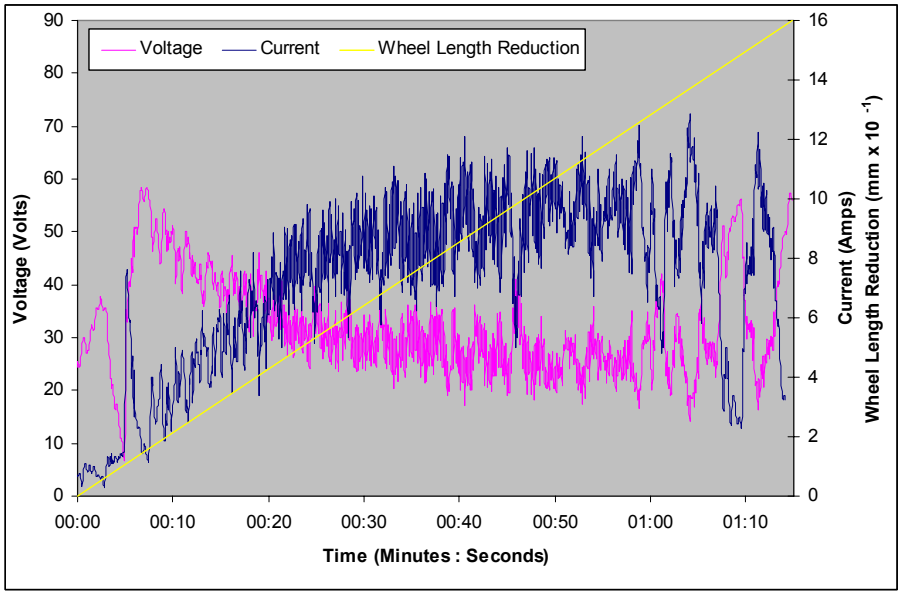

Figure 129 - Elid power and wheel length reduction recorded during electro-discharge truing
(Elid power supply set to 90V,40I, 10% or 50% - RNB08 ball, #12000 MRB-CBN wheel, Run no. 50)

Voltage and current levels fluctuated violently as a result of the electrical discharge and a rapid wheel length reduction rate of 1.3 mm per minute was recorded. The current research recorded considerably larger rates of wheel material removal compared to the reviewed literature on EDT. This rate is dependent on a number of factors, including consistently maintaining the touch point position, and the particulate build up insulating the ball's surface. An increased truing rate is achieved when higher power values are used. However, in order to minimize damage to the wheel's grinding surface, reducing the power levels to the minimum setting towards the end of the truing operation is

recommended. In order for the EDT process to work most effectively, the grinding zone should be flooded with fluid; resulting in a combination mechanism of electro-discharge truing process and aggressive electrolytic dressing. Normal superfinishing speeds can be used. The final accurate form of the wheel is created after the bedding-in process.

The extent of the damage that EDT causes to the wheel's surface was not fully evaluated; however there was never any detrimental effect on superfinishing performance after truing was performed, or any noticeable difference compared to the non-Elid truing methods tested. EDT was successfully used to accurately, rapidly, easily and cost effectively form the required shape of new and damaged wheels. EDT is the recommended method of forming the required shape of the wheel and is considered better than the diamond coated truing ball. Electro-discharge truing was also found to be effective for use with CIB-D wheels.

15.3 Pre-process dressing

15.3.1 Elid Power Data

After truing, a wheel's surface should be conditioned before it is used. Pre-dressing is particularly important prior to Elid 3 superfinishing, as a stable and non-conductive insulating layer must be introduced onto the wheel's surface, to enable dressing to continue during the superfinishing process.

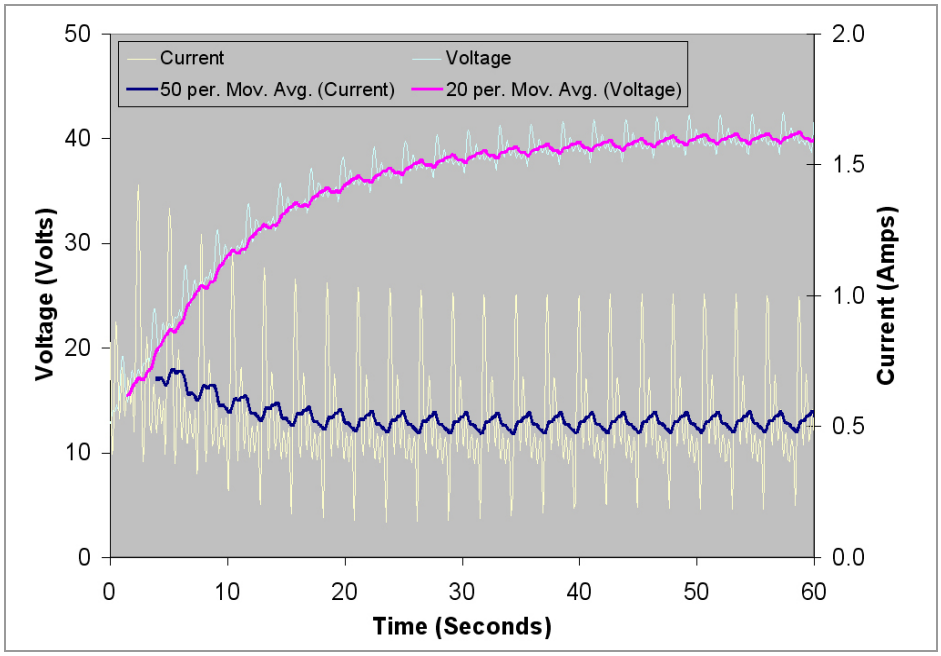

Figure 130 - Elid Pre-dressing power activity. – Graph of initial 60 second period for run no. 40. - [20I, 60V, 10% Duty, #12,000 MRB-CBN, 0.2 mm gap].

Figure 130 displays typical electrical behaviour for pre-process dressing. The rise in voltage and fall in current follows the trend discussed previously by other authors. However the rate at which the voltage reaches its maximum is only a fraction of what has been presented in the literature. This rapid stabilization of Elid power values occurred whenever dressing was performed using a separation gap and was largely unaffected by any of the parameters investigated. The copper-resin bonded MRB wheels dressed more quickly than the CIB wheel measured. This is to be expected as copper will rapidly form a thin oxide layer. The electrode coverage is larger than normally employed for Elid grinding or lap-polishing; as larger current density increases electrolytic erosion, this would result in a faster rate of power value stabilisation.

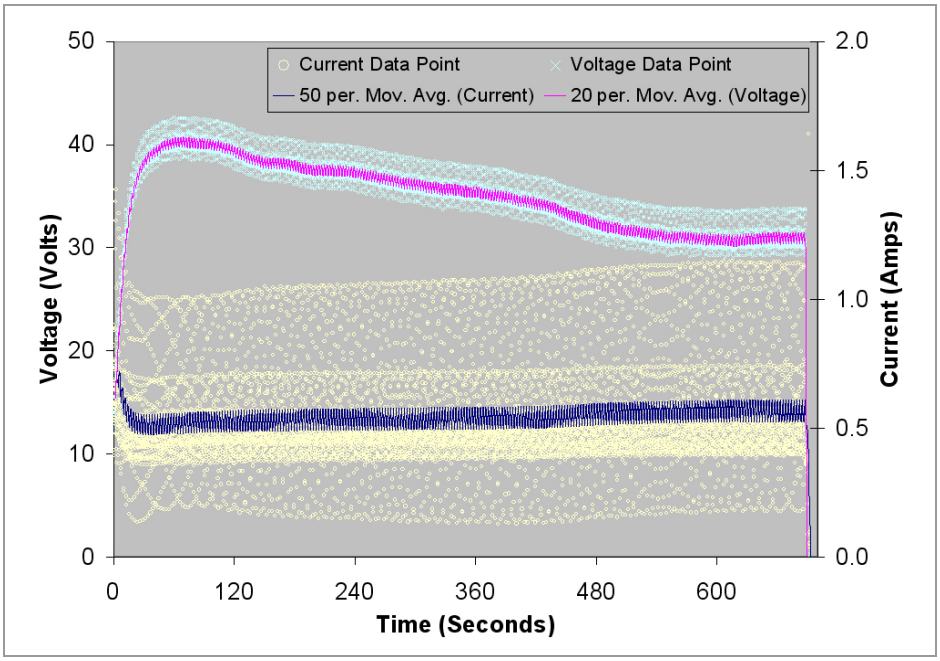

Figure 131 - Elid Pre-dressing power activity. - Graph of entire pre-dressing period for run no. 40. - [#12,000 MRB-CBN wheel dressed with a 0.2 mm gap after EDT using 20I, 60V, 10% Duty].

Assessment of the Elid power levels when pre-process dressing the wheels over a longer time period showed that after the resistance has reached a maximum, it is often seen to gradually reduce, even though the conditions have not changed (figure 131). The voltage rises in the short term as the wheel becomes dressed, but over a longer period the voltage declines. This electrical behaviour was consistently recorded on numerous occasions; however the reason for the declining voltage after was not identified. No improvement was observed in the wheel's performance when pre-dressing was allowed to continue past the point of maximum voltage.

The required time that pre-process dressing should be conducted for is dependent upon many factors. A wheel that has had no prior electrolysis performed on it will require a longer time for the current and voltage levels to plateau, than one which has been previously used and is entirely or partially electrolytically dressed. If pre-dressing is stopped and then restarted, the power levels will resume at their previous level. The size of the electrode gap only made a surprisingly small difference to the Elid power values, until direct electrical contact is made between the ball and wheel (Elid 3). There was some evidence that a larger gap produced slower wheel dressing. Ultimately pre-dressing should be continued until the voltage and current levels have stabilized.

15.3.2 Effect of pre-dressing on the wheel surface

The visual appearance of a set of RNB08 Elid 3 wheels after electro-discharge truing and pre-process dressing varied quite considerably (figure 132), even though the electrical behaviour recorded was very consistent. This is due to the formation of differing quantities of copper oxides and compounds at the wheels' surfaces.

Figure 132 - Variation in wheel appearance after electro-discharge truing and then pre-process dressing the set of wheels

When the wheel is electro-chemically dressed, the copper bond material undergoes an oxidation reaction where the atoms are ionised, lose electrons, and go into solution. Corrosion occurs because copper ions leave the wheel. However, as the copper is consumed various solid by-products are formed. Also retained at the surface are the wheel's resin bonding constituent and the CBN abrasives.

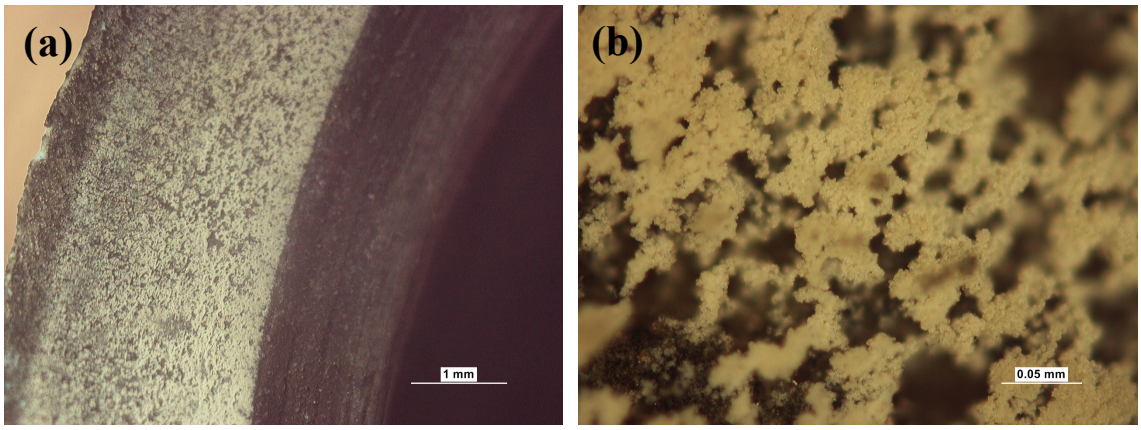

Figure 133 - Optical microscope images of an MRB wheel's surface after dressing.

The erosion of the metallic bond material from the surface of the wheel renders it non-conductive. This insulating layer prevents further oxidation, increasing the Elid voltage as described earlier. The smaller abrasives (4 to 0.13 μm) of the #4000 to #120,000 wheels are entirely held within the insulating surface layer. The larger size of the abrasives (30 μm) in the #500 wheel means that they can remain anchored in the bulk material of the wheel.

Figure 134 illustrates the various surfaces and deposits that occur at the wheel's grinding surface.

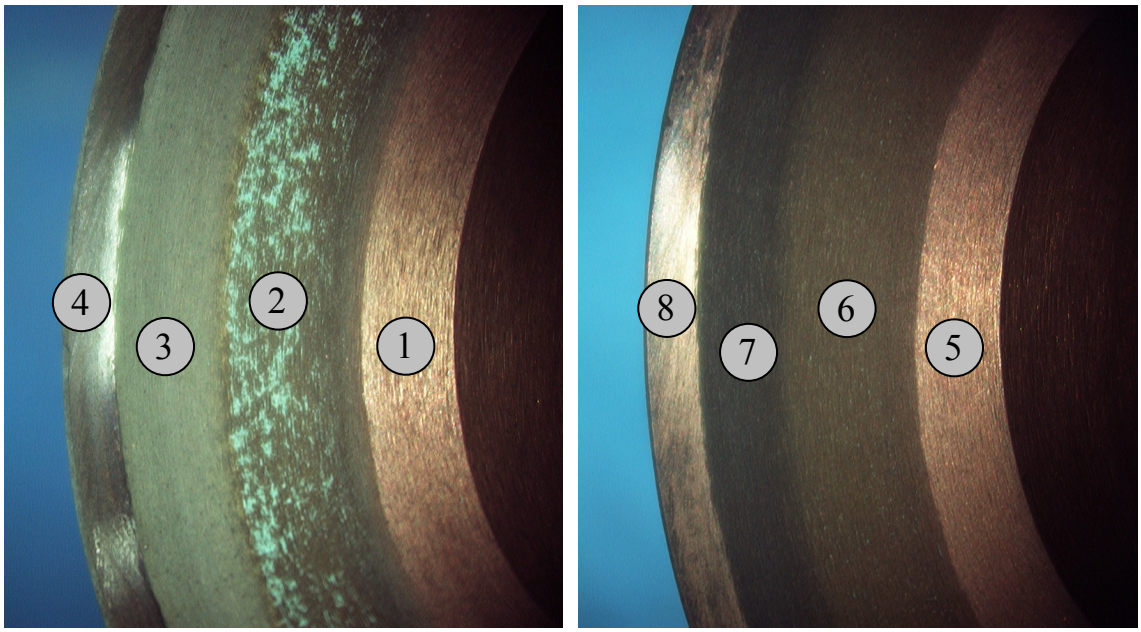

Figure 134 - Variation in the appearance of MRB wheels during their use. –
(1 & 5) New / Undressed wheel surface. (2, 6) Wheels appearance after pre-dressing.
(3 & 7) pre-dressed again. (4 & 8) Glazed wheel surface after superfinishing

15.4 Elid Superfinishing

When superfinishing is started, the surface of the wheel is dramatically altered once again. The insulating layer at the grinding surface of the wheel is compacted and, depending on what type of Elid is used and how effective it is, the wheel either remains in an effective well-dressed condition, or degrades as it develops a shiny glazed appearance.

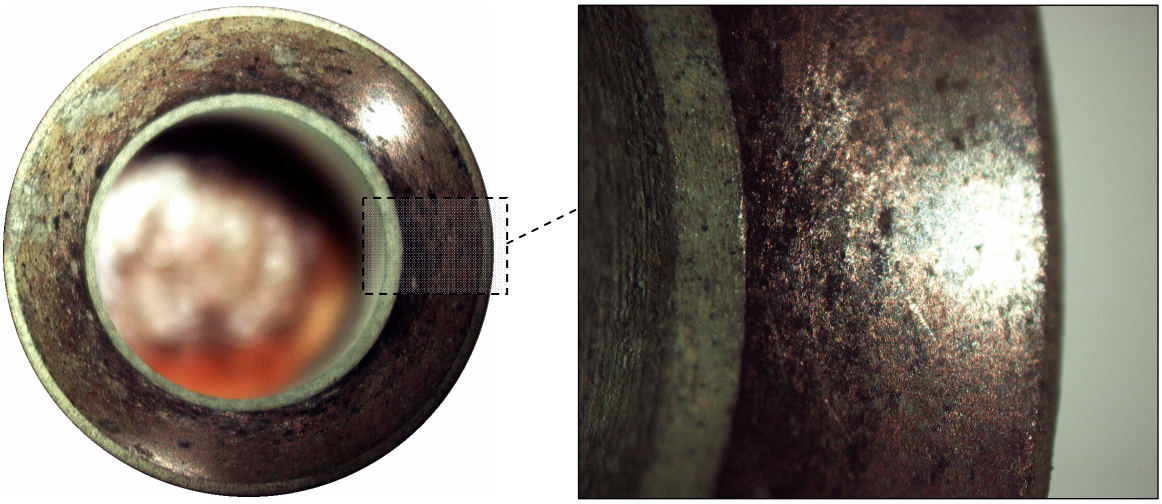

Figure 135 - Example of a glazed wheel surface – [#8000 MRB-CBN wheel]

If a periodic cycle of separate Elid dressing and non-Elid superfinishing (Elid 2) is used, the wheel develops a glazed appearance over the course of the run, but recovers the open structure as its surface is redressed. This cycle of glazing and recovery causes the wheel to wear and thus the performance of the wheel is maintained. A fully glazed wheel is shown in figure 135 and additional wheel pictures in appendix F.

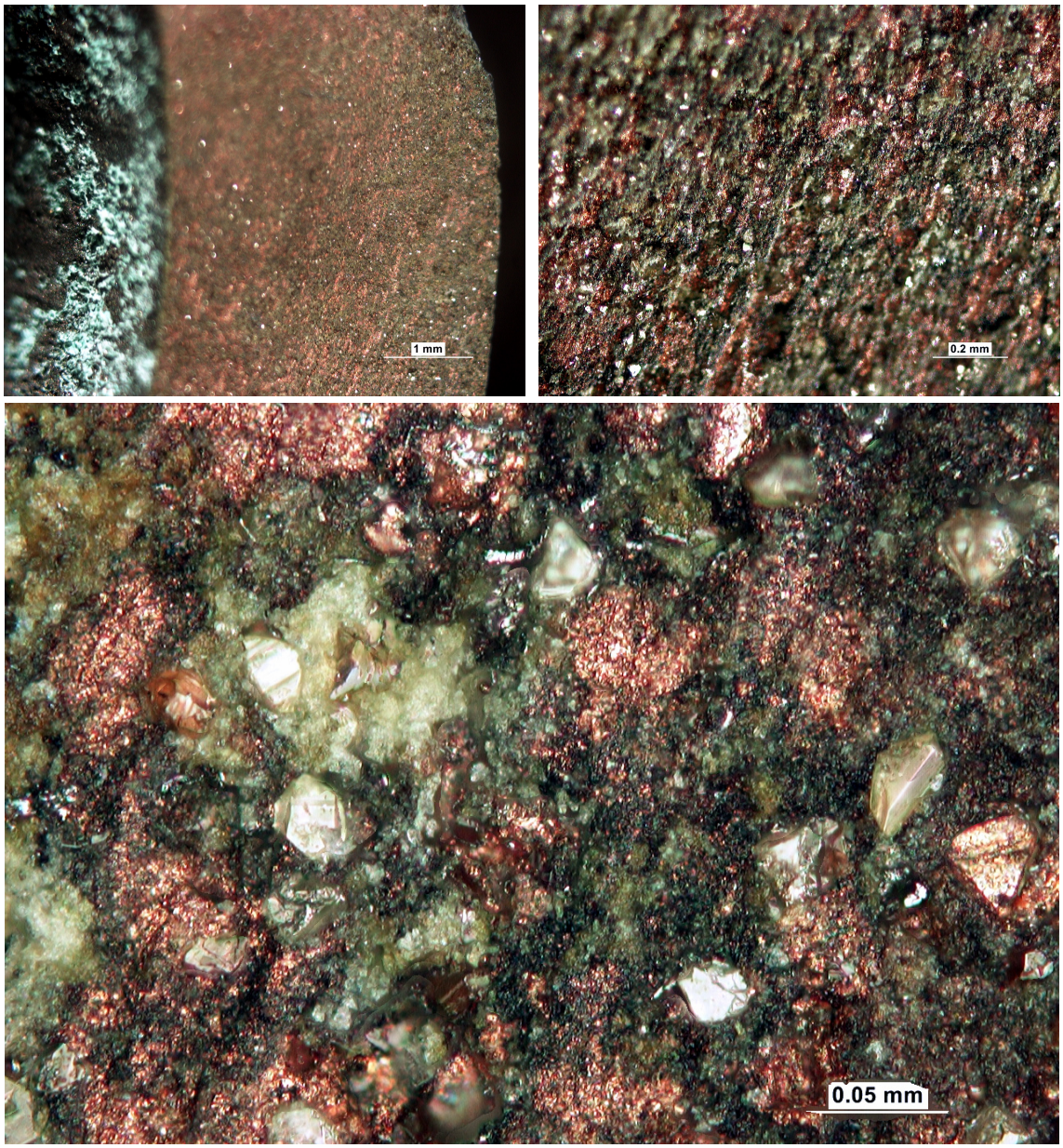

Figure 136 - High magnification optical image (Montage) of a #500 MRB-CBN wheel's surface after Elid 3 superfinishing.

When using the Elid system in an Elid 3 configuration, non-conductive constituents at the surface of the wheel provide a dynamic separating gap that allows newly revealed areas of copper at or near the surface of the wheel to be oxidized. Figure 136 shows a

high magnification image of a #500 MRB wheel's surface after Elid 3 superfinishing. As the surface was rough it was outside the depth of field of the microscope and 'Montage' imaging software was used to compile numerous pictures. The wheel was not glazed or loaded and was producing good surface finish and removal rates before the picture was taken. The copper bond material, although oxidised and eroded away, is still present at the surface. The abrasive is clearly visible.

When Elid 1 is used, the wheel's surface is continually maintained in an open, well-dressed condition during processing (figure 137). Pre-dressing is not required when Elid 1 superfinishing as the time is better spent running the wheel in during processing.

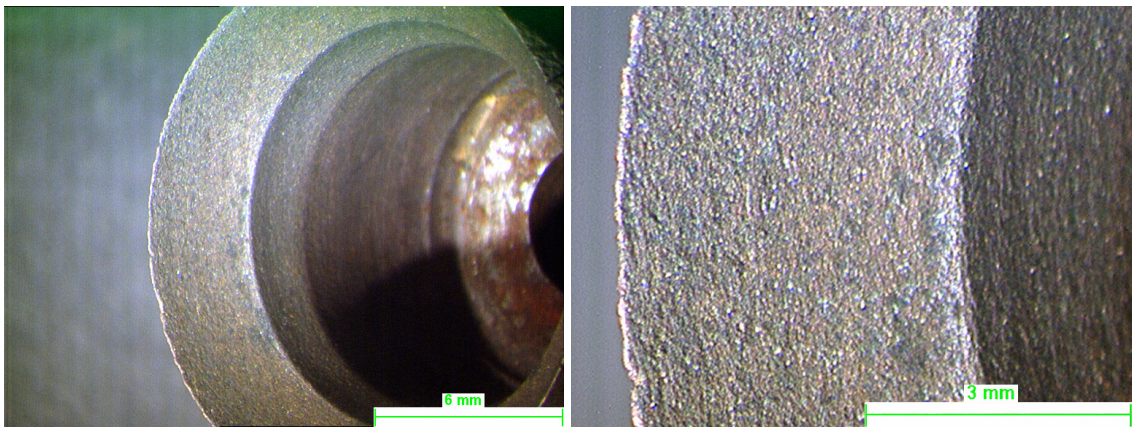

Figure 137 - Example of a well-dressed wheel surface after superfinishing with Elid 1. [#500 wheel]

Chapter 16 - General Ball Quality

Using optical and electron microscopes, talysurf and interferometer measurements, this chapter investigates the appearance and surface quality of balls produced using Elid. The results relate to standard hardened steel balls Elid processed with MRB-CBN wheels. The range of surfaces produced is shown, including the possible ball defects. (Additional pictures and talysurf profiles are provided in appendices G & H). The ball material and wheel type fundamentally influence the superfinishing process. The quality of the surface produced is dependent on a number of factors, the most influential of which are the following:

(1) the size of the abrasive used in the superfinishing wheel (30 to 0.14 μm)
(2) the wheel's condition, both in terms of how well it is dressed (free-cutting to glazed) and whether it is excessively chipped
(3) correct system set-up (wheel trueness, ball to wheel alignment & conformity)
(4) superfinishing operation (how and when Elid is used)

The type of Elid used does not directly influence ball surface quality, other than by affecting the wheel's condition. Processing parameters have only a limited influence on the visual appearance. Slight changes to the condition of the wheel, or adjustments to the superfinishing set-up, overshadow the effects of changing the processing speeds and forces.

16.1 Surface Finish

Initial Elid 3 testing at NMB provided information on the typical surface finish produced by the various abrasive size MRB-CBN wheels (figure 138) and demonstrated that the goal of 10 nm Ra was certainly achievable. Profilometry measurements taken at both NMB and Cranfield showed an improvement in Ra surface finish in all Elid superfinished balls. The #500 mesh Elid wheel, containing 30 μm abrasives, produced comparable results to the standard NMB superfinishing processes. Wheels #4000 to #20,000 (4 to 0.8μm) all produced similar values; the best recorded being 2 nm Ra using the #8000 wheel. In this case the finest abrasive wheel did not produce the smoothest surface. The strong dependence on exacting set-up and wheel condition is responsible for a greater degree of variation than is caused by the comparative closeness between these abrasive sizes.

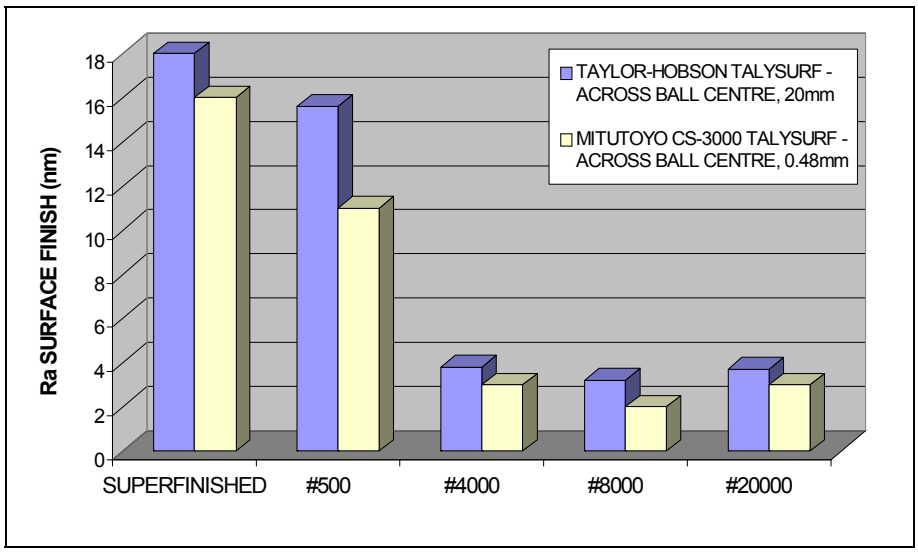

Figure 138 - Surface finish vs. abrasive size from initial tests conducted at NMB using RNDEB14 balls, Elid 3, and MRB-CBN wheels

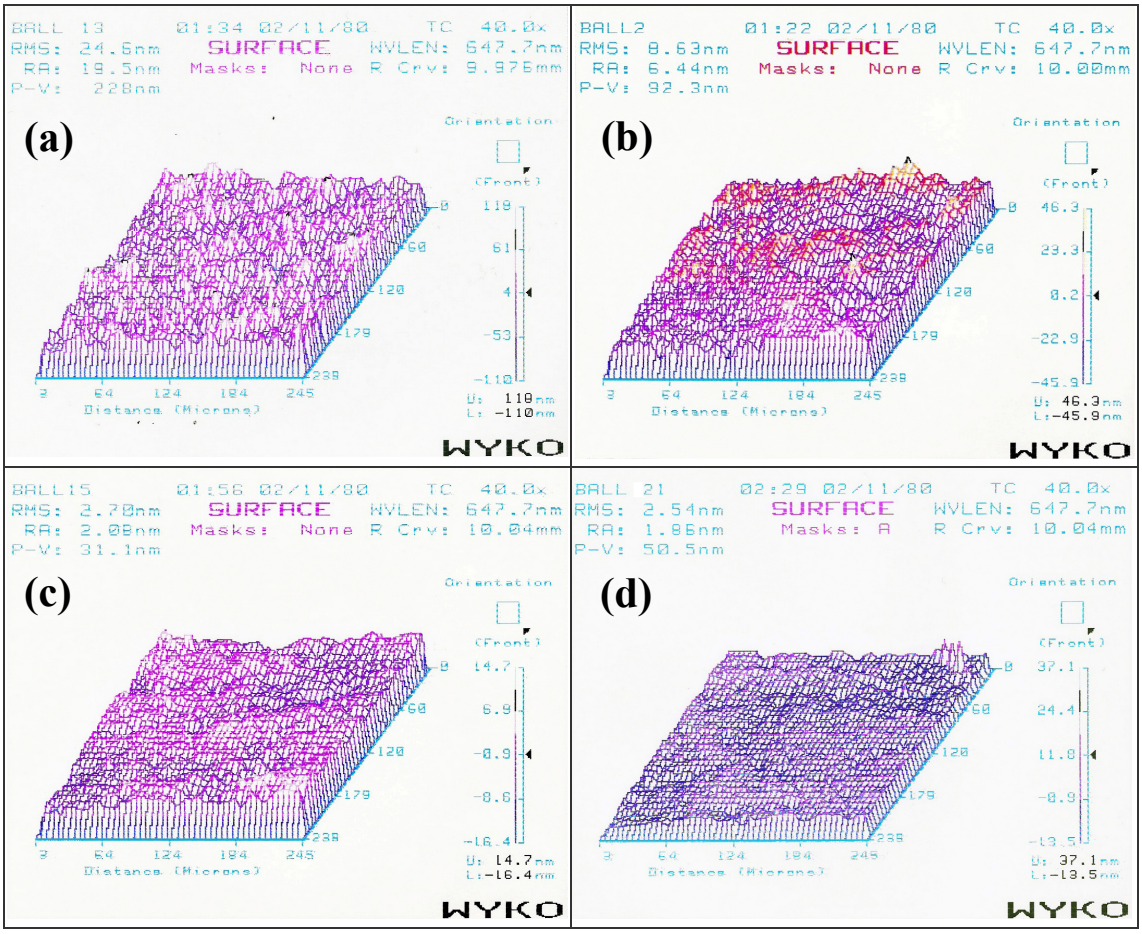

Figure 139 - Surface profile examples for balls produced using (a) #500 (b) #2,000 (c) #12,000 and (d) #120,000 MRB-CBN Elid wheels. [Wyko phase shift interferometer]

Based on the initial graph of surface finish versus abrasive size, two further MRN-CBN wheels (#2000 & #120,000) were ordered for testing with RNB08 balls on Tetraform. The slightly larger abrasives (8 μm) in the #2000 wheel significantly reduced the processing time required whilst still maintaining the ability to achieve high quality, sub 10 nm Ra, surface finishes. The #120,000 wheel (0.13 μm) produced comparatively similar finish results to the #4000 to #20,000 wheels. This suggests that when Elid 3 superfinishing there is a drop off in the importance of the abrasive as its size is reduced and that, ultimately, the limit in terms of surface finish for the Elid 3 process has been reached.

16.2 Microscopy

Figure 140 demonstrates the range in visual appearance that can be achieved when Elid superfinishing with MRB-CBN wheels of different abrasive sizes and wheel conditions. Figure 140a represents one of the roughest balls produced in this research and figure 140c one of the highest quality balls.

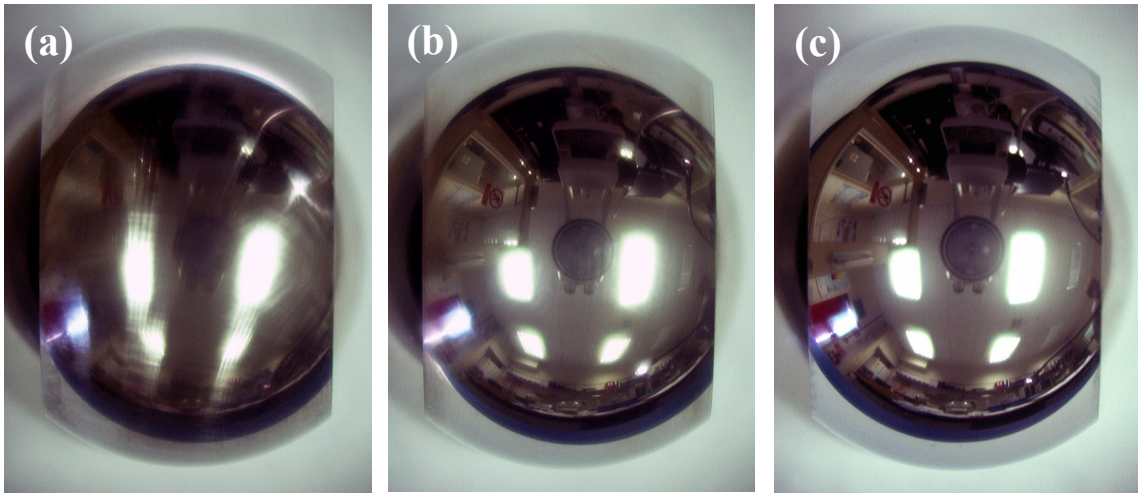

Figure 140 - Pictures of RNB08 balls comparing the visual quality of their spherical surface. - (a) Ball produced with a free-cutting #500 MRB-CBN wheel, (b) Ball produced with a glazed #500 MRB-CBN wheel, (c) Highest quality Elid superfinished ball produced with a #12,000 MRB-CBN wheel

16.2.1 Ball surface produced with a #500 MRB-CBN wheel

When using a #500 wheel in a free-cutting well-dressed condition, distinct grinding marks appear on the ball's surface (figure 141). It has an appearance that is approximately equivalent to the standard honed finish. However, when the wheel becomes glazed, as a result of ineffective or insufficient dressing, the surface produced is greatly improved and is comparable in quality to a standard NMB superfinished surface (figure 142).

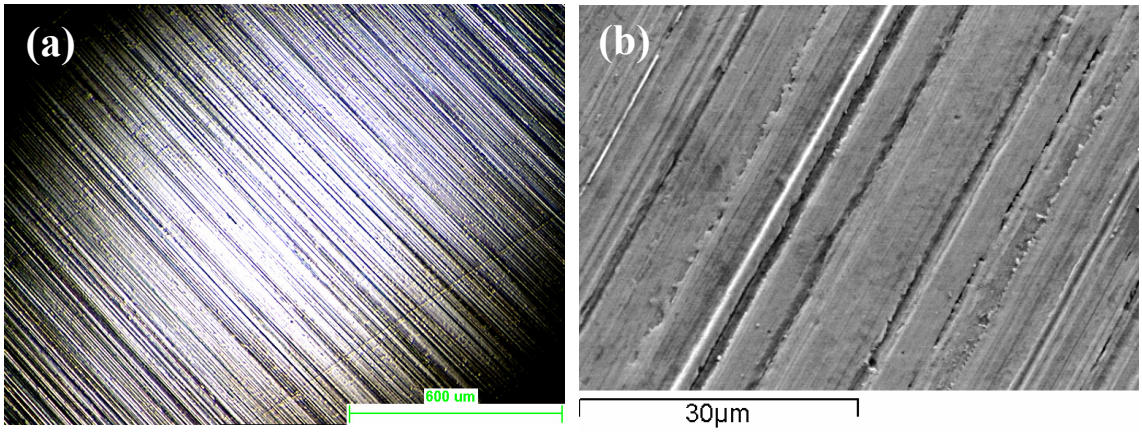

Figure 141 - Pictures displaying the typical quality of a ball's surface when produced using a #500 MRB-CBN wheel in a free-cutting condition. - (a) Low mag. optical microscope image, (b) SEM image.

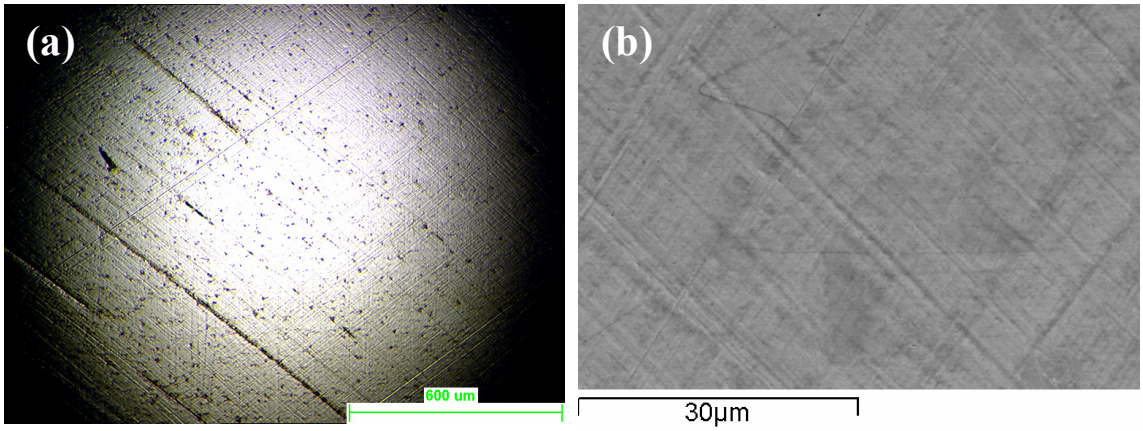

Figure 142 - Pictures displaying the typical quality of a ball's surface when produced using a #500 MRB-CBN wheel in a glazed condition. - (a) Low magnification optical microscope image, (b) SEM image.

As the wheel glazes, its surface becomes smooth, the abrasive dulls and wear flats are formed. This turns the grinding mechanism from one where material is removed and the surface is scored with grinding marks, to one where the surface features are flattened and material is not removed. There is an improvement in surface finish associated with a lack of grinding marks.

16.2.2 Ball surface produced with a #2000 MRB-CBN wheel

Of particular promise is the high quality and repeatability of surfaces produced with a #2000 MRB-CBN (8 µm) wheel. As the quality is satisfactory and a relatively large abrasive is used, the processing time can be reduced (60 seconds from honed when either Elid 2 or Elid 3 superfinishing). Again the surface quality of the ball is dependent on the condition of the wheel. In a free-cutting condition, very fine grinding marks are just visible to the naked eye and can be seen clearly with a microscope (figure 143).

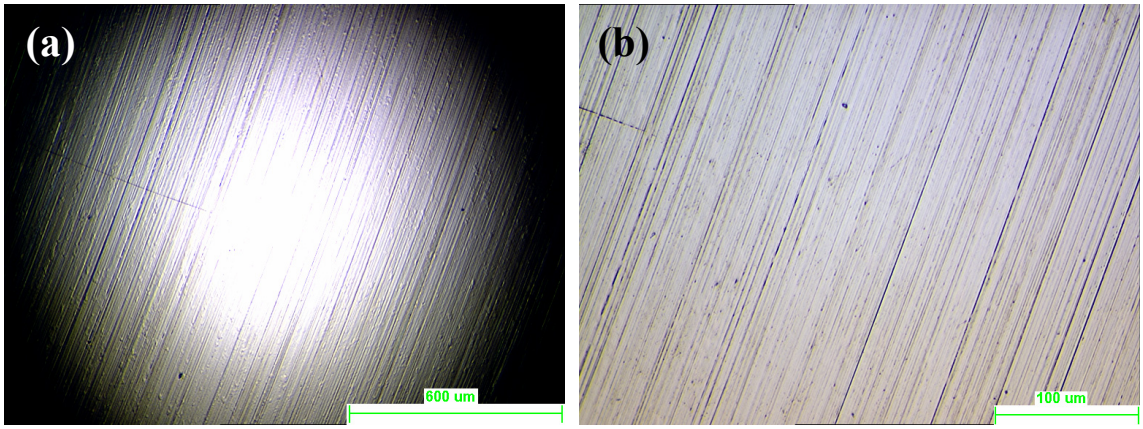

Figure 143 - Optical microscope image displaying the typical quality of a ball's surface when produced using a #2000 MRB-CBN wheel in a free-cutting condition. - (a) Low magnification, (b) High mag.

When the wheel is glazed the surface produced appears to be of the highest quality and very similar to those produced with finer abrasive wheels (figure 144). However, superfinishing with a glazed wheel is less effective at cutting the carbides in the surface of the ball, which increases the surface roughness.

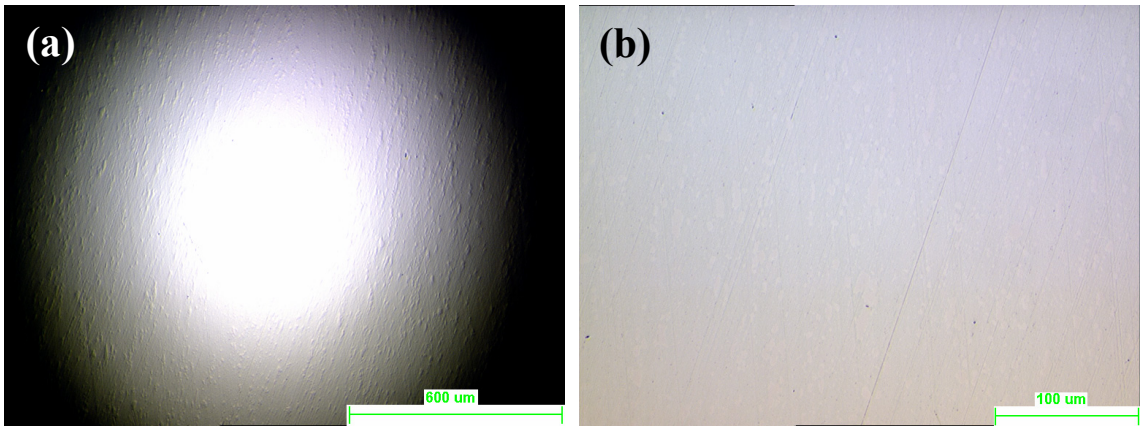

Figure 144 - Optical microscope image displaying the typical quality of a ball's surface when produced using a #2000 MRB-CBN wheel in a glazed condition. - (a) Low magnification, (b) High magnification

When Elid superfinishing using #2000 wheels and finer, a visually improved surface quality and a sharp mirror surface finish is achieved. The reflectivity of a surface does not necessarily denote an improvement in surface quality. However throughout this research, analysis under the microscope has been in very good agreement with the talysurf measurements. Visual inspection, including basic methods of magnification and comparison, provide an easy way to assess the surface quality during experimentation or a production batch. The required quality of a ball can be determined by the absence of surface features visible under the microscope.

16.2.3 Ball surface produced with a #12,000 MRB-CBN wheel

Generally the quality of the surfaces produced with wheels ranging in mesh size from #4000 to #120,000 (4µm - 0.13µm) have been of an equivalent standard (figure 145). Quality depends as much on the idiosyncrasies of a particular set-up as on the size of the abrasives used.

Compared to the larger abrasive wheels, the condition of the #12,000 wheel has less influence on ball finish. The grinding marks produced are very small, therefore uncut carbides become the predominant factor in determining the surface roughness of the ball. The benefits gained from reducing the very fine grinding marks through glazing are largely eliminated by the inefficient cutting of the materials carbide phase.

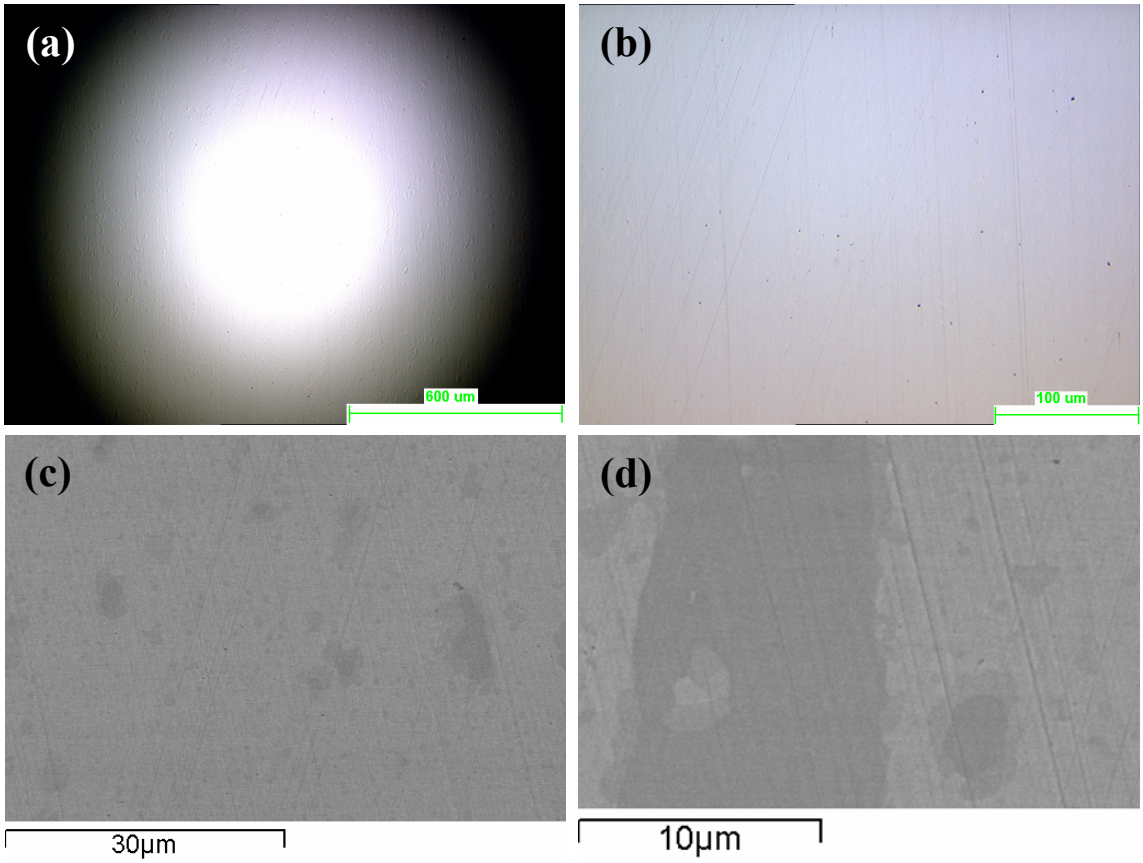

Figure 145 - Pictures displaying the typical quality of a ball's surface when produced using a #12,000 MRB-CBN wheel. - (a & b) Low and high magnification optical microscope images, (c & d) SEM images

16.2.4 Ball Hardness and Structure

There was no difference in the hardness measured on the ball's spherical surface before and after Elid superfinishing. There was no evidence of surface smearing and the carbides were effectively cut, rather than remaining protruding or being plucked from the ball's surface.

16.3 Comparison of standard NMB and Elid superfinished balls

When comparing Elid with standard superfinished balls, results show an improvement in Ra surface finish in all Elid superfinished balls (figures 146 - 148), except for those produced using a #500 wheel. Likewise additional finish parameters Rq, Rp, Rv, Rz, and Rt also reduce. Surface slope (Rdq) is generally reduced through Elid superfinishing. This parameter is often considered an important factor in reducing friction, adhesion and wear; lower values achieving lower friction. Averaging data sets records a general increase in kurtosis (Rku) when Elid superfinishing. Although smaller, the surface perturbations can be sharper. The skew of the surfaces assessed varied with no pattern identified.

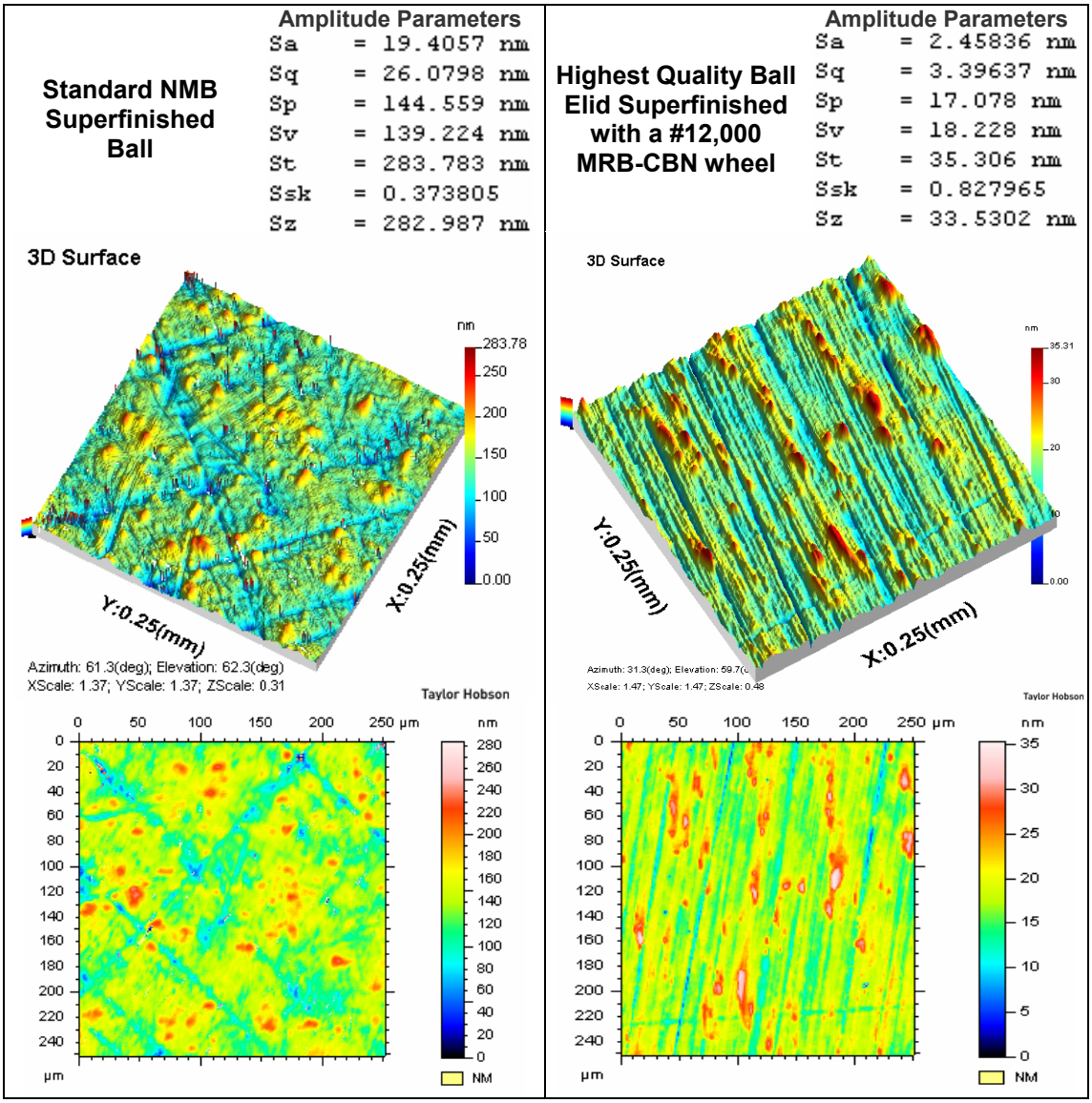

Figure 146 - Comparison of standard NMB and Elid superfinished ball surfaces

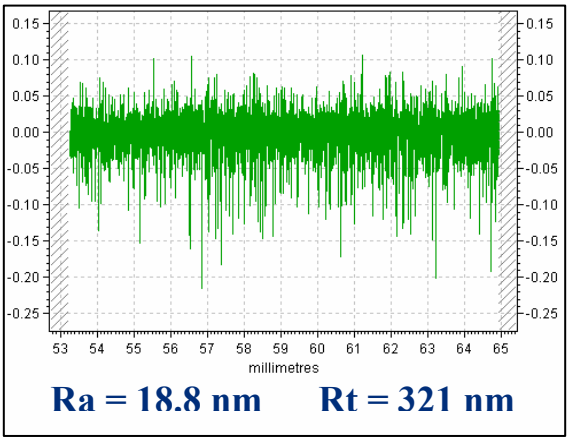

Figure 147 - Standard NMB Superfinished

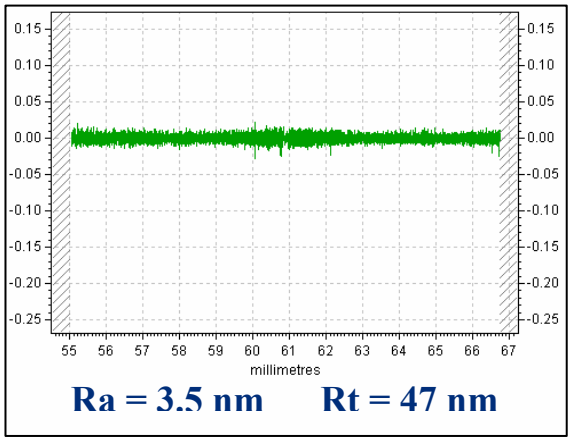

Figure 148 - Elid Superfinished #8000 wheel

16.4 Variation in Surface Quality

Data from a variety of experimental runs is combined in figure 149 in order to demonstrate the range and consistency of ball surface finish. All surfaces are fully formed by the individual wheels, with the data representing the range and variance in surface finish resultant when Elid 3 superfinishing with wheels of differing abrasive sizes. The two lines represent the roughest and smoothest surface finish results achievable across the abrasive range.

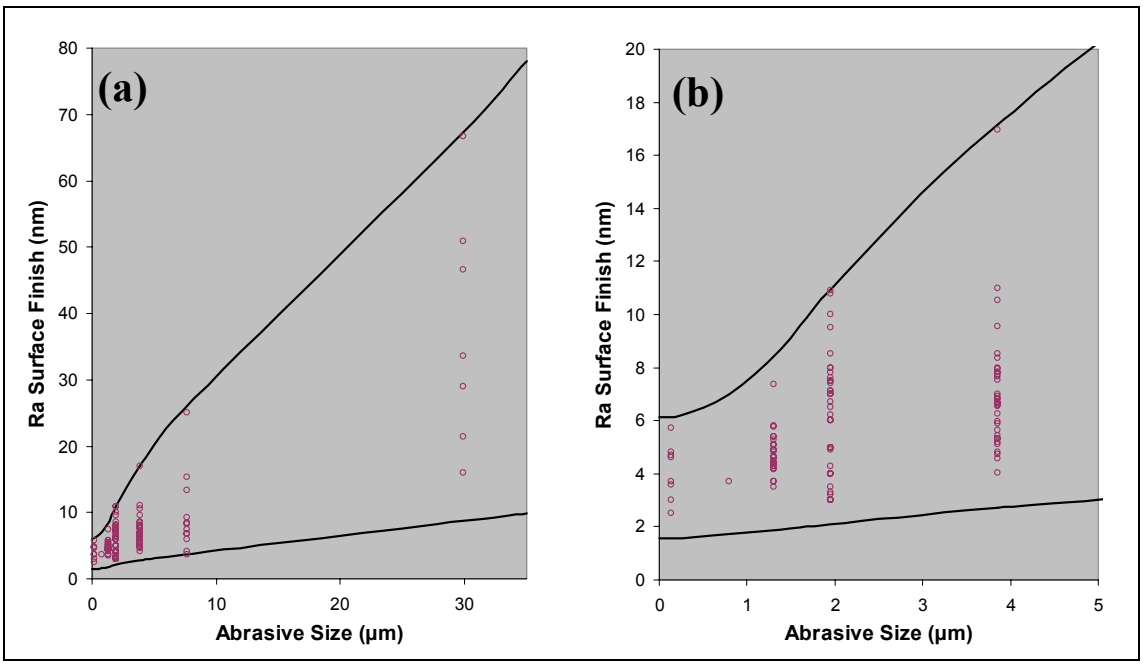

Figure 149 - Surface finish V's abrasive size from a variety of experimental runs -
(a) Full graph, (b) magnified fine abrasive portion of the same graph. [talysurf measurements]

Elid surfaces produced during experimental runs (Elid 3) have been consistently of a very high standard during some experiments but of a lesser and inconsistent quality during others. The development of the process ultimately reduced these inconsistencies. The variation in ball quality that occurred within a batch when processing using the same parameters is shown in figure 150. This provides a visual impression of the consistency of the surface produced.

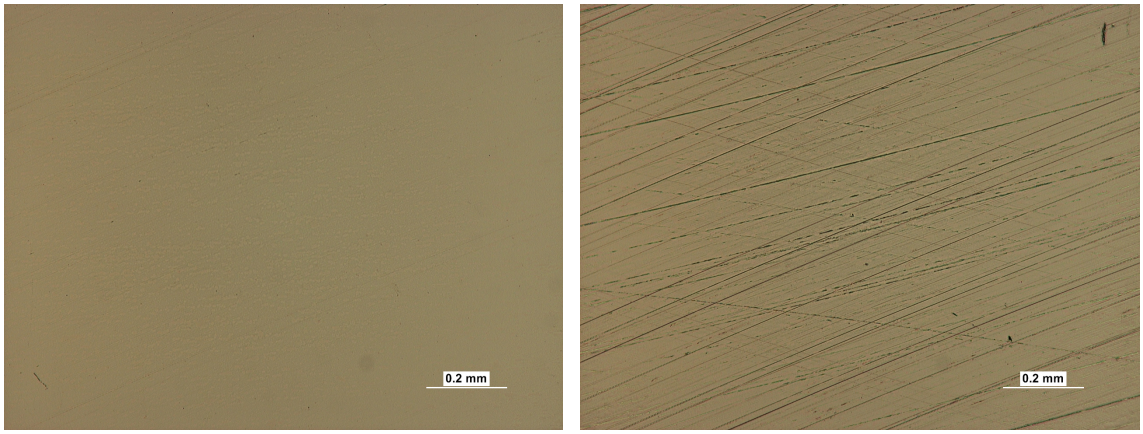

Figure 150 - Variation in ball quality within a batch of RBFB16AB balls produced with a #20,000 MRB-CBN wheel and Elid 3 - (a) Highest quality ball produced, (b) Lowest quality ball produced.

16.5 Analysis of Ball Defects & Deposits

A number of defects can be introduced onto a ball's spherical surface during standard production and as a direct result of the Elid superfinishing process. The defects discussed in this section are not insurmountable problems and their presence can be either reduced or eliminated.

16.5.1 Deposits on the surface of the ball

Through the use of Elid, three different copper deposits have been electro-chemically deposited onto the surface of various balls. Although distinct in appearance, EDX analysis revealed that they are all forms of copper.

(1) Figure 151 an adhered layer of copper plate, reddish gold in appearance.
(2) Figure 152 a black powder of copper particles that can easily be removed.
(3) Figure 153 a semi-adhered layer of copper oxides and compounds, which is black / green in appearance and can be removed if cleaned.

These deposits appear both in isolation and in conjunction with each other and form as a result of the reduction reaction occurring at the cathode (the ball). When considering the deposits that form on the surface of the ball, it is worth noting the similarity of Elid to an electro-plating process. The oxidation reaction at the anode (the wheel) involves copper ions being removed into the electrolyte fluid. Copper, in particular, can easily reform at the anode. Whether, and how, the copper ions combine with electrons at the ball determines the formation.

Although the controlling factors were not identified, the exact conditions during Elid processing are thought to determine the formation. The confined environment of this type of superfinishing restricts the access of superfinishing fluid to the grinding interface, and may concentrate the soluble and non-soluble oxide or salt. Deposit formation throughout testing was somewhat erratic. On some occasions deposits formed very easily and at other times they did not. Although all deposits have been seen when both new and old fluid it used, new fluid appears to increase the ease with which deposits can form. Other Elid 3 systems that used copper-based wheels referred to in the literature review did not highlight the problem of depositing copper onto the workpiece. They did not have the additional problem of restricted fluid penetration and access; however it is believed that they would have experienced problems with deposits.

Figure 151 shows pictures of an adhered layer of copper which has plated-out on the ball's surface. Picture (a) was taken with a plain white background reflected in the ball's surface in order to reveal the defects more clearly. The same ball, as it appears to the naked eye, is shown in appendix G4 along with additional pictures of the various copper deposits. EDX analysis of the deposit on this ball showed a marked increase in copper content when compared to a standard NMB superfinished ball from the same batch.

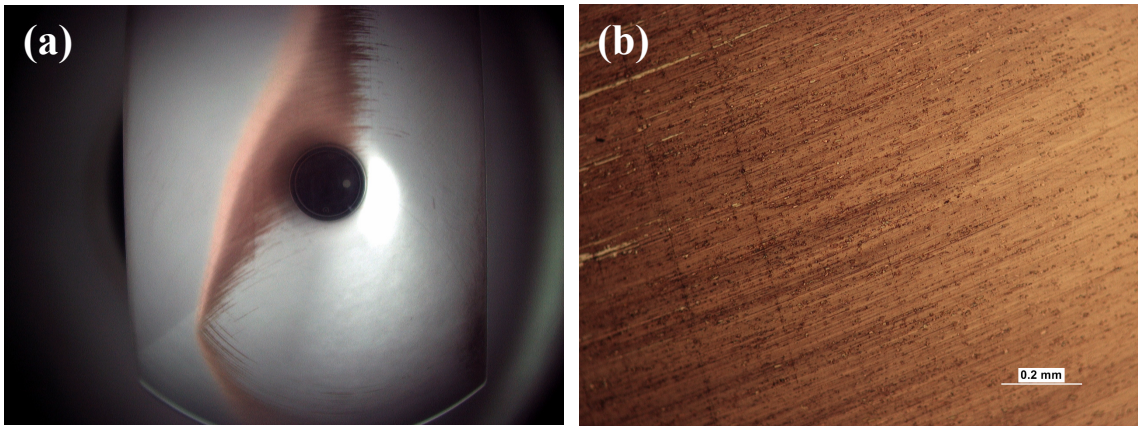

Figure 151 - Pictures of copper which has plated-out onto the surface of an RNDEB14 ball after Elid processing with an #8000 MRB-CBN wheel. (a) Full ball picture, (b) Optical microscope image

The second deposit is a black powder, which forms on the surface of the ball when Elid dressing is performed with a separation gap between the ball and wheel. With the appearance and characteristics of black soot (figure 152), this layer can be easily removed. Transferring it onto conductive tape and analysis with EDX revealed that these were copper particles of short range order.

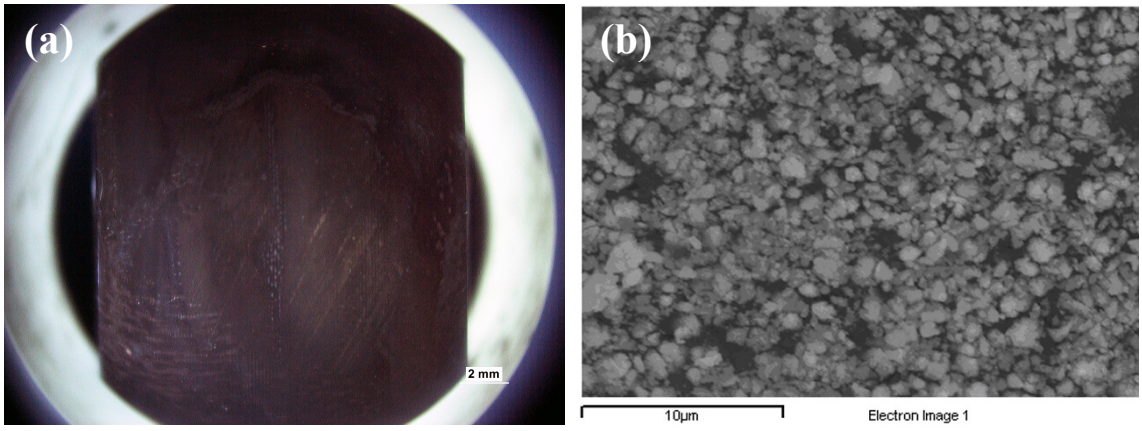

Figure 152 - Black powder of copper particles which formed on the surface of a ball after EDT followed by pre-process dressing. (a) Full ball picture, (b) SEM image of powder transferred to conductive tape.

Figure 153 shows a ball surface produced after Elid superfinishing with an #8000 MRB-CBN wheel. The surface is free from defects and is of the usual high quality on the right side. On the left side there is a semi-adhered black-green coating of copper, that has formed on top of a layer of adhered copper plate. Although quite sticky, the black-green deposit can be wiped off the ball's surface using an alcohol-based cleaning fluid. Again this deposit can form in isolation and appears quite distinct when viewed under a microscope.

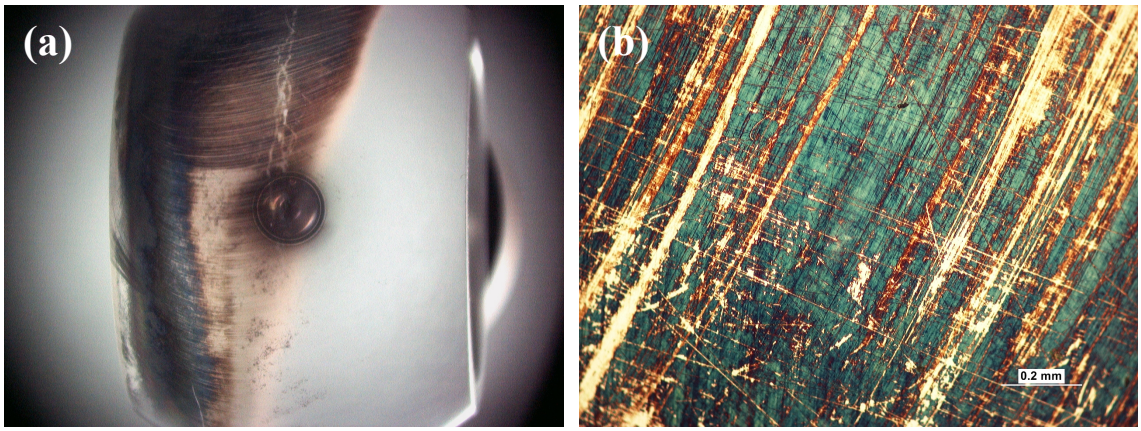

Figure 153 - Pictures of electro-chemically deposited copper on the surface of an RNDEB14 ball after Elid superfinishing with an #8000 MRB-CBN wheel. (a) Full ball picture, (b) Optical microscope image

When Elid superfinishing, the various copper deposits are only able to build up where the ball is not in contact with the wheel. If the wheel and ball make full contact, the wheel removes the deposits as they are formed, even if aggressive dressing occurs. When pre-process dressing with a separation gap, the copper can be evenly distributed over the surface of the ball. The deposits form on the ball in the most energy efficient place, that is, the closest point where grinding contact between the ball and wheel is broken. This occurs predominantly at the edges of the spherical surface.

Figure 154 shows the initiation of the black-green, semi-adhered copper deposit forming on the edge of the ball's spherical surface. When Elid 3 superfinishing a batch of 22 balls with an #8000 wheel, this mottled green deposit appeared on 13 of the balls. When measured, the surface finish in this area resulted in an Ra value of 48 nm; ten times greater than the unaffected area of the bearing. The size and shape of the mottling appears to match the carbide phase of the material. The electrolytic fluid had recently been changed.

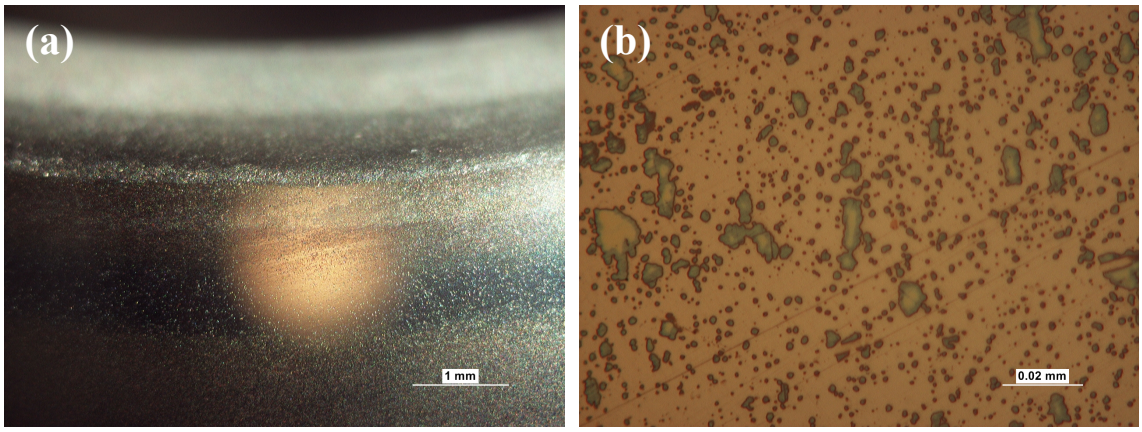

Figure 154 - Pictures of a mottled green deposit semi-adhered to an RNDEB14 ball after Elid processing with an #8000 MRB-CBN wheel. Optical microscope images at the edge of the ball's spherical surface. (a) Low magnification image, (b) High magnification image

When Elid 1 superfinishing, the problem of copper depositing onto the ball still remains, even though the ball is insulated from the Elid power supply. Copper still deposits when full grinding contact does not occur, because the ball is surrounded by a negative electric field and is in close proximity to high power-carrying elements.

In addition to depositing material at the edge of the ball, the creation of an electro-chemical cell between the ball and its fixturing can result in oxidation of the ball at its edge. This manifests itself as etching of the ball's surface, which appears to correspond to a preferential attack on the chromium carbide phase.

Turning the Elid power supply off 2 to 30 seconds before the end of the superfinishing cycle eliminates the problem of deposit formation, providing the entire surface of the ball comes into contact with the wheel. Within this time any deposits formed on the ball are removed by the abrasive action of the superfinishing process or mechanically transferred back onto the wheel's surface.

16.5.2 Pitting

During Elid 3 superfinishing, electrical sparking can occur between the ball and wheel because the anode and cathode are in dynamic contact with each other. The electrical discharge can cause pitting on the surface of a ball (figure 155) and therefore must be prevented.

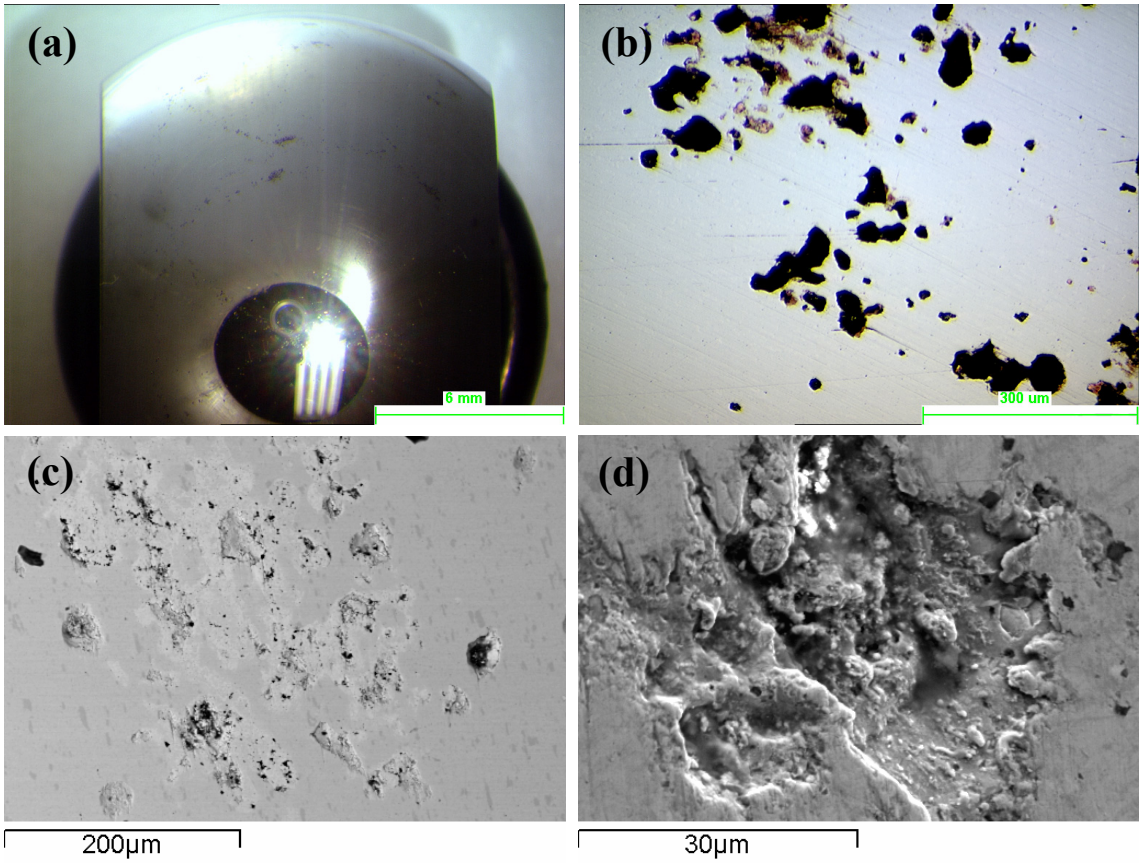

Figure 155 - Pictures of electrical sparking damage to an RNB08 ball's surface after Elid 3 superfinishing. (a) Full ball picture, (b) Optical microscope image, (c) Backscatter SEM image, (d) SEM image of crater

Pitting occurs very extensively on balls used for electrode discharge truing but it has also been observed during superfinishing. It occurs most prevalently when grinding contact is either initiated or broken, with the power supply switched on. For this reason the Elid power must be off, or directed away from the grinding zone, when contact is in transition.

As reported in Elid 3 honing and grinding literature, using reduced power levels minimizes but does not eliminate this problem. To reduce the risk of electrical sparking occurring when Elid 3 superfinishing, low electrical power settings are used (low open voltage and current). However, this also reduces the aggressiveness and effectiveness of the Elid dressing.

During Elid 1 superfinishing the ball is insulated from the electrical circuit; during Elid 2 the power supply is off when superfinishing. As a result they are much less susceptible to sparking damage and it was not generally an issue.

16.5.3 Burning

Workpiece burning (figure 156) was observed when superfinishing with the #500 wheel but not with the finer mesh wheels. This is the reverse of what might be expected, as finer abrasive wheels are generally less efficient at removing heat from the grinding zone.

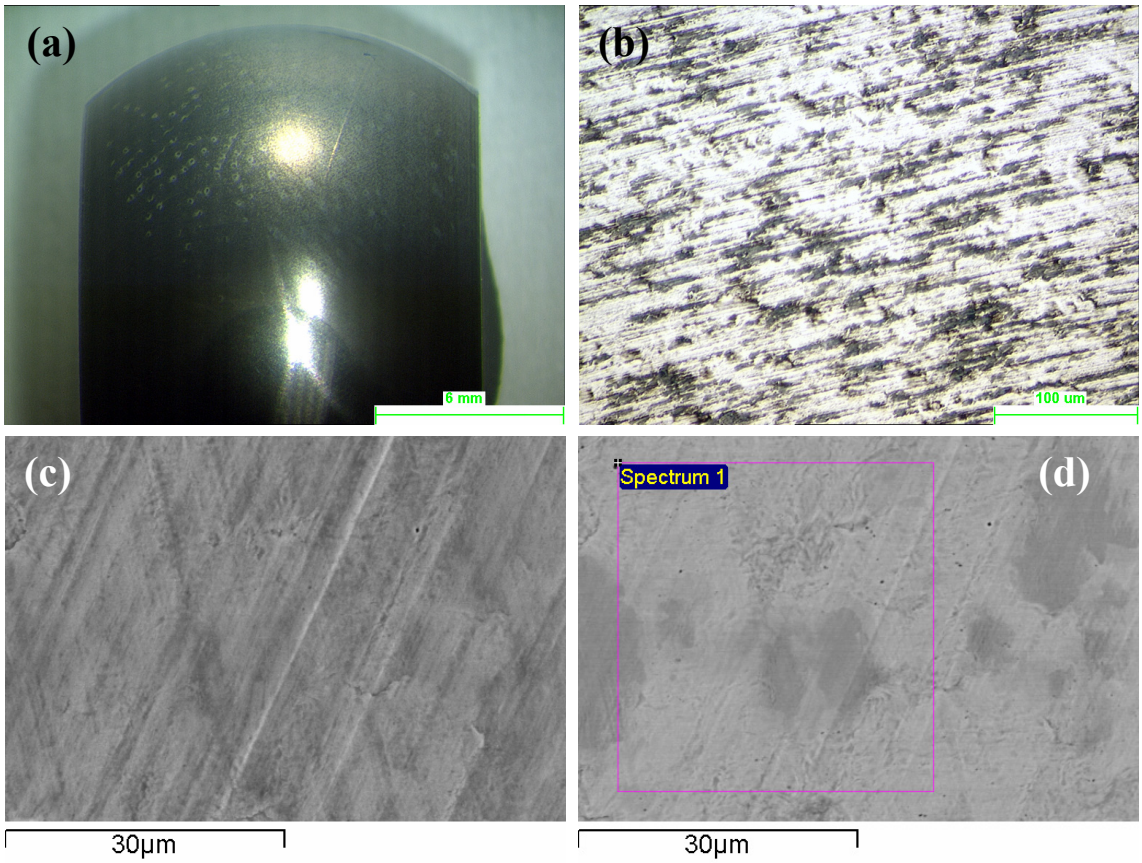

Figure 156 - Pictures of burning on the surface of an RNB08 ball after Elid superfinishing with a #500 MRB-CBN wheel - (a) Full ball picture, (b) Optical microscope image, (c) SEM image, (d) Backscatter SEM image

Slightly elevated levels of copper were recorded (1.55 wt%) when a burnt surface was analysed using EDX, however it is not believed to be a copper deposit, as the surface of the ball becomes blackened when processing with the Elid power switched off. This has also been observed when Elid is not used, ruling out the possibility of it being Elid related. The burning of the surface is related to the condition of the wheel and a decrease in the ball material removal rate. It was most prevalent when the wheel was glazed, and when both the wheel wear and ball material removal rates were almost zero. This caused wear flats to form on the CBN abrasives, increasing localised friction and heat. The burning of the surface when using a #500 MRB-CBN wheel was a persistent problem which contributed to this wheel being considered ineffective and ultimately unusable.

16.5.4 Digs

Digs on the surface of the ball have been observed sporadically throughout Elid superfinishing runs and have also been seen on standard NMB superfinished samples.

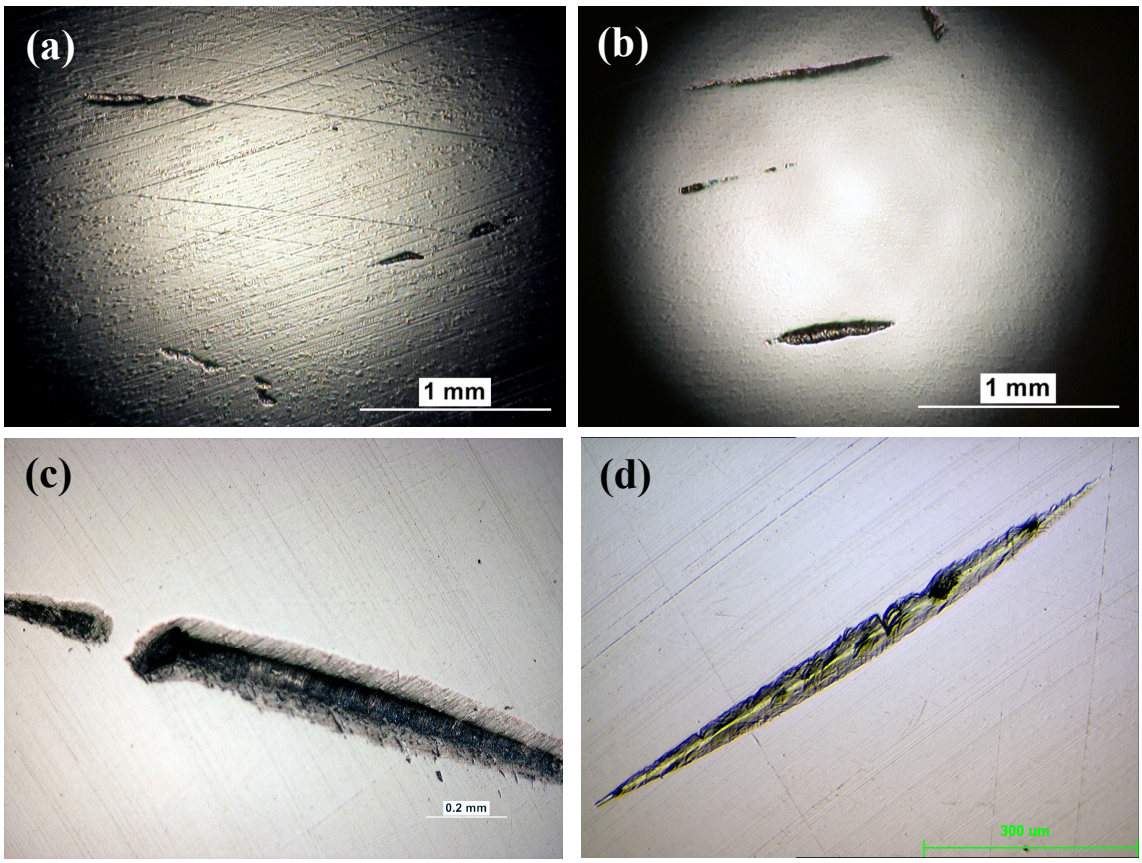

Figure 157 - Optical microscope image of digs on the surface of various balls.
(a) on standard NMB superfinished ball, (b, c, d) on Elid superfinished balls

Shown in figure 157, they have been recorded as large as 2 mm in length, occurring both in isolation and in small groups. They generally appear to be elongated in the same direction as the grinding marks. Possible causes include: (1) re-circulation of old large abrasives, (2) snagging of broken wheel edges, and (3) plucking of carbides.

Figures 157b & c show digs which are thought to have been introduced somewhere in the standard NMB process chain, then subsequently Elid superfinished. The dig in figure 157d was introduced by Elid superfinishing. The impact that digs have on the life of a bearing is not considered to be excessively large, as they are valleys contained within an otherwise smooth surface.

16.5.5 Ball Storage Damage

Damage can be caused to the balls' spherical surface as a result of poor storage and handling. Although the balls are hardened, their mirror surface finish is more vulnerable to damage. Even measuring a ball's O/D with a comparator gauge or micrometer can introduce identifiable marks. Figure 158 shows the damage that was caused as a result of swarf rubbing against a ball which was poorly stored.

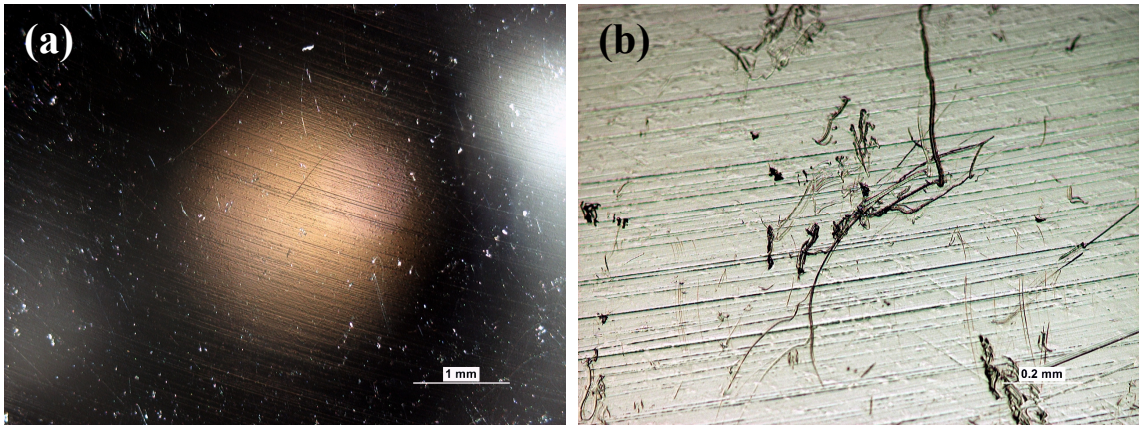

Figure 158 - Optical microscope images of damage to an RBFB16AB ball's surface caused by poor storage. (a) Low magnification image taken with additional lighting to highlighting the balls damaged surface, (b) Medium magnification image.

Defects introduced onto the ball's surface after Elid processing can reduce or negate the benefits of achieving a super smooth surface. If the surface is damaged before Elid processing, additional processing time may be required in order to fully remove the defects. The balls should be inspected after complete bearing assembly and additional consideration should be given to protecting the balls during storage and swaging, as well as sealing the bearing unit during its use.

Chapter 17 - System Set-up

The spherical form of the ball is self-generated during superfinishing. However, there are a number of elements that can affect it. Ensuring that there is accurate alignment, good concentricity and full conformity between the ball and wheel is fundamental when superfinishing spherical bearings. When these factors are not achieved the balls will possess inadequate sphericity and poor surface finish will be achieved. Even slight errors will result in an uneven pressure distribution between the ball and wheel. Larger errors can result in the superfinishing process moving from an area contact to a line or point contact. The metal-resin wheels used for this process are fragile and geometric errors in set-up often result in wheel failure.

17.1 Ball to Wheel Conformity

The contacting surfaces form a perfect area contact, assuming there is perfect alignment and concentricity. When correct alignment exists but the diameter of the wheel's grinding surface is larger than that of the ball, a circular line contact results between ball and wheel (figure 159). As there is no superfinishing contact at the edge of the ball, a usable product is not produced. Balls produced under these conditions (figure 160) show a cross hatch patterning over the centre region of the ball, with a circumferential line at the ball edges indicating the point where contact was lost. If left unchecked, the wheel will eventually wear so that it will conform enough to contact the ball at the edges.

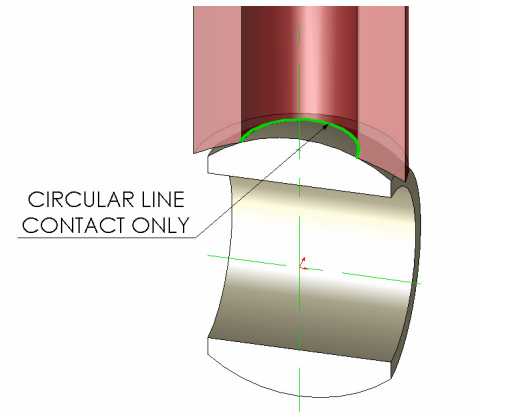

Figure 159 - Wheel's grinding surface diameter larger than that of the ball. (Over-formed)

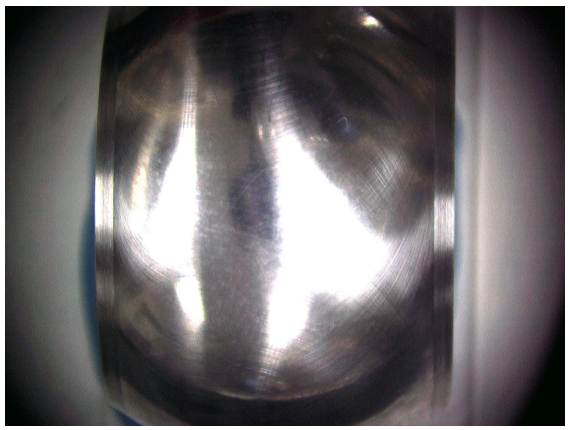

Figure 160 - Example of ball produced with an over-formed wheel. [#500 MRB-CBN, Elid 3]

In a similar manner, when the diameter of the wheel's grinding surface is smaller than that of the ball, a circular line contact is made which extends over the edges of the ball (figure 161). As the entire surface of the ball can be ground with this circular line contact, a usable, though not ideal, output is achieved from the start. As the wheel wears full contact will occur between the ball and wheel.

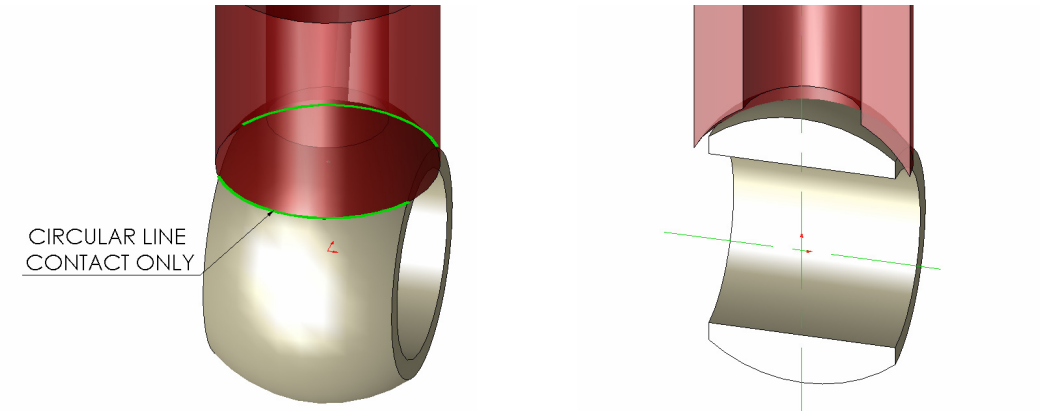

Figure 161 - Wheel's grinding diameter too small. (Under-formed)

When full contact is lost between the ball and wheel during processing, copper deposits are likely to form on the ball's surface, as previously discussed. The conformity between ball and wheel also affects the fluid's ability to penetrate the grinding interface and thus the effectiveness of Elid 3 and the process as a whole. Better surface finish results have been achieved when increased conformity exists.

Unlike conventional superfinishing, the superabrasive Elid wheels used do not self-sharpen and wear at a slower rate. This slower rate inhibits the degree to which the wheel beds into the ball being processed. This results in the ball predominantly adopting the form of the wheel, taking into account the degree of misalignment, concentricity etc. However, as new balls are continually introduced during a set of experiments or during a production run, it is the shape of a batch of balls that will ultimately determine the shape of the wheel.

Processing a ball at the upper end of the O/D tolerance causes the wheel to be under-formed relative to the nominal ball size. This can cause problems when a batch of balls at the lower end of the O/D tolerance is processed. Wheels are more likely to fail, or chip at the edges, when they are under-formed.

Balls that are ‘up at the edges’ make initial contact with the wheel at the edges; the area of contact moving inwards as form is created (figure 162 a&b). The cylindrical grinding operation intentionally processes balls to be ‘up at the edges’, as this ensures that the form is generated most effectively by the subsequent honing operation. When balls are ‘down at the edges’, parallel line contact is initially achieved in the centre of the ball which progresses outwards as the ball’s spherical form is created (figure 162 c&d).

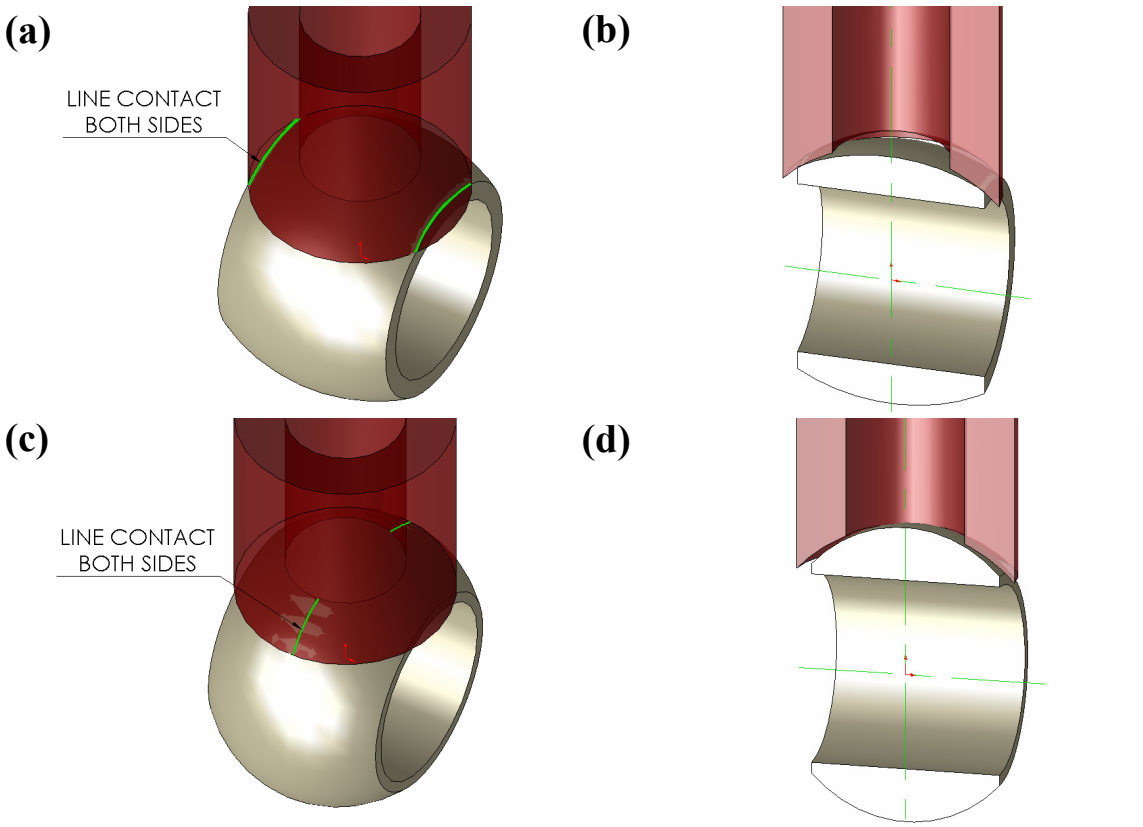

Figure 162 - Error in ball form. – (a & b) Balls with an input form that is ‘up at the edges’. (c & d) Balls with an input form that is ‘down at the edges’.

17.2 Ball & Wheel Alignment

A combination of superfinishing marks and roundness results can be used to determine that the correct geometric set-up is achieved. When the correct geometric set-up is realized a cross hatch patterning of superfinishing marks is formed on the surface of the ball. The grinding pattern is visible to the naked eye when using coarse abrasive wheels such as the #500 but not when finer mesh wheels are used.

When running with an x-axis misalignment, a point contact is made in the plane shown in figure 163. As wheel wear occurs, the wheel's grinding diameter will increase and conform to a line contact in this plane. The wheel will not wear to achieve an area contact. A ball produced with an x-axis misalignment is typified by a cross hatch patterning on one side of the ball only. X-axis misalignment will eventually result in the ball being elliptical rather than spherical. When running with a y-axis misalignment, a point contact is made in a perpendicular plane (figure 164). This progresses to a line contact and there is an increase in the wheel's grinding diameter. Once again area contact is not achievable. A ball produced with a y-axis misalignment is typified by pronounced half arc patterning, on the centre of the ball only.

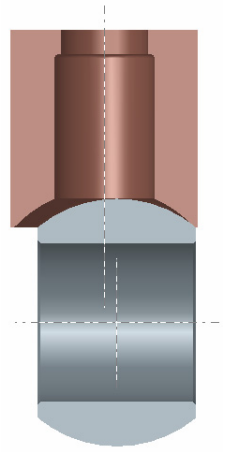

Figure 163 - X-axis misalignment

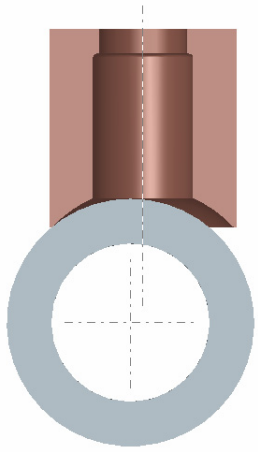

Figure 164 - Y-axis misalignment

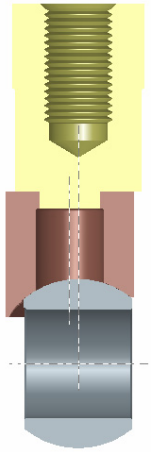

Figure 165 - Poor wheel concentricity

Wheel concentricity errors where the rotation of the wheel is on the centreline of the ball can cause significant problems if the wheel has not been trued or has not worn into the rotational path. Once it has worn in, full spherical conformity will be achieved (figure 165) even though concentricity remains poor. Accurate *ball* concentricity is required in order to maintain full conformity and produce round balls. A small amount of error can be accounted for by the spindle deflection and spring loaded wheel

The accuracy with which alignment must be achieved is dependent on the stiffness of the system. The ball faces are ground with a relatively large 76 μm tolerance bandwidth on the spherical centreline. As the balls are manufactured from a datum point on either of the ball faces, the system must be able to accommodate this potential error. In addition, the bore is ground to a concentricity tolerance to the spherical of 25 μm. The fixturing described in chapter 13 must be able to accommodate these potential errors, in addition to installation and spindle rotational errors. The use of a roller-centric fixturing method, an alternative fixturing method employed at NMB to produce spherical bearing balls, does not constrain the ball in such a manner.

17.3 Ball to Wheel Speed Ratio

Converting spindle speeds (rpm) to comparative wheel surface speeds (m/s) provides a more consistent comparison between balls of differing size. Wheel speed is calculated as the speed of the wheel at its O/D. For example, tests outlined in chapter 23 investigated wheel speeds of 3, 4 and 5 metres per second which converted to 3341, 4454 and 5568 rpm respectively. Similarly ball speed is calculated as the speed of the ball at its crown relative to a static wheel. For RNB08 balls, speeds of 1, 2 and 3 metres per second convert to 963, 1926 and 2889 rpm respectively. The ratio of these speeds controls the pattern of grinding marks introduced onto the ball's surface. Variation in spindle speeds in chapter 23 resulted in wheel to ball speed ratios of 1:1, $1^2/_3$:1, 2:1, 3:1, and 5:1, although a greater range was investigated over the course of the research.

The relative speed between the ball and wheel varies considerably depending on the point of measurement. The speed at the inner edge of the wheel is lower than the outer edge, and the speed of the ball at the crown is larger than at the edges. The combined speed of the wheel and ball (the true grinding speed) on one side (the right) is higher than on the other (the left). The ball is 'up ground' with a higher relative speed due to the addition of the ball speed to the wheel speed at the right edge. Depending on the ball and wheel speed used, the subtraction of the ball speed from the wheel speed either results in a lower relative speed as the ball is 'down ground', or as with the standard honing process, a negative value as the actual grinding direction is reversed. At the middle of the ball, the wheel's motion is perpendicular to that of the ball. The final superfinishing pattern is a skewed cross hatch with the combined speed determining the degree of skew or reversion of grinding direction (figure 166).

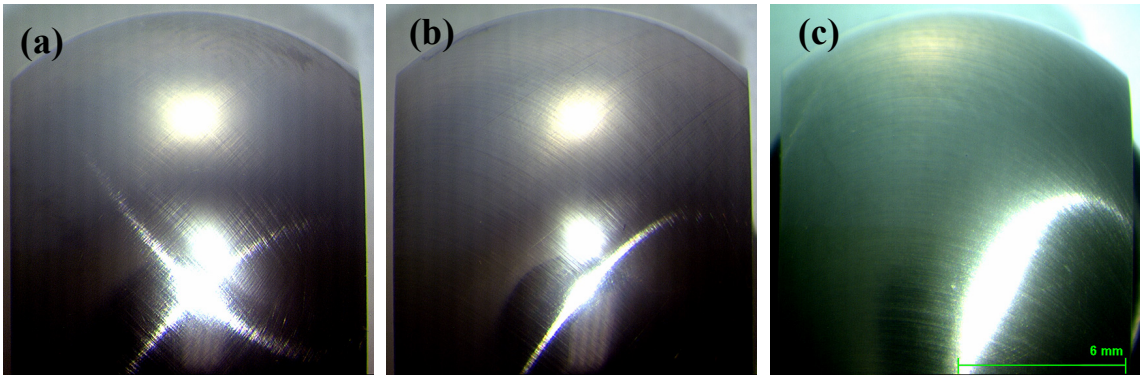

Figure 166 - Pictures showing the degree of skew to the cross hatch pattern resultant from various wheel : ball ratios. – (a) Standard honed ball estimated 1 : 1 ratio, (b) #500 Elid 1 superfinished 1.3 : 1 ratio, (c) Darmann Number 2 wheel 5 : 1 ratio.

17.4 Initial investigation of System Compliance

The machine tool including the ball and wheel are of course not rigid bodies; the compliance of the system in reality reduces the effects of poor set-up to some extent. Mounting the superfinishing wheel against a rubber washer is standard practice for the current NMB honing process. This adds flexibility to the superfinishing system, lessening the influence of errors in alignment and aiding full conformity between the ball and wheel. The use of a rubber washer was tested on the Grieshaber machine at NMB in order to investigate whether added flexibility would improve results when Elid superfinishing.

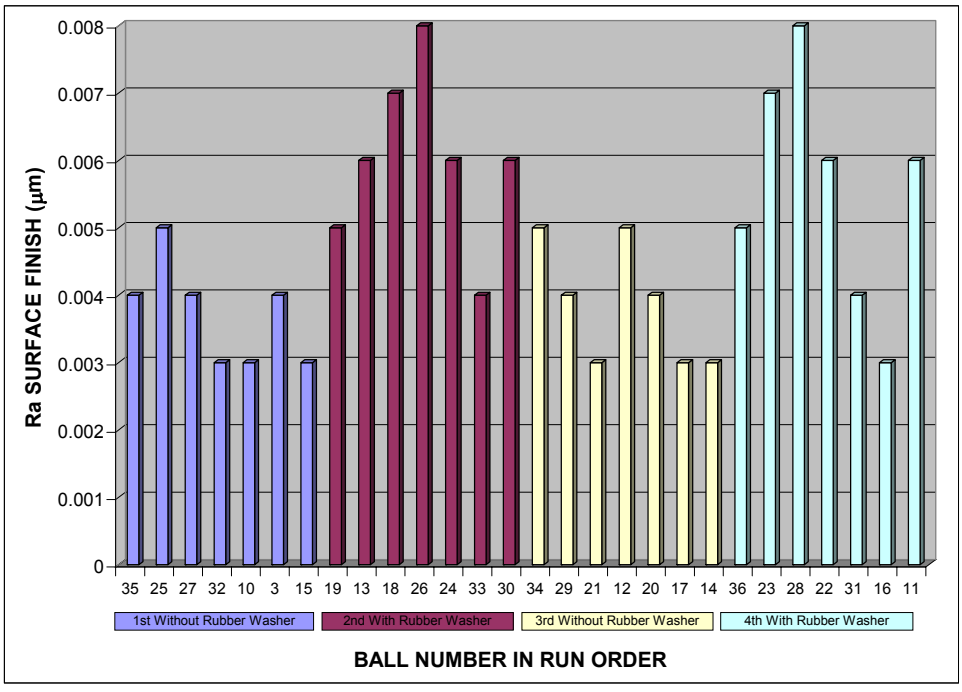

Figure 167- Final Ra surface finish results of RBFB16AB balls showing variation with and without the use of a rubber washer - [Measured across ball centre, Mitutoyo talysurf]

The results, shown in figures 167 & 168, demonstrate that the rubber washer did not improve ball surface finish. On average Ra values of 3.8 nm without, and 5.8 nm with the rubber washer were achieved.

Finish	Without Rubber Washer	With Rubber Washer
Ra (nm)	3.8	5.8
Rq (nm)	4.9	7.4
Rsk	-0.17	0.05
Rku	3.5	3.2
Rp max (nm)	15	24
Rv max (nm)	22	24
Rz (nm)	25	35
Rt (nm)	37	49
Rdq (deg)	0.004	0.004

Figure 168 - Mean ball surface finish values - (RBFB16AB Balls measured 'across' on a Mitutoyo CS-3000 Talysurf)

Roundness	Mean	STDEV	Maximum
Without rubber washer	1.78	0.38	2.25
With rubber washer	2.13	0.42	2.49
Additional tests with an extended run time	4.83	2.93	9.07

Figure 169 - P-V Roundness values (µm) - RBFB16AB Balls measured 'Up & Down' on a Mitutoyo TalyRound

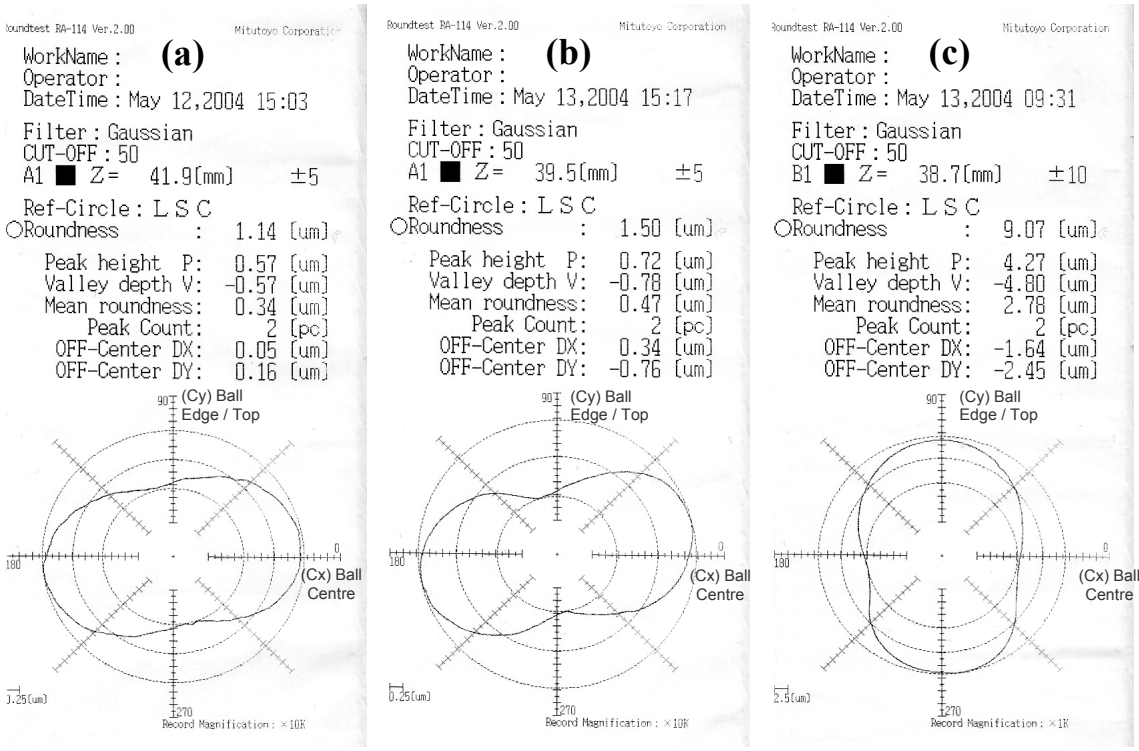

Figure 170 - Roundness measurements taken on RBFB16AB balls after Elid 3 superfinishing. – (a) Best result without rubber washer, (b) Best result with rubber washer, (c) Worst result extended period without washer.

Ball roundness appeared to be slightly worsened by the incorporation of the rubber washer (figure 169). However results generally degraded over the 28 runs possibly because of changes in the wheel shape. Although still within drawing tolerance, Elid runs both with and without the rubber washer produced poorer roundness results than the standard superfinishing processes. Also shown in figures 169 & 170, the poorest results, well in excess of tolerance, were observed when an excessively long run time was used. Balls that had been subjected to a longer run time were ‘up at the edges’ whereas all the other balls were ‘down at the edges’ (figure 170). The more material is removed from the ball the worse the form became. Balls only remained within roundness tolerance because insufficient material was removed to dramatically degrade their form.

On this occasion the results clearly showed a negative effect associated with the use of a rubber washer. This was later determined to be as a result of the rubber washer increasing wheel concentricity / runout and not due to increasing the flexibility in the system. Results presented in chapter 28 demonstrate that a flexible system is better.

Chapter 18

Initial Assessment of Wheel Spindle Power Usage

Assessing the power used by the wheel spindle during superfinishing can provide useful in-process information about various aspects of this process. A set of tests was conducted on spindle power monitoring early in the research and the results are outlined in this chapter.

18.1 Free Running Power Usage

The stated maximum power output of Tetraform's vertical (z-axis) wheel spindle is 2 KW. The range 0 to 10 volts is set to 150% of this figure, 298.4 Watts per Volt. Figure 171 shows the spindle power usage from start-up to 6000 rpm. As would be expected a large amount of power is used initially to reach the required speed and then a lower and constant power usage is used to maintain a particular speed.

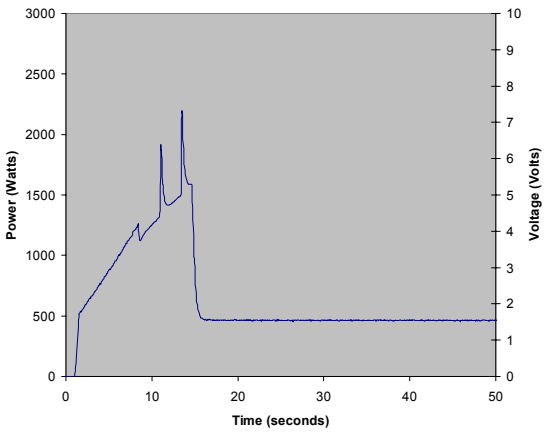

Figure 171 - Plot showing the change in wheel spindle power usage during start-up to 6000 rpm

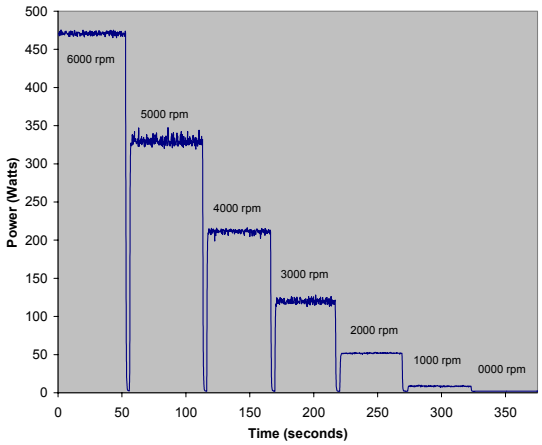

Figure 172 - Plot showing the free running wheel spindle power usage for various spindle speeds

A larger power requirement is called for when maintaining a faster speed compared with a slower speed and this is illustrated in figure 172. Although relatively slight changes to spindle speed produce large differences in the amount of power required, it is easy to accurately and repeatedly control this factor. The amount of signal noise changed when the spindle was set at differing speeds. There is also a small time delay after a speed is selected, until the power levels return to stable values.

This was seen as the power used dropped to zero each time the speed was reduced. This effect was reversed when spindle speed was increased; power levels spiked and then levelled off after about five seconds.

18.2 Effect of Applied Contact Load

As the wheel is brought into dynamic contact with the ball, an increase in power is recorded. The larger the force between the ball and wheel the more power is required to drive the spindles. Figure 173 below illustrates how changes in the contact load affect the power used by the wheel spindle.

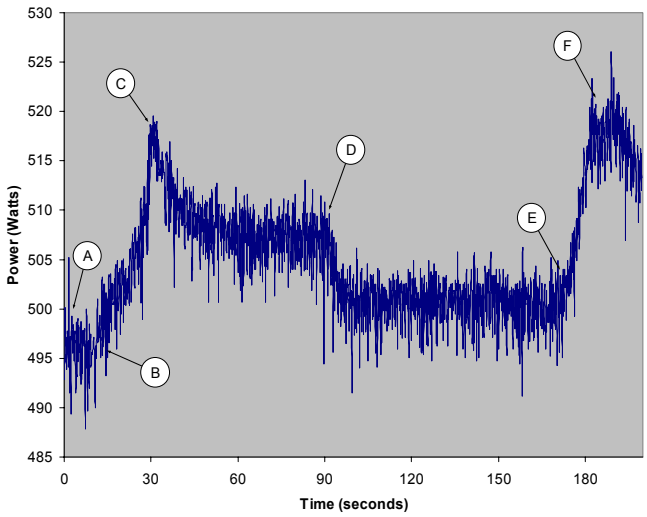

A	Spindles running (6000, 963 rpm). No grinding contact.
B	Contact is made and the spring is slowly compressed
C	5 mm compression reached (50 N, 0.375 MPa). parameters unchanged for 60 seconds
D	Wheel Spindle moved upwards to 2.5 mm displacement (30 N, 0.218 MPa)
E	Wheel Spindle displacement increased to 10 mm (92.5 N, 0.685 MPa)
F	10 mm displacement reached

Figure 173 - Effect of applied load on wheel spindle power - [Run 004, No Elid used]

The effect that the applied load has on spindle power is influenced by the contact conditions between the ball and wheel. As outlined later, variation in these conditions caused the gradual decline in spindle power usage after points (C) and (F).

18.3 Effect of Ball Speed

The ratio of ball to wheel speed also affects the machine power as illustrated in figure 174. The test was run with no Elid used and no electrical contacts in place. The wheel spindle speed was 5215 rpm, and three ball spindle speeds of 700, 963 and 1541 rpm were used. These correspond to ratios of wheel O/D speed to ball O/D speed of 5½:1, 4:1 and 2½:1 respectively.

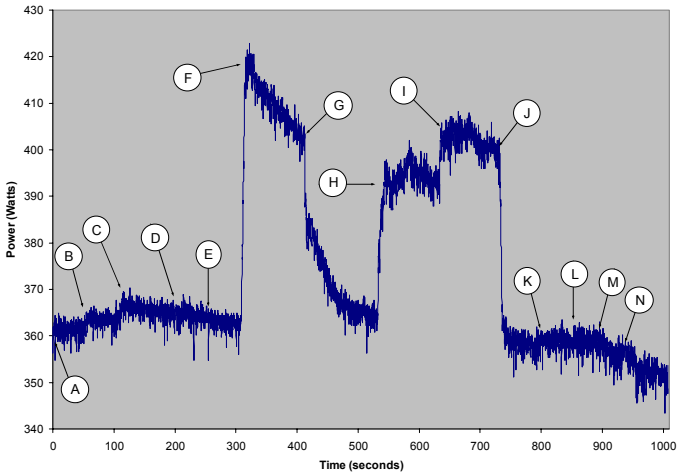

A	Spindles running with no fluid or grinding contact. Wheel : Ball ratio 4:1
B	The fluid is turned on
C	Touch point contact made. (Spark-out conditions, no load).
D	Wheel : Ball ratio reduced to 2½ : 1
E	Wheel : Ball ratio increased to 5½ : 1
F	50 Newtons load applied and held constant for 100 seconds.
G	Wheel : Ball ratio is decreased to 2 ½ : 1 and held for 100 seconds.
H	Wheel : Ball ratio increased to 4 : 1.
I	Wheel : Ball ratio increased to 5½ : 1
J	Load removed and moved back from the touch point position.
K	Wheel : Ball ratio deceased to 4 : 1
L	Wheel : Ball ratio deceased to 2½: 1
M	Wheel moved completely off the ball.
N	Finally the fluid is turned off

Figure 174 - Wheel spindle power usage during changing wheel to ball speed ratio. - [Run 036, No Elid]

The graph demonstrates that larger ball to wheel ratios / slower ball speeds, increase the power used by the wheel spindle. Under simplified conditions of perfect alignment and conformity, the effect of ball spindle speed would be cancelled out on the wheel spindle. However, such conditions are rare and problems such as misalignment between the ball and wheel can cause an increase in pressure on one side of the ball. This means that ball spindle speed will affect the wheel spindle power usage. As discussed in later chapters, the influence of the processing mechanism and its effectiveness also cause ball speed to affect spindle power.

18.4 Influence of Fluid Application

The application of fluid into the grinding interface can cause variation in power values. The exact positioning and repeatability of fluid application into the system is difficult to achieve. Figure 175 shows the difference that fluid positioning can make on wheel spindle power usage. As the fluid is turned on at point (B) a corresponding rise in machine power occurs. Altering the exact position that the fluid hits the grinding interface has the effect of altering the power reading. The largest increases in power are seen at F & G, which correspond to the fluid being directed towards the balancing ring of the wheel fixturing. In addition, a change in power, attributed to a fluid contribution, has been seen when the ball spindle is turned on. This changes the flow dynamic of the fluid entering the grinding interface. These effects need to be taken into account when assessing each individual superfinishing runs. Values should be allowed to stabilize in a dwell position (0.2 mm separation between ball and wheel), prior to applying the grinding force. The effects of fluid on the process are considered in greater detail in chapter 24.

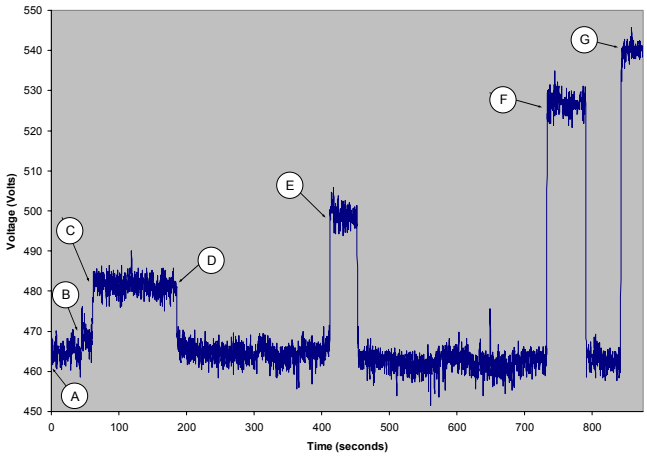

A	Spindles running (6000, 963 rpm). No fluid, grinding contact or electrical contacts in place.
B	The fluid is directed at the grinding interface and turned on.
C	Fluid nozzle position moved but still directed towards the grinding interface.
D	Nozzle is directed away from the interface and rotating fixturing.
E	Fluid directed towards the grinding interface and positioned to achieve highest power level.
F / G	Fluid directed towards balancing ring of wheel fixturing.

Figure 175 - Effect of fluid application on wheel spindle power - [010, 010b & 011]

18.5 Electrical Contacts and Interference

The wheel's electrical connection required for Elid consists of a piece of copper rubbing against the wheel fixturing. This applies an extra frictional force and as would be expected the larger the force, the greater the additional power requirement to drive the spindle. Although values remain stable during normal operation, when the electrical contacts have been moved and then repositioned there is a measurable power difference as it beds itself into its new position.

Due to the fine nature of the superfinishing undertaken there is a reasonably high degree of signal noise within which the required information is held. The spindle power monitoring equipment was affected by the machine tool's power systems and the Elid system. This aspect became less influential as the research progressed, as interference issues were resolved and the amount of power used during optimized Elid 1 runs was proportionally much higher. Increasing the time per measurement from 10 per second to 1 per second smoothed the signal.

18.6 Ball to Wheel Alignment and Conformity

Figures 176 & 177 display changes in the wheel spindle power usage during movement or misalignment of the ball / wheel. No Elid was used and the wheel had a shiny glazed appearance at the start of both tests.

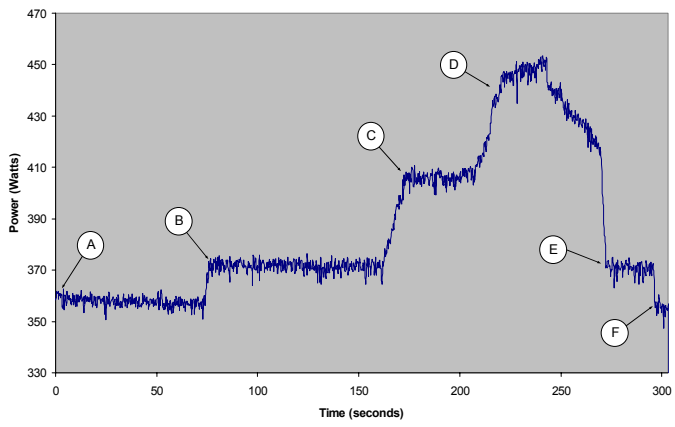

A	Spindles running (5215, 963 rpm), Fluid on, at the touch point
B	Spring is compressed 5 mm (50N load applied, 0.375 MPa)
C	X-axis moved by 10 µm
D	X-axis moved an additional 15µm
E	X-axis moved back to the zero misalignment position
F	The load is removed back to touch point position.

Figure 176 - Wheel spindle power usage as the x-axis is moved during superfinishing. - [037]

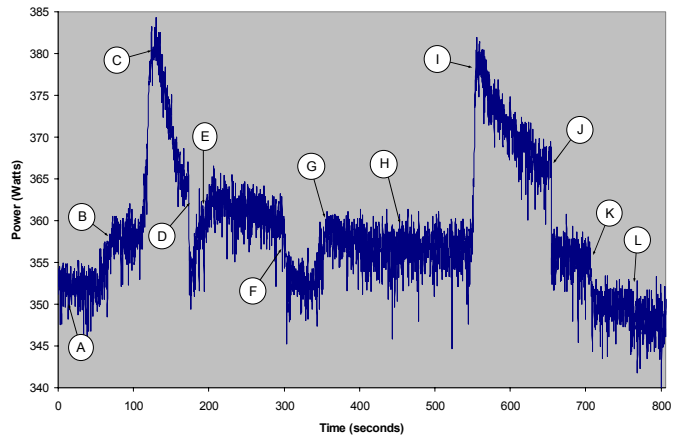

A	Spindles running (5215, 963 rpm).
B	The fluid is turned on and touch point contact made (no load, x axis =132.3305)
C	Spring is compressed 5 mm (50 N load applied, 0.218 MPa)
D	Load removed & x-axis moved by + 25µm (x axis = 132.3055)
E	Load reapplied. (50 N)
F	Load removed & x-axis moved by - 50µm (x axis = 132.3555)
G	Load reapplied. (50 N)
H	Traverse -50 µm (x axis = 132.3305)
I	Traverse -25µm (x axis = 132.2755)
J	Back to touch point (x axis = 132.2755)
K	Wheel fully off.
L	Finally the fluid is turned off

Figure 177 - Wheel spindle power as the x-axis is misaligned prior to superfinishing - [038]

A significantly larger increase in power occurred during run 037 (figure 176) than during run 038 (figure 177). Two possible reasons for this are as follows:

(1) The procedure used when running test 037 involved traversing the spindle when grinding with the load still applied. This was similar to taking a conventional grinding cut. Run 038 involved removing the load before traversing and then reapplying the load. This is a constant force process operating under conditions of slight misalignment and as a result the forces involved should be lower.

(2) Conducting test run 037 caused the ball to wheel conformity to change. Traversing the wheel spindle causes an increase in the diameter at the surface of the wheel. By the start of run 038 the wheel is already 'over-formed'. This effect is illustrated by considering what happens at point (H) in figure 177. There is no increase in power recorded even though the spindle is traversed 50 µm with the load still applied. This was due to the wheel's spherical grinding surface already being large enough to accommodate a 50 µm change in x-axis movement without placing the wheel under excessive load. At point (I) there was a sharp increase in power as the x-axis displacement was increased by +25 µm further than it has been moved before.

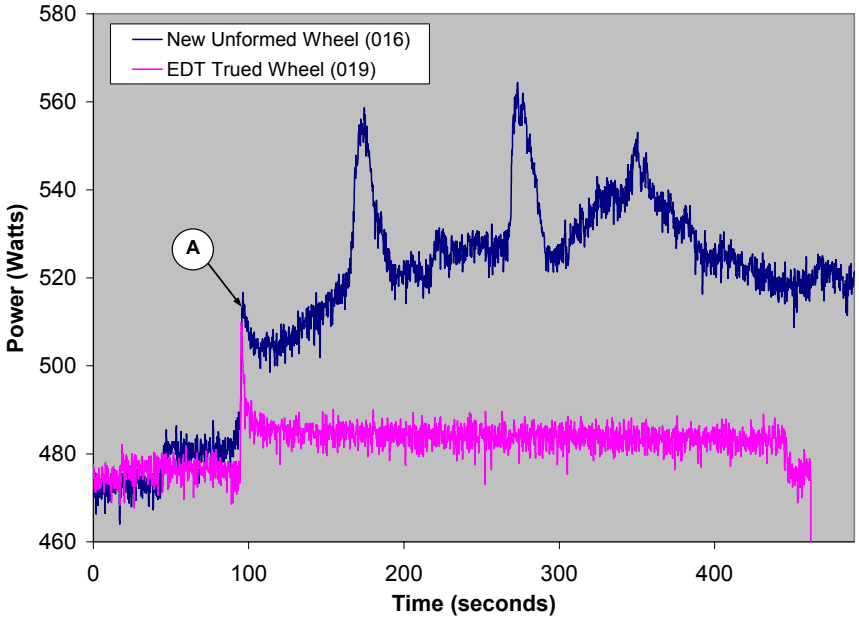

Figure 178 - Wheel spindle power with differing ball to wheel conformity. - [Load applied at (A)]

Figure 178 once again looks at conformity of the ball and wheel. The graph illustrates the difference in power when superfinishing with a new and 'under-formed' #500 wheel, compared to after it has been formed by electro-discharge truing. Substantially higher power values are seen as a result of grinding with a new and un-trued wheel. On inspection of the wheel after run 016 the edges were chipped. It is possible that the spikes in power recorded during test 016 correspond to the edges of the wheel breaking.

18.7 The Condition of the Wheel

Elid can be used to alter / control the condition of the wheel and thus affect the process. As stated before, the condition of the wheel is an important factor that determines superfinishing characteristics, removal rate and surface finish. The universal power cell provides an in-process method of assessing whether the wheel is dressed sufficiently and is adequately polishing the surface of the ball.

Figure 179 illustrates both the effect of electrical interference during Elid 2 dressing (C to D) and how the wheel condition changes once non-Elid superfinishing has begun. In this case it takes approximately 50 seconds before the power levels stabilize.

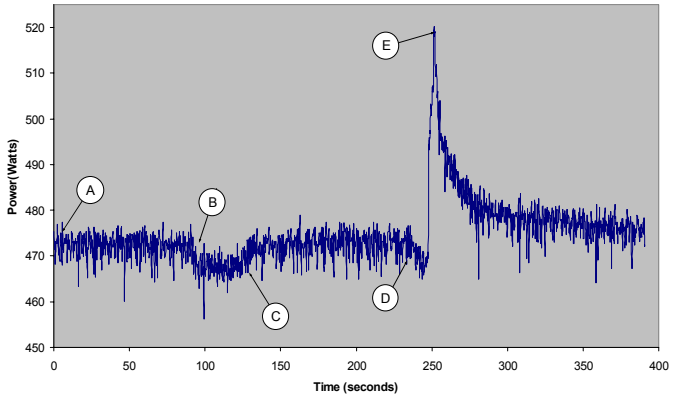

A	Superfinishing with 50N load applied
B	Load removed, fluid left on
C	Elid on, Dress wheel gap of 0.2 mm
D	Elid off.
E	50 N load is reapplied and superfinishing restarted

Figure 179 - Wheel spindle power resulting after dressing a wheel using Elid - [008]

18.8 Wheel Condition & Effect of Applied Load

The effect of load on power usage is also influenced by wheel condition. A glazed wheel produces a less marked increase in power when compared with a wheel that has been recently dressed. This is demonstrated in figure 180. Prior to run 034 the wheel had been used for an extended period without re-dressing (36 minutes). The surface of the wheel had a very shiny green / copper appearance. Prior to run 035 the wheel was given a two minute pre-process dress before repeating under the same conditions. The pre-process dressing revealed a cleaner, newer, speckled brown surface to the wheel. On this occasion it took approximately 1 minute for the power levels to match those of the previous run. On inspection of the wheel after run 035 the wheel once again had a very glazed and shiny appearance.

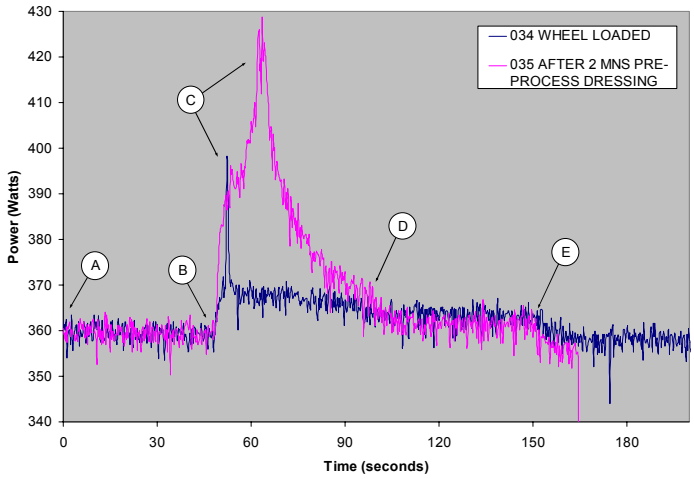

A	Spindles running (6000, 963 rpm), fluid on, at touch point position (no load)
B	The load is applied.
C	spring compressed 10 mm. (92.5 N, 0.685 MPa)
D	Force reduced to 42N, 0.311 MPa
E	Force begun to be reduced back to touch point.

Figure 180 - Wheel spindle power under changing wheel conditions and load – [034, 035]

When considering a grinding process controlled by a predetermined depth of cut, an increase in power use would be expected when a wheel is removing material less efficiently. This would result from an increase in force as the wheel struggles to remove material in pace with its feed rate. With this superfinishing system the normal force is independent of material removal rate and thus remains constant regardless of wheel condition. The rotational reaction force inhibiting the wheel spindle is dependent on friction at the grinding interface. This force is decreased when the wheel is glazed, resulting in lower power values.

18.9 Spindle Power Measurements

To account for any drift in the power values and the influence of fluid during superfinishing, it is important to measure free running periods at the start and end of the run. As an example of this, figure 181 shows the spindle power profile recorded during a combined Elid 2 + Elid 3 superfinishing run.

The spindle power recorded during the Elid 3 superfinishing period is adjusted based on the slope of the free running periods before and after. Various aspects of the data are assessed including the average, maximum, slope, minimum, starting period and final period (figure 182).

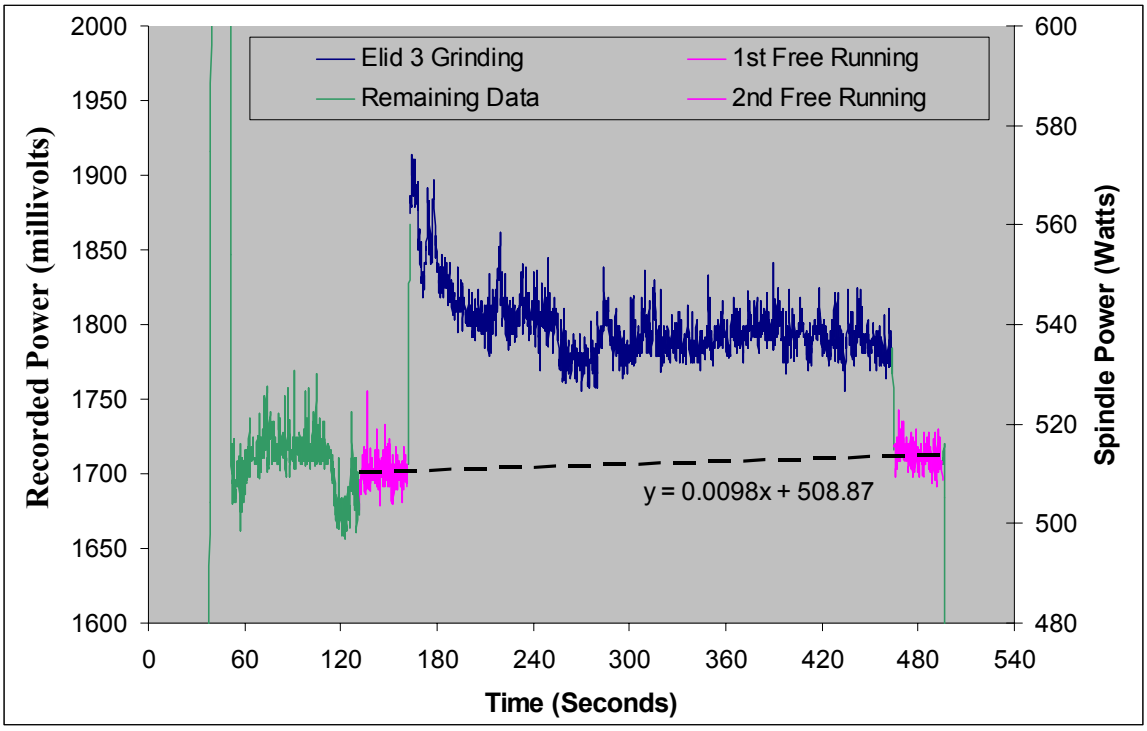

Figure 181 - Measurement of wheel spindle power change during superfinishing

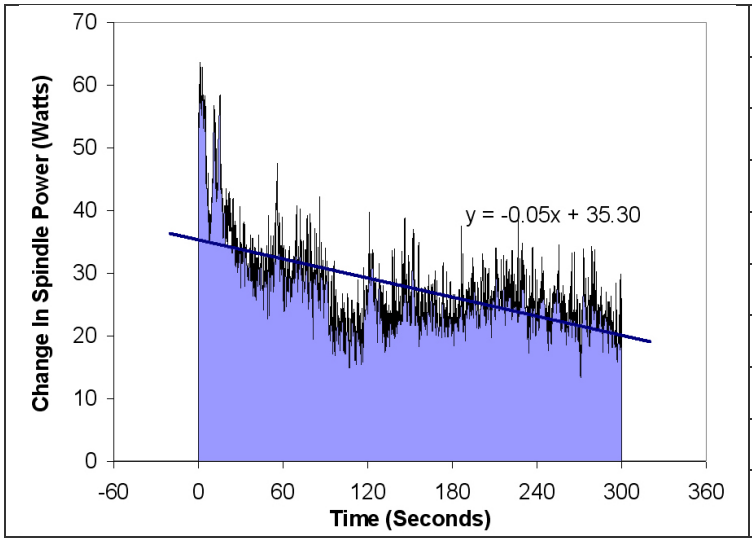

Mean = 27.7 watts
Maximum = 63.4 watts
Minimum = 13.4 watts
Initial Power = 43.5 watts
Final Power = 23.0 watts
Slope = -3.0 watts / minute (-0.05 watts / second)
Area under graph = (0.00232 kw.h), (8352 Joules)
Total material removal = (0.3 µm off O/D), (0.9 mg), (0.7 mm^3 by volume)
Specific Grinding Energy = 11931 Joules / mm^3
Resultant ball finish of this run = 4.3nm Ra Talysurf, (3.4nm Ra Wyko)

Figure 182 - Measurement of wheel spindle power change during superfinishing

Chapter 19 - Elid 3 Performance

Elid 3 is an electrode-less type of in-process dressing where the anode (the wheel) and the cathode (the ball) are in dynamic contact with each other. Superfinishing using Elid 3 was the original proposed solution to produce sub 10 nm Ra balls, because of the restricted access involved in spherical superfinishing. The majority of time was spent investigating this type of Elid and several hundred runs were conducted using it. Elid 3 processing was conducted on balls ranging from 20 to 48 mm in diameter. There was no observable difference in the performance of the Elid 3 superfinishing process when applied to balls of differing size. Factors such as ball roundness and surface output quality are, for the most part, not a function of the type of Elid used but a refection on how effectively it works; i.e. how the type of Elid affects the condition of the wheel.

19.1 Elid 3 Power Activity

The distinct power activity associated with Elid 3 is demonstrated in figure 183, which shows the Elid power values recorded when conducting a three minute pre-process dress of the wheel (period A) directly followed by ten minutes Elid 3 superfinishing (C and D). After the initial pre-dressing period, when grinding contact was made (point B) the current rapidly increased, voltage rapidly declined and electrical resistance was greatly reduced. The Elid was ‘active’ during period (C); albeit at a low level. During period (D) the Elid system was ‘inactive’. When this occurred the Elid system had little or no effect on dressing the wheel.

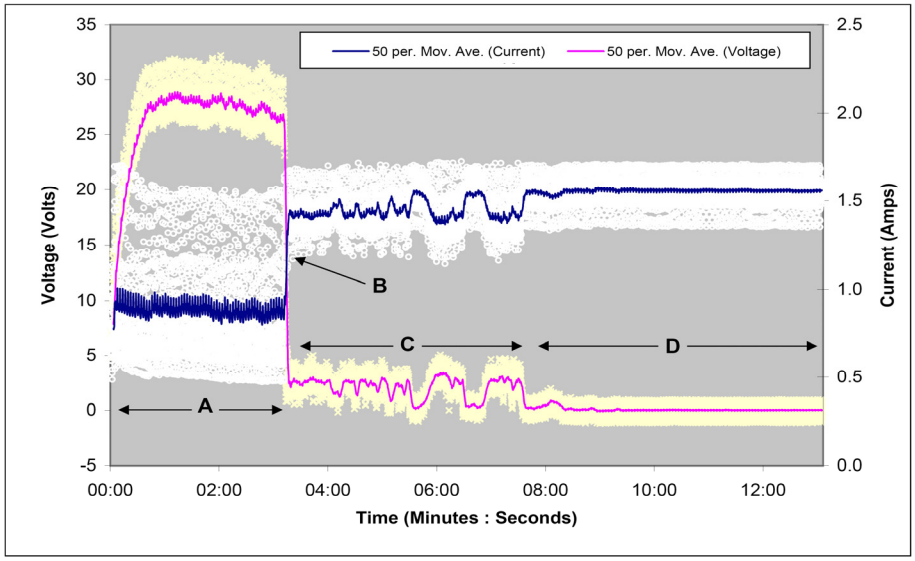

Figure 183 - Distinct regimes of Elid power activity - pre-dressing followed by Elid 3 superfinishing [Elid power supply set to 60V,20I, 10% - RNB08 ball, #12,000 MRB-CBN wheel, run number 003]

When the load has been applied and processing started, the Elid system should gradually erode the wheel's bond material to reveal fresh abrasives. However this only occurs when the Elid system is actively working (period C). The Elid power data shows that the system does not consistently maintain the wheel's condition in a stable manner. A breakdown of the oxide / resin insulating layer results in direct metal to metal contact between the ball and wheel. At this point electrolysis cannot occur and the wheel is not being dressed, which restricts its ability to recover (period D).

The exact conditions at the surface of the wheel are complex. The dynamic contact between the anode and cathode makes Elid 3 less effective at dressing than other types of Elid. The effectiveness of the process is also influenced by the fluids ability to penetrate the grinding interface. Stopping and performing a pre-process dress of the wheel with a separation gap, re-forms the insulating layer at the surface of the wheel. The breakdown of the wheel's condition when superfinishing is a fundamental problem with the Elid 3 process.

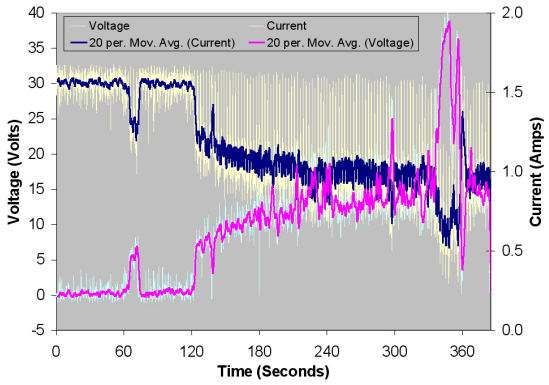

Figure 184 - Very Active Elid 1 power activity

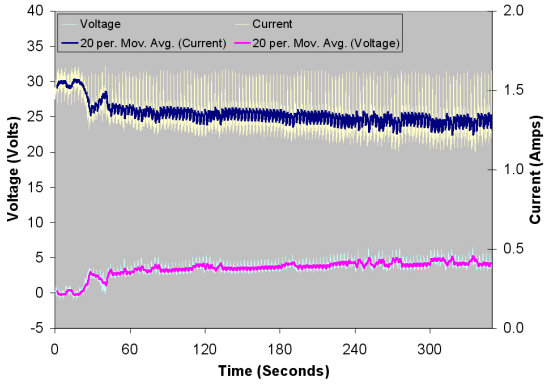

Figure 185 - Active Elid 1 power activity

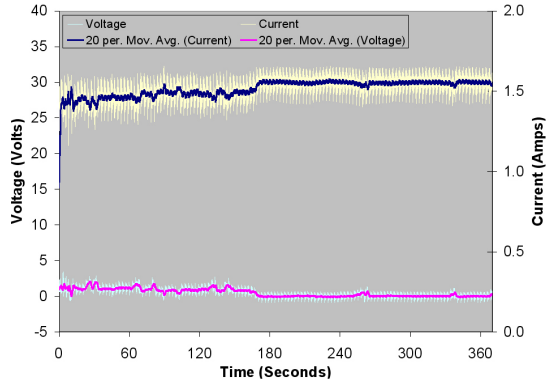

Figure 186 - Inactive Elid 1 power activity

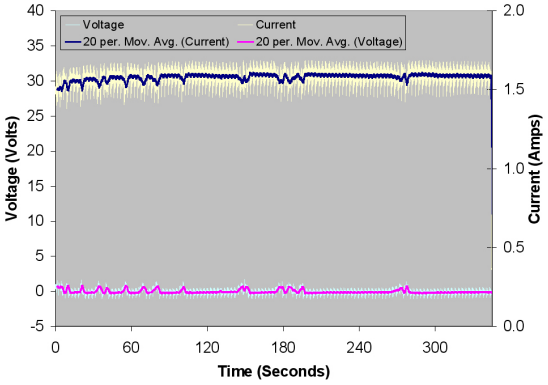

Figure 187 - Very Inactive Elid 1 power activity

Figure 184 shows an example of a very active period of dressing occurring during Elid 3 superfinishing. A #500 wheel was used with this test and it is often the case that a more pronounced change in Elid power values is recorded when a coarser abrasive wheel is used. This is probably due to the size of the abrasive assisting in the formation of a separation gap within which electrolysis can occur. The Elid power supply values recorded during this test run show that there is a reasonably good degree of resistance between the ball and the wheel, and that erratic but effective in-process dressing is occurring. During very active periods of Elid power, thus effective dressing, wheel spindle power and material removal rates were noticeably higher. Various runs showed that inactive periods (figure 187) resulted in low or declining spindle power and low ball material removal rates.

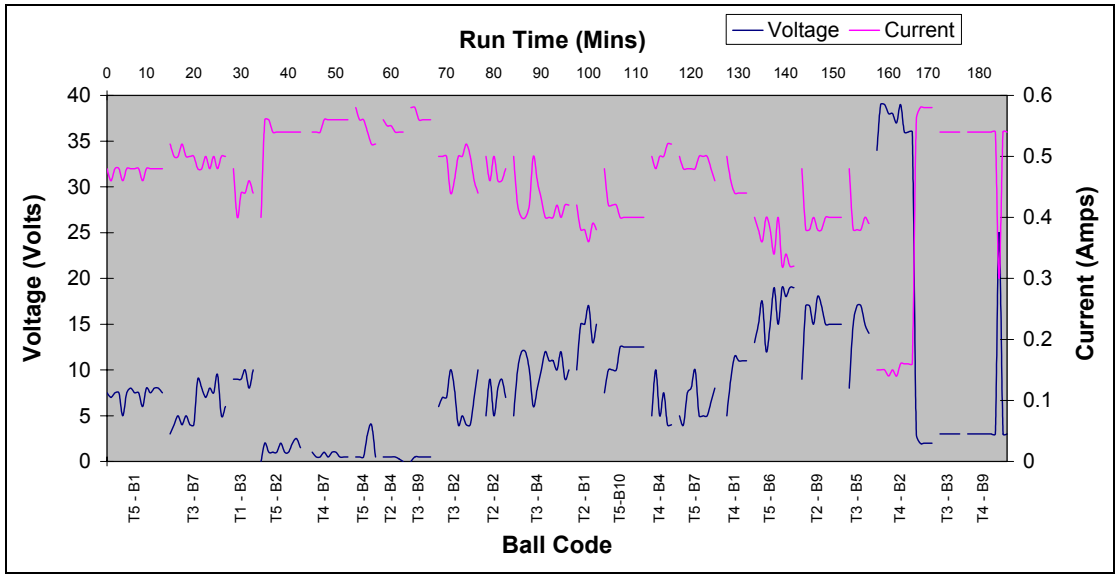

Figure 188 - Voltage and current levels recorded throughout Elid 3 testing of RNDEB14 balls at NMB

An example of larger scale Elid 3 power supply values is shown in figure 188. Each break in the lines represents the end of one run and the start of the next. Assessment of this data did not reveal a statistically significant general correlation between average Elid 3 power levels and material removal. It is possibly not how high the power levels are but how dramatically they fluctuate that is important.

19.2 Elid 3 Surface Generation Rates

In order to evaluate the required processing time, the rate of surface generation when Elid 3 superfinishing with wheels of differing mesh sizes was investigated. Twenty seven RBFB16AB balls were subjected to processing times ranging from 40 seconds to 12 minutes. As figure 189 shows, the rate of surface finish improvement declined as steady state levels began to be reached. For the #20,000 wheel, a processing time of around 10 minutes was required.

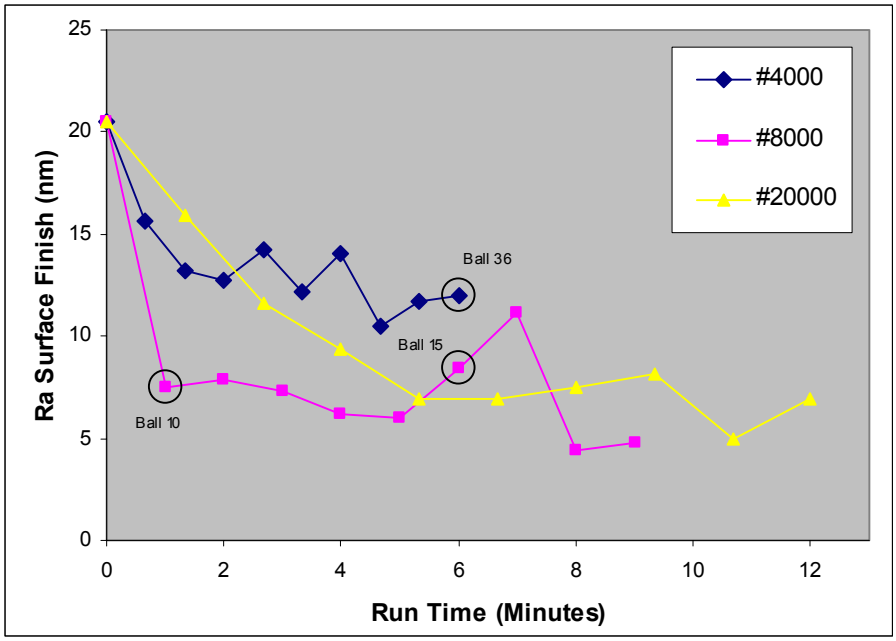

Figure 189 - Rate of spherical surface generation. -
[Taylor Hobson talysurf, across batch of RBFB16AB balls]

Anticipating a faster generation rate with the #4,000 wheel, a shorter time interval was used between data points. After 6 minutes the surface finish values were substantially higher than the 3nm Ra that the wheel is capable of producing. Microscope analysis of the surface produced by the #4000 wheel revealed that after 6 minutes it was not fully generated; making the #4000 wheel the slowest at forming a surface on this occasion. Microscope analysis was in good agreement with the surface finish results produced. Vastly differing surface quality often existed over the spherical surface of the ball as it is in the process of being formed by a particular wheel (figure 190), with additional Ra measurements, taken on a separate day, varying by up to 8 nm. This variation in re-measurement was an effect of the relatively large influence of the point of measurement when a ball's surface is part way through being processed.

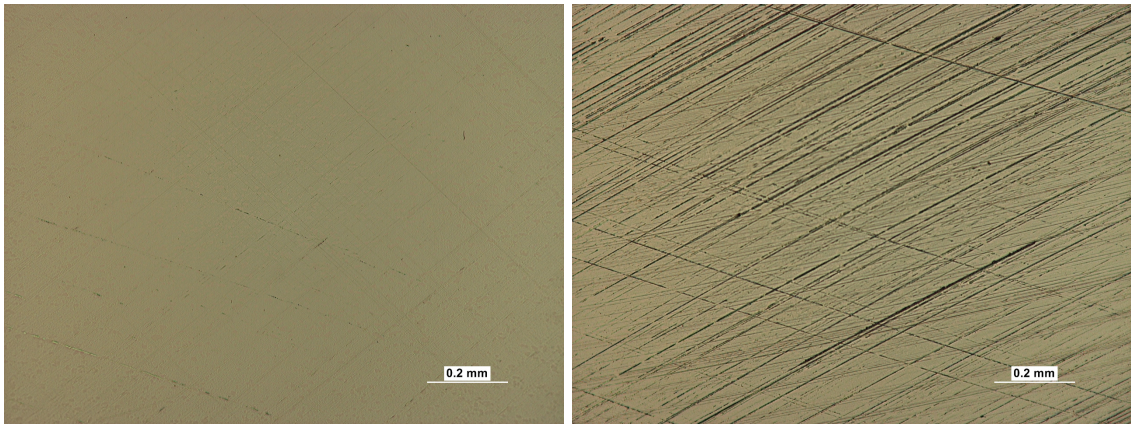

Figure 190 - Optical microscope pictures of ball 15 part way through surface generation. - (a) Showing the area of best surface quality, (b) Showing the area of worst surface quality

The processing times were excessively long for all the wheels tested. However the surface finish and appearance of ball no.10, superfinished for 60 seconds with the #8000 wheel, was of similar quality to the other eight balls that had longer processing runs. Overall this set of tests was not considered successful, due to the large amount of variation in the talysurf readings relative to the small improvement in surface finish and uncertainty about the processing time required.

A second attempt at measuring surface generation rate was performed under closely controlled experimental conditions on the precision controlled Tetraform C. A repetition of the generation plot was provided by adding additional runs. Figure 191 shows the ball surface generation and corresponding ball material removal when Elid 3 superfinishing with a #12,000 wheel. A rapid improvement in surface finish is recorded in the first minute's superfinishing. The rate of improvement gradually slowed, until after 10 minutes the surface was fully generated. Material removal continued to occur after the surface was fully generated. The reduced removal rate recorded after steady state surface finish was reached, was a result of the changing wheel condition and not a result of the difference in ball surface finish.

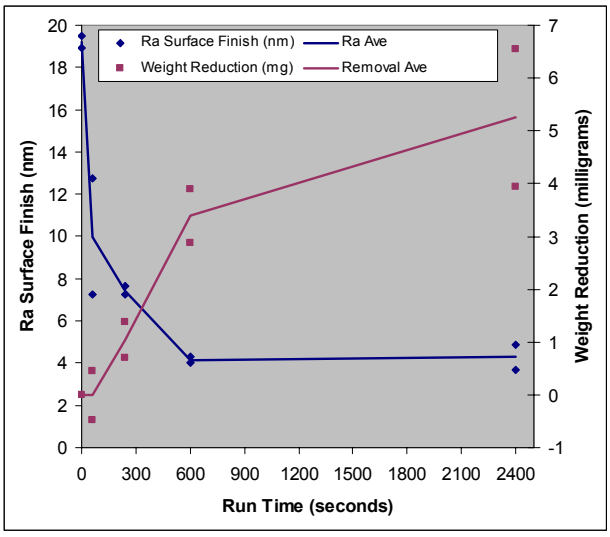

Figure 191 - Ball surface generation rate & corresponding material removal over time

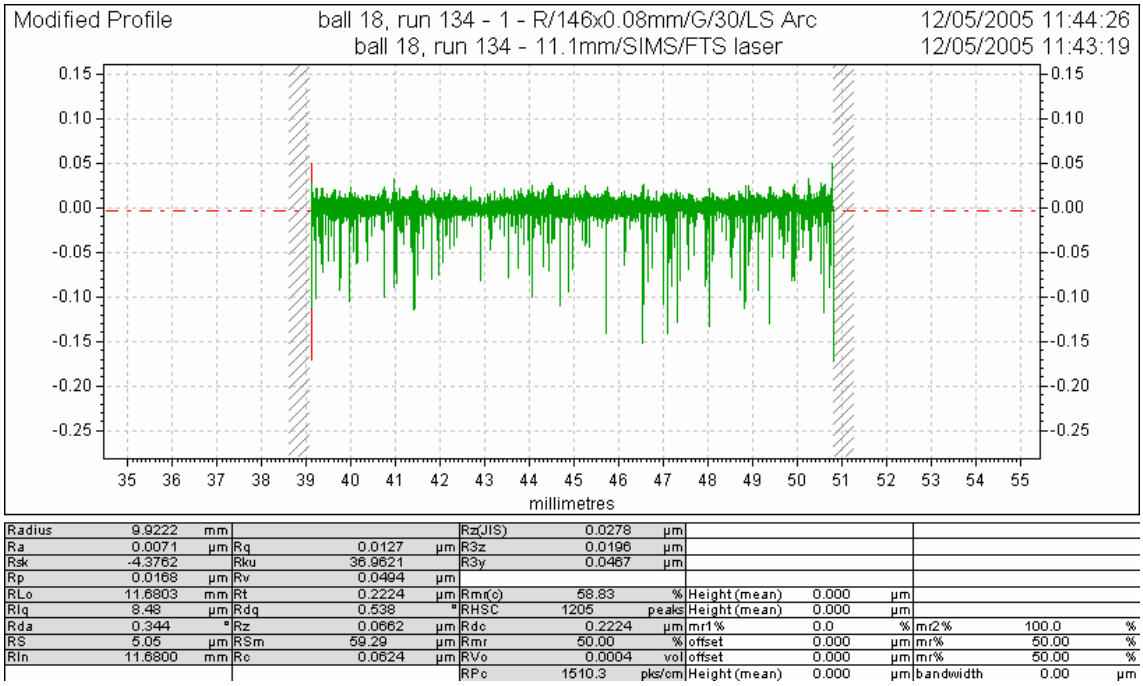

Radius	9.9222	mm			Rz(JIS)	0.0278	µm							
Ra	0.0071	µm	Rq	0.0127	µm	R3z	0.0196	µm						
Rsk	-4.3762		Rku	36.9621		R3y	0.0467	µm						
Rp	0.0168	µm	Rv	0.0494	µm									
RLo	11.6803	mm	Rt	0.2224	µm	Rmr(c)	58.83	%	Height (mean)	0.000	µm			
Rlq	8.48	µm	Rdq	0.538	°	RHSC	1205	peaks	Height (mean)	0.000	µm			
Rda	0.344	°	Rz	0.0662	µm	Rdc	0.2224	µm	mr1%	0.0	%	mr2%	100.0	%
RS	5.05	µm	RSm	59.29	µm	Rmr	50.00	%	offset	0.000	µm	mr%	50.00	%
Rln	11.6800	mm	Rc	0.0624	µm	RVo	0.0004	vol	offset	0.000	µm	mr%	50.00	%
						RPc	1510.3	pks/cm	Height (mean)	0.000	µm	bandwidth	0.00	µm

Figure 192 - Surface finish profile part way through being processed demonstrating consistent material removal from the ball's spherical surface.

Surface profiles corresponding to the previous graph showed that the barrelled surface prior to grinding has a finish of around 19 nm Ra. After superfinishing for 1 minute the surface peaks have been removed and a finish value of 7 nm is reached (figure 192). The fully formed surface records a value of 4 nm Ra. Although this level is of a very high quality, problems exist with the stability of the Elid 3 process and its ability to produce consistent surface generation and removal rates.

19.3 Ball Material Removal

Removal rates have a large influence on required processing time. An accurate estimate of the process time required to fully form a new surface can be taken by equating removal rate to peak to valley roughness, Rz or Rt. For a honed surface the average Rz and Rt values are 0.3 and 0.8 μm respectively. When the amount of material removed from a ball's radius approaches these values (x2 for O/D), the original surface features have been removed. There are also both surface form errors and surface finish improvement involving non-material removal mechanisms to contend with. However, in terms of this process, material removal correlates well with surface generation.

When using Elid 3, a very slow rate of material removal was recorded from the start of testing. An average O/D reduction of 85nm per minute, maximum of 0.44 μm /min, was recorded over 22 runs performed on RNDEB14 balls with the #8000 wheel. Both removal rates and spherical surface generation rates produced irregular values. This suggests that stable superfinishing had not been achieved. Removal rates were substantially lower than reported in comparative literature.

19.3.1 Various Elid 3 Comparisons

Experimental runs on RNB08 balls which looked at the rate and consistency of ball material removal during Elid 3 superfinishing are shown in figure 193. All the runs were conducted with the same processing parameters (5 minutes run time, 67.6N load, wheel speed 5215 rpm, ball speed 963 rpm) and the ball input and output remained consistently within a range of 3.5 to 5.2 nm Ra. The consistency of material removal during some Elid 3 only tests is problematic, as there were two runs (140a & 140f) where no material was removed. If this was a production run then the surface of these balls would not be improved from the input quality. The inconsistency in removal rate achieved highlights a significant problem. A 0.6 micron reduction in the balls O/D converts to a required processing time of 5 minutes at the fastest removal rate of 0.117 μm/min, 14 minutes at the average removal rate 0.044 μm/min, and indefinitely for the slowest removal rate of zero.

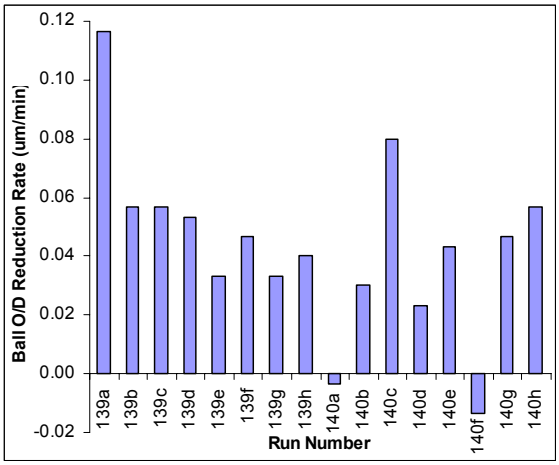

Figure 193 - Ball material removal consistency when processing using Elid 3. [Result inaccuracy: max=0.08 µm, standard error = 0.0049 µm]

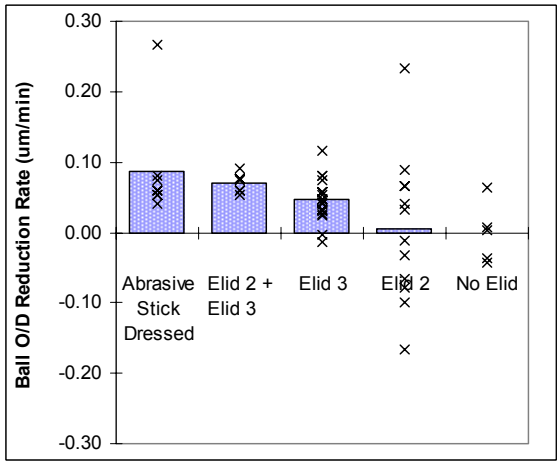

Figure 194 - Material removal of various methods of wheel dressing. – [#12,000 MRB-CBN wheel]

These Elid 3 results were then compared to various alternative ways of dressing the wheel (figure 194). Again measurements were taken at five-minute intervals. This represents both a cycle time for one ball using these dressing methods with the #12,000 wheel and the minimum superfinishing time required to achieve a material removal quantity that can be measured to any degree of accuracy.

- On average no material was removed from the ball when Elid was not used. The highest recorded change in spindle power during these non-Elid runs was only 4 watts (figure 195).

- The combination of Elid 2 and a #12,000 wheel resulted in the material removal being effectively zero (chapter 20). These runs used the ball being processed for the Elid 2 dressing stage and as a result electrolytically deposited copper formed on the ball during dressing and was then transferred back to the wheel during superfinishing. As a result the amount of material removed varied around the zero mark.

- When combining Elid 2 and Elid 3, material removal slightly increased and critically no runs recorded zero material removal. Spindle power typically declined when superfinishing was started as the condition of the wheel degraded (figure 195). The use of Elid 3 prevented spindle power falling to zero.

- Comparisons with all types of Elid showed that, when using a #12,000 wheel, a dressing stick was more of an effective method of dressing in terms of material removal, but there are other problems associated with its use (chapter 20).

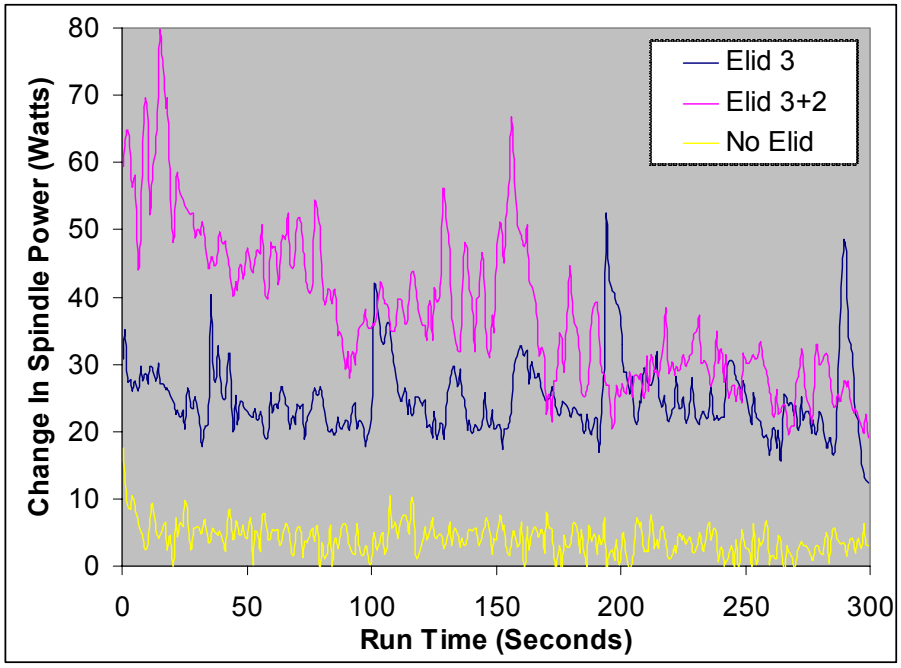

Figure 195 - Typical wheel spindle power profiles corresponding to figure 194 / type of Elid used.

When superfinishing using Elid 3 there is a very small but nevertheless measurable increase in material removal and wheel spindle power levels compared to when no Elid is used. The mere fact of having electricity flowing, even when direct metal to metal contact occurs, provides a minimal amount of dressing allowing some material to be removed. Although capable of generating a ball's surface in 10 minutes, this amount of removal is minute in comparison with what can be achieved when the wheel is being effectively dressed by a working Elid superfinishing system such as Elid 1.

The magnitude of spindle power recorded during Elid 3 superfinishing relates to a combination of the processing parameters used and the condition of the wheel. More aggressive processing parameters and a well-dressed wheel increase spindle power. As the dressing effectiveness for Elid 3 ranges from low to worthless, the spindle power increase resulting from superfinishing is often unpronounced.

19.3.2 *Influence of Abrasive Size on Elid 3 Ball Material Removal*

Plotting the removal rates recorded for a variety of experimental sets using different abrasive sizes revealed a large degree of variation (figure 196). Although parameters do change from point to point, the data clearly illustrates that consistent material removal is not being achieved. The line represents the upper limit of removal rates recorded for particular abrasive sizes. As the material removal can fall to zero when the wheel condition is poor, the minimum removal rate is zero. As would be expected the smaller abrasive wheels produced a lower maximum material removal rate. The minimum rate for all wheels is zero. Experiments with the #4000 mesh wheel found removal rates to be broadly independent of the surface finish produced. This is not the case with the #500 mesh wheel.

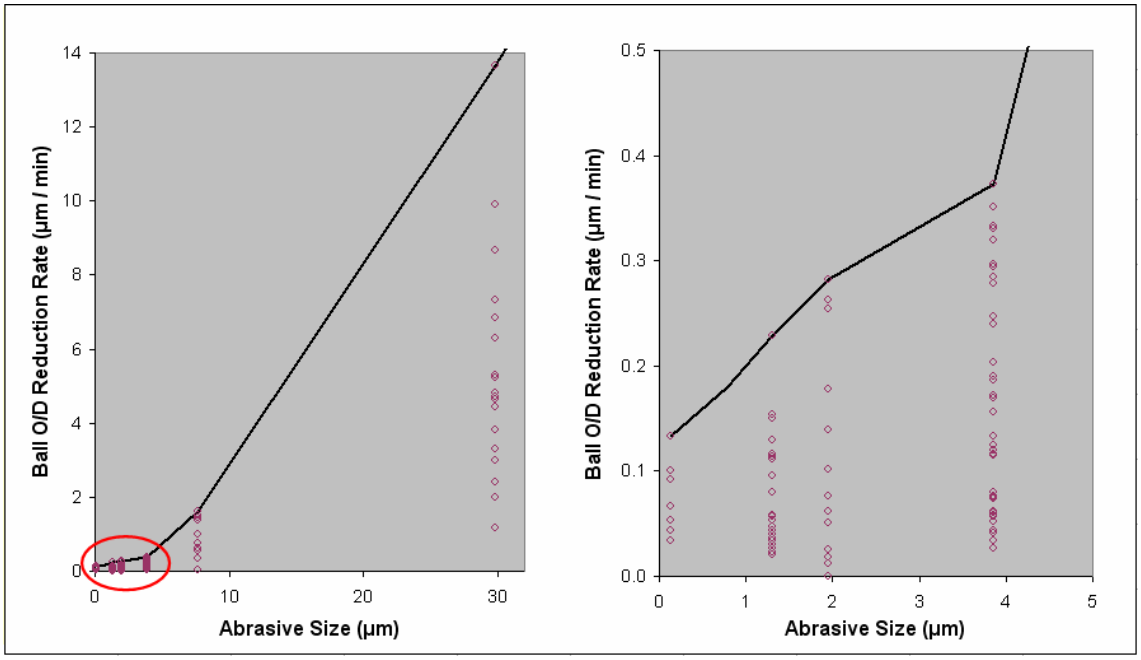

Figure 196 - Ball material removal rates versus abrasive size for a variety of Elid 3 experimental sets

19.4 Wheel Wear when Elid 3 superfinishing

Wheels were measured after completing Elid 3 runs that lasted for several hours but no wheel wear was observed. This was the case regardless of abrasive size. Any wear that did occur must have been less than 25 µm per hour; a rate that is unacceptable and indicative of a dressing method / process that is not working as it should. Superfinishing using Elid 3 was ultimately deemed to be an ineffective method of producing balls and better options were developed for wheel dressing.

Chapter 20

Elid 2, Rate of Wheel Glazing & Recovery

It has already been established in previous sections that the condition of the wheel is a fundamental factor in this process. Superfinishing using MRB wheels without employing any form of dressing is unacceptable. Elid 2 (interval dressing) is performed periodically as a separate stage at the start of a superfinishing cycle and restores the wheel's grinding surface to its optimum condition, after it has been degraded to some extent through use. It is essentially the same as the pre-process dressing operation, but as the required dressing time is dependent on the condition of the wheel at the start, the dressing times for Elid 2 are shorter. It is important to know the rate at which the wheel condition and processing efficiency degrade, in order to determine the required time between dressings. It is also important to know how long the wheel takes to recover after superfinishing to determine the required Elid 2 dressing time.

20.1 Material Removal

Figure 197 shows the rate at which ball material removal declined for a #2000 MRB-CBN wheel. As material removal ultimately ceases when using Elid 2 exclusively, there is a maximum limit on how much material a wheel is capable of removing per dressing cycle (figure 198), before the abrasive dulls and the wheel becomes glazed. Additional processing time at this point will not yield any further improvement.

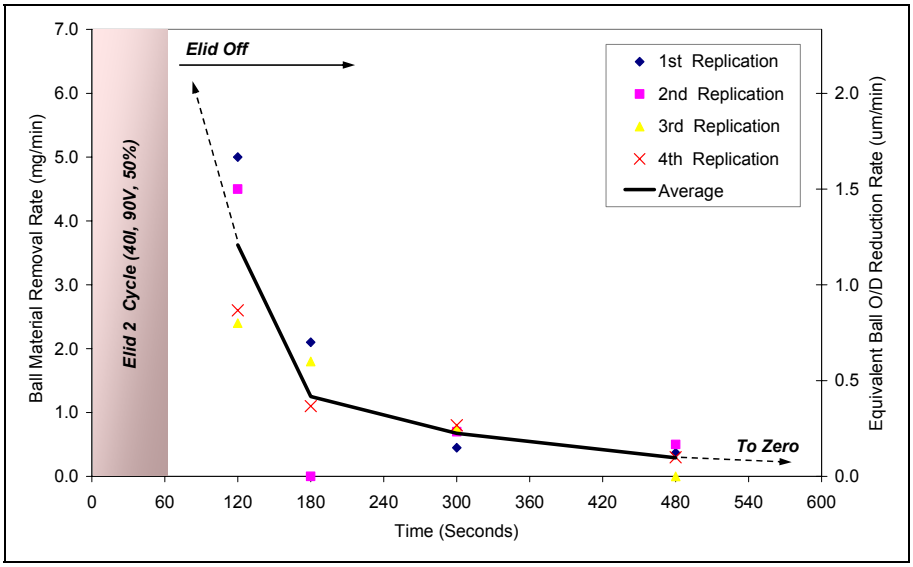

Figure 197 - Declining ball material removal rate when Elid 2 superfinishing using a #2000 MRB-CBN wheel. [Standard superfinishing parameters as in figure 95]

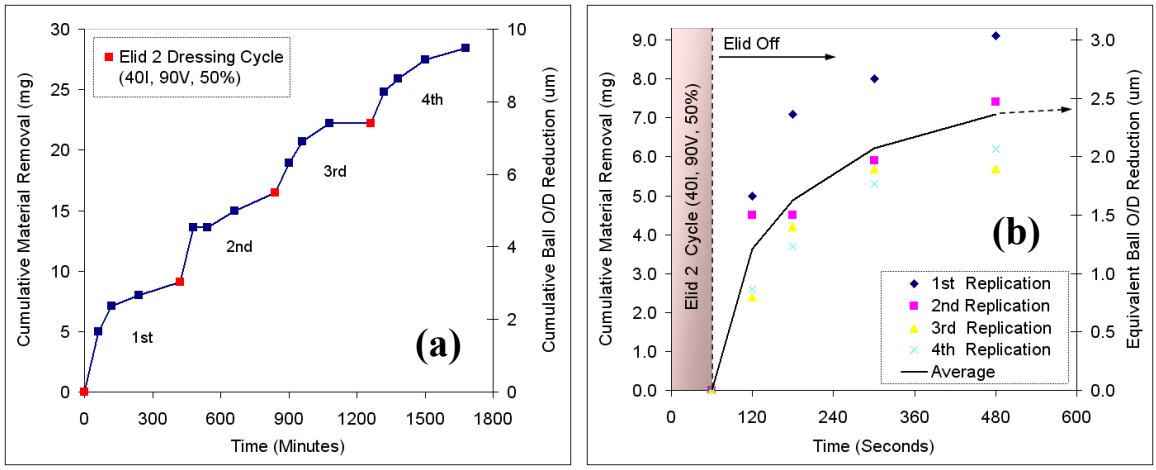

Figure 198 - Deterioration of a #2000 MRB-CBN wheels ability to removal ball material when superfinishing without Elid but after conducting a one minute Elid 2 dressing cycle.
(a) Cumulative ball material removal (b) Cumulative ball material removal per dressing cycle.

It is necessary to remove 1 to 2 microns off the ball's O/D in order to fully remove honed or barrelled surface features. A #2000 MRB-CBN wheel is able to remove this quantity of material before it becomes glazed and further material removal is halted. The material removal per dress is insufficient when processing with abrasives smaller than the #2000 wheel. A #12,000 wheel glazes over too quickly and would require more than one Elid 2 dressing cycle to be performed per ball. Surface finishes generated with wheels larger than the #2000 mesh do not reach the required level of sub 10 nm Ra. In addition, processing with a #500 wheel did not appear to remove more ball material per dressing cycle.

Ball surface finish improves as material removal flattens, therefore a balance must be struck between processing efficiency and ball quality. In this instance this was achieved by using the #2000 wheel until material removal had ceased and glazing had just begun (the crest of the flat region on figure 198b). The use of the #2000 MRB-CBN wheel is investigated further in the final grinding cycle chapter 28.

Elid 2 dressing should be carried out once per ball, in order to maintain a consistent wheel condition and produce balls of similar quality. Dressing after processing several balls would add variability to the process. More material would be removed and a worse finish achieved with the first balls than with subsequent balls. Dressing more than once per ball would be time consuming and inefficient. In an automated process, dressing could be conducted while balls were being loaded and unloaded, or while an in-process ball form measurement was being taken.

20.2 Spindle Power Data

Spindle power levels provide good information on the condition of the wheel and therefore on the required Elid 2 cycle times. Figure 199b shows the power data corresponding to one of the replications above. Spindle power usage during superfinishing reduces as the wheel becomes glazed.

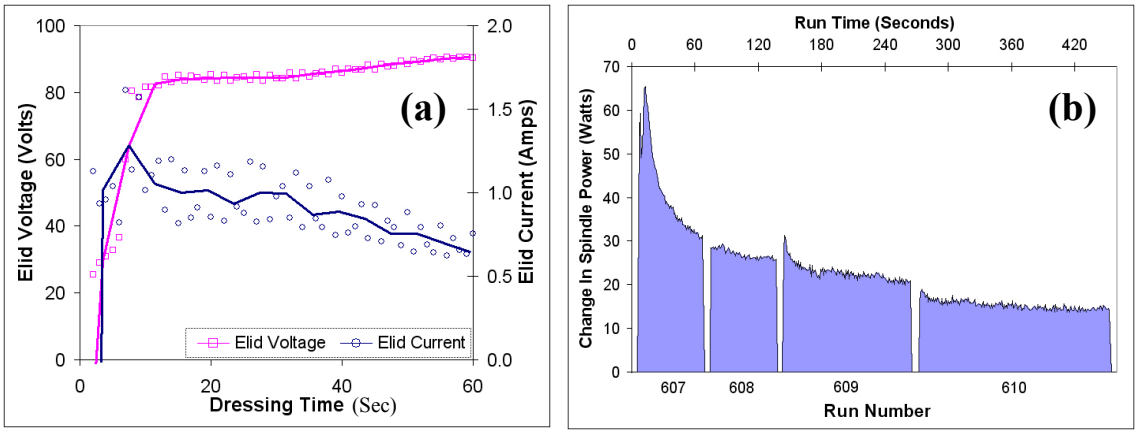

Figure 199 - Corresponding wheel spindle and Elid power values to material removal data (a) Elid power values during Elid 2 dressing cycle, (b) Declining spindle power after Elid 2 dressing cycle.

Assessment of spindle power revealed that the wheel's condition degraded and the material removal rate declined more rapidly when aggressive processing parameters were used and less rapidly when non-aggressive parameters were used. The ball material removed per dressing cycle remained relatively constant.

According to the literature, spindle speeds should be reduced during dressing. Reducing spindle speed allows a smoother flow of fluid between the inter-electrode gap. However, when this was tested no significant difference was observed in the wheel dressing efficiency and it is not worth the time taken to slow down the spindles during each dressing cycle.

20.3 Elid Power Data

Because MRB wheels contain a large proportion of copper they dress very quickly. Elid power data showed that the Elid current and voltage stabilised rapidly. This indicated that the wheel was dressed. Higher Elid power values increase the aggressiveness of dressing.

The Elid power levels did not demonstrate a prolonged flat level (figure 199a); however additional dressing time would not be beneficial as the bottom line is that the material removal performance has recovered. This recovery is demonstrated in figure 198a, as material removal recommences after performing each Elid 2 dressing. An Elid 2 dressing time of 1 minute is sufficient for the performance of the wheel to recover.

20.4 Wheel Wear

During the 28 minute run time using Elid 2 (figure 198a) the #2000 wheel reduced by 6.8 microns in length. The wheel can be considered to wear a consistent amount for each dressing cycle; an average wheel wear rate of 1.7 µm /minute per dressing cycle was recorded.

20.5 Role of Abrasive Size

The rate at which a wheel glazes and stops removing ball material is dependent in part on the size of the abrasive in the wheel. Large abrasives take longer to stop cutting than small abrasives because they dull less rapidly.

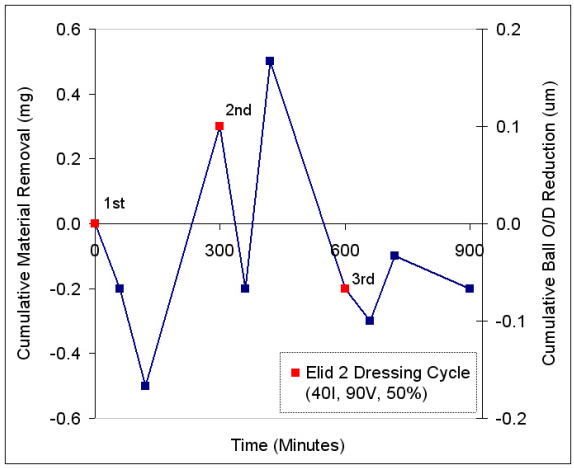

Figure 200 - Cumulative ball material removal

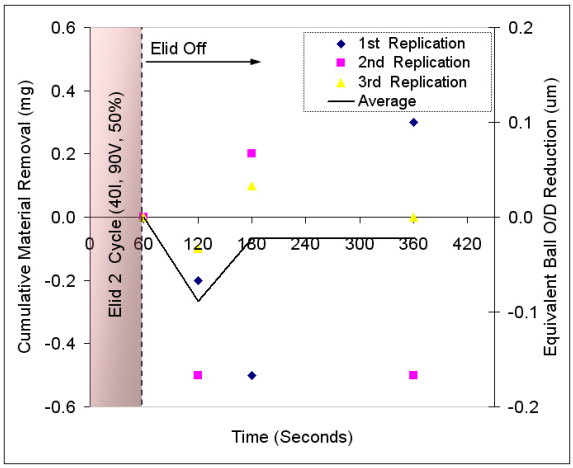

Figure 201 - Rate of wheel glazing Elid 2 evaluated through ball material removal per dressing cycle.

The small amount of variation observed around the zero material removal value in figures 200 & 201, shows that material is not being removed from the ball during Elid 2 processing with a #12,000 MRB-CBN wheel. Corresponding spindle power showed a low flat level (figure 202).

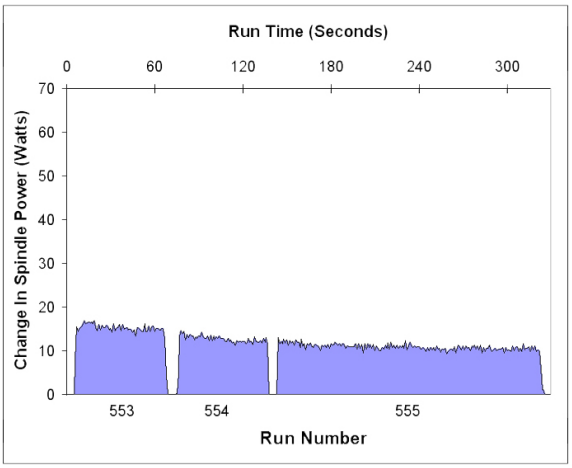

Figure 202 - Corresponding wheel spindle power after Elid 2 dressing cycle - [#12,000]

Additional runs conducted in a similar manner to those outlined above showed that the #12,000 wheel was capable of removing a very small amount of material and experienced a very rapid spindle rundown period, before glazing. The material removal was still insufficient, therefore the combination of Elid 2 and a #12,000 wheel is not a practical option.

20.6 Dressing stick

One traditional method of dressing is the use of a dressing stick. When correctly shaped, a dressing stick can be used to both form the shape of the wheel and condition the surface. The use of a dressing stick was evaluated on a #12,000 wheel.

Superfinishing runs conducted after dressing with a stick revealed that the wheel's form was poor. Complete area contact between the ball and wheel was not achieved. A higher removal rate was recorded for the first run compared to subsequent runs conducted after the wheel was re-dressed with the stick (figure 203). At the rates of material removal achieved, a processing time in the region of 10 minutes would be required to produce each ball.

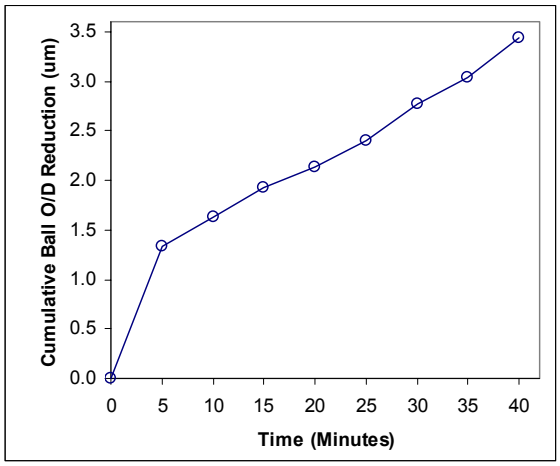

Figure 203 - Cumulative material removal when only using a dressing stick before superfinishing. – [#12,000 MRB-CBN wheel, standard parameters]

As with Elid 2 dressing there is a limit to the amount of material that can be removed per dressing cycle. In order to maintain material removal rates, re-dressing needs to be repeated prior to superfinishing every ball, if not a few times per ball. A proposition that unless automated is not practicable.

Chapter 21

Optimisation of Combined Elid 2 + 3 Superfinishing

As outlined in previous chapters, the main problem with Elid 3 superfinishing is the inadequate dressing and erratic maintenance of the wheel's condition. With Elid 2 superfinishing a #12,000 wheel was inadequate at removing ball material. In an attempt to overcome these problems, combined Elid 2 and Elid 3 was used with a #4000 MRB-CBN wheel. Prior to beginning each Elid 3 superfinishing run, a one minute Elid 2 cycle was conducted.

A replicated full factorial experiment was conducted to investigate the effect of applied load and spindle speed on performance (figure 204). In total 40 runs were conducted on 20 balls that were measured before being re-used. It was not possible to fully randomise the design in terms of spring stiffness. Numerous responses were analysed including the in-process information of Elid and wheel spindle power values, ball material removal rates, ball surface inspection, and form and finish measurements.

Factors Under Investigation	Low Level	Centre Level	High Level
(A) Ball Spindle Speed @ Crown (m/s)	0.625	1	1.375
(B) Wheel Spindle Speed @ O/D (m/s)	2.5	3.5	4.5
(C) Superfinishing Contact Pressure (MPa)	0.3	0.6	0.9
(D) Spring Stiffness Rating (N/mm)	8.41	14.16	19.91

Figure 204 - Factors under investigation - [Run details: 1 minute Elid 2 dressing cycle conducted before the start of each 10 minute Elid 3 superfinishing run. Elid power turned off 10 seconds before the end of each superfinishing run. 20I, 60V, 50% Duty. #4000 MRB-CBN wheel].

21.1 Ball Surface Finish Results

The most basic way to assess the effect of the changes made to the four factors is to compare their mean values produced with runs involving the use of low, medium and high levels. The mean values for the average talysurf Ra response are shown in figure 205, along with the individual data points. Each data point consists of the average of two Ra finish measurements, one taken across the ball and one around the ball. The effects recorded were not dramatic compared to the natural variation that the process produces, however a trend emerged for contact pressure.

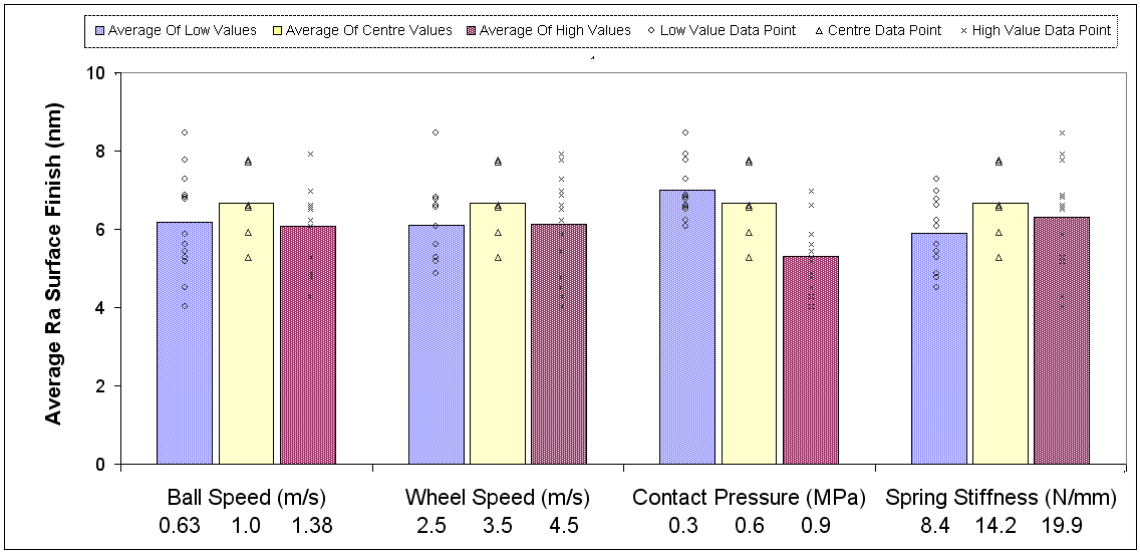

Figure 205 - Column graphs of raw results versus factor levels for ball Ra surface finish. - [Data points are an averaged reading of Taylor Hobson talysurf measurements taken around and across the ball's crown]

A statistical software package 'Design Expert' was used to analyse surface finish and various other responses. As is demonstrated by the effects table and graph (figure 206), when assessing the surface finish response only contact pressure produced a large enough effect to be statistically significant.

Model Term	Standardised Effect	Sum Of Squares	Percent Contribution
A - Ball Speed	-0.198	0.176	0.44
B - Wheel Speed	0.229	0.097	0.24
C - Pressure	-1.677	18.918	47.36
D - Stiffness	0.264	0.381	0.95
AB	0.331	1.088	2.72
AC	0.417	1.330	3.33
AD	0.093	0.057	0.14
BC	-0.067	0.018	0.04
BD	-0.147	0.116	0.29
CD	-0.341	0.925	2.32
ABC	0.115	0.050	0.12
ABD	-0.036	0.015	0.04
ACD	0.024	0.002	0.00
BCD	0.010	0.000	0.00
ABCD	-0.271	0.496	1.24
Curvature	0.455	1.591	3.98
Lack Of Fit		10.477	26.23
Pure Error		4.210	10.54
Lenth's ME	0.739	Lenth's SME	1.176

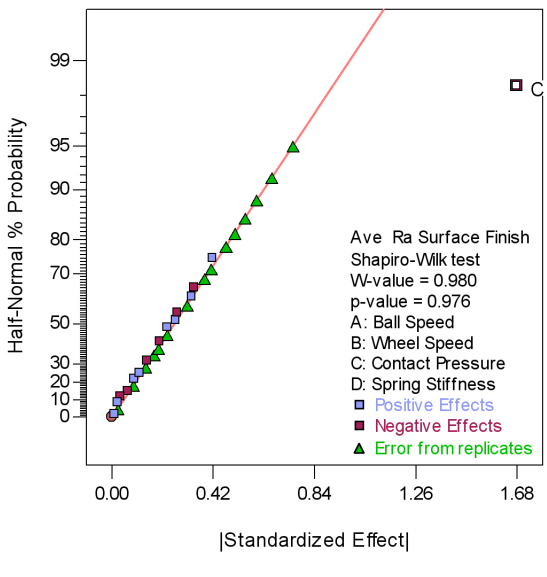

Figure 206 - Effect measurements of the various factors and interaction for Average ball Ra surface finish response. - (a) Effects Table, (b) Half-Normal Probability Plot Versus Standardized Effect

The relatively large influence of the main effect 'C' is demonstrated as it lies off the line on the graph. A 'p-value' that is greater than 0.1 for the Shapiro-Wilk test demonstrates

the normality of the remaining data. The achieved value of 0.976 demonstrates that the unselected terms are normally distributed. The effects table shows the standardized effect (the response change that occurs when a factor is altered from the low to the high level), the sum of squares for the terms (the quantity of information attributed to a term as it is changed) and the percentage contribution (based on the sum of squares and the assumption that terms possess the same degrees of freedom).

The exclusion of terms which produce non-significant effects improves the model accuracy; therefore all the other effects and interactions apart from the main effect C were removed from the Anova table (figure 207).

Source	Sum of Squares	Deg. Of Freedom	Mean Square	F Value	p-value Prob > F
Block	0.16	1	0.16		
Model	**19.12**	**1**	**19.12**	**28.522**	**< 0.0001**
C - Pressure	**18.92**	**1**	**18.92**	**28.226**	**< 0.0001**
Curvature	1.39	1	1.39	2.077	0.1603
Residual	19.44	29	0.67		
Lack of Fit	15.23	25	0.61	0.579	0.8246
Pure Error	4.21	4	1.05		
Cor Total	40.11	32			

Model Statistics		
Std. Dev.		0.82
Mean		6.22
C.V. %		13.16
PRESS		25.47
R-Squared		0.496
Adj R-Squared		0.478
Pred R-Squared		0.339
Adeq Precision		6.277
Average Ball Ra Surface Finish (nm)	=	+ 7.818 - 2.794 * C

Figure 207 - ANOVA Table, Model statistics, and optimisation equation (C in MPa) for the response of 'Average ball Ra surface finish' - [Factors that surpass a 95% confidence interval are highlighted and statistically significant. Partial sum of squares - Type III]

The 'F-Values' for both the model and factor C (contact pressure) are statistically significant. 'Prob > F' values smaller than 0.05 indicate that model terms are significant and values larger than 0.1 indicate that they are not. In the case of contact pressure there is a less than 0.01% chance that an 'F-Value' as large as 28.226 would be due to noise. The curvature, a measure of the difference of the average factorial and average centre points, is not significant for the surface finish response.

As shown in figure 208, Ra surface finish improves (decreases) as contact pressure increases. The optimisation equation shown in figure 207 describes the model behaviour.

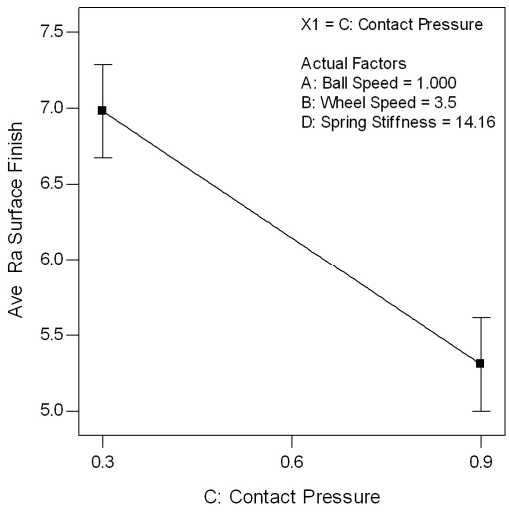

Figure 208 - Effect of contact pressure on finish

21.1.1 Model Adequacy

As demonstrated in the Anova table (figure 207) the model is significant. As desired there is only a 0.01% chance that a 'Model F-Value' as large as 28.522 would be due to noise. In terms of lack of fit, a significant value is undesirable and means that the variation of the design points about their predicted values is more than the variation of the replicates about their mean values. The model's 'Lack of Fit F-Value' (0.579) is not significant relative to the pure error. There is an 82.46% chance that a value as large as this would occur due to noise.

The 'Adjusted R-Squared' value shows that 47.8 % of the variability in this experiment is caused as a result of the model factors, i.e. in this case 47.8 % is due to changes made to the contact pressure. The 'Predicted R-Squared' value provides an indication of the predictive capability of the model. The model can be expected to explain 33.9 % of the variability in predicting new surface finish observations. Values of this size are adequate for identifying the basic magnitude of the important effects and interactions, as well as their direction. However they would ideally be in excess of 0.7 in order to accurately model this process for the identification of the precise optimum of the control parameters. The 'Predicted R-Squared' and 'Adjusted R-Squared' values are in reasonable agreement and are within the recommended 0.2 of each other. The 'Adequate Precision' ratio of 6.277 indicates an adequate signal to noise ratio; values greater than 4 are desirable and usually indicate that the model is reasonably effective at prediction.

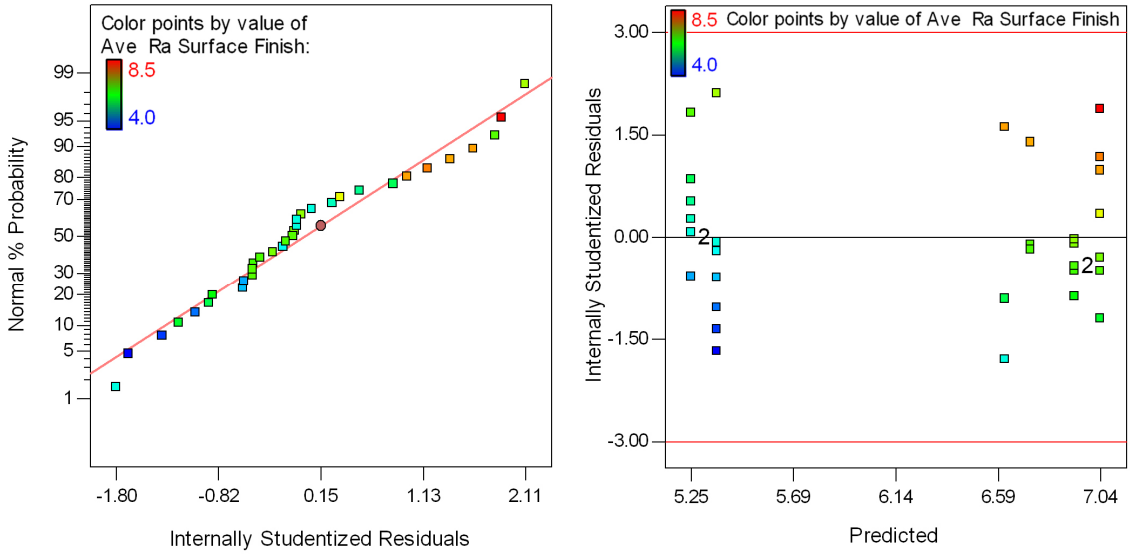

Figure 209 - Model diagnostic and influence plots for the average ball Ra surface finish response (a) Normal probability plot of studentized residuals, (b) Studentized residuals versus predicted values.

The plots of normal probability versus residuals and residuals versus predicted value are satisfactory for this response (figure 209). The residuals are normally distributed and their variance is consistent. For all factors consistent variance is observed at high, medium, and low levels, as well as for both blocks. Additional plots that checked the model satisfy that it is indeed adequate (appendix I1). As indicated by the Box Cox plot there was no need to perform a data transform. It was necessary to remove a few outlying surface finish data points from the analysed data set. These higher values were caused as a result of sparking damage to the ball during processing and the talysurf profiles clearly display their cause and presence.

21.1.2 Additional Finish Parameters

Talysurf average readings for Rq, Rp, Rz, Rt and Rdq all clearly show the sole significant result; larger contact pressures produce better surface finishes. The response for Rku suggests that high contact pressure reduces kurtosis; the strength of the effect falling between the Bonferroni and t-value limits (p-value 0.0339). The model for Rsk was not significant. There were no particular differences when comparing talysurf measurements taken solely in one direction (either across or around the ball centre) with the averaged result described above.

21.2 Wheel Spindle Power Results

Assessment of the wheel spindle power showed that contact pressure, wheel speed and the third order interaction ABC were significant effects. Figure 210 presents this data (average change in wheel spindle power usage during superfinishing) and figure 211 shows the statistical model for this response.

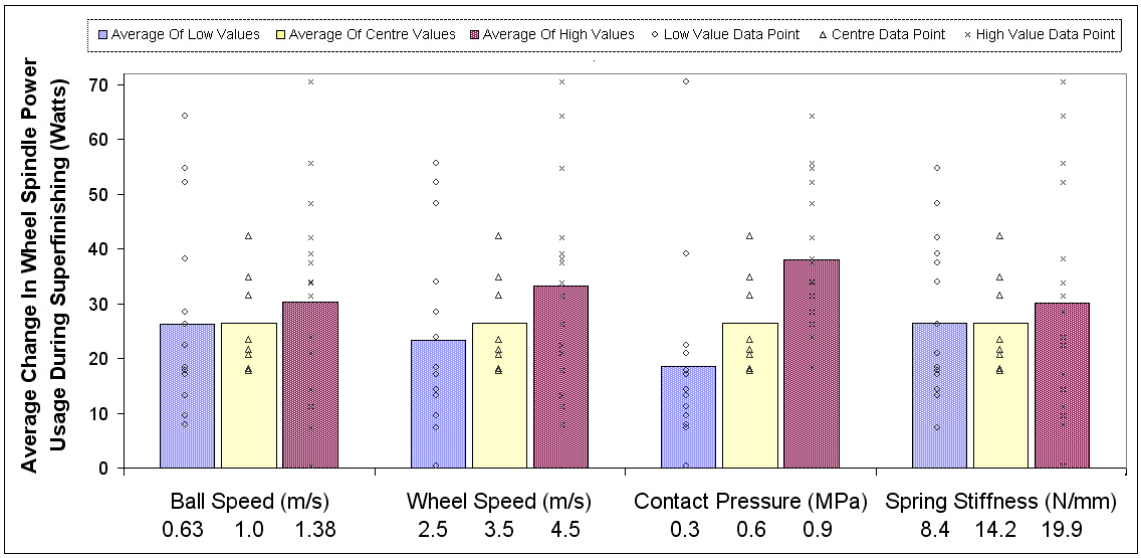

Figure 210 - Column graphs of raw results versus factor levels for the response 'average change in wheel spindle power usage during superfinishing'

As shown in the Anova table the model is significant, the lack of fit and curvature are not. The significant main effect and interactions are demonstrated by the Pareto chart (figures 211a), effects table, and plot of half normal probability versus standardized effect (appendices I2 & I3). On the Pareto chart, effects that are above the Bonferroni corrected t-value limit are almost definitely significant and those below the standard t-value limit are unlikely to be significant.

Once again factor C (contact pressure) produced a marked effect; the wheel spindle understandably using more power when a higher load is applied to the ball. This effect can be easily observed in real-time as spindle power is measured in-process. Figure 211 (c & d) shows how spindle power increased when wheel speed and contact pressure were increased at a ball speeds of 0.625 m/s and 1.375 m/s. These graphs agree with data assessing the optimisation of Elid 1 superfinishing (chapter 23).

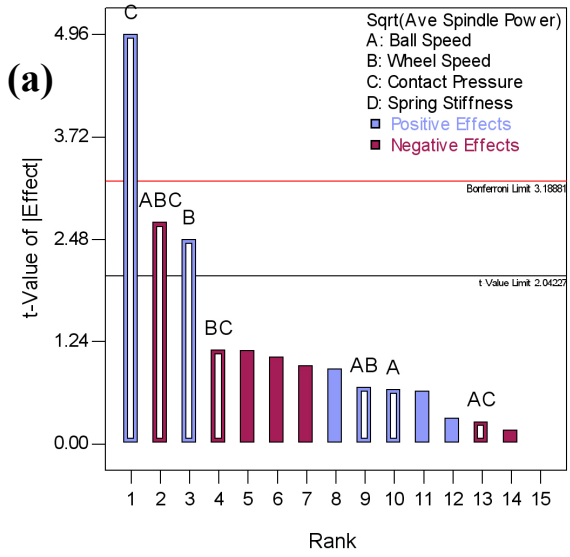

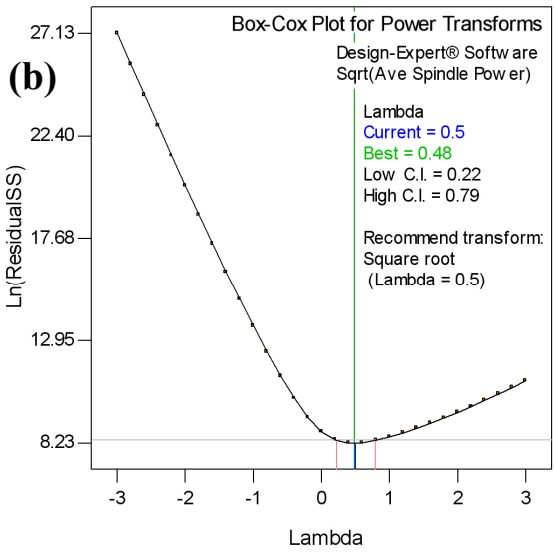

Source	Sum of Squares	Deg. Of Freedom	Mean Square	F Value	p-value Prob > F
Block	1.94	1	1.94		
Model	**56.16**	**7**	**8.02**	**5.751**	**0.0003**
A - Ball	0.60	1	0.60	0.432	0.5158
B - Wheel	**8.60**	**1**	**8.60**	**6.166**	**0.0188**
C - Pressure	**34.32**	**1**	**34.32**	**24.599**	**< 0.0001**
AB	0.65	1	0.65	0.469	0.4987
AC	0.10	1	0.10	0.072	0.7906
BC	1.80	1	1.80	1.292	0.2647
ABC	**10.08**	**1**	**10.08**	**7.229**	**0.0116**
Curvature	0.01	1	0.01	0.009	0.9242
Residual	41.85	30	1.40		
Lack of Fit	37.08	24	1.55	1.944	0.2085
Pure Error	4.77	6	0.79		
Cor Total	99.96	39			

Model Statistics	
Std. Dev.	1.18
Mean	5.04
C.V. %	23.42
PRESS	77.13
R-Squared	0.573
Adj R-Squared	0.473
Pred R-Squared	0.213
Adeq Precision	7.444

SQRT (Aveage Spindle Power Change) =

+ 10.637
- 11.149 * A
- 2.382 * B
- 10.747 * C
+ 3.375 * A * B
+ 16.968 * A * C
+ 4.199 * B * C
- 4.990 * A * B * C

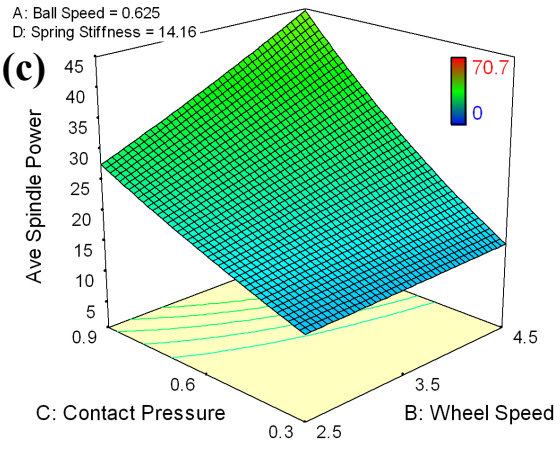

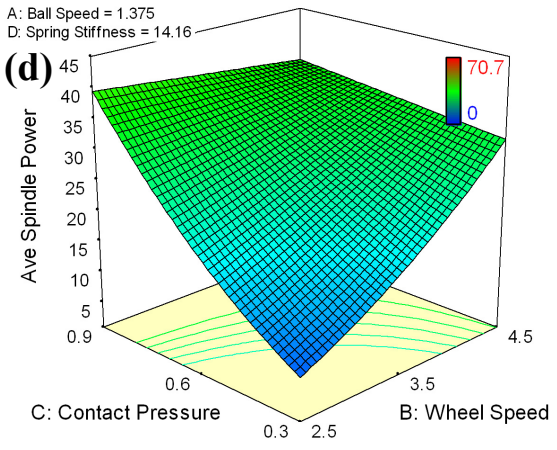

Figure 211 - Model for Drift adjusted wheel spindle power change during superfinishing response. - (a) Pareto chart of effects, (b) Box cot plot recommending transformation based on best lambda value, ANOVA table, Model statistics, and optimisation equation, 3D surface plots (c - Low ball speed), (d - High ball speed)

There was a third order interaction (ABC) that also surpassed the 0.05 threshold of statistical significance. As hierarchical factor selection is required, A, BC, AC and AB are also selected. The addition of all of these non-significant terms, whilst being required to maintain hierarchal factor selection, resulted in the predicted R-squared value of 0.213 not being as close to the 0.473 adjusted R-squared value as would normally be expected. Three factor interactions are rare in factorial design involving numeric factors and can be caused by an outlying data point. In this instance the residuals are normally distributed; there are no outlying data points, or large blocking effects. The 'Design Expert' software package recommended a square root transformation (Figure 211b) which was applied to the data of this response.

The influence that the factors have on spindle power varies from the start of a run to the end of a run. The significance of the effects B and ABC are below the 0.05 threshold of statistical significance when the initial power level is assessed (figure 212b) but increase to above the threshold when a run's final spindle power level is assessed (figure 212c). Conversely, an increase in contact pressure C, has a more pronounced effect on spindle power at the start of a run than at the end of a run (figure 212a).

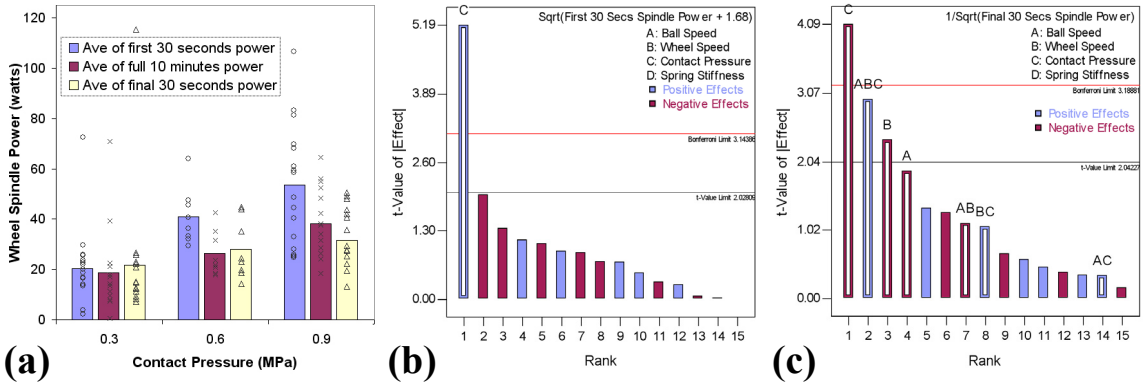

Figure 212 - Graphs showing the significant effects when assessing different portions of the runs spindle power profiles. (a) Raw data for contact pressure, (b) Analysis of the first 30 seconds, (c) Analysis of the final 30 seconds.

As demonstrated by figure 213 the slope of a run's spindle power profile is affected by the contact pressure. During run 256 for example (figure 213a), the spindle power declined over the 10 minute run at a rate of 4.21 watts per minute. A gradual decline in spindle power during a run is characteristic of a wheel that is not being maintained effectively and is therefore becoming glazed. Assessing the spindle power slope profiles for all the experimental runs revealed that when a higher contact pressure is used the condition of the wheel declines more rapidly.

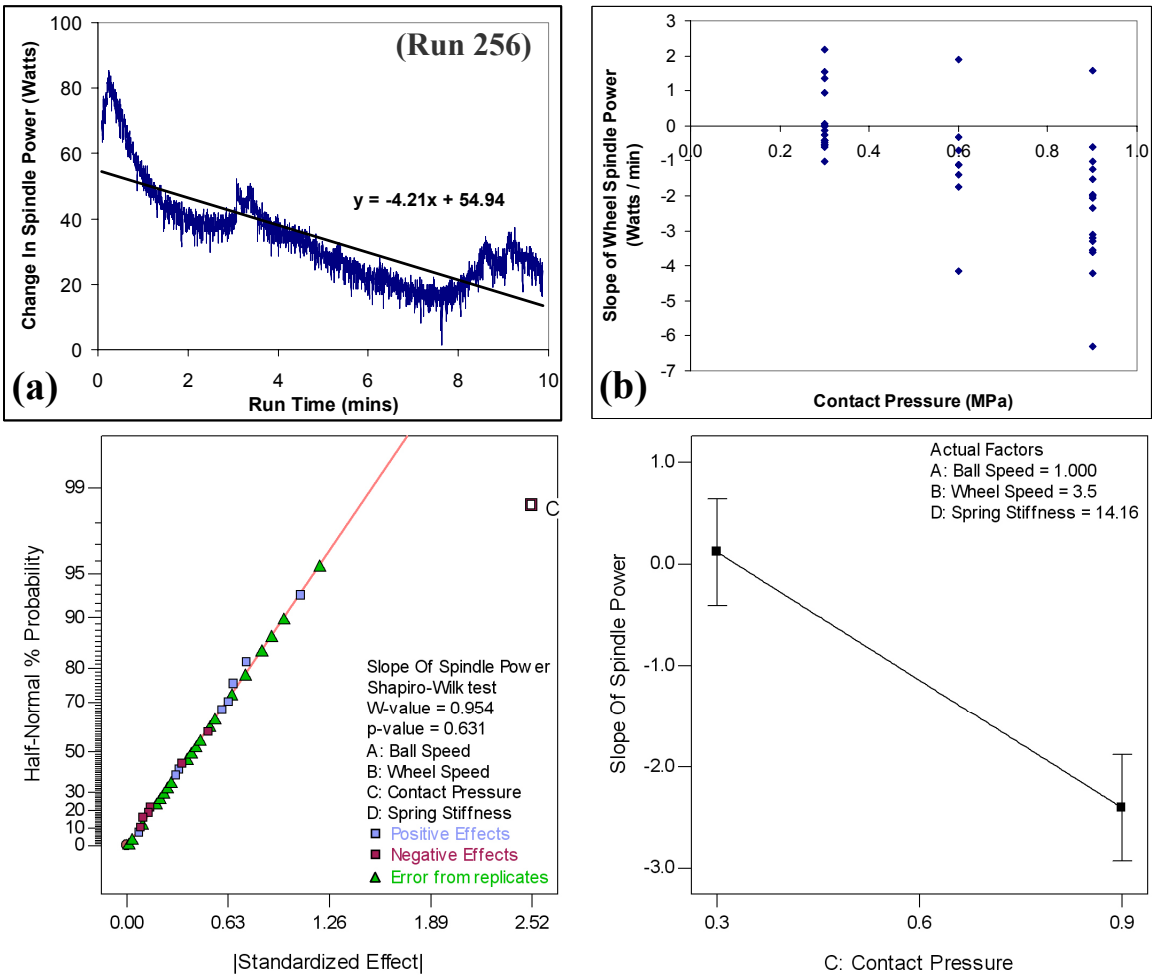

Source	Sum of Squares	Deg. Of Freedom	Mean Square	F Value	p-value Prob > F
Block	2.47	1	2.47		
Model	**47.68**	**1**	**47.68**	**21.266**	**< 0.0001**
C - Pressure	**47.57**	**1**	**47.57**	**21.215**	**< 0.0001**
Curvature	0.03	1	0.03	0.012	0.9135
Residual	76.23	34	2.24		
Lack of Fit	56.53	28	2.02	0.615	0.8233
Pure Error	19.71	6	3.28		
Cor Total	126.41	37			

Model Statistics	
Std. Dev.	1.50
Mean	-1.20
C.V. %	125.22
PRESS	95.89
R-Squared	0.385
Adj R-Squared	0.367
Pred R-Squared	0.226
Adeq Precision	6.245
Slope Of Spindle Power (watts / min) =	+ 1.381 - 4.207 * C

Figure 213 - Slope measurements and model for the response 'Slope of wheel spindle power usage during superfinishing (watts / minute). (a) Example of a run with a declining spindle power profile (Run 256), (b) Effect of contact pressure on the wheel spindle power slope for the Elid 3 factorial experimental runs.

21.3 Ball Waviness

Assessment of waviness average (Wa), produced a number of significant effects involving ball speed, wheel speed, and spring stiffness. Contact pressure did not affect ball form. Although the data was un-replicated and only consisted of 20 measurements, as opposed to the usual 40, the model was adequate to describe the effects observed.

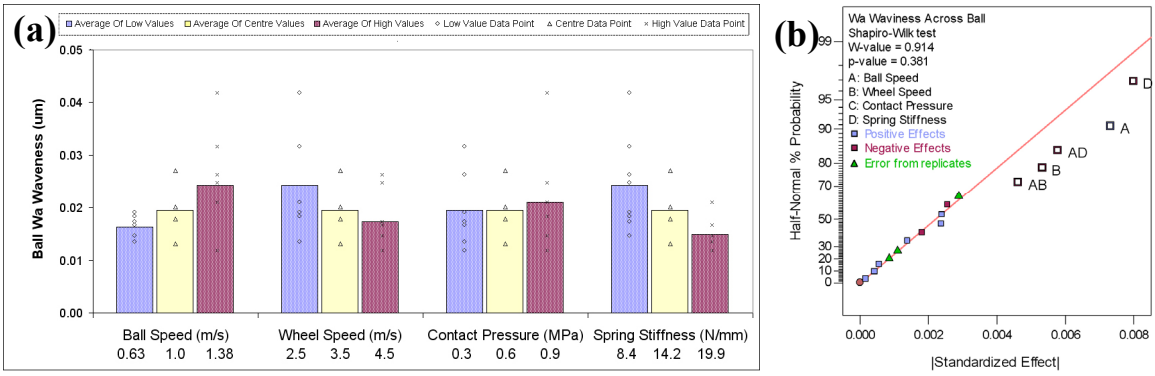

Source	Sum of Squares	Deg. Of Freedom	Mean Square	F Value	p-value Prob > F
Model	**0.00085**	**5**	**0.000171**	**10.982**	**0.0006**
A - Ball	**0.00020**	**1**	**0.000195**	**12.576**	**0.0046**
B – Wheel	**0.00010**	**1**	**0.000103**	**6.658**	**0.0256**
D - Stiffness	**0.00023**	**1**	**0.000233**	**14.981**	**0.0026**
AB	**0.00008**	**1**	**0.000078**	**5.007**	**0.0469**
AD	**0.00012**	**1**	**0.000122**	**7.842**	**0.0173**
Curvature	0.00000	1	0.000001	0.065	0.8036
Residual	0.00017	11	0.000016		
Lack of Fit	0.00007	8	0.000009	0.263	0.9420
Pure Error	0.00010	3	0.000033		
Cor Total	0.00102	17			

Model Statistics	
Std. Dev.	0.0039
Mean	0.0201
C.V. %	19.607
PRESS	0.0004
R-Squared	0.833
Adj R-Squared	0.757
Pred R-Squared	0.619
Adeq Precision	10.091

Wa Waviness Across Ball (µm) =

- 0.01249
+ 0.05260 * A
+ 0.00366 * B
+ 0.00068 * D
- 0.00644 * A * B
- 0.00140 * A * D

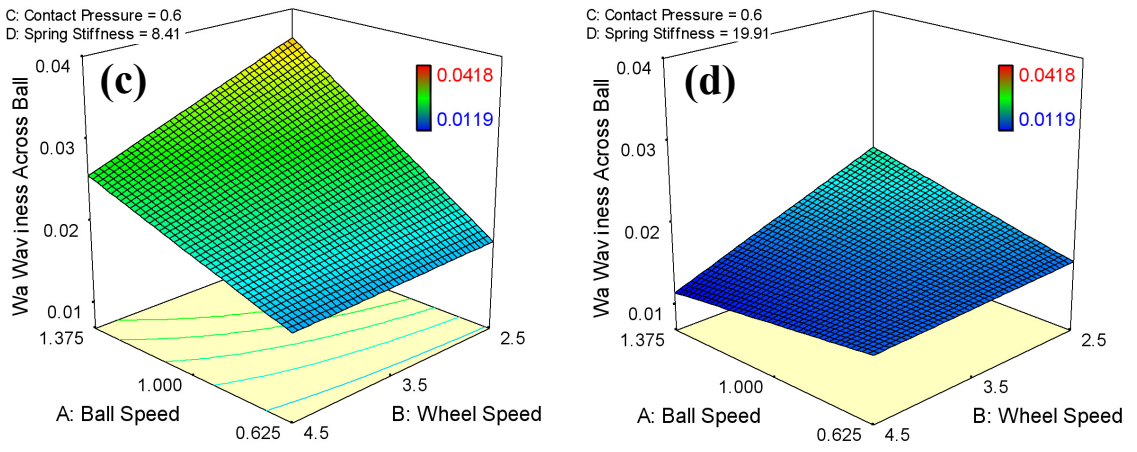

Figure 214 - Model for ball Wa waviness response. - ANOVA table, Model statistics, and optimisation equation (a) Low spring stiffness, (b) High spring stiffness

The lowest waviness result was achieved when a fast ball speed, a fast wheel speed and a stiff spring were used (figure 214). The individual effect of ball speed, whereby a slower speed improves waviness, can become subsumed by the effect of the ball-wheel and ball-stiffness interaction. Processing using a fast wheel speed and a slow ball speed resulted in the highest speed ratio (5:1) and produced grinding marks that were flat across the ball and possessed little skew to their pattern. The stiffer spring is believed to react better to any errors in ball concentricity.

As standard NMB superfinished balls were used the input waviness was already low. Assessment of waviness considered how the form of the ball was affected whilst levels of surface finish were improved. The Elid superfinished balls tested were of equivalent quality in terms of the amount of variation, as well as the general magnitude of waviness results, to those produced using standard NMB methods. Assessment of the peak to valley waviness parameter Wt produced a model of similar character to the Wa model.

21.4 Elid Power Data

None of the Elid power responses assessed produced any effects that were large enough to be distinguishable from the noise of the model. The response 'average Elid voltage during superfinishing' is shown in figure 215. The Elid power response can take several minutes to adopt levels consistent for the particular combination of factors under investigation. Superfinishing with a run time of 10 minutes is sufficiently long for this to have occurred. Nevertheless, assessment of the Elid voltage level at the end of each superfinishing run did not produce a satisfactory model with any significant effects.

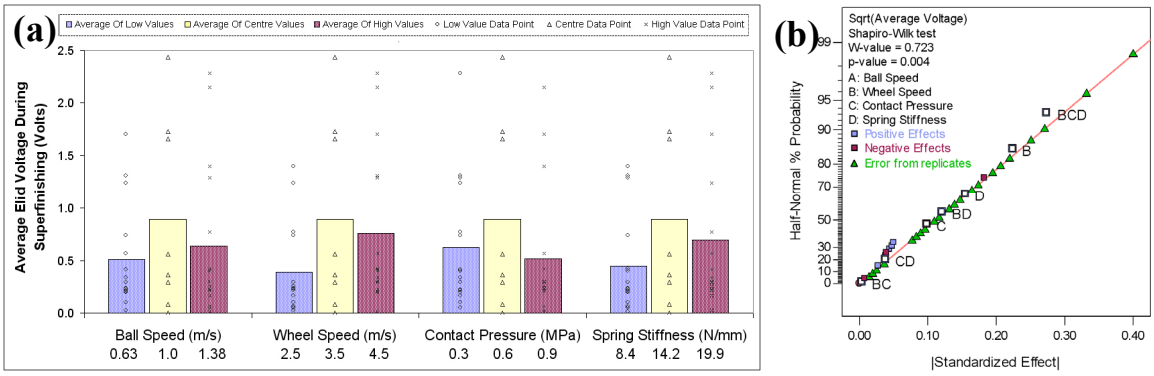

Figure 215 - Model for the Average Elid voltage during superfinishing response. - (a) Column graph of raw results, (b) Graph of effects

The voltage was measured to a high degree of accuracy compared to the variation observed and demonstrated that when Elid 3 superfinishing, the voltage level is not influenced by spindle speed, applied load or spring stiffness. The variation in values, being relatively small during this set of tests, is a result of other factors.

During Elid 3 superfinishing, a breakdown of the insulating layers results in the direct flow of current and produces a voltage reading of zero volts. The consistently low levels of voltage recorded during this experiment (zero to 6.9 volts, zero to 2.4 volts average over the 10 min runs, zero to 5.6 for average of final 30 seconds) demonstrate that the system was not maintaining the wheel's condition effectively.

21.5 Ball Material Removal

As shown in the Anova table (figure 216) the 'p-value' for the ACD interaction is less than 0.05, indicating that the effect is different from zero at a 95% confidence level. However as the 'p-value' for the model is not significant it can be concluded that none of the factors or interactions under investigation has a statistically significant effect on ball material removal.

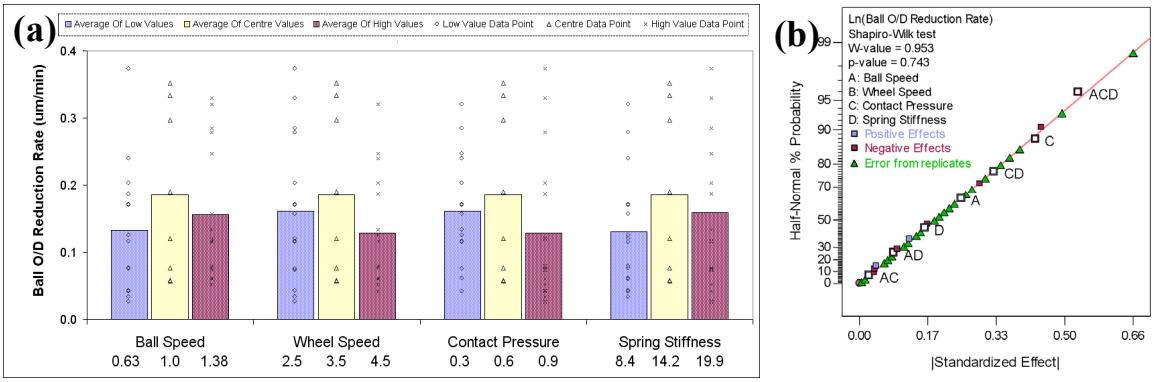

Source	Sum of Squares	Deg. Of Freedom	Mean Square	F Value	p-value Prob > F
Block	0.012	1	0.012		
Model	5.340	7	0.763	1.482	0.2113
A - Ball	0.492	1	0.492	0.955	0.3362
C - Pressure	1.465	1	1.465	2.847	0.1019
D - Stiffness	0.203	1	0.203	0.393	0.5352
AC	0.005	1	0.005	0.009	0.9248
AD	0.055	1	0.055	0.107	0.7459
CD	0.857	1	0.857	1.665	0.2068
ACD	**2.264**	**1**	**2.264**	**4.399**	**0.0445**
Curvature	0.379	1	0.379	0.736	0.3976
Residual	15.442	30	0.515		
Lack of Fit	11.307	24	0.471	0.684	0.7671
Pure Error	4.135	6	0.689		
Cor Total	21.173	39			

Model Statistics	
Std. Dev.	1.50
Mean	-1.20
C.V. %	125.22
PRESS	95.89
R-Squared	0.385
Adj R-Squared	0.367
Pred R-Squared	0.226
Adeq Precision	6.245

Figure 216 - Model for rate of ball O/D reduction response. - (a) Column graph of raw results, (b) Graph of effects, ANOVA table, Model statistics, and optimisation equation

None of the factors produced an effect even though a large number of runs was conducted and the measurement accuracy was sufficient relative to the quantity of material removed (maximum error for data points in figure 216a is $\pm$ 0.027 µm/min, standard error is $\pm$ 0.0012 µm/min). The combination of Elid 2+3 dressing and the #4000 wheel did, however, prevent any runs recording zero material removal.

21.6 Wheel Wear

During the 6.67 hours of total superfinishing time for this set of tests, the wheel length was reduced by 0.46 mm, equating to 1.15 µm per minute. Assuming that the rate of wheel wear is consistent and considering the small size of the abrasives used (4.0 µm), a new layer of sharp abrasives would be revealed every 3½ minutes.

Touch point at the start of testing = 2.920 mm
Touch point at the end of testing (ball 7) = 3.380 mm
½ the difference in ball O/D between touch points = 0 µm
Wheel length reduction = 460 µm
Total superfinishing run time = 6.67 hours
Average wheel wear = 11.5 µm per ball / run or 1.15 µm per minute

As previously identified, Elid 3 superfinishing alone results in effectively zero wheel wear. The vast majority of wear that occurred during this set of tests can therefore be confidently attributed to the inclusion of a one minute Elid 2 conditioning cycle prior to each run. Following this cycle, when superfinishing contact is initiated it is likely that the wheel would wear the total amount for the 10 minute run almost immediately.

It is not just achieving a larger quantity of wheel wear that is required, but achieving it at a rate that is steady relative to the size of the abrasive. This is where the in-process gradual wear of the wheel using Elid 1 (chapter 22) provides benefits over conventional dressing, Elid 2, or the ineffective dressing of Elid 3.

21.7 Correlations for Elid 2 + 3 Superfinishing

Figure 217 shows the correlations between some of the responses analysed. Values of 1 or -1 indicate either a perfect positive or perfect negative correlation. A value of zero indicates no correlation. In order to be statistically significant, in excessive of a 95% confidence level, a value greater than 0.445 or less than -0.445 is required.

Correlation Matrix Using Excels CORREL Function $Correl(X,Y)=\frac{\sum(x-\bar{x})(y-\bar{y})}{\sqrt{\sum(x-\bar{x})^2\sum(y-\bar{y})^2}}$	Average Current	Average Voltage	Slope Of Spindle Power	Average Spindle Power	Ball O/D Reduction Rate	Ra Surface Finish (Average)	Rsk Surface Finish (Average)	Rku Surface Finish (Average)	Rp Surface Finish (Average)	Rt Surface Finish (Average)	Rdq Surface Finish (Average)	Wt Waviness (Across Ball)	Wa Waviness (Across Ball)
Average Current	1.00												
Average Voltage	-0.93	1.00											
Slope Of Spindle Power	-0.02	0.00	1.00										
Average Spindle Power	-0.32	0.24	-0.64	1.00									
Ball O/D Reduction Rate	-0.32	0.27	0.03	0.37	1.00								
Ra Surface Finish (Average)	-0.02	0.05	0.70	-0.37	0.22	1.00							
Rsk Surface Finish (Average)	-0.08	0.01	0.27	-0.26	-0.04	0.12	1.00						
Rku Surface Finish (Average)	-0.15	0.21	-0.21	0.37	0.18	-0.05	-0.86	1.00					
Rp Surface Finish (Average)	-0.23	0.24	0.63	-0.27	0.41	0.87	0.30	-0.03	1.00				
Rt Surface Finish (Average)	-0.24	0.30	0.46	-0.19	0.29	0.46	-0.31	0.57	0.60	1.00			
Rdq Surface Finish (Average)	-0.14	0.23	0.63	-0.30	0.44	0.76	0.03	0.16	0.85	0.69	1.00		
Wt Waviness (Across Ball)	0.03	-0.03	0.03	-0.09	0.38	-0.47	0.43	-0.38	-0.16	-0.09	-0.06	1.00	
Wa Waviness (Across Ball)	-0.06	0.09	-0.03	-0.03	0.38	-0.29	0.38	-0.23	-0.01	0.10	0.13	0.87	1.00

Figure 217 - Correlation matrix for some of the responses analysed -
[Correlation in excess of 0.5 are coloured red, and points of interest highlighted yellow]
[Correlation equation x and y are the sample means 'average(array1)' and 'average(array2)'].

- As usual Elid current closely mirrors Elid voltage (Correlation function = -0.93) (figure 218).
- Although both factors can be used to describe the condition of the wheel and unlike in other experimental sets, there was no correlation between spindle power and Elid activity. There is however evidence of a direct relationship from the profiles recorded during each run, (figure 219).
- The slope of spindle power correlates reasonably well with surface finish parameters Ra (figure 218), as well as Rp and Rdq. This correlation is due the fact that spindle power decline denotes wheel glazing and that glazed wheels produce better surface finishes.
- Unusually there was no correlation between the rate of ball material removal and spindle power.
- Ball material removal did not correlate with any of the other responses investigated (Elid or spindle power, ball form or finish).
- As they are simply a different analysis of the same data, many of the surface finish parameters correlate.
- Likewise ball waviness parameters Wa and Wt correlate with each other, however not with any of the other responses.

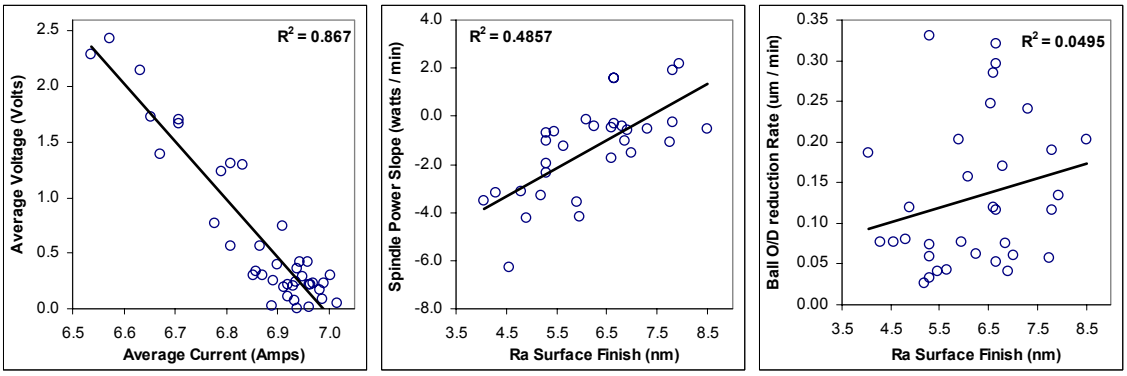

Figure 218 - Correlations between various responses

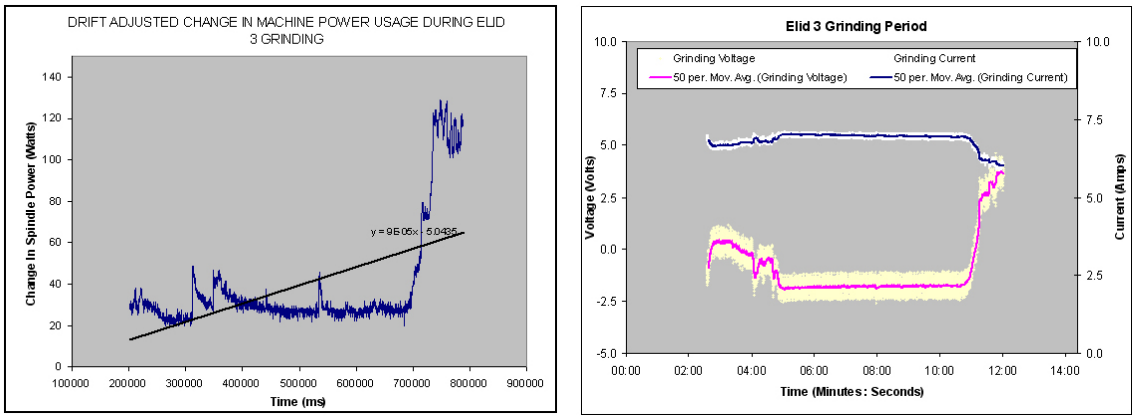

Figure 219 - Example of correlation in real time between spindle and Elid power

21.8 Chapter Conclusions

The results from this experiment are marked as much by the absence of strong effects and correlations as by their presence. The influence that spindle speed and applied load had on the various responses was surprisingly small.

The inclusion of Elid 2 dressing had a number of beneficial effects. It returned the wheel to a well-dressed condition, lessening the influence of the previous run, improving the stability of the process and increasing the rate of ball material removal. Assessment of the Elid power activity during superfinishing revealed that Elid 3 was erratic and largely ineffective at maintaining the condition of the wheel; this was not improved by changing the various factors. The effects recorded can be attributed equally to the degradation of the wheel's condition after Elid 2 dressing and to the influence of Elid 3 superfinishing.

21.8.1 Spindle Power

The fact that an Elid 2 cycle was used influenced spindle power results considerably and caused the surface finish to be linked to the slope of spindle power. There is a steeper slope decline, strongly indicating a faster rate of wheel glazing, when high pressure is used compared to when low pressure is used. Runs conducted when the applied load was high also recorded statistically higher spindle power; therefore more work has gone into the ball. When comparing levels at the beginning and end of runs, there is a larger relative difference when a high load is used.

21.8.2 Material Removal

Although the use of Elid 2 did improve processing stability it did not aid the assessment of how factors influence ball material removal. Elid 2 refreshes the condition of the wheel, allowing an amount of material to be removed before the wheel becomes glazed and is incapable of further material removal (chapter 20). This should occur well within the 10 minute run time conducted here, regardless of what processing parameters are used. Elid 2 not only increased material removal but also masked the effects under investigation. This, combined with the unpredictability of Elid 3, resulted in no significant effects being observed for this response.

21.8.3 Surface Finish

Surface finish results obtained in this experiment are contrary to those described in the literature, where surface finish benefited, through a reduced grit depth of cut, from a lower applied load.

In the current research, surface finish improves when contact pressure increases for the following reasons:

(1) *Geometry* - When a high load is used the ball and wheel will knit together better during processing. This increases the evenness of the ball and wheel area contact as the spindles deflect under load.

(2) *Wheel Condition* - From its original well-dressed condition at the start of a run, the wheel will become more glazed, more quickly, when contact pressure is high than when it is low. As a result, the wheel will provide more of a burnishing action by the end of the run. The wheel will have been superfinishing in a glazed condition for longer which produces a better finish. Assessment of spindle power supports this argument.

21.8.4 Optimised Elid 2+3 Parameters

For optimum results the factors investigated should be set as outlined in figure 220. Ball speed should be slow, wheel speed should be fast, contact pressure should be high and a stiff spring should be used.

Required Response	Ball Speed	Wheel Speed	Contact Pressure	Spring Stiffness
Lowest Surface Finish	Any	Any	High	Any
Highest Spindle Power	Slow	Fast	High	Any
Lowest Waviness	Debatable	Fast	Any	Stiff
Highest Elid Voltage	Any	Any	Any	Any
Highest Material Removal	Any	Any	Any	Any

Figure 220 - Optimum selection of parameters based on Elid 2+3 superfinishing data

Chapter 22 - Elid 1 Performance

Following the poor performance of Elid 3, a new fixturing method was designed in order to test the use of the more conventional Elid 1. The details of the system developed are outlined in the experimental. This type of Elid has a number of advantages over electrode-less Elid 3; it allows a wider range of metal bonded wheels to be used, as well as improving overall Elid simplicity and performance. There are some restrictions on the size / type of balls that can be processed, i.e. no high angle balls, nothing smaller than size RNB08.

22.1 Elid Power

Because there is a separation gap between anode and cathode when an Elid 1 setup is employed, there is a large resistance in the electro-chemical cell. The Elid power results follow typical behaviour for Elid 2, or pre-process dressing, with the addition of the grinding surface of the wheel being gradually worn away while superfinishing. Voltage remains stable and high, current remains low and the wheel is continually maintained close to its fully dressed condition (figure 221). When fresh sites of the wheel's copper bond are uncovered while superfinishing, the equilibrium of the electro-chemical cell is affected, causing a decrease in resistance. After a period of time the superfinishing process achieves its own equilibrium, balanced by the electro-chemical erosion of the wheel's bond and the gradual mechanical wearing of the wheel.

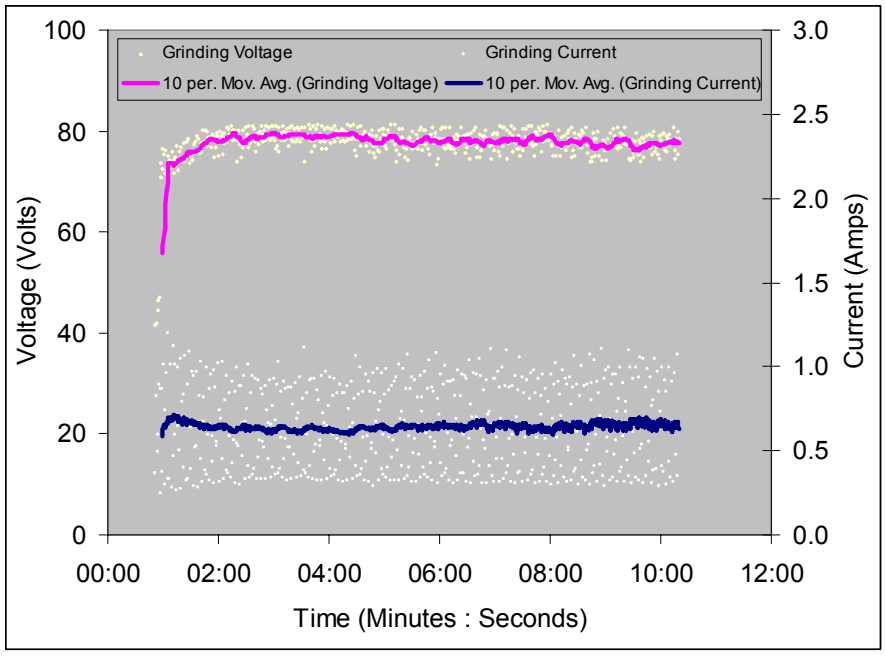

Figure 221 - Typical Elid power activity during Elid 1 superfinishing. - [40I, 90V, 50%]

22.2 Ball Material Removal (#12,000 MRB-CBN)

Using the Elid 1 system significantly improved the ball material removal rate. However stability was not improved, as zero removal was recorded on some runs (figure 222). It appeared that stable superfinishing conditions were not achieved during many of the initial tests. In figure 223 the Elid 1 material removal rate is compared against those achieved when using the Elid power supply in various different ways, as previously discussed in chapters 19 & 20.

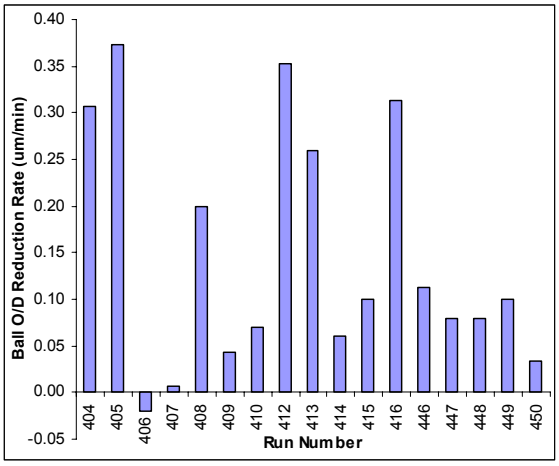

Figure 222 - Ball material removal consistency when processing using Elid 1. [Result inaccuracy: max=0.05 µm, norm=0.017 µm]

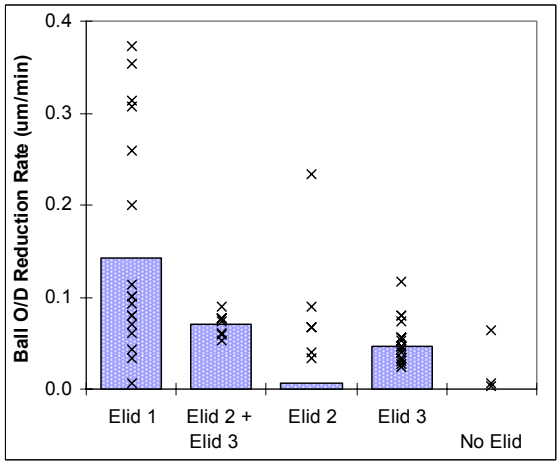

Figure 223 - Ball material removal rates for various Elid configurations

There are two main elements which combine to cause a vast increase in processing efficiency when Elid 1 superfinishing, but do not improve Elid 3 efficiency. These are increased Elid power settings, and optimization of spindle speeds and applied force. When high Elid power settings (40A, 90V, 50% duty) are used in conjunction with Elid 1, there is a significant improvement in the rate of ball material removal compared to when low power settings (20A, 60V, 10% duty) are used. The application of these high power values in an Elid 3 configuration did not lead to an increase in processing efficiency (figure 224). In fact, using high power values with Elid 3 has the additional adverse effect of increasing the chances of sparking between the ball and wheel.

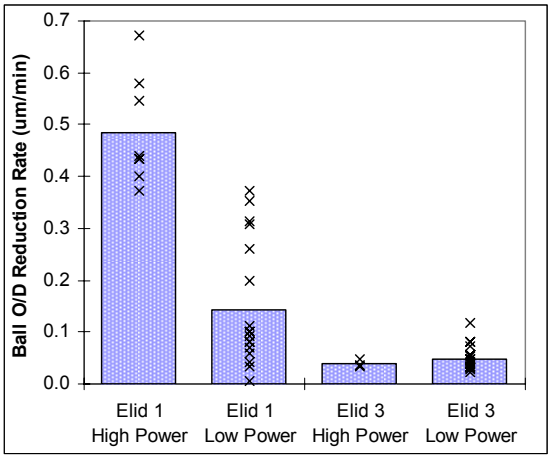

Figure 224 - Ball material removal rates at high (40A, 90V, 50% duty) and low (20A, 60V, 10% duty) power values

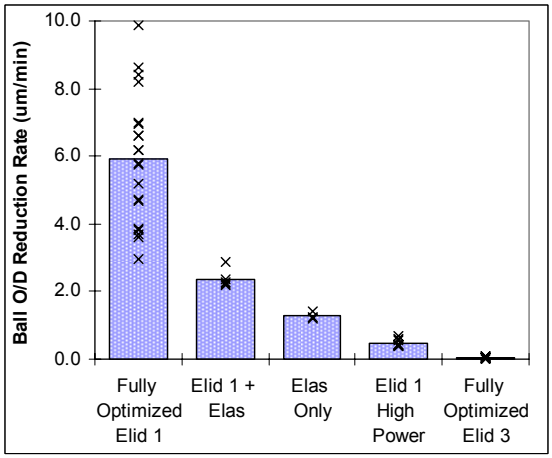

Figure 225 - Ball material removal rates when using a fully optimized Elid 1 and fully optimized Elid 3 parameters. (#12,000 MRN-CBN)

When the Elid 1 aggressiveness was increased further by using a duty of 70% instead of 50%, there was another major jump in removal rate. This increased the working current during processing from 0.6 - 0.8 amps to 1.2 - 1.8 amps. This substantial increase in Elid aggressiveness improved the condition of the wheel and caused the spindle power usage to increase from around 100 to 200 watts.

Optimization of spindle speeds and applied forces for Elid 1 is outlined in chapter 23. Figure 225 shows the ball O/D reduction rate after full optimization of processing parameters for both Elid 3 and Elid 1 superfinishing. When all aspects of the Elid 1 superfinishing process had been optimized (chapter 28), spindle power values of up to 350 watts were reached.

22.2.1 Influence of Abrasive Size

The material removal data from Elid 1 runs using different MRB-CBN wheels is shown in figure 226. These results reveal an unusual but beneficial trend. The rate of material removal is largely unaffected by the abrasive size used. This is because the Elid 1 superfinishing process can be made to work extremely effectively with smaller abrasives but remains relatively ineffective when larger abrasives are used. This means that the finest abrasives can be used and very high levels of surface finish achieved, without sacrificing processing efficiency.

Around 70 Elid 1 runs were conducted with the #500 MRB-CBN wheel that varied numerous factors. Whereas the performance of the finer abrasive wheels improved dramatically as the process was optimized, the #500 wheel did not.

The lines which display the maximum achieved ball material removal rates when Elid 1 and Elid 3 are used, ultimately converge. At some point the abrasive is either too small or too large to effect a change in material removal.

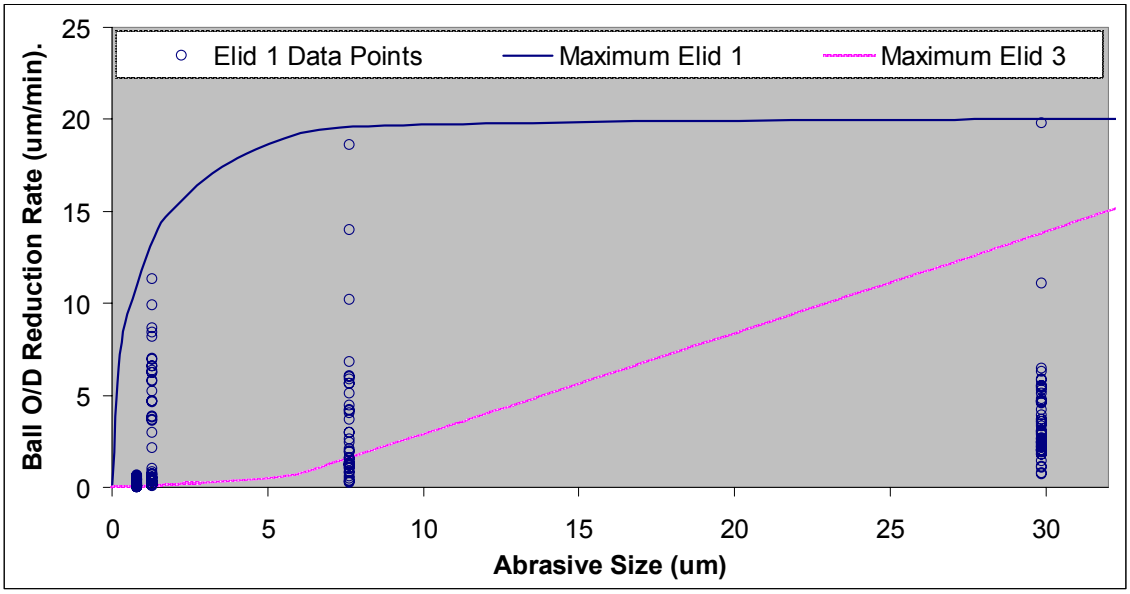

Figure 226 - BMRR vs. abrasive size and a variety of experimental sets

It is believed that the high material removal rate achieved using Elid 1 is due to the way that the wheel wears. The continual erosion / oxidation of the wheel's surface allows new / sharp abrasives to be revealed and then easily ejected when worn. When a #500 wheel (30 µm abrasive) is used, the rate at which worn abrasives are ejected and new abrasives are revealed is slower.

An interesting continuation to this work would be to explore the material removal and resultant ball surface finish that can be achieved with the use of the smallest abrasive MRB-CBN wheels available (#120,000 to #3,000,000).

22.3 Ball Output Quality

Ball form is not a function of the type of Elid used. However, better wheel dressing (thus larger rates of material removal) causes the form of the ball to be increasingly dependent on the processing run.

Copper deposits were found on the surface of some Elid 1 superfinished balls, when the system was not aligned correctly. This is despite the fact that when Elid 1 superfinishing, the ball is insulated and is not involved in the electrical circuit. This is probably due to fluid collecting in the central space of the wheel and becoming concentrated with copper ions, combined with the close proximity of high power carrying elements.

The surface finish of balls produced when using Elid 1 reflect the fact that the wheel is well-dressed. As a result the surface finish is slightly worse than when using Elid 3 or Elid 2. This disparity in surface finish is greater when using larger abrasive wheels such as the #2000, where the difference between a well-dressed and a glazed wheel is more pronounced (chapter 16). One option to overcome this is to achieve the improved removal rates of Elid 1 at the start of a run, then allow the wheel to glaze towards the end of a processing cycle.

22.4 Elid 1 - Rate of Wheel Glazing & Recovery

The rate of wheel glazing and recovery was clearly of particular importance when Elid 2 superfinishing and it is also of relevance to Elid 1. Elid 1 superfinishing with a #12,000 MRB-CBN wheel achieved a good rate of ball material removal for the standard parameters selected (figure 227). One minute after turning the Elid power supply off, ball material removal had declined to zero. When the Elid power was turned back on, effective ball material removal was restarted within seconds.

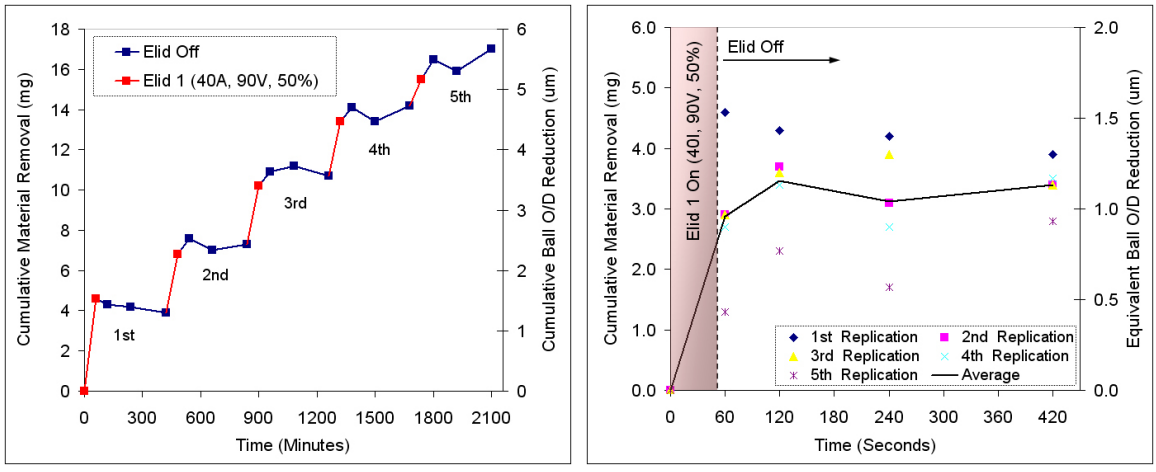

Figure 227 - Deterioration of a #12,000 MRB-CBN wheels ability to remove ball material when Elid 1 is turned off and ability to recover when it is turned on. - (a) Cumulative material removal, (b) Cumulative ball material removal per dressing cycle. [Standard parameters as in figure 95]

When the Elid 1 system is on, the substantially inflated spindle power usage value (figure 228 a & c) shows that the wheel is being continually dressed and maintained in a heightened free-cutting state. The spindle power data shows how rapidly the spindle power level declines when the Elid system is turned off. The decline in spindle power corresponds to the ball material removal levels shown in figure 227.

When Elid 1 superfinishing is re-initiated, the wheel's condition is restored very rapidly; the spindle power only takes a few seconds of steep climbing to reach static levels after the load has been applied (run 534, figure 228c). There was no recovery period for the first run of this set of tests (run 530, figure 228a) as the wheel was not glazed prior to beginning.

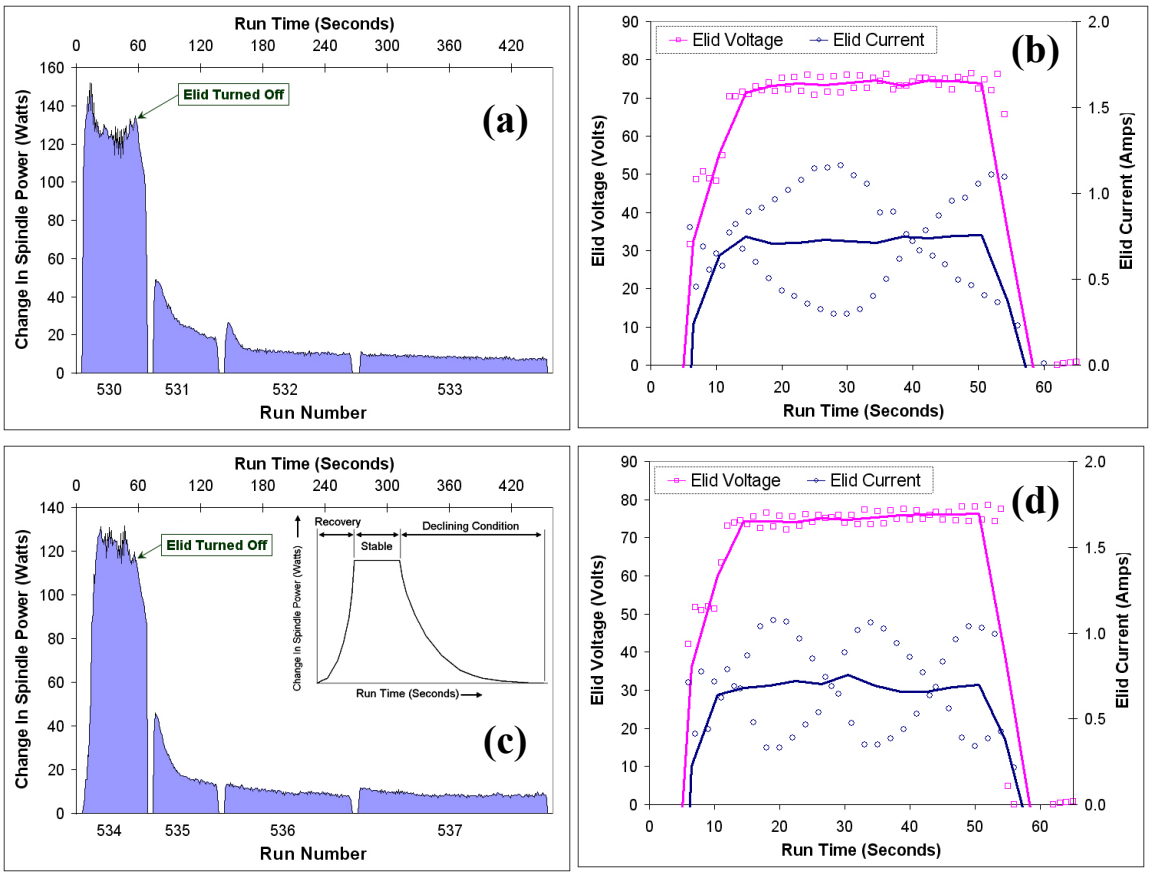

Figure 228 - Graphs showing the rate of wheel glazing and recovery when Elid 1 superfinishing with a #12,000 MRB-CBN wheel. – Graphs corresponded to material removal information provided in figure 227. (a) Wheel spindle power data for 1st replication, (b) Elid power data for 1st replication. (c) Wheel spindle power data for 2nd replication, (d) Elid power data for 2nd replication.

The Elid power supply achieves stable (flat) levels seconds after Elid 1 processing is restarted (bearing in mind that it takes a few seconds for the Elid power levels to fully power up when the power supply is turned on).

Chapter 23

Optimization of Elid 1 superfinishing parameters

Using a #12,000 (1.31 µm) MRB-CBN wheel in an Elid 1 configuration, the factors wheel speed, ball speed and contact pressure were investigated (figure 229). Results from this experiment were analysed using 'Design Expert' and are summarised below with additional information provided in appendix J.

Factors Under Investigation	Low Level	Centre Level	High Level
(A) Ball Spindle Speed at Crown (m/s)	1.0	2.0	3.0
(B) Wheel Spindle Speed at O/D (m/s)	3.0	4.0	5.0
(C) Superfinishing Contact Pressure (MPa)	0.5	1.0	1.5

Figure 229 - Factors under investigation - [Run Details: Elid 1 superfinishing for 10 mins. Elid turned off 30 seconds before the end of each grinding run. 40l, 90V, 50% Duty. #12,000 MRB-CBN wheel].

23.1 Ball Material Removal Rate

Compared with chapter 21, where combined Elid 2 + Elid 3 was employed, the use of Elid 1 resulted in the material removal rates being on average 2.7 times larger, despite the fact that the abrasive was 2.9 times smaller. This is because the wheel was effectively maintained in a well-dressed condition during all the runs. In addition to the higher average rates of material removal, when Elid 1 was used all three of the factors under investigation produced significant main effects. Material removal increased when using a low ball speed, a low wheel speed, and a high contact pressure (figure 230).

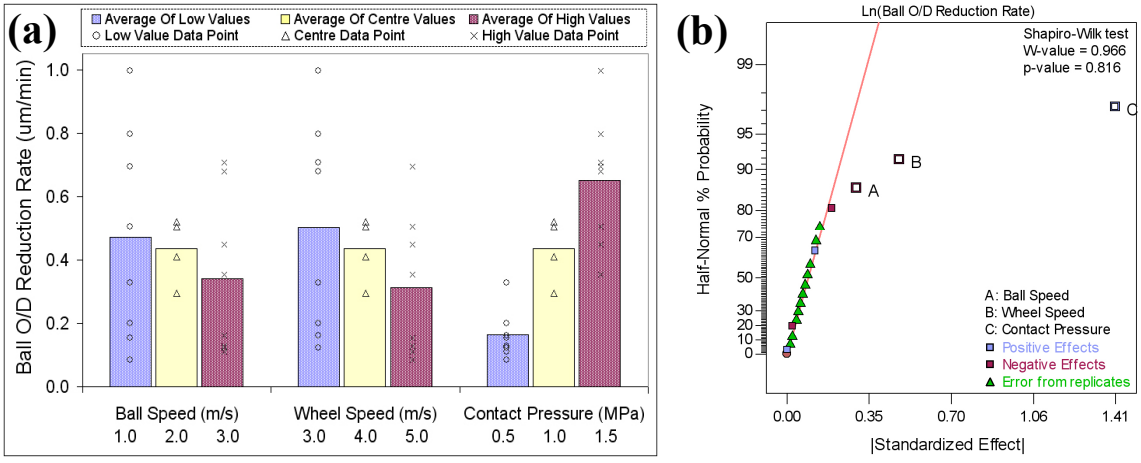

Figure 230 - Model for the Ball O/D reduction response. (a) Graph of raw results, (b) Graph of effects

The model was significant and accurately described the strong effects observed (figure 231). Curvature was significant for the ball material removal model. A log data transform was applied to this data set.

Source	Sum of Squares	Deg. Of Freedom	Mean Square	F Value	p-value Prob > F
Model	**9.23**	**3**	**3.077**	**54.146**	**< 0.0001**
A - Ball	**0.36**	**1**	**0.356**	**6.272**	**0.0243**
B - Wheel	**0.93**	**1**	**0.930**	**16.360**	**0.0011**
C - Pressure	**7.94**	**1**	**7.945**	**139.808**	**< 0.0001**
Curvature	**0.34**	**1**	**0.340**	**5.981**	**0.0273**
Residual	0.85	15	0.057		
Lack of Fit	0.21	4	0.053	0.901	0.4959
Pure Error	0.64	11	0.058		
Cor Total	10.42	19			

Model Statistics	
Std. Dev.	0.24
Mean	-1.12
C.V. %	21.34
PRESS	1.52
R-Squared	0.915
Adj R-Squared	0.899
Pred R-Squared	0.850
Adeq Precision	18.373

Ln (Ball O/D Reduction Rate) µm/min =
- 1.329
- 0.149 * A
- 0.241 * B
+ 1.409 * C

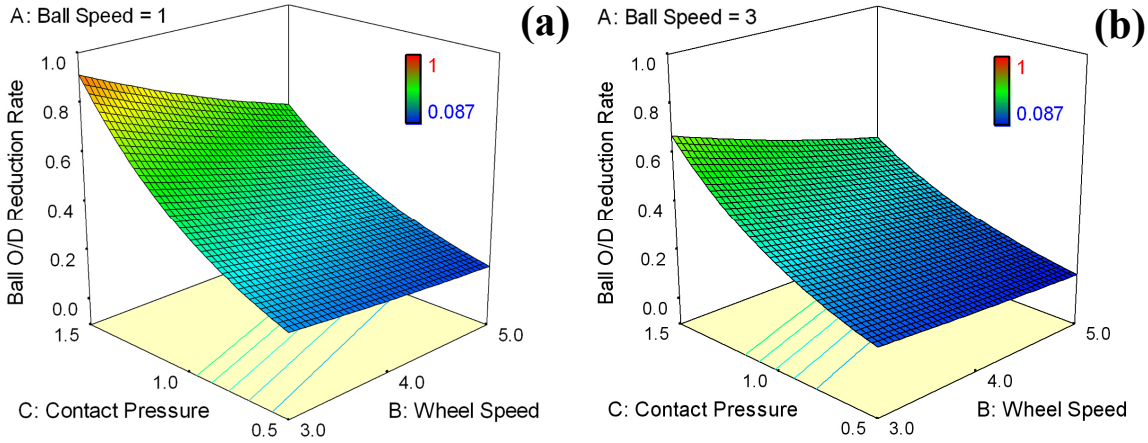

Figure 231 - Model for the Ball O/D reduction response. - ANOVA Table, Model statistics, and optimisation equation, 3D surface graphs of wheel speed and contact pressure for (a) Ball speed of 1.0 m/s, (d) Ball speed of 3.0 m/s.

When the condition of the wheel is effectively maintained, the influence that the processing parameters have on material removal becomes significant. As a result processing parameters are able to be optimized for maximum material removal, in addition to the generally higher removal rate that occurs when using Elid 1. The process has to work harder to maintain the wheel's condition when ball material removal is high. This is because aggressive processing parameters degrade the wheel faster, as illustrated by the Elid power and wheel spindle power responses. The Elid power supply recorded a lower voltage and the surface of the wheel was coarse and open, therefore the spindle power was higher.

23.2 Elid power values

The Elid power supply responses were assessed as changes were made to spindle speed and contact pressure. As usual the current response was mirrored by the voltage (voltage is shown in figure 232). Contact pressure had a strong effect; the effect of wheel speed was statistically significant but less pronounced, falling between the Bonferroni and T-Value limits (appendix J5). Neither the ball speed, nor any interactions, had a statistically significant effect (figure 232a). The curvature of this response was not significant relative to the noise.

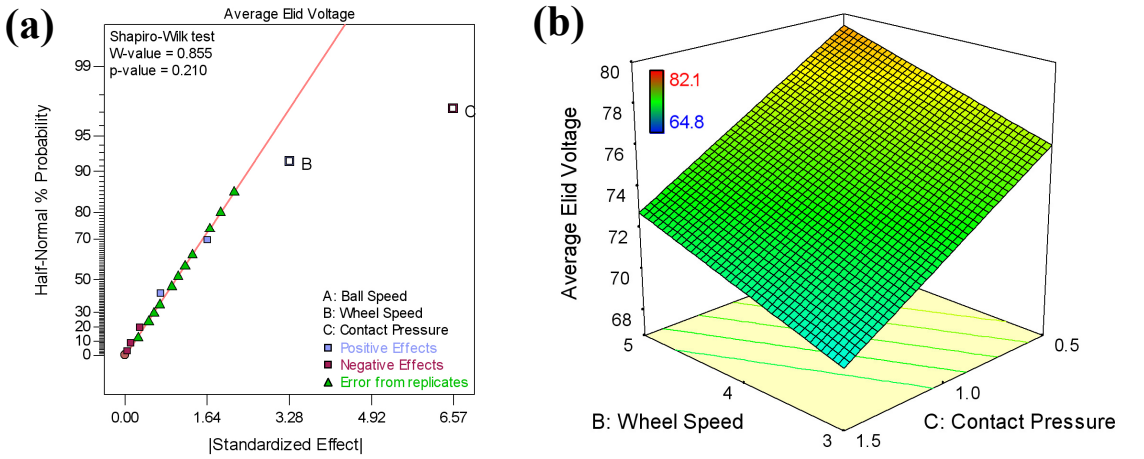

Source	Sum of Squares	Deg. Of Freedom	Mean Square	F Value	p-value Prob > F
Model	**215.99**	**2**	**107.99**	**15.95**	**0.0002**
B - Wheel	**43.51**	**1**	**43.51**	**6.43**	**0.0221**
C - Pressure	**172.48**	**1**	**172.48**	**25.47**	**0.0001**
Curvature	3.91	1	3.91	0.58	0.4581
Residual	108.34	16	6.77		
Lack of Fit	13.41	5	2.68	0.31	0.8964
Pure Error	94.93	11	8.63		
Cor Total	328.25	19			

Model Statistics	
Std. Dev.	2.60
Mean	74.28
C.V. %	3.50
PRESS	169.74
R-Squared	0.666
Adj R-Squared	0.624
Pred R-Squared	0.477
Adeq Precision	8.477

Average Voltage (Volts) During Superfinishing = + 74.472 + 1.649 * B - 6.567 * C

Figure 232 - Model for the average Elid voltage during superfinishing response. –
(a) Graph of effects, (b) 3D surface graph, ANOVA Table, Model statistics, & optimisation equation.

As demonstrated in the analysis of variance table, there was only a 0.02% chance that a "Model F-Value" this large could occur due to noise. The model statistics, as well as the diagnostic plots of the data, indicate that the model is adequate at describing the effects shown.

A high voltage occurs when the wheel's surface is thoroughly oxidised, usually indicating that the wheel is in a good condition. When Elid 1 superfinishing with un-aggressive processing parameters, there is little change to the wheel's surface and therefore little change to the Elid power values. When aggressive processing parameters are used the surface of the wheel is worn away faster. The lower voltage levels that directly correspond to a higher rate of material removal occur as the Elid system is oxidising freshly revealed portions of the copper wheel.

Unlike superfinishing with Elid 3 there is no breakdown in the Elid mechanism when Elid 1 is used. As a result, a low voltage (relative to the voltage level selected) signifies that the Elid 1 system is working hard and rapidly eroding the wheel's metallic bonding material. Due to this continual refreshment of the abrasives there is a correlation between low Elid voltage and high ball material removal, high spindle power, and high surface finish. This is the reverse of Elid 3 where due to the breakdown in dressing there is lower ball material removal and lower spindle power when the voltage is low.

Elid power values are a somewhat complex way to assess the Elid process and they can appear contradictory. The higher the Elid power values used the higher the voltage will remain, as it will have more strength to oxidize the wheel as it wears. Therefore it will show a less pronounced response (still maintaining high values) when the copper at the surface of the wheel is revealed. When Elid 2 dressing or when pre-conditioning the wheel, a high voltage indicates that the wheel is well-dressed, or at least as well-dressed as it is going to get. This is because there is no mechanical method of removing the oxidized and non-conductive material from the surface of the wheel.

23.3 Wheel Spindle Power

Figure 233 shows the model for average spindle power during superfinishing. As with the ball material removal and Elid power responses, the system is working most aggressively when the ball and wheel spindle are running slowly and the contact pressure is large.

Source	Sum of Squares	Deg. Of Freedom	Mean Square	F Value	p-value Prob > F
Model	**142.77**	**5**	**28.55**	**45.52**	**< 0.0001**
A – Ball	**37.48**	**1**	**37.48**	**59.75**	**< 0.0001**
B - Wheel	1.54	1	1.54	2.46	0.1408
C - Pressure	**92.96**	**1**	**92.96**	**148.19**	**< 0.0001**
AB	**5.26**	**1**	**5.26**	**8.38**	**0.0125**
AC	**5.53**	**1**	**5.53**	**8.81**	**0.0109**
Curvature	1.12	1	1.12	1.79	0.2036
Residual	8.16	13	0.63		
Lack of Fit	0.22	2	0.11	0.15	0.8607
Pure Error	7.94	11	0.72		
Cor Total	152.05	19			

Model Statistics	
Std. Dev.	0.79
Mean	6.70
C.V. %	11.81
PRESS	19.18
R-Squared	0.946
Adj R-Squared	0.925
Pred R-Squared	0.873
Adeq Precision	19.267

SQRT(Average Spindle Power) Watts =
+ 8.302
- 2.648 * A
- 1.457 * B
+ 7.172 * C
+ 0.573 * A * B
- 1.176 * A * C

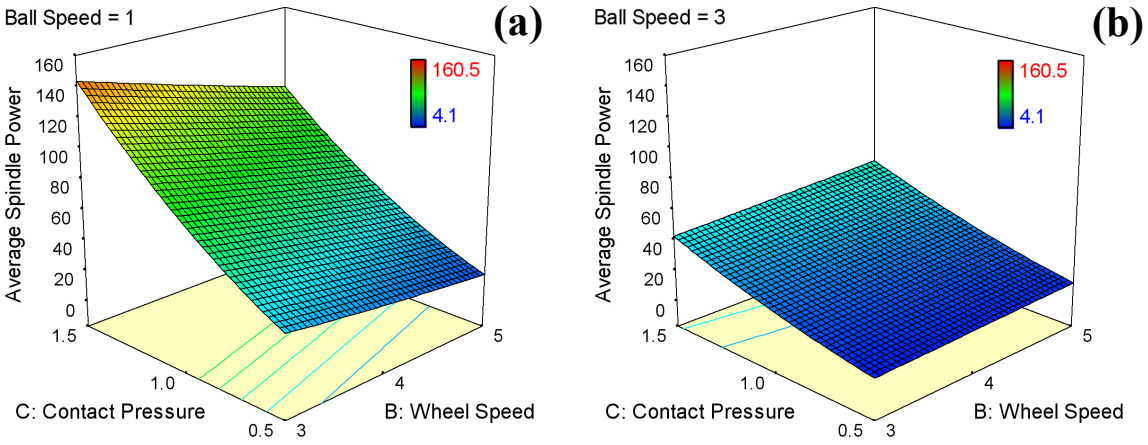

Figure 233 - Model for the 'average wheel spindle change during superfinishing' response. – ANOVA Table, Model statistics, and optimisation equation, 3D surface graph for (a) Ball speed of 1.0 m/s, (b) Ball speed of 3.0 m/s.

Assessment of the slope of the wheel spindle power profiles (appendix J7), showed that a slower ball speed produced a more pronounced decline in wheel spindle power during the runs. A declining spindle power signifies that the wheel condition is deteriorating over a run. The most pronounced decline in spindle power levels (-6.26 watts / min), occurred when contact pressure was high, and ball and wheel speeds were low.

23.4 Surface Finish

Ball surface finish was assessed extensively and with the utmost care and precision. Assessment included the following measurements:

- Five separate Wyko phase shift interferometer measurements for each of the 20 balls / runs. Evaluating the best, worst, and average values for parameters Ra, RMS, Rt, RpMax, RvMax.
- Talysurf measurements taken across, as well as around the centre, of each of the 20 balls. Evaluating parameters Ra, Rq, Rsk, Rku, Rp, Rv, Rz, Rt, and Rdq, for measurements across, around, as well as their average.
- A combined measure of surface finish which took the average of the 5 Wyko and added it to the average of the Talysurf surface measurements around and across the ball (totalling 140 finish measurements on 20 balls).

The models for the best Wyko Ra reading per ball and the talysurf Ra reading across the ball are demonstrated below, with various others shown in appendix J8.

23.4.1 Wyko Phase Shift Interferometer

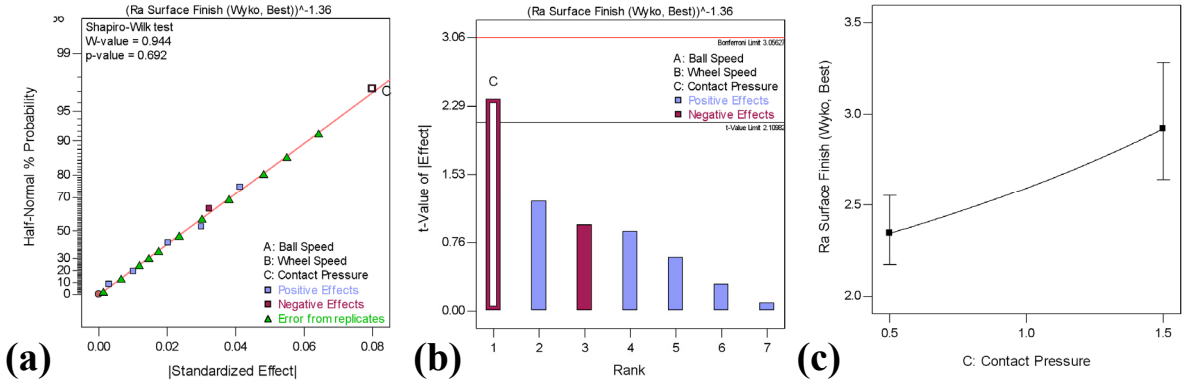

Source	Sum of Squares	Deg. Of Freedom	Mean Square	F Value	p-value Prob > F
Model	**0.026**	**1**	**0.026**	**5.636**	**0.0296**
C - Pressure	**0.026**	**1**	**0.026**	**5.636**	**0.0296**
Curvature	0.001	1	0.001	0.237	0.6326
Residual	0.080	17	0.005		
Lack of Fit	0.017	6	0.003	0.505	0.7923
Pure Error	0.062	11	0.006		
Cor Total	0.107	19			

Model Statistics		
Std. Dev.		0.068
Mean		0.277
C.V. %		24.685
PRESS		0.120
R-Squared		0.249
Adj R-Squared		0.205
Pred R-Squared		-0.137
Adeq Precision		3.065
(Wyko Finish, Ra nm)^-1.36	=	+ 0.3545 - 0.0812 * C

Figure 234 - Model for the response 'Wyko Interferometer Ra surface Finish (Best Values)'. (a & b) Graphs of effects, (c) Effect of contact pressure on surface finish, ANOVA Table, Model statistics, and optimisation equation

Assessment of the best Wyko interferometer Ra readings per ball (figure 234) shows that surface finish improves when contact pressure is reduced. The model is significant, however, the negative predicted R-Squared value implies that the overall mean is a better predictor than the model, and the adequate precision ratio of 3.06 indicates an inadequate signal.

Assessment of the average of 5 Wyko measurements per ball, as well as the additional surface finish parameters RMS, Rt, RpMax, RvMax, either showed no significant effects or showed that lower contact pressure produced improved finish.

23.4.2 Talysurf

Surface finish talysurf measurements produced various models where wheel speed had a weak but consistent effect. As demonstrated in figure 235 surface finish improved when a faster wheel speed was used. The combined measure of surface finish produced no significant effects for parameters Ra, Rq, & Rt.

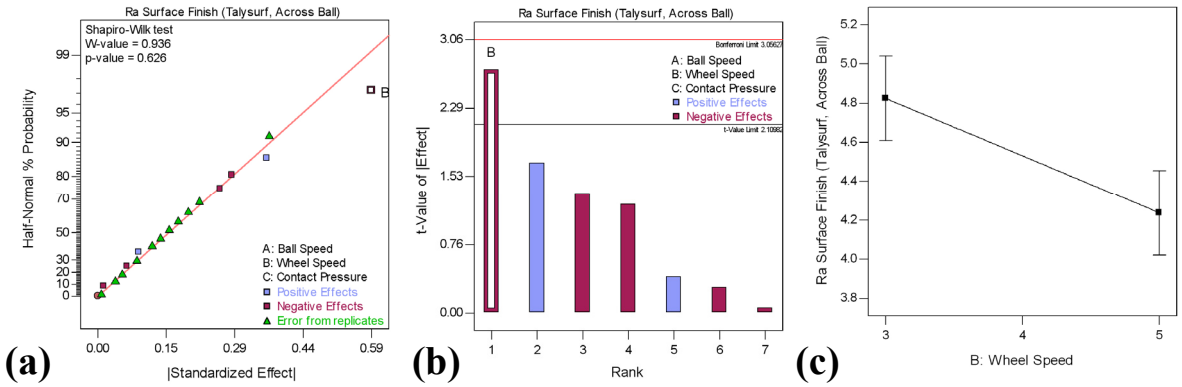

Source	Sum of Squares	Deg. Of Freedom	Mean Square	F Value	p-value Prob > F
Model	**1.381**	**1**	**1.381**	**7.419**	**0.0144**
B - Wheel	**1.381**	**1**	**1.381**	**7.419**	**0.0144**
Curvature	0.253	1	0.253	1.360	0.2596
Residual	3.164	17	0.186		
Lack of Fit	1.179	6	0.196	1.089	0.4259
Pure Error	1.985	11	0.180		
Cor Total	4.798	19			

Model Statistics	
Std. Dev.	0.43
Mean	4.48
C.V. %	9.64
PRESS	4.51
R-Squared	0.304
Adj R-Squared	0.263
Pred R-Squared	0.007
Adeq Precision	3.516
Ra Surface Finish (nm) Talysurf, Across Ball =	+ 5.706 - 0.294 * B

Figure 235 - Model for the response 'Taylor Hobson talysurf Ra Finish (Across Values)'. - (a & b) Graphs of effects, (c) Effect of contact pressure on surface finish, ANOVA Table, Model statistics, and optimisation equation

None of the surface finish parameters produced a particularly strong effect that would indicate a definite course of action. However several effects were observed that were consistent and in excess of the 95% threshold of statistical significance. According to the literature, better surface finishes are achieved when a high wheel speed and low contact pressure is used. Although the influence of the processing parameters is not dramatic, this is also the case when superfinishing using Elid 1. Any influence that these effects have is very small and would only result in a batch average Ra being a nanometre or so better. While balls within the batch naturally varied by more than this amount.

It is advantageous that surface finish is not overly influenced by the processing parameters and material removal is strongly influenced. This allows processing parameters to be set to maximize processing efficiency, whilst not being in conflict with surface finish, which is not ordinarily possible.

It is likely that the condition of the wheel is influencing the resultant surface finish through its dependence on processing parameters. The highest quality surface finish was achieved when less aggressive parameters were selected. An improvement in finish corresponds to the same parameters (low contact pressure and high wheel speed) which achieve low ball material removal, low spindle power, and high Elid voltage. Conversely, when the condition of the wheel is allowed to become glazed, a higher contact pressure improves surface finish.

23.5 Ball Form

Error in the balls' spherical form was assessed using a Taylor Hobson TalyCenta, taking roundness measurements around and 'up & down' the ball, as well as Talysurf waviness measurements taken around and across the ball. Prior to beginning testing, the form was reasonably good as the balls from chapter 21 were re-used. The quantity of material removed from the balls (0.8 to 10 µm) was sufficient for the form to be substantially influenced, if not fully generated, by this set of Elid 1 superfinishing runs.

Unlike the previous assessment of combined Elid 2+3, none of the factors under investigation produced any statistically significant effects. There was no consistency between the different measurements to suggest that either high or low factor levels are better for ball form. Combined measures of ball roundness and waviness also did not produce significant effects. Any levels or combinations of spindle speeds and contact pressure can be used to achieve the required levels of ball roundness.

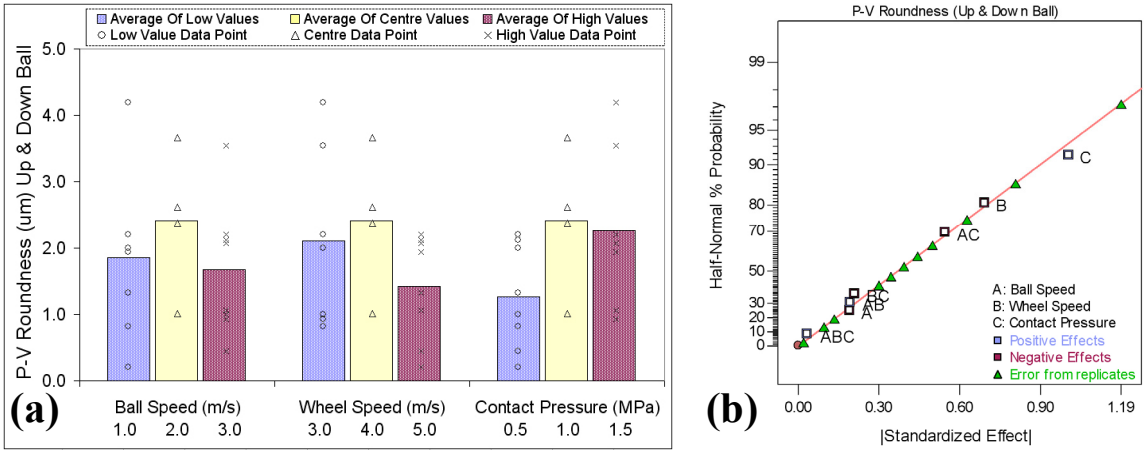

Figure 236 - Model for the 'Roundness up and down ball' response. –
(a) Column graph of raw results, (b) Graph of Effects.

Roundness measurements taken 'up and down' the ball, the standard NMB assessment method, are shown in figure 236. The runs conducted in this section have had the effect of slightly degrading ball form. Some of the balls produced were in excess of the 2.5 µm roundness tolerance. Ball waviness values measured across the ball were considerably worse than those measured around the ball and well in excess of typical values (figure 237). As demonstrated by the correlation in section 23.7, the more material that was removed from the ball the worse the form became. The degradation of form is thought to be due to the stiff grinding system that was used in these runs.

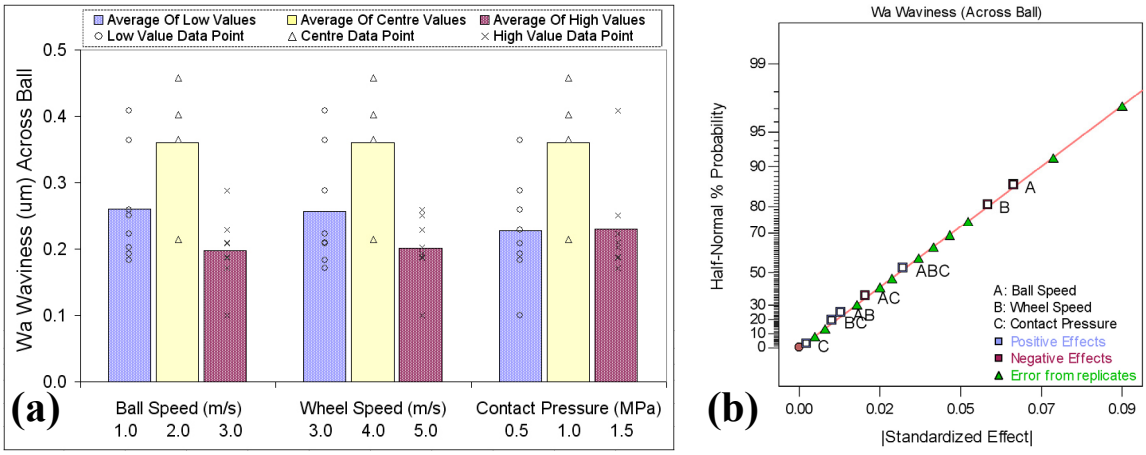

Figure 237 - Model for the 'Wa waviness across ball' response. –
(a) Column graph of raw results, (b) Graph of Effects.

23.6 Wheel Wear

The wheel wore a total of 861 microns during the 200 minutes of superfinishing running time. This rate of wheel wear (4.3 µm/min) is both acceptable to maintain the condition of the 1.3 µm abrasive wheel and acceptable in terms of the life of the wheel. Each wheel is capable of producing a few thousand balls in its life (figure 238).

Wheel Used = #12,000 MRB-CBN (1.3 µm)

Wheel Wear
- Total length reduction = 0.861 mm
- Total by volume = 104.465 cubic mm
- Average rate = 4.3 µm off length per min

Ball Material Removal (all Balls)
- Total of O/D = 82.5 µm
- Average rate = 0.413 µm off O/D per min
- Total by weight = 247.5 mg
- Total by volume = 31.936 cubic mm

G-ratio = 0.306

Figure 238 - Wheel wear statistics

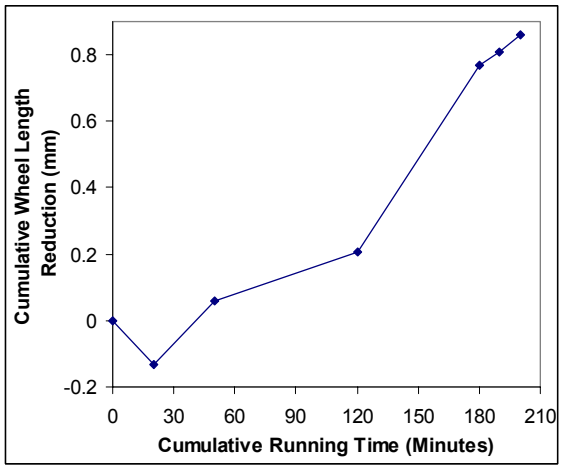

Figure 239 - Wheel wear versus run time during Elid 1 superfinishing factorial experiment

23.7 Correlations for Elid 1 superfinishing

Figure 240 shows the correlation matrix for a selection of the major responses. Correlations that are statistically significant in excess of 95% confidence, are shown in bold red type. A selection of correlation graphs are provided in appendix J9.

Correlation Matrix Using Excels CORREL Function $Correl(X,Y)=\frac{\sum(x-\bar{x})(y-\bar{y})}{\sqrt{\sum(x-\bar{x})^2\sum(y-\bar{y})^2}}$	Average Current	Average Voltage	Slope Of Spindle Power	Average Spindle Power	Ball O/D Reduction Rate	Ra Surface Finish (Wyko Best)	Ra Surface Finish (Talysurf Average)	Rsk Surface Finish (Talysurf Average)	Rku Surface Finish (Talysurf Average)	Rp Surface Finish (Talysurf Average)	Rt Surface Finish (Talysurf Average)	Rdq Surface Finish (Talysurf Average)	Wt Waviness (Across Ball)	Wa Waviness (Across Ball)	Wa Waviness (Around Ball)	P-V Roundness (Up & Down Ball)	P-V Roundness (Around Ball)	Ball Concentricity
Average Current	**1.00**																	
Average Voltage	**-0.97**	**1.00**																
Slope Of Spindle Power	-0.20	0.28	**1.00**															
Average Spindle Power	**0.65**	**-0.68**	**-0.71**	**1.00**														
Ball O/D Reduction Rate	**0.70**	**-0.77**	**-0.45**	**0.86**	**1.00**													
Ra Surface Finish (Wyko Best)	**0.54**	**-0.59**	0.08	0.26	**0.50**	**1.00**												
Ra Surface Finish (Talysurf Average)	**0.46**	**-0.45**	0.31	-0.04	0.22	**0.79**	**1.00**											
Rsk Surface Finish (Talysurf Average)	0.00	-0.03	-0.05	0.17	0.16	0.18	0.00	**1.00**										
Rku Surface Finish (Talysurf Average)	0.00	0.01	0.14	-0.23	-0.14	-0.05	0.10	**-0.97**	**1.00**									
Rp Surface Finish (Talysurf Average)	**0.45**	**-0.46**	0.41	-0.07	0.24	**0.73**	**0.89**	0.21	-0.07	**1.00**								
Rt Surface Finish (Talysurf Average)	0.36	-0.33	0.25	-0.09	0.10	0.19	0.44	**-0.78**	**0.82**	0.36	**1.00**							
Rdq Surface Finish (Talysurf Average)	0.31	-0.27	0.09	0.05	0.18	0.37	**0.56**	-0.23	0.27	0.37	**0.47**	**1.00**						
Wt Waviness (Across Ball)	0.33	-0.37	**-0.49**	0.36	0.22	0.01	0.03	0.07	-0.14	-0.06	-0.08	-0.36	**1.00**					
Wa Waviness (Across Ball)	0.31	-0.34	-0.44	0.31	0.18	-0.02	0.03	-0.02	-0.05	-0.06	-0.01	-0.38	**0.99**	**1.00**				
Wa Waviness (Around Ball)	-0.01	0.00	0.28	-0.27	-0.13	-0.01	0.09	0.22	-0.15	0.31	-0.06	0.07	-0.28	-0.26	**1.00**			
P-V Roundness (Up & Down Ball)	**0.75**	**-0.78**	-0.30	**0.56**	**0.54**	0.29	0.21	0.13	-0.17	0.28	0.15	-0.11	**0.63**	**0.64**	0.14	**1.00**		
P-V Roundness (Around Ball)	-0.08	0.00	0.02	-0.22	-0.14	-0.24	-0.27	0.17	-0.15	-0.08	-0.11	-0.05	-0.10	-0.16	0.24	-0.05	**1.00**	
Ball Concentricity	-0.35	0.22	-0.27	-0.05	-0.04	0.05	-0.26	0.05	-0.04	-0.33	-0.33	-0.05	-0.19	-0.24	-0.16	-0.37	0.37	**1.00**

Figure 240 - Correlation matrix for some of the major responses analysed.

23.7.1 Ball Form

Correlations associated with ball roundness ‘up and down the ball’ show that an improved ball form is achieved with the following responses:

- A higher Elid voltage level (Correlation function = -0.777).
- A lower average spindle power level (0.556)
- A lower material removal rate (0.554)
- Lower waviness measured across the ball (0.632 for Wt & 0.636 for Wa).

Elid voltage and spindle power are thought to correlate largely as a result of their relationship with ball material removal. There may however be an additional reason why the Elid voltage correlation is stronger. When the ball is less round it would increase fluid access to the wheel’s grinding surface, possibly reducing resistance (lower voltage). It could also cause more wheel wear (more dressing, lower voltage).

The only correlation between the measurements of ball form is between roundness up and down the ball and waviness across the ball. Generally the other measures of ball form did not produce significant correlations. Measures of ball form around the ball (roundness and waviness) did not correlate with each other or with any other response assessed.

23.7.2 Elid power responses (Voltage)

The Elid power responses correlate with several of the other responses. High Elid voltage correlates with low Elid current, low spindle power, low material removal, low surface finish and low roundness.

23.7.3 Material removal

As usual, an increase in the material removal rate correlates closely with an increased average spindle power level (0.860). The rate of material removal is increased as a result of the increased rate of wheel erosion (lower voltage), but tends to decline as the wheel's condition degrades (negative spindle power slope). There is some evidence that surface finish is improved when a low material removal rate is achieved (0.50).

23.7.4 Surface Finish

Measurements taken with Wyko phase shift interferometer correlated most accurately with talysurf measurements taken around the centre of the ball. There is no statistically significant correlation between average spindle power level and ball surface finish. This contrasts with previously analysed datasets in which lower power levels produced better finishes. Lower voltage (greater wheel erosion and more newly-revealed sharp abrasives) increases surface finish.

23.7.5 Ball Concentricity

The concentricity of the freely rotating ball on the ball spindle ranged between 2 and 50 μm during these tests. None of the responses assessed correlated with the concentricity of the ball's motion.

23.8 Additional Factorial Experiments - Wheel Spindle Power

A confidence and understanding of the wheel spindle power response allowed optimization of processing parameters for various wheel types and abrasive sizes to be conducted over a few simple runs (figure 241a). Wheel spindle power levels were substantially higher when a smaller abrasive was used (figure 241 b,c,d). This helps to explain why the process fails to be effective when abrasives larger than 8 μm (#2000 wheel) are used for Elid 1 superfinishing. Runs were conducted with the Elid power supply set to its maximum level.

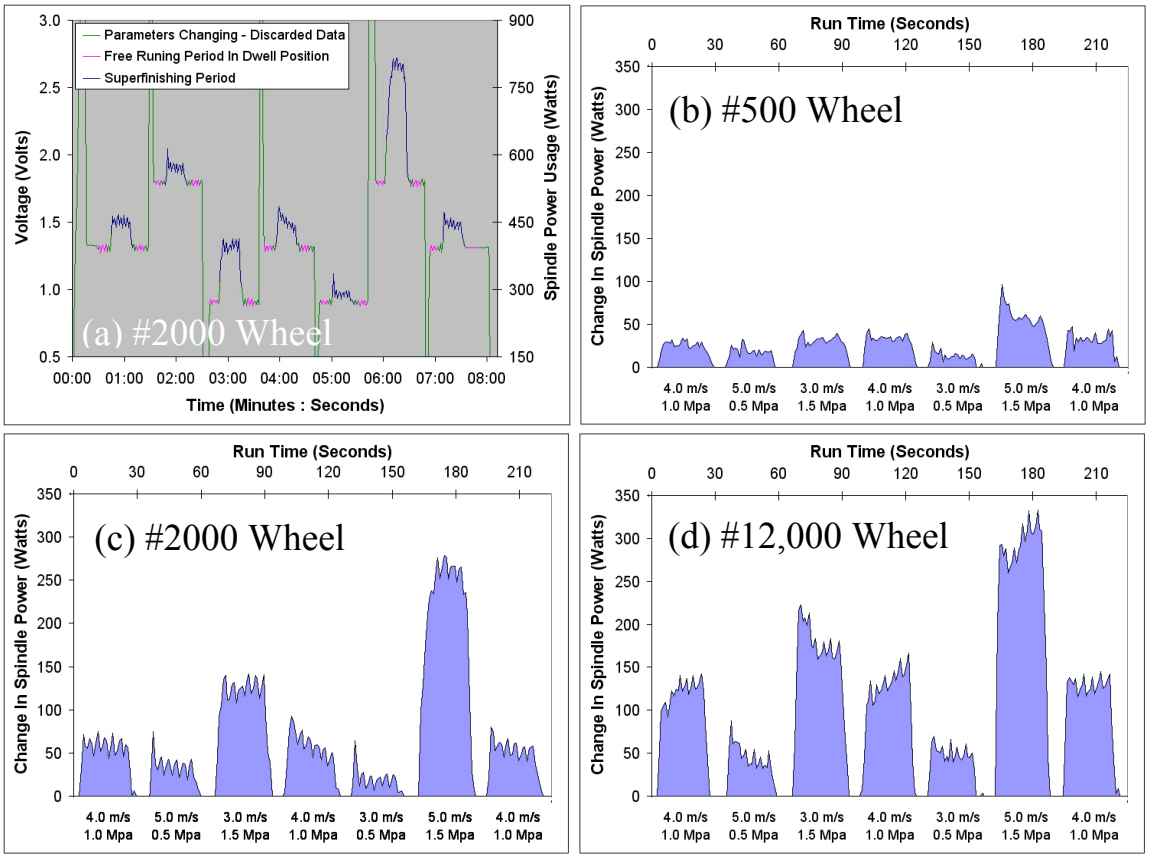

Figure 241 - Wheel spindle power data from Speed-Force program runs - (a) Raw wheel spindle power data for run 766, (b, c & d) Drift adjusted spindle power data for #500, #2000, & #12,000 MRB-CBN wheels. [Details: Runs 874, 766, 931, full power Elid 1, ball speed 963rpm or 1.0 m/s,)

Factorial assessment of these runs produced models that described the effects on spindle power very accurately (figures 242 & 243). The highest spindle power was unequivocally achieved when wheel spindle speed was high and contact pressure was high. This is contrary to what was found earlier in this chapter where the highest spindle power was achieved when a slow wheel speed was used.

As the highest spindle power was associated with the largest material removal, the wheel spindle speed should be set high in order to maximize efficiency. The most plausible reason for the disparity between these results and those outlined previously, is that the larger Elid power settings employed in these runs allowed the wheel's condition to be maintained even with a faster wheel speed.

The Elid power data was left on as the parameters were changed, which caused the Elid voltage to climb as the wheel surface recovered. During superfinishing the Elid current and voltage levels corresponded to the spindle power levels. When the spindle power was high, the current was high and voltage was low. The aggressive processing parameters caused fresh sites of copper to be revealed at the surface of the wheel and in turn lowered Elid voltage. The lowest Elid voltage occurred with a fast wheel speed as this corresponded to the most aggressive processing parameters.

Source	Sum of Squares	Deg. Of Freedom	Mean Square	F Value	p-value Prob > F
Model	**24.55**	**3**	**8.183**	**85.571**	**< 0.0001**
A - Ball	**0.55**	**1**	**0.548**	**5.728**	**0.0219**
B - Wheel	**2.48**	**1**	**2.479**	**25.927**	**< 0.0001**
C - Pressure	**21.52**	**1**	**21.523**	**225.059**	**< 0.0001**
Curvature	0.04	1	0.044	0.463	0.5003
Residual	3.54	37	0.096		
Lack of Fit	0.69	10	0.069	0.654	0.7556
Pure Error	2.85	27	0.106		
Cor Total	28.13	41			

Model Statistics	
Std. Dev.	0.31
Mean	3.97
C.V. %	7.79
PRESS	4.44
R-Squared	0.874
Adj R-Squared	0.864
Pred R-Squared	0.842
Adeq Precision	26.397

Ln(Average Wheel Spindle Power) Watts =
+ 1.082
- 0.140 * A
+ 0.321 * B
+ 1.894 * C

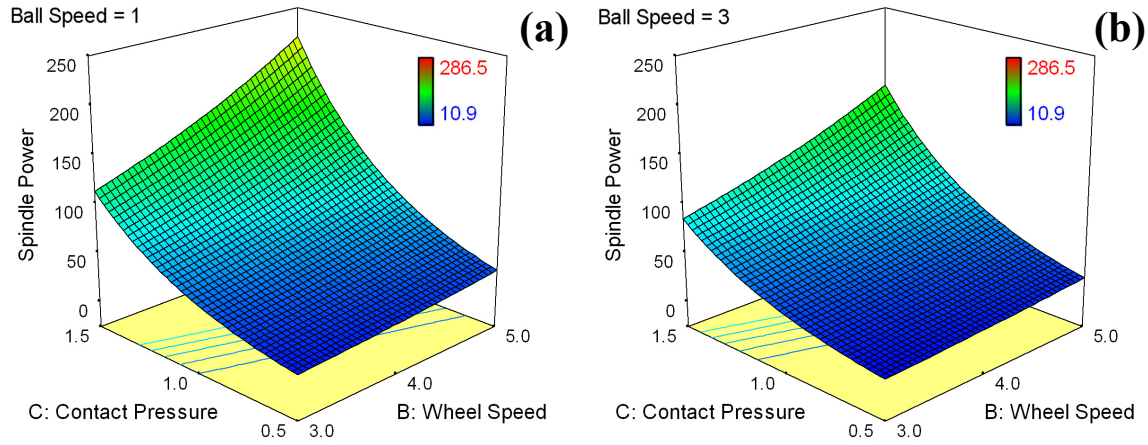

Figure 242 - Model for the average wheel spindle power response - #2000 MRB-CBN wheel. - ANOVA Table, Model statistics, and optimisation equation, 3D surface graphs of wheel speed and contact pressure for (a) Ball speed of 1.0 m/s, (d) Ball speed of 3.0 m/s.

Source	Sum of Squares	Deg. Of Freedom	Mean Square	F Value	p-value Prob > F
Model	**2999**	**4**	**749.78**	**71.52**	**< 0.0001**
A - Ball	**97**	**1**	**96.51**	**9.21**	**0.0084**
B - Wheel	**627**	**1**	**627.15**	**59.82**	**< 0.0001**
C - Pressure	**2068**	**1**	**2068.41**	**197.29**	**< 0.0001**
BC	**207**	**1**	**207.06**	**19.75**	**0.0005**
Curvature	47	1	47.10	4.49	0.0511
Residual	**157**	**15**	**10.48**		
Lack of Fit	**60**	**9**	**6.65**	**0.41**	**0.8894**
Pure Error	**97**	**6**	**16.23**		
Cor Total	**3203**	**20**			

Model Statistics	
Std. Dev.	3.24
Mean	26.90
C.V. %	12.04
PRESS	289.14
R-Squared	0.950
Adj R-Squared	0.937
Pred R-Squared	0.908
Adeq Precision	26.560

Average Wheel Spindle Power = + 10.819 - 2.626 * A - 1.079 * B - 6.974 * C + 8.308 * B * C

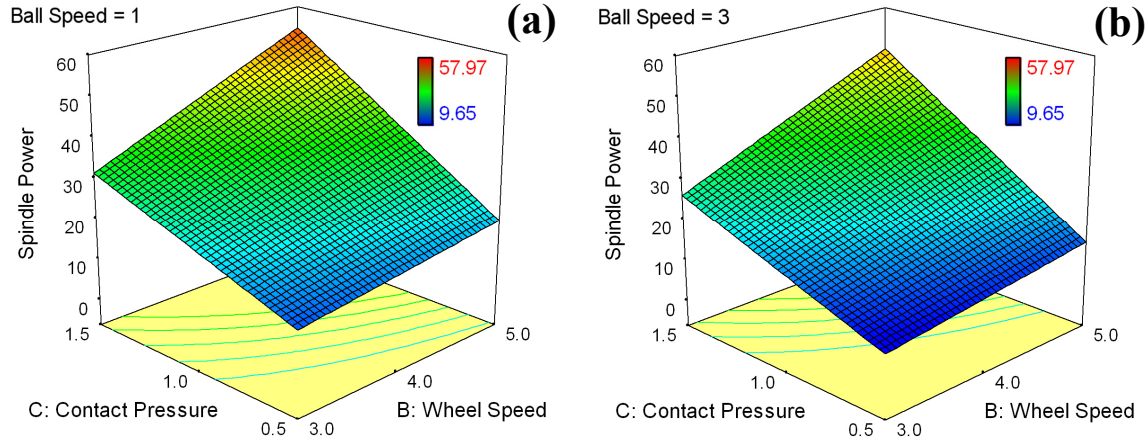

Figure 243 - Model for the average wheel spindle power response. - #500 MRB-CBN wheel - ANOVA Table, Model statistics, and optimisation equation, 3D surface graphs of wheel speed and contact pressure for (a) Ball speed of 1.0 m/s, (d) Ball speed of 3.0 m/s.

23.9 Optimised Elid 1 Parameters

Based on all the findings from this chapter, the factors investigated should be set as outlined in figure 244 in order to provide optimum results when using Elid 1 (along with maximum Elid power settings including duty ratio). The interplay between the use of Elid and processing parameters makes the optimum selection of parameters change. Improved surface finish, for example, can also be achieved by maintaining a high contact pressure and turning the Elid off for a period at the end of a superfinishing run. This aspect is explored in chapter 28.

Required response	Ball Speed	Wheel Speed	Contact Pressure
Lowest Surface Finish	Any	Fast	Low
Highest Spindle Power	Slow	Fast	High
Lowest Form Error	Any	Any	Any
Lowest Elid Voltage	Any	Fast	High
Highest Material Removal	Slow	Fast	High

Figure 244 - Optimum selection of parameters based on Elid 1 superfinishing data

Chapter 24

Influence of Fluid on Elid Superfinishing Performance

A D-optimal experimental design was used to investigate the influence of fluid type, age, and method of application, on Elid 1 superfinishing performance (figure 245). This design was selected as it maximizes the efficiency of the experiment. Further details can be found by reviewing references [96, 97, 98]. It was not possible to fully randomise the design in terms of fluid type and age. A total of 20 runs was completed; the same ball was reloaded onto the machine in the same position for each run. Each run used a #20,000 MRB-CBN wheel dressed with Elid 1 and lasted for a total of 10 minutes.

FACTORS	LEVELS		
Fluid Type	Old CEM	Dowel	New CEM
Nozzle Size (inches)	1/4" - flood application		1/16" - high pressure application
Number of Nozzles	1		2
Position of Nozzles	Edge		Centre

Figure 245 - Factors and levels investigated. - [Run Details: Elid 1, 40l, 90V, 50% Duty, #20,000 MRB-CBN wheel. 5215 rpm wheel speed, 963 rpm ball speed, 2.75 mm contact pressure, Each superfinishing run lasted 10 minutes, Elid being turned off for the final 30 seconds. Elid 1 Used]

The application of the fluid was either through a small nozzle (1/16") that produced a high pressure application or a large nozzle (1/4") that produced a flood application (figure 246). Fluid was aimed at the ball / wheel interface and directed either at the edge of the ball or at the centre of the ball (figure 247).

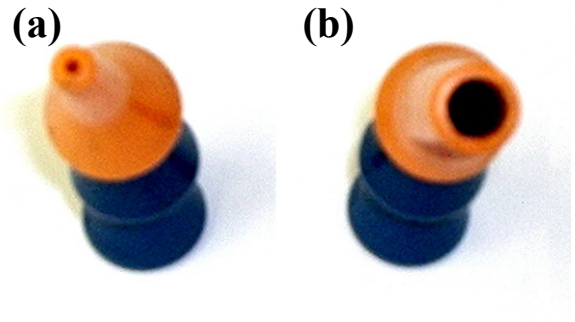

Figure 246 - Size of nozzles used during testing. - (a) 1/16" nozzle, (b) 1/4" nozzle.

The number of nozzles was also tested. When one nozzle was used it was always the front nozzle. During these runs the remaining nozzle (of the same size) was simply directed away from the grinding zone. This approach maintained an even and consistent pressure and flow of fluid so that the effects of nozzle size and number were independent. When two nozzles were used, one was positioned at the front and one at the back.

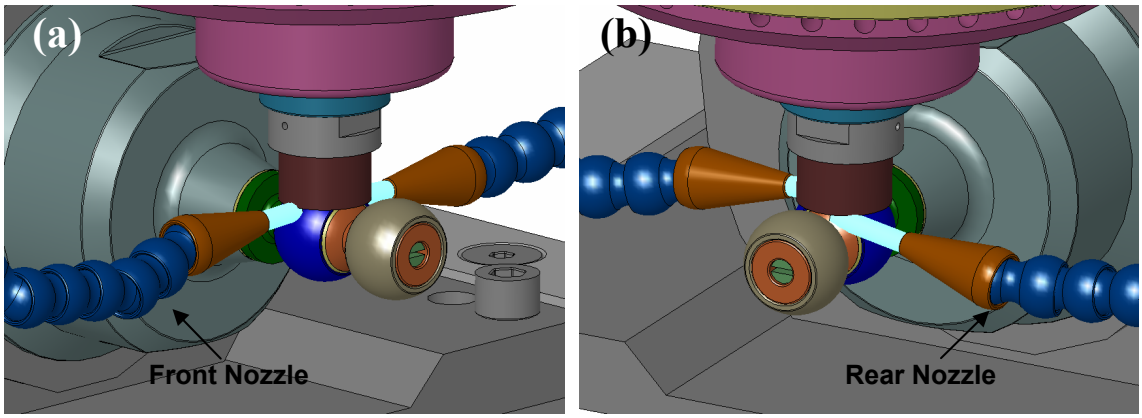

Figure 247 - Figures showing the positioning of the nozzles during Fluid Experiment. - (a) Two nozzles at centre, (b) Two nozzles at edges

Figure 248 shows the conductivity and pH levels of the different fluids, after dilution, tested before and after use. A 50:1 ratio of tap water to fluid was used, as recommended in the literature. The pH levels recorded were broadly similar to what was used and recommended in the literature. As the ion concentration of the fluid rises, the conductivity rises. The conductivity of the fluids rose during use.

Fluid Measured	Fluid Conductivity (millisiemens)	Fluid pH
Tap Water	0.363	6.8
Old Noritake CEM - @ Start	2.33	10.14
Old Noritake CEM - @ End (+60 minutes Elid 1 use)	2.35	10.13
New Dowel - @ Start	1.028	8.6
New Dowel - @ End (+70 minutes Elid 1 use)	1.152	8.73
New Noritake CEM - @ Start	1.465	10.8
New Noritake CEM - @ End (+70 minutes Elid 1 use)	1.637	10.69
Re-measure of **New** Noritake CEM - @ End (after 7 months storage).	3.01	9.62
Noritake CEM - @ Start Of RBFB16AB runs @ NMB	2.460 ms/cm	9.5
Noritake CEM - @ End Of RBFB16AB runs @ NMB (+167 minutes Elid 3 use)	2.580 ms/cm	9.5

Figure 248 - Conductivity & pH measurements of the electrolytic superfinishing fluids under investigation.

The effects tables for the various responses measured are shown in appendix K1. Generally fluid type was the factor that caused the largest effect, followed by nozzle size. The number of nozzles and nozzle position generally caused a less pronounced effect. All four of the responses produced models that were sufficiently accurate at describing the effects shown. Influence and diagnostic plots were all satisfactory and within limits for these models. Predicted values accurately matched actual values; studentized residuals were normally distributed and maintained consistent variance.

24.1 Elid Power data

The results from the average Elid voltage response are shown in figure 249. The model and model terms A, C, D, and AC were statistically significant. Using the Dowel fluid always resulted in a high voltage regardless of the other factors. The larger ¼" nozzle size reduced voltage, particularly when using the new and old CEM fluids. The number of nozzles used only had a small influence, slightly lowering voltage across the board when two were used.

Source	Sum of Squares	Deg. Of Freedom	Mean Square	F Value	p-value Prob > F
Model	**1475.4**	**6**	**245.9**	**73.67**	**< 0.0001**
A - Fluid Type	**626.9**	**2**	**313.5**	**93.92**	**< 0.0001**
C - Nozzle Size	**580.2**	**1**	**580.2**	**173.82**	**< 0.0001**
D - No. of Nozzles	**21.6**	**1**	**21.6**	**6.47**	**0.0245**
AC	**102.6**	**2**	**51.3**	**15.37**	**0.0004**
Residual	43.4	13	3.3		
Cor Total	1518.7	19			

Model Statistics	
Std. Dev.	1.83
Mean	82.80
C.V. %	2.21
PRESS	101.88
R-Squared	0.971
Adj R-Squared	0.958
Pred R-Squared	0.933
Adeq Precision	23.913

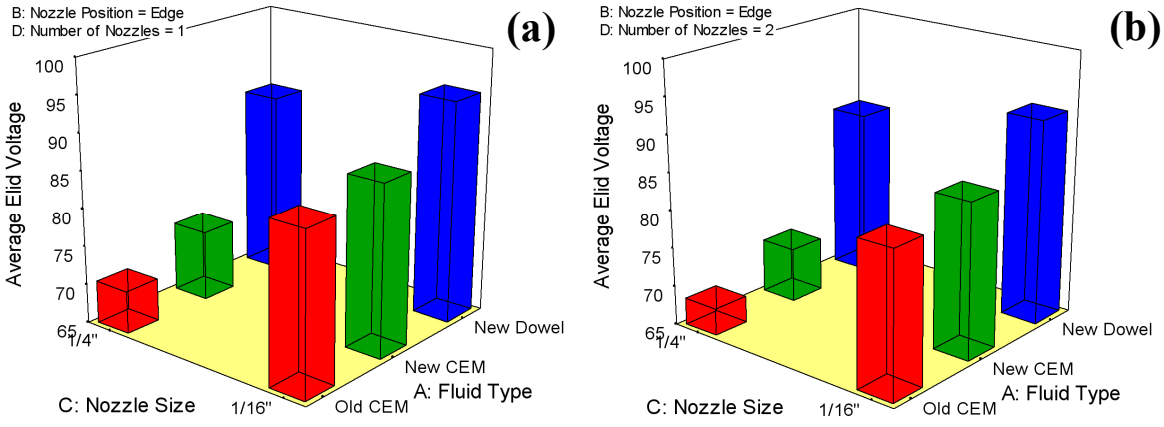

Figure 249 - Average Elid voltage response model. - Anova table, model statistics,
(a) Effect of fluid type and nozzle size (one nozzle), (b) Effect of fluid type and nozzle size (two nozzles).

For the Elid current model (appendix K3), the terms A, B, C, D, BD, and CD were significant after the recommended power transformation had been applied to the data set. Nozzle position produced higher current when two nozzles were directed towards the edge than when they were directed towards the centre, particularly when old CEM fluid was used. The lowest voltage and highest current, representing the most effective dressing, was achieved when using old CEM fluid with two large nozzles positioned to deliver fluid to the edge.

24.2 Wheel Spindle Power

When assessing spindle power usage, fluid type and nozzle size as well as the interaction between them were significant model terms (figure 250). The use of new CEM fluid and a large nozzle achieved the highest spindle power levels.

Source	Sum of Squares	Deg. Of Freedom	Mean Square	F Value	p-value Prob > F
Model	**37131**	**5**	**7426**	**35.25**	**< 0.0001**
A - Fluid Type	**29272**	**2**	**14636**	**69.47**	**< 0.0001**
C - Nozzle Size	**2705**	**1**	**2705**	**12.84**	**0.0030**
AC	**2945**	**2**	**1473**	**6.99**	**0.0079**
Residual	2949	14	211		
Cor Total	40080	19			

Model Statistics	
Std. Dev.	14.51
Mean	80.57
C.V. %	18.02
PRESS	5887.11
R-Squared	0.926
Adj R-Squared	0.900
Pred R-Squared	0.853
Adeq Precision	13.867

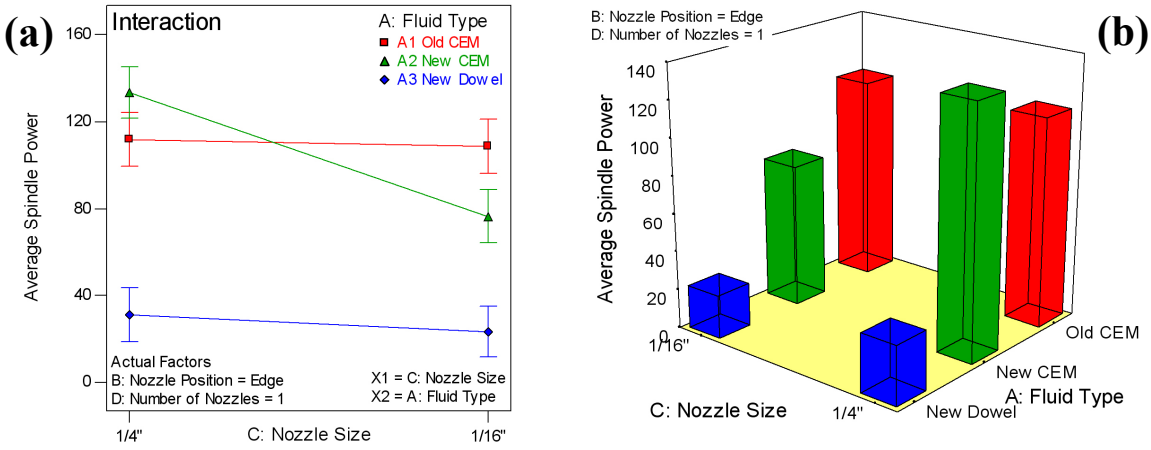

Figure 250 - Model results for the response, 'Average change in wheel spindle power during superfinishing' (watts). - Anova table and model statistics, (a) Graph demonstrating the AC interaction, (b) Effect of fluid type and nozzle size (One nozzle, edge position).

24.3 Material Removal

As shown in the Anova table (figure 251) factors A, B, C, AC, and BD produced statistically significant effects. The rates of ball material removal were in line with those achieved previously using the same parameters.

The effect of fluid type was only distinguishable when the larger nozzle size was used. The highest rate of ball material removal was achieved when the CEM fluid was used. It was necessary to perform the required runs for each fluid type before it was changed. The effect of fluid was therefore influenced by the running order. The use of the Dowel fluid had an undeniable effect on the process; in particular it was less effective at

allowing the Elid system to dress the wheel. As a result Elid current and spindle power were lower, and material removal was reduced. As the Dowel fluid was the second type tested, this deterioration of the wheel had a negative impact on the results achieved with the final (new CEM) fluid.

Source	Sum of Squares	Deg. Of Freedom	Mean Square	F Value	p-value Prob > F
Model	**0.3693**	**8**	**0.0462**	**73.5**	**< 0.0001**
A - Fluid Type	**0.1029**	**2**	**0.0514**	**81.9**	**< 0.0001**
B - Nozzle Position	**0.0061**	**1**	**0.0061**	**9.7**	**0.0099**
C - Nozzle Size	**0.0862**	**1**	**0.0862**	**137.3**	**< 0.0001**
D - No. of Nozzles	0.0007	1	0.0007	1.1	0.3131
AC	**0.1118**	**2**	**0.0559**	**89.0**	**< 0.0001**
BD	**0.0057**	**1**	**0.0057**	**9.0**	**0.0119**
Residual	0.0069	11	0.0006		
Cor Total	0.3762	19			

Model Statistics	
Std. Dev.	0.025
Mean	0.152
C.V. %	16.483
PRESS	0.024
R-Squared	0.982
Adj R-Squared	0.968
Pred R-Squared	0.935
Adeq Precision	27.341

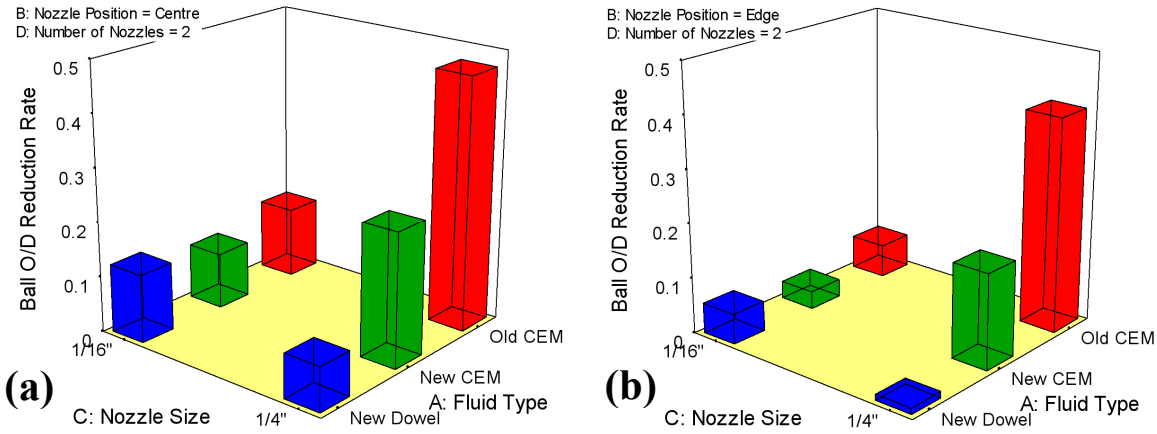

Figure 251 - Model results for the response 'Ball O/D reduction rate' (µm/min). - Anova table and model statistics, (a) Effect of fluid type and nozzle size (two nozzles, centre position), (b) Effect of fluid type and nozzle size (two nozzles, edge position)

The results for ball material removal when only one nozzle was used parallel those above. There is little difference between the application of fluid towards the edge or centre; both graphs following the same form as in figure 251 and achieving intermediate values.

The highest rate of ball material removal was achieved when old CEM fluid was used in conjunction with two centrally positioned $^{1}/_{4}$" nozzles. The lowest removal rate and worst result occurred when two $^{1}/_{16}$" nozzles were used to apply Dowel fluid to the edge of the ball-wheel interface. Whereas assessment of the power responses provides information about what the process is doing, the rate of ball material removal is the bottom line and factors should be selected to maximize this.

24.4 Surface Finish Results

Levels of surface finish achieved when using the Dowel fluid were equivalent to those produced with the Noritake CEM fluid. A total of only three finish measurements were taken when the dowel fluid was used. A much greater number of measurements would be required in order to detect the small difference between them and differentiate which fluid actually produced better surface finish.

24.5 Wheel Wear

Levels of wheel wear produced when the Dowel fluid was used were indistinguishable from the wheel wear when either the old or new CEM fluid was used. These measurements were in line with others taken when Elid 1 superfinishing.

24.6 General Performance

As demonstrated by figure 252 and appendix K2 the responses are related and correlate. High material removal is achieved when low Elid voltage and high spindle power are present. A more effectively dressed wheel increases the friction / cutting energy at the grinding interface making the wheel spindle power requirements larger.

Correlation Matrix Using Excels CORREL Function	Average Current	Average Voltage	Average Spindle Power	Ball O/D Reduction Rate
Average Current	1.00			
Average Voltage	-0.97	1.00		
Average Spindle Power	0.70	-0.80	1.00	
Ball O/D Reduction Rate	0.81	-0.80	0.54	1.00

Figure 252 - Correlations between responses.

Although Dowel fluid worked effectively as a coolant and lubricant, it was significantly less effective as an Elid electrolyte than the Noritake CEM. The reduced overall performance of the Dowel fluid was partly due to foaming. This was particularly pronounced when a high pressure application was used and the even flow of fluid between the anode and cathode reduced dressing effectiveness. As old fluid achieved superior results compared to new fluid, the issue of how often to change the fluid is not based on material removal performance. However if fluid is not aerated through frequent use it can become stagnant and is a breeding ground for bacteria. Appropriate biocides can be used to prevent this.

Chapter 26

Electrolytically Assisted Superfinishing

Most forms of abrasive processing have at some point been combined with the large number of electro-chemical machining techniques (ECM) to form various hybrid processes. Electrolytically assisted grinding is one of the best known and although currently out of favour, is a well established technique that uses the electro-chemical corrosion of a workpiece to assist the abrasive action of the wheel. Electrolytically assisted superfinishing was investigated as part of a series of measures undertaken to improve the inadequate ball material removal rates that were achieved early in the research using Elid 3.

The Elid power supply can be used in a number of different ways other than for its conventional role of wheel dressing. This chapter looks at the various methods of electro-chemically eroding the ball's spherical surface during superfinishing. The methods available include those described in figure 273. A brief assessment of Elid 3R, Elas, and Elas combined with Elid, was conducted in order to gauge their potential benefit.

Name	Brief Details
Elid 3R	Uses the same set-up as described for usual Elid 3 superfinishing but with the polarity of the power supply reversed. The ball is made the anode and the wheel the cathode.
Elid 3A	Elid 3 processing using an alternating current instead of a pulsed dc waveform. As a result both the wheel and the workpiece are oxidized.
Elas	'Electrolytically Assisted Superfinishing' – Superfinishing with a static, separate, electrode positioned to oxidise the surface of the ball during superfinishing.
Elas + Elid	A combination of Elas and Elid which enables the wheel to be dressed and the ball's surface to be oxidised during superfinishing.

Figure 273 - Various electrolytically assisted superfinishing methods

Two methods were developed in order to examine the performance of combined Elas and Elid. When the ball is insulated from the electrical circuit (figure 274a) it acts to self-regulate the balance between the proportion of the current which acts to corrode the wheel and that which corrodes the surface of the ball.

Configuration (A) weights the split of current so that the largest proportion is concentrated on dressing the wheel. The split with configuration (B) is weighted towards oxidation of the ball's surface.

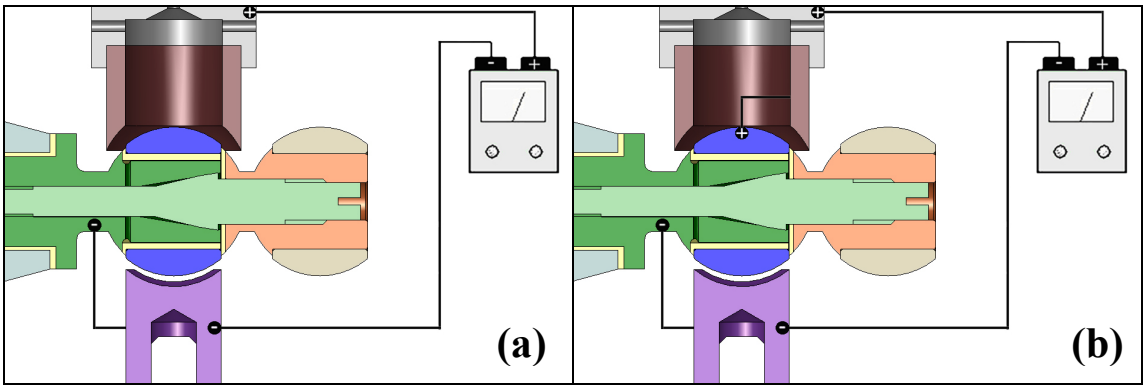

Figure 274 - Diagrams of Elas + Elid system Configurations. - (a) Positive wheel, negative fixturing & separate electrode, neutral / insulated ball, (b) Positive wheel & ball, negative fixturing & separate electrode

26.1 Ball Output Quality

All methods of electrolytically assisted superfinishing tested caused the ball's surface to oxidize and preferentially etched the ball at the exposed carbides. Oxidising of the ball, as shown in figure 275, can cause discolouration and pitting on its surface. The quality is therefore lower and the surface finish much rougher. Because of this problem, systems involving oxidation of the ball's surface should only be used at the start of a cycle and not towards the end. Further superfinishing is then able to remove this surface defect, allowing normal levels of finish to be achieved. Although not quantified there may be an improvement in the ball's corrosion resistance when this method is used.

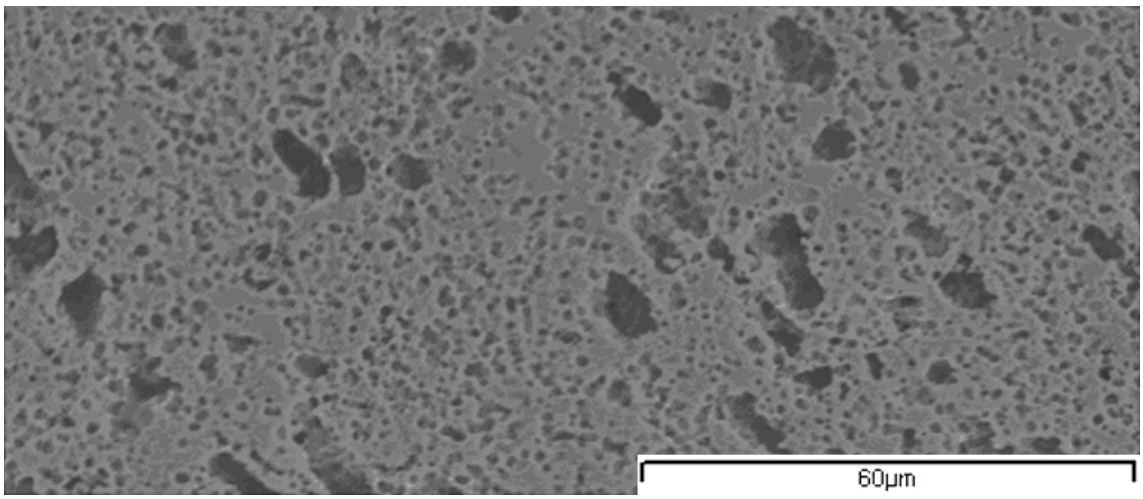

Figure 275 - SEM image of an RNB08 ball's surface after being oxidised with the Elid power supply

26.2 Ball Material Removal

The rate at which material was removed from the ball increased with the addition of an electrode which oxidised the surface of the ball during superfinishing, when compared to Elid 3. The stability of an Elid 3 system is improved when used in conjunction with Elas, as the material being removed from the ball's surface is turned into a friable oxide. This also applies to the condition of the wheel and the stability of material removal.

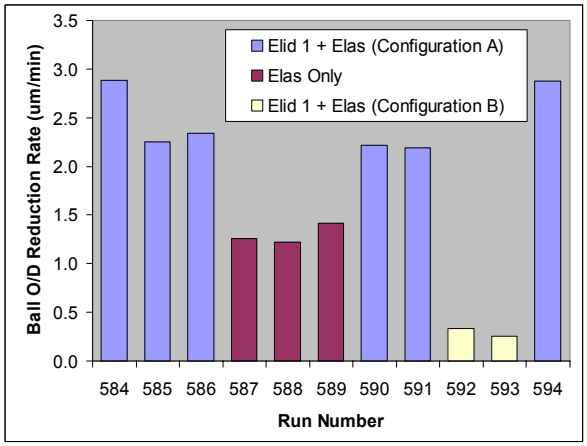

Figure 276 - Rate of ball material removal using Elas. [#12,000 MRB-CBN]

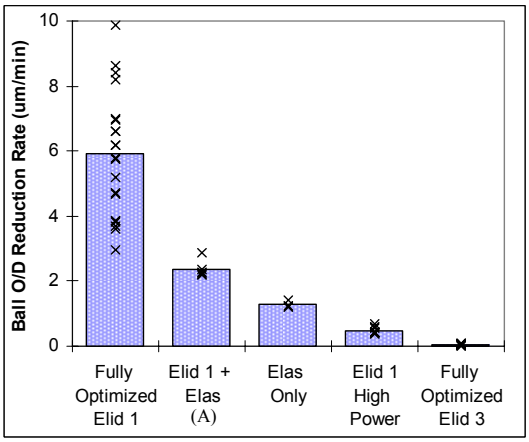

Figure 277 - Comparison of ball material removal rate for Elas and Elid types [#12,000 MRB-CBN]

When there is no provision for the wheel to be dressed (Elas only), the MRB-CBN wheel quickly becomes glazed. Ball material removal still continues, however the removal mechanism is not based on abrasion. Combining Elas and Elid requires appropriate levels of power to be split between dressing the wheel and corroding the ball. Configuration A achieved higher material removal rates than the other Elas set-ups (figure 276), because the power supply was concentrated on dressing the wheel. However, as figure 277 demonstrates, the material removal rate with the best Elas set-up was significantly lower than it was with fully optimised Elid 1.

Like Elid 1, Elas is more efficient when an increased superfinishing load and more aggressive electrical parameters are used. There was a problem in getting an even gap between the separate electrode and the surface of the ball. This caused one side of the ball to corrode faster than the other which may possibly throw out the roundness of the ball.

26.3 Spindle & Elid Power values

The in-process information recorded during Elas and combined Elas + Elid runs is shown in figures 278 and 279. As demonstrated by the lower spindle power and higher Elid power values recorded, configuration B did not dress the wheel effectively.

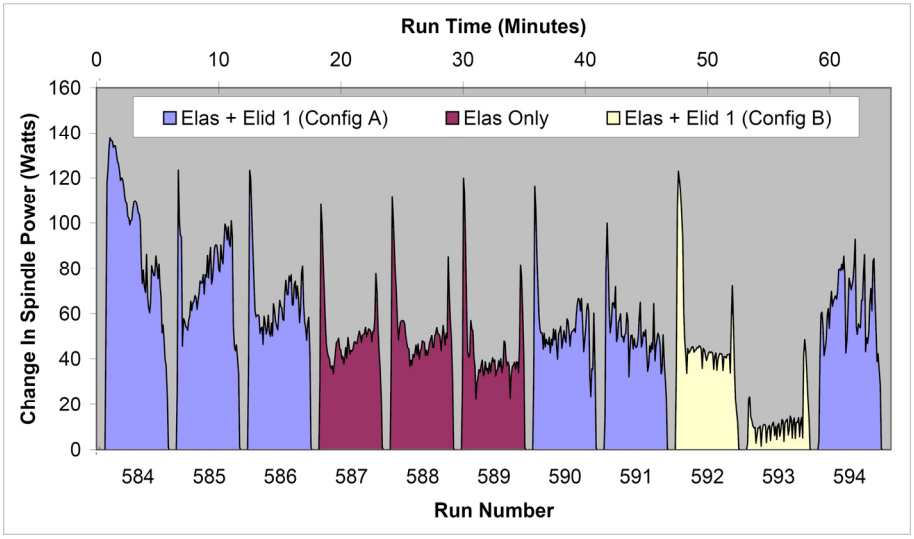

Figure 278 - Drift adjusted change in wheel spindle power usage during various superfinishing runs involving the use of Elas and combined Elas + Elid 1 superfinishing. - [ws 5215, bs 962, 68N] (1 averaged data point per 5 seconds)

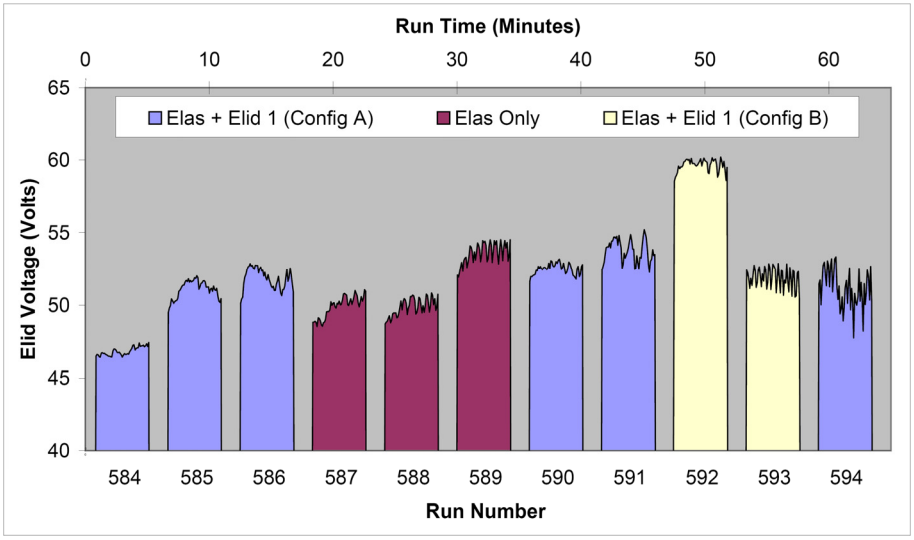

Figure 279 - Elid electrical behaviour recorded during various superfinishing runs involving the use of Elas and Combined Elas + Elid 1 superfinishing. – [90V, 40I, 50%] (1 averaged data point per 5 seconds)

26.4 Processing using Elid 3R

When using Elid 3R the direct electrical contact between the negative wheel and the positive ball resulted in a voltage of zero and a current of 20 amps. As there was direct electrical flow only a very limited difference in ball material removal was achieved. As there was no provision for the wheel to be dressed after the initial minute of Elid 2 dressing, the spindle power usage was low and declined to zero as the condition of the wheel became rapidly glazed.

In the same manner as Elid 3 superfinishing, the fact that electricity is flowing, albeit almost entirely uninterrupted, through the wheel and ball, makes a small material removal rate achievable (figure 280). This rate is equivalent to the rate that is achieved when the electrical flow direction is reversed. Ultimately this is not working and cannot be considered real electrolytic superfinishing.

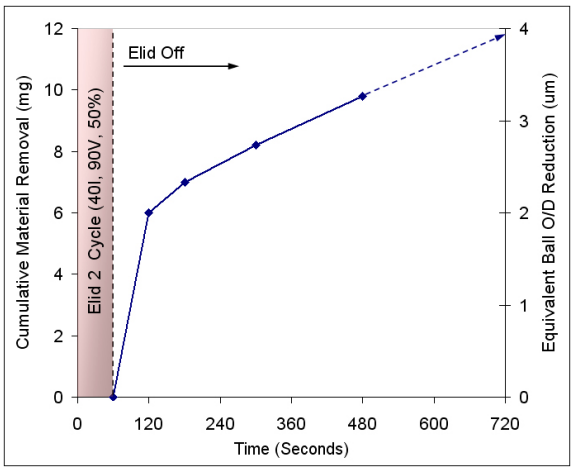

Figure 280 - Decline in material removal after Elid 2 dressing when superfinishing using Elid 3R - [#2000 MRB-CBN wheel]

26.5 Conclusions

The use of combined Elid and Elas offered some advantages over Elid 3, in terms of increased material removal and reduced processing times. However the approaches outlined above are overly elaborate and time-consuming, and appear to offer no benefit over using Elid 1 and 2. These methods of producing balls would require further study and development to ascertain whether they could be a suitable method of producing spherical bearing balls. A separate power supply could be used for Elid and Elas to solve problems of balance between wheel dressing and workpiece oxidation.

Chapter 27

Superfinishing of Titanium Balls & Ball Coatings

In order to address the fundamental drive towards weight reduction in the bearing industry, the potential benefits of Elid superfinishing were investigated on titanium balls. The commonly used titanium alloy IMI 318 was tested, the basic composition of which is Ti-6Al-4V.

There are various surface treatments available to improve the life of both metal to metal and lined bearings. Many of these can be used in conjunction with the improved surface finish and quality that Elid superfinishing can provide. The use of various ball coatings improves bearing performance, extending life and improving corrosion resistance. This section summarizes tests performed on titanium balls and various ball coatings.

27.1 Elid 3 Superfinishing of Chrome-Coated Titanium Balls

Using an #8000 MRB-CBN wheel, a brief assessment of the potential of Elid 3 superfinishing was conducted on one of the various chrome coatings used at NMB. Testing was performed on RBJB208 EXP/D3 titanium balls which had been chrome-coated with Poeton's Apticote 100T applied to a thickness of 0.2mm.

27.1.1 Microscopy

Figure 281 shows the initial Apticote 100T chrome surface, as well as its appearance after Elid 3 superfinishing. As only the uppermost surface peaks were initially in contact with the wheel, the rate of surface improvement was quite rapid with Elid 3 superfinishing. After the first few minutes of superfinishing (figure 281c), improvement slowed dramatically. The surface was not fully formed even after 28 minutes active Elid 3 superfinishing (figure 281d).

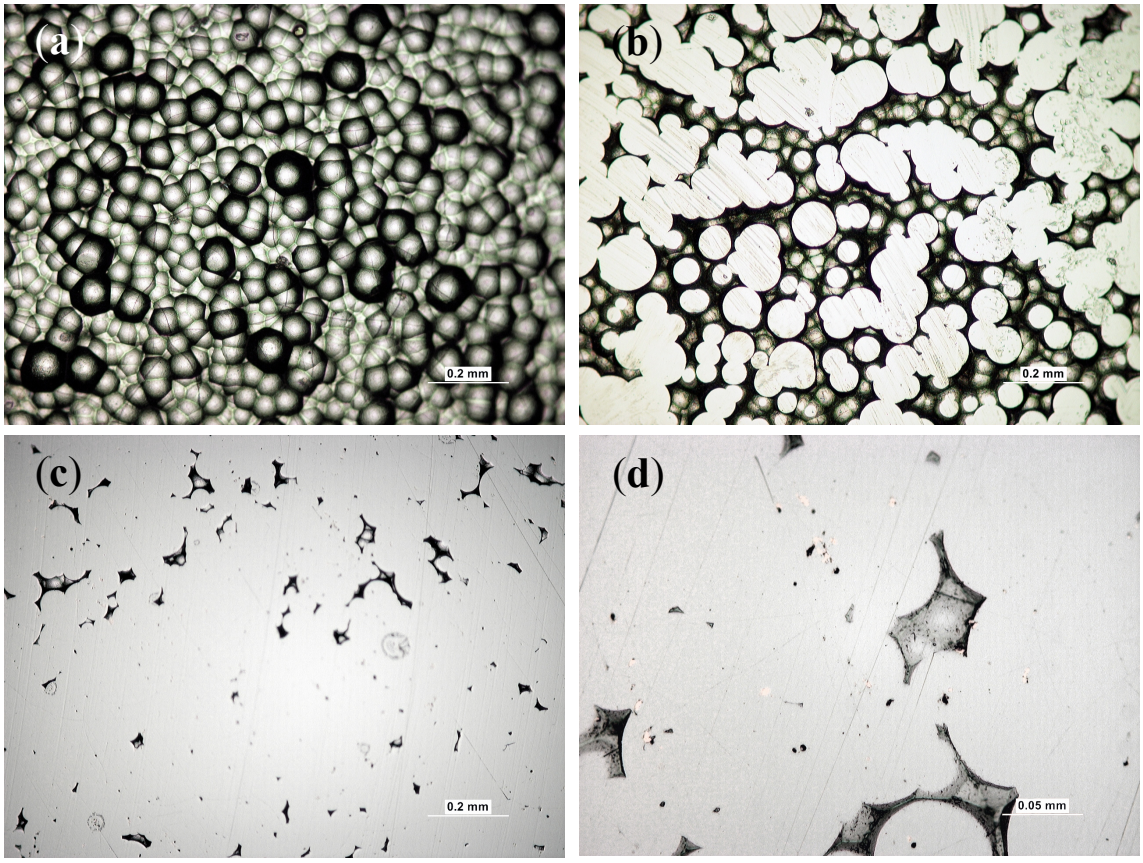

Figure 281 - Pictures of an Apticote chrome-coated titanium ball (RBJB208 EXP/D3) at three points during an Elid 3 superfinished cycle with an #8000 MRB-CBN wheel. - (a) Un-ground / as-received surface, (b) superfinished for 170 secs, (c) superfinished for 28.3 mins, (d) higher mag. after 28.3 mins.

This set of tests was conducted at the very start of the research, before the Elid 1 fixturing had been developed or larger abrasive wheels tested. As a result ball material removal rates were very low and the original surface was not fully removed by the runs conducted. However, all indications were that a flawless ball surface would have been achieved eventually, or been attained if a more efficient method of Elid processing was used.

The ball was designed to run against an uncoated titanium race (metal to metal bearing), with a molybdenum disulphide-based dry film lubricant (Lube-Loc 5306). Cracking of the as-received surface, typically found with chrome coatings, can be seen at larger magnification and has the beneficial effect of holding lubricant at the surface. One option that could be considered is if the Apticote chrome surface was only partially formed as this would provide a very smooth surface to reduce wear, but also have pockets within which oil can be retained.

27.1.2 Other Information

The Elid 3 system employed displayed the usual profile of active and inactive periods of Elid 3 superfinishing (as described in chapter 19). Pronounced Elid activity was recorded when superfinishing the ball shown in figure 281c & d. Unlike later tests conducted on stainless steel balls, there was no electrolytically deposited copper on the surface of the chrome-coated balls. This was despite there being both poor alignment and conformity between the ball and wheel during these tests. The surface undulations and poor form of the ball would have encouraged fluid access into the grinding interface, possibly aiding Elid activity. There was no measurable difference in wheel length when measured with a digital calliper.

27.1.3 Roundness Measurements

Prior to being Elid superfinished, the spherical form of the balls was in excess of the standard 2.5 μm tolerance. The balls' roundness ranged between 15.35 μm to 5.45μm when measured around the ball centre, and between 40.31 μm to 49.11 μm when measured across the ball. These high values were a result of coating the balls directly after turning; a consequence of using titanium as the balls' substrate material.

After Elid 3 superfinishing, with processing times ranging from 85 seconds to 28 minutes, the roundness of the balls was not significantly improved. A range of 34.63 μm to 49.65 μm was recorded when measured across the ball. Due to poor ball roundness there was a large variation in material removal recorded from the ball edge to the centre. The material was exclusively removed from the centre whilst the edges remained unpolished. Again the slow material removal rate prevented the final levels of form being achieved.

27.1.4 Required processing cycle for chrome-coated titanium balls

The processing cycle for chrome-coated balls, and resultant output quality, would not be significantly different from standard steel balls. The required processing time is strongly dependent on the input surface finish, roundness, and geometry of the ball. The balls should be as round as possible prior to coating, in order to increase superfinishing efficiency and maintain an even coating thickness over the spherical surface after processing.

Generally the processing recommendations given in chapter 28 apply. The dimensions of these (RBJB208 EXP/D3) balls would have allowed them to be processed using Elid 1. However in order for this approach to be successful, cylindrical grinding may be required prior to Elid 1 superfinishing to control O/D tolerance. If a ball's dimensions prevent Elid 1 processing then conventional cylindrical grinding and honing should be performed, prior to Elid 2 superfinishing with a #2000 MRB-CBN wheel.

Due to environmental considerations, the use of thick chrome coatings in new bearing development projects is restricted / discouraged. Nevertheless, processing other thick ball coatings may be used as a manner of achieving a highly polished surface on titanium substrate balls. After the ball has reached the required finish and form accuracy it can be given a final coating, possibly Balinit C, depending on the required application.

27.2 Balinit C® Coating after Elid Superfinishing

In combination with the improved surface finish that Elid superfinishing provides, a Balinit C coating can be applied onto the balls of lined bearings requiring the longest lifespans. Applied to the spherical surface of a ball by Balzers Ltd, it has a stated Knoop hardness of 1000 HK. The Balinit C coating is a low temperature PVD process, involving an initial chrome adhesion layer, followed by a hardwearing 1 to 1.5 μm tungsten carbide and graphite coating. As it is applied using physical vapour deposition the surface finish after coating is highly dependent on the initial surface finish. This coating is therefore the final finishing operation and applied after Elid superfinishing.

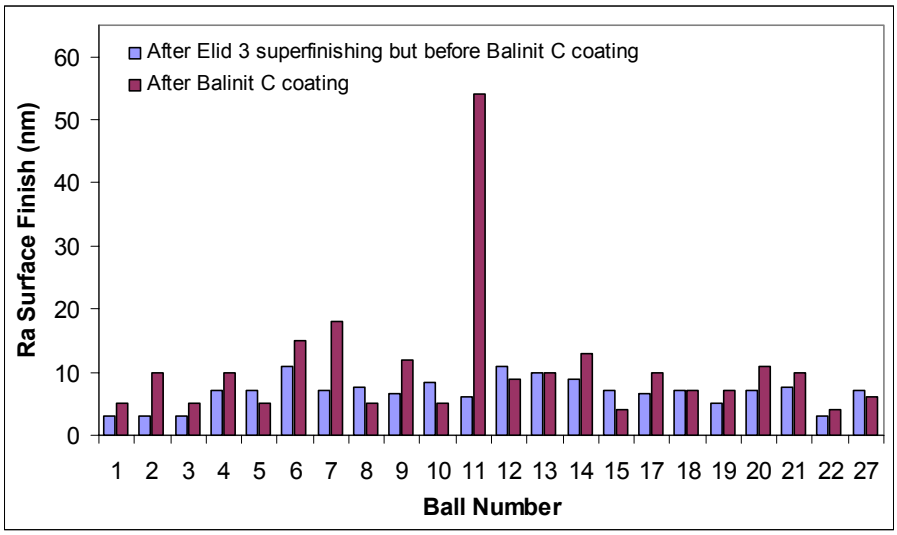

Figure 282 - Graph of Ra surface finish before and after Balinit C coating.

Twenty-two steel balls were coated with a Balinit C coating after being Elid 3 superfinished at NMB with an #8000 MRB-CBN wheel. The surface finish of these balls was assessed before and after coating (figure 282). There was an average increase in Ra surface finish of 4 nm, however one of the balls worsened to a much greater extent than this. After coating there were circumferential marks around the centre of 11 of the balls' spherical surfaces that were not present prior to coating. It is not known if this is a problem that can be avoided or prevented, however it highlights the fact that the balls should be assessed after coating and the negative aspect of no longer being in direct control of the final ball processing operation.

27.3 Elid 3 Superfinishing on Uncoated Titanium Balls

27.3.1 Ball Input Condition

Testing was conducted on titanium balls in the fully annealed, as-received, condition. The balls were only turned prior to beginning Elid superfinishing tests and the turning marks were visible (figure 283a).

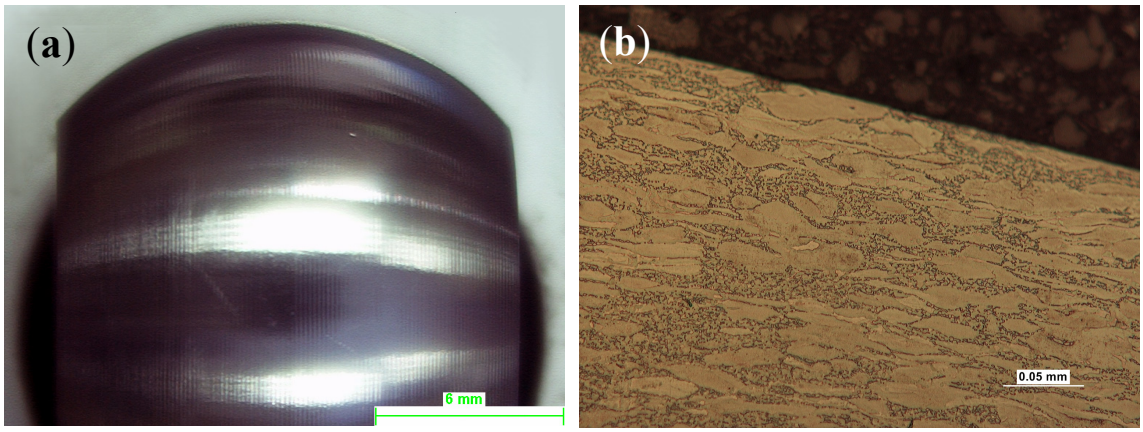

Figure 283 - Picture of the MNRFB08GA titanium balls used for testing. - (a) Full ball in as-received condition [surface finish across ball of 1.0 µm Ra, 5.3 µm Rt, Roundness up & down ball of 12 µm], (b) sectioned ball demonstrating Ti-6Al-4V material structure up to the spherical surface.

Figure 283b shows the etched bulk material structure of a sectioned titanium ball with lighter elongated hcp alpha grains and the darker bcc beta phase. At the spherical surface of the ball, no subsurface damage was visible. Hardness measurements taken of the lighter phase recorded lower values (264 Hv) than the darker, speckled, region (322 Hv). Measurements taken on the balls' spherical surfaces before superfinishing varied between 313 and 458 Hv and remained within this range after Elid superfinishing was conducted.

27.3.2 Elid 3 Superfinishing with MRB-CBN Wheels

Testing on titanium balls was initially conducted at NMB in Lincoln using MRB-CBN wheels and Elid 3. A variety of experimental parameters were tested (Spindle speeds, applied force, Elid settings, fluid application, etc), however at no point did the wheel achieve a stable Elid insulating layer. The voltage display on the Elid power supply remained at zero as the ball and wheel were in direct metal to metal contact with each other.

The prepared Elid surface of the wheel was stripped away within seconds of grinding contact being made. Excessive wheel wear was recorded during superfinishing, with the length of the wheel reducing at a rate of up to 1 mm per minute. After superfinishing, both the surface of the ball and the wheel appeared smeared and scuffed (figure 284). The surface of the ball was irregular and very poor. It also appeared pitted and had copper transferred onto it.

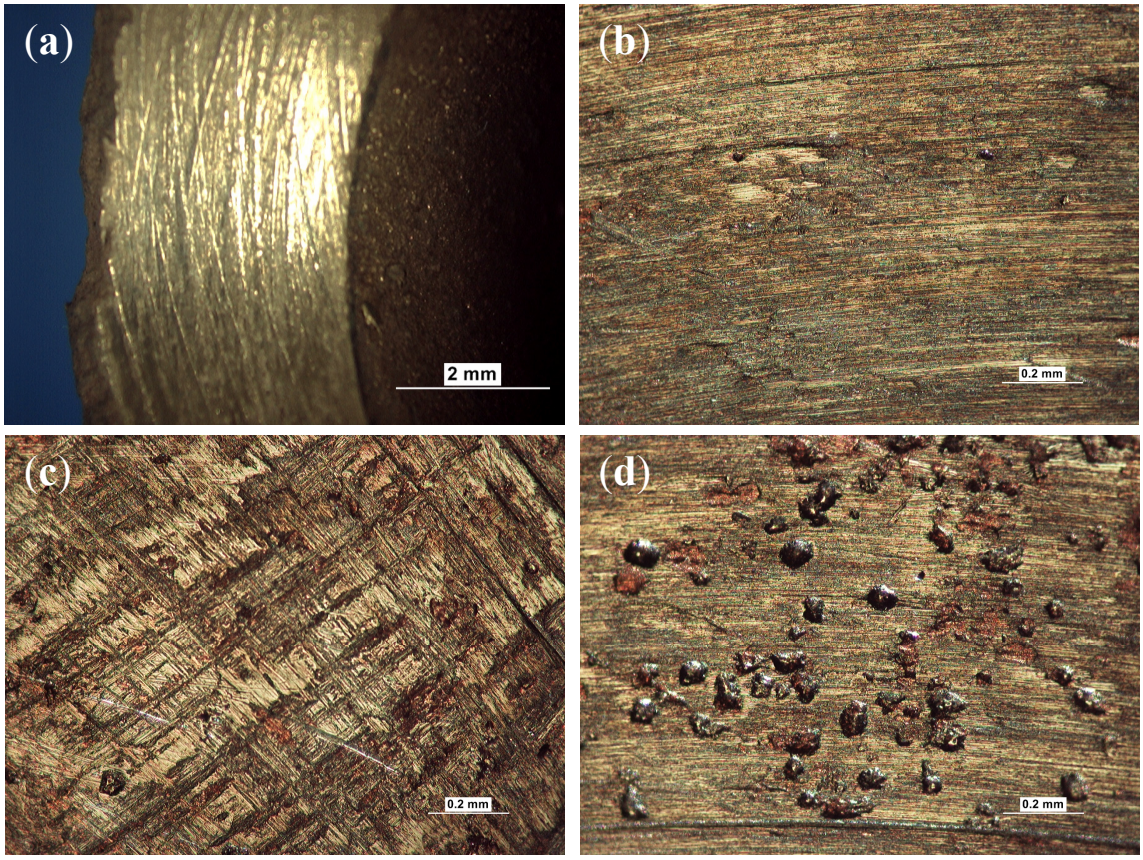

Figure 284 - Pictures of a titanium ball and #20,000 MRB-CBN wheel after 450 seconds Elid 3 superfinishing on the as-received surface. - (a) Wheel surface after superfinishing (b) Smoothest part of the ball's surface (c) Ball Edge, (d) Pitting on the ball's surface.

Processing titanium is notoriously difficult and is particularly so for this application as achieving a very good surface finish is the main requirement. As previously discussed the area contact between the ball and wheel inhibits fluid access which is more problematic when using titanium because of its limited ability to dissipate heat. To ensure the effects recorded were a result of the ball material, several steel balls were tested alongside the titanium balls. The steel balls achieved an effective Elid layer and polished to a good surface finish. The (Fuji Die KFSI-2) MRB-CBN wheels are entirely unsuitable for superfinishing directly onto titanium. As testing was deemed unsuccessful, other processing options were investigated.

27.4 Elid 3 Superfinishing of Nitron-Coated Titanium Balls

A Nitron-"O" coating, applied by Tecvac (figure 285), is used on large metal to metal titanium bearings to improve their wear performance. The coating consists of a nitrogen diffusion layer into the titanium ball's surface which supports a 1 to 4 microns thick, very hard (3000 Hk), PVD coating of TiN.

The nitrogen enriched layer has a depth of 20 μm over which the hardness declines to the bulk material value. In the context of this research the coating was tested to determine whether the altered surface structure would assist superfinishing prior to the ball being recoated.

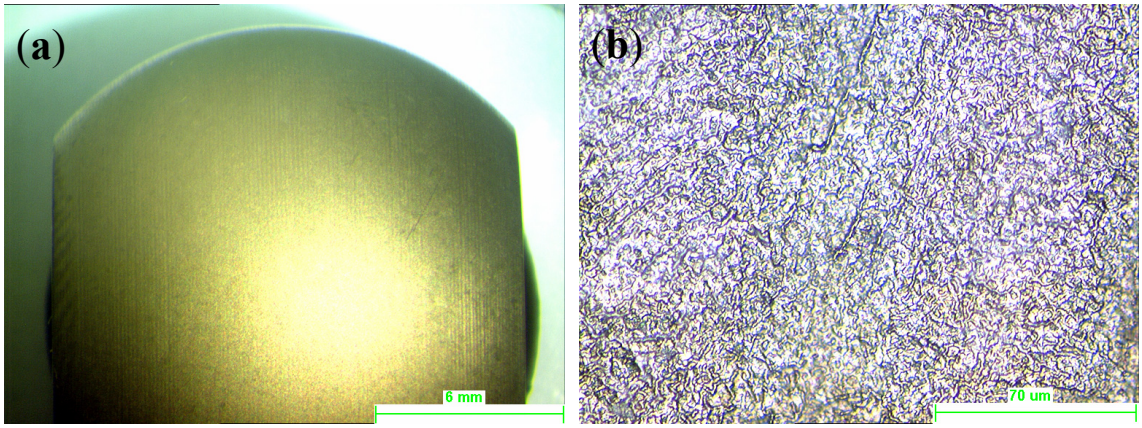

Figure 285 - Optical microscope pictures of a Nitron-"O" coated titanium IMI 318 ball used for testing. (a) Full ball picture MNRFB08GA, (b) High magnification picture of the ball's spherical surface.

Hardness testing was conducted on the Nitron coated titanium balls before and after Elid superfinishing. When a low load of 50g was used, the indenter penetrated the coating to a depth of around 1.7 microns; approximately equal to the recommended 10% of the depth of the coating thickness. Hardness values ranged from 593 to 841 Hv.

After Elid 3 superfinishing the surface of the balls was stripped away. Again various control parameters were varied and the highest quality ball produced is shown in figure 286. Nitron coating the surface of the titanium balls did not improve the process. Again the Nitron coated titanium balls did not achieve a stable Elid layer.

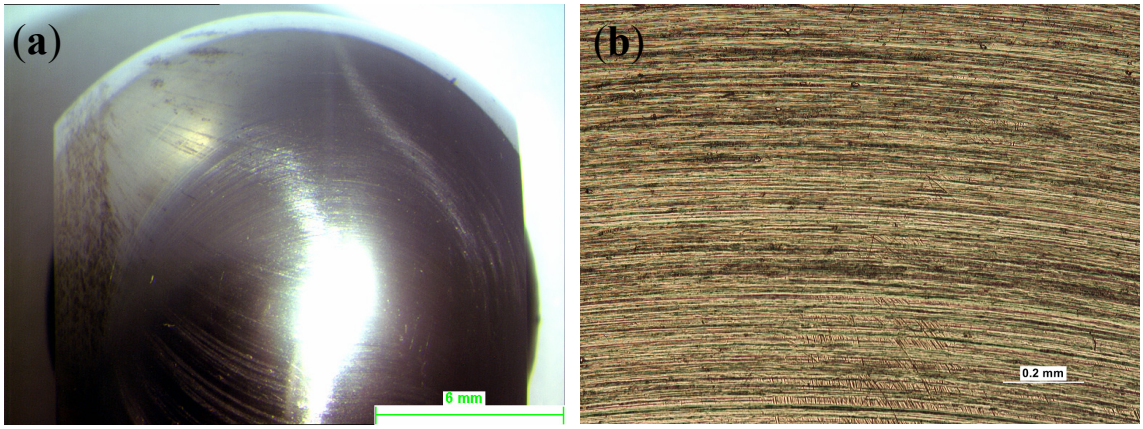

Figure 286 - Optical microscope pictures of a Nitron-"O" coated titanium IMI 318 balls after Elid 3 superfinishing with a #20,000 MRB-CBN wheel. - (a) Full ball picture MNRFB08GA, (b) Highest quality portion of the ball's spherical surface

27.5 Tests by Fuji Die

After discussion with the wheel manufacturer Fuji Die, an attempt was made to develop a more suitable wheel to Elid 3 finish titanium. This took the form of the conventional #2000 copper resin wheel, but with an increased amount of porosity (KFSI-2Q-CBN). Fuji Die tested it in a less demanding Elid 1 cylindrical surface grinding configuration and as it performed unsuccessfully the wheel was not ordered. The second part of the tests used Elid 1 ground nitride-coated titanium samples with a #8000 cast iron bonded diamond wheel (FCI). This was more successful, achieving a surface finish of 4.7 to 5.6 nm Ra. A #2000 CIB-D wheel was ordered and tested at Cranfield.

27.6 Additional Tests on Uncoated Titanium Balls

The development of the Elid superfinishing system at Cranfield enabled uncoated titanium balls to be tested easily using a number of different processing methods. A number of different wheels, processing parameters, and applications of the Elid power supply were briefly evaluated (figure 287).

Factor Tested	Details
Wheel Type	#2000 CIB-D, #8000 MRB-CBN, #8000 MRB-AlO, #8000 MRB-CeO, Darmann No 2, Darmann No 4.
Elid Application	No Elid, and various combinations of Elid 1, Elid 2, and Elas
Spindle Speeds (rpm)	Wheel speeds (5215, 3000, 1000, 100). Ball speeds (963, 600)
Applied Force	From zero up to 67.6 Newtons
Fluid Application	Low pressure, high pressure.

Figure 287 Parameters evaluated on uncoated / untreated RNB08 titanium balls

27.6.1 Elid 1 Superfinishing with a #2000 CIB-D Wheel

As outlined in the literature, research has been conducted into Elid *grinding* of Ti6Al4V using cast iron bond diamond wheels. Despite the inherent difficulties some success was achieved. The recommendations made were followed / investigated for the researched application of Elid *superfinishing*.

Elid 2 dressing for 5 minutes followed by Elid 1 superfinishing, resulted in an unacceptably high rate of wear in the #2000 CIB-D wheel (average wheel length reduction of 0.857 mm/min). Even though the wheel's surface was continually and aggressively oxidized by the Elid system, it had a metallic appearance after processing (figure 288a). As occurred with the other wheels tested, the Elid prepared grinding surface of the wheel was easily stripped away. The large wear of this wheel highlighted an additional problem of using CIB wheels with this application. As a CIB wheel wears, a burr forms at its outer edge (figure 288b) which does not break off. This caused sparking between the wheel and fixturing, and required repeatedly filing down.

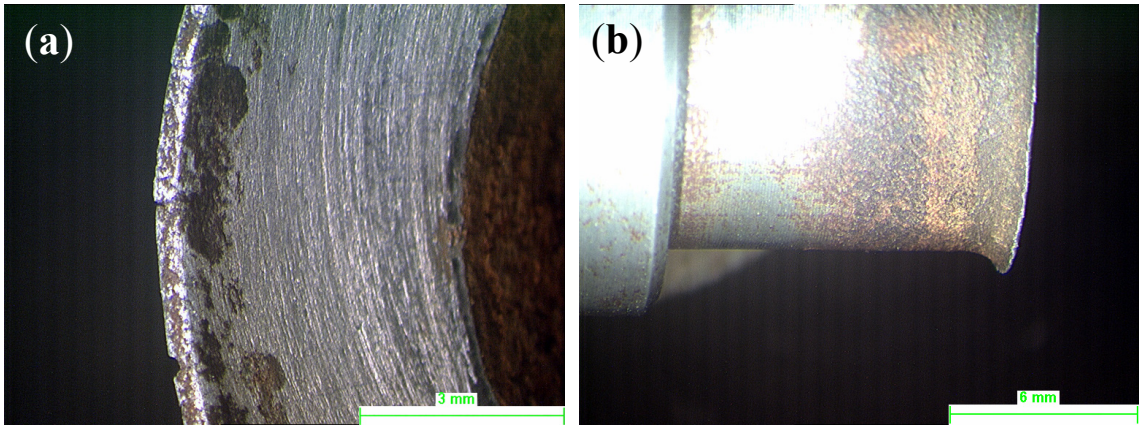

Figure 288 - Pictures of a #2000 CIB-D Elid 1 wheel. - (a) wheel's surface stripped of Elid oxidized layer after Elid 1 superfinishing titanium, (b) burr formed on the edge of the wheel as the wheel wears.

The ball's weight reduced by 17mg (equivalent to 10 µm off the balls O/D). However micrometers measurement indicated that there was no change in the ball's size at its centre. The wheel spindle power usage was reasonably high; recording an average power increase from superfinishing of 115 watts during these various runs. The surface of the ball after superfinishing was of a poor quality and appeared slightly oxidized. The normal processing parameters used on steel (ws 5215 rpm, bs 963 rpm, 67.6 N) were too aggressive for processing titanium. The tests suggested that Elid superfinishing with a CIB-D wheel would not be an effective method of producing high quality titanium balls.

Some runs were conducted where the oxidation of the ball's surface was encouraged by using Elas in combination with Elid, as described in the previous chapter. However as demonstrated by figure 289, the superfinishing process was not improved.

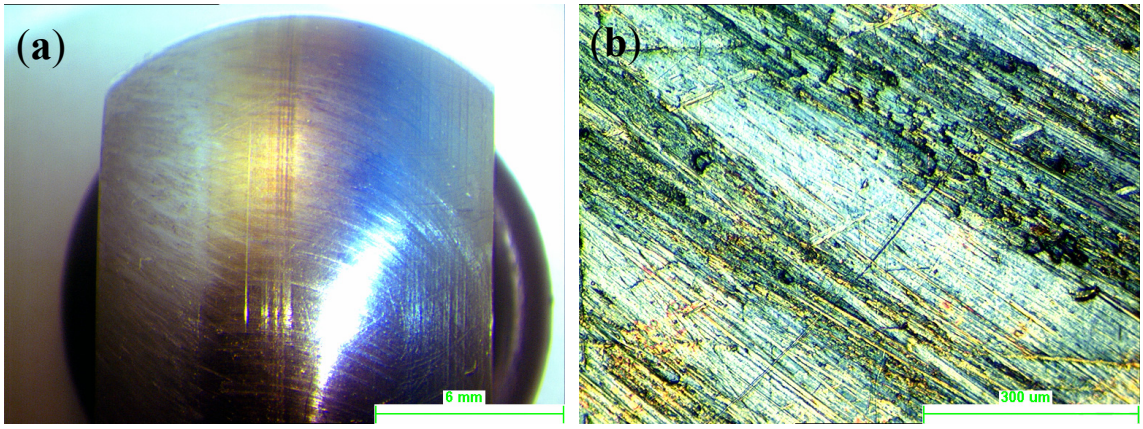

Figure 289 – Ball's surface produced with a #2000 CIB-D wheel. [Oxidation on the ball's surface remains visible as no grinding contact was made during this Elas + Elid 1 superfinishing run]. - (a) Full ball picture, (b) Optical microscope picture

27.6.2 Superfinishing Titanium with MRB wheels

The #8000 MRB-CeO, MRB-AlO, and MRB-CBN wheels used on steel balls in chapter 25 were also tested on titanium.

Cerium oxide is a low hardness, highly friable, lapping abrasive that has been previously studied for Elid 1 lap-polishing of titanium. Processing with aggressive processing parameters (ws-5215, bs-963, 67.6N), the wear rate of the MRB-CeO wheel was very high (1.39 mm/min). Reducing the speeds and load (ws-1000, bs-600, 28N) arrested the excessive wheel wear to a rate that averaged at 0.025 mm/min. The surface of the balls produced was however of a poor quality (figure 290).

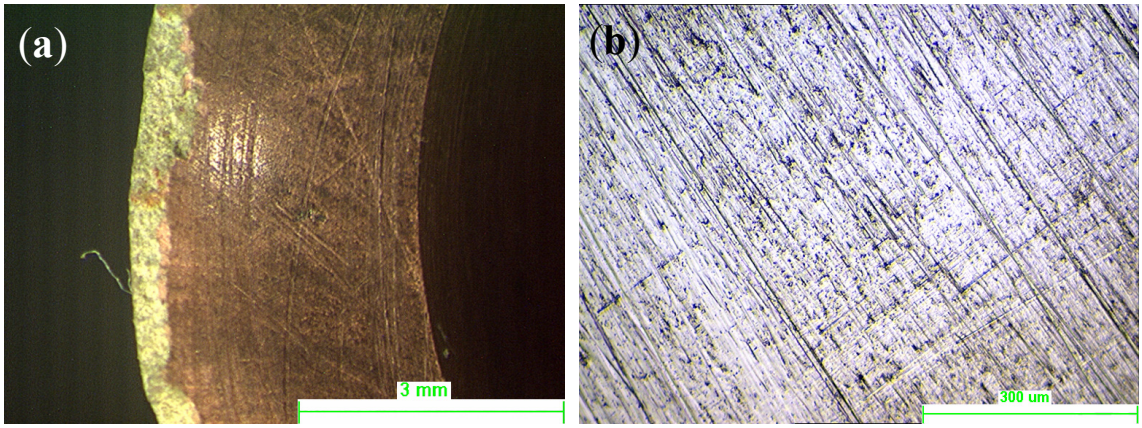

Figure 290 - Picture of a titanium ball surface and the #8,000 MRB-CeO wheel used to produce it. [No-Elid used, ws 1000, bs 600, 28N]. - (a) Wheel's grinding surface after superfinishing (b) Smoothest part of the titanium ball surface

Neither superfinishing with Elid 1, nor the oxidation of the ball's surface using Elas, managed to improve ball surface quality or ball material removal rate. The best results were achieved when no Elid was used at all.

In comparison with the Cerium oxide wheel, processing using either the MRB-AlO or the MRB-CBN wheels made no significant difference to the results. The application of a Molybdenum disulphide powder to the titanium ball and MRB-CBN wheel did not improve the surface quality to the required levels. Whilst suitable for use on steel and with Elid 3, copper is not the correct wheel bonding material for processing titanium.

27.6.3 Superfinishing Using Darmann Wheels

Using either of the Darmann wheels resulted in catastrophic wheel wear. Runs conducted with a minimum spring compression of 0.5mm (28N) resulted in an average wear of 0.490mm and 0.442mm respectively for wheels No.2 and No.4. Increasing the spring compression to 1 mm resulted in increased wear (No.2 = 0.981mm, No.4 = 0.538mm). Due to the un-aggressive processing parameters used, the spindle power usage only increased slightly (~7 watts) when the superfinishing load was applied (figure 291). The spindle power declined during the processing run as the wheel wore away and caused the load to reduce. At the end of the run the spindle was typically only using 2 watts more than free running.

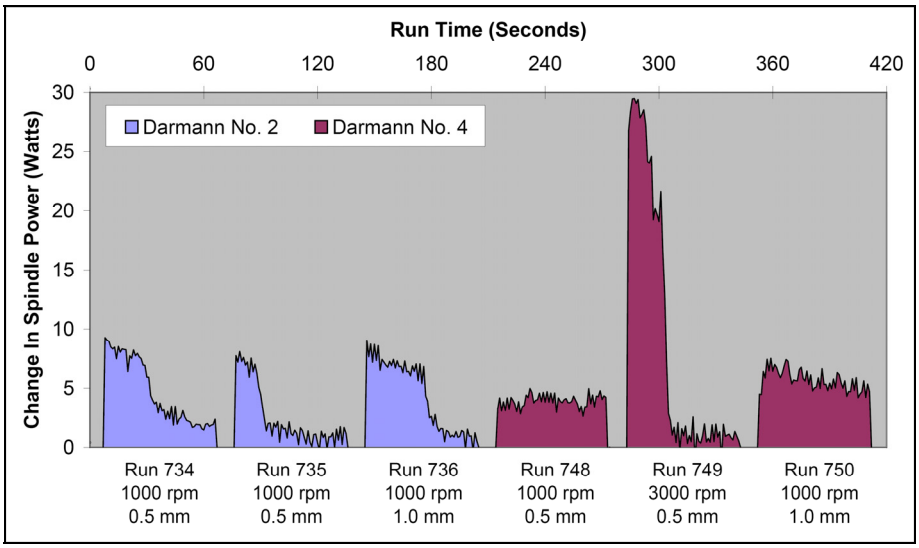

Figure 291 - Wheel spindle power data from runs using Darmann wheels No.2 and No.4 on RNB08 titanium balls - [Details: ball speed 600 rpm, ball input as output]

The surface quality produced, although not particularly good, was the best achieved in this research on titanium (figure 292). Material was being removed from the surface of the ball (no.2 average 9.7 µm/min, no 4 average 4.5 µm/min). The grinding marks were relatively coarse but regular and consistent when the No.2 wheel was used. More of a polishing action with finer, slightly smeared grinding marks appeared when the No.4 wheel was used. The surface quality was best on the right side of the ball where the relative ball to wheel speed is larger, but was not as good on the left.

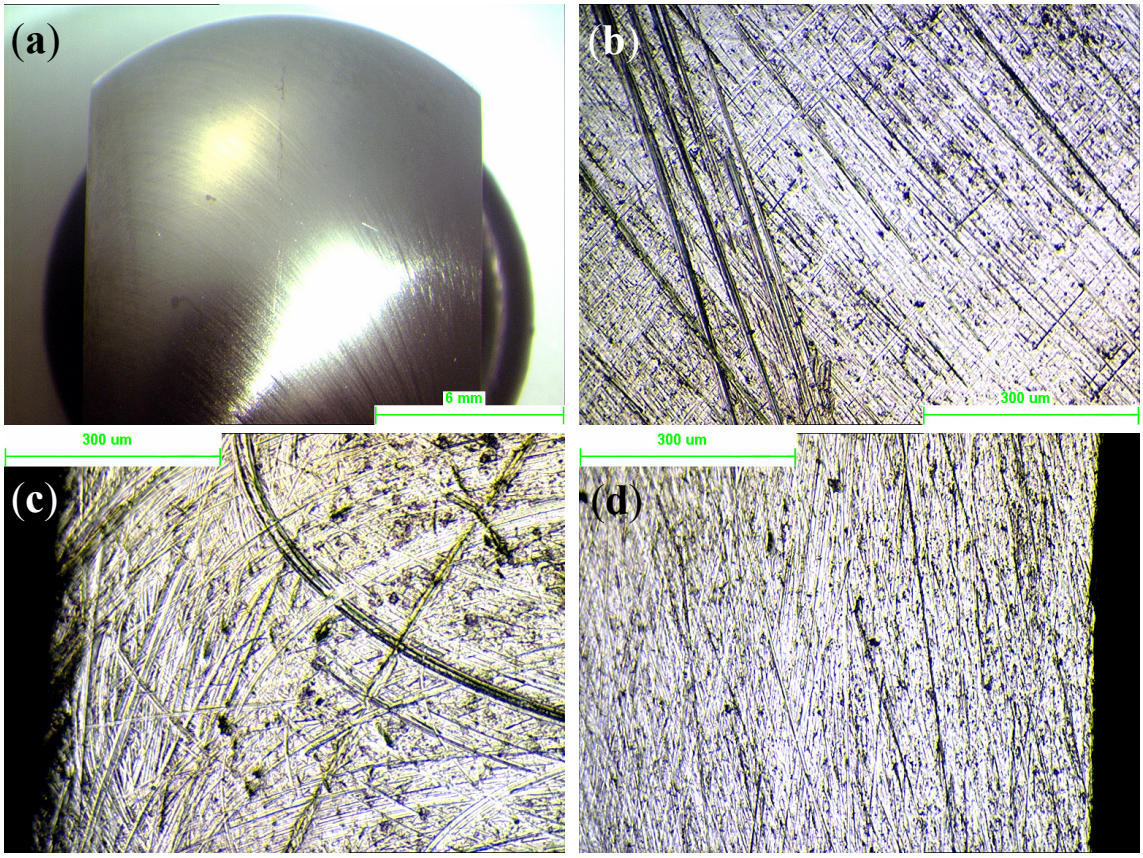

Figure 292 - Titanium ball after superfinishing with a Darmann No. 4 wheel on the as-received surface. (a) Full ball, (b to d) balls surface at centre, LH edge, RH edge.

27.7 Conclusions of Tests on Titanium Balls

As demonstrated in this chapter, no satisfactory processing option was found for processing directly onto titanium. The main problems being excessive wheel wear and very poor quality ball finishes. Results were somewhat improved when very slow speeds and light loads were used. Better results were achieved when Elid was not used, as wheels that wear excessively do not benefit from being electrolytically dressed. Processing on a thick chrome coating offered a usable and effective processing solution for titanium balls.

Chapter 28

Evaluation of Optimised Processing Cycles

This chapter evaluates various optimised processing cycles, in order to assess and compare which achieve the best quality end product by the most efficient means. Testing involved an exhaustive 160 runs conducted on 32 balls taken from various stages in the conventional process chain. Comparisons were made between five different wheel types, stiff and flexible wheel mountings, and the type of Elid used. The full range of responses, as outlined in the experimental, was measured at various points during a ball's typical processing cycle. Testing was carefully conducted to ensure that all the cycles being evaluated were sustainable and results obtained were truly representative. For example, results obtained while Elid 2 superfinishing were only recorded after conducting a number of dummy runs. These ensured the wheel's condition was representative of what it would be if it had been used to produce an entire batch of balls in this manner. The cycles selected represent the best available options to efficiently produce high quality balls. Figure 293 outlines the factors tested.

Factor Tested	Details
Ball Input	After – Heat-treatment, Cylindrical grinding, Honing, Barrelling
Number Of Stages	One, two, three, or four processing stages after heat-treatment
Processing Parameters	Applied Load (0.5 & 1.5 MPa) with Elid Setting (Off & 40A, 90V, 70%)
System Set-up	Stiff / Flexible Wheel Mounting
Elid Type	Elid 1, Elid 2, None
Wheel Type & Abrasive Size	Fujidie Elid wheels (#500, #2000, & #12000 MRB-CBN). Darmann non-Elid wheels, No.2 - (10µm SIC+AlO) & No.4 - (5µm AlO)

Figure 293 - Details of the factors investigated

Ball processing is subject to differing requirements depending on the input state of the ball and whether it is used to just improve ball finish or also used to generate ball roundness and O/D tolerance. For example, when processing cylindrically ground balls, roundness and finish both require improvement. This can be achieved by two different wheels sequentially, one for roughing which achieves the form and another for finishing. Alternatively it is possible to achieve form and finish in one operation with one wheel.

As discussed previously, conflicting processing parameters are required to achieve maximum efficiency and optimal ball quality. Rather than compromise it is possible to apply parameters for maximum efficiency at the start of a ball processing cycle (High load, aggressive Elid) and optimal quality setting at the end of the cycle (Low Load, no Elid). Aggressive Elid creates a free-cutting wheel, which coupled with the application of high loads, dramatically increases material removal but at the expense of form and finish. Turning the Elid off glazes the wheel improving the ball surface finish; reducing the load improves ball form.

28.1 Superfinishing of Heat-treated Balls

Seven heat-treated balls were used to evaluate three possible cycles where ball form and finish both require improvement.

Cycle A. Darmann No.4 wheel without Elid used for both form and finish.

Cycle B. Darmann No.2 wheel without Elid primarily for form improvement, followed by a #12,000 MRB-CBN wheel using Elid 1 for final finishing.

Cycle C. #500 MRB-CBN wheel primarily for form improvement, followed by a #12,000 MRB-CBN wheel for final finishing. Both conducted using Elid 1.

28.1.1 Ball Material Removal

Between 10 and 20 microns must be removed from the O/D of a turned and heat-treated ball in order to fully generate the required form and surface finish. It is also necessary to remove the heat affected zone created by the heat-treatment process, but this element is not considered here. The material removed from the ball during processing is shown in figure 294. Results obtained through ball weight measurement are generally mirrored by micrometer measurements (appendix M).

The Darmann No.4 wheel (**Cycle A**) experienced a very rapid initial rate of material removal as the rough surface of the ball self-sharpened the wheel. After this initially large removal rate, virtually no further wheel material was removed. Therefore this wheel is only capable of surface improvement and not bulk material removal. After 600 seconds the remnants of the heat-treated surface still remained in a band around the centre. The wheel was unable to remove the final 5% of the heat-treated surface without an excessively long processing time (five further minutes) at an increased load.

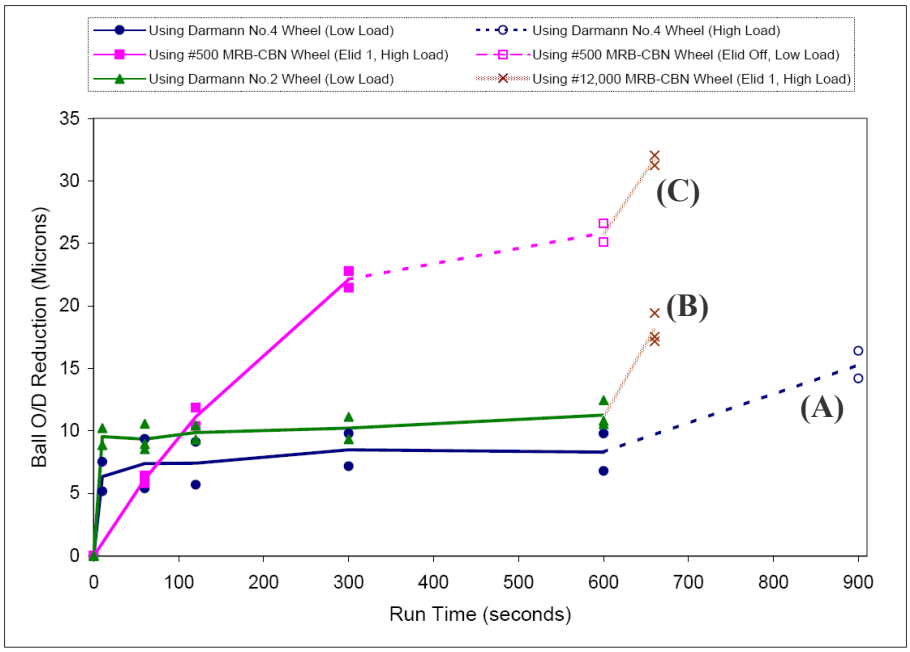

Figure 294 - Cumulative ball material removal during the superfinishing of heat-treated balls 83 to 89 [weight measurements converted to O/D reduction]

The Darmann No.2 wheel (**Cycle B**) exhibited the same characteristics of rapid initial material removal followed by an inability to remove bulk ball material. When switching to the 12,000 MRB-CBN wheel at the 600 second point, rapid material removal recommenced (figure 294), finishing off the balls.

Previous experimentation revealed that when using the #500 MRB-CBN wheel (**Cycle C**), the material removal rate is not considerably affected by the input condition of the ball. This result is confirmed by this wheel achieving a consistent rate of material removal into the bulk material of the ball. After 300 seconds the load was reduced and the Elid turned off. This resulted in a reduction in the ball material removal rate. After 600 seconds the #12,000 wheel was again employed for final finishing.

28.1.2 Wheel Wear

In an attempt to minimize wheel wear, a factor previously found to be critical, a low load was used during the initial stages as this had reduced wear in earlier tests. The wheel wear recorded with both the Darmann wheels, particularly No.2, was unacceptably large in the initial period of superfinishing (figure 295). It is this rapid wear of the wheel which was responsible for the rapid ball material removal rate in the early stages of the processing cycle. After approximately 10 seconds no further significant wheel wear occurred, even when the load was increased.

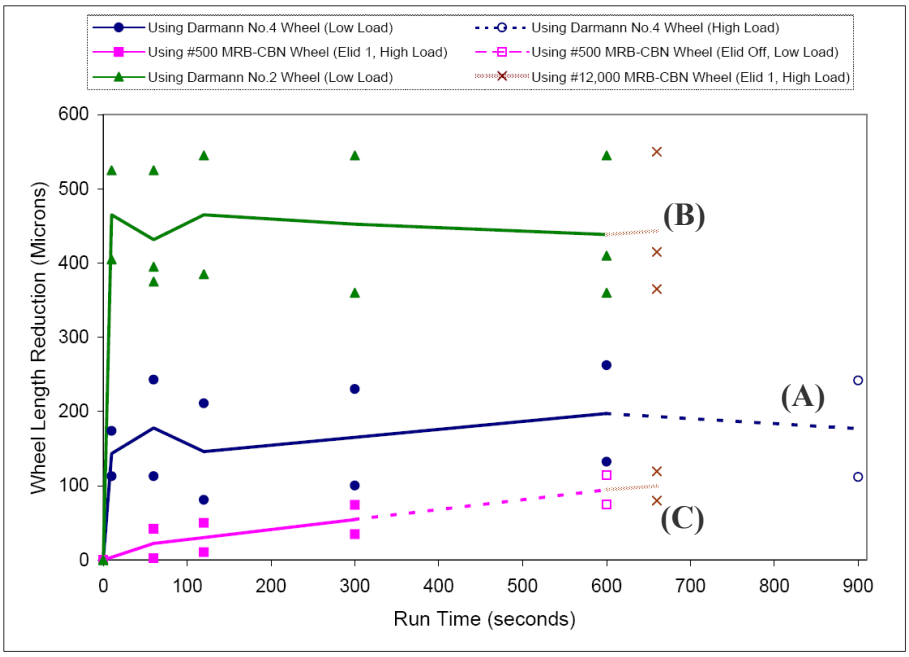

Figure 295 - Cumulative wheel wear during the superfinishing of heat-treated balls 83 to 89

The length reduction of the No.2 wheel per ball is approaching 0.5 mm. A wheel will only be able to produce around 30 balls at this unacceptable rate of wear. Using the No.4 wheel the wear rate is slightly less, producing ~75 balls per wheel, in one processing operation to finished ball quality. The wear recorded while using the #500 MRB-CBN wheel was larger than previous readings but still acceptable, improving the finish of approximately 1000 heat-treated balls per wheel, not including set-up.

Standard batches of balls are between 50 and 200 balls; a wheel should last at least this long as this in order to avoid additional set-up time. The fact that the Darmann wheels are relatively inexpensive compared to the Elid wheels should be considered when deciding what rates of wheel wear are reasonable. Each No.2 wheel costs from £10.79 (5units), to £2.52 (100units) and wheel No.4 costs from £11.58 (5units), to £3.31 (100units). A mounted #2000 MRB-CBN wheel costs £122.09, although purchasing in larger batches and reusing mountings may reduce the costs.

28.1.3 Roundness

Both ball roundness (figure 296) and ball waviness measurements (appendix M1) were taken over the same ball track after each run and measured in accordance with the method described in chapter 13. Roundness values improve very quickly from the turned and heat-treated starting condition, and all the wheels achieved the required 2.5 µm tolerance requirement within 60 seconds (figure 296). Once the form has been impressed onto the ball, its level remains within the 2.5 µm tolerance band.

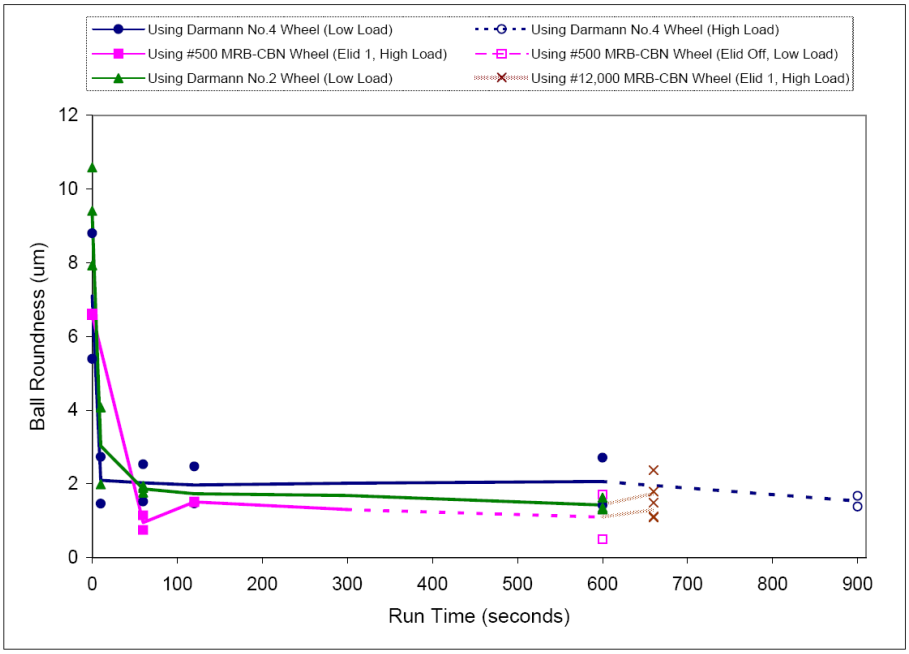

Figure 296 - Change in ball roundness during the superfinishing of heat-treated balls 83 to 89 [Taylor Hobson TalyCenta, up & down ball]

28.1.4 Surface Finish

Surface roughness analysis was measured using both a Taylor Hobson talysurf and a Wyko phase shift interferometer. The full range of finish parameters were recorded and analysed, with Ra results presented in figure 279. The talysurf measurement traced the same profile across the centre of the ball from one edge to the other each time processing was stopped. Along with an assessment of roughness taken across the entire ball's width, measurements were also taken on parts of the ball that were fully formed. Wyko interferometer readings were averaged from various measurements taken across the ball's width.

When assessing the roughness across the entire ball width, the Darmann wheels initially improved ball finish very rapidly. However, as a result of the portion of heat-treated surface that was not able to be removed, further finish improvement became very slow. The No.4 wheel completely generated the ball after 15 minutes, the final 5 of which were using a high load. Even slower progress was made with the No.2 wheel, until it was finished with a #12,000 MRB-CBN wheel using Elid 1.

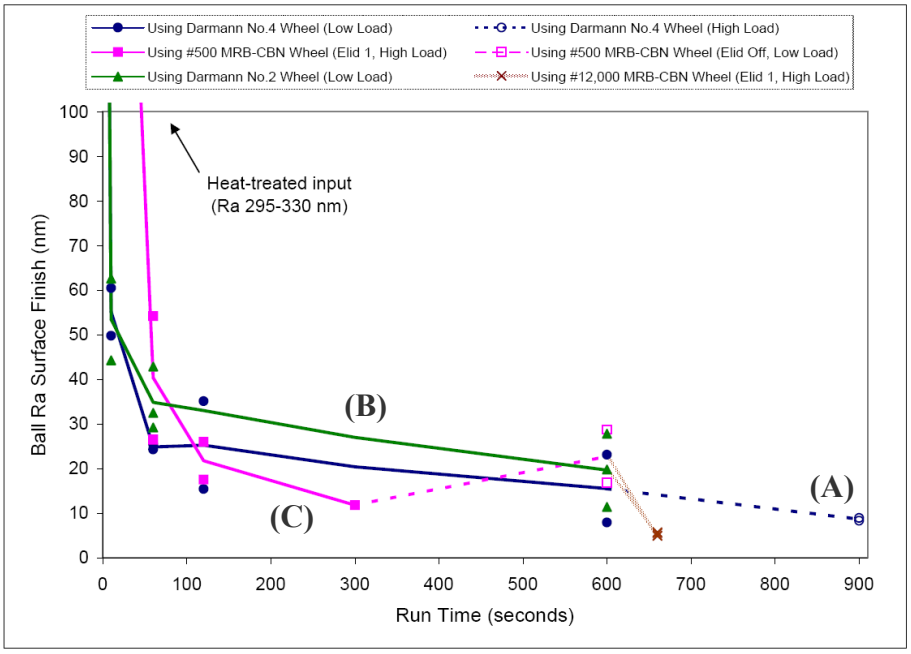

Figure 297 - Change in ball Ra surface finish during the superfinishing of heat-treated balls 83 to 89 [Taylor Hobson talysurf across centre of entire ball width]

Between one and two minutes into its cycle the #500 wheel surpassed the level of surface finish of the Darmann wheels. After five minutes the ball's surface was fully generated. At this point the load was reduced and Elid turned off, in order to facilitate an improvement in ball form and finish. Superfinishing with a glazed #500 wheel, caused the surface of the ball to burn, which is the reason for the surface finish worsening at 600 seconds. This has been discussed further in chapter 16.

28.2 Superfinishing Of Cylindrically Ground Balls

After heat-treatment, the next stage on a standard processing route would be for the balls to be cylindrically ground. The cylindrical grinding process removes 100 microns from a heat-treated ball's O/D, which consists of the heat damaged surface. In addition, the ball's form and finish is slightly improved, although it is still a long way from meeting the final requirements. In order to fully remove the cylindrical grinding marks a further 5 to 10 microns must be removed from the ball's O/D. Three cycles were evaluated on seven balls, using Elid 1 for both form and finish improvement. All three cycles were conducted using maximum efficiency parameters at the start and optimum quality settings at the end.

Cycle D. #12,000 MRB-CBN wheel with a flexible mounting
Cycle E. #2,000 MRB-CBN wheel with a flexible mounting
Cycle F. #2,000 MRB-CBN wheel with a stiff mounting

28.2.1 Ball Material Removal

There is a close grouping of the replicated data points and all the cycles followed a relatively linear trend for both maximum efficiency and optimum quality parameters (figure 298). This shows that the Elid 1 process is stable and that ball material is being removed at a consistent rate.

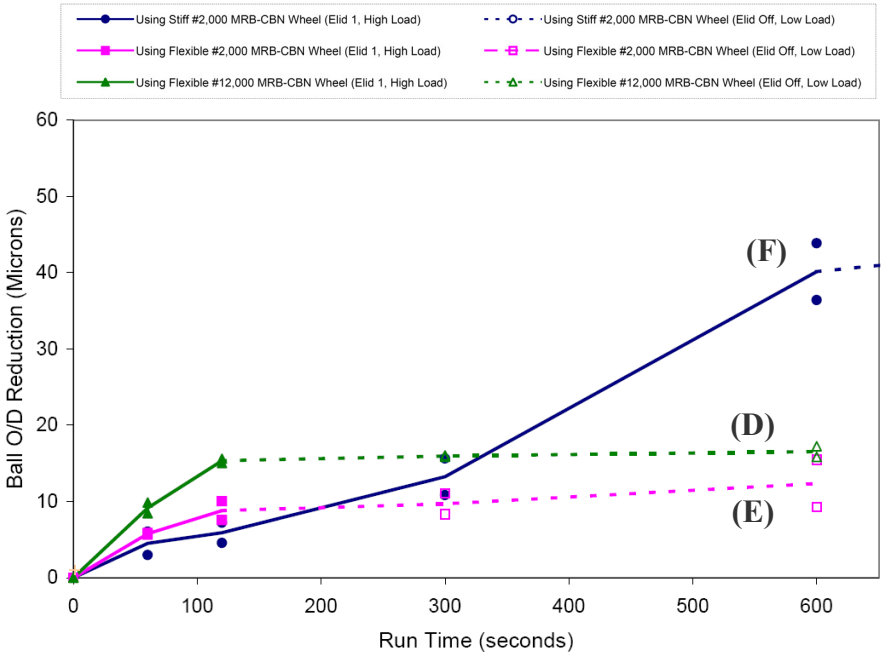

Figure 298 - Cumulative ball material removal during the superfinishing of cylindrically ground balls 75 to 81 [weight measurements converted to O/D reduction]

The #12,000 MRB-CBN wheel (**Cycle D**) removed material particularly quickly during this set of experiments, actually removing material faster than the larger abrasive #500 & #2000 wheels. This demonstrates that it is possible to get a high rate of material removal even with a very fine abrasive wheel. The material removal capacity of the #12,000 wheel is effectively zero when the load is reduced and Elid turned off.

When the flexible system was used, the #2000 wheel (**Cycle E**) performed adequately, achieving the required 5 to 10 micron O/D reduction in 120 seconds. This was enough to fully remove the cylindrical grinding marks. After 120 seconds only a very slight increase in material removal was recorded with optimum quality parameters.

Using the stiff mounted system (**Cycle F**), 40 μm had to be removed in order to fully generate the entire surface of the ball. This was because it could not adapt to the slight misalignment and removed most of the material from the edge of the ball. This is a result of the stiff system's inability to adapt to minor ball to wheel misalignment during processing.

Surface generation rate, and thus ultimately processing time, is strongly dependent on not only the ball material removal rate but also whether this material is removed evenly from the ball's surface (figure 299). This is dependent on whether correct ball to wheel alignment is achieved; however increasing the system flexibility allows a greater degree of misalignment to be tolerated (figures 300 & 301). The stiff system is over-constrained when superfinishing, the flexible system uses the ball-wheel interface as a self-centring constraint. Although the diagrams exaggerate the degree of misalignment, an error in the order of ~25 microns using the rigid system produces 'out of round' balls (figure 302). A 76 μm manufacturing tolerance exists from the ball faces to the ball centreline. This coupled with errors in ball or wheel installation, can add up. The flexible system can deal with misalignments approaching 100 microns, although wheel failure becomes increasingly likely at this level.

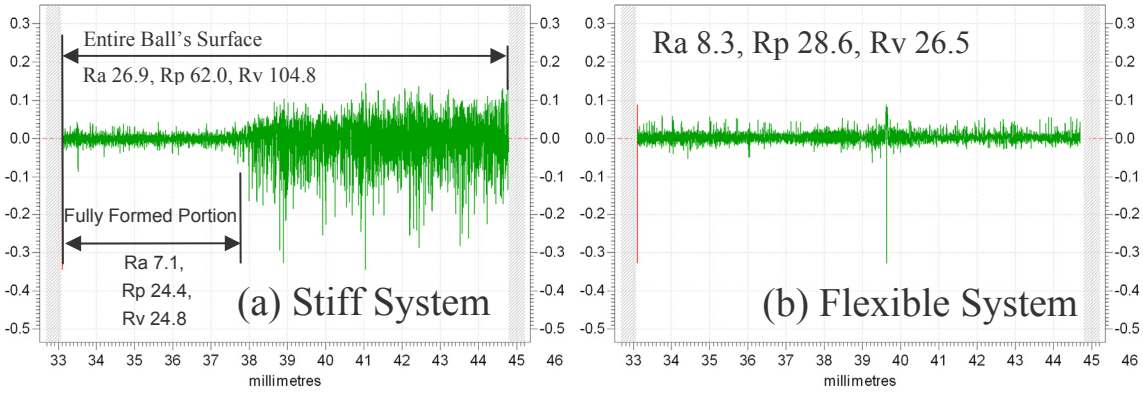

Figure 299 - Talysurf roughness profile examples, across centre of entire ball. - (a) Stiff system: material removed form the LHS only, balls surface not improved on the RHS. (b) Flexible system: material removed evenly from the entire ball's surface, ball's surface fully generated.

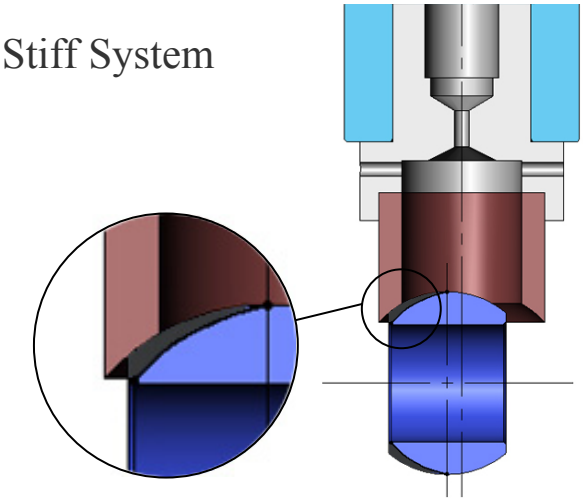

Figure 300 – Illustration of material removal from one side of the ball only

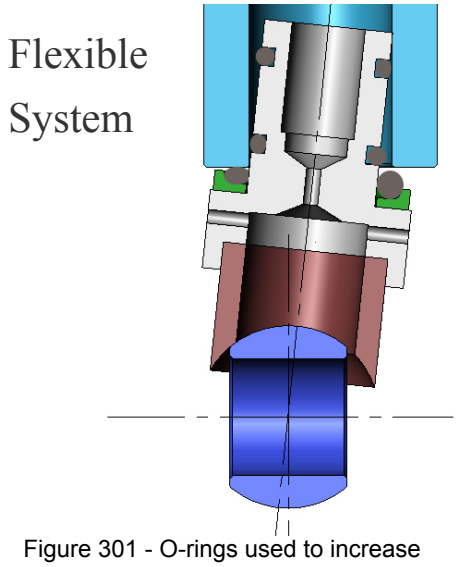

Figure 301 - O-rings used to increase system compliance

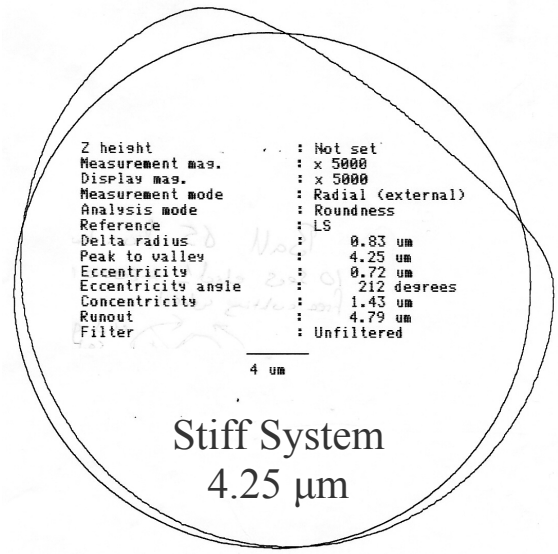

Figure 302 - Roundness measurement when material is being removed from one side only (Stiff System)

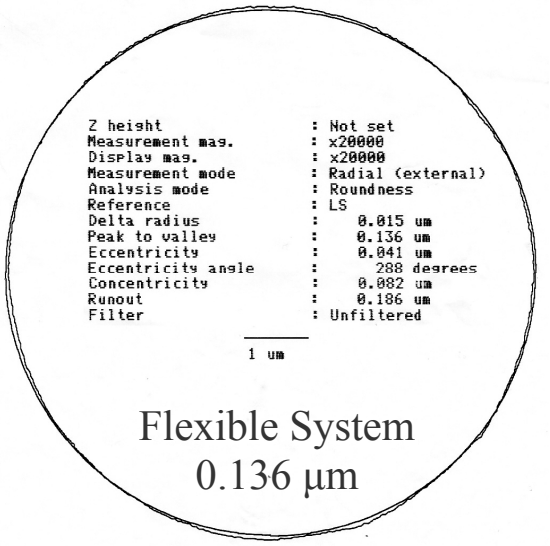

Figure 303 - Roundness measurement of the best achieved roundness (Flexible system)

28.2.2 Roundness

Ball roundness is clearly affected by uneven material removal from the surface of a ball as demonstrated by cycle **(F)** in figure 304. An error in the ball's form will eventually resolve itself into a new centreline. Both the flexible mounted wheels (**Cycles D & E**) achieve the required 2.5 micron roundness within 60 seconds and the flexible #2000 wheel achieves very high quality results. Reducing the load does not appear to further improve roundness. The grouping consistency of the flexible mounted cycles is very good once form has been fully generated.

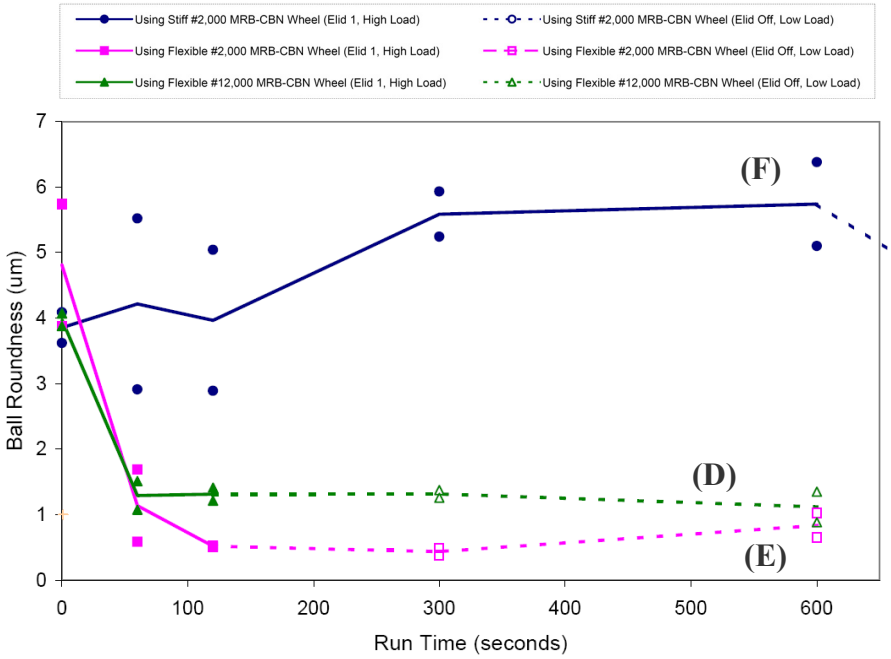

Figure 304 - Change in ball roundness during the superfinishing of cylindrically ground balls 75 to 81 [Taylor Hobson talycenta, up & down ball]

28.2.3 Surface Finish

Finish results (figures 305 & 306) show that the ball's surface is fully formed by the #12,000 wheel after less than 60 seconds. The flexible #2000 wheel has a lower removal rate which takes between 60 and 120 seconds. The stiff system takes at least 600 seconds with the proportion of completed surface across the ball driving the gradual reduction in surface finish.

Surface finish results recorded with the Wyko interferometer are more accurate but only measure a small concentrated area of the ball's surface (250 μm^2). The results reveal the excellent levels of surface finish achieved, the differences between the wheel mesh sizes, as well as the effects of finishing parameters.

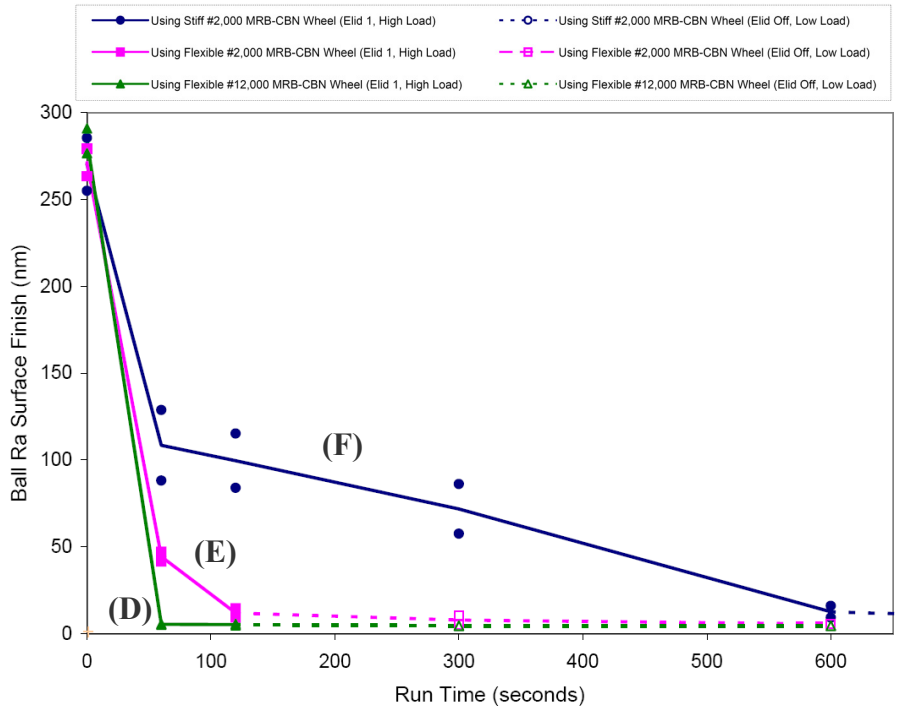

Figure 305 - Change in ball Ra surface finish during the superfinishing of cylindrically ground balls 75 to 81 [Taylor Hobson talysurf across centre of entire ball width]

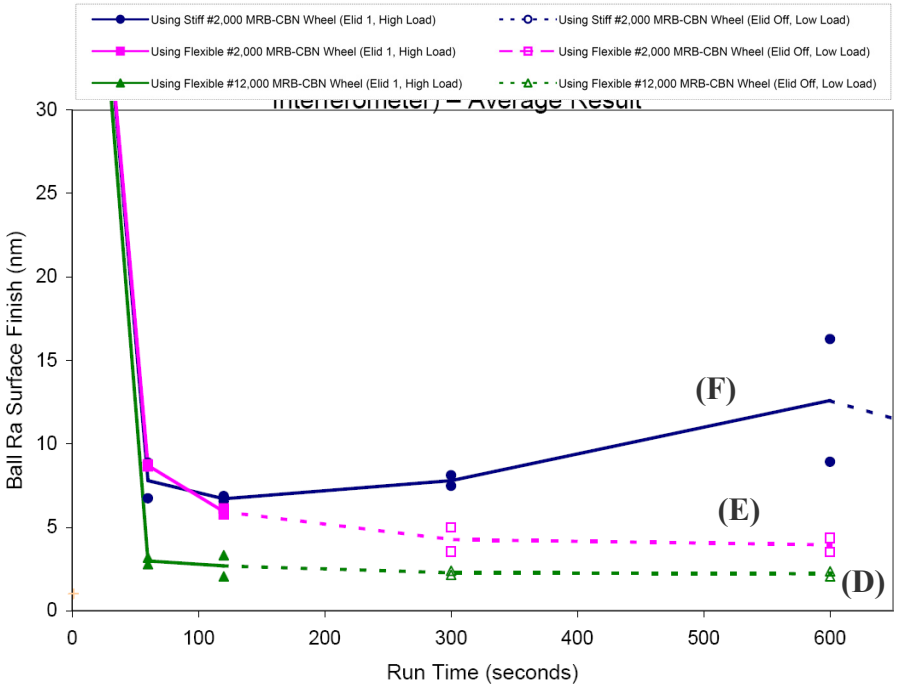

Figure 306 - Change in ball Ra surface finish during the superfinishing of cylindrically ground balls 75 to 81 [Wyko phase shift interferometer – Average of three readings]

Balls superfinished with the #12,000 wheel are clearly the best, achieving around 2 nm Ra. There was no real difference when the #12,000 wheel became glazed through turning Elid off. There was, however, a noticeable improvement in both visual appearance and ball surface finish results when the #2000 wheel became glazed. Although glazed #2000 wheels do provide an improvement in finish, it can take a prohibitively long time. The time can be reduced if the load remains high but this will not ultimately be better than simply using a finer abrasive wheel.

28.3 Superfinishing Of Honed Balls

The conventional processing route after cylindrical grinding is honing. Honed balls possess the required form accuracy but levels of finish, although much improved, still require refining. Again the #2000 MRB-CBN wheel is used to evaluate stiff and flexible systems, using Elid 1. In addition the #2000 MRB-CBN wheel is evaluated using Elid 2.

Cycle G. #2,000 MRB-CBN wheel with a flexible mounting using Elid 2
Cycle H. #2,000 MRB-CBN wheel with a flexible mounting using Elid 1
Cycle I. #2,000 MRB-CBN wheel with a stiff mounting using Elid 1

28.3.1 Ball Material removal

As shown in figure 307 the material removal varied quite considerably between runs considering they all used the same wheel. In order to fully eliminate all the honing marks approximately 1 to 2 microns requires 'evenly' removing from the O/D of the ball. Elid 2 (**Cycle G**) achieved a considerably higher removal rate at the start of processing than at the end and the required quantity of material was removed by the 10 second mark. Visual inspection and surface finish results confirmed that the original honed surface had been fully removed. As is the nature of Elid 2, the removal rate declined over time. It was lower during the second run and was effectively zero after the load was reduced.

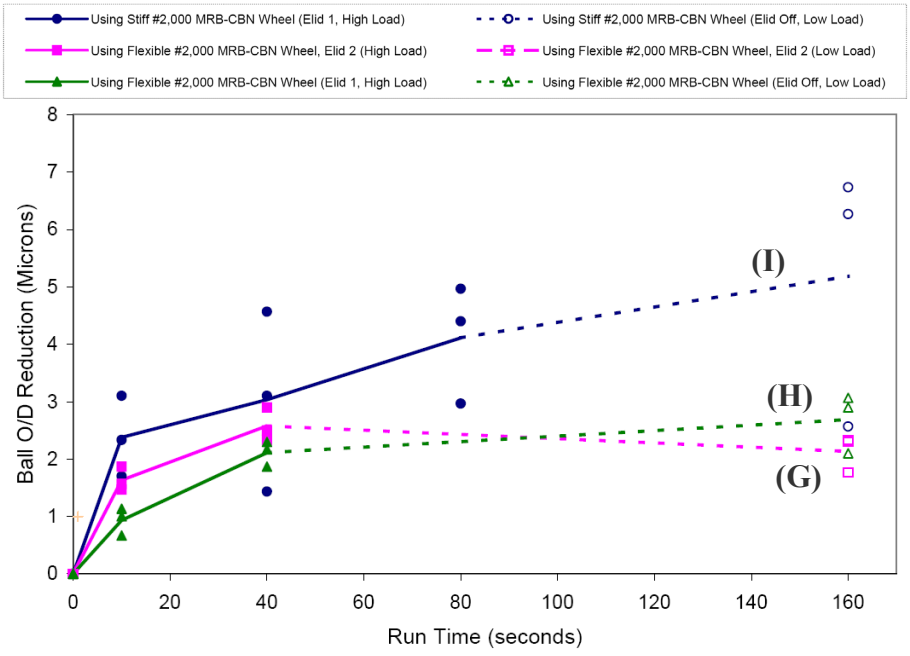

Figure 307 - Cumulative material removed from ball O/D during processing
[From Ball Weight Measurements]

When processing using the flexible system with Elid 1 (**Cycle H**), the surface took longer to fully generate, between 10 and 40 seconds, due to the initial removal rate being lower. Processing with the stiff system and Elid 1 (**Cycle I**) recorded the highest initial removal rate but removed material unevenly from the ball's surface. As a result one of the balls was finished within 10 seconds; the other two tested were still not evenly completed after 160 seconds.

28.3.2 Roundness

The ball roundness generated by the standard honing process was maintained to a very high standard when the flexible mounting was used (**Cycles G & H**), i.e. below 1 micron (figure 308). An extremely good result (0.233 µm) was recorded using Elid 2. When additional measurements were taken on this ball no other track recorded higher results. The best result on this ball was measured up and down the ball at the dot +90 degrees and recorded 0.136 µm roundness (figure 303).

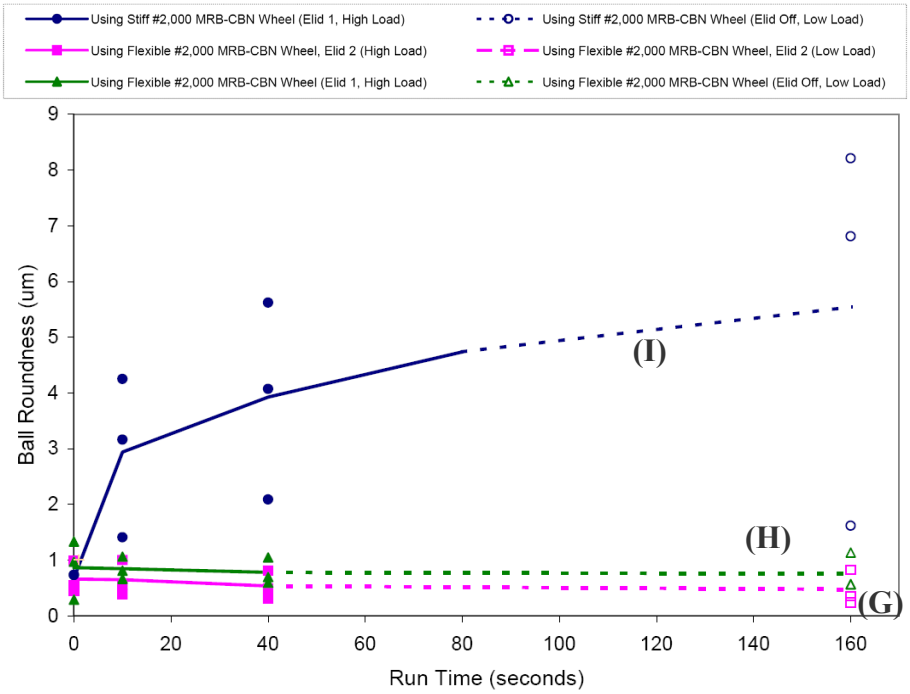

Figure 308 - Ball roundness - T.H. talycenta, up & down ball

The use of the stiff mounting (**Cycle I**), throws off the form considerably. Only one of the balls superfinished with the stiff system achieved good roundness results and an even finish. This variation is probably due to this ball's centreline lining up accurately with the wheel's centreline.

28.3.3 Surface Finish

The surface finish results (figures 309 & 310) agree with the estimate that 1.5 µm requires removing evenly from the balls O/D. The flexible system using Elid 1 had not entirely removed all the honing marks after 10 seconds. By the 40 second mark both the flexible Elid 1 and Elid 2 cycles, as well as one of the stiff system balls, are effectively achieving the same result (7nm Ra). Levels of finish are slightly improved by switching to optimum quality parameters.

In accordance with conventional grinding wisdom, evidence was provided in chapter 17 that demonstrated an improvement in surface finish when using a rigid system. However, this is not the case here. Not only are the entire balls' profiles worse, but measurements taken on the fully formed portions of the balls are also worse, when using the stiff system (figure 310 & appendix M3).

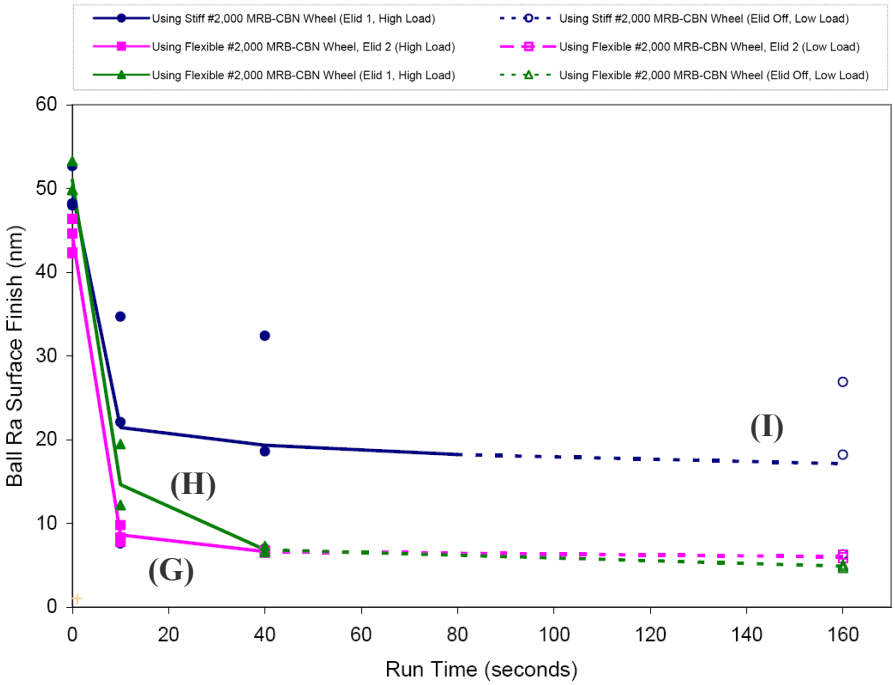

Figure 309 - Ball Ra surface finish (T.H talysurf) across entire ball centre

When using Elid 2 the surface finish improves as the wheel goes from a free-cutting, high material removing condition at the start of the cycle, to a glazed, polishing condition at the end. One additional advantage of the Elid 2 cycle is that at no point is the ball involved in the electro-chemical circuit. This eliminates the possibility of stray deposits of copper, which can occur in error with the use of Elid 1.

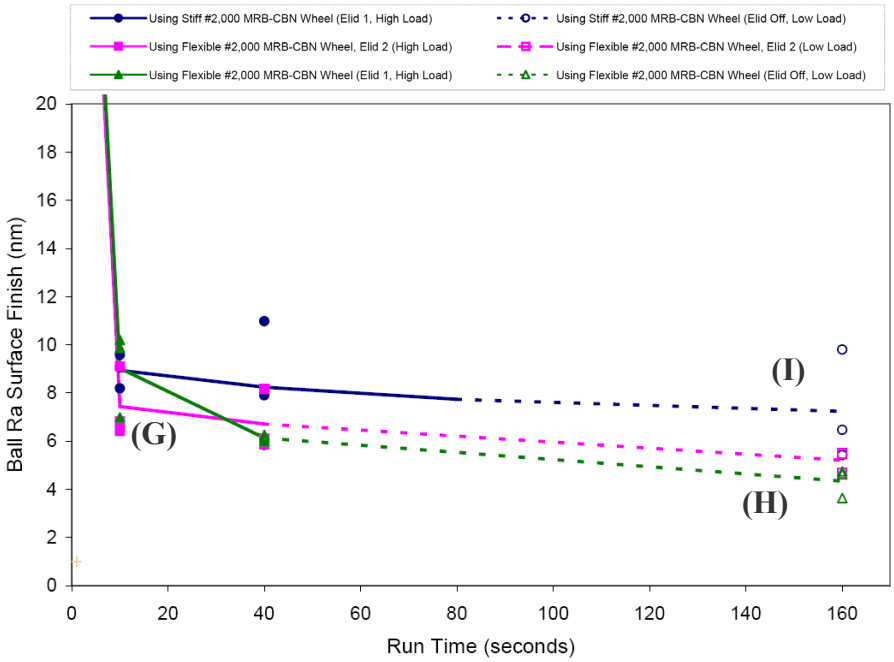

Figure 310 - Ball Ra surface finish (Wyko phase shift interferometer) – average result

28.4 Superfinishing Of Barrelled Balls

Previous experimentation has revealed that after barrelling, 1 micron must be removed in order for the surface to be fully formed. At this stage the required level of roundness has been achieved and is maintained during processing (appendix M4). Two cycles were evaluated for improvement of ball surface finish only.

Cycle J. #12,000 MRB-CBN wheel using Elid 1 and a high initial load for a period of 40 seconds.

Cycle K. Darmann wheel No.4 used without Elid. Low initial load increased after 10 seconds.

28.4.1 Ball Material Removal

The #12,000 MRB-CBN wheel, combined with Elid 1 and a high load (**Cycle J**), rapidly removed material from the balls and consistently achieved the one micron O/D reduction in 10 seconds (figure 311). The surface finish results shown in figures 312 & 313 also demonstrate that the surface was fully formed after 10 seconds. The disadvantage of a 10 second process cycle is that there is insufficient time to dress the wheel. This length of cycle would not sustain the condition of the wheel over an entire batch of balls. When final finishing parameters were used (low load, no Elid), the material removal rate dropped to zero.

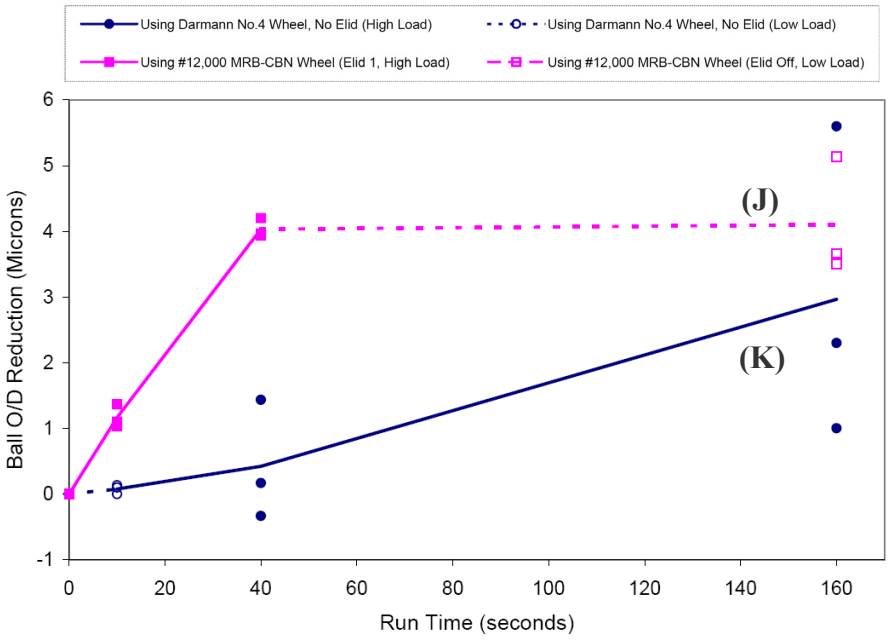

Figure 311 - Cumulative Material Removed From Ball O/D During Processing [From Ball Weight Measurements]

The removal rate with the Darmann No.4 wheel was less marked (**Cycle K**), although with the application of a high load, bulk material could slowly be removed. Material removal was inconsistent between the runs on the three balls.

28.4.2 Wheel Wear

As the smooth input quality of the barrelled balls did not abrade the Darmann wheel, wheel wear remained low. A negligible quantity of material was removed from the wheel's length after processing the 3 balls (12 μm in 8 minutes).

The #12,000 MRB-CBN wheel also achieved a low rate of wheel wear when processing barrelled balls, but unlike the Darmann wheels, wheel wear was also low when processing the rougher cylindrically ground input. A combined assessment of wheel wear for both barrelled and cylindrically ground balls (cycles D and J), produced an average wheel wear rate of 9.3 μm/min with the #12,000 wheel. At this rate, a 10 second run time would enable ~10,000 balls to be produced per wheel. In other words, wear is not the issue; truing and failure are what limits wheel life.

28.4.3 Surface Finish

Ball surface finish values produced with the #12,000 wheel (**Cycle J**) were very regular and remained constant after the 10 second processing time (figures 312, 313 & appendix M4). Talysurf readings of just below 5nm Ra were recorded compared to interferometer readings of between 1.35 to 3.12 nm Ra. With the #12,000 MRB-CBN wheel, surface finish did not improve drastically when optimal quality parameters were selected.

Visual inspection of balls produced using the Darmann No.4 wheel (**Cycle K**) showed that complete surface finish generation took 160 seconds, although the ball's surface finish was markedly improved after 40 seconds.

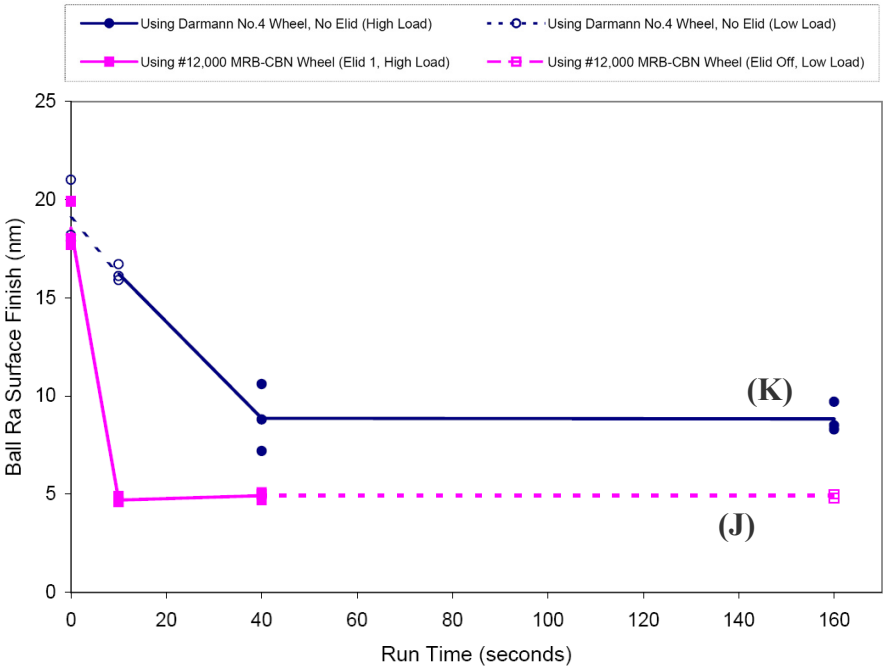

Figure 312 - Ball Ra Surface Finish (T.H Talysurf) Across Entire Ball Centre

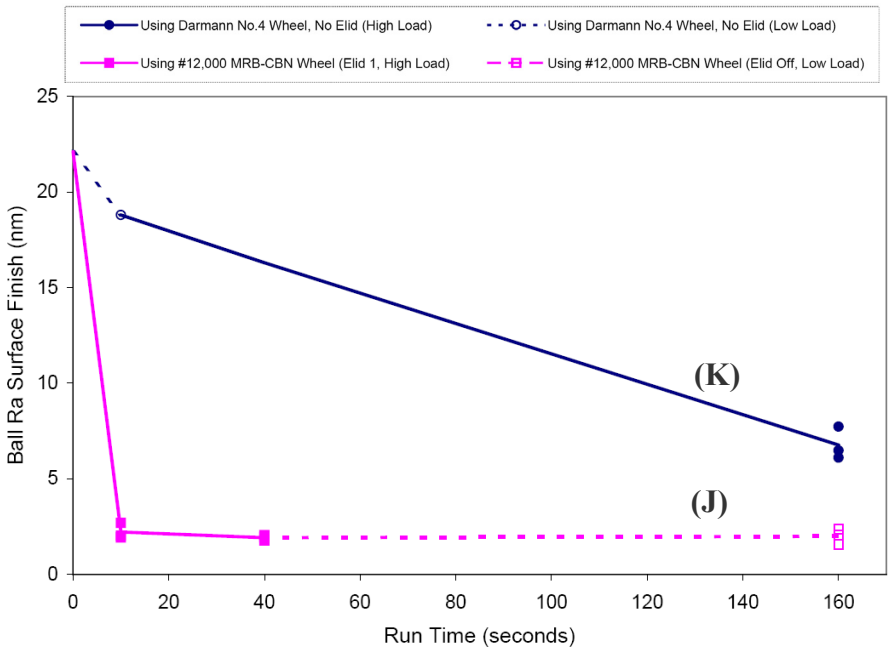

Figure 313 - Ball Ra Surface Finish (Wyko Phase Shift Interferometer) – Average Result

28.5 General Comparisons

General comparisons between the various processing cycles evaluated in this chapter are presented in figures 314 to 317, with graphs showing additional data in appendix M5.

28.5.1 Processing Parameters

Material removal results (figure 314) show that there is a dramatic reduction when optimum quality parameters are selected. This corresponds to the wheel spindle power data (appendix M5), where a reduction in the power usage is recorded when these parameters are used.

A reduction in the applied load has previously been found to improve ball roundness. However the results in this chapter do not show a significant improvement (figure 315). As there is only a trivial advantage gained by reducing the applied load and doing so incurs a large cost on processing efficiency, it should not be done.

In terms of surface finish (figures 316 & 317) the results reveal a small improvement when using optimum quality parameters. This improvement is associated with the glazing of the wheel when Elid is turned off, which creates a polishing / burnishing action. This only produces a minimal improvement considering the extra processing time required and is therefore of questionable benefit. However an improved rate and more pronounced effect of a final polish with a glazed wheel will occur if the load is maintained at a high level throughout.

Glazing provides the most benefit when using the #2000 wheel. Using the coarser #500 wheel when it is glazed can result in the ball's surface burning. When very fine abrasives are used (#12,000 wheel), there is no improvement in surface finish. It is anticipated that a better surface finish could be obtained with a free-cutting #120,000 wheel than one which has been allowed to glaze.

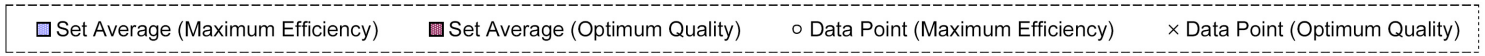

Figure 314 Comparison of ball O/D reduction rate - [Weight reduction]

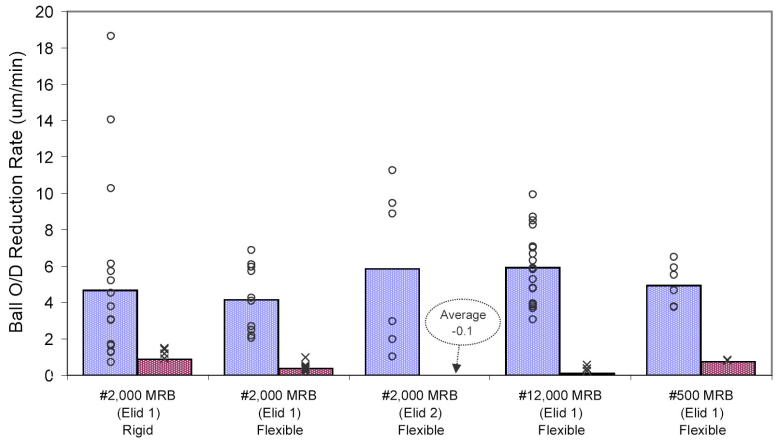

Figure 315 Comparison of ball roundness - [Talycenta, up & down ball]

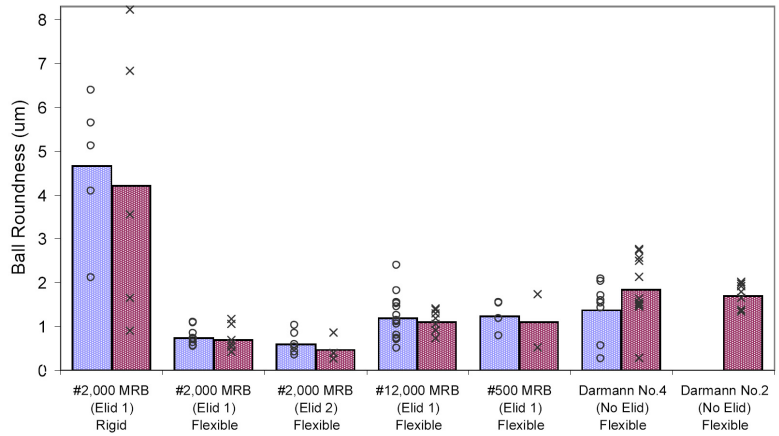

Figure 316 Comparison of ball Ra surface finish - [Taylor Hobson talysurf, across ball centre, on fully formed portion of balls surface]

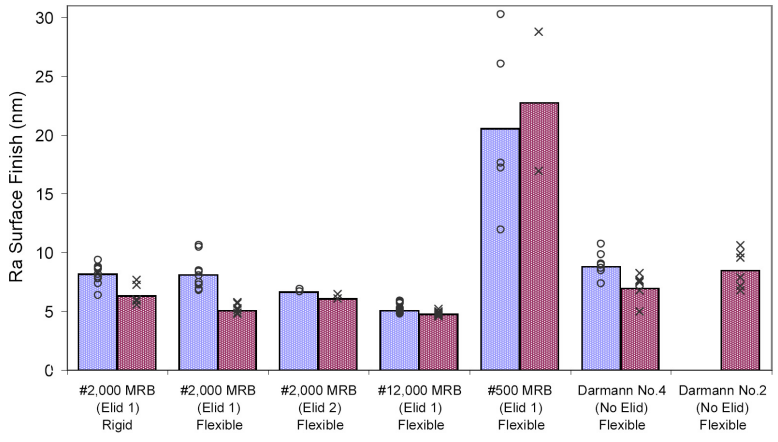

Figure 317 Comparison of ball Ra surface finish - [Wyco phase shift interfometer, average of reading taken on fully formed surface]

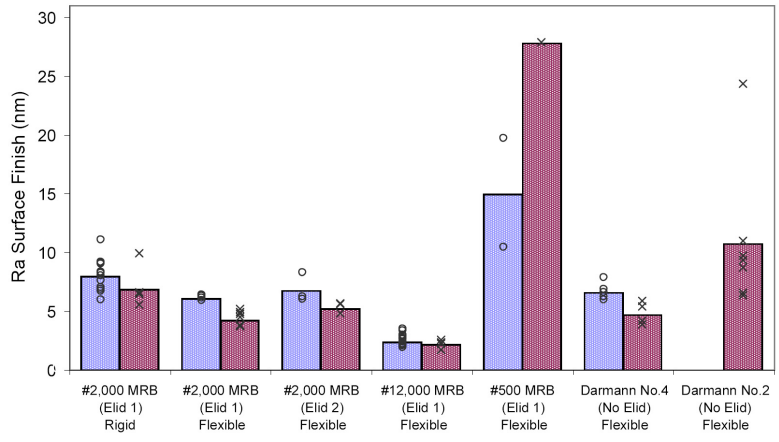

28.5.2 System Set-up

A comparison between stiff and flexible systems is provided in columns 1 & 2, figures 314 to 317. While material removal remains on average the same, results are more consistent when the flexible system is used. As the material is removed unevenly from the surface of the ball when employing the stiff system, the amount that actually requires removing increases dramatically. This in turn causes processing time to multiply. Ball roundness is considerably worsened when employing the stiff system, as a result of its inability to adapt to minor ball to wheel misalignment during processing.

Contrary to the results provided in chapter 17, the surface finish is improved when the flexible system is used. There is no demonstrated disadvantage in using the flexible system and its use provides improved ball quality and a less stringent requirement on system set-up. Therefore a degree of flexibility should be employed.

28.5.3 Elid Type

Elid 2 is used when there is insufficient room to fit a separate electrode. When using Elid 2 superfinishing the material removal rate degrades from the point of initial contact. The removal rate is high and comparable to Elid 1 superfinishing at the start of the run, due to the 30 second pre-process dressing of the wheel creating a well-dressed, free-cutting wheel surface. At the end of the run the wheel has begun to glaze and material removal has ceased. The surface finish produced using Elid 2 is better than when Elid 1 is employed. Both achieve very good roundness results.

28.5.4 Abrasive Size

In line with previous Elid 1 measurements, MRB-CBN wheels ranging from #500 to #12,000 achieve very similar removal rates. There is more variation in ball material removal between data points within sets, than between wheels of different abrasive sizes.

Ball roundness results are similar between all flexible wheel types. Any slight differences are probably dependent upon the exactitudes of the new installation and truing of the wheels, and are not necessarily a true depiction of whether one wheel is better than another. The flexible #2000 MRB-CBN achieved both the best single ball roundness and lowest average readings.

As expected wheels with smaller abrasives produce finer surface finishes. Balls processed with the #12,000 MRB-CBN wheel are clearly the best in terms of finish. Balls produced with the #500 wheel do not reach the required standard and thus require subsequent processing. In addition the finish produced with the #500 wheel is subject to a large amount of variability. Apart from the #500 MRB-CBN wheel, surface finish results are very consistent.

28.5.5 Wheel Type

Ball material removal is fundamentally different when using Elid and Darmann wheels. This is because the Darmann wheels self-sharpen and Elid wheels do not. The CBN in Elid wheels cuts carbides in the ball better than the conventional abrasives used in Darmann wheels, resulting in better surface finish. Visual appearance and values of roughness on balls produced by the No.4 wheel are approximately equivalent to balls produced by a #2000 MRB-CBN wheel. Like the #500 MRB-CBN wheel, the No.2 wheel does not achieve the level of surface finish required from this research and would require an additional finishing stage.

28.6 Processing Options

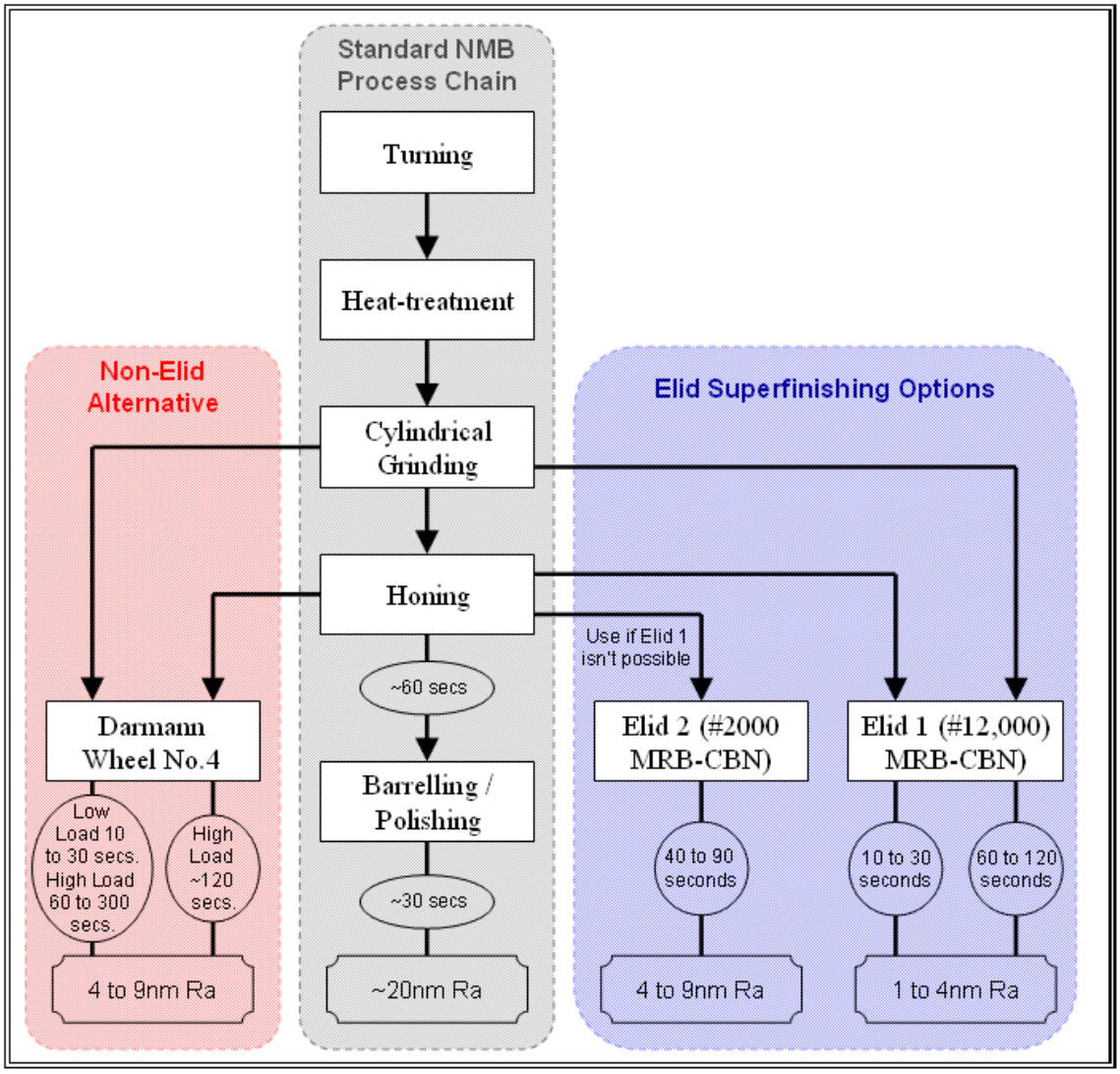

Figure 318 - Process chain options

28.6.1 Ball Input

Superfinishing directly after heat-treatment is not possible for two reasons.

(1) Approximately 0.1 mm must be removed from the surface of the ball, to get rid of the heat-treated heat affected layer. Elid processing is unable to remove this quickly enough and Darmann wheels are incapable of bulk material removal.

(2) The balls do not possess the required 12 µm O/D tolerance bandwidth at this stage. As superfinishing is a constant force process it does not possess the ability to improve O/D consistency.

Balls should be Elid superfinished either after cylindrical grinding or after conventional honing.

If used after cylindrical grinding, Elid superfinishing needs to maintain the O/D tolerance and achieve the desired levels of finish and roundness. One potential problem is the variability of material removal rate widening the 12 μm O/D tolerance, during the removal of the 5 to 10 microns which comprise the cylindrical grinding marks and errors in ball form. This is not an issue for non-Elid superfinishing methods (conventional abrasives), as the self-sharpening mechanism regulates the quantity of ball material removed. Elid 1 superfinishing removes bulk ball material and is not self-regulating. This problem is not insurmountable and can be overcome by monitoring of processing efficiency (Elid power, spindle power, O/D gauging).

After honing, balls only require finish improvement and therefore only need a short run time. This is not long enough to throw out the O/D tolerance. Allowing a degree of system flexibility enables even surface finish generation across the ball's entirety.

Standard barrelling and super-polishing operations are superfluous when an Elid ground finish is required. This is because the peak to valley roughness of the surface profile of honed and polished balls is relatively similar. Virtually the same amount of material will need removing regardless of whether the input ball is honed, barrelled or super-polished.

28.6.2 Two stage finishing process

In order to alleviate problems with ball and wheel alignment and conformity, a roughing operation that generates the form and a finishing operation which produces the final surface finish should ideally be done consecutively on the same machine. Either a coarse Elid wheel (#500) or a conventional non-Elid wheel that would work with a water-based fluid could be used prior to finishing. Alternatively balls could be honed by the normal means and transferred to a separate machine for Elid finishing, with special attention paid to system alignment. Processing for finish improvement only would use #2000 to #20,000 MRB-CBN wheels and a short processing time. The preferred two stage option from cylindrically ground is conventional honing followed by either a #12,000 wheel using Elid 1 or a #2000 wheel using Elid 2 if there are space constraints.

28.6.3 Single stage finishing process

Processing for form and finishing improvement with #2000 to #20,000 MRB-CBN wheels would require a longer processing run. Elid processing benefits from longer run times where the wheel and ball have time to bed into each other and the Elid can be active for a long time. Generating form and finish in a one stage process is achievable and although the total cycle time may be longer, the processing would be less problematic. The best single stage option from cylindrically ground uses a #12,000 wheel and Elid 1.

28.6.4 Processing Using #500 MRB-CBN Wheel (Elid 1)

Processing with the #500 MRB-CBN wheel offers no advantage in terms of efficiency over using either a #2000 or #12,000 MRB-CBN wheel. Due to the large abrasive size it is incapable of achieving the required levels of surface finish.

28.6.5 Processing with the Darmann 2 wheels

Superfinishing with the Darmann 2 wheel is a direct alternative to honing in a two stage process. It can provide finishes comparable to barrelling / superpolishing but requires further processing in order to reach sub 10nm finishes. As this wheel was designed for use with a water-based fluid, subsequent Elid finishing can be completed on the same machine. However, the overriding disadvantage is that wheel wear is unacceptably high.

28.6.6 Processing with the Darmann 4 wheels

As this wheel is a direct alternative to Elid processing and is capable of achieving the required levels of surface finish in a single stage, an oil-based fluid can be used. The optimum cycle for this wheel is 10 to 30 seconds at low load followed by 1 to 5 minutes at high load. This would assist in the removal of any remaining un-generated ball surface whilst reducing catastrophic wheel wear.

28.6.7 Processing Using #2000 MRB-CBN Wheel (Elid 2 and 1)

The #2000 MRB-CBN wheel has been proven, both in previous experiments and during this one, to be ideally suited for use on an Elid 2 cycle. This experiment has shown that the processing times of 30 seconds dressing followed by 10 – 60 seconds superfinishing

can be used for improving the finish of honed balls. This cycle should be used on balls where the ball width prevents the use of Elid 1 superfinishing. Wheel dressing could be performed while a new ball is being installed or while in-process measurement is being carried out. Elid 2 with a #2000 MRB-CBN wheel can only remove a few microns per dressing cycle and is not suitable for use as a single stage on cylindrically ground balls.

Using the #2000 wheel with Elid 1 offers no advantage over using the #12,000 wheel. It does not increase material removal rates and cannot easily achieve surface finishes below 5 nm Ra.

28.6.8 Processing Using #12,000 MRB-CBN Wheel (Elid 1)

The #12,000 wheel can be used for final finishing in a two stage process or as a single stage cycle after cylindrical grinding.

Final finishing with this wheel can be achieved in as little as 10 - 30 seconds. The use of a processing cycle that only lasts for 10 seconds does present some problems. The Elid system must be off when the load is applied and removed, and ideally turned off at least a few seconds before the end of the processing cycle, in order to ensure that there is no electro-chemically deposited copper remaining on the ball. In addition, the Elid system takes approximately 5 seconds to power up. Maintaining the wheel in the heightened free-cutting state that using high power Elid 1 provides, becomes increasingly difficult if the wheel does not have a reasonably long length of uninterrupted time in which it is dressed. The solution to this could be to leave the power supply on but switch it away from the grinding area when required. The wheel could retreat to a position where additional Elid dressing is performed while the ball auto loading system loads the next ball.

When the #12,000 wheel is used to generate both form and finish (single stage process) it benefits from a slightly longer run time (60 - 120 seconds), avoiding the problems outlined above. It is essential that constant material removal is maintained.

This wheel produces the highest quality balls in processing times that are comparable to both the use of larger abrasive wheels and to current honing and polishing times. The use of the #12,000 presents itself as a very attractive method of producing spherical bearing balls.

CONCLUSIONS & FUTURE WORK

Chapter 29 - Conclusions

The goals outlined in the introduction have, for the most part, been realized and the vast majority of problems encountered with this process have been overcome. This research has ultimately provided a process that can repeatedly produce balls with surface finishes of between 1 to 4 nm Ra. Although ball roundness values as good as 0.136 μm have been achieved, in reality ball form can be considered to reside within the standard tolerance of 2.5 μm and is comparable to the standard honing technique. Material removal rates have been increased by around 100 times from the start of the research. This results in a vastly reduced processing time (down from 10 minutes to 10 seconds) to achieve the quality stated above. Elid superfinishing can be used after cylindrical grinding as a single finishing stage alternative to the conventional honing and polishing operations, or after honing as part of a two stage finishing process.

This research has demonstrated that using Elid provides control of wheel wear and condition, and ultimately ball material removal. However significant differences in performance were revealed between the types tested.

- When no Elid is used, material removal rates and spindle power levels fall to zero as the wheel rapidly becomes glazed and stops cutting effectively. Processing with MRB-CBN wheels without electrolytic dressing is not sustainable.
- Elid 3 (electrode-less) superfinishing does not work effectively, is inefficient and erratic. Stable and consistent grinding conditions were not achieved using this method.
- Elid 1 proved to be the most effective type of Elid tested, aggressively dressing the wheel. This type should be used where size constraints allow with a #12,000 MRB-CBN wheel, on honed or cylindrically ground balls.
- Elid 2 (periodic Elid dressing) was considered successful and can be used where an Elid 1 arrangement is not possible, with a #2000 MRB-CBN wheel on honed input balls.

There are three main elements which were combined to make the Elid superfinishing process work efficiently. If any of these were not correct, then processing times were found to be excessively long.

Wheel condition - As the super-abrasive Elid wheels do not rely on a self-sharpening mechanism it is control of Elid power values (Elid aggressiveness) that influences dressing, determining wheel wear and therefore material removal efficiency. Without effective dressing a wheel will not maintain a free-cutting condition but will become glazed, reducing material removal efficiency.

System set-up - Although once set up correctly and operating effectively balls of consistently high quality can be relied upon, the set-up process can be difficult and time-consuming. Achieving correct ball to wheel alignment and concentricity is essential to ensure full conformity. Problems with ball and wheel spindle alignment can result in poor finish and form, longer processing times and, in extreme cases, wheel failure. The wheel should be given a degree of flexibility in order prevent the system from becoming over constrained and to allow it to account for errors in set-up. Electro-discharge truing (EDT) followed by bedding-in of the wheel was found to be an effective method of truing the wheel.

Processing parameters - When employing MRB-CBN wheels with either Elid 1 or Elid 2, the best processing parameters to use are the following:

- The Elid power supply should be set to maximum, in order to aggressively dress the wheel. It should only be turned on after initial grinding contact is made. It should be turned off (or the flow of electricity directed away from the grinding zone), before the end of a processing cycle in order to prevent various ball defects.
- After the required ball material has been removed, the Elid power supply should be turned off to glaze the wheel and further improve the surface finish. The amount of superfinishing time conducted without Elid on should be based on the need for efficiency or quality.
- The superfinishing load should be high in order to maximize processing efficiency; however there are limits due of the increased likelihood of wheel failure at higher loads. A pressure between the wheel and ball of ~1.5 MPa is recommended. The load should remain high during the final stage of a processing cycle when the Elid is turned off, in order to gain the most benefit from processing with a glazed wheel.

- The wheel speed should be fast; RNB08 balls used 5.0 m/s at wheel O/D. The ball speed should be slow (1.0 m/s at ball O/D). This produces a large wheel to ball speed ratio, resulting in a flattened cross hatch pattern on the ball's surface. Speeds and forces make a big difference to performance when a wheel is well-dressed but not when it is glazed.
- The Noritake CEM fluid produced the best overall performance compared to the other fluids tested. A low pressure application ensuring laminar flow of fluid between electrodes is better than a high pressure application, as it allows for more aggressive and constant Elid dressing.

The power monitoring equipment provided useful information in assessing whether or not effective processing conditions were achieved. When the Elid superfinishing process was accurately set up, monitored and carefully controlled, most of the problems experienced such as surface defects, wheel failure and process variability were eliminated.

Chapter 30 - Future Work

30.1 Continued Development of Superfinishing System

Although the Elid system can be employed on a relatively basic machine tool, a more sophisticated set-up is required in order to fully utilize its capabilities. Suggestions for improvement are:

- Incorporate the Elid power supply into machine CNC program, allowing power supply to be turned off and on automatically as required.
- Feedback control of Elid and spindle power data into machine CNC program to allow wheel condition to be maintained with more stability through the Elid. Allow spindle power data to determine required processing time.
- Incorporate in-process measurement of ball form (size and roundness) via a gap sensor, in order to maintain O/D tolerance.
- Force sensors that can monitor ball to wheel misalignment.
- Feedback system to account for differences in ball production batch sizes. Self-centring of the wheel to the ball.
- The use of a low magnification optical assessment of ball surface quality on or next to machine to highlight ball defects and monitor surface quality.
- Wheels that are protected against breakage by a supporting mounting, which holds the wheel and applies a compressive stress to the wheels O/D.
- The development of an Elid fixturing that uses the roller centric method.
- The inclusion of rotational motion between the ball and wheel. Dressing when the ball and wheel angle is at extremes. This would enable Elid superfinishing to be used on small balls and ball pins.
- A more precise and controllable method of applying load (e.g. air pressure).
- The use of a spherical air bearing in the wheel fixturing to allow for misalignments.
- Incorporate flexibility into the wheel fixturing in order to achieve the correct degree of compliance / stiffness.
- Safety considerations – interlock of Elid power supply preventing the risk of electrocution.

30.2 Roundness and further finish improvement

Currently the 2.5 μm tolerance does not require precision machining practice to be followed. Assessment should be made of the effect of form error on bearing life. If the effect is found to be important, roundness could be improved by focusing on improving ball form and the factors that affect ball form, in the same way that this PhD has focused on improving ball surface finish. Form errors consistently less than 0.5 μm could be a goal of future work.

It should be possible to further improve the ball's surface finish to an anticipated production repeatable sub 1nm Ra quality. This could be tested using finer abrasives (#120,000 to #3,000,000 wheels) maintained in a free-cutting condition with Elid 1, using ball materials with a finer dispersion of carbides (e.g. Cronidur 30®). Efficiency may not be excessively affected by undertaking this; however it is of unproven benefit to bearing life.

30.3 Additional Testing

The performance of the non-Elid Darmann wheel No.4 should be tested with the use of an oil-based cutting fluid as per its recommended use. Further investigate and optimize superfinishing with this wheel by balancing input roughness and bonding strength to achieve sufficient but not excessive wheel wear.

Various other options could be considered for testing on titanium balls. These are (1) the use different fluids, possibly the Dowel electrolytic fluid or even a cryogenic coolant combined with Elid 1; (2) the use of alternative titanium materials, heat-treatments or different coatings; (3) the use of different, non-Elid, wheel types.

Further investigation should be carried out into the relationship between very fine surface finishes and extended bearing life, including testing the higher quality Elid finished balls against other bearing liners and materials.

The findings of this research could be applied to other applications where long life is required, such as bearing bushes, ball pins and prosthetic joints.

REFERENCES

[1] http://www.nmb-minebea.co.uk (Accessed 25th April 2007).

[2] http://www.minebea.co.jp/english/product/machinery/1181969_2090.html (Accessed 25th April 2007).

[3] Hutchings, I.M. (2001). *Tribology - friction and wear of engineering materials.* Butterworth-Heinemann, Department of Material Science and Metallurgy, University of Cambridge.

[4] *A self-lubricating bearing,* (2005).
GB Patent, GB2406622

[5] Shaw, M.C. (1996). *Principles of abrasive processing.* Clarendon press, Oxford, Oxford series on Advanced Manufacturing.

[6] Metzger, J.L. (1986). *Superabrasive grinding.* Butterworth-Heinemann, London.

[7] Knight, P. (2000). *Enhanced surface finishing of bearing raceway.* PhD thesis, Cranfield University, School of Industrial and Manufacturing Science, Cranfield.

[8] McKee, R. L. (1982). *Machining With Abrasives*. Van Nostrand Reinhold Company, Wokingham, Berkshire, England.

[9] ME477 Manufacturing Processes, Lecture 19, Grinding & Abrasive Processes, (2006). http://www.egr.msu.edu/classes/me477/hinds/Lecture%20Originals (Accessed 25th April 2007).

[10] King, R. I. (1986). *Handbook of modern grinding technology*. Chapman and Hall, New York.

[11] *National and International Size Standards – Macrogrits.*
http://www.uama.org/Abrasives101/101Standards.html (Accessed 25th April 2007).

[12] Itoh, N., Ohmori, H., Morijasu, S., Kasai, T. and Karaki-Doy, T. (1998). Finishing characteristics of brittle materials by ELID lap grinding using metal-resin bonded wheels. *International Journal of Machine Tools and Manufacture,* 38(7), 747 -762.

[13] Shore, P. (1990). State of the Art in "Damage Free" Grinding of Advanced Engineering Ceramics. *British Ceramic Proceedings*, 46, 189 - 200. Cited in [93].

[14] Malkin, S. (1989). *Grinding technology - theory and application of machining with abrasives.* Ellis Horwood, Chichester, UK.

[15] Wills, H. J. (1943). *Fine Grinding And Lapping*. Machineries Yellow Back Series 19, Machinery Publishing Co, London.

[16] Schwarz, J. *For Superfinishing Excellence, Start With The Right Finish*
http://www.mmsonline.com/articles/129804.html (Accessed 1st April 2007).

[17] Puthanangady T. K. and Malkin, S. (1995). Experimental investigations of the superfinishing process. *Wear*, 185(1-2), 173-182.

[18] Dundas, B. *Cup Wheel Superfinishing*.
http://www.mmsonline.com/articles/0203rt2.html (Accessed 25th April 2007).

[19] Keshavan, S. (2004). *Cup Wheel Finishing: A Cost-Effective Alternative to Double Disk Grinding.* 1st Annual Manufacturing Technology Summit, Michigan, Society of Manufacturing Engineers.
http://www.sme.org/cgi-bin/get-pdf.pl?/gmn/tp/2004/TP04PUB355.pdf (Accessed 25th April 2007).

[20] Hwang T. W., Evans, C.J. and Malkin, S. (1999). Size effect for specific energy in grinding of silicon nitride. *Proceedings of the 1999 12th International Conference on Wear of Materials*, WOM-99, 225-229, 862-867.

[21] Pavel, R. Pavel, M. Marinescu, I. (2004). Investigation of pre-dressing time for ELID grinding technique. *Journal of Materials Processing Technology,* 149, 591-596.

[22] Ohmori, H. (2005) *ELID Grinding and Micro-machining Processes* - tutorial notes (unpublished) Lamdamap 7th International Conference, 27th-30th June 2005, Cranfield University.

[23] Lim H. S., Fathima K., Senthil Kumar, A. and Rahman M. (2002). A fundamental study on the mechanism of electrolytic in-process dressing (ELID) grinding. *International Journal of Machine Tools and Manufacture*, 42(8), 935-943.

[24] Kramer, D. *EcoDress – a new grinding technique for modern cutting materials* http://www.agathon.com/en/default.htm (Accessed 1st April 2005).

[25] Murata, R., Okano, K. and Tsutsumi, C. (1985). Grinding of structural ceramics. *Milton C. Shaw Grinding Symposium PED,* 16, 261-272. Cited in [23].

[26] Ohmori, H. and T. Nakagawa, T. (1990). Mirror surface grinding of silicon wafers with electrolytic in-process dressing. *Annals of the CIRP,* 39(1), 329-332. Cited in [23].

[27] General information about Elid grinding. http://www.nexsys.co.jp/contents_e/technology.htm (Accessed 25th April 2007).

[28] Rahman, M., Senthil Kumar, A., Lim, S.H. and Fatima, K. (2003). Nano finish grinding of brittle materials using electrolytic in-process dressing (Elid) technique. *Sadhana - Academy Proceedings in Engineering Sciences*, 28(5), 957-974.

[29] Lee, E-S. (2000). A study on the mirror-like grinding of die steel with optimum in-process electrolytic dressing. *Journal of Materials Processing Technology*, 100, 200-208.

[30] Itoh, N., Ohmori, H., Kasai, T. and Karaki-Doy, T. (1998). Study of precision machining with metal resin bonded wheel on ELID-lap grinding. *International Journal of Electrical Machining,* 3, 13-18.

[31] Matsuzawa, T., Ohmori, H. and Itoh, N. (1999). Development and grinding effect of ELID3 grinding method. *1st International Conference on Precision Engineering and Nanotechnology (euspen),* 282-285.

[32] Fathima, K., Senthil Kumar, A., Rahman, M. and Lim, H. S. (2003). A study on wear mechanism and wear reduction strategies in grinding wheels used for ELID grinding, *Wear*, 254(12), 1247-1255.

[33] Itoh, N. and Ohmori, H. (1996). Grinding characteristics of hard and brittle materials by fine grain lapping wheels with Elid. *Journal of Materials Processing Technology*, 62(4), 315-320.

[34] Nano Surface Generation by ELID Grinding http://www.eng.nus.edu.sg/EResnews/0402/sf/sf_3.html (Accessed 25th April 2007).

[35] Lee, E-S. (1997). A study on the analysis of grinding mechanism and development of dressing system by using optimum in-process electrolytic dressing. *International Journal of Machine Tools and Manufacture*, 37(12), 1673-1689.

[36] Sawada, K., Yamamoto, A., Ohmori, H., Yutaka, Y., Moriyasu, S. and Muramatsu, Y. (2001). Study on ELID grinding for quartz blank. *RIKEN Review No. 34*, Focused on Advances on Micro-mechanical Fabrication Techniques. Material Fabrication Laboratory, RIKEN. http://www.riken.go.jp/lab-www/library/publication/review/pdf/No_34/34_029.pdf (Accessed 25th April 2007).

[37] Shih, A. J., Clark, W. I. and Akemon, J. L. (2001). Wear of the blade diamond tools in truing vitreous bond grinding wheels Part II. Truing and grinding forces and wear mechanism. *Wear*, 250-251(1), 593-603.

[38] Shih, A. J. (2000). An experimental investigation of rotary diamond truing and dressing of vitreous bond wheels for ceramic grinding. *International Journal of Machine Tools and Manufacture*, 40(12), 1755-1774.

[39] Wang, X., Ying, B. and Liu, W. (1996). EDM dressing of fine grain super abrasive grinding wheel. *Journal of Materials Processing Technology*, 62(4), 299-302.

[40] Qian, J. and Ohmori, H. (2001). Internal mirror grinding with a metal/metal-resin bonded abrasive wheel. *International Journal of Machine Tools and Manufacture,* 41(2), 193-208.

[41] Zhang, C., Ohmori, H. and Wei, L. (2000). Small-hole machining of ceramic material with electrolytic interval-dressing (ELID-II) grinding. *Journal of Materials Processing Technology,* 105(3), 284-293.

[42] Qian, J., Li, W. and Ohmori, H. (2000). Precision internal grinding with a metal-bonded diamond grinding wheel. *Journal of Materials Processing Technology,* 105(1), 80-86.

[43] Qian, J., Kim, G-n., Ohmori, H. and Jeong, H. D. (2000). Internal Cylindrical Grinding with Super Abrasive Wheel and Electrolytic In-process Dressing. *Journal of the Korean Society of Precision Engineering,* 17(4), 156-162.

[44] Qian, J., Li, W. and Ohmori, H. (2000). Cylindrical grinding of bearing steel with electrolytic in-process dressing. *Precision Engineering,* 24(2), 153-159.

[45] Zhang, C., Ohmori, H. and Wei, L. (2000). Precision shaping of small diameter wheels using micro electric discharge truing (MEDT) and hole-machining of Al2O3 material. *International Journal of Machine Tools & Manufacture*, 40, 661-674.

[46] Ohmori, H., Li, W., Makinouchi, A. and Bandyopadhyay, B. P. (2000). Efficient and precision grinding of small hard and brittle cylindrical parts by the centerless grinding process combined with electro-discharge truing and electrolytic in-process dressing. *Journal of Materials Processing Technolog*y, 98(3), 322-327.

[47] Wang, Y., Zhou, X-J. and Hu, D-J. (2006). An experimental investigation of dry-electrical discharge assisted truing and dressing of metal bonded diamond wheel. *International Journal of Machine Tools and Manufacture*, 46(3-4), 333-342.

[48] Brynn Hibbert, D. (1993). *Introduction to electrochemistry.* Mackays of Chatham, Chatham. Macmillan Physical Science Series.

[49] Ohmori, H. and Nakagawa, T. (1997). Utilisation of nonlinear conditions in precision grinding with ELID (electrolytic in-process dressing) for fabrication of hard material components. *CIRP Annals - Manufacturing Technology*, 46(1), 261-264.

[50] Askeland, D. R. (1996). *The science and engineering of materials*, 3rd ed. Chapman and Hall, London.

[51] Hong, C. and Li James, C. M. (2000). Anodic metal matrix removal rate in electrolytic in process dressing, I, two-dimensional modeling. *Journal of Applied Physics*, 87(6), 3151-3158. Cited in [21].

[52] Hong, C. and Li James, C. M. (2000). Anodic metal matrix removal rate in electrolytic in process dressing, II, Protrusion effect and three-dimensional modeling. *Journal of Applied Physics,* 87(6), 3159–3164. Cited in [21].

[53] Ahn, J-H., Kim, H-Y., Seo, H-Y. and Paik, I-H. (2001). In-process measurement of ELID grinding status - thickness of insulating layer. *Korean Society of Mechanical Engineers international journal*, 15(9), 1268-1273.

[54] Bifano, T., Krishnamoorthy, R., Caggiano, H. and Welch, E. (1995). Fixed-load electrolytic dressing with bronze bonded grinding wheels. *Manufacturing Science and Engineering,* MED 2(1), 329-348.

[55] Lee, E.-S. (2000). The effect of optimum in-process electrolytic dressing in the ultraprecision grinding of die steel by a superabrasive wheel. *International Journal of Advanced Manufacturing Technology*, 16(11), 814-821.

[56] Ueda, T., Sakamoto, S. and Sugita, T. (1996). Effective of coolant of water-solution in Superfinishing - application of electrolytic in-process dressing. *Japan Society Precision Engineering*, 62(2), 252 – 257 (in Japanese).

[57] Elid wheel manufacturers and CEM fluid suppliers http://www.fujidie.co.jp (Accessed 6th August 2006).

[58] Dowel Fluid manufacturers http://www.chemsearch.com/viewArticle.asp?countryName=UK&language_id=4&language=English&country=UK&article_id=1921 (Accessed 25th April 2007).

[59] Turley, D. M. (1985). Factors affecting surface finish when grinding titanium and a titanium alloy (Ti-6Al-4V). *Wear,* 104(4), 323-335.

[60] Itoh, N., Nemoto, A., Katoh, T. and Ohmori, H. (2004). Eco-friendly Elid Grinding Using Metal-Free Electro-Conductive Resinoid Bonded Wheel. *JSME International Journal,* 47(1), 72-78.

[61] Mizutani, M., Komoturi, J., Nagata, J., Katahira, K. and Ohmori, H. (2003). Surface finishing for biomaterials: application of the ELID grinding method. *International Journal of Modern Physics B*, 17(8-9), 1395-400.

[62] Manufacturers of truing ball and Elid wheels http://www.wendtgroup.com (Accessed 25th April 2007).

[63] Wang, S. H. (2000). *Investigation Into The Grinding Of Titanium Alloys*, PhD thesis, Cranfield University, School of Industrial and Manufacturing Science, Cranfield.

[64] Mizutani, M., Komotori, J., Katahira, K., Watanabe, Y. and Ohmori, H. (2004). Improvement of Corrosion Resistance and Mechanical Properties of the Biomaterial Ti-6AL-4V Alloy by ELID Grinding. *Key Engineering Materials,* Advances in Abrasive Technology, 257-258, 473-476.

[65] Stephenson, D. J., Veselovac, D., Manley, S. and Corbett, J. (2001) Ultra-precision grinding of hard steels. *Precision Engineering,* 25(4), 336-345.

[66] Ohmori, H., Lin, W., Moriyasu, S. and Yamagata, Y. (2001). Microspherical lens fabrication by cup grinding wheels applying ELID grinding. *RIKEN Review No. 34,* Focused on Advances on Micro-mechanical Fabrication Techniques. Materials Fabrication Laboratory, RIKEN. http://www.riken.go.jp/lab-www/library/publication/review/pdf/No_34/34_003.pdf (Accessed 25th April 2007).

[67] Ball, M.J., Murphy, N.A. and Shore, P. (1992). Electrolytically assisted ductile-mode diamond grinding of BK7 and SF10 optical glasses. *Proceedings of SPIE - The International Society for Optical Engineering*, 1573, 30-38.

[68] Nagata, J., Komoturi, J., Katahira, K. and Ohmori, H. (2001). Effect of surface roughness on corrosion response of stainless steel polished by ELID grinding method. *Keio University ELID Grinding Project, RIKEN*, 30, 176-181.

[69] *Electrodeless electrolytic dressing grinding method and apparatus,* (2000). U.S. Patent, 6 162 348.

[70] *Method and apparatus for grinding curved surfaces,* (2001). European Patent Application, EP1078714B1.

[71] Okuyama, S., Yonago, M., Kitajima, T. and Suzuki, H. (2001). A basic study on the combination machining of ELID-grinding and EDM-experiments of combination machining using a pulse power-source. *Journal of the Japan Society of Precision Engineering*, 67(3), 407-12. (in Japanese) Cited in [28].

[72] Ohmori, H. and Nakagawa, T. (1995). Analysis of mirror surface generation of hard and brittle materials by ELID (electrolytic in-process dressing) grinding with superfine grain metallic bond wheels. *Annals of CIRP - Manufacturing Technology*, 44(1), 287-290.

[73] Trucks, H. E. *Machining Titanium Alloys* http://www.titanium.com/titanium/tech_manual/tech2.cfm (Accessed 25th April 2007).

[74] Machado, A.R. and Wallbank, J. (1990). Machining of titanium and its alloys: A review. *Proceedings of the Institution of Mechanical Engineers, Part B*: Management and Engineering Manufacture, 204(1), 53-60.

[75] Kahles, J. F., Field, M., Eylon, D. and Froes, F. H. (1985). Machining of Titanium Alloys. *Journal of Metals*, 37(4), 27-35.

[76] Chandrasekar, S. and Shaw, M. C. (1983). Cutting Fluid Performance In Fine Grinding. *Wear*, 86, 139-149.

[77] Katahira, K., Watanabe, Y., Ohmori, H. and Kato, T. (2002). ELID grinding and tribological characteristics of TiAlN film. *International Journal of Machine Tools & Manufacture,* 42, 1307-1313.

[78] Stephenson, D.J., Sun, X. and Zervos, C. (2006). A study on ELID ultra precision grinding of optical glass with acoustic emission. *International Journal of Machine Tools and Manufacture*, 46(10), 1053-1063.

[79] Jayakumar, T., Mukhopadhyay, C. K., Venugopal, S., Mannan S. L. and Raj B. (2005). A review of the application of acoustic emission techniques for monitoring forming and grinding processes. *Journal of Materials Processing Technology,* 159(1), 48–61.

[80] Warren, A.W. and Guo, Y.B. (2007). Acoustic emission monitoring for rolling contact fatigue of superfinished ground surfaces. *International Journal of Fatigue*, 29(4), 603-614.

[81] McSpadden, S. B. and Hughes G. R. *A Systematic Method for Grinding Wheel Performance Evaluation.* http://www.ornl.gov/~webworks/cppr/y2001/pres/116758.pdf (Accessed 25th April 2007).

[82] Deiva Nathan, R., Vijayaraghavan, L. and Krishnamurthy, R. (1999). In-process monitoring of grinding burn in the cylindrical grinding of steel. *Journal of Materials Processing Technology*, 91(1-3), 37-42.

[83] Savage, M. D. and Chen, J. C. (2002). Multiple Regression-Based Multilevel In-Process Surface Roughness Recognition System in Milling Operations. *The Journal of Technology Studies,* 28-34. http://scholar.lib.vt.edu/ejournals/JOTS/Winter-Spring-2002/pdf/savage.pdf (Accessed 25th April 2007).

[84] van der Bijl, R-J. M., van Brug, H., Fähnle, O. W. and Braat, J. J.M. (2001) Applicability of iTIRM for roughness reduction monitoring. *Optical Manufacturing and Testing III, Proceedings of SPIE - The International Society for Optical Engineering,* 4451, 340-344. http://www.optica.tn.tudelft.nl/publications/docs/2001%20pdf%20files/2_25_2004_12_33_38Applicability.pdf (Accessed 25th April 2007).

[85] van der Bijl, R-J. M., Fähnle, O. W., van Brug, H. and Braat, J. J.M. (2000). In-process monitoring of grinding and polishing of optical surfaces. *Applied Optics.* 39(19), 3300-3303.

[86] *Apparatus for optically monitoring surface finish of ground workpieces,* (1987). U.S. Patent, US4693038.

[87] *BLUM in-process wheel wear assessment - LaserControl NT* http://www.blum-novotest.com/e/products/lasercontrol.html (Accessed 25th April 2007).

[88] Lee, E-S. (2000). A study of the development of an ultraprecision grinding system for mirror-like grinding. *International Journal of Advanced Manufacturing Technology*, 16, 1-9.

[89] Kramer, D. (1999). ECD (electrochemical in-process controlled dressing) a new method for grinding of modern high-performance cutting materials to highest quality. *Annals of CIRP*, 265-268.

[90] Pfluger, J. A., (2002). *The "EcoDress"-grinding process opens new horizons in the machining of ultra-hard cutting materials.* www.agathon.ch/en/aktuelles/aag_EcoDress_e.pdf (Accessed 25th April 2007).

[91] Boland, R. (1999). Computer control and process monitoring of Electrolytic In-Process Dressing of metal bond fine diamond wheels for NIF optics. *Optical Manufacture and Testing III, Proceedings of SPIE - The International Society for Optical Engineering*, 3782(20-23), 61-69.

[92] Bifano, T. G. and Fawcett, S. C. (1991). Specific grinding energy as an in-process control variable for ductile-regime grinding. *Precision Engineering*, 13(4), 256-262.

[93] Arai, S. (2004). *Surface Integrity Control of Piezoelectric Materials in Ultra Precision Grinding on the basis of Machine Design Assessment*. Cranfield University, School of Industrial & Manufacturing Science.

[94] Leadley, D. R. (1997). *Quantum Hall Effect*. http://www.warwick.ac.uk/~phsbm/qhe.htm (Accessed 25th April 2007).

[95] *LC-UPC - universal power cell - Full Range Data Sheet PDF file.* http://www.vydas.co.uk/PDF/LC/LC-UPCdatasheet-2-v.pdf (Accessed 25th April 2007).

[96] Manufacturers of non-Elid wheels tested http://www.darmann.com/index.html (Accessed 25th April 2007).

[97] Montgomery, D. C. (2001). *Design and Analysis of experiments,* 5th ed. Wiley, Massachusetts.

[98] *Electronic Statistics Textbook* http://www.statsoft.com/textbook/stathome.html (Accessed 25th April 2007).

[99] *Design expert software, manual and tutorials* http://www.statease.com/soft_ftp.html (Accessed 25th April 2007).

[100] Surface finish parameters definitions http://www.taylor-hobson.com/faq.asp (Accessed 25th April 2007).

[101] Marking System - page 6 http://www.swaty.si/fileadmin/Katalog/pdf/ANGLESKI.pdf (Accessed 25th April 2007).

[102] Colton, J. S. *Manufacturing Processes and Systems* - Grinding ME 6222 http://www.me.gatech.edu/jonathan.colton/me4210/grinding.pdf (Accessed 1st April 2007).

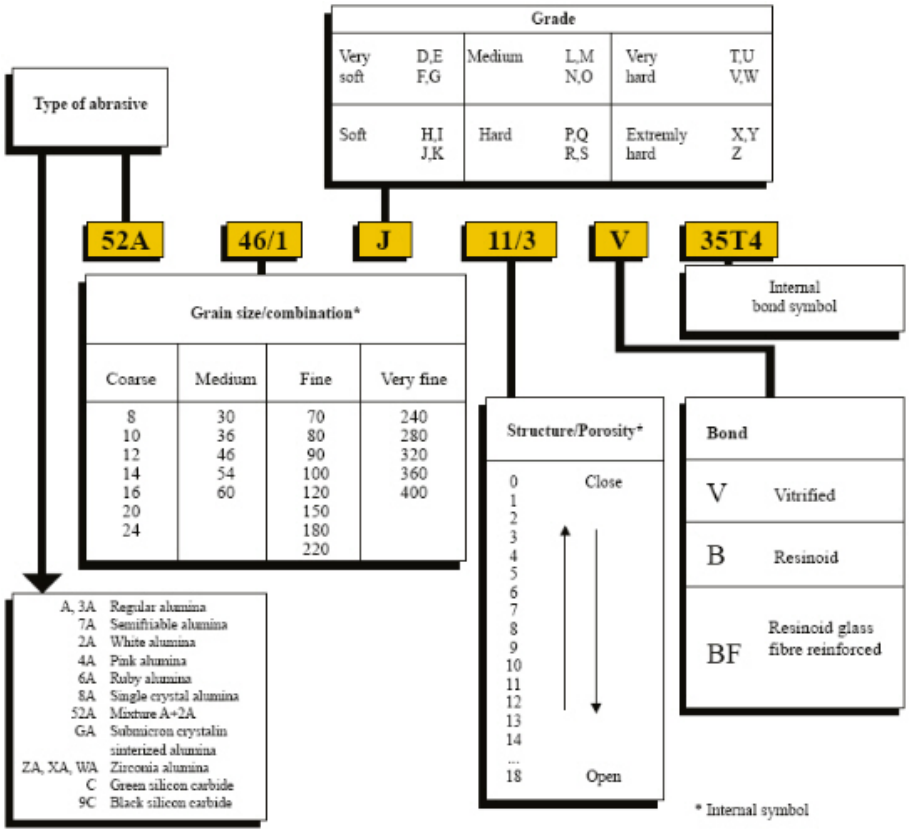

Appendix A1 - Conventional abrasive wheel specification - [101]

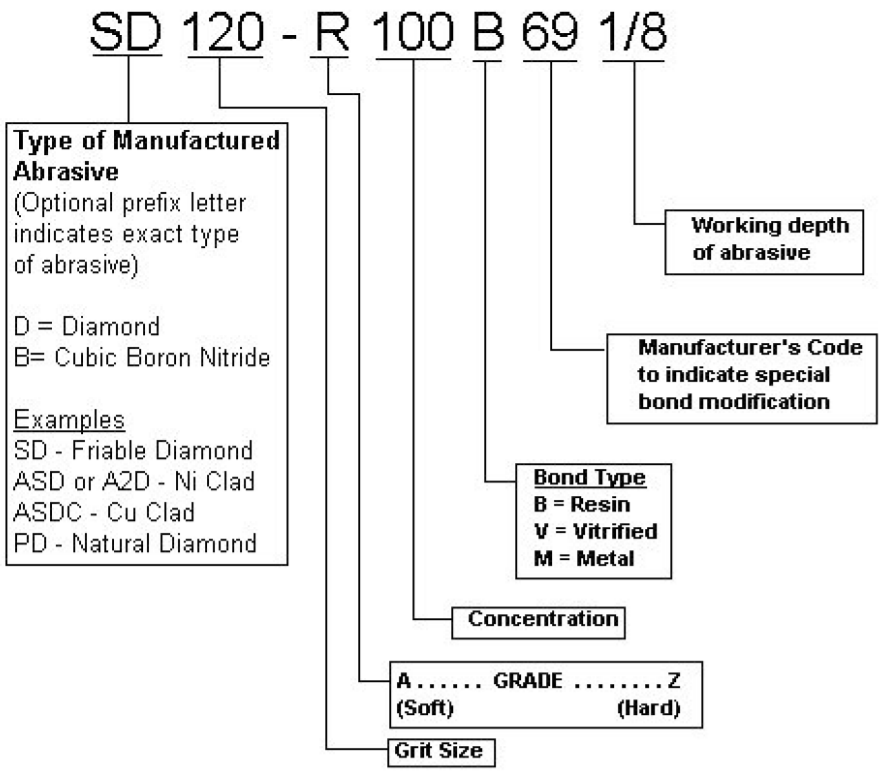

Appendix A2 - Superabrasive wheel specification - [102]

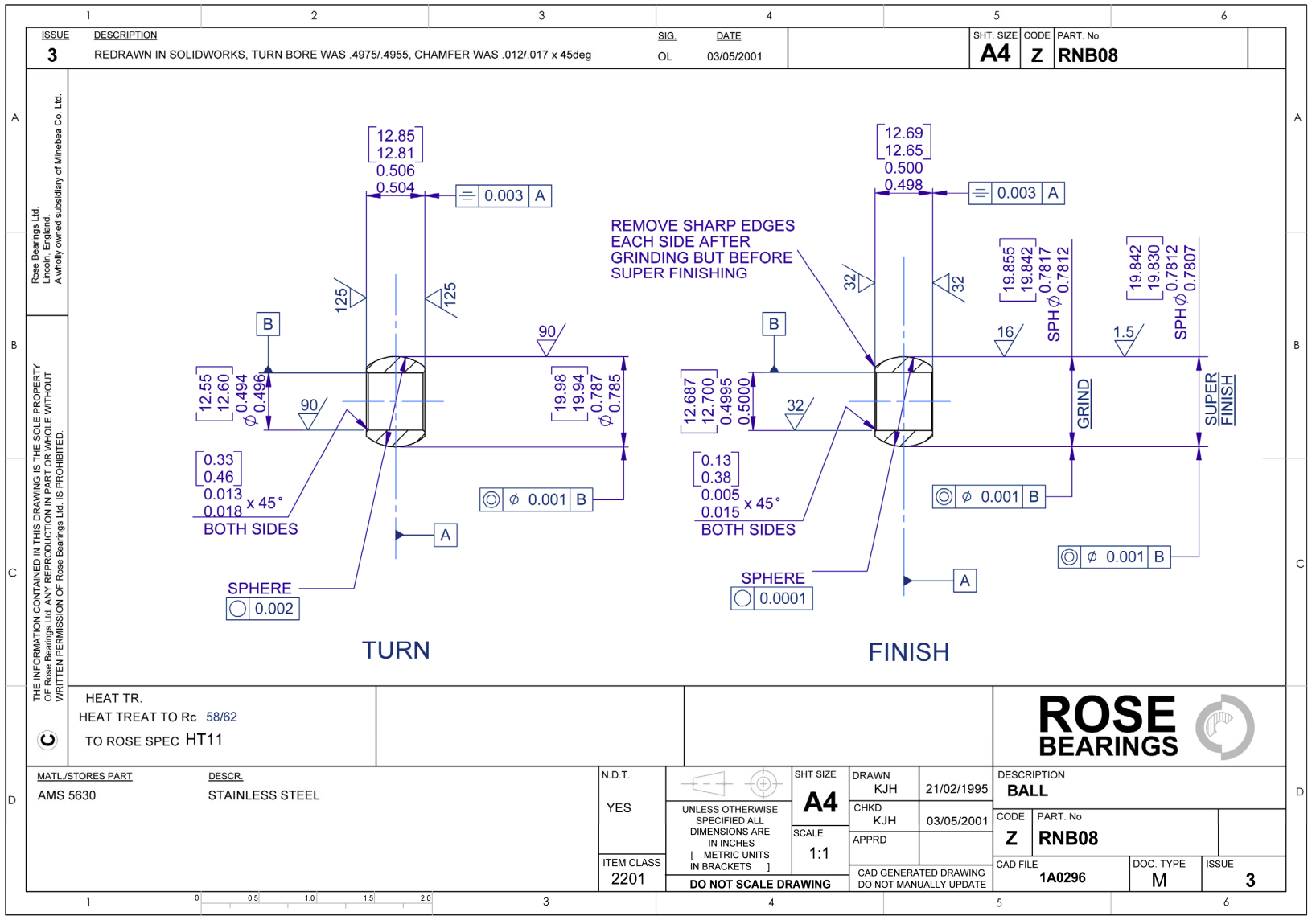

Appendix B1 – RNB08 Manufacturing Drawing

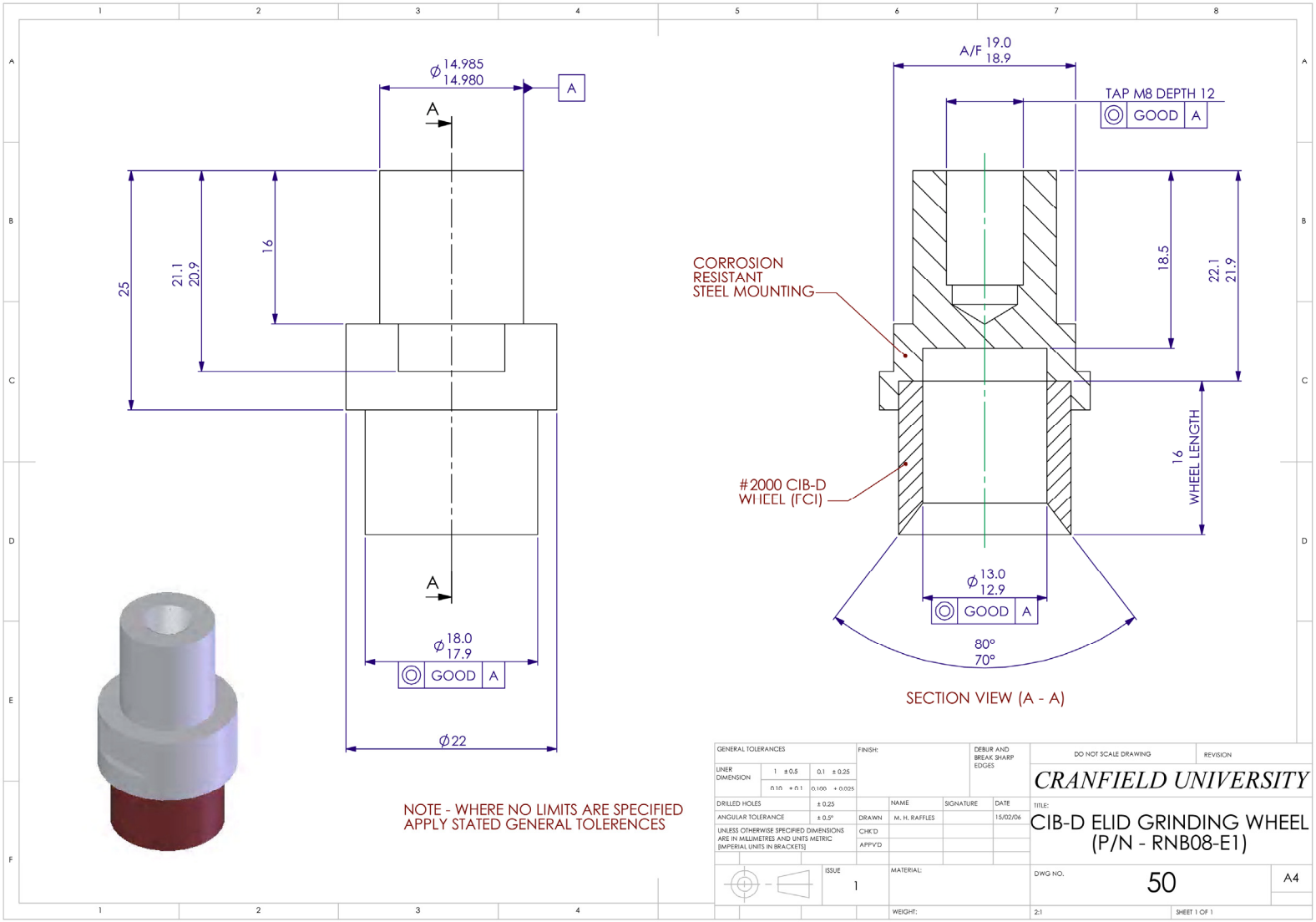

Appendix B2 – Elid 1 wheel for RNB08 balls

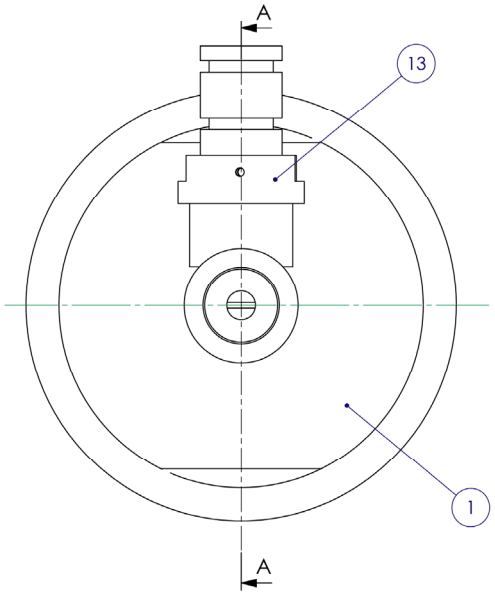

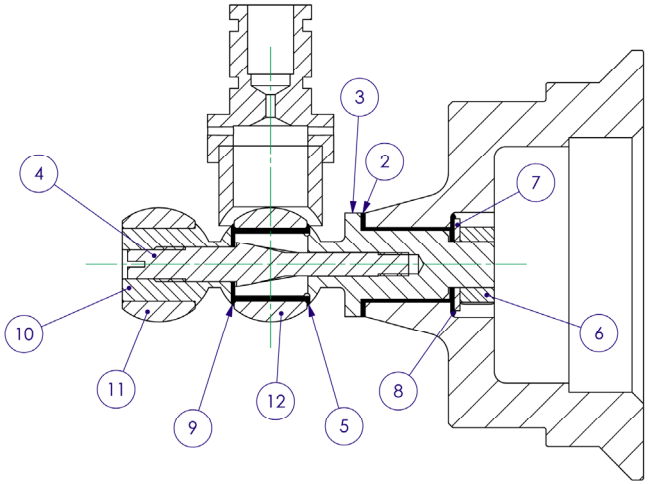

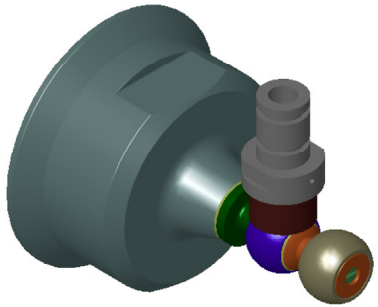

PART NO.	PART DISCRIPTION (DRAWING NO.)	MATERIAL / MANU.	QUANTITY
13	KFSI-2 GRINDING WHEEL (STD PART)	MRB-CBN	1
12	ZRNB08 BALL (STD PART)	AMS5630	1
11	TRUING BALL (STD PART)	AMS5630	1
10	ELECTRODE (022)	CRES STEEL	1
9	ELECTRODE INSULATION (021)	NYLON	1
8	NUT INSULATION (020)	NYLON	1
7	WASHER (STD PART)	STEEL	1
6	M8 NUT (STD PART)	STEEL	1
5	INNER COLLET INSULATION (019)	NYLON	1
4	COLLET LOCKING PIN (018)	CRES STEEL	1
3	INNER BALL COLLET (017)	USEN 31	1
2	OUTER COLLET INSULATION (016)	NYLON	1
1	OUTER BALL COLLET (015)	USEN 31	1

GENERAL TOLERANCES

LINER DIMENSION: 1 ±0.5 | 0.1 ±0.25 | 0.10 ±0.1 | 0.100 ±0.025

DRILLED HOLES ±0.25

ANGULAR TOLERANCE ±0.5°

UNLESS OTHERWISE SPECIFIED DIMENSIONS ARE IN MILLIMETRES AND UNITS METRIC (IMPERIAL UNITS IN BRACKETS)

FINISH:

DEBUR AND BREAK SHARP EDGES

DO NOT SCALE DRAWING

REVISION

CRANFIELD UNIVERSITY

	NAME	SIGNATURE	DATE
DRAWN	M. H. RAFFLES		09/09/05
CHK'D			
APP'V'D			

MATERIAL:

WEIGHT:

TITLE: COLLET ASSEMBLY

DWG NO. 024

A3

SCALE:3:2

SHEET 1 OF 1

Appendix B3 – General assembly drawing of Elid 1 ball fixturing

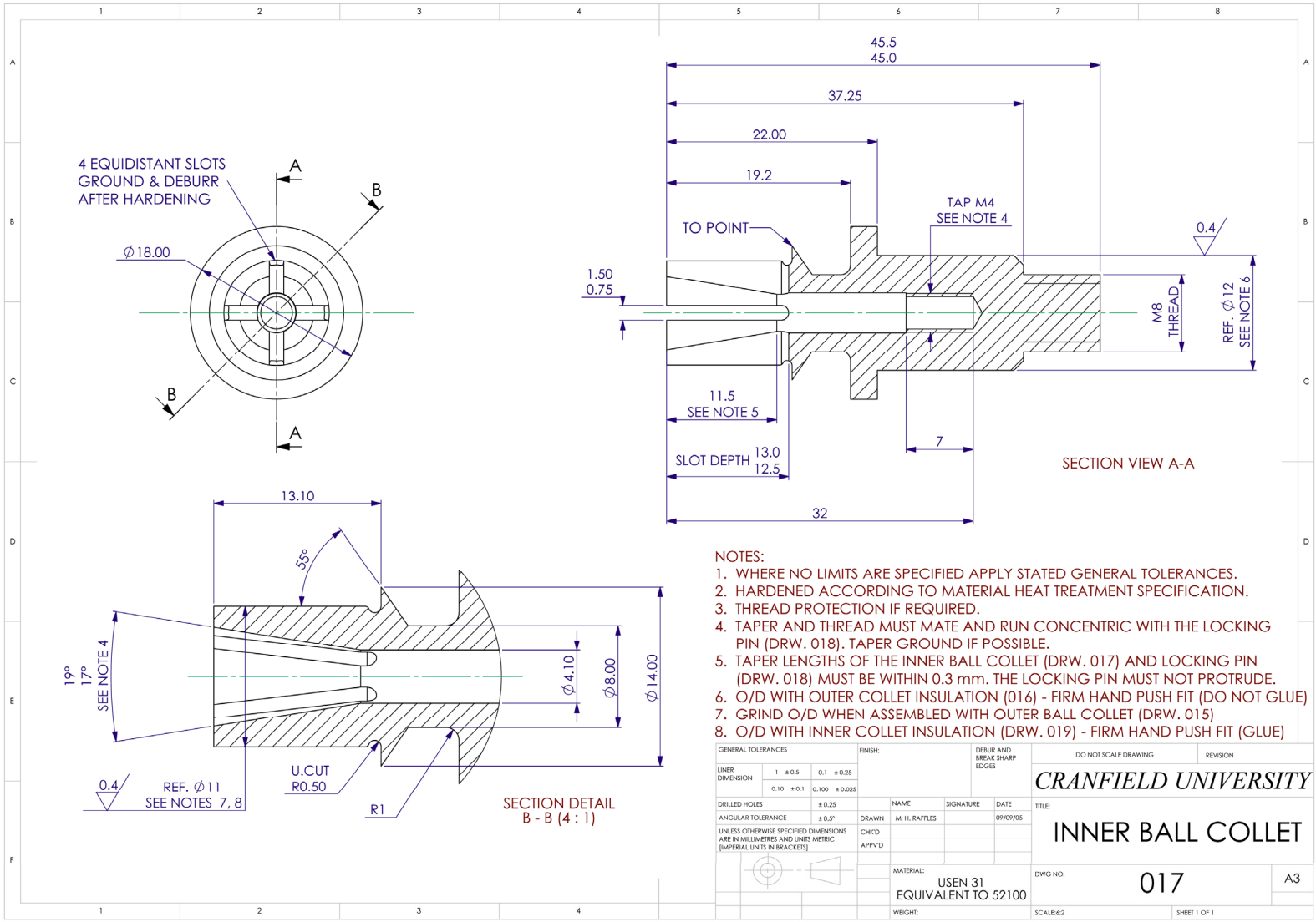

NOTES:

1. WHERE NO LIMITS ARE SPECIFIED APPLY STATED GENERAL TOLERANCES.
2. HARDENED ACCORDING TO MATERIAL HEAT TREATMENT SPECIFICATION.
3. THREAD PROTECTION IF REQUIRED.
4. TAPER AND THREAD MUST MATE AND RUN CONCENTRIC WITH THE LOCKING PIN (DRW. 018). TAPER GROUND IF POSSIBLE.
5. TAPER LENGTHS OF THE INNER BALL COLLET (DRW. 017) AND LOCKING PIN (DRW. 018) MUST BE WITHIN 0.3 mm. THE LOCKING PIN MUST NOT PROTRUDE.
6. O/D WITH OUTER COLLET INSULATION (016) - FIRM HAND PUSH FIT (DO NOT GLUE)
7. GRIND O/D WHEN ASSEMBLED WITH OUTER BALL COLLET (DRW. 015)
8. O/D WITH INNER COLLET INSULATION (DRW. 019) - FIRM HAND PUSH FIT (GLUE)

GENERAL TOLERANCES		FINISH:	DEBUR AND BREAK SHARP EDGES	DO NOT SCALE DRAWING	REVISION
LINER DIMENSION	1 ±0.5 0.1 ±0.25 0.10 ±0.1 0.100 ±0.025			CRANFIELD UNIVERSITY	
DRILLED HOLES	±0.25		NAME / SIGNATURE / DATE	TITLE:	
ANGULAR TOLERANCE	±0.5°	DRAWN	M. H. RAFFLES / 09/09/05	INNER BALL COLLET	
UNLESS OTHERWISE SPECIFIED DIMENSIONS ARE IN MILLIMETRES AND UNITS METRIC (IMPERIAL UNITS IN BRACKETS)		CHK'D			
		APPV'D			
		MATERIAL: USEN 31 EQUIVALENT TO 52100		DWG NO. 017	A3
		WEIGHT:		SCALE:6:2	SHEET 1 OF 1

Appendix B4 – Inner ball Collet

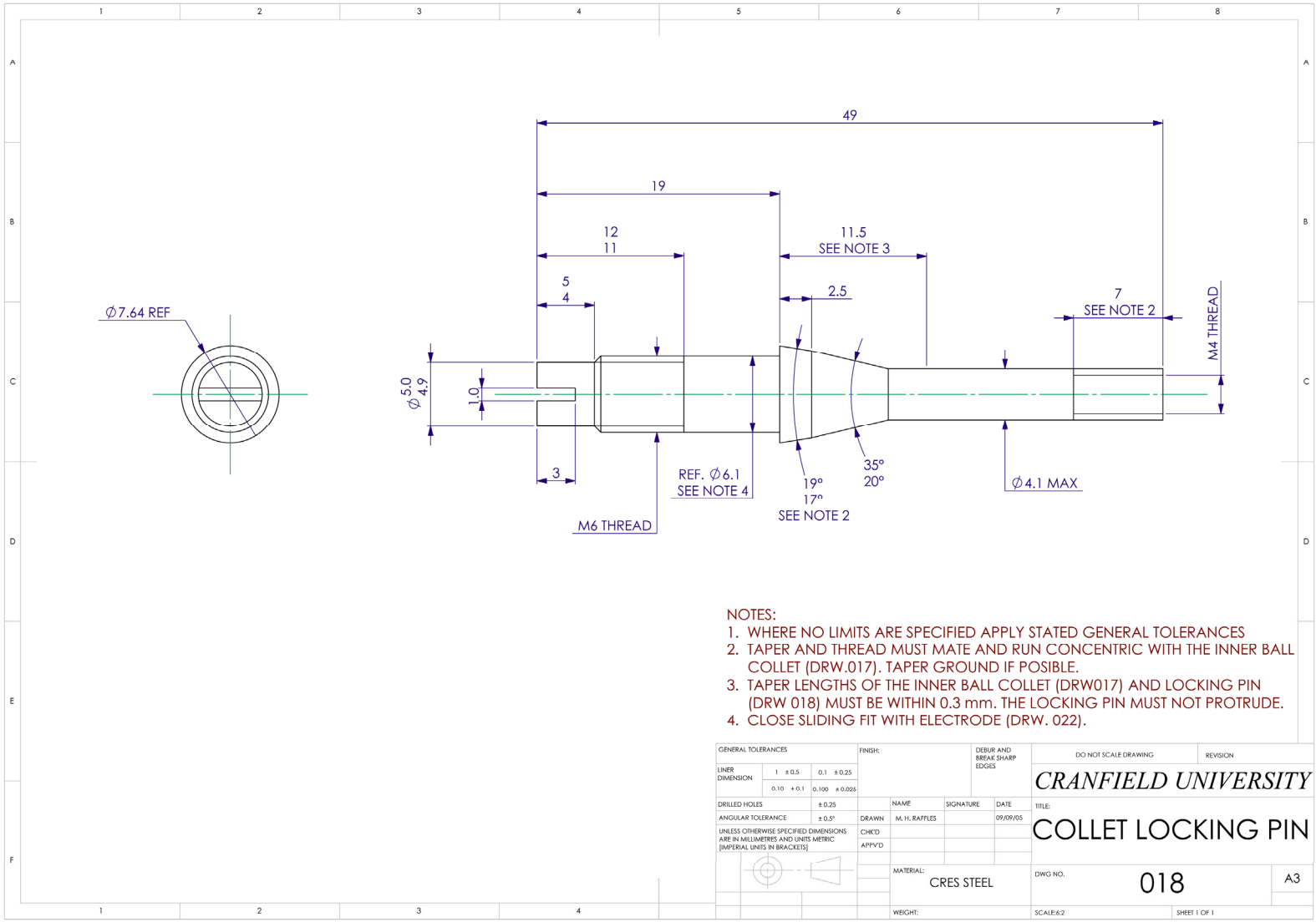

NOTES:

1. WHERE NO LIMITS ARE SPECIFIED APPLY STATED GENERAL TOLERANCES
2. TAPER AND THREAD MUST MATE AND RUN CONCENTRIC WITH THE INNER BALL COLLET (DRW.017). TAPER GROUND IF POSIBLE.
3. TAPER LENGTHS OF THE INNER BALL COLLET (DRW017) AND LOCKING PIN (DRW 018) MUST BE WITHIN 0.3 mm. THE LOCKING PIN MUST NOT PROTRUDE.
4. CLOSE SLIDING FIT WITH ELECTRODE (DRW. 022).

GENERAL TOLERANCES		FINISH:	DEBUR AND BREAK SHARP EDGES	DO NOT SCALE DRAWING	REVISION
LINER DIMENSION	1 ±0.5 / 0.1 ±0.25 / 0.10 ±0.1 / 0.100 ±0.025			CRANFIELD UNIVERSITY	
DRILLED HOLES	±0.25		NAME / SIGNATURE / DATE	TITLE:	
ANGULAR TOLERANCE	±0.5°	DRAWN	M. H. RAFFLES / 09/09/05	COLLET LOCKING PIN	
UNLESS OTHERWISE SPECIFIED DIMENSIONS ARE IN MILLIMETRES AND UNITS METRIC (IMPERIAL UNITS IN BRACKETS)		CHK'D			
		APPV'D			
		MATERIAL: CRES STEEL		DWG NO. 018	A3
		WEIGHT:		SCALE:6:2	SHEET 1 OF 1

Appendix B5 – Collet locking pin

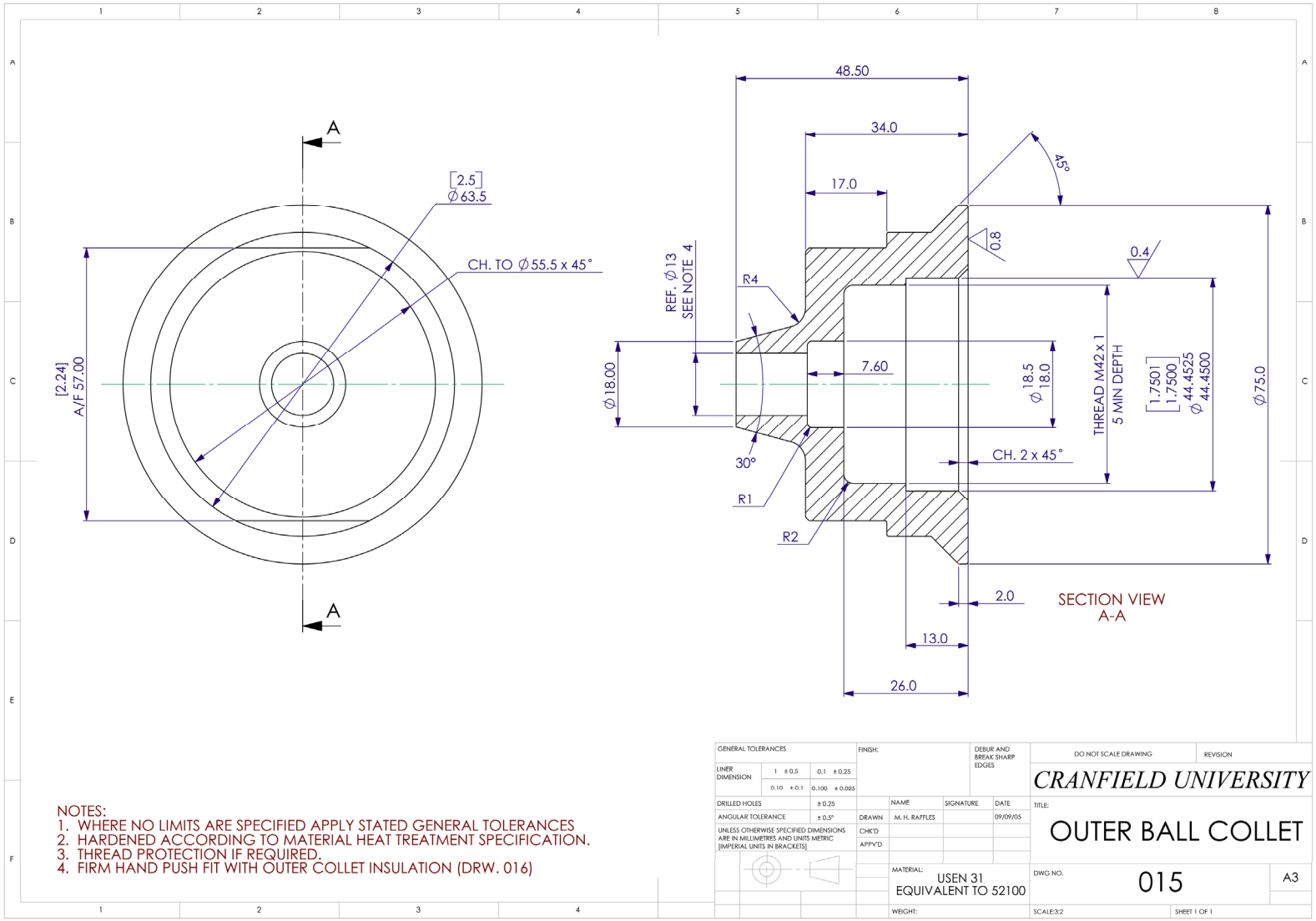

NOTES:
1. WHERE NO LIMITS ARE SPECIFIED APPLY STATED GENERAL TOLERANCES
2. HARDENED ACCORDING TO MATERIAL HEAT TREATMENT SPECIFICATION.
3. THREAD PROTECTION IF REQUIRED.
4. FIRM HAND PUSH FIT WITH OUTER COLLET INSULATION (DRW. 016)

GENERAL TOLERANCES		FINISH:		DEBUR AND BREAK SHARP EDGES	DO NOT SCALE DRAWING / REVISION
LINER DIMENSION	1 ±0.5 / 0.10 ±0.1 / 0.1 ±0.25 / 0.100 ±0.025				CRANFIELD UNIVERSITY
DRILLED HOLES	±0.25		NAME	SIGNATURE / DATE	TITLE: OUTER BALL COLLET
ANGULAR TOLERANCE	±0.5°	DRAWN	M. H. RAFFLES	09/09/05	
UNLESS OTHERWISE SPECIFIED DIMENSIONS ARE IN MILLIMETRES AND UNITS METRIC (IMPERIAL UNITS IN BRACKETS)		CHK'D			
		APPV'D			
		MATERIAL:	USEN 31 EQUIVALENT TO 52100		DWG NO. 015 / A3
		WEIGHT:			SCALE:3:2 / SHEET 1 OF 1

Appendix B6 – Outer ball collet

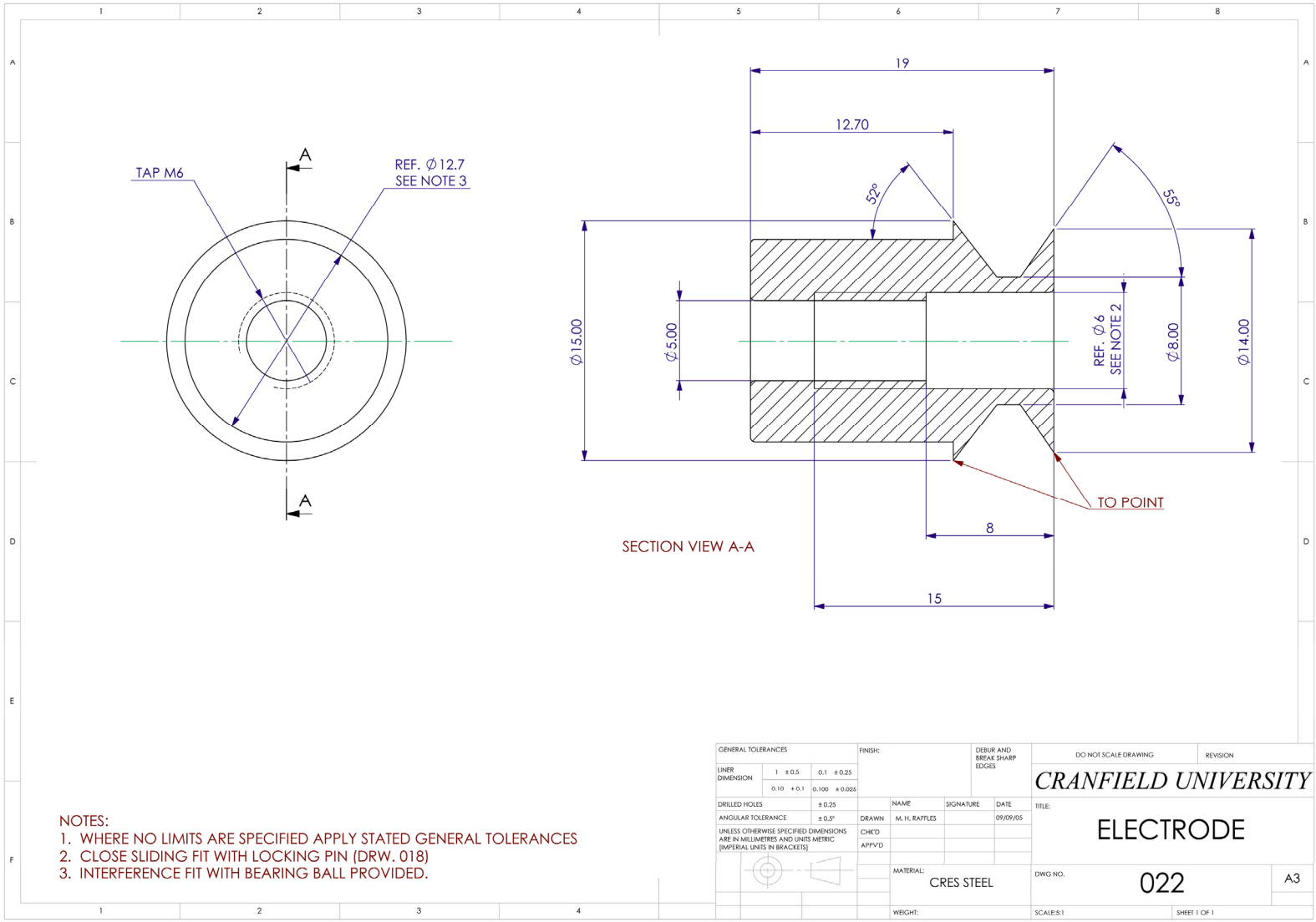

NOTES:
1. WHERE NO LIMITS ARE SPECIFIED APPLY STATED GENERAL TOLERANCES
2. CLOSE SLIDING FIT WITH LOCKING PIN (DRW. 018)
3. INTERFERENCE FIT WITH BEARING BALL PROVIDED.

GENERAL TOLERANCES		FINISH:	DEBUR AND BREAK SHARP EDGES	DO NOT SCALE DRAWING	REVISION
LINER DIMENSION	1 ±0.5 0.1 ±0.25 0.10 ±0.1 0.100 ±0.025			CRANFIELD UNIVERSITY	
DRILLED HOLES	±0.25		NAME / SIGNATURE / DATE	TITLE:	
ANGULAR TOLERANCE	±0.5°	DRAWN	M. H. RAFFLES / 09/09/05	ELECTRODE	
UNLESS OTHERWISE SPECIFIED DIMENSIONS ARE IN MILLIMETRES AND UNITS METRIC (IMPERIAL UNITS IN BRACKETS)		CHK'D			
		APPV'D			
		MATERIAL: CRES STEEL		DWG NO. 022	A3
		WEIGHT:		SCALE:5:1	SHEET 1 OF 1

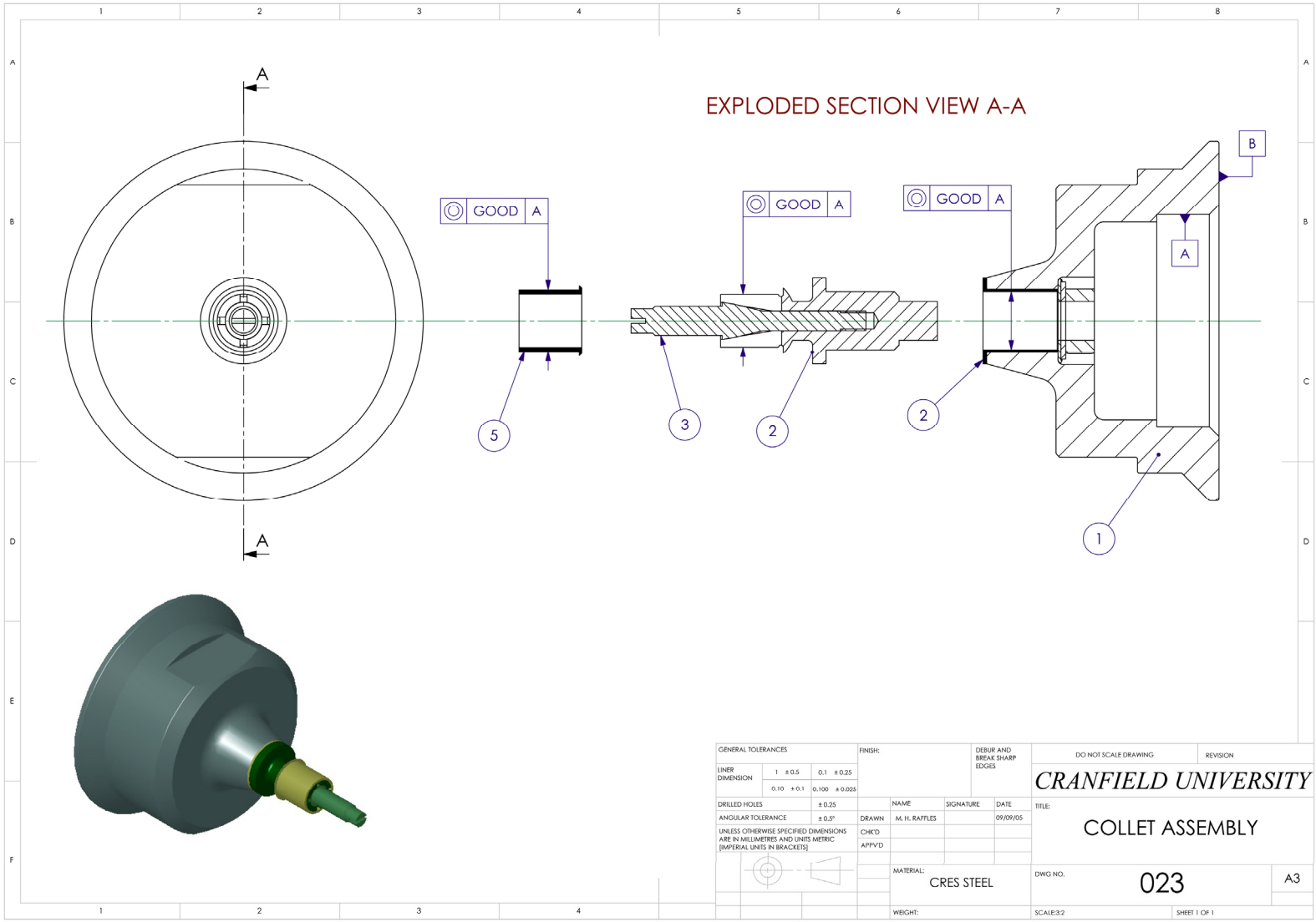

Appendix B8 – Ball Collet sub-assembly

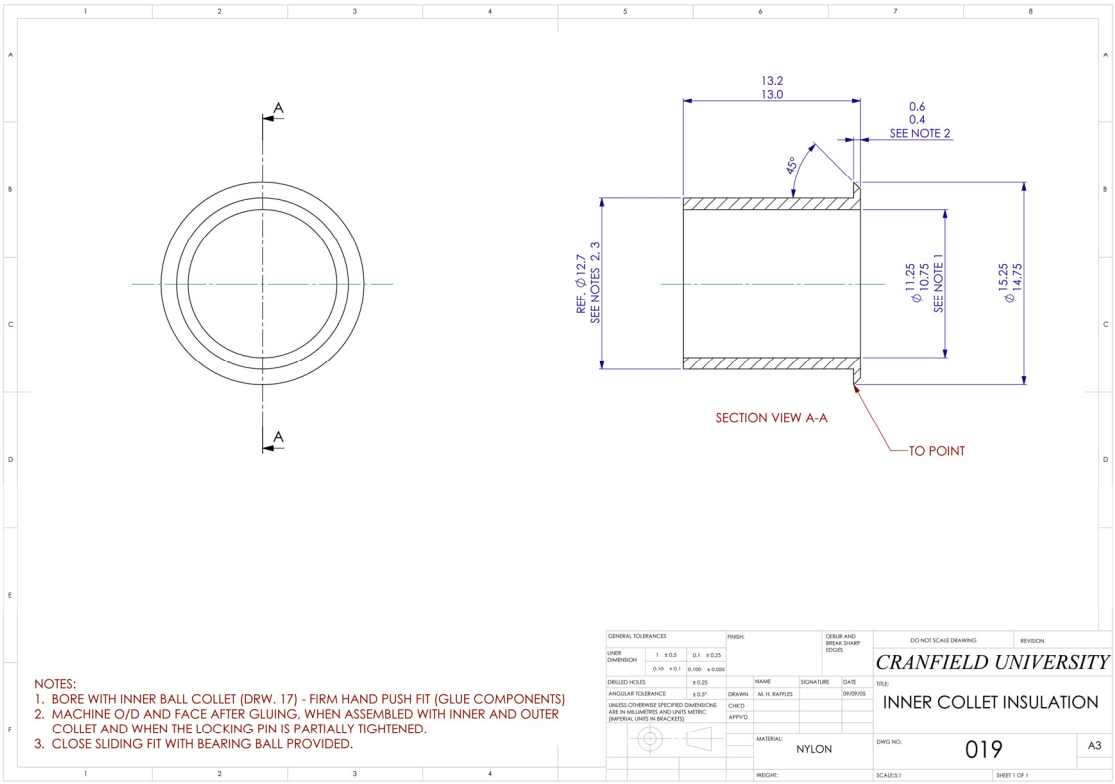

Appendix B9 – Inner collet insulation

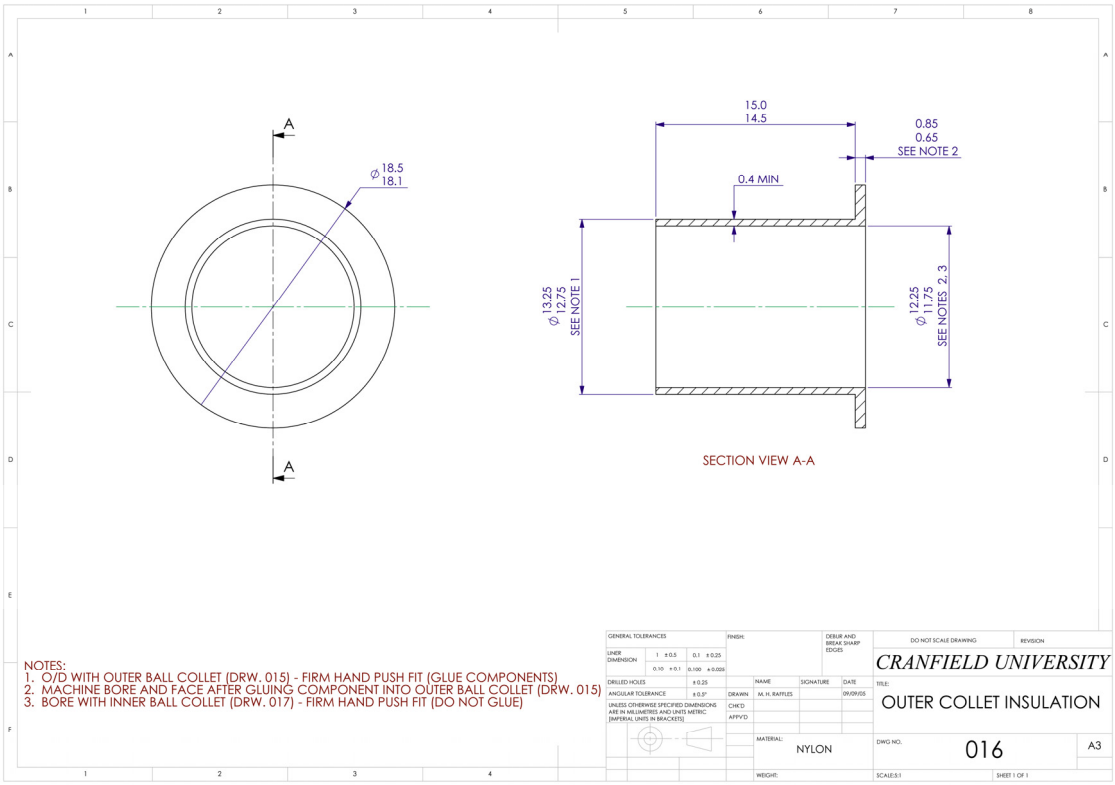

Appendix B10 – Outer collet insulation

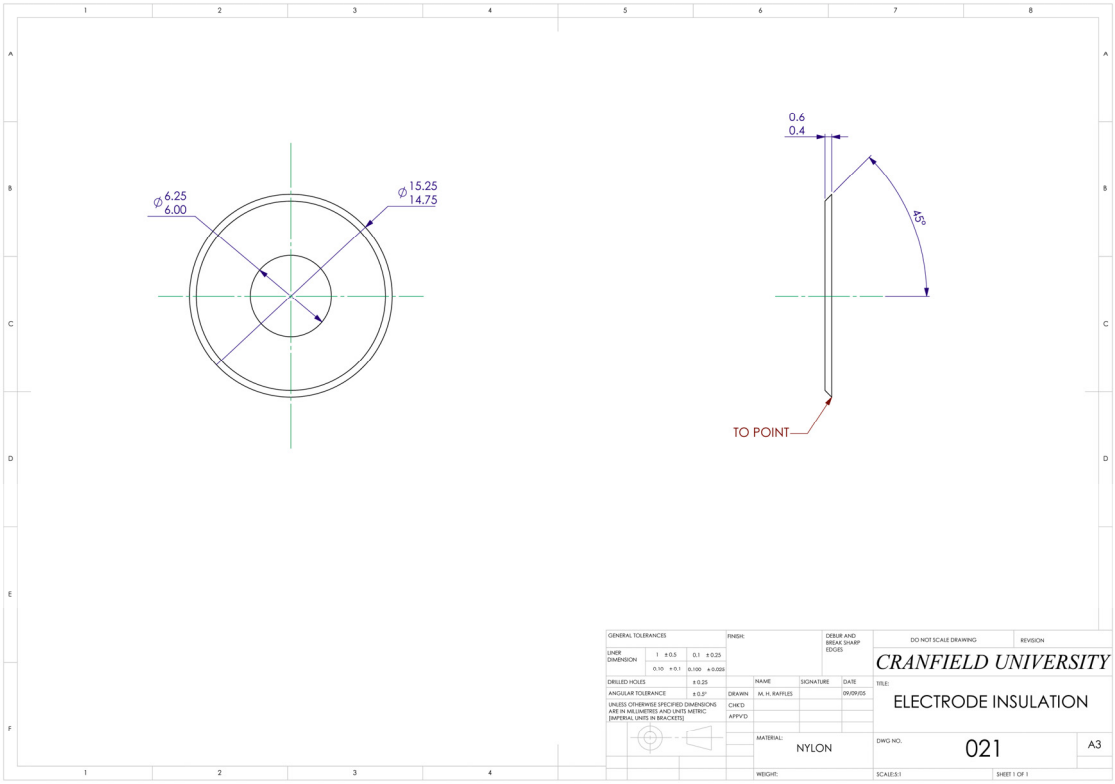

Appendix B11 – Electrode insulating washer

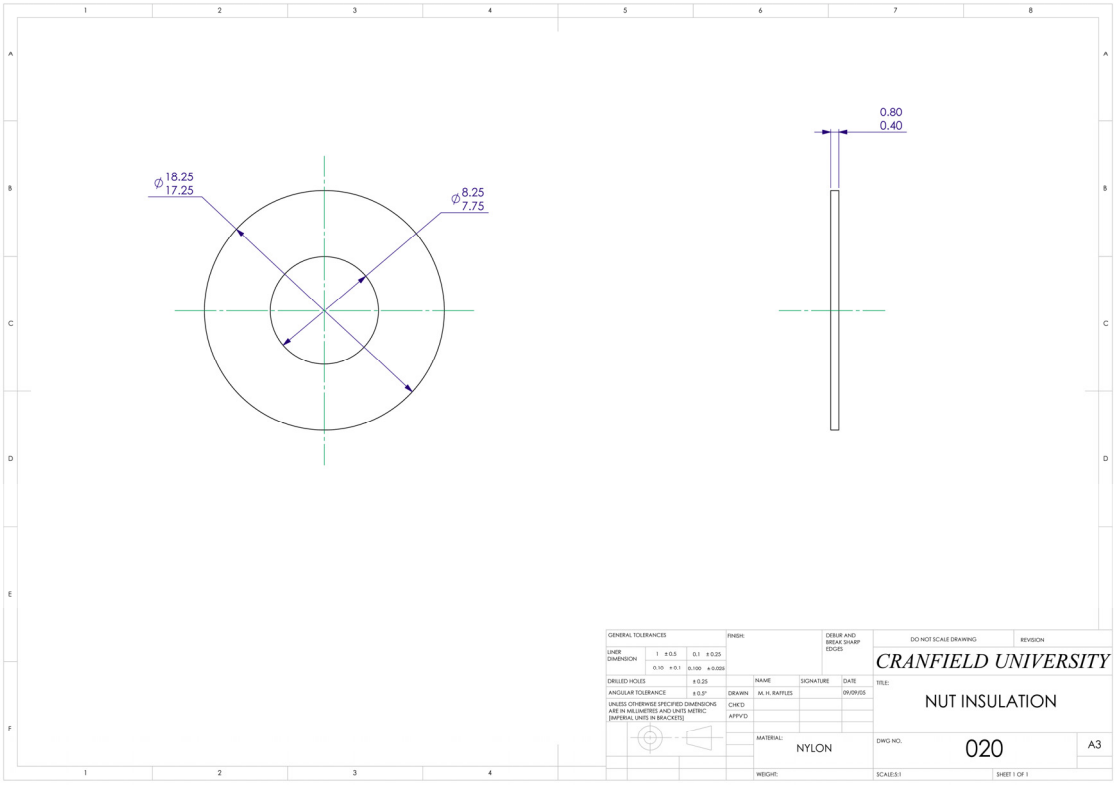

Appendix B12 – Nut insulation

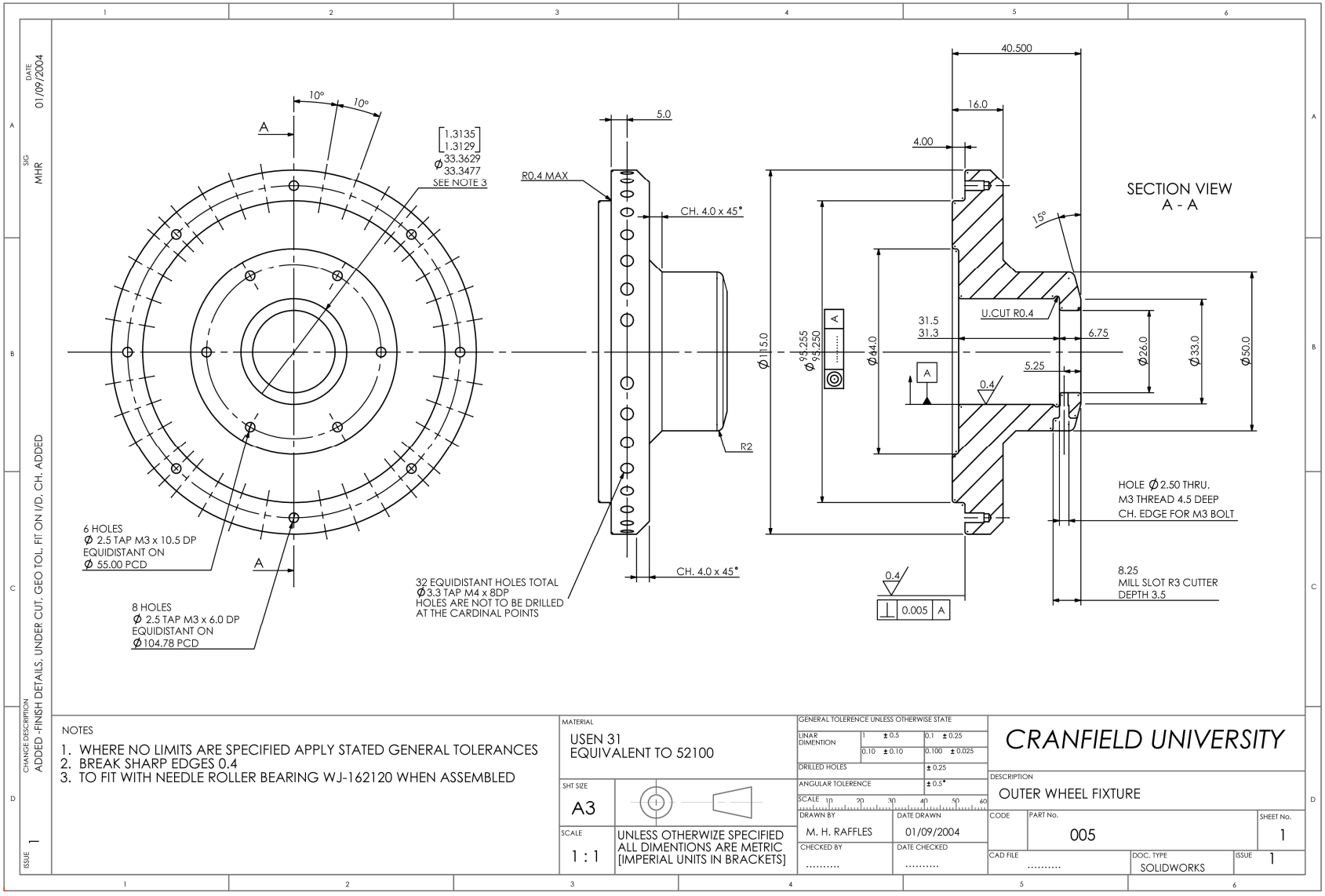

NOTES

1. WHERE NO LIMITS ARE SPECIFIED APPLY STATED GENERAL TOLERANCES
2. BREAK SHARP EDGES 0.4
3. TO FIT WITH NEEDLE ROLLER BEARING WJ-162120 WHEN ASSEMBLED

MATERIAL	USEN 31 EQUIVALENT TO 52100
SHT SIZE	A3
SCALE	1 : 1
	UNLESS OTHERWIZE SPECIFIED ALL DIMENTIONS ARE METRIC [IMPERIAL UNITS IN BRACKETS]
GENERAL TOLERENCE UNLESS OTHERWISE STATE	
LINAR DIMENTION	1 ± 0.5 ; 0.1 ± 0.25 ; 0.10 ± 0.10 ; 0.100 ± 0.025
DRILLED HOLES	± 0.25
ANGULAR TOLERENCE	± 0.5°
SCALE	10 20 30 40 50 60
DRAWN BY	M. H. RAFFLES
DATE DRAWN	01/09/2004
CHECKED BY	.....
DATE CHECKED	.....

CRANFIELD UNIVERSITY

DESCRIPTION	OUTER WHEEL FIXTURE
CODE	
PART No.	005
SHEET No.	1
CAD FILE	.....
DOC. TYPE	SOLIDWORKS
ISSUE	1

CHANGE DESCRIPTION	SIG	DATE	ISSUE
ADDED -FINISH DETAILS, UNDER CUT, GEO TOL, FIT ON I/D, CH. ADDED	MHR	01/09/2004	1

Appendix B13 – Outer wheel fixturing

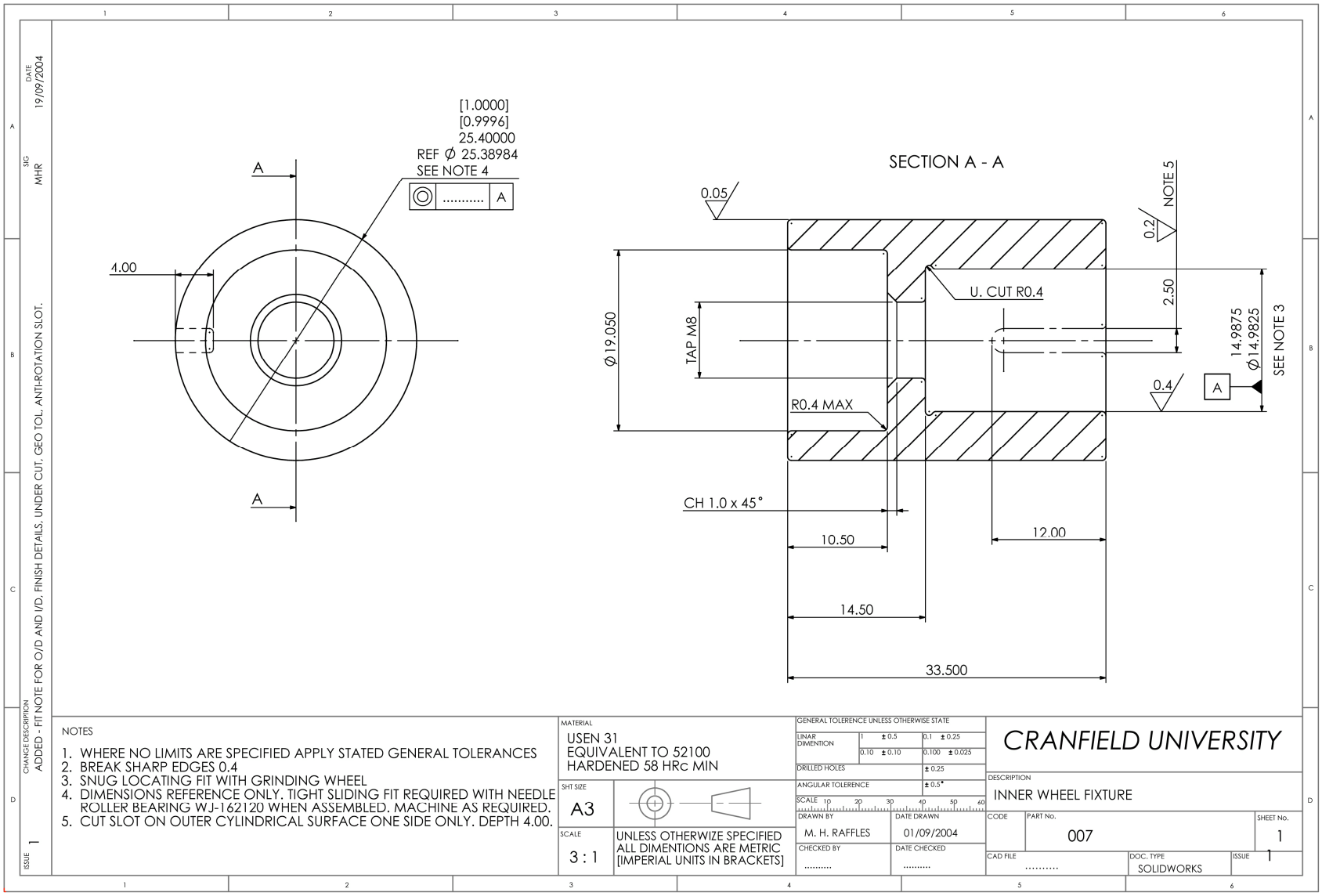

NOTES

1. WHERE NO LIMITS ARE SPECIFIED APPLY STATED GENERAL TOLERANCES
2. BREAK SHARP EDGES 0.4
3. SNUG LOCATING FIT WITH GRINDING WHEEL
4. DIMENSIONS REFERENCE ONLY. TIGHT SLIDING FIT REQUIRED WITH NEEDLE ROLLER BEARING WJ-162120 WHEN ASSEMBLED. MACHINE AS REQUIRED.
5. CUT SLOT ON OUTER CYLINDRICAL SURFACE ONE SIDE ONLY. DEPTH 4.00.

ISSUE	1
CHANGE DESCRIPTION	ADDED - FIT NOTE FOR O/D AND I/D. FINISH DETAILS. UNDER CUT. GEO TOL. ANTI-ROTATION SLOT.
SIG	MHR
DATE	19/09/2004
MATERIAL	USEN 31 EQUIVALENT TO 52100 HARDENED 58 HRc MIN
SHT SIZE	A3
SCALE	3 : 1
UNLESS OTHERWIZE SPECIFIED ALL DIMENTIONS ARE METRIC [IMPERIAL UNITS IN BRACKETS]	
GENERAL TOLERENCE UNLESS OTHERWISE STATE	
LINAR DIMENTION	1 ± 0.5 · 0.1 ± 0.25 · 0.10 ± 0.10 · 0.100 ± 0.025
DRILLED HOLES	± 0.25
ANGULAR TOLERENCE	± 0.5°
SCALE	10 20 30 40 50 60
DRAWN BY	M. H. RAFFLES
DATE DRAWN	01/09/2004
CHECKED BY	.....
DATE CHECKED	.....
CRANFIELD UNIVERSITY	
DESCRIPTION	INNER WHEEL FIXTURE
CODE	
PART No.	007
SHEET No.	1
CAD FILE	.....
DOC. TYPE	SOLIDWORKS
ISSUE	1

Appendix B14 – Inner wheel fixturing

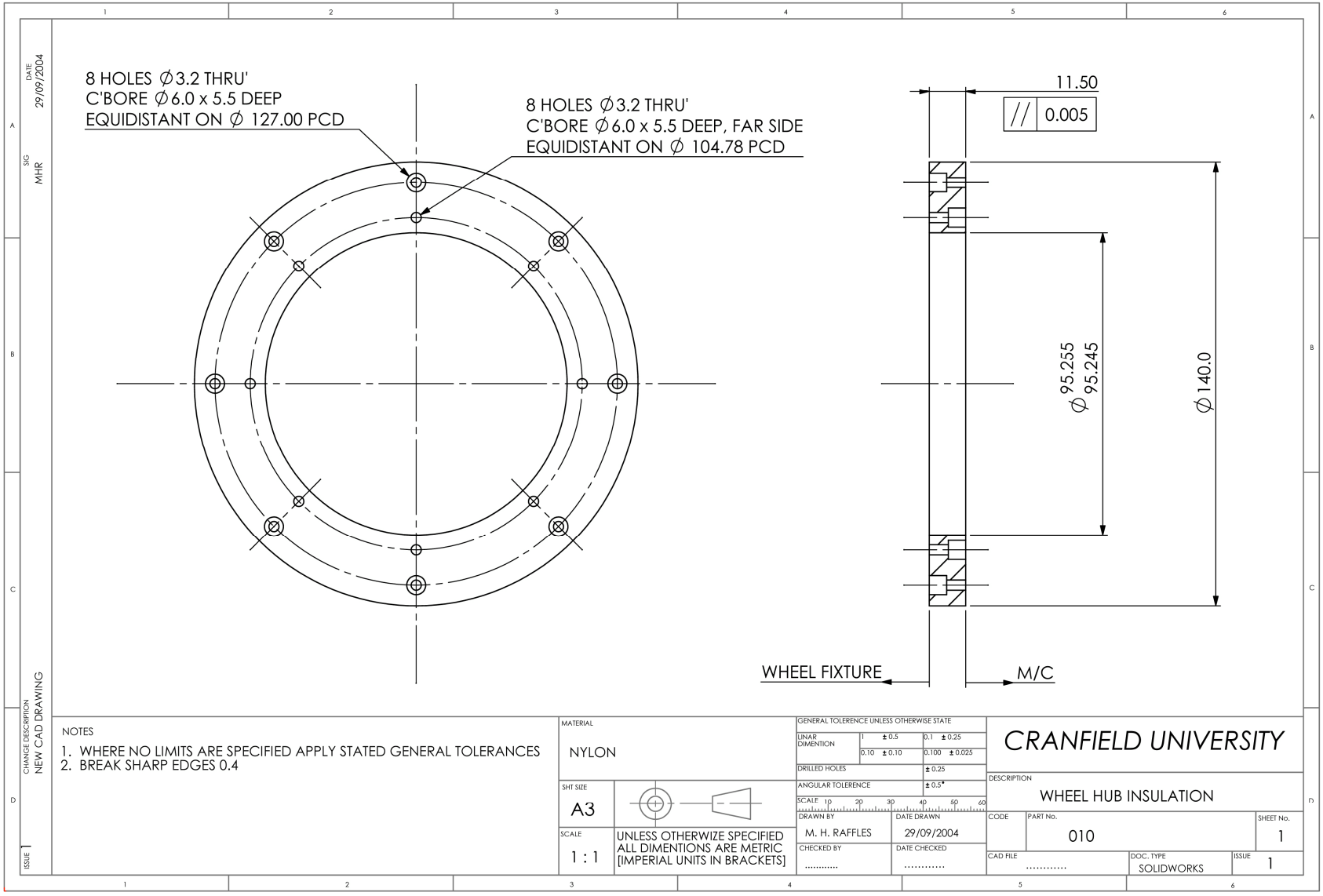

Appendix B15 – Wheel hub insulation

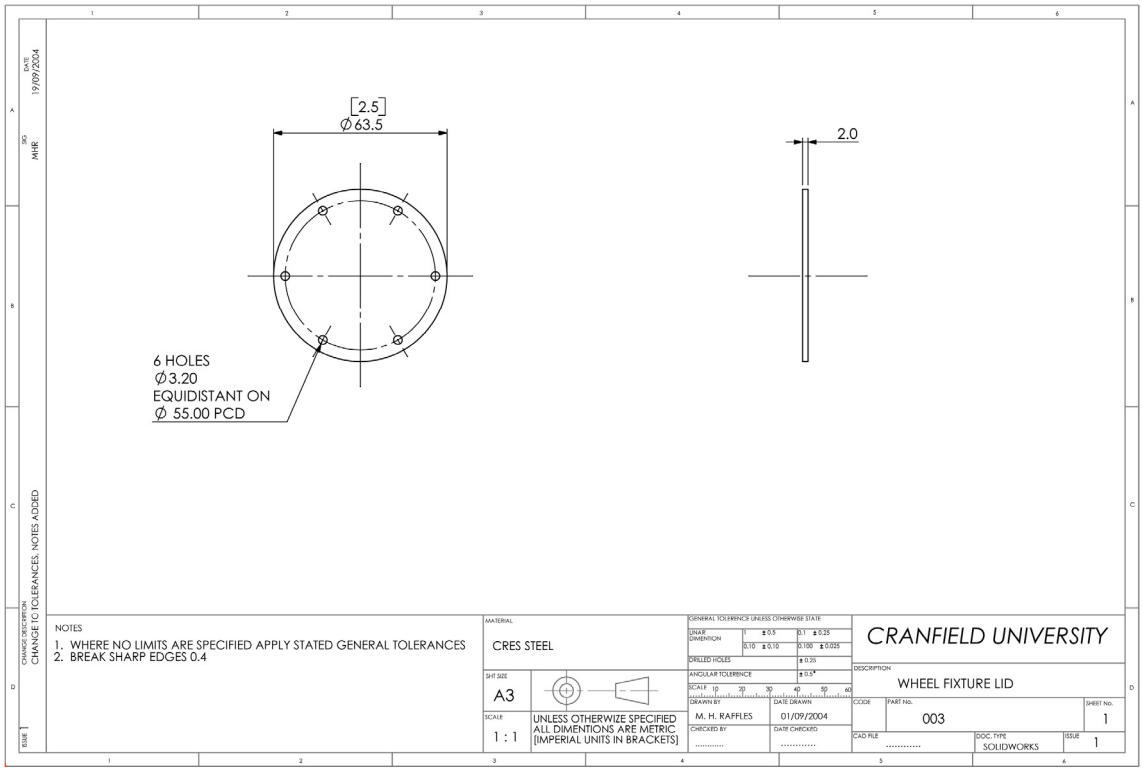

Appendix B16 – Wheel fixturing lid

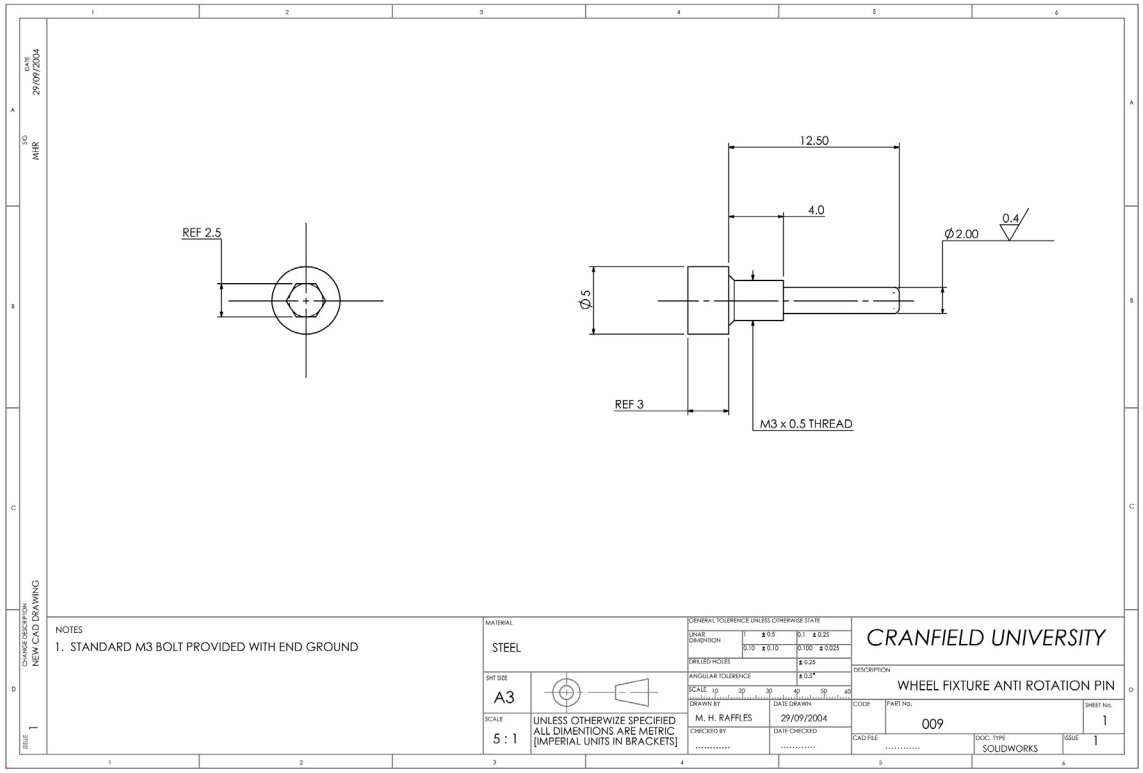

Appendix B17 – Wheel fixturing anti-rotation pin

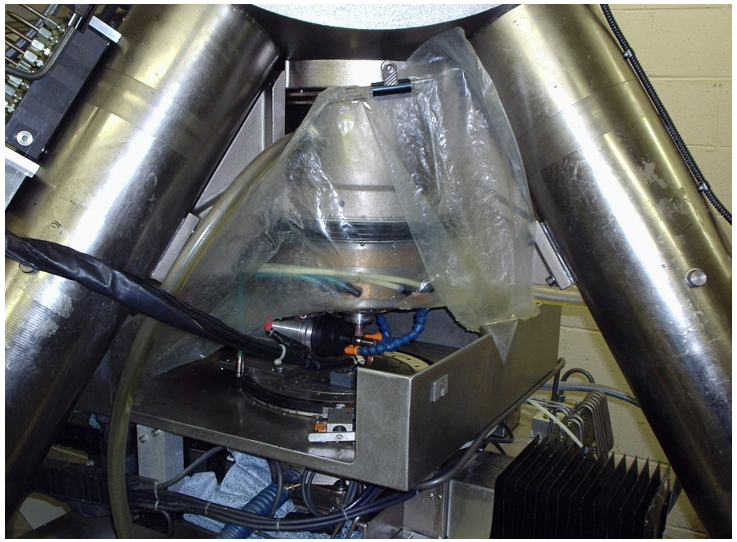

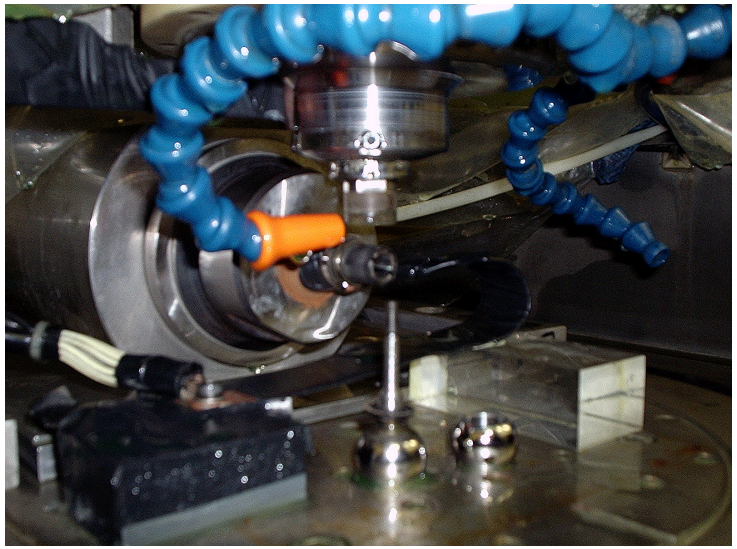

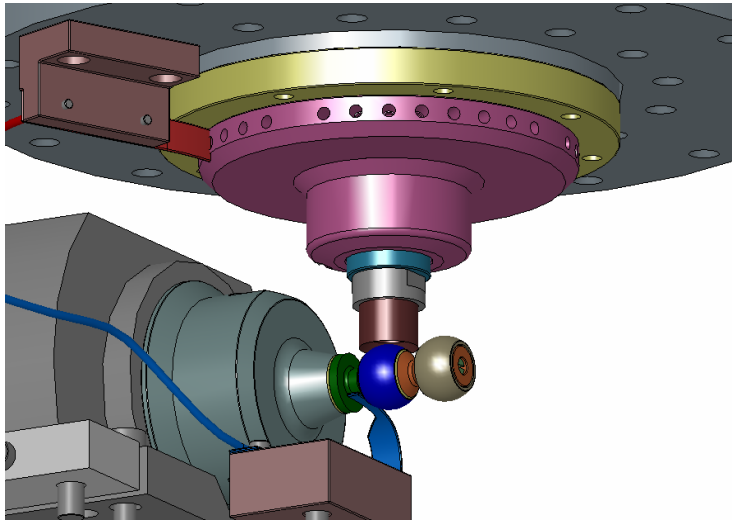

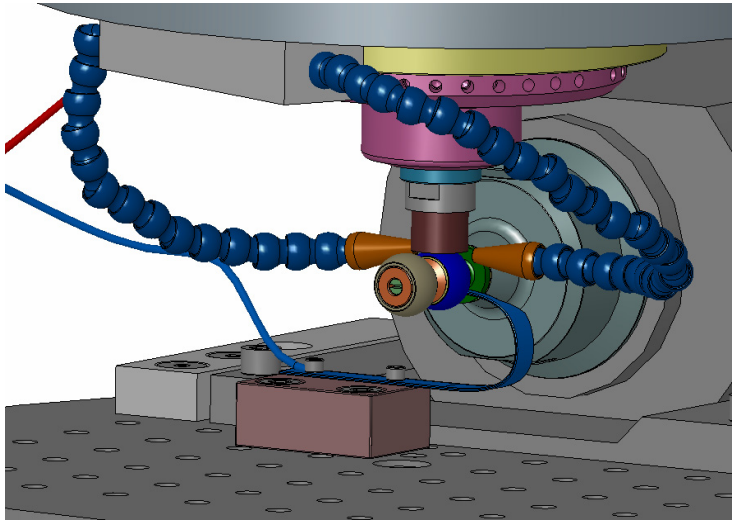

Appendix C1 – Additional pictures of Elid 1 superfinishing system at Cranfield

Appendix C2 – Additional pictures of Elid 3 superfinishing system at NMB –
(a) Elid power supply at NMB, (b) Fluid delivery

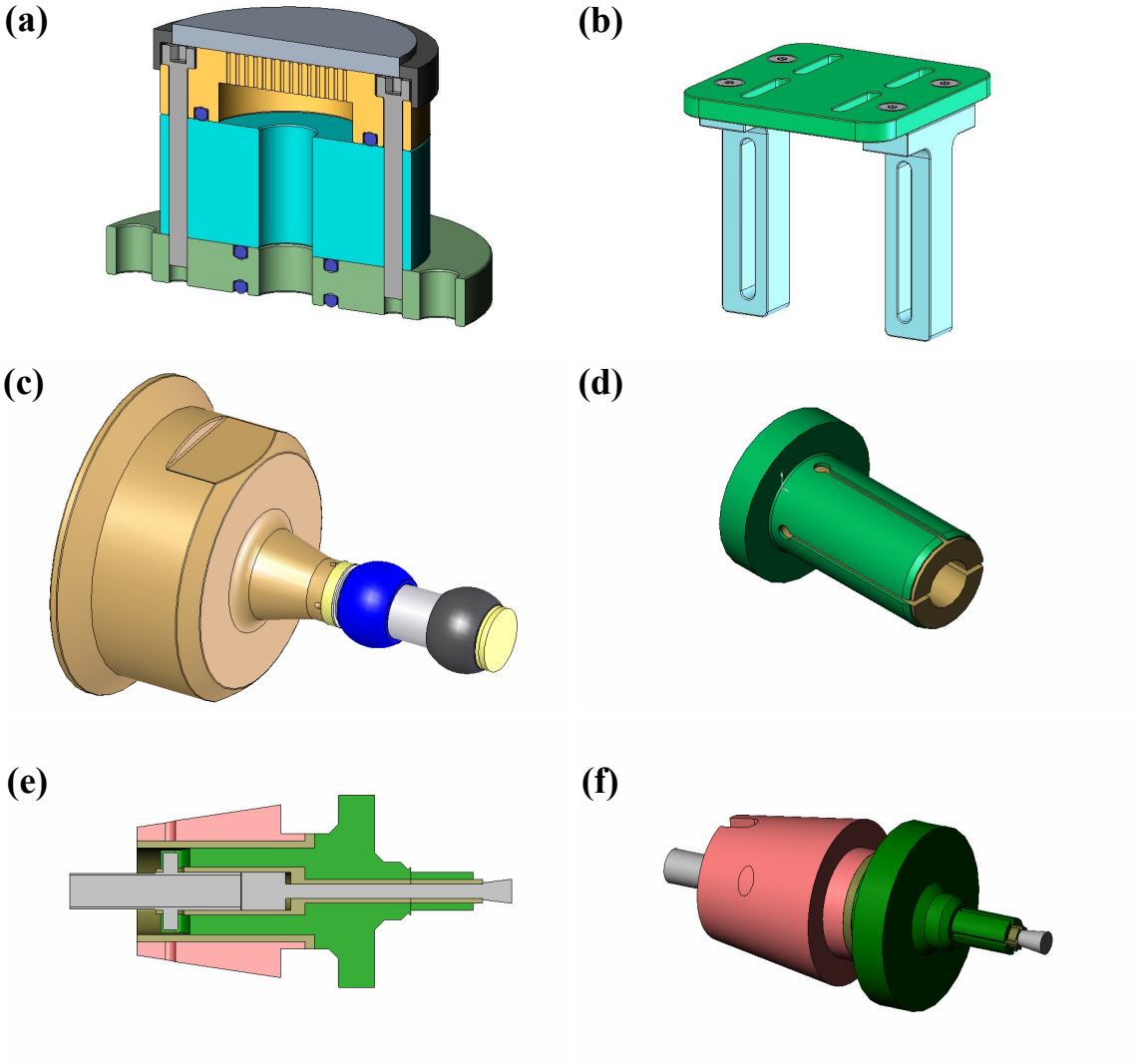

Appendix C3 – Additional fixturing produced –
(a) Vacuum chuck designed for superfinishing flat samples (b) Bracket designed for Blum laser,
(c) Original Elid 3 fixturing designed at Cranfield, (d) Collet for RBFB16AB balls at NMB
(e & f) Collet for MNRFB08GA balls at NMB

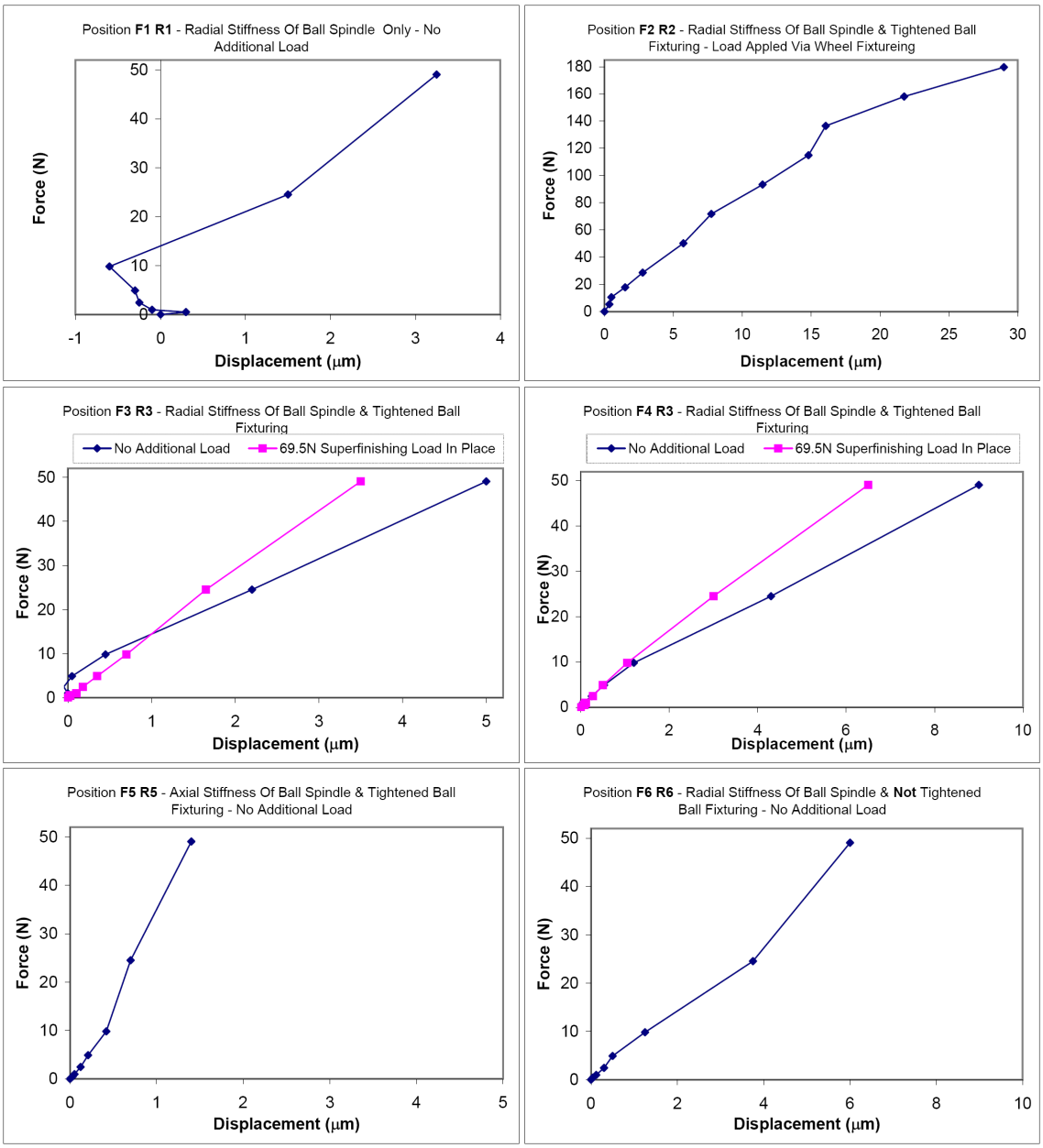

Appendix D1 - Graphs showing force displacement measurements taken on the ball spindle and Elid 1 ball spindle fixturing.

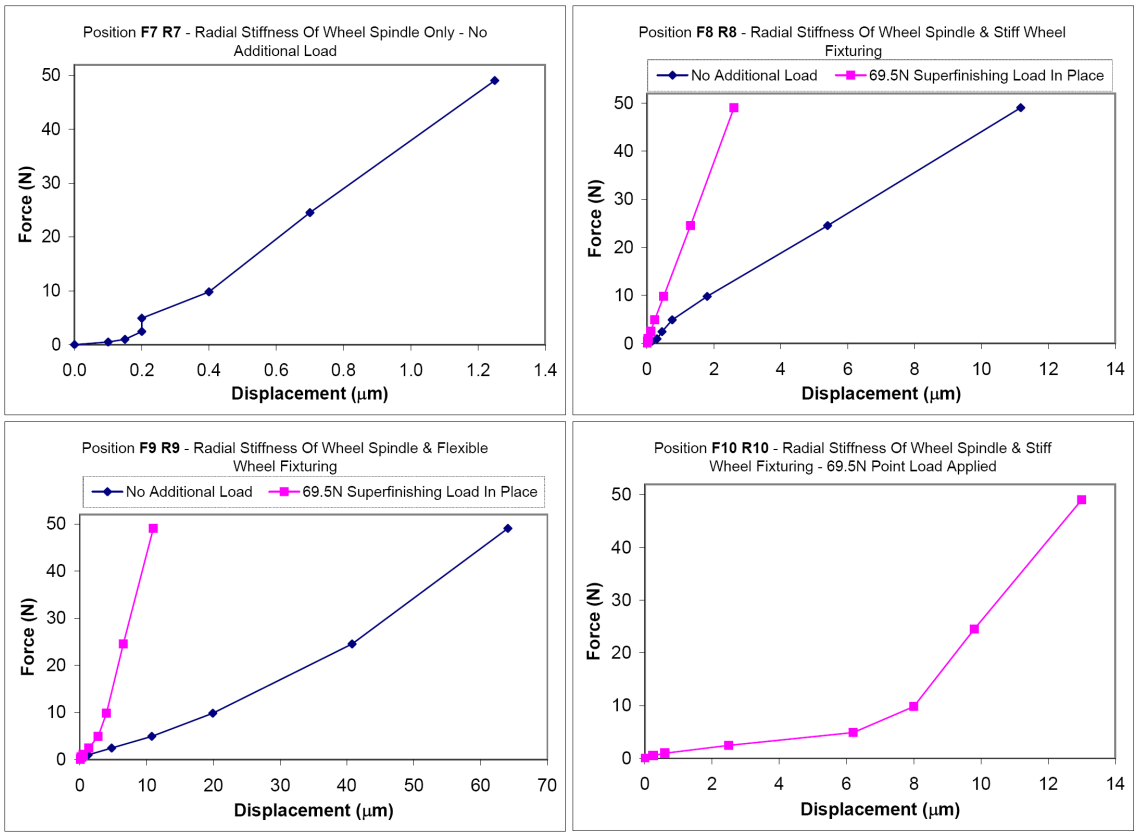

Appendix D2 - Graphs showing force displacement measurements taken on the wheel spindle and Elid 1 wheel spindle fixturing.

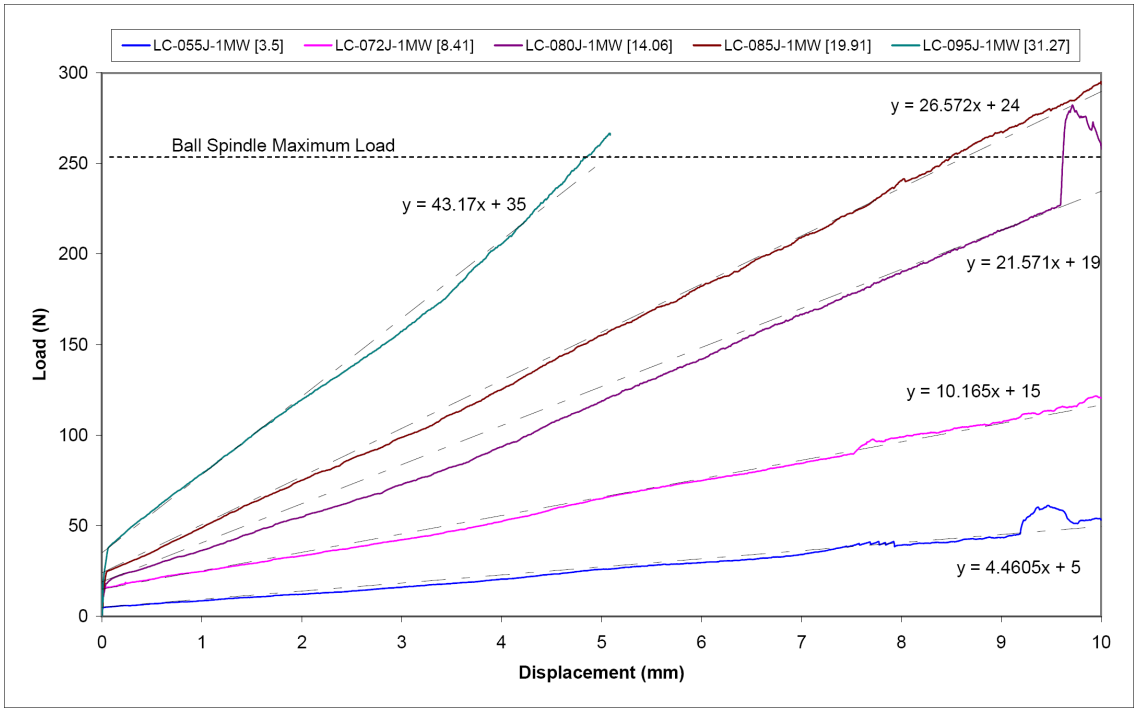

Appendix D3 - Static compression test of Cranfield wheel fixturing spring stiffness

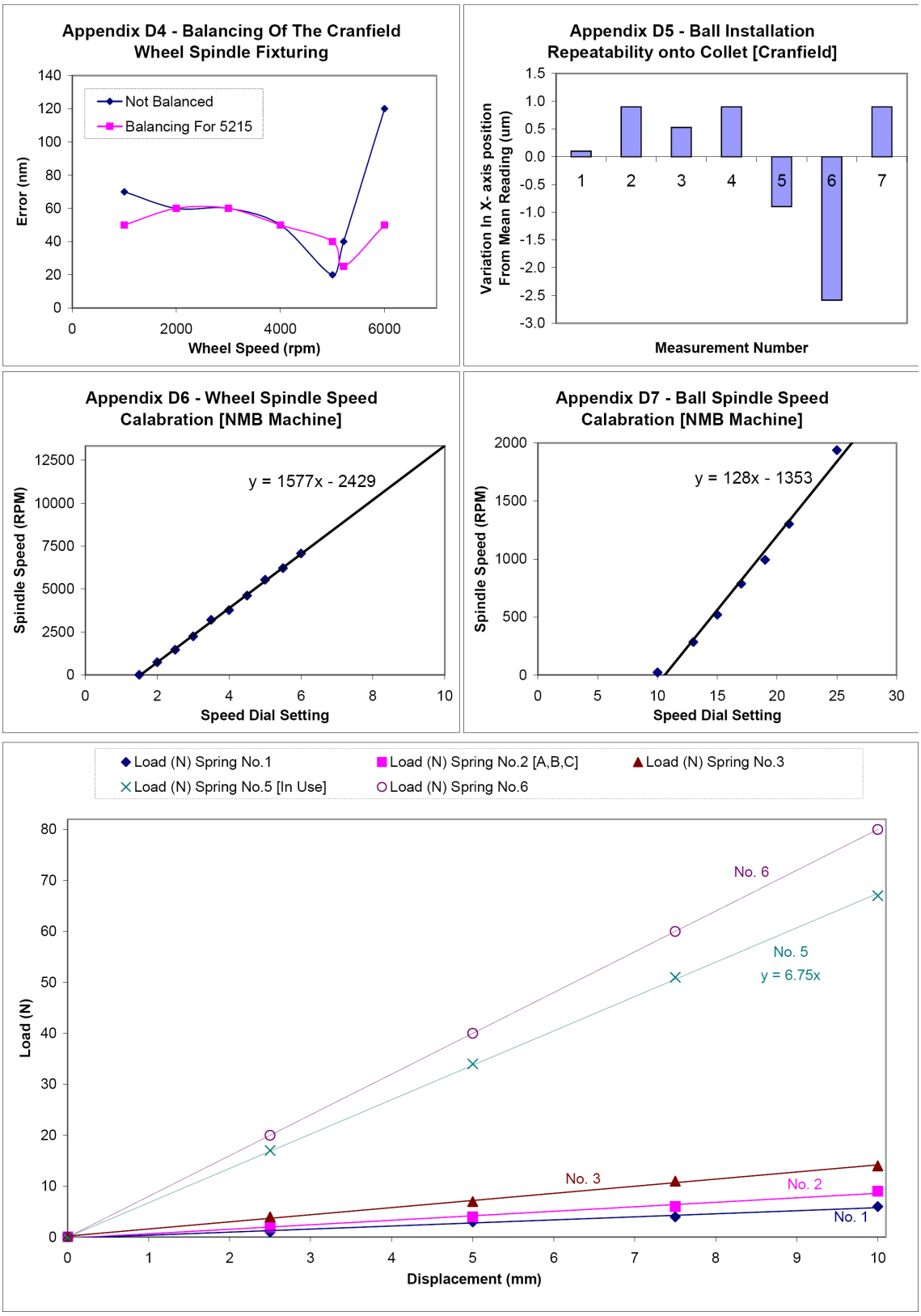

Appendix D8 - Static compression test of springs used at NMB

Heat-treated

Cylindrically Ground

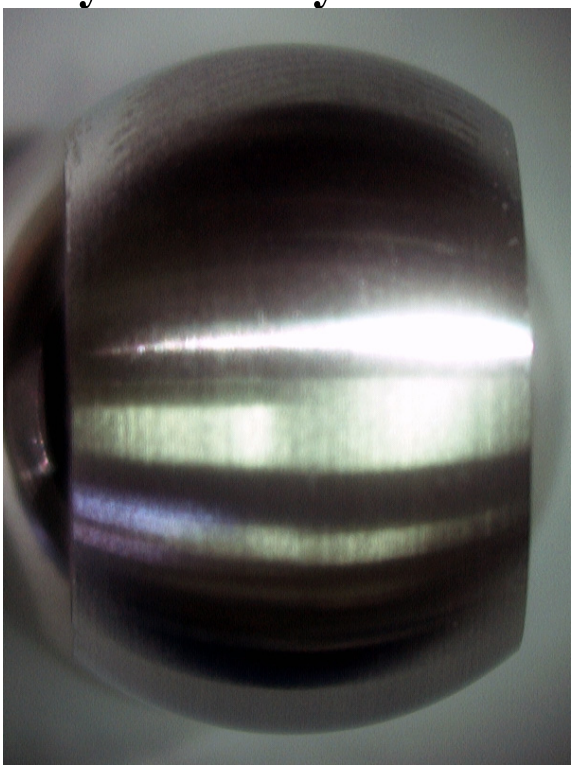

Honed

Barrelled

Appendix E1 - Pictures of RNB08 balls at various points in the NMB ball production chain.

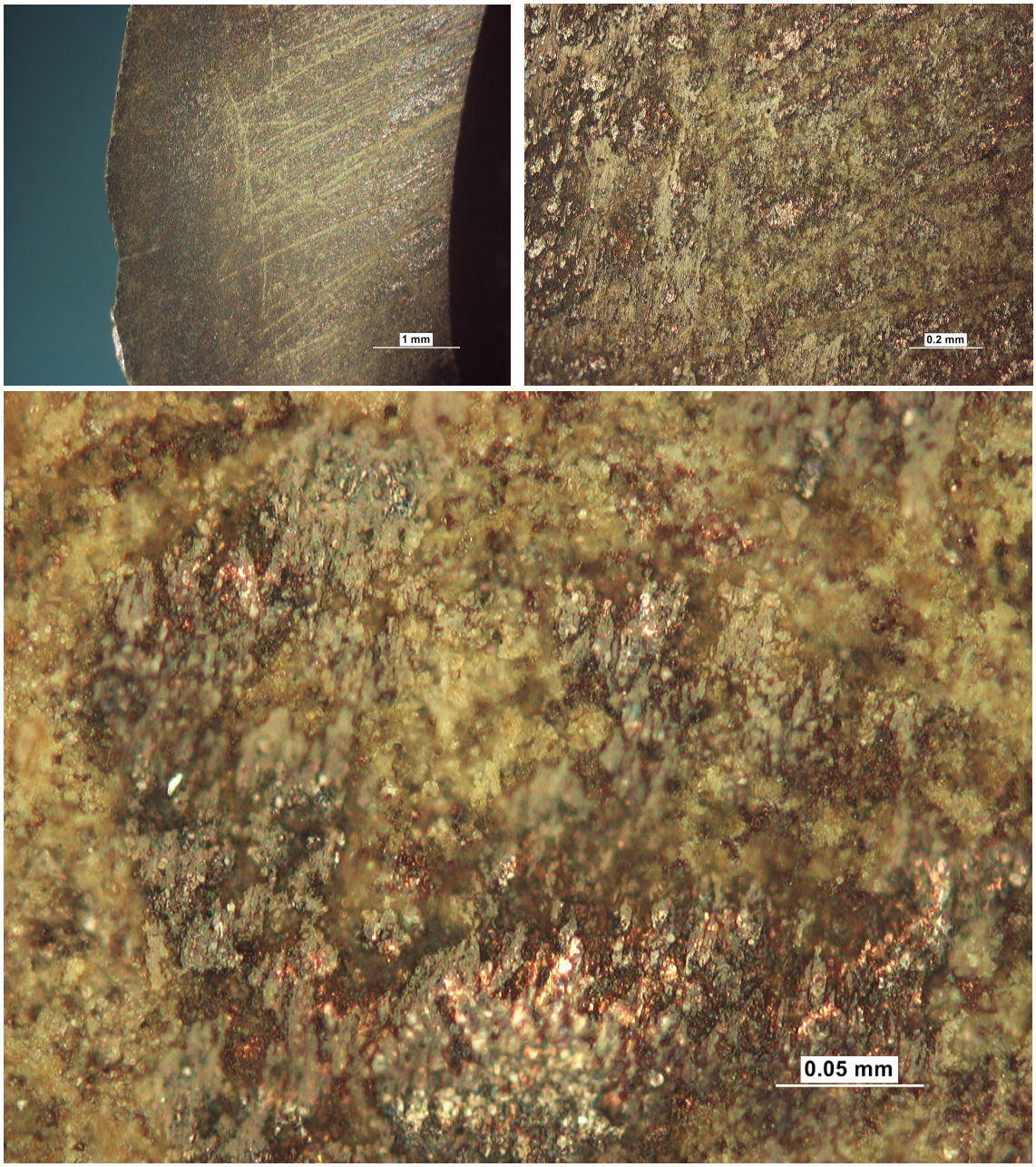

Appendix F1 - High magnification optical image (Montage) of a #4000 MRB-CBN wheel's surface after Elid 3 superfinishing.

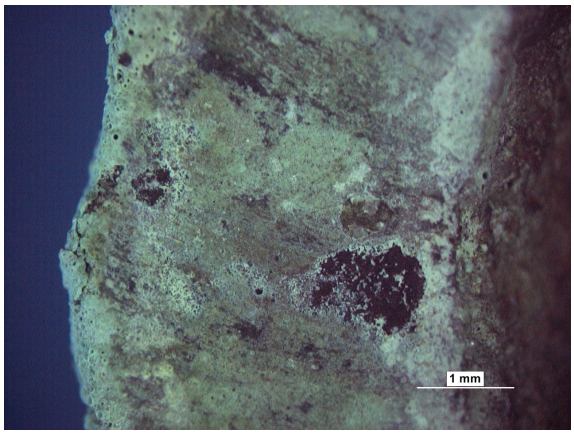

Appendix F2 - Wheel surface after electro-discharge truing and aggressive pre-dressing

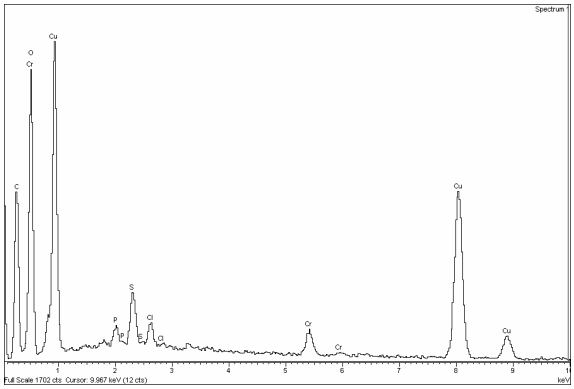

Appendix F3 - Analysis of blue deposit that is formed on the surface of a wheel when Elid pre-process dressing

Appendix F4 - Example of a glazed wheel surface [#8000 MRB-CBN wheel]

Appendix F4 – Examples of well-dressed wheels.

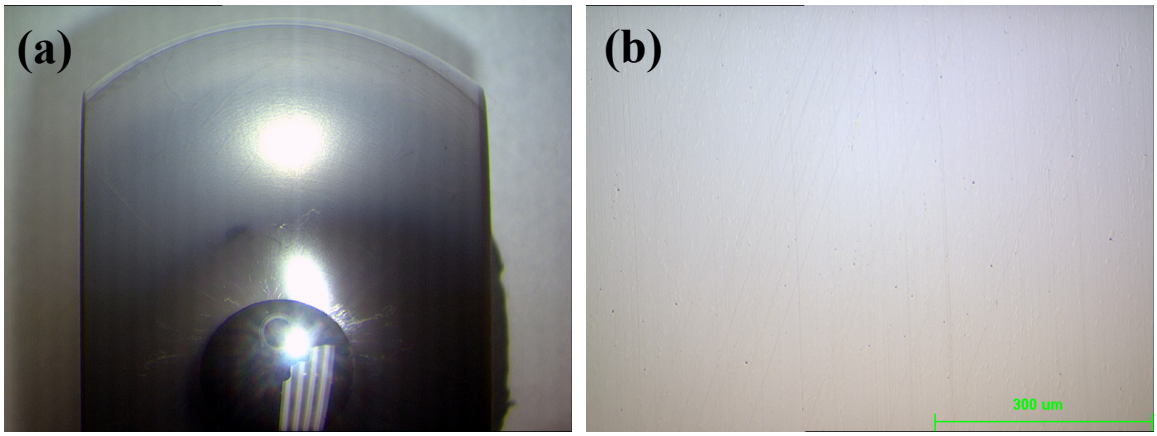

Appendix G1 - Additional pictures demonstrating typical ball surface quality when using a #12,000 MRB-CBN wheel. - (a) Full ball picture, (b) medium mag optical microscope image.

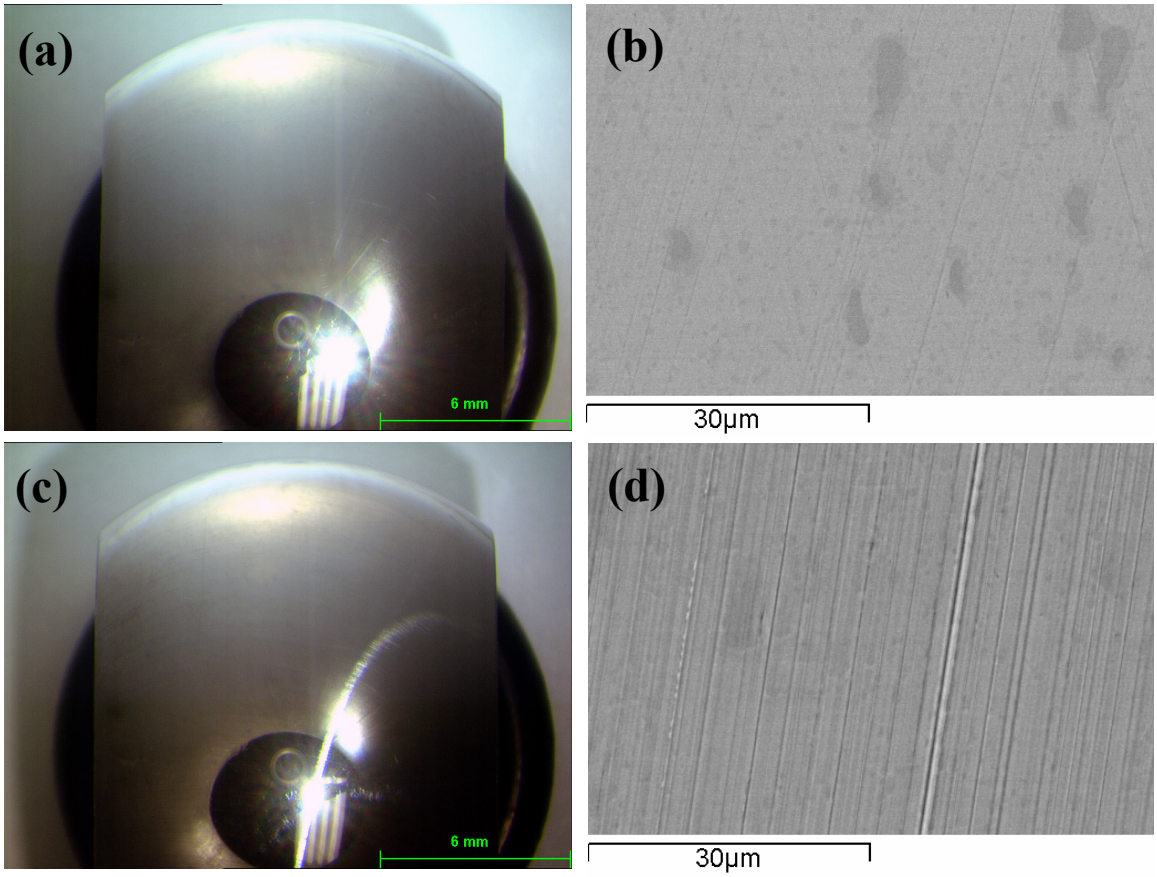

Appendix G2 - Additional pictures demonstrating the ball surface quality produced using a #2,000 MRB-CBN wheel of varying condition. (a & b) Glazed wheel, (c & d) Free-cutting wheel.

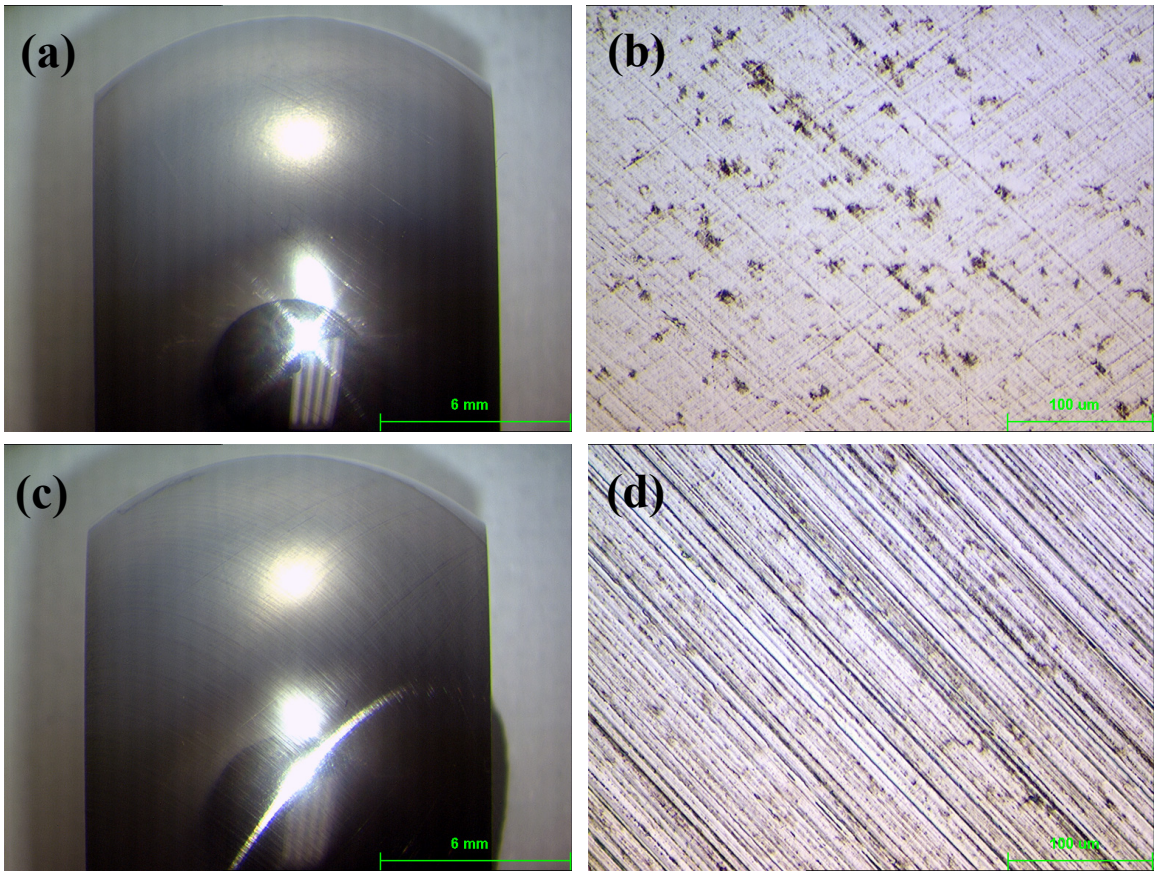

Appendix G3 - Additional pictures demonstrating the ball surface quality produced using a #500 MRB-CBN wheel of varying condition. (a & b) Glazed wheel, (c & d) Free-cutting wheel.

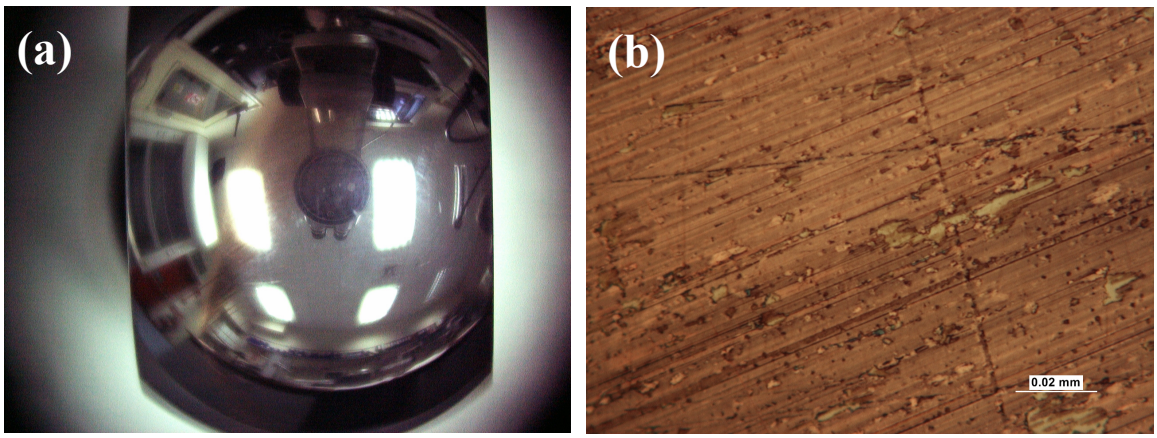

Appendix G4 - Pictures showing an adhered layer of copper on the surface of an RNDEB14 ball after Elid superfinishing. (a) Full ball picture, (b) Optical microscope image

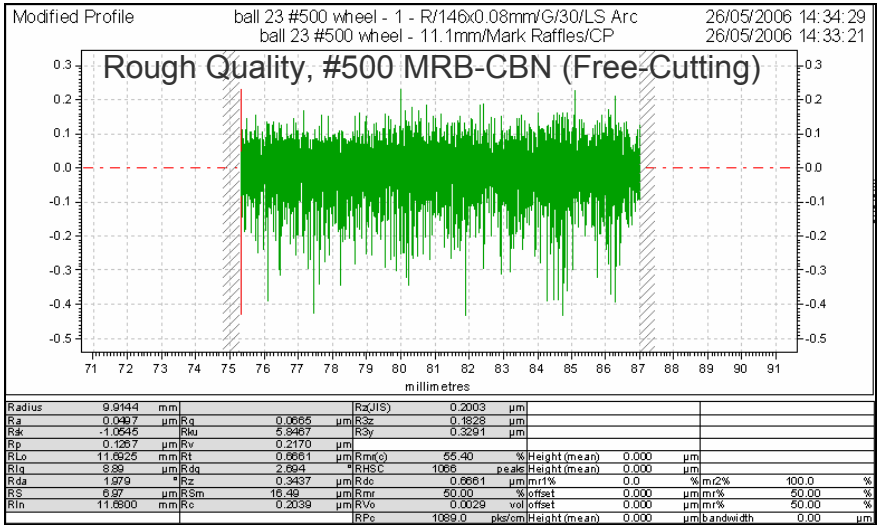

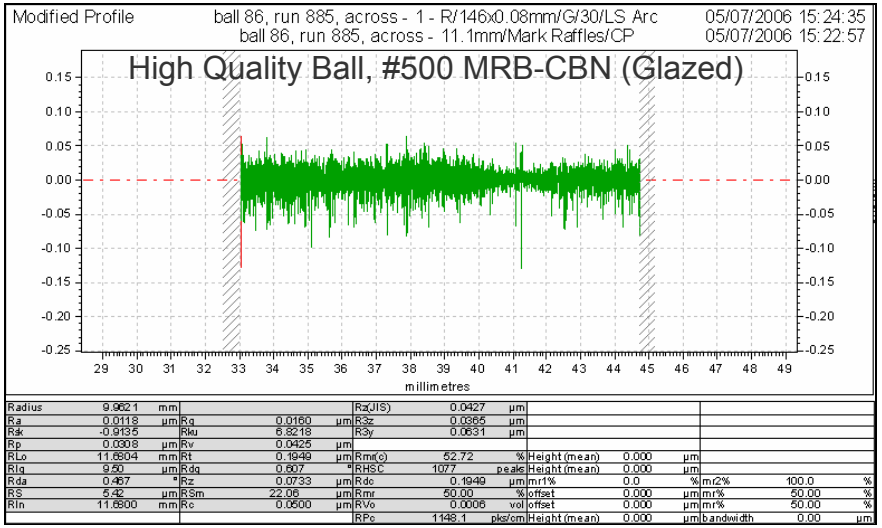

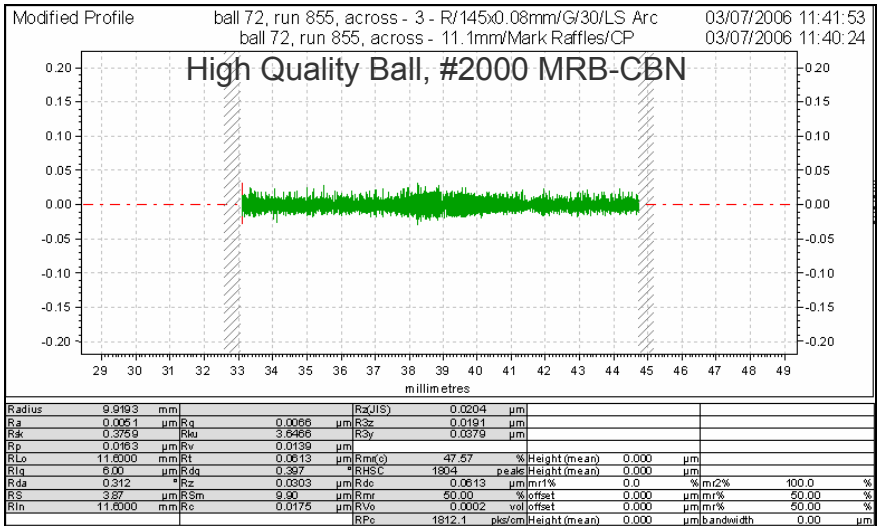

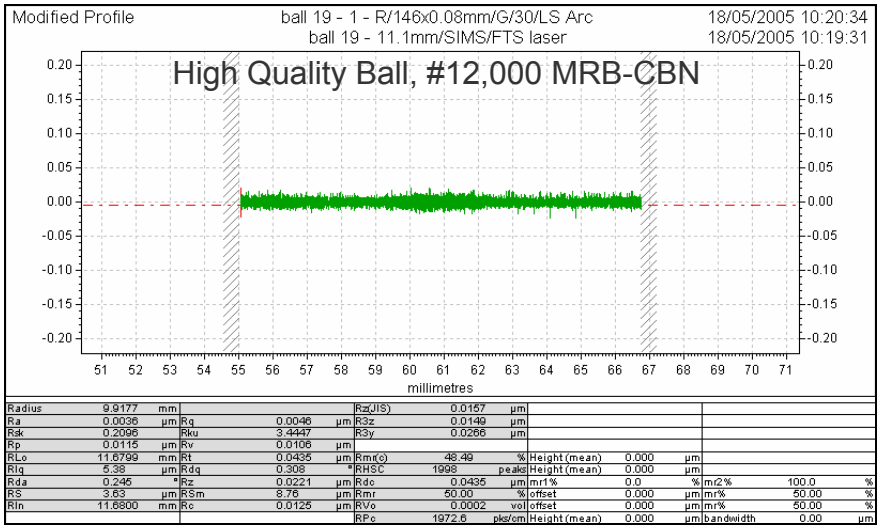

Appendix H - Surface roughness profiles of balls after processing using various MRB-CBN wheels. - [Taylor Hobson talysurf, Across ball]

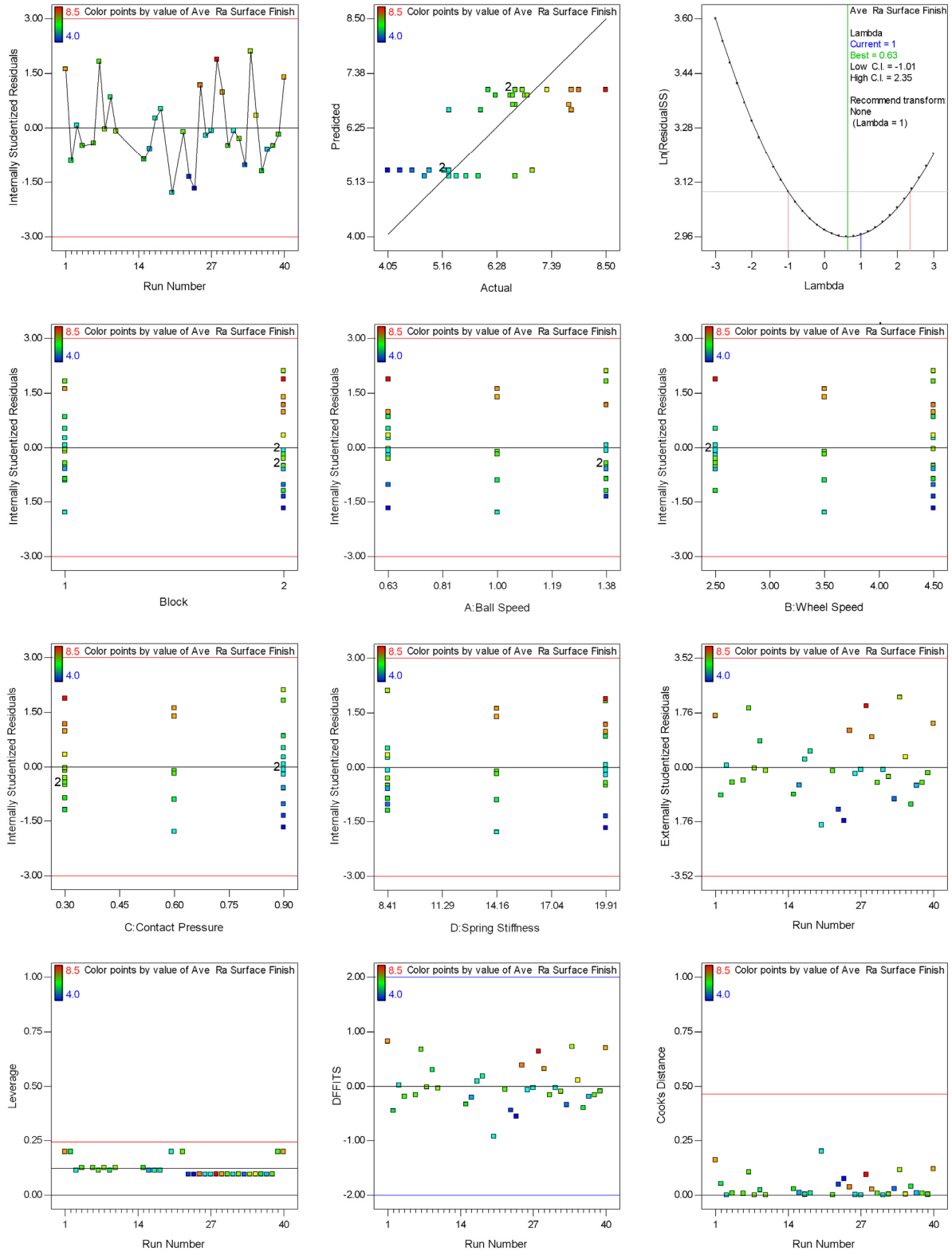

Appendix I1 - Various diagnostic and influence graphs demonstrating the validity of the model which expresses the average ball Ra surface finish response

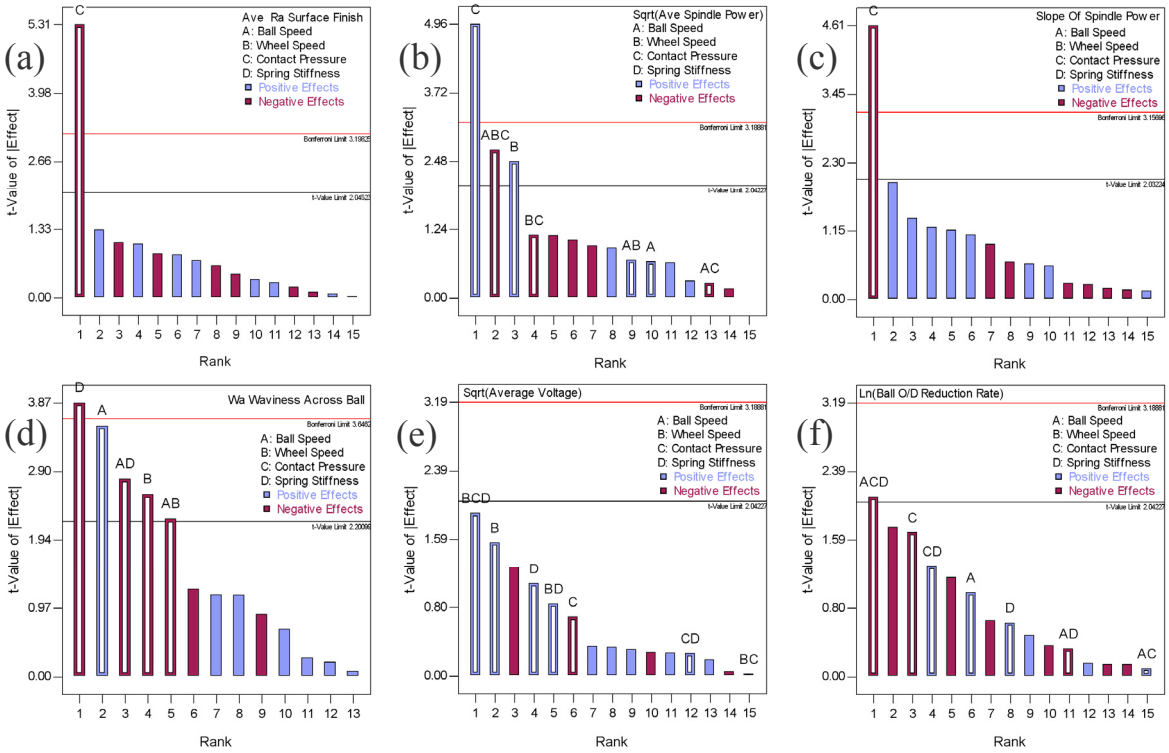

Appendix I2 - Pareto charts of various responses. – [Due to the transformation applied the graphs spindle power, voltage and O/D reduction show an inverted effect].

Average ball Ra surface finish			
Model Term	Standardised Effect	Sum Of Squares	Percent Contribution
A - Ball	-0.198	0.176	0.44
B - Wheel	0.229	0.097	0.24
C - Pressure	-1.677	18.918	47.36
D - Stiffness	0.264	0.381	0.95
AB	0.331	1.088	2.72
AC	0.417	1.330	3.33
AD	0.093	0.057	0.14
BC	-0.067	0.018	0.04
BD	-0.147	0.116	0.29
CD	-0.341	0.925	2.32
ABC	0.115	0.050	0.12
ABD	-0.036	0.015	0.04
ACD	0.024	0.002	0.00
BCD	0.010	0.000	0.00
ABCD	-0.271	0.496	1.24
Curvature	0.455	1.591	3.98
Lack Of Fit		10.477	26.23
Pure Error		4.210	10.54
Lenth's ME	0.739	Lenth's SME	1.176

Average Change In Wheel Spindle Power Usage			
Model Term	Standardised Effect	Sum Of Squares	Percent Contribution
A - Ball	0.275	0.603	0.62
B - Wheel	1.037	8.602	8.78
C - Pressure	2.071	34.317	35.01
D - Stiffness	0.131	0.138	0.14
AB	0.286	0.654	0.67
AC	-0.112	0.100	0.10
AD	-0.470	1.770	1.81
BC	-0.475	1.802	1.84
BD	0.005	0.000	0.00
CD	0.378	1.142	1.16
ABC	-1.123	10.085	10.29
ABD	0.266	0.568	0.58
ACD	-0.438	1.535	1.57
BCD	-0.394	1.241	1.27
ABCD	-0.072	0.041	0.04
Curvature	0.040	0.013	0.01
Lack Of Fit		30.649	31.26
Pure Error		4.769	4.86
Lenth's ME	0.940	Lenth's SME	1.470

Slope Of Wheel Spindle Power			
Model Term	Standardised Effect	Sum Of Squares	Percent Contribution
A - Ball	0.747	3.880	3.13
B - Wheel	0.079	0.013	0.01
C - Pressure	-2.524	47.568	38.38
D - Stiffness	0.328	0.131	0.11
AB	0.636	3.272	2.64
AC	-0.148	0.248	0.20
AD	1.085	7.180	5.79
BC	-0.346	1.333	1.08
BD	0.596	1.979	1.60
CD	-0.139	0.018	0.01
ABC	0.665	3.301	2.66
ABD	0.309	0.445	0.36
ACD	-0.089	0.004	0.00
BCD	-0.104	0.013	0.01
ABCD	-0.509	1.935	1.56
Curvature	0.060	0.141	0.11
Lack Of Fit		32.776	26.44
Pure Error		19.707	15.90
Lenth's ME	1.185	Lenth's SME	1.861

Wa Waviness Across Ball			
Model Term	Standardised Effect	Sum Of Squares	Percent Contribution
A - Ball	0.0077	0.000195	21.61
B - Wheel	-0.0056	0.000103	11.44
C - Pressure	0.0015	0.000001	0.16
D - Stiffness	-0.0084	0.000233	25.75
AB	-0.0048	0.000078	8.60
AC	0.0025	0.000010	1.09
AD	-0.0060	0.000122	13.48
BC	-0.0027	0.000027	3.00
BD	0.0025	0.000016	1.77
CD	0.0004	0.000000	0.01
ABC	-0.0019	0.000015	1.61
ABD	0.0006	0.000001	0.12
ACD	0.0002	0.000000	0.01
BCD	Aliased		
ABCD	Aliased		
Curvature	0.0000	0.000002	0.20
Lack Of Fit		0.000000	0.00
Pure Error		0.000100	11.12
Lenth's ME	0.0082	Lenth's SME	0.0145

Average Elid Voltage During Superfinishing			
Model Term	Standardised Effect	Sum Of Squares	Percent Contribution
A - Ball	0.038	0.012	0.18
B - Wheel	0.222	0.395	6.20
C - Pressure	-0.098	0.076	1.20
D - Stiffness	0.154	0.189	2.96
AB	0.044	0.015	0.24
AC	0.027	0.006	0.09
AD	0.047	0.018	0.28
BC	0.004	0.000	0.00
BD	0.120	0.115	1.80
CD	0.038	0.011	0.18
ABC	-0.181	0.262	4.11
ABD	0.050	0.020	0.31
ACD	-0.039	0.012	0.19
BCD	0.271	0.589	9.24
ABCD	-0.008	0.000	0.01
Curvature	0.121	0.118	1.84
Lack Of Fit		3.989	62.59
Pure Error		0.546	8.57
Lenth's ME	0.302	Lenth's SME	0.473

Rate Of Ball O/D Reduction			
Model Term	Standardised Effect	Sum Of Squares	Percent Contribution
A - Ball	0.248	0.492	2.32
B - Wheel	-0.166	0.220	1.04
C - Pressure	-0.428	1.465	6.92
D - Stiffness	0.159	0.203	0.96
AB	-0.293	0.686	3.24
AC	0.024	0.005	0.02
AD	-0.083	0.055	0.26
BC	-0.036	0.011	0.05
BD	-0.037	0.011	0.05
CD	0.327	0.857	4.05
ABC	-0.442	1.565	7.40
ABD	0.041	0.013	0.06
ACD	-0.532	2.264	10.70
BCD	0.122	0.119	0.56
ABCD	-0.093	0.069	0.32
Curvature	0.218	0.379	1.79
Lack Of Fit		8.613	40.70
Pure Error		4.135	19.54
Lenth's ME	0.541	Lenth's SME	0.847

Appendix I3 - Tables of effects for a variety of the responses assessed

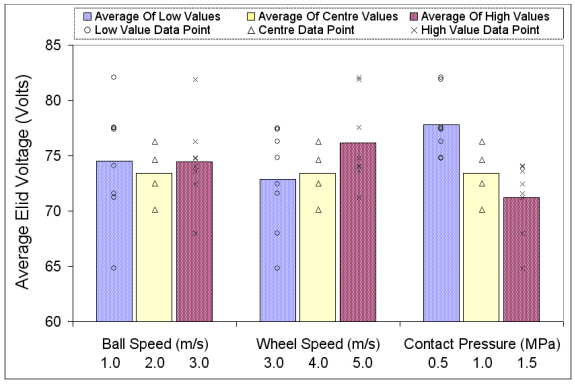

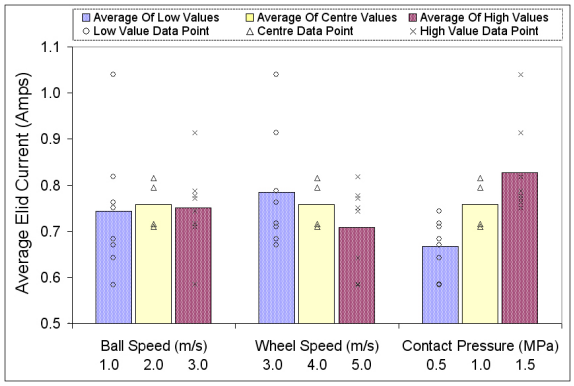

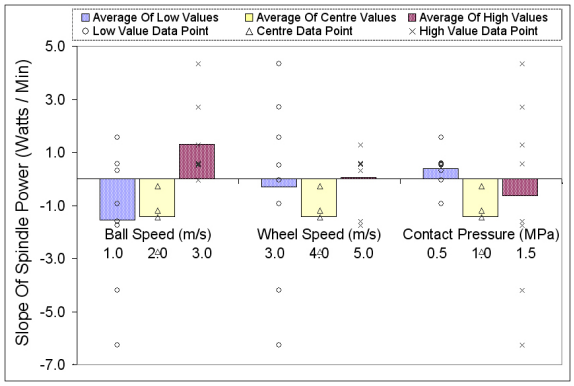

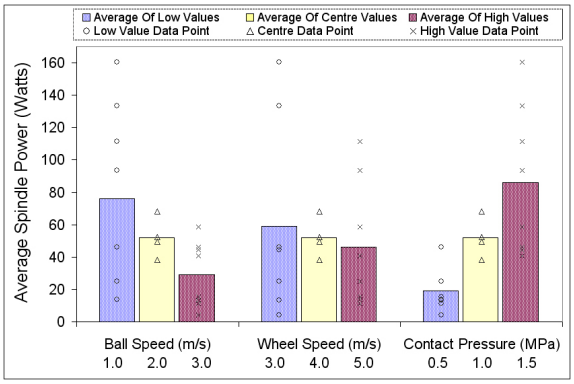

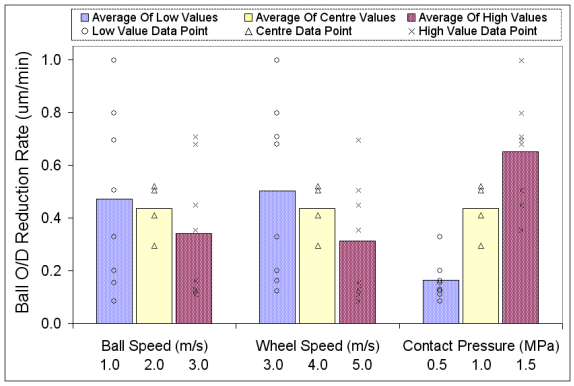

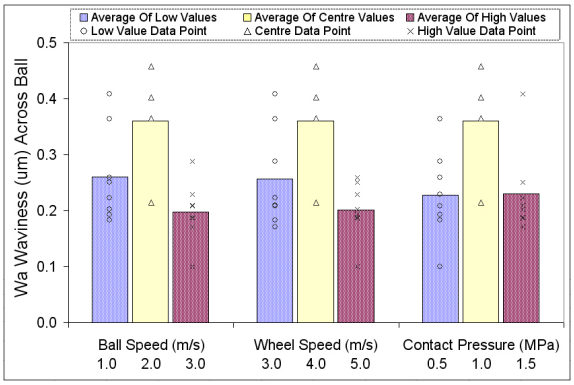

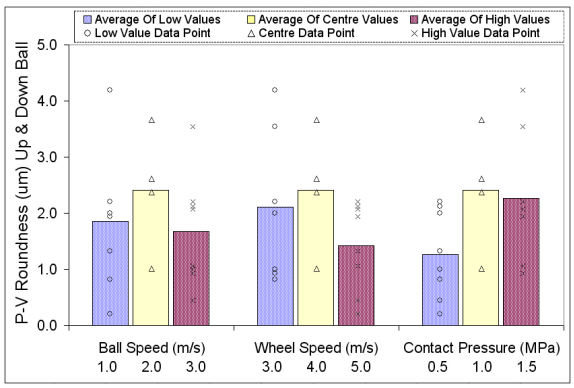

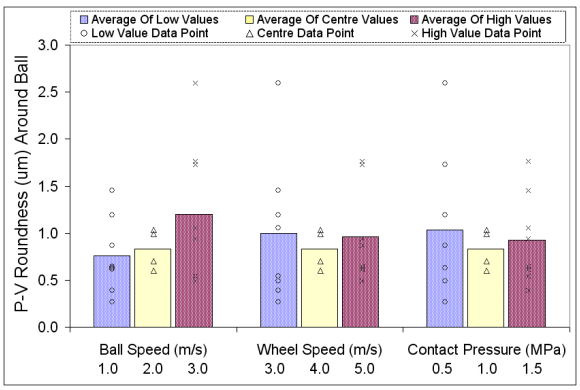

Appendix J1 - Column graphs of raw results versus factor levels for various responses.

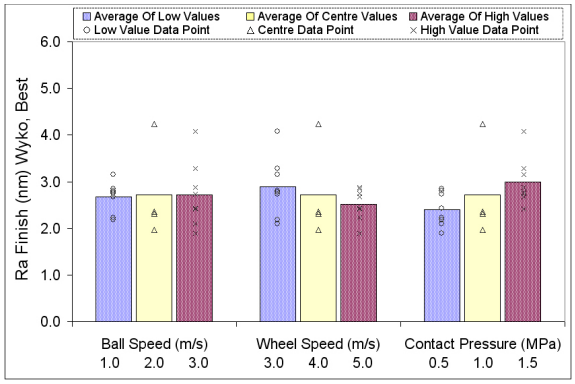

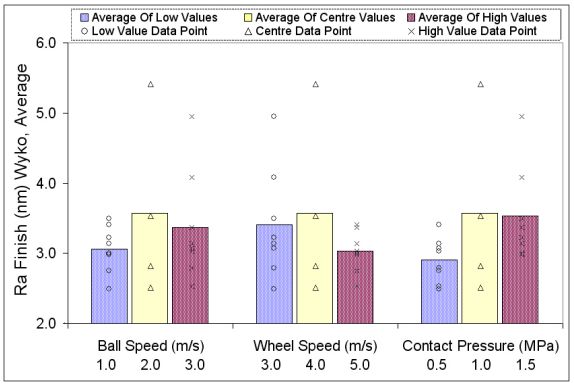

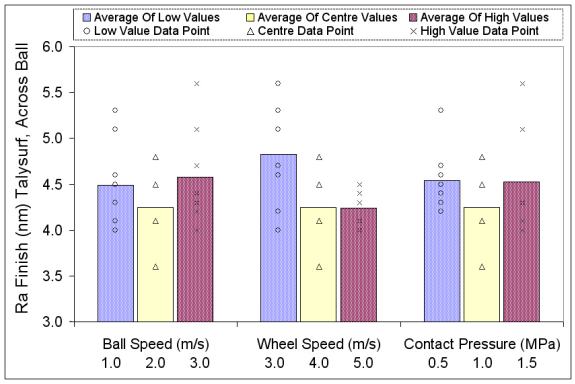

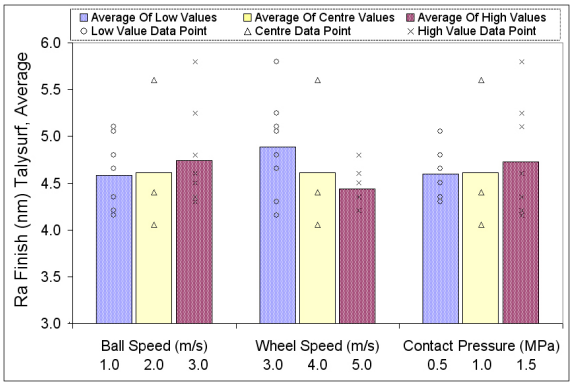

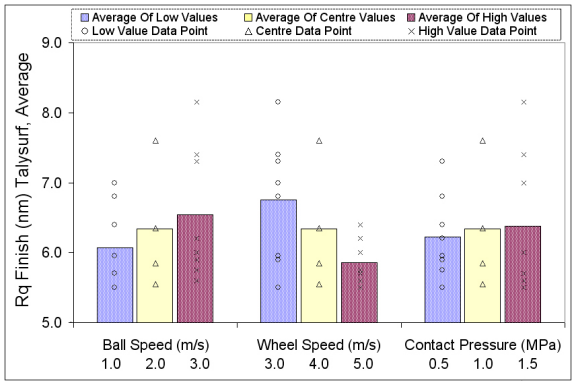

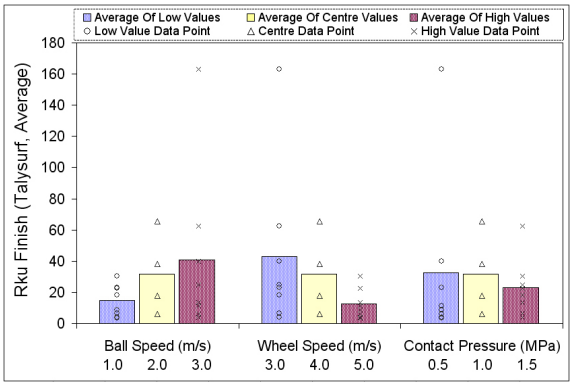

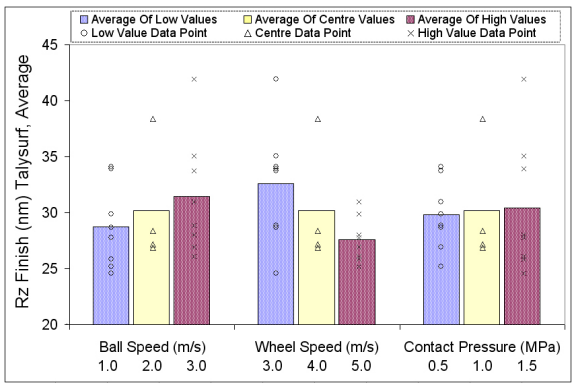

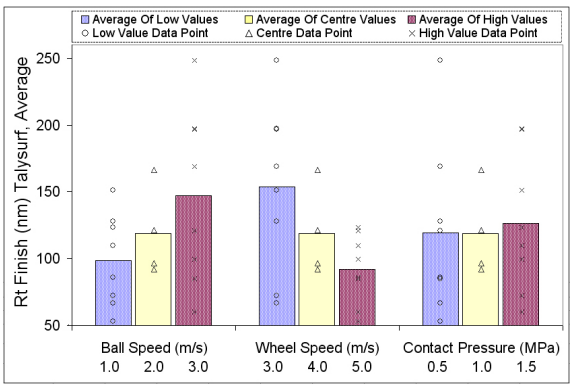

Appendix J2 - Column graphs of raw results versus factor levels for various responses.

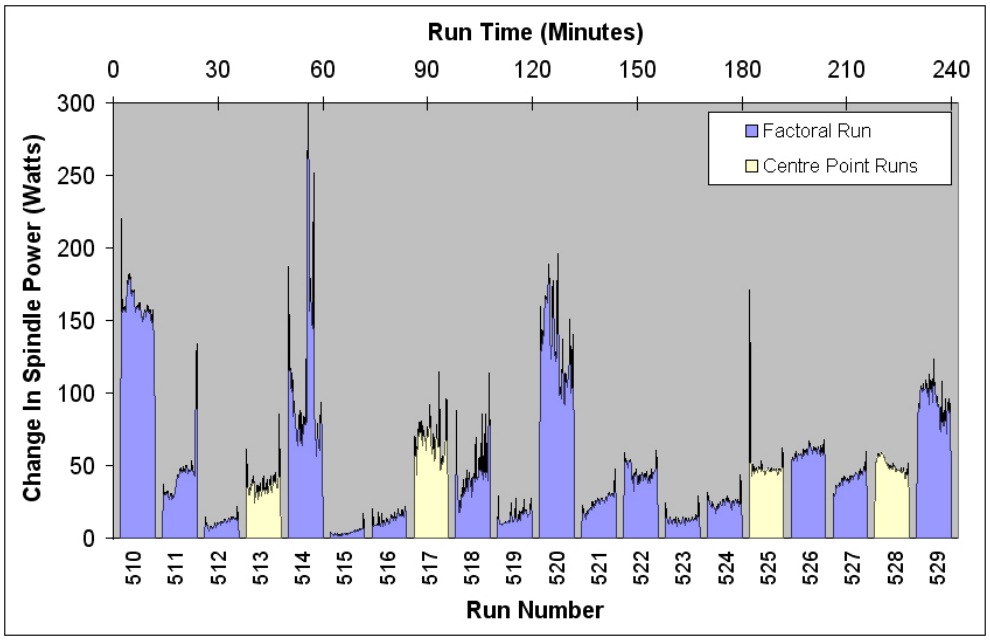

Appendix J3 - Spindle data recorded over the various runs

Average Elid Voltage During Superfinishing			
Model Term	Standardised Effect	Sum Of Squares	Percent Contribution
A - Ball	-0.05	0.01	0.00
B - Wheel	3.30	43.51	13.25
C - Pressure	-6.57	172.48	52.55
AB	-0.12	0.06	0.02
AC	1.65	10.92	3.33
BC	0.72	2.06	0.63
ABC	-0.30	0.36	0.11
Curvature	-2.57	3.91	1.19
Lack Of Fit		0.00	0.00
Pure Error		94.93	28.92
Lenth's ME	2.90	Lenth's SME	4.26

Average Elid Current During Superfinishing			
Model Term	Standardised Effect	Sum Of Squares	Percent Contribution
A - Ball	0.007	0.000	0.09
B - Wheel	-0.076	0.023	11.24
C - Pressure	0.161	0.103	49.75
AB	0.014	0.001	0.38
AC	-0.037	0.005	2.65
BC	-0.020	0.002	0.78
ABC	0.006	0.000	0.08
Curvature	0.001	0.000	0.21
Lack Of Fit		0.000	0.00
Pure Error		0.072	34.81
Lenth's ME	0.082	Lenth's SME	0.120

Slope Of Wheel Spindle Power			
Model Term	Standardised Effect	Sum Of Squares	Percent Contribution
A - Ball	2.85	32.48	31.38
B - Wheel	0.35	0.49	0.48
C - Pressure	-1.01	4.09	3.96
AB	-1.48	8.82	8.52
AC	2.82	31.82	30.74
BC	0.12	0.06	0.06
ABC	-1.59	10.17	9.82
Curvature	-1.12	5.43	5.25
Lack Of Fit		0.00	0.00
Pure Error		10.14	9.80
Lenth's ME	2.22	Lenth's SME	3.25

Average Change In Wheel Spindle Power Usage			
Model Term	Standardised Effect	Sum Of Squares	Percent Contribution
A - Ball	-3.06	37.48	24.65
B - Wheel	-0.62	1.54	1.01
C - Pressure	4.82	92.96	61.14
AB	1.15	5.26	3.46
AC	-1.18	5.53	3.64
BC	-0.23	0.22	0.14
ABC	-0.01	0.00	0.00
Curvature	0.42	1.12	0.74
Lack Of Fit		0.00	0.00
Pure Error		7.94	5.22
Lenth's ME	1.46	Lenth's SME	2.14

Rate Of Ball O/D Reduction			
Model Term	Standardised Effect	Sum Of Squares	Percent Contribution
A - Ball	-0.299	0.356	3.42
B - Wheel	-0.482	0.930	8.92
C - Pressure	1.409	7.945	76.22
AB	0.122	0.059	0.57
AC	-0.025	0.002	0.02
BC	0.002	0.000	0.00
ABC	-0.193	0.148	1.42
Curvature	0.069	0.340	3.26
Lack Of Fit		0.000	0.00
Pure Error		0.642	6.16
Lenth's ME	0.318	Lenth's SME	0.467

Wa Waviness Across Ball			
Model Term	Standardised Effect	Sum Of Squares	Percent Contribution
A - Ball	-0.063	0.016	9.30
B - Wheel	-0.056	0.012	7.21
C - Pressure	0.002	0.000	0.01
AB	0.012	0.001	0.35
AC	-0.019	0.002	0.89
BC	0.010	0.000	0.22
ABC	0.031	0.004	2.18
Curvature	0.010	0.055	32.09
Lack Of Fit		0.000	0.00
Pure Error		0.082	47.76
Lenth's ME	0.088	Lenth's SME	0.130

Ball Roundness Up & Down Ball			
Model Term	Standardised Effect	Sum Of Squares	Percent Contribution
A - Ball	-0.190	0.145	0.66
B - Wheel	-0.690	1.906	8.72
C - Pressure	1.001	4.010	18.35
AB	0.192	0.147	0.67
AC	-0.544	1.182	5.41
BC	-0.209	0.175	0.80
ABC	0.033	0.004	0.02
Curvature	0.629	1.345	6.15
Lack Of Fit		0.000	0.00
Pure Error		12.942	59.22
Lenth's ME	1.096	Lenth's SME	1.607

Ra Ball Surface Finish (Best Wyko Reading)			
Model Term	Standardised Effect	Sum Of Squares	Percent Contribution
A - Ball	0.010	0.000	0.40
B - Wheel	0.042	0.007	6.57
C - Pressure	-0.081	0.026	24.64
AB	0.030	0.004	3.47
AC	-0.033	0.004	4.01
BC	0.021	0.002	1.58
ABC	0.003	0.000	0.03
Curvature	0.001	0.001	1.04
Lack Of Fit		0.000	0.00
Pure Error		0.062	58.26
Lenth's ME	0.084	Lenth's SME	0.124

Ra Surface Finish Across Ball (Talysurf)			
Model Term	Standardised Effect	Sum Of Squares	Percent Contribution
A - Ball	0.088	0.031	0.64
B - Wheel	-0.588	1.381	28.78
C - Pressure	-0.013	0.001	0.01
AB	-0.063	0.016	0.33
AC	0.363	0.526	10.96
BC	-0.263	0.276	5.75
ABC	-0.288	0.331	6.89
Curvature	-0.109	0.253	5.28
Lack Of Fit		0.000	0.00
Pure Error		1.985	41.38
Lenth's ME	0.547	Lenth's SME	0.802

Appendix J4 - Tables of effects for a variety of the responses assessed.

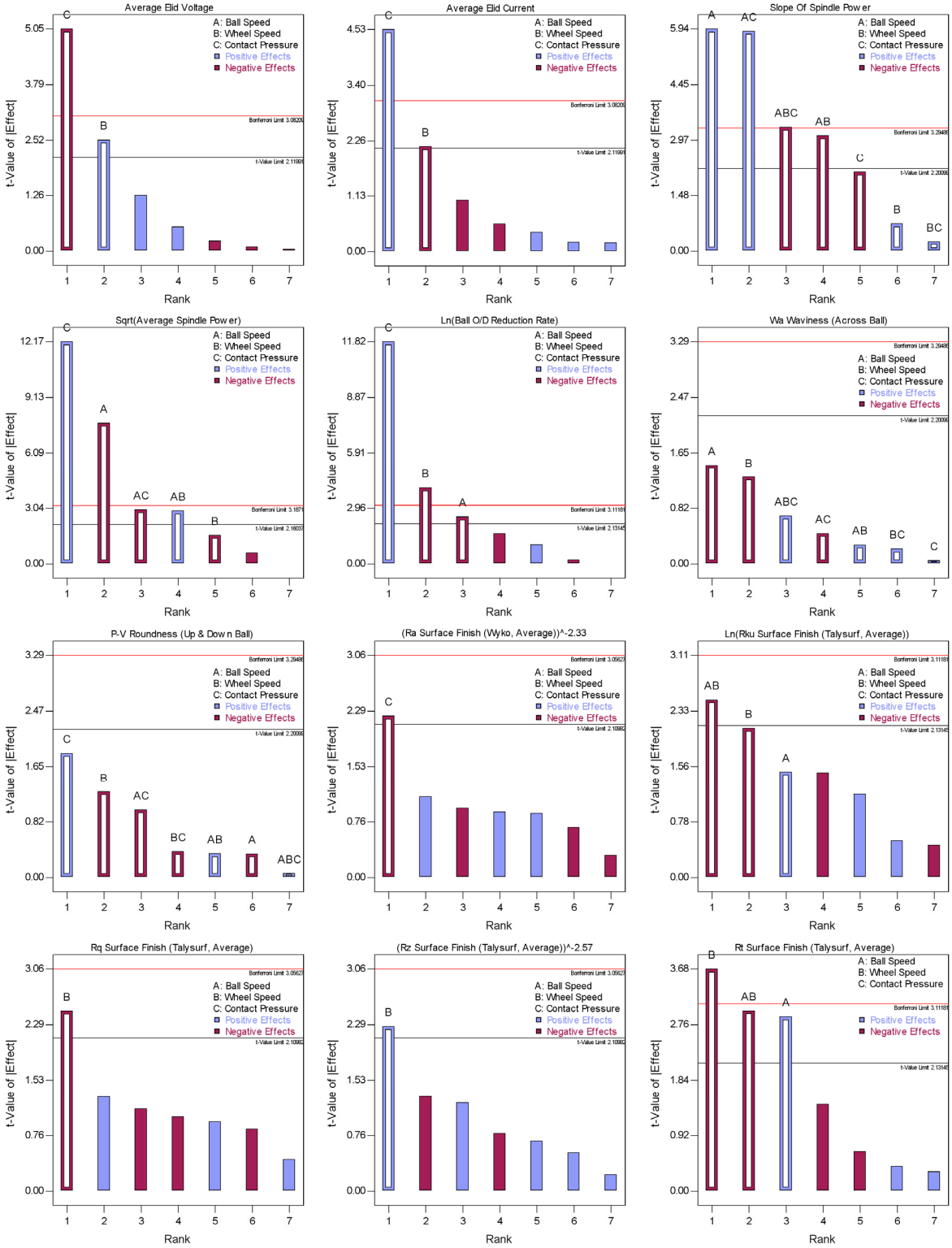

Appendix J5 - Pareto charts for a variety of the responses assessed.
[N.B. Data transformation can invert effect shown].

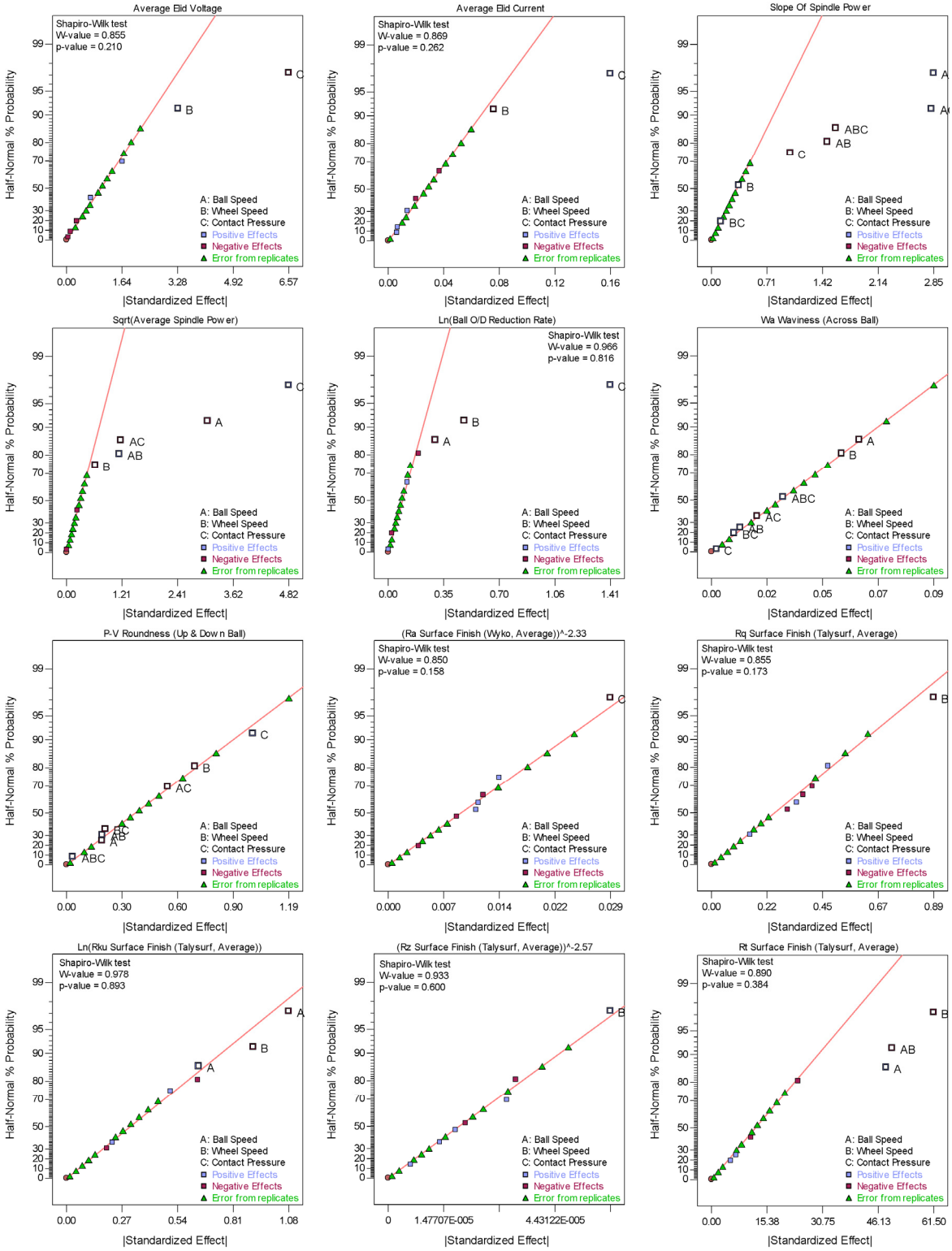

Appendix J6 – Half normal probability plots for a variety of the responses assessed.
[N.B. Data transformation can invert effect shown].

Source	Sum of Squares	Deg. Of Freedom	Mean Square	F Value	p-value Prob > F
Model	**87.93**	**7**	**12.56**	**13.626**	**0.0001**
A – Ball	**32.48**	**1**	**32.48**	**35.233**	**< 0.0001**
B – Wheel	0.49	1	0.49	0.535	0.4800
C - Pressure	4.09	1	4.09	4.440	0.0589
AB	**8.82**	**1**	**8.82**	**9.568**	**0.0102**
AC	**31.82**	**1**	**31.82**	**34.517**	**0.0001**
BC	0.06	1	0.06	0.062	0.8077
ABC	**10.17**	**1**	**10.17**	**11.026**	**0.0068**
Lack of Fit	5.43	1	5.43	5.890	0.0336
Pure Error	10.14	11	0.92		
Cor Total	103.50	19			

Model Statistics	
Std. Dev.	0.96
Mean	-0.37
C.V. %	257.01
PRESS	33.60
R-Squared	0.897
Adj R-Squared	0.831
Pred R-Squared	0.657
Adeq Precision	13.584

Slope Of Wheel Spindle Power (watts / min) =

10.280
- 4.802 * A
- 1.648 * B
- 19.885 * C
+ 0.852 * A * B
+ 9.197 * A * C
- 3.308 * B * C
- 1.594 * A * B * C

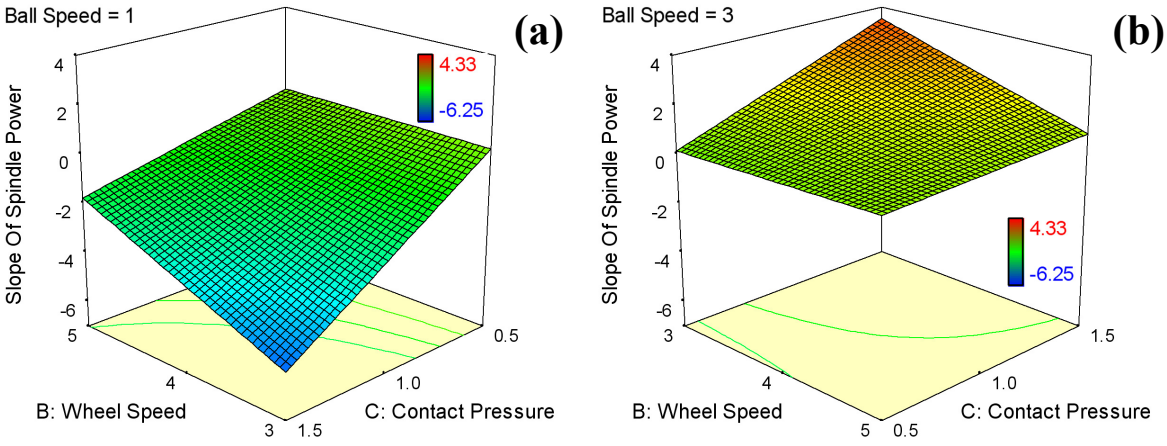

Appendix J7 - Model for the 'slope of spindle power' response. - ANOVA Table, Model statistics, and optimisation equation, 3D surface graph for ball speed of (a) 1.0 m/s, (b) 3.0 m/s.

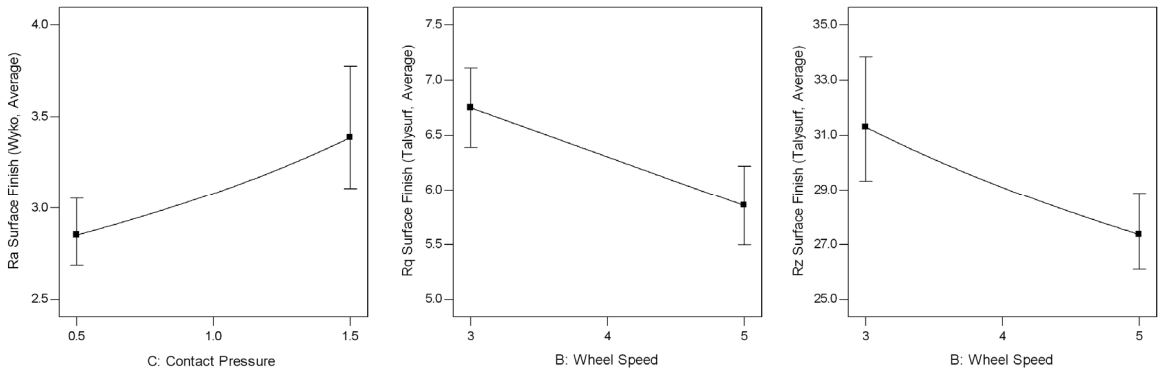

Appendix J8 - Additional graphs of surface finish results

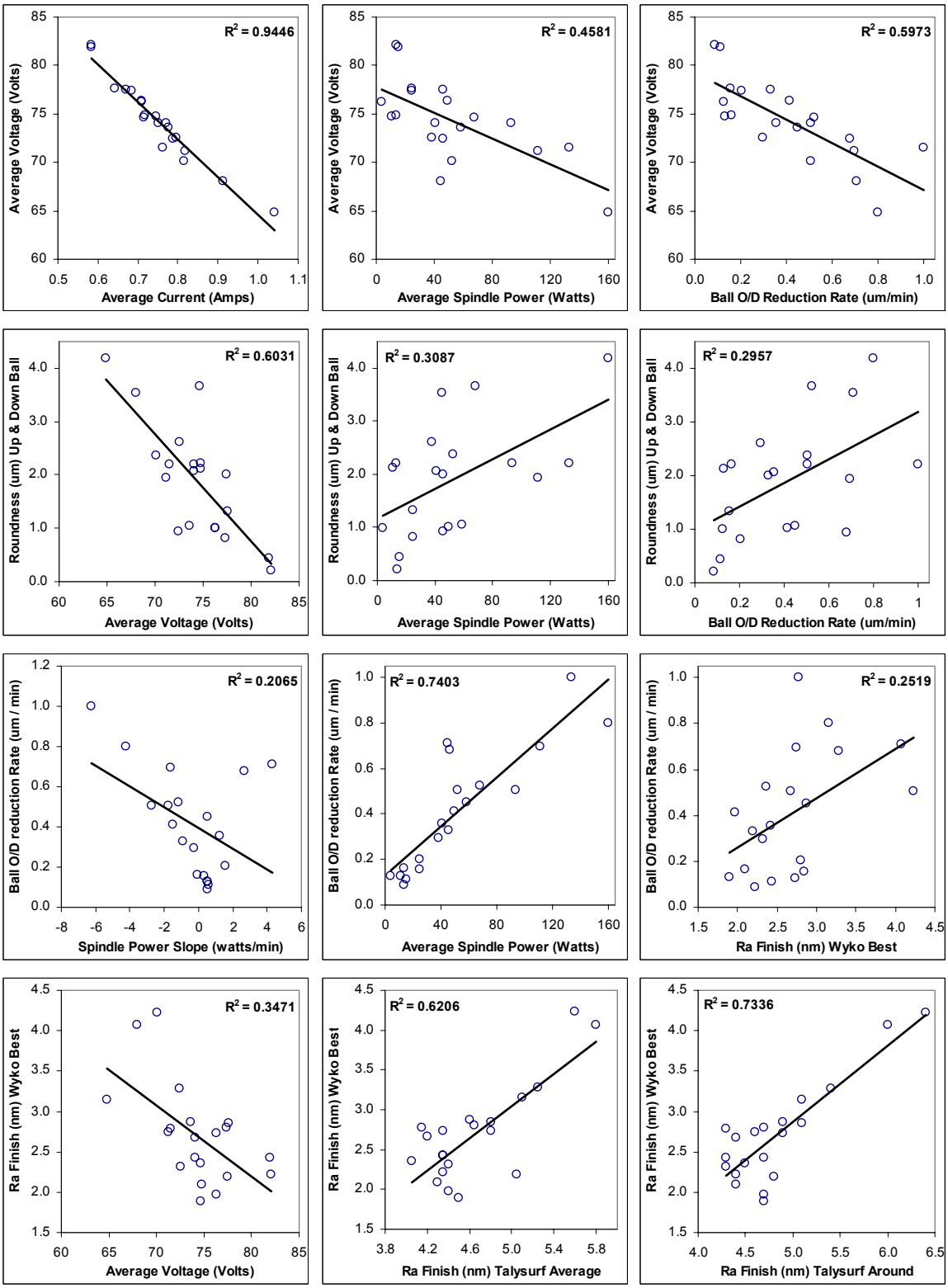

Appendix J9 - Selection of graphs showing the correlations between the responses

Average Elid Voltage During Superfinishing Response			
Model Term	Deg. Of Freedom	Sum Of Squares	Percent Contribution
A - Fluid Type	2	791.4	52.11
B - Nozzle Position	1	1.7	0.11
C - Nozzle Size	1	564.1	37.14
D – No. of Nozzles	1	17.3	1.14
AB	2	5.4	0.36
AC	2	102.6	6.76
AD	2	1.1	0.07
BC	1	0.0	0.00
BD	1	8.4	0.56
CD	1	11.9	0.79
ABC	2	1.5	0.10
ABD	0	Aliased	
ACD	2	11.9	0.79
BCD	1	1.4	0.09
ABCD	0	Aliased	
Residuals	0	0.0	

Average Elid Current During Superfinishing Response			
Model Term	Deg. Of Freedom	Sum Of Squares	Percent Contribution
A - Fluid Type	2	13.76	60.65
B - Nozzle Position	1	0.18	0.80
C - Nozzle Size	1	7.61	33.54
D – No. of Nozzles	1	0.52	2.30
AB	2	0.07	0.30
AC	2	0.03	0.11
AD	2	0.01	0.05
BC	1	0.02	0.10
BD	1	0.23	1.03
CD	1	0.13	0.58
ABC	0	Aliased	
ABD	2	0.01	0.07
ACD	2	0.11	0.48
BCD	1	0.00	0.01
ABCD	0	Aliased	
Residuals	0	0.00	

Average Change In Wheel Spindle Power Response			
Model Term	Deg. Of Freedom	Sum Of Squares	Percent Contribution
A - Fluid Type	2	31480	78.54
B - Nozzle Position	1	8	0.02
C - Nozzle Size	1	2705	6.75
D – No. of Nozzles	1	79	0.20
AB	2	374	0.93
AC	2	2945	7.35
AD	2	236	0.59
BC	1	796	1.99
BD	1	148	0.37
CD	1	5	0.01
ABC	2	1118	2.79
ABD	0	Aliased	
ACD	2	186	0.46
BCD	1	0	0.00
ABCD	0	Aliased	
Residuals	0	0	

Rate Of Ball O/D Reduction Response			
Model Term	Deg. Of Freedom	Sum Of Squares	Percent Contribution
A - Fluid Type	2	0.137	36.43
B - Nozzle Position	1	0.020	5.43
C - Nozzle Size	1	0.090	23.88
D – No. of Nozzles	1	0.000	0.01
AB	2	0.001	0.33
AC	2	0.116	30.91
AD	2	0.001	0.17
BC	1	0.000	0.01
BD	1	0.006	1.51
CD	1	0.000	0.00
ABC	2	0.004	1.06
ABD	2	0.001	0.23
ACD	0	Aliased	
BCD	1	0.000	0.03
ABCD	0	Aliased	
Residuals	0	0.000	

Appendix K1 - Tables of effects for the various responses assessed

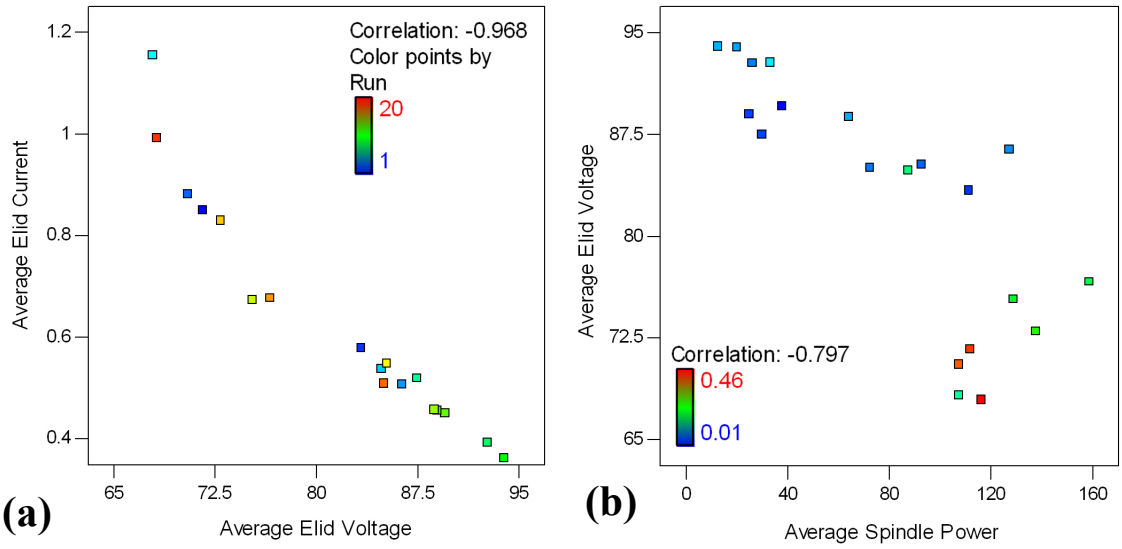

Appendix K2 - Correlations between responses.
(a) Coloured by run order, (b) Coloured by material removal rate

Source	Sum of Squares	Deg. Of Freedom	Mean Square	F Value	p-value Prob > F
Model	**22.432**	**7**	**3.205**	**152.005**	**< 0.0001**
A - Fluid Type	**11.491**	**2**	**5.745**	**272.529**	**< 0.0001**
B - Nozzle Position	**0.138**	**1**	**0.138**	**6.557**	**0.0250**
C - Nozzle Size	**8.119**	**1**	**8.119**	**385.100**	**< 0.0001**
D - No. of Nozzles	**0.522**	**1**	**0.522**	**24.764**	**0.0003**
BD	**0.240**	**1**	**0.240**	**11.389**	**0.0055**
CD	**0.130**	**1**	**0.130**	**6.190**	**0.0285**
Residual	0.253	12	0.021		
Cor Total	22.685	19			

Model Statistics	
Std. Dev.	0.145
Mean	2.452
C.V. %	5.922
PRESS	0.742
R-Squared	0.989
Adj R-Squared	0.982
Pred R-Squared	0.967
Adeq Precision	35.848

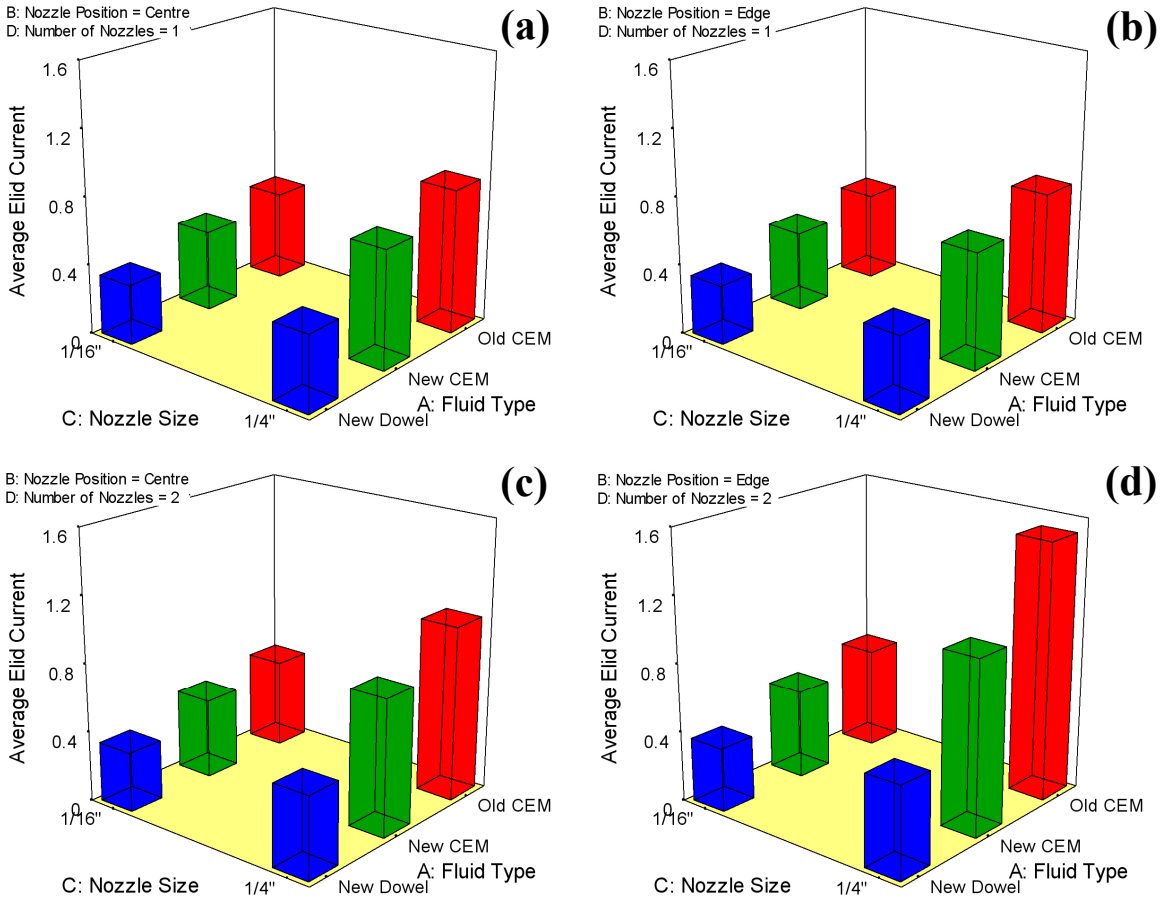

Appendix K3 - Average Elid current response model. - Anova table, model statistics, (a) One nozzle, centre position, (b) One nozzle, edge position, (c) Two nozzles, centre position, (d) Two nozzles, centre position. [Power transform applied lambda = -1.39. Actual current (amps) shown in graphs.]

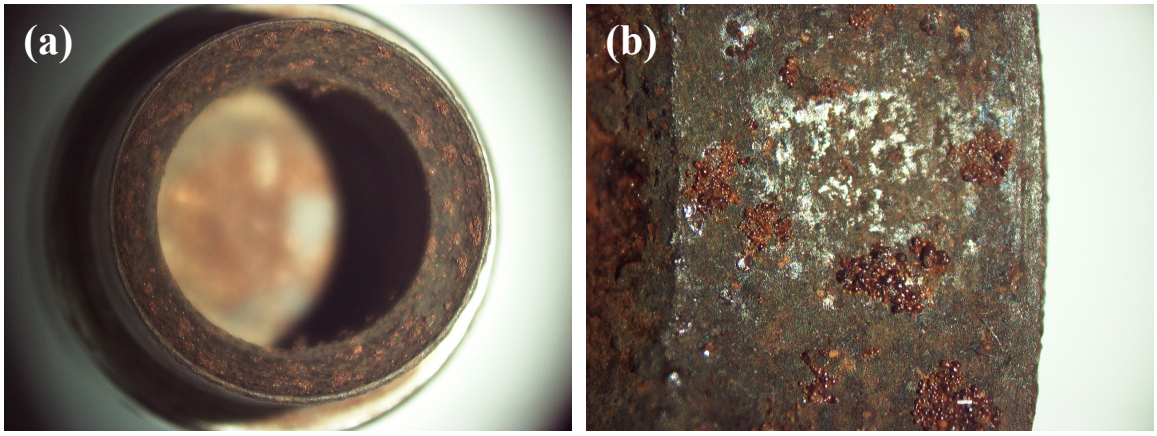

Appendix L1 - CIB-D wheel's surface after pre-process dressing –
(a) Full wheel picture, (b) Low magnification image

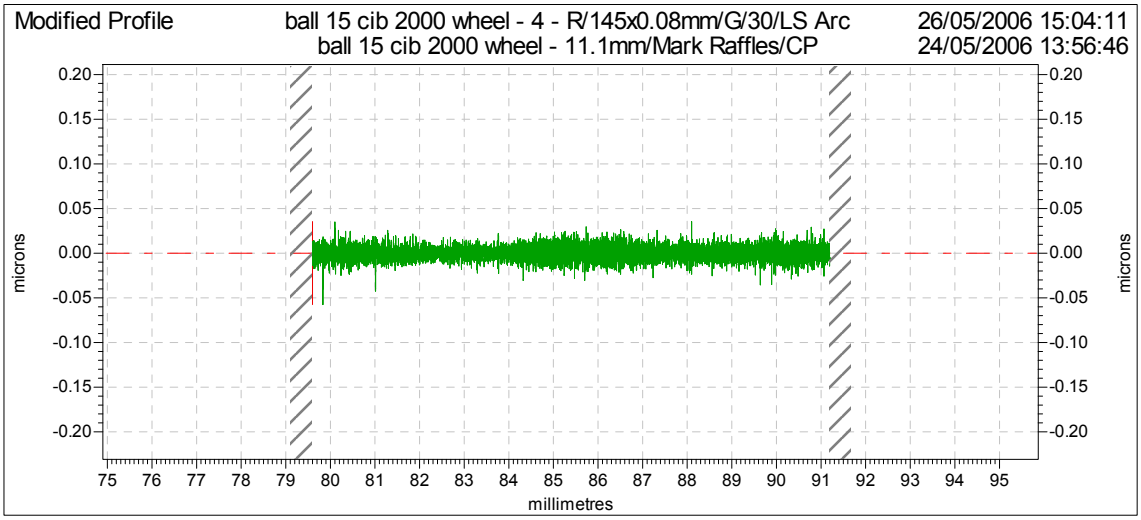

Radius	9.9068	mm				Rz(JIS)	0.0249	µm					
Ra	0.0057	µm	Rq	0.0074	µm	R3z	0.0237	µm					
Rsk	-0.1370		Rku	4.2824		R3y	0.0405	µm					
Rp	0.0177	µm	Rv	0.0181	µm								
RLo	11.6001	mm	Rt	0.0930	µm	Rmr(c)	50.21	%	Height (mean)	0.000	µm		
Rlq	6.00	µm	Rdq	0.442	°	RHSC	1747	peaks	Height (mean)	0.000	µm		
Rda	0.350	°	Rz	0.0358	µm	Rdc	0.0930	µm	mr1%	0.0	%	mr2%	100.0 %
RS	3.99	µm	RSm	12.41	µm	Rmr	50.00	%	offset	0.000	µm	mr%	50.00 %
Rln	11.6000	mm	Rc	0.0224	µm	RVo	0.0003	vol	offset	0.000	µm	mr%	50.00 %
						RPc	1742.2	pks/cm	Height (mean)	0.000	µm	bandwidth	0.00 µm

Appendix L2 - Highest quality surface roughness profile across an
RNB08 ball produced with a #2000 CIB-D wheel (Run 686)

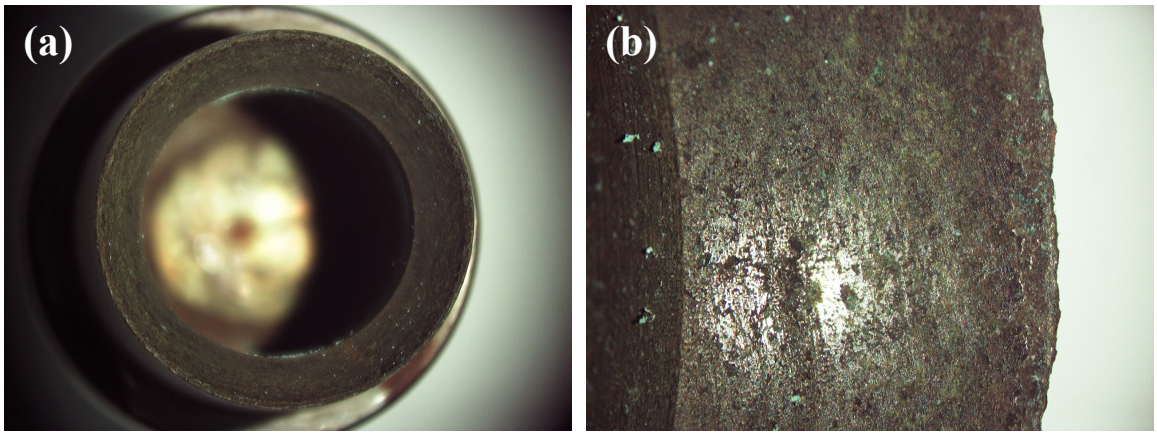

Appendix L3 - MRB-ALO wheel's surface after Elid 1 grinding –
(a) Full wheel picture, (b) Low magnification image

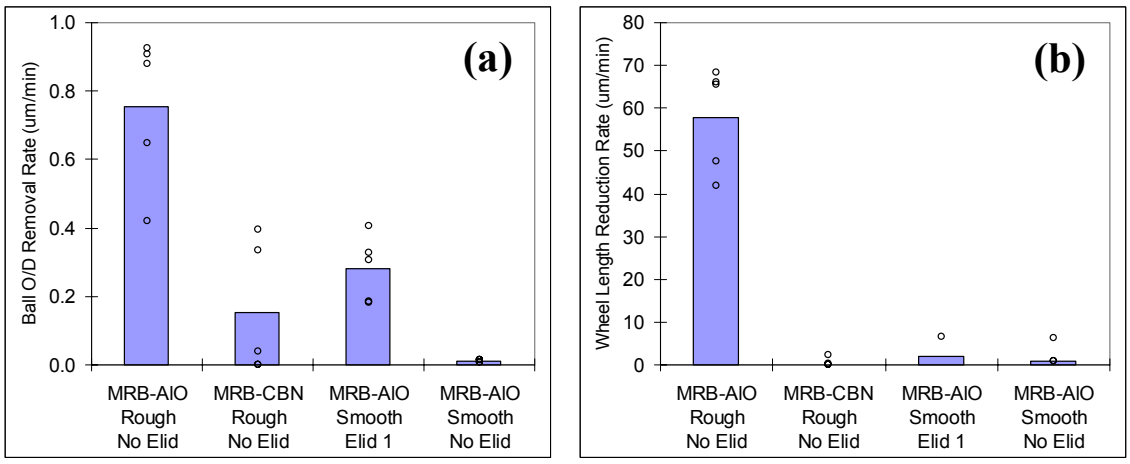

Appendix L4 – Effect of ball starting condition and the use of Elid on the rate of:
(a) Ball material removal and (b) Corresponding wheel wear (#8000 MRB-AlO wheel)

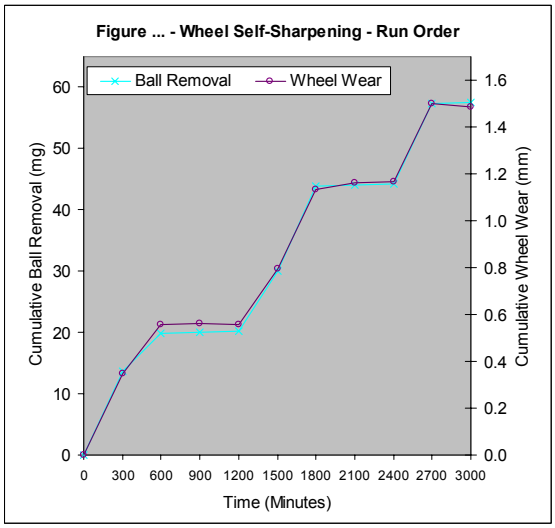

Appendix L5 - Correlation between wheel wear and ball material removal (#8000 MRB-AlO)

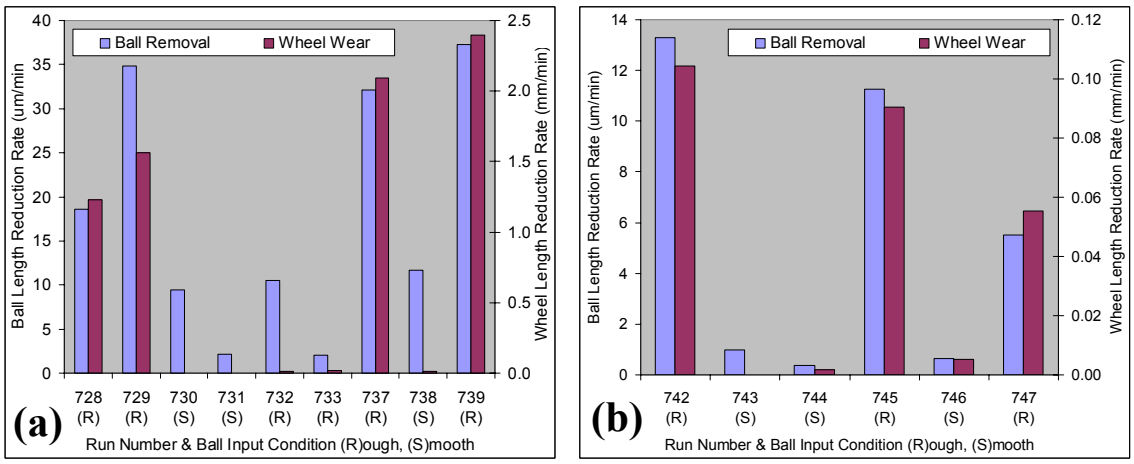

Appendix L6 - Ball material removal and wheel wear according to ball starting condition (a) Darmann No.2 wheel, (b) Darmann No.4 wheel

Appendix M1 - Superfinishing Of Heat Treated Balls 83 to 89

Cumulative Material Remove From Ball O/D During Processing
[From Ball Micrometer Measurements]

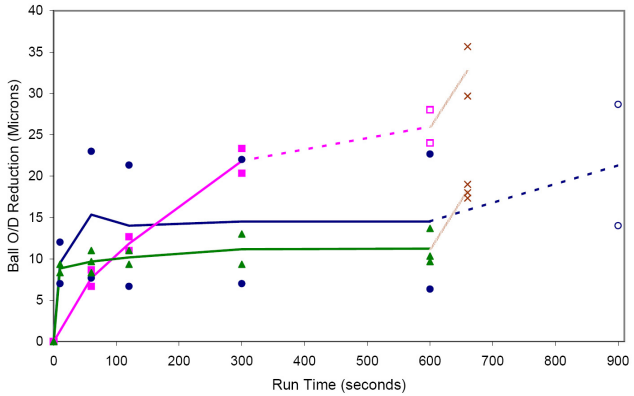

Ball Ra Surface Finish (T.H Talysurf) Across Ball Cnt of Good
Position / Fully Formed

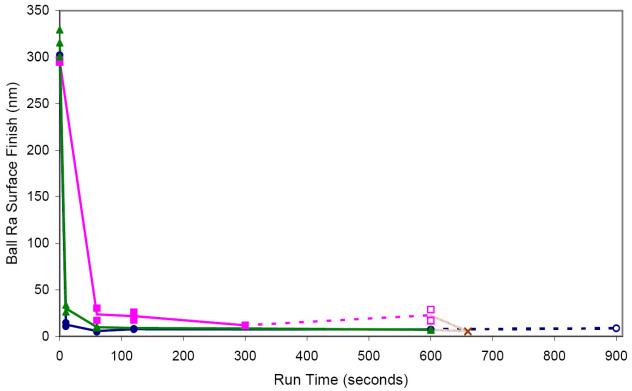

Ball Waviness - T.H. TalyCentre, Up & Down Ball

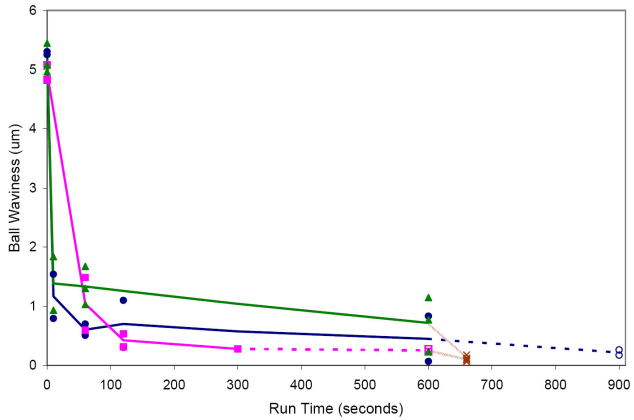

Ball Ra Surface Finish (Wyko Phase Shift Interferometer) – Average Result

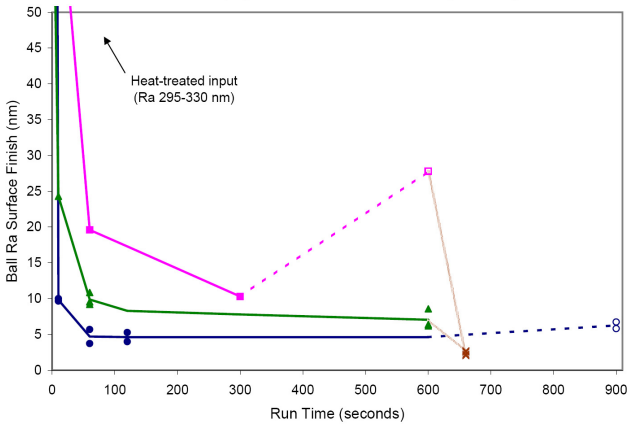

Appendix M2 - Superfinishing Of Cylindrically Ground Balls 75 to 81

Cumulative Material Remove From Ball O/D During Processing
[From Micrometer Measurements]

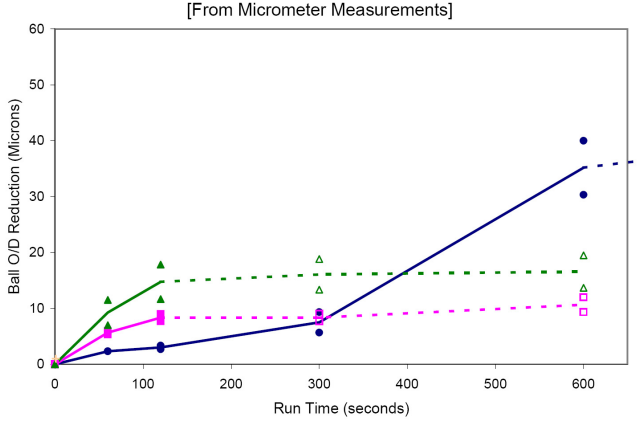

Figure … - Ball Rz Surface Finish (T.H Talysurf) Across Entire Ball Cnt

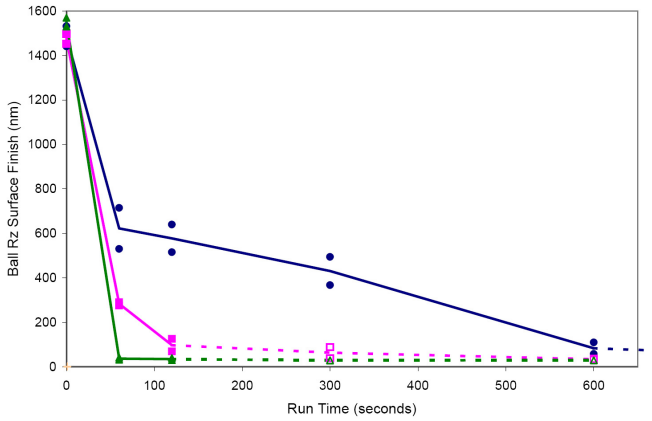

Ball Waviness (Talysurf) Across Entire Ball Centre

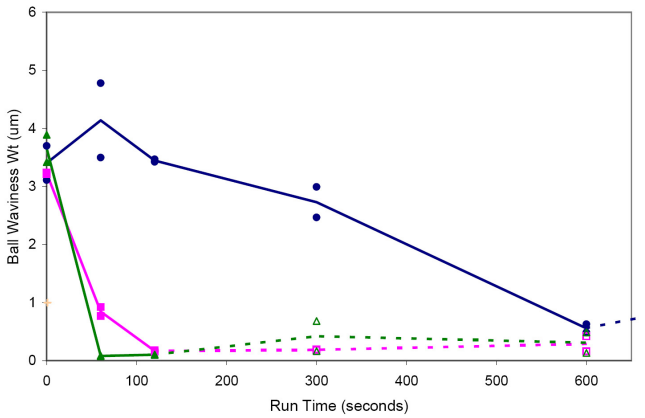

Ball Ra Surface Finish (T.H Talysurf) Across Ball Cnt of Good Position / Fully Formed

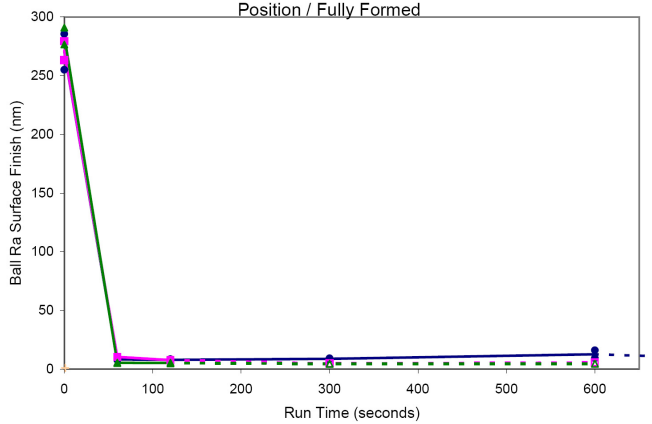

Appendix M3 - Superfinishing Of Honed Balls 64 to 72

Cumulative Material Remove From Ball O/D During Processing
[From Micrometer Measurements]

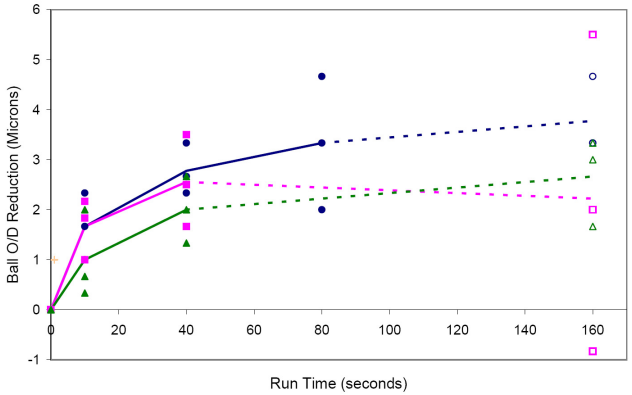

Ball Ra Surface Finish (T.H Talysurf) Across Ball Cnt of Good
Position / Fully Formed

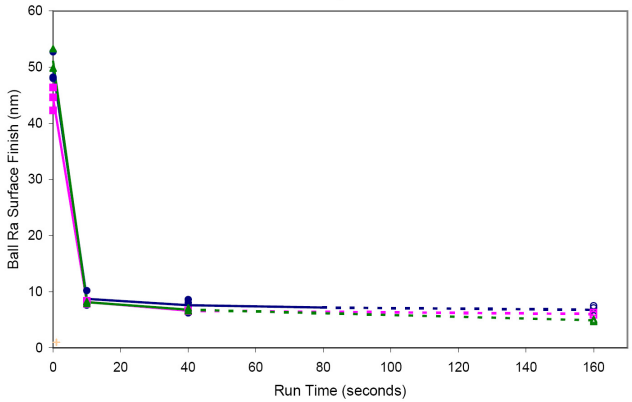

Ball Waviness (Talysurf) Across Entire Ball Centre

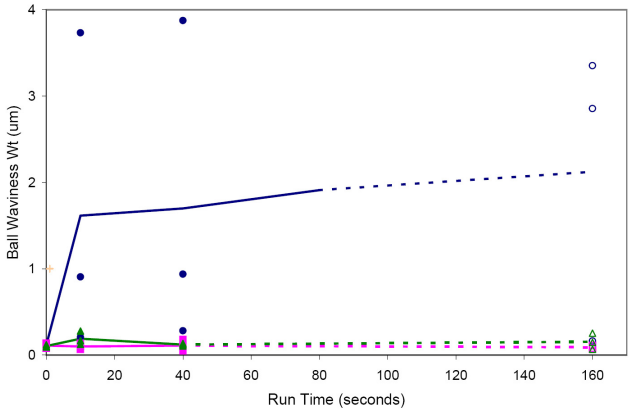

Drift Adjusted Average Power Increase During Grinding Run

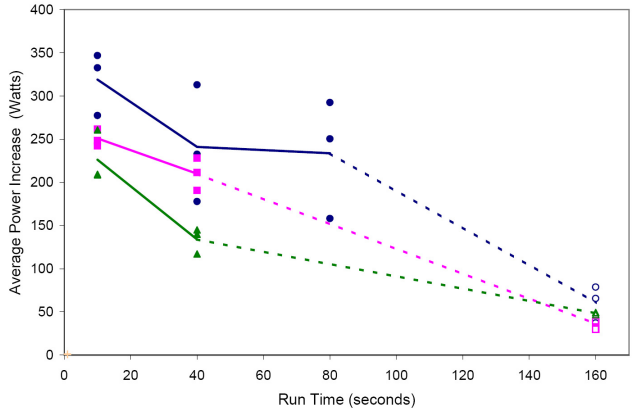

Appendix M4 - Superfinishing Of Barrelled Balls 50, 51, 52, 56, 57, and 58

Cumulative Material Remove From Ball O/D During Processing
[From Micrometer Measurements]

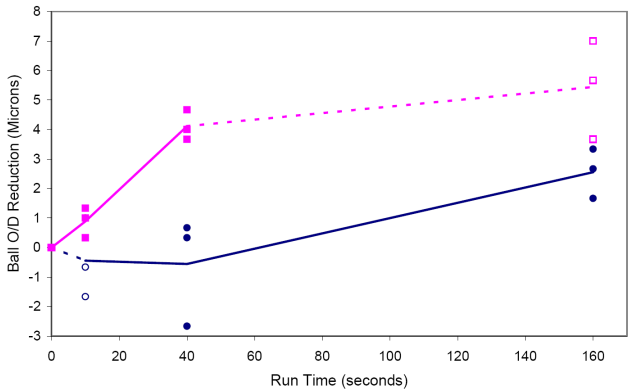

Ball Rz Surface Finish (T.H Talysurf) Across Entire Ball Cnt

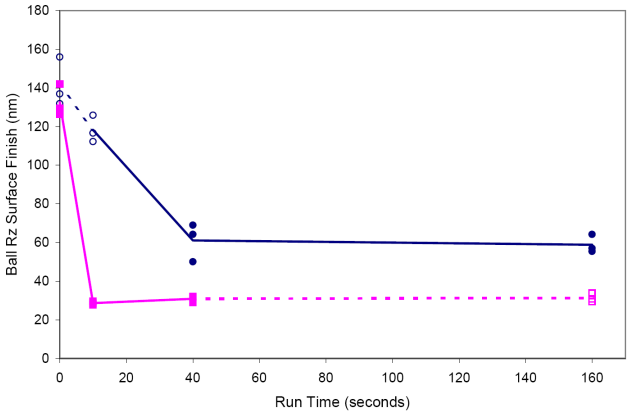

Ball Waviness (Talysurf) Across Entire Ball Centre

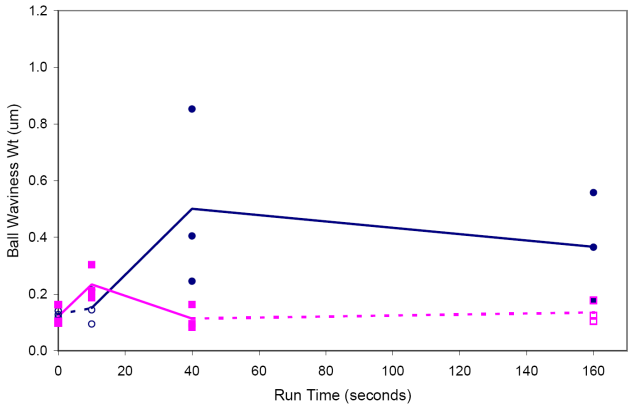

Ball Roundness - T.H. TalyCentre, Up & Down Ball

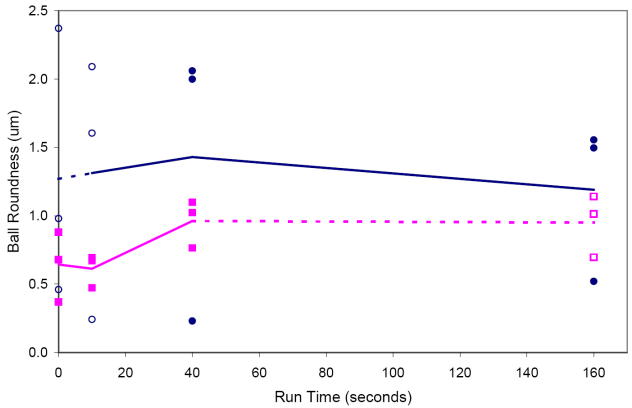

Appendix M5 - Various General Comparison Graphs